

Thèse présentée en vue de l'obtention du grade de docteur en Science

SYNTHESIS, PHYSICAL PROPERTIES AND SUPRAMOLECULAR
ORGANIZATION OF B-DOPED MOLECULAR MATERIALS

SIMON KERVYN DE MEERENDRE

NOVEMBER 2012



UNIVERSITY OF NAMUR

NAMUR

FACULTES DES SCIENCES

Laboratoire de Chimie Organique des Matériaux Supramoléculaires

“Satisfaction of one's curiosity is one of the greatest sources of happiness in life.”

Dr. Linus Pauling

Acknowledgements

My first thanks goes to *Professor Dr. Davide Bonifazi* for giving me the opportunity to work in his lab, at the beginning of his career, on many interesting and challenging projects. I appreciated his advices as well as his encouragement during my Ph.D. study. I especially thank him for giving me the opportunity to present my work and to widen my knowledge by attending interesting group meetings and conferences abroad.

Professor Dr. Alain Krief dedicated his time to my training more than 6 years ago, when I started my master thesis in his group. His many suggestions helped me to successfully achieve the different projects, throughout the years of this Ph.D., more particularly during the synthesis of the DDDD system of hydrogen bonding. I am also very grateful to *Dr. Adrian Kremer*, *Dr. Riccardo Marega*, *Dr. Stefan Mohnani*, and more particularly *Dr. Irene Georgiou*, for the proof-reading and many helpful suggestions on this manuscript.

The helpful collaboration with several research groups was also a key factor in the achievement of this work.

I thank the group of *Professor Dr. Johan Wouters*, with a great help from *Bernadette Norberg*, who has resolved all X-ray diffraction structures, in the University of Namur.

Many thanks go to with *Dr. Gianluca Accorsi*, in the group of *Dr. Nicola Armaroli*, CNRS, Bologna, Italy, who studied photophysical properties of borazine derivatives.

Special thanks go to the group of *Professor Dr. Giovanni Costantini* from the University of Warwick in the United Kingdom, which performed the surface analysis, using STM instrument. Many thanks go to *Nataliya Kalashnyk* for the STM experiments.

OLED devices fabrication was completed in the lab of *Professor Dr. Franco Cacialli*, in UCLondon, United Kingdom, I am grateful to him and his group for welcoming me and teaching me engineering techniques during a two weeks stay.

During a stay in the group of *Dr. Takashi Nakanishi*, in the NIMS institute from Tsukuba in Japan, the properties of borazine•fullerene cocrystal were probed, I thank him for the extraordinary welcome and a good collaboration during this stay.

In addition, I would like to acknowledge the group of *Dr. Pascal Gerbaux* at the University of Mons for measuring mass spectra.

Of course, this project wouldn't have been completed without the funding from F.R.I.A. (Fonds pour la Recherche dans l'Industrie et l'Agriculture) and from the University of Namur.

Many thanks go to all the people working in the University of Namur. More particularly, I would like to acknowledge *Alain Burlet* and *Giuseppe Barbera*, technician for the organic chemistry labs. This project would have been finish without the advices and help from *Dr. Praveen Ganesh* and the help of *Florence Valtin*, who worked during her master thesis on the synthesis of boronic acid derivatives. Obviously, the whole lab has his share for the good working atmosphere: *Dr. Stefan Mohnani*, *Dr. Simone Armani*, *Dr. Adrian Kremer*, *Dr. Riccardo Marega*, *Dr. Chiara Fabbro*, *Dr. Claudia Aurisicchio*, *Benoit George*, *Laura Maggini*, *Arnaud Delforge*, *Daphné Stassen*, *Laure-Elie Carloni*, *Valentina Corvaglia*, *Rosaria Vulcano*, *Federica De Leo*, *Silvia Forensi*, *Florent Pineux*, *Jonathan Tasseroul*.

Finally, I would like to thank my family and friends for their extraordinary support throughout the thesis.

Table of contents

List of abbreviations	IV
Abstract	VII
1. Introduction	3
1.1 Boron Connected to Aryl Units	3
1.1.1 Derivatives Used in Chemicals Sensing	7
1.1.2 Steric Protection of Borane Derivatives	4
1.2 Boron Inserted into Aryl Units	10
1.2.1 Borabenzene	10
1.2.2 Boranaphthalene and Higher Acenes	12
1.2.3 Borepin and Boroles	13
1.3 Boron-Nitrogen Pair Inserted into Aryl Units	15
2. Borazines-Borazenes, Synthesis, Photophysical Properties, Surface Study and Implementation in OLEDs	22
2.1 Introduction	22
2.1.1 Synthetic Strategies and Photophysical Properties of Borazine Rings	23
2.1.1.1 Synthesis of Borazine Rings by Dehydrogenation of Aminoborane	24
2.1.1.2 Synthesis of Borazine Rings from Halogeno Borane	24
2.1.1.3 Synthesis of Borazine Rings by the Reduction of Multiple Bonds Using Borane	27
2.1.1.4 Synthesis of Borazine Rings from Nucleophiles Reacting with Boronic Esters	27
2.1.1.5 Synthesis of Differently Substituted Borazine Rings	28
2.1.2 Reactivity of the Borazine Ring	28
2.1.3 Stability of the Borazine Ring	29
2.1.4 Synthesis of Borazenes	30
2.2 Synthesis	32
2.2.1 Synthesis of Hexaphenyl Borazine	32
2.2.2 Synthesis of Borazines Stable toward Moisture	33
2.2.3 Synthesis of Sterically Hindered Borazenes	37
2.2.4 Differently Substituted Borazine on the Boron atoms	45
2.3 Crystal Structures-Polymorphism	48
2.3.1 Crystal Structure of Hexaphenylborazine 169	48
2.3.2 Crystal Structures and Polymorphs of B-trimesityl-N-triphenylborazine 173	49
2.4 UV-Vis Absorption and Fluorescence Properties	51
2.4.1 Analysis of the Doping Effect: HPBenzene vs HPBorazine	51
2.4.2 UV-Vis Absorption and Fluorescence Properties in Solution and in the Solid State of Borazine 173	52
2.4.2.1 UV-Vis Absorption and Fluorescence in Solution	52
2.4.2.2 Fluorescence in the Solid State	55
2.4.3 UV-Vis Absorption and Fluorescence Properties in Solution and in the Solid State of Extended Borazine 176	56

2.4.4 UV-Vis Absorption and Fluorescence Properties in Solution and in the Solid State of Differently Substituted Borazine 196	57
2.5 UHV-STM Characterization of Borazines on Au and Cu Surfaces	58
2.5.1 Surface Study of HPborazine 169	58
2.5.2 Surface Study of B-trimesityl-N-triphenylborazine 173	59
2.5.3 Surface Study of Differently Substituted Borazine 196	59
2.6 OLEDs and LECs, Constructions and Characterizations	60
2.7 Borazine-Fullerene cocrystal	62
2.7.1 Structural Studies	63
2.7.2 Photophysical Properties	64
2.8 Conclusions and Outlooks	66
3. Boronic Acid Derivatives as new Scaffold for H-Bonded Supramolecular Architectures	68
3.1 Introduction	68
3.1.1 Hydrogen Bond Features	68
3.1.1.1 Hydrogen Bond Definition	68
3.1.1.2 Hydrogen Bond Strength	69
3.1.1.3 Hydrogen Bond Geometry	71
3.1.1.4 Hydrogen Bond Distances	75
3.1.1.5 Multiple Hydrogen Bonds	75
3.1.1.5.1 Effect of the Number of Hydrogen Bonds on the Binding Constant	75
3.1.1.5.2 Effect of the Secondary Interactions on the Binding Constant	75
3.1.2 Characterization of the Hydrogen Bond	76
3.1.2.1 Stoichiometry of the Complex: Job's Plot	76
3.1.2.2 Determination of the Thermodynamic Parameters by NMR Spectroscopy	77
3.1.2.3 Determination of the Thermodynamic Parameters by ITC	78
3.1.3 Boronic Acids Features	79
3.1.3.1 Boronic Acids-Boroxines	80
3.1.3.1.1 Equilibrium Between Boronic Acid and Boroxine Forms	80
3.1.3.1.2 Distinction between Boronic acid and Boroxine Forms by Spectroscopic Methods	81
3.1.3.1.3 Parameters Favoring the formation of Boroxine	81
3.1.3.2 Conformations of the Boronic Acids	82
3.1.3.3 Boronic acids in Supramolecular Chemistry	83
3.1.3.3.1 Boronic Esters	83
3.1.3.3.2 Spiroborates	84
3.1.3.3.3 Boroxines	85
3.1.3.3.4 Hydrogen Bonded Complexes	86
3.2 Synthesis	89
3.2.1 Synthesis of Boronic Acids (DD Systems)	90
3.2.2 Synthesis of Multiple Boronic Acid (DDDD Systems)	92
3.2.3 Synthesis of Hydrogen Bond Acceptors	97
3.3 Equilibrium between Boronic Acids and Boroxines	98
3.3.1 Analysis of Boroxines by ¹ H NMR Spectroscopy	98
3.3.2 Analysis of Boroxines by IR Spectroscopy	101
3.3.3 Temperature Effects on Complexation	101
3.4 Crystal Structures Study	103

3.4.1 Crystal Structures of Boroxines	103
3.4.2 Crystal Structures of Self-Interacting Boronic Acids	105
3.4.3 Crystal Structures of Complexes	108
3.4.3.1 Complexes with Pyridyl or Naphthyridine as Acceptors (1:1 Stoichiometry)	108
3.4.3.2 Bidentate Hydrogen Bond Motifs	114
3.5 Binding Constant Measurement by ITC	117
3.6 Conclusions and Outlooks	122
4. Experimental part	123
4.1 Instrumentation	123
4.2 Materials and General Methods	123
4.3 Experimental Procedures	124
4.3.1 Borazine and Borazene Derivatives	124
4.3.2 Boronic Acid Derivatives	130
Appendix I - Crystal structures	138
Appendix II – NMR Spectra	155
Bibliography	194
<i>Curriculum Vitae</i>	211

List of Abbreviations

Å	Angstrom (1 Å = 10 ⁻¹⁰ m)
aq.	aqueous
br.	broad (NMR)
Bu	butyl
<i>n</i> -BuLi	<i>n</i> -Butyllithium
<i>tert</i> -BuLi	<i>tert</i> -Butyllithium
°C	degree centigrade (0 °C = 273.16 K)
cal	calorie (1 cal = 4.184 J)
calc.	calculated
CDCl ₃	<i>d</i> -chloroform
CSD	Cambridge structural database
δ	chemical shift (NMR)
d	doublet (NMR)
DDQ	2,3-Dichloro-5,6-Dicyanobenzoquinone
DMF	N,N'-dimethylformamide
DMSO	Dimethyl sulfoxide
ε	extinction coefficient
E ^{1/2}	half-wave potential
<i>e.g.</i>	<i>exempli gratia</i> (latin)-for example
EI	electron impact
ESI	electrospray ionization
Et	ethyl
Et ₂ O	diethylether
EtOAc	ethyl acetate
eV	electron volt (1 eV = 1.602 x 10 ⁻¹⁹ J)
EQE	external quantum efficiency
Φ	quantum yield
Fcc	face-centered cubic
g	gram
HOMO	highest occupied molecular orbital
HPLC	high performance liquid chromatography
HR	high resolution

Hz	Hertz (s^{-1})
<i>i.e.</i>	<i>id est</i> (latin)-that is to say
IR	infrared
ITC	isothermal titration calorimetry
ITO	indium tin oxide
J	Joule
<i>J</i>	coupling constant (NMR)
k	kilo (10^3)
K	Kelvin
λ	wavelength
λ_{abs}	wavelength of absorption
λ_{em}	wavelength of emission
LEC	light emitting electrochemical cell
LUMO	lowest unoccupied molecular orbital
m	multiplet (NMR)
M	molarity (mol L^{-1})
MALDI	matrix assisted laser desorption-ionization
Me	methyl
MeCN	acetonitrile
MeOH	methanol
min.	minutes
μL	microliter
mol	mole
m.p.	melting point
MS	mass spectrometry
MW	microwave
NLO	non-linear optics
NMR	nuclear magnetic resonance (spectroscopy)
OLEDs	organic light emitting diodes
ppm	part per million
STM	scanning tunneling microscopy
q	quartet (NMR)
r.t.	room temperature
s	second, singlet (NMR)

t	triplet (NMR)
TBAF	tetrabutylammonium fluoride
TBS	tert-butyl silane
TEM	transmission electron microscopy
Tf	trifluorosulfonate (triflate)
THF	tetrahydrofuran
TMEDA	tetramethylethylenediamine
UV	ultraviolet
UV-Vis	ultraviolet-visible
V	Volt
vs.	<i>versus</i> (latin) - against

Abstract

π -conjugated structures have been at the center of a growing interest regarding their applications in material science, for OLED, for solar cells and for information storage. In order to extend their applications field, the electronic properties of these molecules can be tuned by substituting the π -conjugated backbone with electron donating or withdrawing groups. An alternative strategy is to tune these properties by replacing the carbon atoms of a compound by heteroatoms. This leads to compounds presenting large arrays of tuned properties. For example, replacing a carbon-carbon pair, in a π -conjugated compound, by a boron-nitrogen pair can lead to bathochromically or hypsochromically shifted fluorescence, which can be exploited for emitting materials in OLED. The objective of the present thesis is to gain a detailed understanding of both the properties and the molecular and supramolecular structures of such compounds.

This thesis is composed of four chapters; the first will present a review of the literature on the subject, the second will focus on the synthesis and properties of molecules where a carbon-carbon pair has been replaced by a heteroatom pair. The third chapter describes the supramolecular assemblies of boronic acids and the final chapter reports the experimental procedures for the synthesis of the product characterized in this thesis.

In *Chapter 1*, the reader is given a brief account of the synthetic strategies and photophysical properties of boron-doped organic molecules. In the first part, the replacement of a carbon atom by a boron atom, introducing an electronic vacancy in the molecule, is described. The second part gives examples of the replacement of a carbon-carbon pair by a boron-nitrogen pair, which leads to dramatic changes in the emission properties of the molecules.

In *Chapter 2*, a brief account of synthetic strategies and reactivity, crystal structure and photo-physical properties of borazine derivatives is presented, followed by their UHV-STM studies, implementation inside the luminescent layer of an OLED and the structural and photophysical study of a borazine·fullerene cocrystal. Firstly, the synthesis of hexaarylborazine derivatives are described. It was noticed that hexaphenylborazine **169** hydrolyzed into phenylboronic acid **170** (Figure 3) upon standing in non-anhydrous solvent or upon standing at air. Stable compounds are needed for applications in material sciences, such as OLED. Therefore, the synthesis was refocused on stable borazine **173** and extended borazine **176**, possessing sterically encumbered substituents, *i.e.* mesityl groups, linked to the boron atoms. The methyl groups on the aryl substituents can be replaced by isopropyl moieties to increase the steric protection around the boron atoms. However, in this case the borazine cycle could not be formed due to the steric clash between the *ortho* substituents and hydrolysis reaction led to the isolation of linear modules constituted of boron-nitrogen bonds, called borazene (*e.g.* molecule **183**, **191** and **192**). This led us to understand the limits between the synthetic availability and the steric protection wanted for borazine derivatives. The hypothetical synthetic pathway for the formation of borazene was further studied. Adding two equivalents of mesityl lithiate on the borazole intermediate, followed by the addition of H₂O, led to differently substituted borazine **196**.

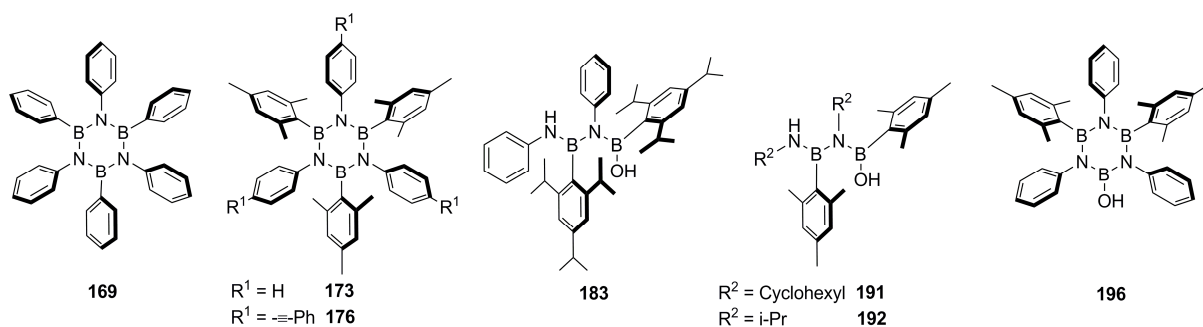


Figure 1 Hexaphenyl borazine **169** sterically protected borazine **173** and **176**, linear borazene **183**, **191**, **192** and differently substituted borazine **196**.

The second section of *Chapter 2* details this steric protection, the bond distances, the angles and the crystal packing, probed by means of X-ray diffraction. While hexaphenylborazine **169** does not possess *ortho* substituents, the methyl groups of borazine **173** and **194**, or isopropyl groups of borazene **183** sterically encumbered the boron atoms. The nucleophilic attack of H₂O molecules on the boron centers, which would lead to the hydrolysis of the boron-nitrogen bonds, is therefore prevented by the substituents. The crystal structures obtained for the borazine derivatives revealed a planar cycle surrounded by substituents nearly perpendicular to the plane of the heterocycle (dihedral angles from 60° to 83°). As a consequence, the substituents are all tilted in one direction, forming a chiral helical structure. In the unit cell, the two turns (clockwise and anti-clockwise) are present since the crystal has grown on achiral substrate. In the fourth section, the adsorptions of borazine on achiral surfaces are described. Another interesting discovery is the formation of polymorphs for borazine **173**, which are reflected by the different fluorescence properties in the solid state.

UV-Vis absorption and fluorescence properties were probed in solution and in the solid state and are the subject of the third section. The fluorescence peak of borazine **169** is hypsochromically shifted ($\lambda_{em} = 328$ nm, $\Delta\lambda = 4$ nm, $\Delta E = 0.05$ eV) respective to hexaphenylbenzene fluorescence peak ($\lambda_{em} = 332$ nm), as expected. The emission of borazine **173** is further shifted in the UV region ($\lambda_{em} = 310$ nm) and the quantum yield is improved (7.7% in CH₂Cl₂ solution). The solid state emissions were probed for each polymorph of the latter compound and revealed a bathochromically shifted emission ($\Delta\lambda = 53$ nm, $\Delta E = 0.59$ eV) for the most compact crystalline polymorph. The presence of polymorphs and the unwanted bathochromic shift in the solid state emission led us to realize the importance of solid state organization inside the OLEDs.

The fourth section describes the adsorption of borazine derivatives on metallic surfaces, which was probed by UHV-STM technique in order to test which electrodes will have a good electrical contact with our compounds. As outlined earlier, two chiral molecules are present in the unit cell of derivatives **169** and **173** in the crystalline state. Upon adsorption on achiral surface, the molecules and the surface form a chiral object. This can be measured by the height differences, respective to the surface, of the aryl group substituting the borazine cycle. The turn can be clockwise or anti-clockwise, with a majority of clockwise turn observed on Cu(111) surfaces for borazines **169** and **173** (Figure 2a and b), which forms regular monolayer. At the contrary, adsorption of asymmetrically substituted borazine **194** on Cu(111) revealed a surprisingly regular arrangement resulting in hexagonal clusters constituted of seven molecules (Figure 2c). This regular pattern is due to the deprotonation of the hydroxyl group by the surface, and subsequent organization of neutral molecules to screen the charged, central molecule.

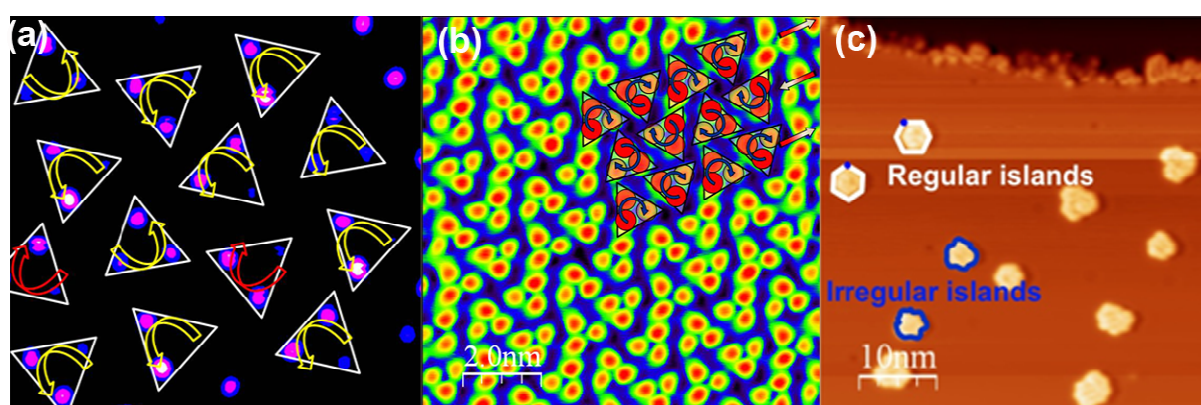


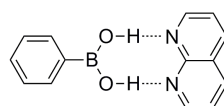
Figure 2 UHV-STM study of borazine derivatives. (a) **169** on Cu(111) The disposition can be clockwise or anti-clockwise following the height gradient. (b) **173** on Cu(111) presenting regular high-packing density, clockwise turns along the different heights of the mesityl substituents. (c) **194** on Cu(111), displaying the regular, hexagonal island constituted of 7 molecules.

Having completed these preliminary studies, the derivative possessing the highest quantum yield (*i.e.* borazine **173**) was implemented into the emissive layer of an OLED. The increase of current density through the device matched the augmentation of light emission. However, the emission profile of the device was bathochromically shifted in the visible

region. This was attributed to a particular aggregation of the chromophore that explains the bathochromic shift of the emission peak, a phenomenon similar to the one observed for the solid state emission of the polymorphs.

Finally, energy transfer between borazine **173** and [60]fullerene was studied. The two compounds were dissolved and crystallized together to form a cocrystal. The structure of the latter was studied by SEM, TEM and powder X-ray diffraction, the 3D crystal structure could not be solved due to crystal twinning. The photophysical properties were probed in solution, revealing no change in the absorption spectra, and in the solid state. Solid-state absorption spectra revealed a hypsochromic shift of the fullerene absorption peak and a quenching of the solid state fluorescence of borazine **173**, indicative of an energy transfer between the borazine and the [60]fullerene.

Chapter 3 describes the synthesis of boronic acids derivatives and latter their self-assembly with hydrogen bond acceptors, probed in solution by means of ITC titration and in the solid state by means of X-ray diffraction. Synthesis of boronic acids, to be used as DD system of hydrogen bond, was straightforward using conventional procedure. While the synthesis of DDDD system, possessing two adjacent boronic acid groups, revealed to be more challenging. Boronic acids derivatives (*e.g.* phenyl boronic acid **170**) are known to be in equilibrium with their anhydride form, called boroxines. Several factors influence the equilibrium, such as the temperature, the substitution by electron withdrawing or donating moieties and the presence of *ortho* groups on the aryl substituting the boronic acid moiety. In this work, the aryl groups were substituted by *ortho* substituents to favor the formation of the acid form. The boroxine forms were probed by ^1H NMR, and IR spectroscopy to detect their presence before ITC titration with a AA system (*i.e.* 1,8-naphthyridine **223**) was carried out. Indeed, the ITC measures the global heat released by the system and the presence of boroxine would lead to the determination of an incorrect value of the binding constant. The ITC measurements provide the values of K_a , ΔG , ΔH , ΔS and the stoichiometry (n) of the complex formed. The trend observed for several derivatives substituted in *ortho* positions, is the increase of K_a when the arylboronic acids are substituted by inductive electron withdrawing atoms (*e.g.* fluorine or chlorine atoms, $\Delta H^\circ = -44.28$ and -48.5 kJ mol^{-1} respectively) as opposed to electron donating groups (*e.g.* methyl or isopropyl groups $\Delta H^\circ = -37.20$ and -37.89 kJ mol^{-1} respectively). The stoichiometry of the complex was further confirmed by X-ray diffraction in the solid state, assuming that the complex formed would be identical in solution. This extensive X-ray study provided also the hydrogen bond lengths and geometry of the complex. The decreased hydrogen bond distances observed, at the solid state, for boronic acid derivatives substituted in *ortho* position by electron withdrawing atoms, could be correlated to the augmentation of enthalpy measured by ITC, in solution.



170•223

Figure 3 Phenylboronic acid (**170**) in complex with 1,8-naphthyridine (**223**).

1. Introduction

During the last decades the research regarding π -conjugated structures has been active and mainly aimed in the creation of new materials, which can be used as organic transistors,^[1] as emitters for non-linear optics (NLO),^[2] and as luminescent compounds for Organic Light Emitting Diode (OLED).^[3] The emission wavelength of organic emitters depends on the energy difference between the Highest Occupied Molecular Orbital (HOMO) and the Lowest Unoccupied Molecular Orbital (LUMO), the HOMO-LUMO gap. Therefore it is desirable to tune this gap, in order to achieve large array of emission wavelengths. To reach this aim, several strategies have been reported, the first being to extend the π -conjugation of the compound. This can be accomplished by increasing the chain lengths of polymers.^[4] In this case, due to the delocalization of the electrons, the $\pi \rightarrow \pi^*$ orbitals are degenerated, reducing the HOMO-LUMO gap. As a result, a bathochromically shifted absorbance is observed.^[4] An alternative strategy is to facilitate the intramolecular charge transfer by substituting the π -conjugated backbone by an electron donating and an electron withdrawing group, this is called the 'push-pull' approach. In particular, these systems are basically constituted by mesomeric donor or acceptor groups interacting through the π -conjugated specie. In this case, the electronic transition is dominated by the $n \rightarrow \pi^*$ transition, which is lower in energy than the $\pi \rightarrow \pi^*$ transition. This result in the reduction of the HOMO-LUMO gap, as observed by the bathochromic shift.^[5-8] Finally, a more dramatic change of the electron density can be achieved by replacing carbon atoms of the backbone by heteroatoms. For example, this strategy has been applied successfully to substitute derivative of perylene by sulfur and selenium atoms.^[9] In this particular case, the derivatives substituted by the heteroatoms revealed a slight hypsochromic shift in the UV-Vis absorption spectra.^[9] As a result, the main objective of this thesis was to probe the properties of organic π -conjugated compounds by taking advantage of the last methodology mentioned. In particular it was envisaged to replace carbon atoms of conjugated systems by heteroatoms, such as boron atoms.

Organoboron compounds have been known and used for decades in applications such as coupling agents in cross-coupling reaction (Suzuki-Miyaura reaction),^[10,11] such as drug compounds including carboranes as pharmacophores in biologically active compounds,^[12,13] and as structural analogues of [60]fullerene.^[14] Nevertheless their use in electronic materials is relatively new.^[15] When a boron atom adopts a position in the compound formerly occupied by a carbon atom, it is electronically equivalent to introducing a trivalent carbocationic species, bearing an empty p orbital perpendicular to the plane of the compound. As a result, by connecting a boron atom to π -conjugated structures, the energy level of their frontier orbital will be affected, due to the conjugation between the empty p orbital of the boron atom with the π orbitals (Figure 1.1a). In the recent years, the field of both the synthesis and material applications of boron-containing organic structures including fluorine sensors,^[16] luminescent compounds in OLED,^[17] and even carboranes for medical applications,^[18] has drawn a great amount of interest from the scientific community and hence a number of reviews have been reported.^[16-18] Therefore, the introduction of this thesis will uncover and report organic compounds in which the boron atom is connected to at least an aryl unit or inserted in an aromatic structure, allowing a conjugation between the empty p orbital of the boron atoms and the π electrons. Most importantly, an additional aim is to provide an overview on the synthesis and applications of compounds with an incorporation of a boron-nitrogen pair, conjugated with π electrons of the rings.

As already mentioned, a first modification of the electronic properties of the material can be accomplished when a boron atom can be connected to aryl groups and this is the subject of *section 1.1*. Due to their electronic deficiency boron atoms can operate as electrophilic centers accommodating anionic species or accepting charges from electron donating bonding units, such as mesomeric donor nitrogen atoms ultimately giving rise to intramolecular charge-transfer phenomena and serve as hole carriers (Figure 1.1c). Taking advantage of these properties it was believed that boron-containing organic architectures seemed to be promising candidates to act as i) molecular sensors for anions detection (mainly fluorides and cyanides); ii) organic materials for NLO applications; and iii) hole transporters and/or emitters for OLEDs.^[19,20] Based on the fact that the conjugation between the p orbital and the π orbitals is cut when the boron atom is tetrasubstituted, borane derivatives

Chapter 1

have been used as molecular sensors. At the ground level, this conjugation between the boron atom p orbital and the backbone of the compound is known to affect principally the LUMO level of the compound and therefore the π^* orbital.^[16,21] Upon addition of fluoride anion or other anions that bind to the empty p orbital, the complex are formed with a tetravalent boron atom (Figure 1.1b).^[16] This leads to a change in the absorption and emission spectra since the boron atom is not anymore conjugated with the π orbitals of the aryl groups. Alternatively, the π -conjugated main chain can also be substituted at one end by an electron deficient boron atom and on the other end by a nitrogen atom, whose lone pair is therefore conjugated with the empty p orbital of the boron, forming a so-called 'push-pull' system (Figure 1.1c). These systems lead to a dramatic change of the emission properties due to the $n \rightarrow \pi^*$ transition. This transition is quenched upon addition of fluoride, which leads to the formation of the tetragonal boron center (Figure 1.1d). As a consequence, the $\pi \rightarrow \pi^*$ transition is activated, leading to the emission of light at higher energy, hence lower wavelength than the $n \rightarrow \pi^*$ transition. The 'push-pull' systems are therefore ideal candidates for fluoride detection as the luminescence of the compound is activated upon detection, so are colorimetric sensors. Research in the NLO field revealed that such push-pull systems (Figure 1.1c) display interesting properties.^[22,23] More particularly, a detailed crystal structure study completed by an investigation of the hyperpolarizability properties have revealed that the capacity of boron moieties to accommodate a negative charge is comparable to the one of the nitro group.^[23] Finally, the modification of the electronic properties of the backbone can be further exploited to dispose of a large array of luminescent compounds for OLED.^[17] The emission of derivatives constituted of boron atoms conjugated with nitrogen atoms is due to the $n \rightarrow \pi^*$ transition. This transition is reflected by a smaller HOMO-LUMO gap, so a bathochromically shifted emission. The wavelength of the emission can therefore be further tuned by modifying the Lewis acidity of the boron by judiciously changing the substituents. Interestingly, these compounds revealed to be also effective as hole transporter material that can be implemented into OLED.^[19,20]

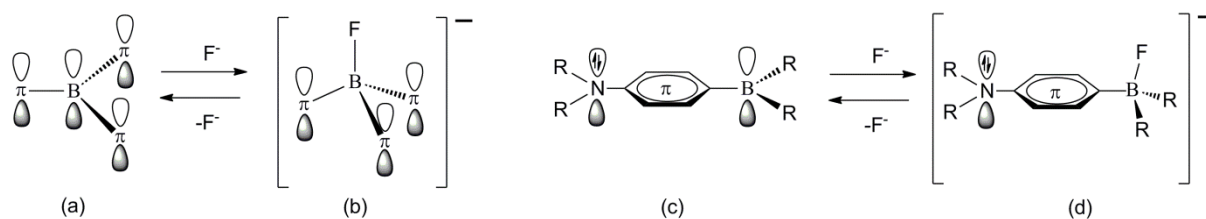


Figure 1.1 Schematic representation of (a) the π conjugation of the empty p orbital of the boron atom and the π orbitals of the conjugated structure, (b) disrupted after the addition of fluoride anion forming a tetrahedral boron complex. Schematic representation of (c) a donor-acceptor system and (d) of the quenching of the conjugation between the nitrogen lone pair and the empty p orbital.

The research regarding boron atoms inserted into aryl units, forming analogues of aromatic structures such as borabenzene, boranaphthalene, and borepin, are presented in *section 1.2*. The electron deficient boron atom can also be incorporated into larger π -conjugated structures, such as nanotubes. The latter are used as metal-free catalyst for O_2 reduction, paving the way for future utilization in fuel-cell.^[24] While smaller structures, such as borabenzene are used in organometallic complexes. The introduction of a boron atom into a six-membered ring results in a six π electrons, negatively charged ring, as the well-known cyclopentadiene anion.^[25] As a consequence, borabenzene and the like boranaphthalene have been used as cyclopentadiene surrogate for metal complexes.^[25,26] At the contrary, replacing a carbon atom by a boron atom into conjugated five or seven membered rings leads to structures with respectively four and eight π electrons. These structures are isoelectronic to the cyclopentadienyl and tropylium cations. Therefore, they are best used as Lewis acids, owing to the presence of the empty p orbital of the boron atom.^[27,28] Finally, the UV and fluorescence properties of boratastilbene,^[29] boraanthracene,^[30] and diboraanthracene^[31] derivatives have been probed. The first species is negatively charged and the emission is dependent on the aggregation behavior in solution. Interestingly, the study reveals that, for this compound, the HOMO is located on the borabenzene ring and the LUMO on the phenyl ring.^[29] At the contrary, the neutral

boraanthracene derivative has a delocalized HOMO and LUMO levels, more similar to the anthracene one but with a smaller band gap.^[30] Polymers of diboraanthracene turn out to be a green solid-state luminescent material.^[31]

Finally, the replacement of a carbon-carbon pair by a boron-nitrogen pair into π -conjugated structures will be presented in *section 1.3*. The boron-nitrogen pair can be introduced into extended π -conjugated structures, such as graphene or nanotubes.^[32,33] The resulting graphene material, where boron-nitrogen pairs have been introduced, is a transparent semiconductor whose conductivity is between the one of graphene, a conductor, and the one of pure boron nitride, an insulator.^[32] The catalytic properties of the nanotubes were doped by the replacement of carbon-carbon pairs by boron-nitrogen pairs, suggesting that the carbon nanotubes could replace costly platinum source for oxygen reduction.^[33] Alternatively, the boron-nitrogen pair can replace a selected carbon-carbon pair in smaller π -conjugated structures. In the literature, several structures are mentioned where the replacement of the carbon-carbon pair by the boron-nitrogen pair (called boron-nitrogen doping) leads to dramatic differences of photophysical properties between the isosteres.^[34,35] Theoretical works suggest that the replacement of the carbon-carbon pair by the more polarized boron-nitrogen pair will be reflected by an increase of the HOMO-LUMO gap,^[36] hypsochromically shifting the fluorescence peak. When the replacement occurs into aromatic modules, such as phenanthrene or benzene, the influence of the boron-nitrogen pair on the fluorescence properties is more complex. For example, two isosteres of phenanthrene, 4a-aza-4b-boraphenanthrene and 9-aza-10-boraphenanthrene reveal bathochromically and hypsochromically shifted emissions respectively.^[34] While, tolane derivatives, where one or two phenyl rings have been substituted for 1,2-azaborine moieties, have bathochromically shifted fluorescence.^[35]

1.1. Boron Connected to Aryl Units

The synthesis of π -conjugated structures where a boron atom has been connected will be presented in this first section, followed by a detail discussion of their properties. As outlined in the introduction, these compounds were mainly used as colorimetric anions sensors.^[16] Their fluorescent properties were also further exploited when implemented into the emissive layer of OLED.^[17] Finally, the ‘push-pull’ systems which revealed to be ideal candidates for NLO applications will be discussed.^[22,23]

1.1.1. Derivatives Used in Chemicals Sensing

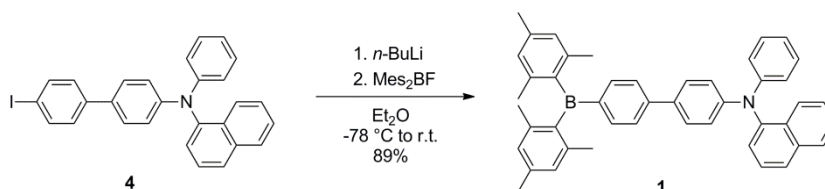
Due to the presence of an empty p orbital and hence their reactivity toward nucleophiles, boron atoms are usually protected by hindered bulky substituents, which provide steric protection. The most common aryl substituents for boron-containing derivatives are mesityl, durene, and 2,4,6-triisopropylphenyl moieties bearing ortho groups which surround the empty p orbital of the boron atom, allowing only small anions (*e.g.* fluoride or cyanide ions) to coordinate with it. As a result, this selectivity has enabled the construction of two types of luminescent chemicals sensors, the ‘turn-off’ and ‘turn-on’ systems. For instance, when the “turn-off” systems are used, the anion binding hampers the formation of any intramolecular charge-transfer states, quenching their emissive properties. On the other hand, anion complexation in “turn-on” sensors exalt their emissive properties (mainly those deriving from $\pi \rightarrow \pi^*$ transitions). In this respect, boron-aryl conjugates **1**, **2** and **3** displayed interesting “turn-on” fluorescent properties. Recently, the group of Bartik,^[37] has demonstrated that titrations in hydroscopic solvents inevitably lead to the formation of HF_2^- from two molecules of TBAF, particularly when concentrations inferior to 10 mM of TBAF are used in hygroscopic solvents. A careful analysis of the titration profiles published in the literature revealed that the conditions of the titrations reported allowed the presence of HF_2^- , which can also bind to the receptor, along with F^- . Hence, the sensitivities of the receptors reported in the literature are related to the combined binding constant of HF_2^- and F^- .

The synthetic pathways for aryl boranes are shown in Schemes 1.1-1.3. While boron compounds bearing two identical aryl groups (such as mesityl groups like in compounds **1**, **2** and **3**) are synthesized by nucleophilic substitution reaction of the

Chapter 1

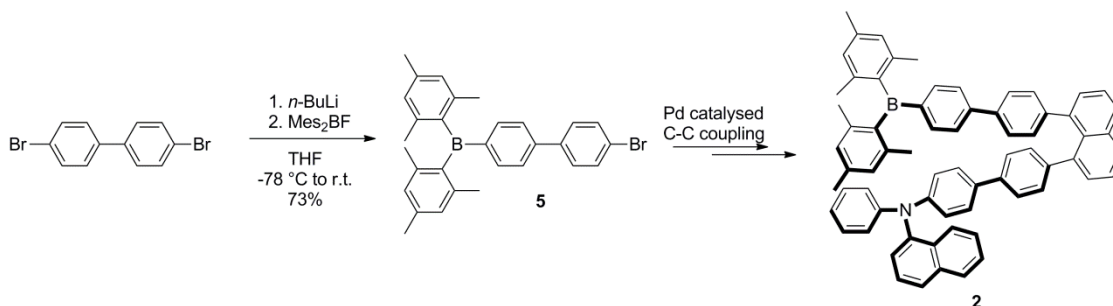
ArLi derivative with Mes₂BF (Schemes 1.1-1.2), boron-phenyl derivatives bearing three identical appends are obtained by reacting the corresponding ArLi with BF₃ (Scheme 1.3).

In particular, compound **1** has been synthesized from precursor **4**, using a metal-halogen exchange reaction followed by substitution with Mes₂BF. Aromatic organo-boron compound **1** has been used as a ‘turn-off’ sensor toward the detection of fluoride anions (sensitivity down to 0.02 mM in CH₂Cl₂).^[38] In addition Wang has also shown its application as an electron transport material and blue emitter in OLED due to its unique photophysical properties ($\Phi = 0.95$, $\lambda_{em} = 513$ nm, $\lambda_{ex} = 377$ nm in CH₃CN; $\Phi = 0.31$, $\lambda_{em} = 451$ nm, $\lambda_{ex} = 390$ nm in the solid state).^[39]



Scheme 1.1 Synthesis of fluoride anion molecular sensor **1**.

Moreover, precursor **5** of the synthesis of compound **2** can be obtained using a similar methodology to the one described for **1** (Scheme 1.2). Pd-catalyzed carbon-carbon cross coupling reaction of **5** with 1,8 diiodonaphthalene furnished aromatic organo-boron compound **2** ($\Phi = 0.98$, $\lambda_{em} = 414$ nm, $\lambda_{ex} = 340$ nm in CH₂Cl₂). In this system, the amine function interacts with the boron-centered electronic vacancy, allowing charge-separation states at the ground state. Upon addition of fluoride ions, the through-space (~10 Å) charge-transfer interaction is broken along with loss of its fluorescence properties. As a result, only aminoaryl-centered $\pi \rightarrow \pi^*$ transitions are activated ($\lambda_{em} = 443$ nm, $\lambda_{ex} = 340$ nm in CH₂Cl₂, Figure 1.2), displaying a ‘turn-on’ sensing activity of compound **2** (fluoride detection limit: 0.015 mM in CH₂Cl₂).^[38]



Scheme 1.2 Synthesis of fluoride sensor **2**.

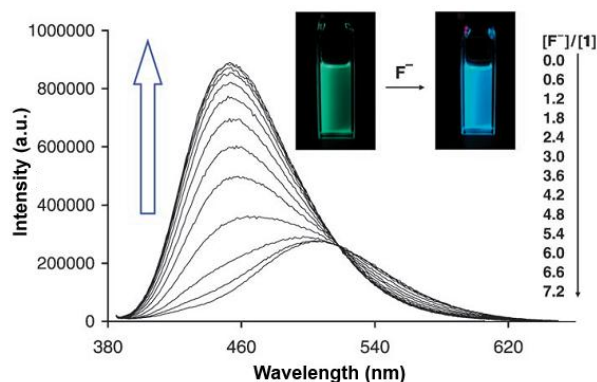


Figure 1.2 Fluorescence titration spectra of compound **2** upon addition of tetrabutylammoniumfluoride (TBAF). Adapted with permission from the Wiley-VCH Verlag GmbH & Co. KGaA. Copyright 2009.^[38]

Wang and co-workers demonstrated that the distance between the donor and the acceptor moieties in these non-conjugated systems can be tuned using a flexible tetrahedral silane linker.^[40] The increased distance ($\sim 10 \text{ \AA}$) between the electron donating and accepting units of compound **3** and the rotational freedom around the carbon-silicon bond diminish the through space charge-transfer process, and thus the enhancement of the emissive properties of the $\pi \rightarrow \pi^*$ excited states (Figure 1.3). In addition, the binding of fluoride anion is also stronger in compound **3** (Figure 1.3) compared to **2**, due to the reduced steric hindrance between the donor and the acceptor moieties.

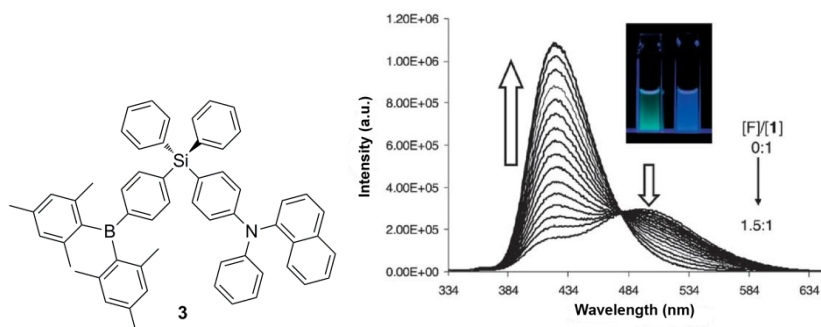
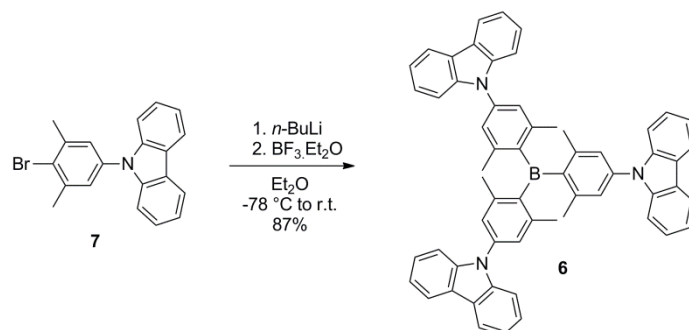


Figure 1.3 Fluoride anion molecular sensor **3** and its fluorescence titration spectra upon addition of TBAF. Adapted with permission from the Wiley-VCH Verlag GmbH & Co. KGaA. Copyright 2009.^[40]

Boron derivative **6** substituted by identical groups is obtained from the nucleophilic addition of lithiated derivative **7** to BF_3 . When more than one donating units are conjugated with the boron center, the *para* substitution leads to a stronger charge transfer interaction as well as weaker electron acceptor abilities compared to its *meta* regioisomer.^[41] This phenomenon is clearly observed in the case of compound **6** (Scheme 1.3), which has been used as a blue emitter ($\Phi = 0.67$, $\lambda_{em} = 476 \text{ nm}$, $\lambda_{abs} = 385 \text{ nm}$, in DMSO) and hole injection material in OLED.^[42]



Scheme 1.3 Synthesis of a C_3 symmetry derivative **6**.

The wavelength of emission of the $\pi \rightarrow \pi^*$ transition in this kind of derivatives can be red-shifted upon increasing the distance between the donor and the acceptor moieties. However, the drawback of this strategy is a resulting decreased efficiency of the through-bond charge-transfer process with regards of the distance.^[43] The group of Müllen elegantly demonstrated that the boron atoms in compound **8a** (Figure 1.4) are conjugated with the π electrons of the aryl groups. As a consequence, the $\pi \rightarrow \pi^*$ electronic transition ($\lambda_{em} = 450 \text{ nm}$, $\lambda_{abs} = 432 \text{ nm}$, in acetone) is quenched upon coordination of the first equivalent of fluoride to the boron atom center. Despite the long distance ($\sim 20 \text{ \AA}$), the negatively-charged tetravalent boron atom acts as a weak donating moiety thus leading to a weak through-bond charge-transfer process. The addition of the second equivalent of fluoride ions quenches the fluorescence and activates the $\pi \rightarrow \pi^*$ transition ($\lambda_{em} = 450 \text{ nm}$, $\lambda_{abs} = 432 \text{ nm}$ in acetone). Interestingly, compound **8b**, an analogue of **8a**, bearing one boron atom and one nitrogen atom was also used as a ‘turn-on’ sensor upon addition of the first equivalent of fluoride anion. Whereas, the charge transfer of compound **8a** is activated upon addition of one equivalent of fluoride and quenched upon the addition of the second equivalent (sensitivity down to 0.01 mM in CH_2Cl_2).^[43]

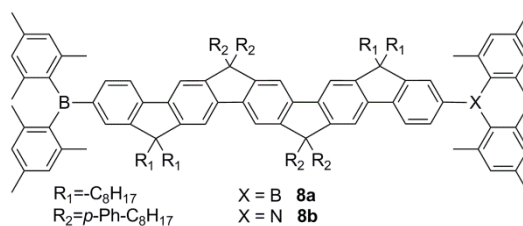
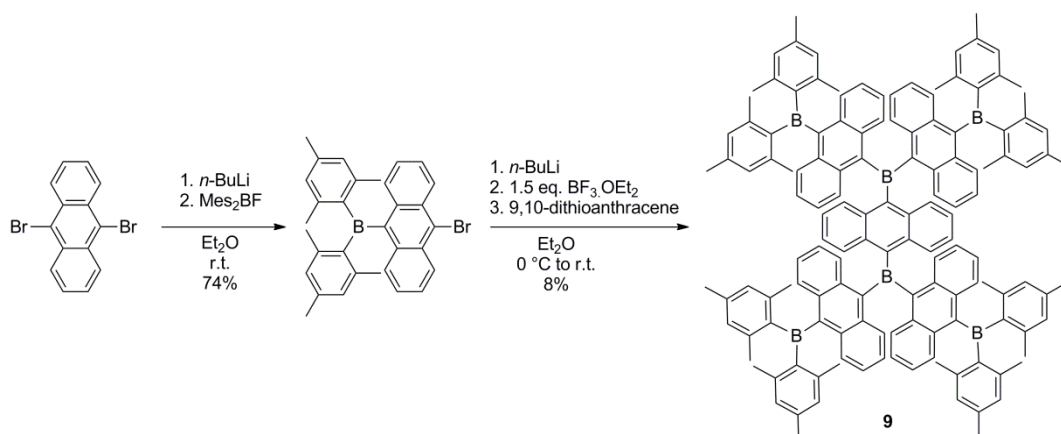


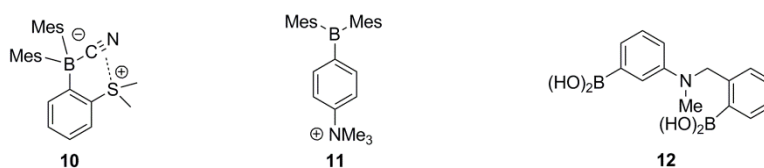
Figure 1.4 Fluoride anion molecular sensors **8a** and **8b**.

The Lewis acidity of the boron atoms is reduced when the mesityl and duryl protecting groups are used, due to the fact that they are substituted by weakly donating methyl groups. One way to overcome this drawback, as reported by the group of Yamaguchi, is to substitute the anthryl moiety by several boron atoms (compound **9**, Scheme 1.4).^[44] Despite the fact that the interplanar angle between the boron plane and the anthracene plane is 53° , a weak electronic conjugation is effective since a substantial bathochromic shift was observed in the UV-Vis spectra of compound **9** ($\lambda_{abs} = 535$ nm, $\Delta\lambda = 65$ nm, in THF) compared to the trianthrylborane derivative ($\lambda_{abs} = 470$ nm, in THF).



Scheme 1.4 Synthesis of the extended boron aryl conjugate **9**.

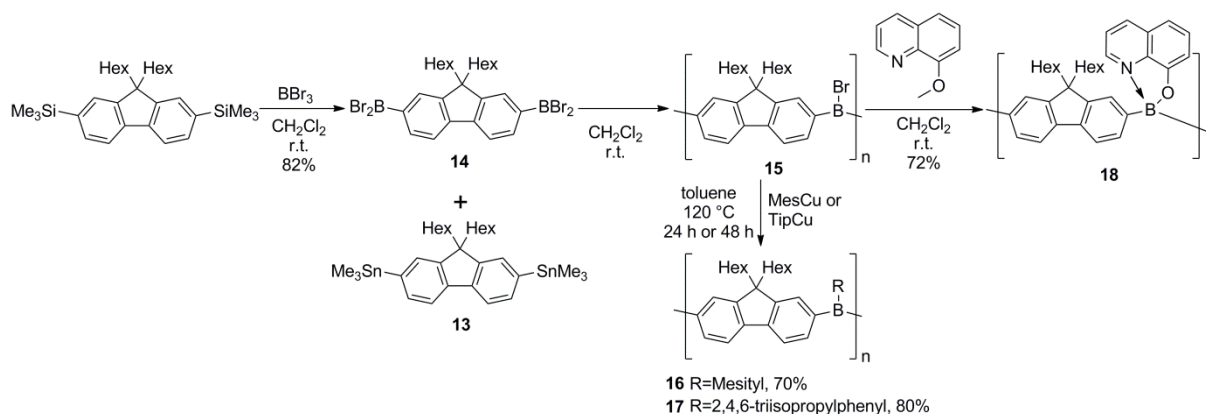
Besides fluoride detection, a few examples of cyanide sensors have also been reported in the literature. For example it was demonstrated that in H_2O compound **10** (Scheme 1.5) is very sensitive to cyanide ions ($\sim 10^8 \text{ M}^{-1}$, $\lambda_{em} = 460$ nm, $\lambda_{ex} = 300$ nm), and nearly inactive toward fluoride anions (4% of fluorescence quenching upon addition of 15 eq.) due to its high hydration enthalpy.^[45] The presence of the sulfonium functional group increases the electrophilicity of the boron center through attractive inductive effect and further stabilizes the cyanide complex by bonding and back-bonding interactions with the CN triple bond.^[45] An enhancement of the electrophilicity of boron atoms has also been evidenced by ammonium-bearing molecular sensor **11**, which binds both fluoride and cyanide ions in organic solvents with an enhanced selectivity toward cyanides ($3.9 \times 10^8 \text{ M}^{-1}$) in $\text{H}_2\text{O}/\text{DMSO}$ (60:40) solutions.^[46] Interestingly, the *ortho* regioisomer of compound **11** revealed to be selective only toward the recognition of fluoride ions as the increased steric hindrance around the boron atom prevents the binding of larger ions, such as the cyanide one.^[46] Furthermore, the group of Houston demonstrated the use of boronic acid derivatives to detect sugars, using the alcohol functionality to reversibly form boronic esters, thus leading to a quenching of the emissive properties. In particular the span between the two boron centers of compound **12**, enables it to be nearly selective toward sialic acid.^[47]



Scheme 1.5 Examples of cyanide sensors **10** and **11** and sugars sensors **12**.

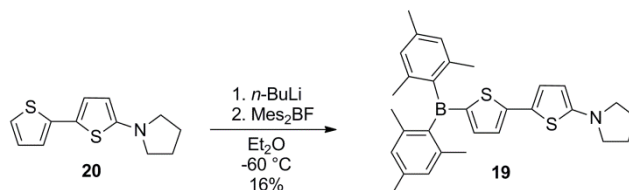
1.1.2. Steric Protection of Borane Derivatives

Boron containing moieties have also been introduced in polymers. One of the examples reported in the literature is outlined in Scheme 1.6, the reaction of fluorenebisstannate **13** with fluorenebisbromine **14**, which can be obtained by reacting its trimethylsilane analogue in the presence of BBr_3 , affords polymer **15**. In this manner, a linking boryl group has been introduced in the polymer backbone. The electronic properties of compound **15** could be tuned by substituting the bromine atom on the boron moiety for aryl groups (from **15** to **16-17**). The boron atoms in polymers **16** and **17** are functionalized with aryl groups, of which the mesityl functions proved to be not bulky enough to protect structure **16** from any degradation upon exposure to air. In contrast, it was shown that the isopropyl *ortho* substituents of **17** result in stable polymers, suggesting that such functional groups are better with regards to protecting the boron moiety. Fluorescence titrations of polymer **17** show a similar detection behavior to that of the bisboron molecular ladder **8**. Namely, after the addition of the first equivalent of fluoride anions, a charge-transfer process occurs between the tetra coordinate boron atoms and the electron deficient center, showing a “turn-on” behavior of the fluorescence signal. Compared to **17** ($\Phi = 0.81$, $\lambda_{em} = 399, 423, 447 \text{ nm}$, $\lambda_{ex} = 371 \text{ nm}$, in CH_2Cl_2), polymer **18** revealed to be weakly fluorescent ($\Phi = 0.21$, $\lambda_{em} = 504, 338 \text{ nm}$, $\lambda_{ex} = 313 \text{ nm}$, in CH_2Cl_2) and its UV-Vis absorption spectrum profile is typical of that of a quinoline compound. From this data, one can conclude that the complexation of the empty *p* orbital of the boron atom by the lone pair of the nitrogen disrupts the π -conjugation along the polymer chain, thus leading to a quenching of the luminescence properties.^[48] An additional reported strategy to dope polymeric structures is to laterally append a substituted boryl moiety.^[49] The boryl substituents revealed to influence the electronic properties of the material if equipped at the *para* or *ortho* positions with respect to the polymer chain.^[49,50]



Scheme 1.6 Synthesis of fluorenyl-based polymers, **16**, **17** and **18** linked by doping boron atoms.

The fluorene moiety can be changed for electron rich substituents such as thiophene (see derivative **19**) and ferrocenyl derivatives. For example, compound **19** (Scheme 1.7) has been prepared by *ortho* lithiation of precursor **20** followed by a nucleophilic addition with Mes_2BF . Although derivative **19** has shown NLO responses ($\beta = 37 \times 10^{-30} \text{ esu}$, $\mu\beta = 148 \times 10^{-8}$, in acetone), it easily degrades within hours upon exposure to light,^[22] thus allowing a limited applicability.

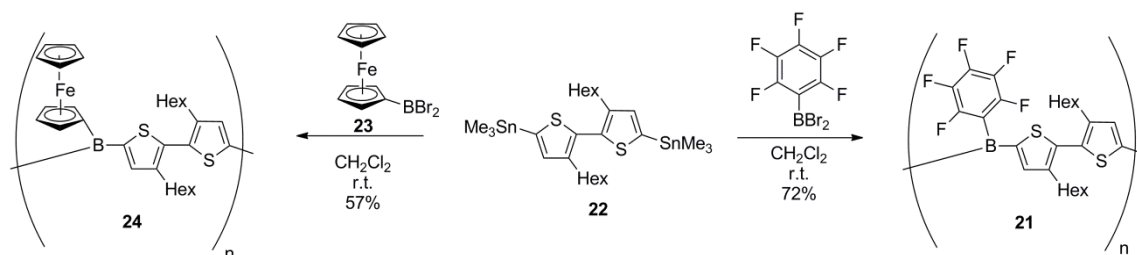


Scheme 1.7 Synthesis of a bithiophene moiety connected to a boryl functional center, compound **19**.

Other substituents than mesityl, duryl, 2,4,6-triisopropylphenyl and anthryl functions can be used to protect the boron center.^[51] However, the resulting polymers are often unstable upon exposure to air. Polymer **21** (Scheme 1.8) was

Chapter 1

synthesized from bis-stannate derivative **22** and $C_6F_5BBr_2$. The attachment of electron withdrawing pentafluorobenzene substituents led to a bathochromic shift in the fluorescence spectra of polymer **21** ($\Phi = 0.15$, $\lambda_{em} = 529$ nm, $\lambda_{ex} = 413$ nm in CH_2Cl_2) compared to the same structure equipped with 4-isopropylphenyl appends ($\Phi = 0.21$, $\lambda_{em} = 491$ nm, $\lambda_{ex} = 391$ nm in CH_2Cl_2). Electron rich ferrocenyl moieties **23** have been also connected to the starting thiophene derivative **22** to furnish polymer **24**, using similar reaction conditions to those used for preparing **21**. Both polymers **21** and **24** have been employed for sensing aromatic amines such as pyridines and picolines. UV and fluorescence (Figure 1.5a and b respectively) titration experiments of samples containing polymer **21** or **24** were used to test the binding capabilities of the polymeric architectures. In particular, the changes in the absorbance and emission spectra profiles for compound **21** showed a strong association with both amines (pyridine and 4-picoline), whereas the response of **24** revealed to be lower, possibly due to a reduced electrophilic character of the boron center.^[51]



Scheme 1.8 Synthesis of polymers **21** and **24** bearing perfluorophenyl and ferrocenyl moieties.

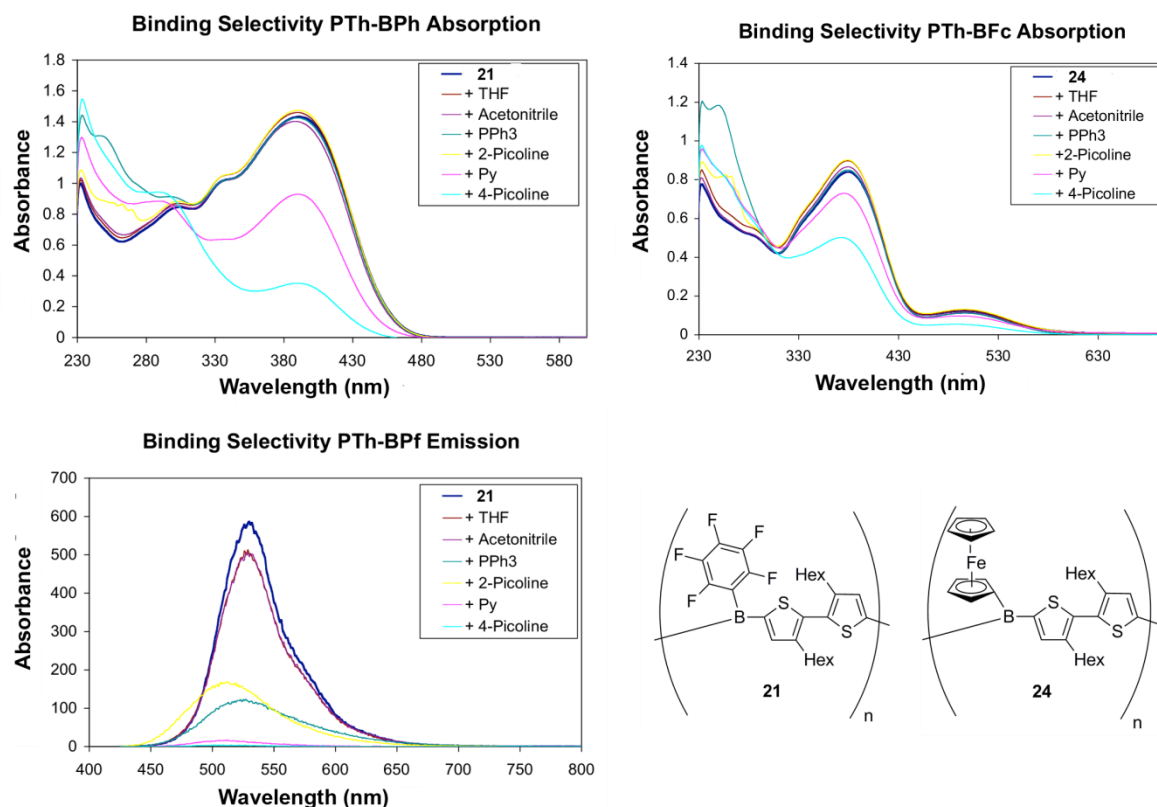
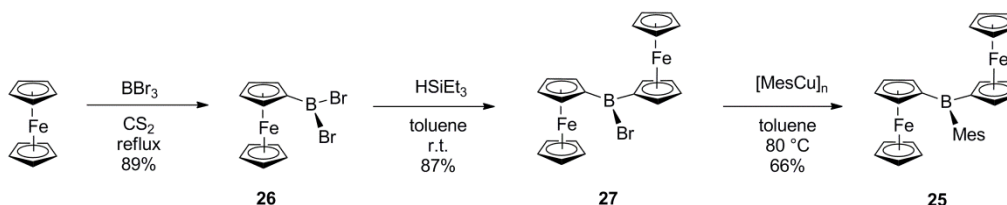


Figure 1.5 Absorbance titration spectra of (a) compound **21**, (b) compound **24** and (c) fluorescence titration spectra of compound **21** upon addition of various aromatic amines. Adapted with permission from the Wiley-VCH Verlag GmbH & Co. KGaA. Copyright 2005.

Boron-doped polymers bearing electron rich substituents have been also synthesized. As model compound, bisferrocenyl borane derivative **25** has been synthesized (Scheme 1.9) to probe the electronic properties of the monomer. Boron ferrocenyl derivative **26**, was prepared in excellent yield (89%) using an established procedure.^[52] Furthermore, it was dimerized *via* homocoupling reaction using $HSiEt_3$ to give bisferrocenyl derivative **27**. Subsequent nucleophilic addition with further

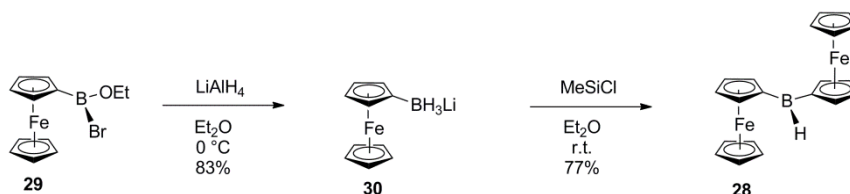
Chapter 1

mesityl cuprate led to compound **25**, in which the mesityl group surrounds the boron atom. The two ferrocenyl entities revealed to electronically communicate *via* the empty *p* orbital of the boron atom, as shown by the presence of two reversible ferrocenyl-centered redox waves measured by cyclic voltammetry ($E^{\circ'} = 45$ mV and 467 mV, at r.t. in CH_2Cl_2 with $\text{NBu}_4[\text{B}(\text{C}_6\text{F}_5)_3]$ as supporting electrolyte using decamethylferrocene as internal standard).^[53]



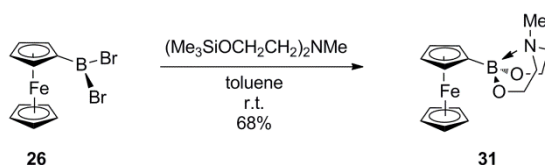
Scheme 1.9 Synthesis of a protected boron bisferrocenyl derivative **25**.

With the aim to study a less hindered polymer as electron deficient analogue of all-carbon structure, bisferrocenyl compound **28** (Scheme 1.10) was synthesized. Boron compound **29** was reduced to give compound **30**, which was further dimerized to bisferrocenyl derivative **28** upon addition of Me_3SiCl . Unfortunately, bisferrocenyl compound **28** revealed to be less stable with respect to derivative **25**, and thus limited investigations were further conducted.^[54]



Scheme 1.10 Synthesis of bisferrocenyl borane **28**.

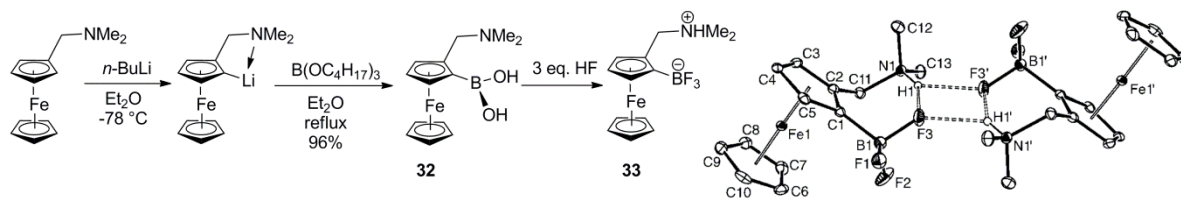
All the molecular structures described so far in this chapter, have been mainly used as molecular sensors to detect fluoride anions, but no example of molecular sensors resistant to detect HF have been reported. In this respect, compound **26** (Scheme 1.11), obtained through an electrophilic substitution as outlined in Scheme 1.8, was transformed into protected boronic ester **31**, which it was thought to be resistant in the presence of HF. However, it was observed that compound **31** degraded upon addition of the acid despite the extra stabilization of the boron center by the nitrogen lone pair (boron-nitrogen distance: 1.735(3) Å).^[55]



Scheme 1.11 Synthesis of protected boron ferrocenyl derivative **31**.

In order to have stable HF sensors, aminoacid **32** (Scheme 1.12) was synthesized through *ortho*-lithiation of the starting ferrocene derivative followed by a nucleophilic substitution reaction with $\text{B}(\text{OC}_4\text{H}_9)_3$ and subsequent hydrolysis of the ester during the workup.^[56] Addition of three equivalents of HF resulted in the isolation of compound **33**, which revealed to dimerize in the solid state (Scheme 1.12) through the formation of intermolecular hydrogen-bonding interactions (hydrogen-fluoride contact distance amount to 2.20 Å).^[55] The selectivity of compound **32** toward HF was investigated by the authors through electrochemical analysis, resulting in opposite responses for HF compared to other acids, like HCl. Thus, the voltammograms of **32** ($E_{1/2} = +37.5$ mV) and **33** ($E_{1/2} = -43$ mV) reveal a cathodic shift upon addition of HF (Figure 1.6 left side). This behavior is consistent with the transformation from a three-coordinate electron-withdrawing boronic acid group into a four-coordinate electron-donating boronate. The reversed situation is found when three equivalents of HCl are added to compound **32** (Figure 1.6 right side). In this case, a significant anodic shift is detected (+149.5 mV) suggesting a possible

protonation of the dimethylamino group without any coordination of the boron center. In addition, the reaction with an excess of fluoride, accomplished by $n\text{Bu}_4\text{NF}$ (Figure 1.6), leads to a voltammetric curve that resembles to the one observed for the authentic sample of **33**, proving then the intrinsic HF selectivity of the boronic acid derivative.



Scheme 1.12 Synthesis and X-ray crystal structure of the HF molecular sensor **32**. Adapted with permission from the Wiley-VCH Verlag GmbH & Co. KGaA. Copyright 2005.

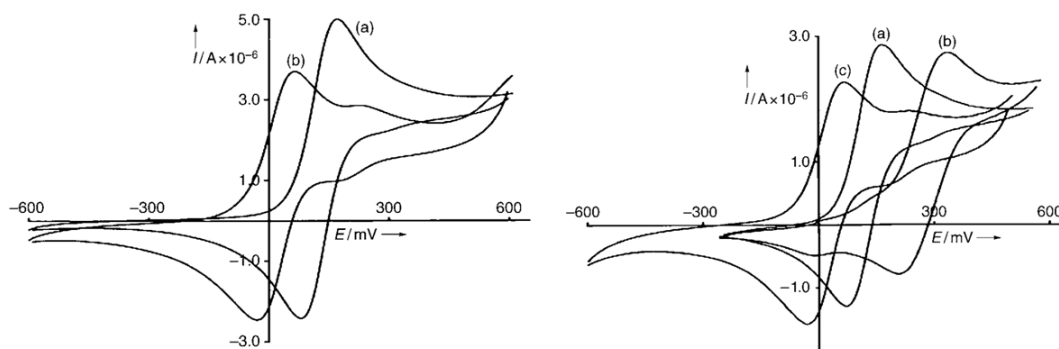


Figure 1.6 Left: Cyclic Voltammograms of (a) **32** and (b) **33** upon addition of HF. Right: Cyclic Voltammograms of (a) **32**, (b) **32** after addition of HCl and (c) **32** after subsequent addition of $n\text{Bu}_4\text{NF}$. Adapted with permission from the Wiley-VCH Verlag GmbH & Co. KGaA. Copyright 2005.

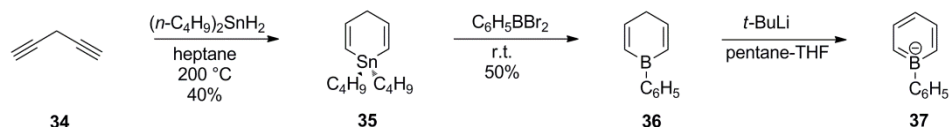
1.2 Boron Inserted into Aryl Units

This section will be focusing on compounds, where a boron atom has been incorporated into the aryl ring. As explained in the introduction, this will result in a more dramatic change of the optoelectronic properties of the compound. The boron heterocycles reported in the literature are constituted of five (*e.g.* boroles), six (*e.g.* borabenzene) or seven (*e.g.* borepin) members. Six-membered rings, with a boron atom incorporated, can be used as cyclopentadiene surrogate for ferrocene complex, since they have the same number of π electrons.^[25] Whereas, five and seven-membered rings are isoelectronic to cyclopentadienyl and tropylium cations respectively. Hence, both the synthesis and applications of the six, seven and five-membered boron heterocycles will be reviewed in this section. In addition, stable derivatives with enhanced stability upon exposure to air can be afforded, by steric protection of the boron atom with mesityl or pentafluorophenyl groups or other sterically encumbered substituents. These sterically hindered groups give enough stability so that the compound is stable upon exposure to air and will also be reported.^[27,57]

1.2.1. Borabenzene

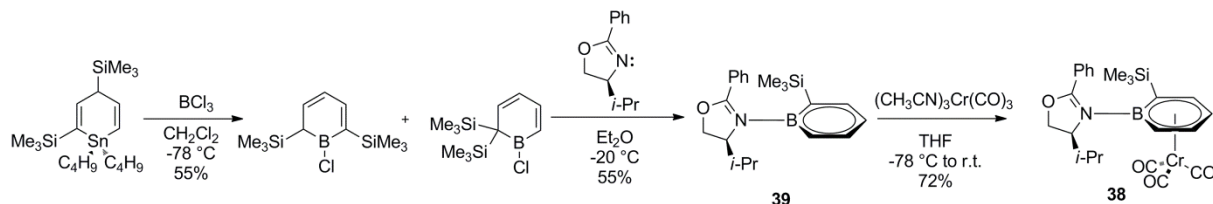
Borabenzene, doped analogue of benzene, has been synthesized and used as a ligand for transition metal complex for decades now.^[25,58,59] The stannohydration of 1,4-diethynyl **34** (Scheme 1.13) gave rise to cyclic compound **35**. The latter is transformed into cyclic borane **36** by a stannate-boron exchange reaction. Finally, deprotonation reaction of **36** with *tert*-BuLi leads to borabenzene derivative **37**, displaying a strong aromatic character.^[60]

Chapter 1



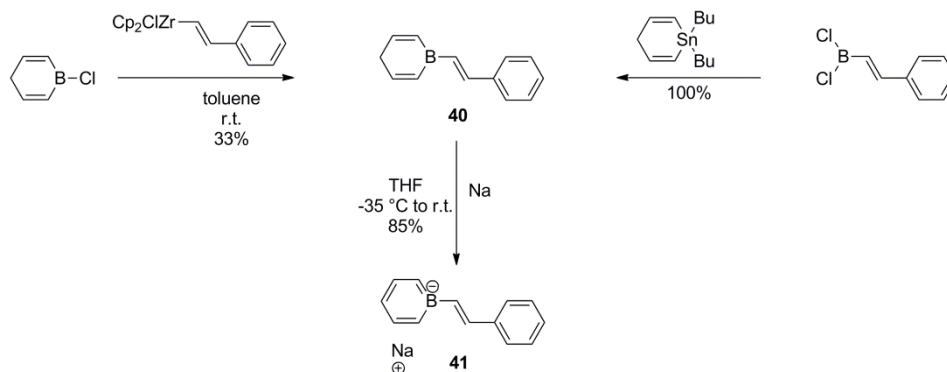
Scheme 1.13 Synthesis of borabenzene **37**.

Recently, the interest for compound **37** and its derivatives has been renewed by its use in chiral Lewis acid complex **38** (Scheme 1.14).^[61] The latter was obtained using a similar synthetic strategy as the one reported in Scheme 1.13, followed by complexation of intermediate **39** with $\{\text{Cr}(\text{CO})_3\}$ complex.



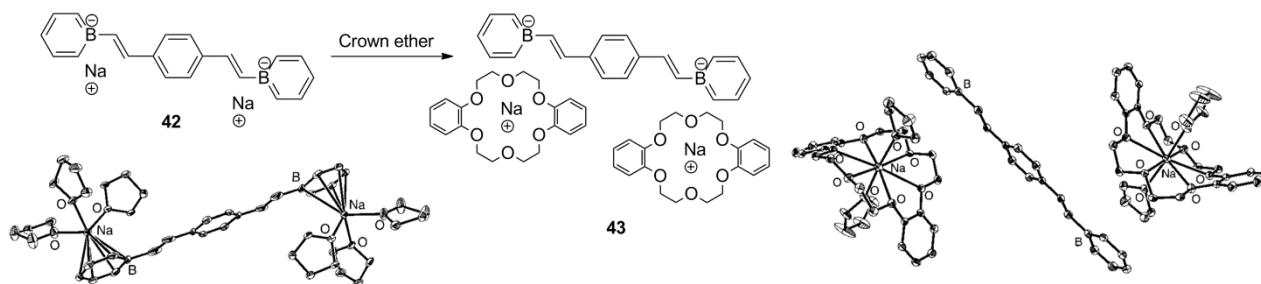
Scheme 1.14 Synthesis of chiral borabenzene complex **38**.

In addition, borabenzene can also be connected to a phenyl ring through a double bond, forming a borastilbene. The latter can be used as ligand for the catalytic polymerization of ethylene.^[62] For example, the synthesis of borastilbene **40** (Scheme 1.15) can be achieved by a transmetalation reaction of the styryl functional group connected to the zirconium (or transmetalation of the stannate derivative, although this synthetic route seems to give rise to a complex mixture of products).^[29] Thus, compound **40** gave, after reaction with metallic Na, fluorescent boratastilbene **41**. The UV-Vis absorption analysis ($\lambda_{\text{abs}} = 357\text{ nm}$, in THF) revealed the presence of a shoulder peak at 400 nm that appears upon dissolution in THF and diminishes with increasing the solution concentration. Upon addition of two equivalents of dibenzo-18-crown-6 in a solution of **41** in THF, the absorption peaks revealed to be red-shifted ($\lambda_{\text{abs}} = 407\text{ nm}$; $\Phi = 0.68$, $\lambda_{\text{em}} = 518\text{ nm}$, in THF) suggesting the presence of molecular aggregates in the solution.^[29]



Scheme 1.15 Synthesis of boratastilbene **41**.

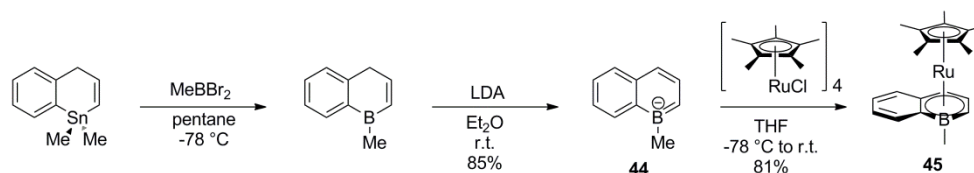
The absorption and emission spectra of the related bisborastilbene **42** ($\Phi = 0.16$, $\lambda_{\text{em}} = 604\text{ nm}$ and $\lambda_{\text{ex}} = 396\text{ nm}$, in THF) also revealed a reduction of the HOMO-LUMO gap upon addition of dibenzo-18-crown-6, as observed for species **43** ($\Phi = 0.44$, $\lambda_{\text{em}} = 534\text{ nm}$, $\lambda_{\text{ex}} = 447\text{ nm}$, in THF), Scheme 1.16.^[63]



Scheme 1.16 Schematic representation and X-Ray analysis of the influence of the counter ion on complexation of bisborastilbene **43**. Adapted with permission from the American Chemical Society. Copyright 2000.

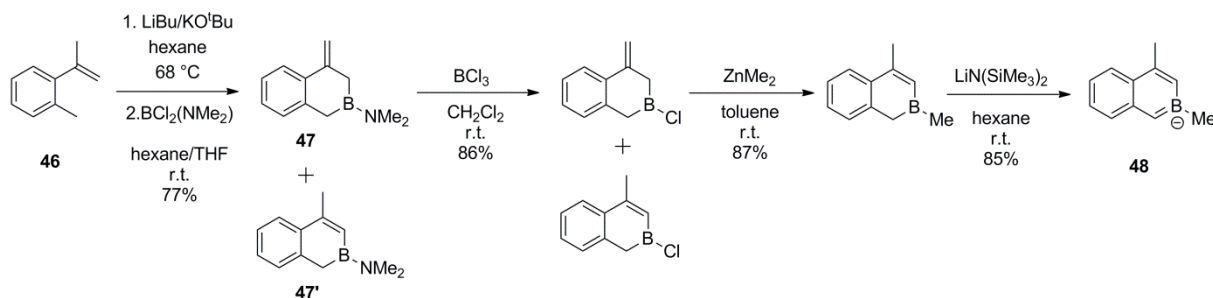
1.2.2. Boranaphthalene and Higher Acenes

Different isomers of boranaphthalene were synthesized and used as ligands for transition-metal coordination complex (**45**). A first approach employs the well explored stannate-boron exchange methodology to synthesize 1-boranaphthalene **44** (Scheme 1.17).^[26]



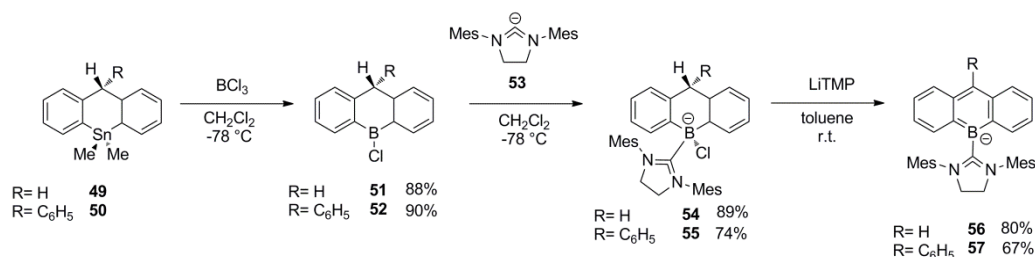
Scheme 1.17 Synthesis of 1-boranaphthalene **44**.

The second synthetic approach involves the ring closure of compound **46** (Scheme 1.18) in presence of $\text{BCl}_2(\text{NMe}_2)_2$. This gives a mixture of isomers **47** and **47'** which further reacts with BCl_3 to chlorinate the boron atom. The crude product was directly subjected to the next reactions to give 2-boranaphthalene **48** in good yield (48% from **46**).^[64]



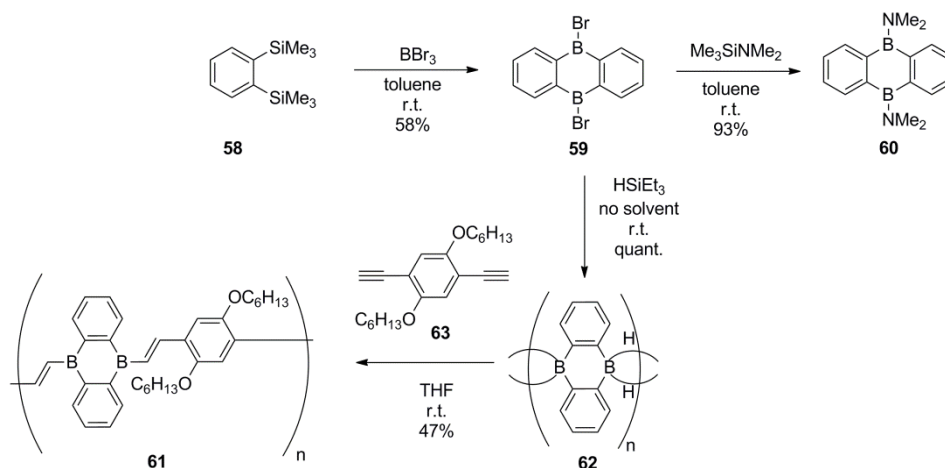
Scheme 1.18 Synthesis of 2-boranaphthalene **48**.

In analogy to the boranaphthalene derivatives, a few synthetic pathways have also been developed to form 9-borananthracene derivatives, the electron deficient analogues of anthracene. This class of compounds can be formed by metal-boron exchange from the corresponding stannate derivative.^[30] Stannate **49** and **50** (Scheme 1.19) react with BCl_3 to give borane derivatives **51** and **52**, which can be substituted by 1,3-dimesityl-4,5-dihydroimidazol-2-ylidene **53** to yield compounds **54** and **55**. Moreover, derivative **54** reacts with a base to form aromatic fluorescent compound **56** ($\lambda_{em} = 597 \text{ nm}$, $\lambda_{ex} = 485 \text{ nm}$, in CH_2Cl_2) for which weak solvatochromism was also observed (12 nm hypsochromic shift in CH_3CN respective to CH_2Cl_2). Notably, both compounds **56** and **57** react quickly with O_2 displaying a great potential as molecular oxygen sensors.^[30]



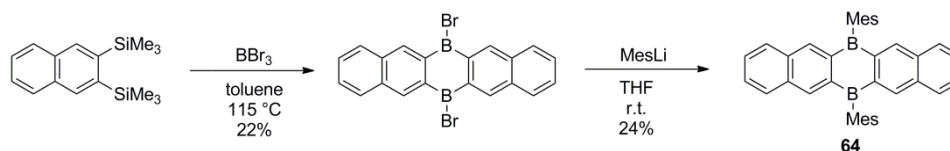
Scheme 1.19 Synthesis of boraanthracenes **56** and **57**.

Using a different synthetic strategy, 9,10-Diboraanthracenes have been synthesized upon dimerization of compound **58** (Scheme 1.20) in the presence of BBr₃. Compound **59**, which is highly sensitive toward moisture, is transformed into derivative **60** in excellent yield (93%) upon addition of Me₃SiNMe₂ in toluene.^[54] Alternatively, compound **59** was further used to prepare polymer **61**. Reaction of **59** with HSiEt₃ led to diboraanthracene hydride polymer **62** (held by agostic bonding interactions between the hydride functions and the boron atoms), which was further transformed into polymer **61**, *via* an hydroboration reaction with 1,4-diethynylphenyl **63**.^[31] Polymer **61** turns out to be weakly fluorescent in the visible region (Scheme 1.20, $\Phi = 0.09$, $\lambda_{em} = 518$ nm, $\lambda_{ex} = 410$ nm, UV-Vis: $\lambda_{abs} = 410, 349, 290$ nm, in toluene).^[31]



Scheme 1.20 Synthesis of 9,10-diboraanthracene **61**.

Following a similar synthetic strategy as that used for preparing the diboraanthracene derivatives, fluorescent ($\lambda_{em} = 464, 435, \text{ and } 410$ nm, $\lambda_{ex} = 330$ nm, UV-Vis: $\lambda_{abs} = 407, 385, 366, 328, 302, \text{ and } 268$ nm, in cyclohexane) diborapentacene **64** (Scheme 1.21) has been also synthesized.^[57] Interestingly, no π - π stacking interactions were observed in the crystal organization of **64** probably due to the presence of the mesityl moieties (typical π -stacks separated of 3.50 Å were observed for the analogue substituted by two methyls groups on the boron atoms).^[57]



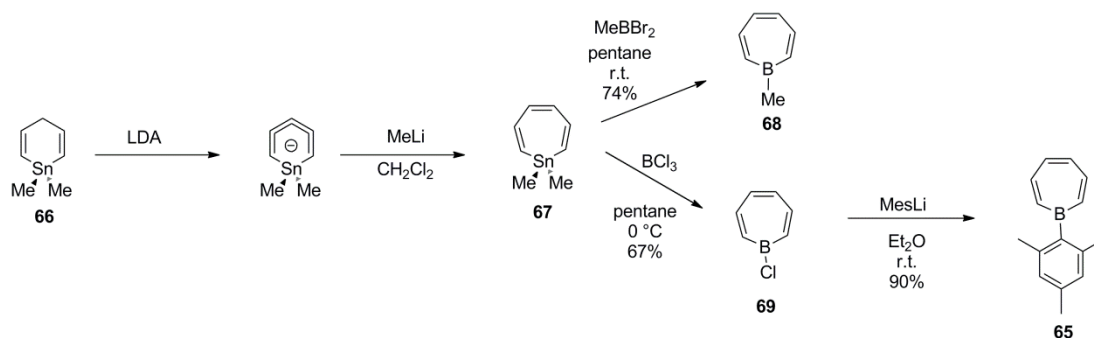
Scheme 1.21 Synthesis of a diborapentacene **64**.

1.2.3. Borepin and Boroles

Larger aromatic cycles such as borepin **65** (a neutral heterocycle isoelectronic to the tropylium cation) have also been reported in the literature (Scheme 1.22). Deprotonation of stannate derivative **66** followed by reaction with MesLi gives stannepin **67**. Reaction of compound **67** in presence of MeBBr₂ affords borepin **68** in good yield while, under the same

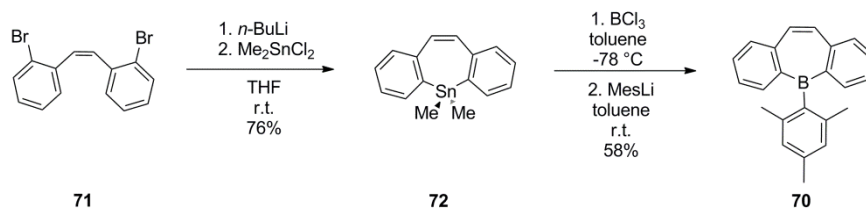
Chapter 1

condition, MesBBr₂ does not afford any products probably due to the steric hindrance of the mesityl group. In this case, an alternative synthetic pathway involving a stannate-boron exchange reaction with BCl₃ (giving chloro-borepin **69**) followed by a nucleophilic addition of MesLi has been employed to prepare mesityl-bearing protected borepin **65**.^[65]



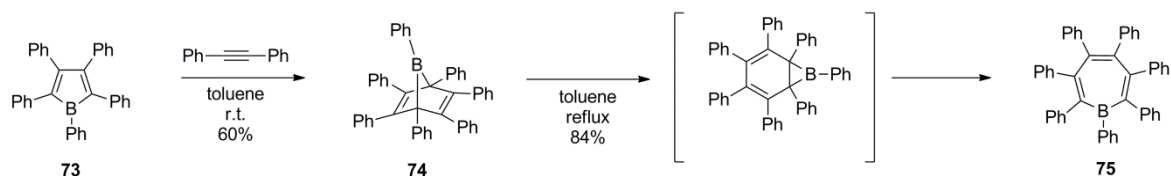
Scheme 1.22 Synthesis of methyl- borepin **68** and mesityl-borepin **65** derivatives.

Using a similar synthetic strategy, borepin **70** was also obtained. After a Li-halogen exchange reaction performed with *n*-BuLi, compound **71** (Scheme 1.23) has been reacted with Me₂SnCl₂ to afford derivative **72**, which gave arylborepin **70** in moderate yield (58%) after reaction with BCl₃ and MesLi using the same synthetic pathway as that outlined in Scheme 1.22.^[27] The conjugation of the empty *p* orbital of the boron with the π orbital reduces the Lewis acidity of compound **70** as demonstrated by competition binding NMR experiments performed by the group of Piers with dimethylamino pyridine.^[27] The fluorescence of derivative **70** ($\Phi = 0.70$, $\lambda_{em} = 400$ nm $\lambda_{ex} = 260$ nm, in CH₂Cl₂) makes it a good candidate for blue emitting OLED.^[27] Others dibenzoborepin derivatives laterally substituted by benzene rings have been reported, amongst them luminescent polymer for OLED.^[66,67]



Scheme 1.23 Synthesis of aryl borepin **70**.

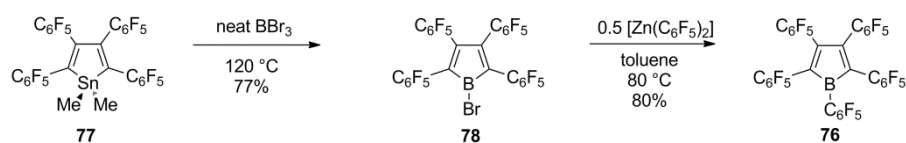
Finally, it has also been demonstrated that borepin cycles can be obtained from borole **73** (Scheme 1.24) upon thermal cycloaddition reaction with bisphenylacetylene in toluene.^[68] The Diels-Alder cycloaddition of **73** with toluene derivative affords boron-bridged compound **74**, which after prolonged heating, undergoes a 1,3-suprafacial-sigmatropic rearrangement followed by a 1,6-disrotatory electrocyclic ring opening to afford borepin **75** in high yield (84%).^[28]



Scheme 1.24 Synthesis of borepin **75** from borole **73**.

With the aim to investigate the Lewis acidity of highly electron-poor boron centers, perfluoroaryl borole **76** (Scheme 1.25) was also synthesized.^[27] Reaction of stannate **77** in neat BBr₃ led to compound **78** which, after treatment with Zn(C₆F₅)₂ gave rise to desired borole **76** in high yield (80%). The Lewis acidity of boroles, heterocyclic analogues of the antiaromatic cyclopentadiene cation, is enhanced compared to the borepin. When one equivalent of CH₃CN is added to a solution of borole **76** and B(C₆H₅)₃ it binds exclusively to the borole (as determined by ¹H NMR spectroscopy), providing

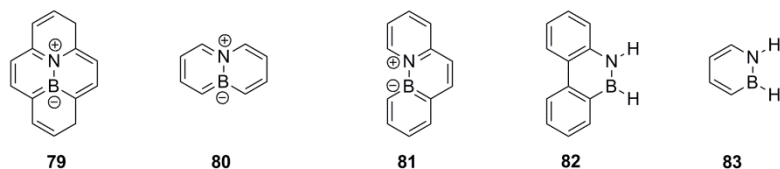
good evidences for its dramatically-enhanced Lewis acidity. Their crystal structures reveal a planar ring with alternated bond length; whether this is due either to a conjugation of the empty p orbital with the π electron or to a packing effect is subject to debate.^[27,69] Boroles are also known to react with potassium in THF to form stable aromatic dianions.^[70]



Scheme 1.25 Synthesis of perfluorinated borole **76**.

1.3. Boron-Nitrogen Pair Inserted into Aryl Units

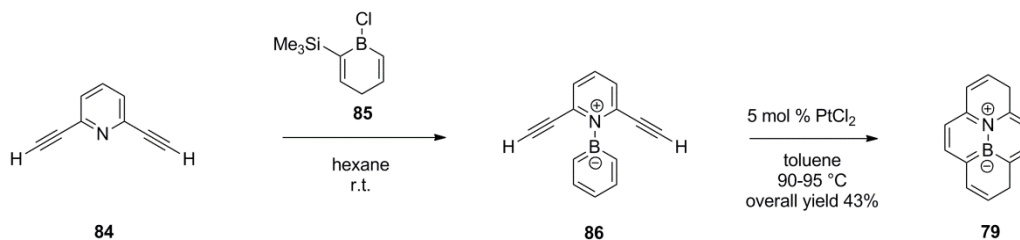
In the previous section, the synthesis of six-membered rings, in which a boron atom has been inserted, has been discussed. However, they present two major drawbacks, the first being that they need to be sterically protected, the second is that they are negatively charged. The steric protection, such as by mesityl groups, prevents π - π stacking interactions.^[57] Hence, the formation of columnar structures, held by π - π stacking, cannot be formed and the compounds cannot be used as anisotropic transporters of electrons.^[71] Furthermore, introducing one boron atom into six-membered rings results in formation of charged species (*e.g.* compounds **41**, **44**, **48**), which have a low solubility in organic media which therefore hampers their utilization. Obviously, a suitable counter ion can enhance this solubility, but this will result in the formation of ionic liquids. These two drawbacks can be addressed by replacing a carbon-carbon pair by a neutral pair, constituted of heteroatoms. One carbon atom can be replaced by an electron deficient boron atom and the other carbon atom by an electron rich nitrogen atom and the pair can be inserted into the aryl unit. The lone pair of the nitrogen atom is partially delocalized into the empty p orbital of the boron atom, reducing its reactivity toward nucleophiles. Also, the π conjugation along the cycle, reduces the electrophilicity of the boron atom. Several groups which have focused their research on the synthesis of heterocyclic derivatives, presented on Scheme 1.26, reported that these compounds do not need steric protection and are stable upon exposure to air and on alumina^[34,72] or silica gel chromatography.^[73] The pioneer research on the synthetic pathway used to insert a boron-nitrogen pair into an arene was achieved by the group of Piers^[34,72,74,75] and by Ashe.^[76-78] Independently, the group of Piers developed the synthesis of 10a-aza-10b-borapyrene **79**,^[72] whereas Ashe and co-workers demonstrated the synthesis of 4a-aza-8a-boranaphthalene **80** (Scheme 1.26).^[78] In addition, the synthesis of two heterocyclic analogues of phenanthrene (**81** and **82**)^[34] was further developed by the group of Piers and the formation of 1,2-dihydroazaborine **83**^[73] was reported by the group of Liu (Scheme 1.26). Unfortunately, the studies on heterocyclic analogues of pyrene **79** and naphthalene **80** were focused on their synthesis and their photophysical properties have not been reported so far in the literature. While the photophysical properties of phenanthrene and benzene were compared to the one of their isosteres **81**, **82** and **83**, the influence of the boron-nitrogen pair on the electronic properties is complex and will be discussed extensively for these derivatives in the following paragraphs.



Scheme 1.26 Heterocyclic analogues of aromatic derivatives: 10a-aza-10b-borapyrene **79**,^[72] 4a-aza-8a-boranaphthalene (**80**),^[78] 4a-aza-4b-boraphenanthrene **81** and 9-aza-10-boraphenanthrene **82**^[34] and 1,2-dihydroazaborine **83**.^[73]

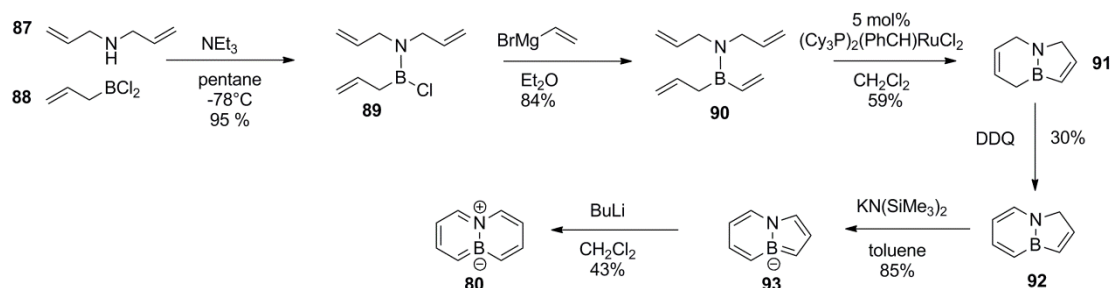
A first possible synthetic pathway is the one described for the synthesis of 10a-aza-10b-borapyrene **79**, which starts with the reaction of pyridine derivative **84** with boracyclohexadiene **85** in the presence of NEt_3 . The Lewis adduct **86** is transformed *in situ* into pyrene derivative **79** by a PtCl_2 catalyzed cycloisomerization. Compound **79** is stable upon exposure to air and can be purified by column chromatography while derivative **86** is reported to be sensitive toward moisture.^[72]

Chapter 1



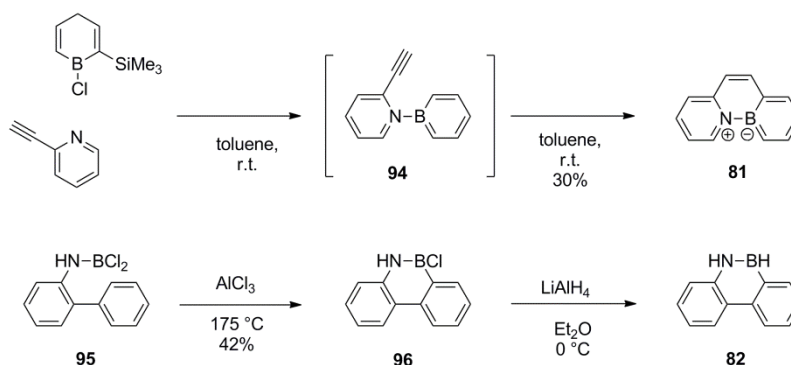
Scheme 1.27 Synthesis of 10a-aza-10b-borapyrene **79**.^[72]

A second synthetic approach for these derivatives has been reported for the synthesis of 4a-aza-8a-boranaphthalene **80** (Scheme 1.28), a sequence similar to the one used later by Liu for the synthesis of 1,2-azaborine (Scheme 1.30). Initially, diallylamine **87** reacts with allylborane dichloride **88** to give **89** in excellent yield (95%). Furthermore, the addition of an allyl Grignard on the boron atom furnishes **90** in average yield (43%). Metathesis reaction using Grubbs catalyst affords **91**, which upon oxidation with DDQ yields **92**. Finally, deprotonation of **92** in the presence of $\text{KN}(\text{SiMe}_3)_2$ gives **93** in good yield (85%), which undergoes reaction with CH_2Cl_2 and BuLi to afford desired derivative **80**.



Scheme 1.28 Synthesis of 4a-aza-8a-boranaphthalene **80**.

The group of Piers^[34] has compared the photophysical properties of two isosteres of phenanthrene. These isosteres were obtained following similar procedures developed for the synthesis of analogues of pyrene and phenanthrene, developed by Ashe^[79] and later used by Piers^[72] for the synthesis of **79**. Lewis adduct **94** was obtained using the same reaction of that outlined in Scheme 1.27. The triple bond moiety reacts, at ambient temperature to give desired derivative **81** in low yield (30%). The synthesis of the other isostere was accomplished following the procedure developed by Dewar.^[79] Starting from Lewis adduct **95**, obtained by addition of BCl_3 to the aniline derivative; phenanthrene **96** is obtained after a Friedel-Craft reaction with AlCl_3 at 175 °C. The latter is then reduced, using LiAlH_4 , to give phenanthrene **82**.^[72]



Scheme 1.29 Synthesis of heterocyclic analogues of phenanthrene, **81** and **82**.

These synthesis were complemented by a crucial study of the photophysical properties. The analysis performed by Piers and co-workers^[72] reveal that the position of the boron-nitrogen pair will determine a hypsochromic or bathochromic shift of the emission profile. In the first case, the boron-nitrogen pair forms double bonds with the carbon atoms (derivative **81**; selected mean bond lengths: C-B: 1.503 Å, C-N: 1.388 Å, B-N: 1.491 Å) and is therefore implicated into the π -conjugation of

the compound. While when the boron-nitrogen pair is introduced at the 9 and 10 positions of the fluorophore, it is not involved in a carbon-boron double bond as observed from the crystal structure (derivative **82**; selected bond lengths: C-B: 1.541 Å, C-N: 1.389 Å, B-N: 1.413 Å). The influences on the emission properties are as followed, isostere **81** has a bathochromically shifted emission ($\lambda_{em} = 450$ nm, $\Delta\lambda = 103$ nm in cyclohexane, $\Phi = 0.58$, Figure 1.7) compared to phenanthrene ($\lambda_{em} = 347$ nm in cyclohexane, $\Phi = 0.09$). This is comparable to the push-pull effect in π -conjugated structures. In particular, the conjugation of the lone pair of electrons of the nitrogen atom into the empty p orbital of the boron atom result in $n \rightarrow \pi^*$ transition for compound **81**, lowering the energy of the transition. Whereas, derivative **82**, whose boron-nitrogen pair is not involved into the π -conjugation, has a hypsochromically shifted emission of only 20 nm ($\lambda_{em} = 327$ nm, $\Delta\lambda = 20$ nm in cyclohexane, $\Phi = 0.61$, Figure 1.7). This shift is due to the increased polarization of the bond in the boron-nitrogen pair, which is reflected by a wider HOMO-LUMO gap. The observed increase of the fluorescence quantum yield upon insertion of a boron-nitrogen pair makes these compounds attractive candidates for OLEDs.^[34]

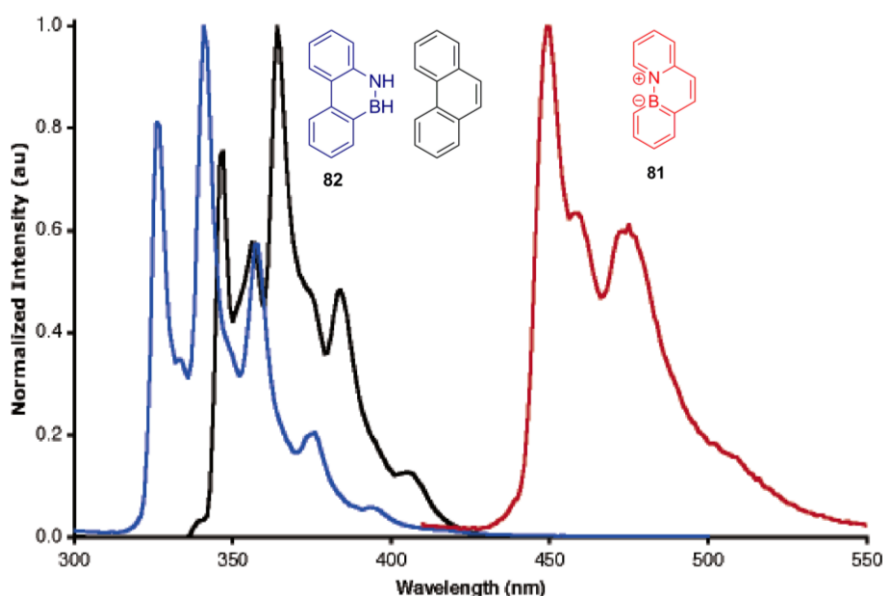


Figure 1.7 Fluorescence emission spectra of phenanthrene (black), **81** (red) and **82** (blue) in cyclohexane. Adapted with permission from the Wiley-VCH Verlag GmbH & Co. KGaA. Copyright 2007.

Lately, the group of Liu performed the synthesis and explored the photophysical properties of azaborine derivatives.^[73] Different research groups made computational predictions about 1,2-azaborine (**83**, Figure 1.8) due to its interest as a π -conjugated analogue of benzene.^[80,81] The chemistry of this heterocycle was explored by Ashe and co-workers, pioneer of the borabenzene synthesis, whose interest span from stibabenzene,^[82] higher acene analogues such as borepin,^[65] pentacene,^[57] oxaborines^[83] and azaborines.^[77] The discovery of protected azaborines derivative, using $\{\text{Cr}(\text{CO})_3\}$ complex as the protecting group,^[84] paved the way for the first synthesis of unsubstituted 1,2-dihydroazaborines by the group of Liu.^[73] It should be noted that if different azaborine derivatives exist, the stability and delocalization of the electrons along the cycles depend strongly on the respective positions of the nitrogen and boron atoms.^[85] The most stable cycle is 1,2-dihydroazaborine^[73,81] **83**, followed by 1,4-azaborine^[81,86,87] analogue **97** and finally 1,3-azaborine^[85] **98** whose derivative has been recently synthesized (Figure 1.8).

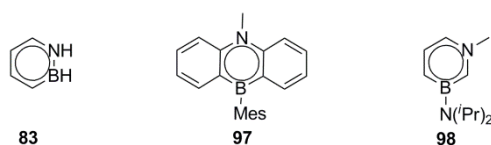
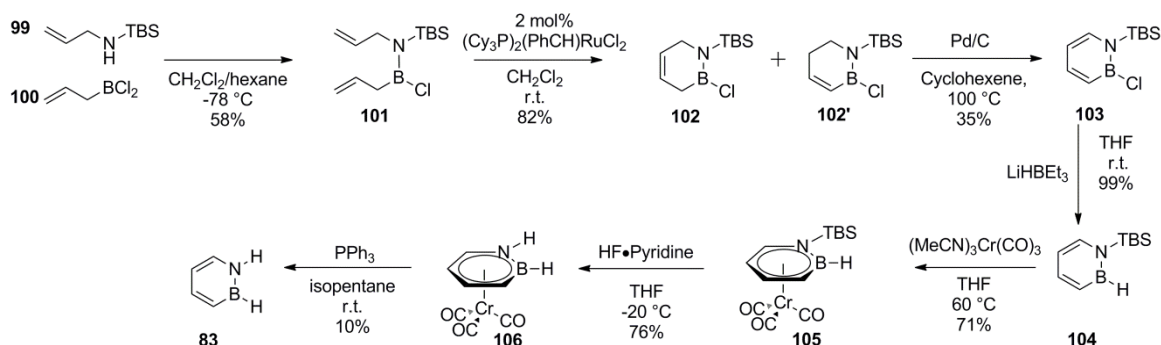


Figure 1.8 Isosteres of benzene ring: 1,2-dihydroazaborine **83**,^[73,88] 1,4-azaborin **97**^[86] and 1,3-azaborin **98**.^[85]

Chapter 1

The synthesis of 1,2-azaborine **83** starts with the reaction of protected allylamine **99** with allyl borane dichloride **100**, affording amino-borane derivative **101** in moderate yield. The latter is condensed in one ring after a metathesis step yielding a mixture of isomers **102** and **102'**. This compound can be further reduced to give 1,2-azaborine **103**, with a TBS-protected nitrogen atom. Furthermore, chloroborane **103** is transformed in nearly quantitative yield into hydroborane **104** after treatment with LiHBEt_3 . The key step in this synthesis is the protection of the 1,2-azaborine ring **104** by $\{\text{Cr}(\text{CO})_3\}$ complex to give derivative **105**. The protection of the ring of **104** allows the use of strong acids ($\text{HF}\cdot\text{pyridine}$) necessary for the removal of the TBS group, without degradation of the azaborine cycle, to afford 1,2-dihydroazaborine **106**. The latter can be deprotected in very low yield (10%) by the use of PPh_3 affording desired 1,2-dihydroazaborine **83**.^[73]



Scheme 1.30 Synthesis of 1,2-dihydroazaborine **83**.

Since the first synthesis of this derivative, many studies outlined the tremendous potential of this isostere of benzene for new pharmacophore,^[88] H_2 storage^[89,90] and material applications.^[35] The research performed in the biological field reveals that compound **83** can bind in the active site of antibacterial enzyme (T4 lysozyme) through π - π stacking interactions with alanine. The lone pair of the nitrogen atom or the empty p orbital of the boron atom are not involved in a specific contact, consistent with the electron conjugation along the cycle. Neither thus the hydrogen atom, connected to the nitrogen atom, is involved in hydrogen bonding, confirming the hydrophobic nature of this compound. The interest of 1,2-azaborine derivatives is therefore to be used as mimic of pharmacophore, which are based on arene, for neutron capture therapy.^[88] The study of 1,2-azaborine derivatives for H_2 storage, revealed that the latter can be dehydrogenated, using palladium on charcoal catalysis, to give the parent unsaturated 1,2-azaborine, releasing H_2 .^[89,90]

Regarding the photophysical properties, the absorption spectra of **83** in pentane reveal bathochromic shift of 14 nm compared to benzene and a much stronger molar absorption coefficient (**83**: $\epsilon = 15632 \text{ M}^{-1}\text{cm}^{-1}$ at 269 nm and $\epsilon = 7459 \text{ M}^{-1}\text{cm}^{-1}$ at 205 nm; benzene: $\epsilon = 971 \text{ M}^{-1}\text{cm}^{-1}$ at 255 nm and $\epsilon = 1299 \text{ M}^{-1}\text{cm}^{-1}$ at 203 nm). These data are consistent with a delocalized aromatic system in the 1,2-dihydroazaborine cycle, as opposed to a cycle constituted of non-conjugated double bond whose absorption spectra would be similar to the one of cyclohexatriene.^[73]

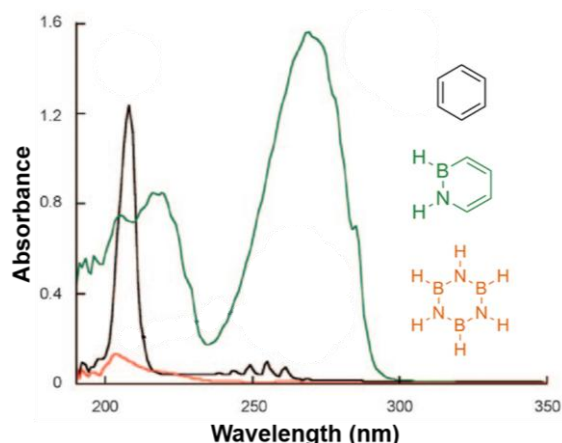


Figure 1.9 UV absorption spectra of 1,2-azaborine **83** (green), benzene (black) and borazine (orange) in pentane, showing the bathochromic shift for azaborine, respective to benzene. Adapted with permission from the Wiley-VCH Verlag GmbH & Co. KGaA. Copyright 2009.

Compound **83** is a liquid, consequently the crystal structure of 1,2-azaborine rings was probed with solid derivative **107**. The crystal structure reveals clear evidence of complete delocalization of electrons along the cycle,^[91] with equalized bond length and a planar cycle (Figure 1.10). The measure resonance stabilization energy suggest an aromatic character,^[89] confirmed by the chemical shift measured by ¹H NMR ($\delta = 8.5$ ppm for N-H, $\delta = 5.0$ ppm for B-H).^[73] However, this delocalization of the lone pair of electrons of the nitrogen atom does not attenuate completely the reactivity of this cycle, which can be functionalized through nucleophilic substitution on halogeno borane derivatives^[92,93] or by exploiting the nucleophilicity of the nitrogen atom.^[92]

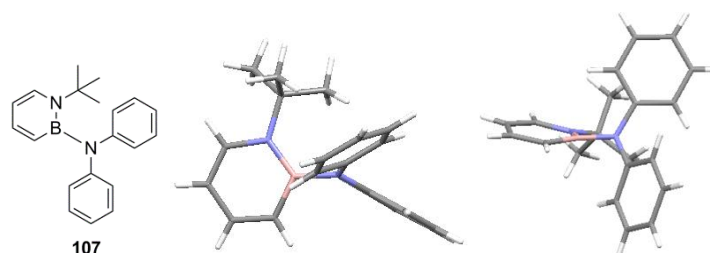
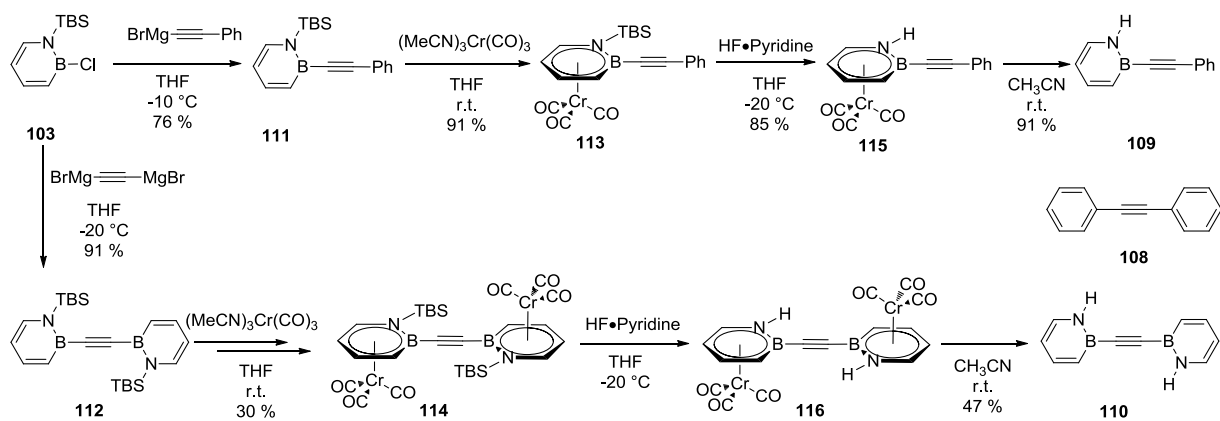


Figure 1.10 Crystal structure of 1,2-azaborine **107** revealing a planar cycle with equalized bond length, suggesting an electron delocalization along the cycle. Representation: capped sticks. Color code: red: O, grey: C, pink: B, white: H, blue: nitrogen. Space group: $P2_1/c$.

This slight red-shift in the absorption spectra of **83**, compare to benzene, is further confirmed by the analysis of analogue of toluene. In order to measure the influence of the 1,2-azaborine ring, the group of Liu synthesized analogues of toluene **108** replacing the phenyl group by one (**109**) or two (**110**) 1,2-azaborine ring (Scheme 1.31).^[35] The synthetic route used the same strategy as developed in Scheme 1.30. Starting from chloroazaborine **103**, the first step is the substitution of chloroborane by phenylethynyl magnesium bromide or ethynyl magnesium bromide to give toluene **111** or **112** respectively. Again the key step is the protection of the azaborine ring by chromium complex to give stable azaborines **113** and **114**. This protection allows the use of HF·pyridine to remove the TBS group in **113** and **114**, to give **115** and **116** respectively. Finally, the removal of the chromium complexes occurs under mild conditions, by stirring in CH_3CN , to give desired toluene derivatives in average (**109**, 41%) or excellent (**110**, 91%) yield.^[35]



Scheme 1.31 Synthesis of tolane analogues, constituted of one (**109**) or two (**110**) 1,2-azaborine ring.

In addition, the absorption spectra of tolane and analogues **109** and **110** were compared. Through UV-Vis absorption spectra it was only observed a broadening of the absorption maximum and no significant bathochromic shift respective to tolane. The change is more noticeable for the emission spectra which are bathochromically shifted of 33 nm for derivative **109** and of 71 nm for tolane analogue **110**. Furthermore, the tolane analogue presented a solvatochromism for the emission spectra, which is more pronounced for compound **110**, consistent with a polarized excited state.^[35] Finally, the fluorescence quantum yield is improving with the doping, starting from 0.7% for tolane, 1.2% for derivative **109** and 2% for product **110**. The compounds are not highly fluorescent nevertheless the relative increase is noticeable (Figure 1.11).^[35]

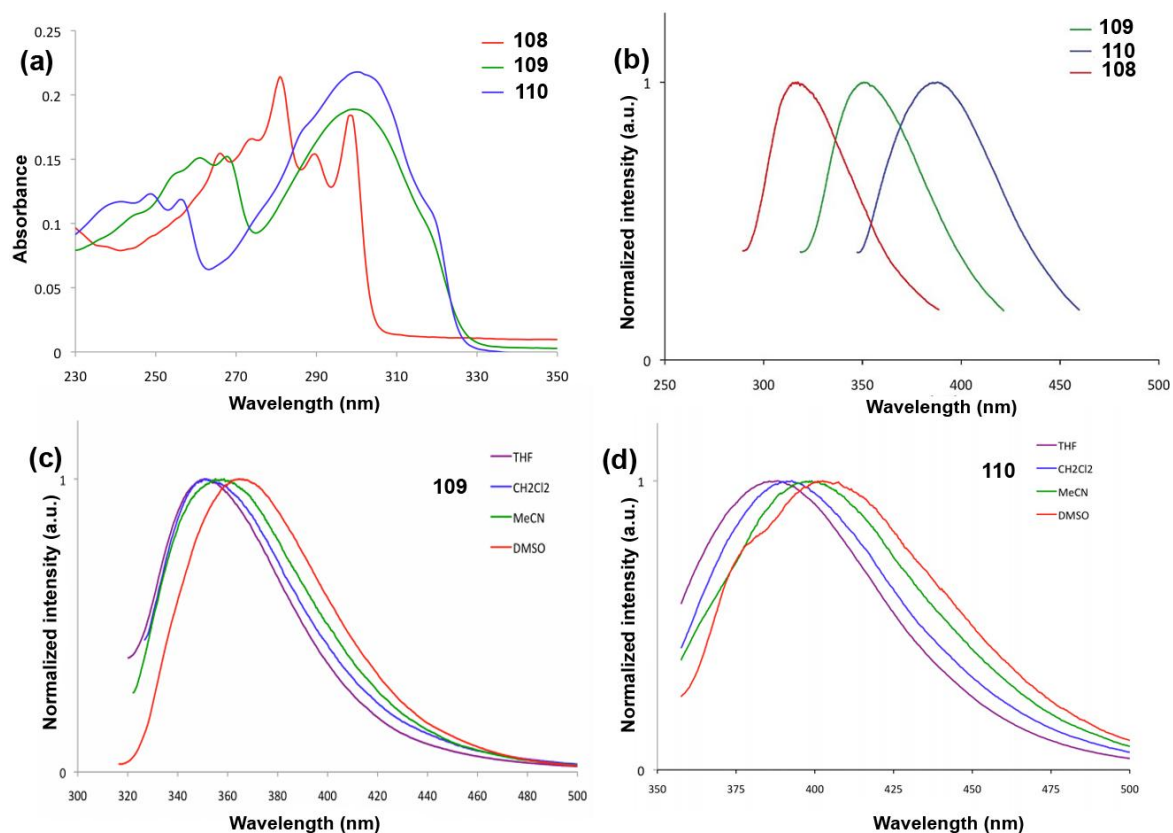


Figure 1.11 (a) UV absorption spectra of tolane **108**, doped tolane **109** and **110** in THF, showing the bathochromic shift of for azaborine, respective to benzene. (b) Comparison of the emission wavelength of the different tolane in THF, showing the red shifted emission of the tolane upon doping: **108** (red), **109** (green) and **110** (blue). (c) Emission spectra of tolane **109** showing solvatochromism only in DMSO. (d) Emission spectra of doped tolane **110** showing solvatochromism. Adapted with permission from the Royal Chemical Society. Copyright 2012.

Chapter 1

In summary, the replacement of a carbon-carbon pair by a more polarized boron-nitrogen pair leads to a complex influence on the photophysical properties of the compound. The isosteres of phenanthrene, **81** and **82**, display respectively a bathochromic and a hypsochromic shifts of the fluorescence. At the contrary, tolane isosteres **109** and **110** both display a bathochromically shifted fluorescence, as well as an increase of the quantum yields. The few examples of fluorescent organic derivatives in the UV region motivated us to aim for hypsochromic shift of the fluorescence by replacing a central benzene ring of π -conjugated structures by analogues containing boron-nitrogen pairs.



2. Borazines-Borazenes, Synthesis, Photophysical Properties, Surface Study and Implementation in OLEDs

The examples described in the introduction chapter outline the important modification of the photophysical properties of π -conjugated compounds, after the insertion of a boron-nitrogen pair. The position of the boron-nitrogen pair into a π -conjugated compound is crucial as it can lead to bathochromic or hypsochromic shifts. A bathochromic shift of the fluorescence is observed for structures where the boron-nitrogen pair is involved in the π -conjugation of the compound, as evidenced by the carbon-boron double bond character identified by crystallography.^[34] At the contrary, a hypsochromic shift of the fluorescence is observed when the boron-nitrogen pair does not form carbon-boron double bonds. The aim of the first part of this thesis involves the synthesis of new UV emitters. Hence, taking into consideration the information described in the introduction, the emitters will be based on the second type of doped π -conjugated structures. A detailed research in the literature revealed that the replacement of the central benzene ring of π -conjugated structures by a heterocycle will be a promising strategy toward our goal. The structures obtained will not possess carbon-boron double bond and should therefore display hypsochromically shifted fluorescence. The synthetic strategies of six-membered heterocycles will be reviewed in this section, with the aim of synthesizing hexaaryl derivatives bearing a central heterocycle.

In the results and discussion part, the synthesis of borazine derivatives and the analysis of their photophysical properties will be extensively described and discussed. Borazines X-ray structures were analyzed in order to understand better the relationship between stability and steric hindrance around the boron atoms. A further study of this led to the discovery of borazenes, linear module constituted of boron-nitrogen bonds. Moreover, the reflection on the hypothetical mechanistic pathway, for the synthesis of the latter, led to the synthesis of differently substituted borazine, on the boron atoms. Furthermore, crystalline structures were also studied to analyze the heterocycle conjugation with peripheral aryl groups (see *section 2.3*). The effective conjugation with the π -conjugated structure has a deep influence on emission properties such as quantum yield and, more importantly, luminescence peak shift, as outlined in the introduction chapter. In addition, the photophysical properties of these heterocycles were later probed in solution and in the solid state, displaying variation of the fluorescence peaks depending on the solid state arrangements (see *section 2.4*). These arrangements were subsequently studied on metallic surfaces by STM techniques to evaluate adsorption properties of the compounds on different metals (see *section 2.5*). This was of crucial importance to choose the suitable metallic cathode when the emitting compound was implemented into the luminescent layer of an OLED (see *section 2.6*). Finally, a donor-acceptor complex was studied, namely a borazine·fullerene cocrystal. The photophysical properties as well as the conductivity probed by time-resolved microwave conductivity (TRMC) presented preliminary results toward applications for solar cells (see *section 2.7*).

2.1 Introduction

Several analogues of benzene, doped with third and fifth row elements are known in the literature such as alumazene^[94] (**117**), phosphinoborine^[95-97] (**118**) and borazine^[98] (**119**) (Figure 2.1). Alumazene derivatives are known to coexist in equilibrium with four-membered rings constituted of alternating aluminum and nitrogen atoms, which can dimerize to form a cube, constituted of four aluminum atoms and four nitrogen atoms.^[94] On the other end, the replacement of aluminum for the lower element in the row, gallium, end up in only four-membered rings constituted of alternating gallium and nitrogen atoms.^[94] In the same manner, phosphinoborine, first discovered by Slota,^[95] are also known to form six-membered rings in equilibrium with the four-membered rings.^[96,97] The latter has been studied as an inorganic analogue of cyclobutadiene but exhibits no evidence of delocalization of the lone pair of the phosphorus atom into the empty p orbital of the boron atom.^[97] Therefore, our choice of stable, six-membered heterocycle analogue of benzene was naturally focused on the borazine cycle (**119**), dubbed inorganic benzene.^[99-101]

The replacement of a carbon-carbon pair by a boron-nitrogen pair results in a more polarized bond, due to the lower electronegativity of the boron atom and the higher electronegativity of the nitrogen atom, respective to carbon atom. Many theoretical calculations predict that this polarization of the bond will be reflected into a wider HOMO-LUMO gap.^[102–104] Based on this hypothesis, the replacement of the central benzene ring of π -conjugated structures by a borazine ring was envisaged, followed by the study on its influence on the photophysical properties. Since its discovery by Stock in 1926,^[98] borazine (**119**), six-membered heterocycle composed of alternating boron and nitrogen atoms, has been forgotten for many years before a surge in interest in the 1960s when they were used as precursor of boron nitride. This boron nitride is the isoelectronic analogue of carbon lattice and exists in the cubic form (c-BN),^[105] a hard material used as an abrasive, in contrary with the hexagonal form (h-BN), a soft material used in cosmetic products.^[106–108] Moreover, boron nitride nanotubes are described in the literature as transparent insulating materials.^[109,110] Whereas mixed structures, composed of carbon, boron and nitrogen atoms, can be obtained to form boron nitride-graphene sheets.^[32] Other nanostructures have also been explored to have a UV emitting material, such as the formation of boron nitride whiskers.^[111] The hexagonal boron nitride, which has a structure similar to graphene, is an emissive material in the UV region (215 nm),^[112] and has been used in LED.^[113] The advantage of the latter over other emissive group three nitrides,^[114] such as gallium nitride, also a UV emitter at 362 nm,^[115] is an emission deeper in the UV. Moreover, the depletion of gallium resource soared the cost of the latter. As a consequence of the impressive array of applications of boron nitride materials, the majority of the literature has been focusing on their utilization with little research devoted to the synthesis of their precursors. Notably, the functionalization of the borazine ring, a well-known precursor of boron nitride, by synthetic methods is seldom discussed in the literature. With the aim of exploiting the fluorescence of boron-nitrogen compounds while keeping the versatility of the organic substituents, which allow fine tuning of the wavelength of emission, the synthetic approaches toward the synthesis of borazine derivatives were explored.

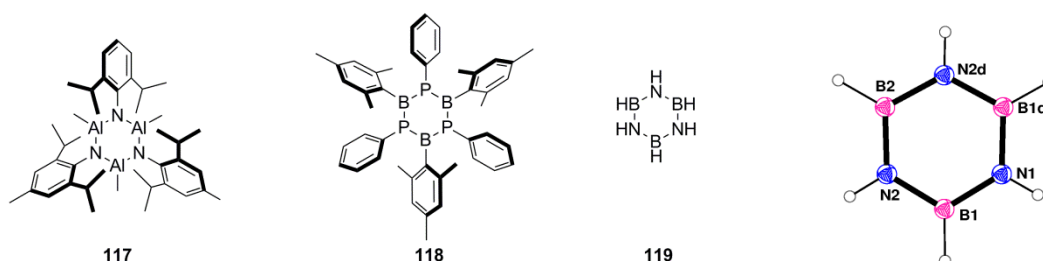


Figure 2.1 Inorganic analogue of benzene: alumazene^[94] (**117**), phosphinoborin^[95–97] (**118**) derivatives, hexahydroborazine^[98] (**119**) and its ORTEP representation of its crystal structure.^[100]

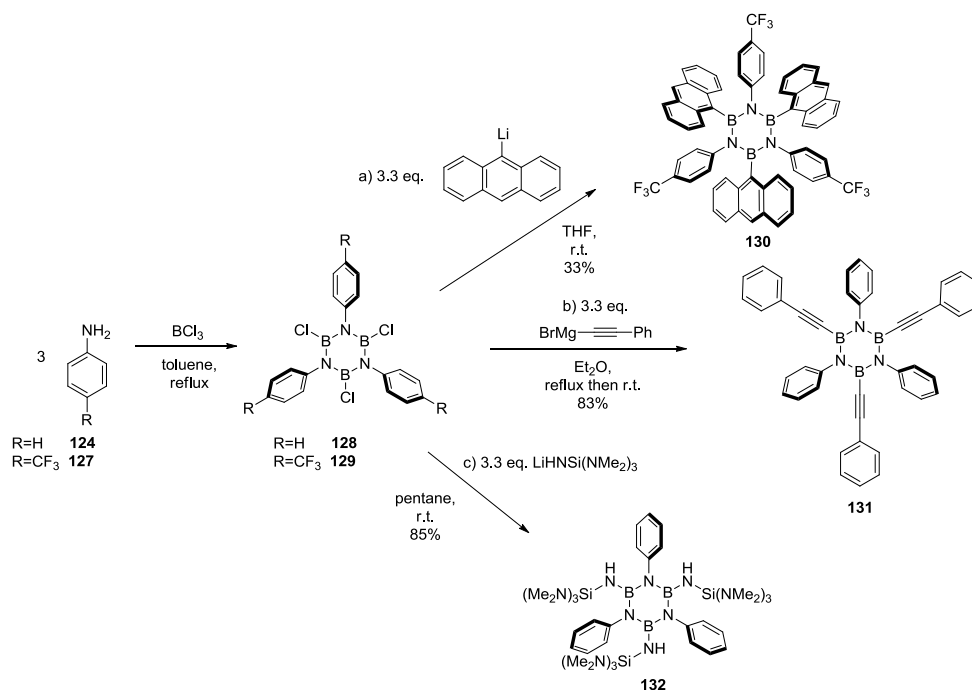
The crystal structure of borazine **119** indicates an equalization of the bond lengths as well as a planar cycle, evidencing a delocalization of the lone pairs of the nitrogen atoms into the empty p orbitals of the boron atoms (Figure 2.16).^[100] The mean boron-nitrogen bond length is of 1.429(1) Å, close to the bond length of 1.40 Å observed for benzene. Even more, the torsion angle is of 0.6(1)° (B1-N1-B1d-N2d), indicating the planarity of the ring. Finally, the mean value of the angles are of 117.1(1)° at the boron atom and of 122.9(1)° at the nitrogen atom, close to the 120° angle observed for benzene.^[100] All these information suggest a strong predominance of the mesomeric form (**119'**) where the lone pairs of the nitrogen atoms are delocalized into the empty p orbitals of the boron atoms, each atoms bearing formal positive and negative charges respectively. For the sake of clarity the mesomeric form **119** will be drawn throughout this work to represent the planar borazine cycles.

2.1.1 Synthetic Strategies and Photophysical Properties of Borazine Rings

The first borazine was discovered by the group of Stock in 1926, while they were studying the reactivity of B_2H_6 **120** with NH_3 **121**.^[98,116] The synthetic strategy outlined in Scheme 2.1 starts with B_2H_6 **120** which reacts with NH_3 **121** at r.t. to

Chapter 2

are highly sensitive toward moisture and are not isolated as such but rather subjected directly to the second reaction step which consists of the nucleophilic substitution on the borazole ring by a Grignard or a lithiate derivative, which leads to hexasubstituted borazine.^[122] This substitution can occur with an aryl (compound **130**, Scheme 2.4),^[122,123] alkyne^[124] (compound **131**, Scheme 2.4) or a protected amine derivative (compound **132**, Scheme 2.4),^[125] leading to a broad range of borazine derivatives.



Scheme 2.4 Outline of the broad range of borazine derivatives that can be obtained through the borazole route. The borazole can be substituted by a) aryl,^[122] b) alkyne^[124] and c) amine^[125] derivatives.

The research conducted by the group of Yamagushi described the use of borazine derivatives as platforms for π -conjugated molecular bundles, resulting in borazine derivatives with a good fluorescence quantum yield.^[122] Nevertheless, the UV-Vis absorption, fluorescence and electrochemistry measured were dominated by the anthracenyl group substituting the boron atom of the borazine ring. This was further evidenced by the comparison of the emission wavelength of the borazine derivatives compared to the one of anthracene. Notably, they revealed a large increase in the fluorescence quantum yield (relative to anthracene) due to the arrangement of the anthracenyl group, perpendicular to the borazine cycle, forced into a rigid conformation which results in an increase of the quantum yield.^[122] The quantum yield of anthracene is of 27% ($\lambda_{em} = 380$ nm, in THF) while they reported quantum yield of 63% ($\lambda_{em} = 397$ nm, in THF) for borazine derivative **130** and 62% ($\lambda_{em} = 397$ nm, in THF) for borazine derivative **133**.^[122]

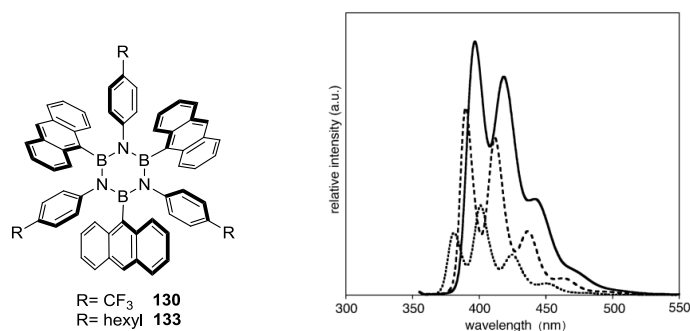


Figure 2.2 Fluorescence spectra of anthracene (dotted line), borazine derivative **130** (solid line) and borazine derivative **133** (dashed line) in THF. Adapted with permission from the American Chemical Society. Copyright 2005.

Chapter 2

Using the same synthetic pathway, Videla and co-workers reported the use of borazine derivatives as neutron scintillation detectors. Indeed, they proved that borazine derivatives became fluorescent upon absorption of neutrons by the boron atoms.^[126,127] Borazine **134** has been found to be an ideal candidate with an absolute quantum yield of 33%, an emission between 350 and 400 nm ($\lambda_{exc} = 254$ nm).

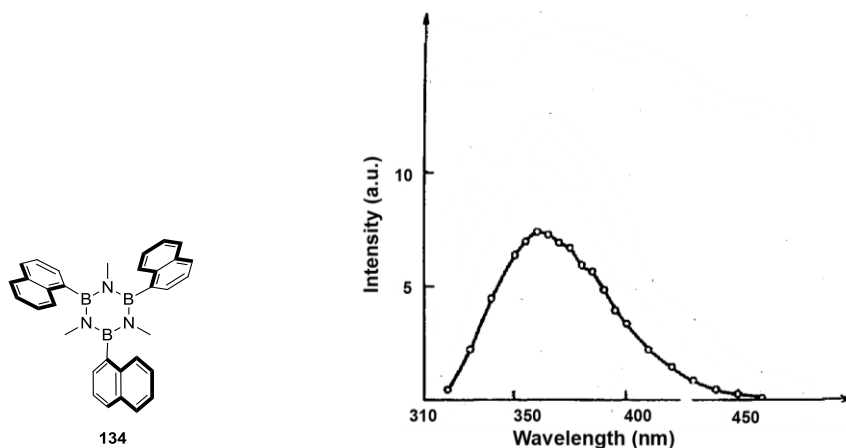
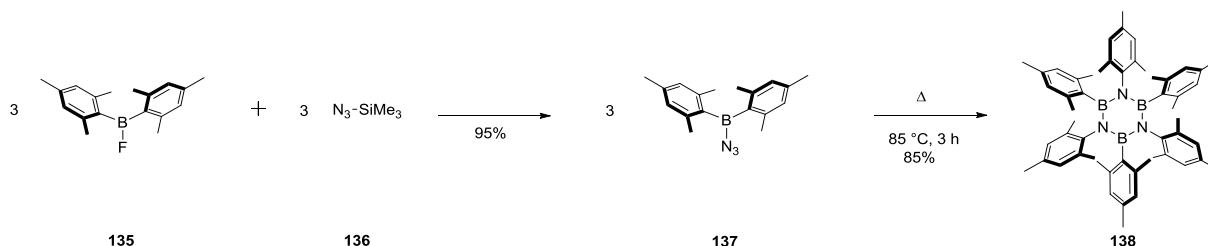


Figure 2.3 Borazine used in neutron scintillation detectors by Videla and the fluorescent spectra of borazine **134**.^[126] Adapted with permission from Pergamon Press Ltd. Copyright 1964.

Finally, the group of Che^[128] reported the first use of B-triphenylborazine derivatives in OLED, which have been also synthesized through the synthetic pathway outlined in Scheme 2.4. Nevertheless, the luminescence reported was the one of zinc complexes. Indeed, they used the borazine derivatives as dopant in the charge transporting layer and not in the emissive layer of the device. This study revealed that the borazine derivatives employed were good electron transporters (10^{-3} cm² V⁻¹ s⁻¹) and display thermal stability up to 200 °C, under N₂ atmosphere.^[128]

Another synthetic pathway taking advantage of the electrophilicity of halogeno borane is detailed in Scheme 2.5.^[129,130] The initial reaction of dimesitylfluoroborane **135** with a protected azide **136**, which substitutes the boron atom, gives intermediate **137**. The latter reacts upon heating, resulting in the shift of one mesityl substituent from a boron to a nitrogen atom and subsequent loss of nitrogen, affording borazine **138** in excellent yield (85%).^[129] The drawback of this synthetic strategy is that it offers no versatility for the choice of the substituents. The substituents on the boron and the nitrogen atoms will always be identical and the known examples are with phenyl, mesityl and perfluorophenyl substituents.^[129]



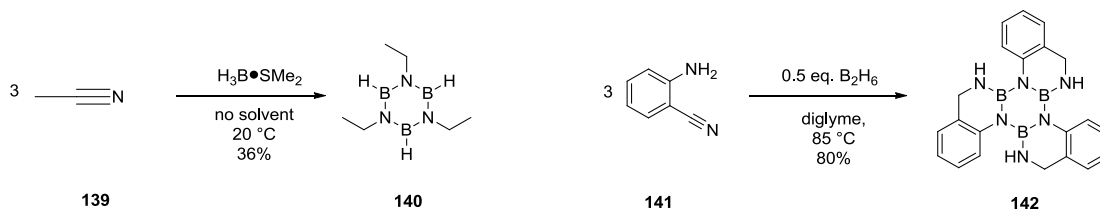
Scheme 2.5 Synthetic strategy used by Paetzold to yield hexasubstituted borazine **138** in two steps.^[129]

2.1.1.3 Synthesis of Borazine Rings by the Reduction of Multiple Bonds Using Borane

The third synthetic strategy exploits the reactivity of borane which can reduce the triple bond of nitrile moieties. Borane forms a Lewis adduct with the nitrogen atom and after subsequent reduction of the triple bond, this leads to the formation of the borazine cycle. For example, the reduction of CH₃CN **139** (Scheme 2.6) with BH₃·SMe₂ complex leads to the formation of trisubstituted borazine **140** (Scheme 2.6).^[131] Starting from an aniline, substituted in *ortho* position by a nitrile group (compound **141**, Scheme 2.6), the Lewis adduct formed leads after heating, to borazine **142** in good yield (80%) (Scheme

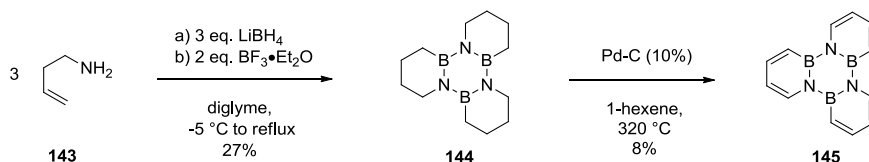
Chapter 2

2.6).^[132] The boron atom is substituted by a mesomeric donor group, which provides an increased stability of the derivative, by reducing its electrophilicity.



Scheme 2.6 Synthetic strategy using the reduction of nitrile and subsequent formation of borazine ring **140** and **142**.

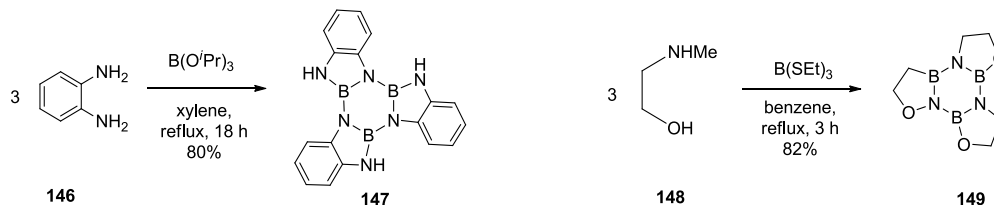
A similar synthetic pathway exploits the reactivity of borohydrides, known to reduce double bonds.^[133] For example, the reaction with an homoallylic amine (**143**) leads to the formation of the only fused alkyl borazine (**144**) reported in the literature.^[134] Unfortunately, the UV-Vis and fluorescence properties were not investigated for this derivative, which was immediately oxidized to form borazine **145** (Scheme 2.7) in low yield (8%), possibly due to the difficulties in isolation. The latter borazine is supposedly conjugated with the double bonds, but once again the properties of this compound were not explored.^[134]



Scheme 2.7 Synthetic approach toward fused conjugated aromatic systems **145** by reduction of double bond with borane.^[134]

2.1.1.4 Synthesis of Borazine Rings from Nucleophiles Reacting with Boronic Esters

Finally, the most attractive synthetic pathway, from the point of view of the ease of reaction conditions, starts from boronic esters, as stable, easy to prepare derivatives. These boronic esters are still electrophilic, despite the presence of three mesomeric donor substituents, and react readily with ditopic nucleophiles such as *ortho*-phenylenediamine,^[135,136] amino alcohol,^[137] or amino mercapto^[138] upon heating. The reaction illustrated in Scheme 2.8, indicates the formation, from *ortho*-phenylenediamine **146**, of borazine **147** in good yield (80%), and the side product being isopropanol.^[135] In the case of amino alcohol **148** the reaction can occur in the presence of $\text{B}(\text{SEt})_3$ to afford hexasubstituted borazine **149** in good yield (82% yield).^[139]



Scheme 2.8 Synthesis of borazine **148** and **149** starting from boronic ester^[135] or thioborane.^[139]

2.1.1.5 Synthesis of Differently Substituted Borazine Rings

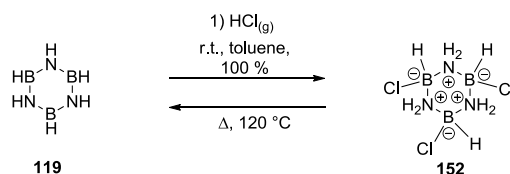
Also notable is the peculiar reactivity of complex **150** (Scheme 2.9) which is reported to yield differently substituted borazine **151** upon addition of BF_3 in Et_2O .^[140] Interestingly, this is the only direct synthesis of differently substituted, on the boron atoms, borazine derivative reported so far in the literature.



Scheme 2.9 First direct synthesis of differently substituted borazine **151**.^[140]

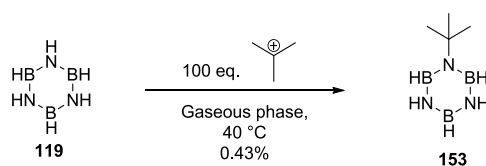
2.1.2 Reactivity of the Borazine Ring

The synthesis of borazines was mainly studied due to their final application as precursor of boron nitride and the functionalization of the heterocycle was seldom explored.^[108,141–144] Consequently, the reactivity of the cycle was not well explored. From the crystal structure, based on the equalization of the boron nitrogen bond length and the trigonal geometry of the boron and nitrogen atoms, one can deduce that the lone pairs of the nitrogen atoms are delocalized into the empty *p* orbitals of the boron atoms. Moreover, the borazine is planar and has equalized bond lengths, as observed from its crystal structure (Figure 2.1).^[100,145,146] However, in strongly acidic conditions, the lone pairs of the nitrogen atoms can be protonated, leading to derivative **152** quantitatively.^[147] The elimination reaction can occur when the latter is heated up to 120 °C to give back borazine **119**.^[147]



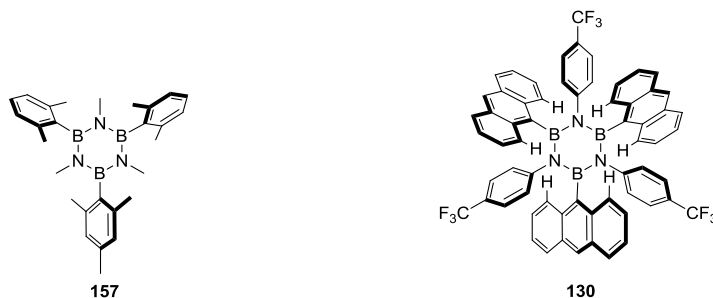
Scheme 2.10 Addition of HCl on the boron-nitrogen bonds of borazine **119**.^[147]

These lone pairs of electrons are thus still slightly nucleophilic and this can be exploited to substitute the nitrogen atoms. Following this strategy, borazine **119** reacts with isobutyl cation, produced by the γ -irradiation of a large excess of butane in gaseous phase, in the presence of oxygen as radical scavenger, to afford derivative **153** (Scheme 2.11) in extremely low yield (0.43%).^[148,149] The latter borazine is now differently substituted.



Scheme 2.11 Asymmetric alkylation of the nitrogen atom of borazine ring **119**.²⁷

The nitrogen atom position can be further functionalized by exploiting the acidity of the hydrogen atoms substituting it. They can be deprotonated in harsh condition, using MeLi to form a reactive, negatively charged nitrogen atom.^[150] Borazine **154** reacts with MeLi to yield complex **155** (Scheme 2.12) where the lithium cation is coordinated by the nitrogen and boron atoms as well as TMEDA.^[151] The lithiate borazine can then be functionalized with an appropriate electrophile. This synthetic strategy was used to synthesize cross linked borazine-phosphane and borazine-arsane derivatives from the reaction of the lithiated analogue of B-trimethyl-N-trihydroborazine with PCl_3 and AsCl_3 .^[152]



Scheme 2.14 Stable borazine reported in the literature, toward hydrolysis (**157**) and on silica gel (**130**).

Other research groups reported the use of chromium complexes, as developed by Ashe and Liu for 1,2-azaborine **83** (*see section 1.3*),^[76] to afford borazine **158** (Figure 2.4).^[158,159] However, even though this strategy works for hexaalkyl borazine, it does not for triaryl borazine **159** (Figure 2.4). It is reported that the chromium will preferably bind to the phenyl substituent than the borazine ring for triphenyl borazine, probably for the same reason reported for triphenyl benzene **160** (Figure 2.4),^[160] where the steric hindrance prevent the chromium complex from binding to the central aryl ring. Moreover, the crystal structure of borazine bound to a chromium complex reveals a puckered geometry for the borazine ring (B-N-B-N dihedral angle: 12°), but less than the one observed for chromium complexes of 1,3,5-triazacyclohexane (C-N-C-N dihedral angle: 67°),^[161] that could suppress the fluorescence. As a comparison, the binding of chromium complexes to aryl ring influence only slightly the planarity of the cycle (C-C-C-C torsion angle: 2.3(6)°).^[162] Consequently, this strategy to afford stable borazines as luminescent emitters was not further used.

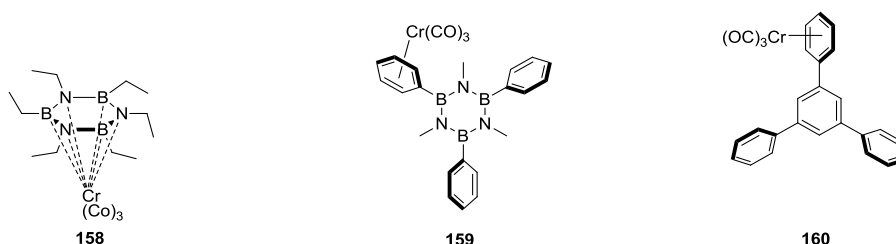
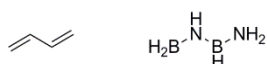


Figure 2.4 Chromium complexes of hexaalkyl borazine **158**, triphenyl borazine **159**, and triphenyl benzene **160**.

2.1.4 Synthesis of Borazenes

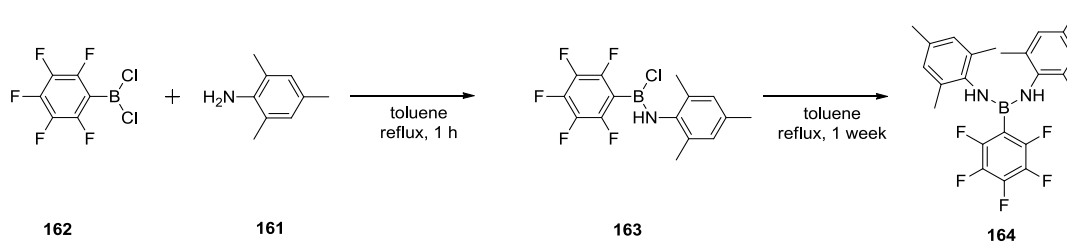
The synthetic strategies for heterocycles six-membered rings have been extensively reported. Nevertheless, linear chain constituted of boron-nitrogen bonds also exist and were studied during this work. Borazenes are linear molecule constituted of alternated boron-nitrogen bonds. They have been synthesized with the aim of studying their properties, as inorganic analogues of butadiene^[163] (Scheme 2.15) or, when inserted into a ring, as analogues of cycloalkyne^[164] and finally as precursors of boron nitride.^[165] More recently, the group of Manners develop the synthesis of boron-nitrogen polymers, starting from aminoborane monomers.^[118,165]



Scheme 2.15 Butadiene and its isostere, borazene derivative.

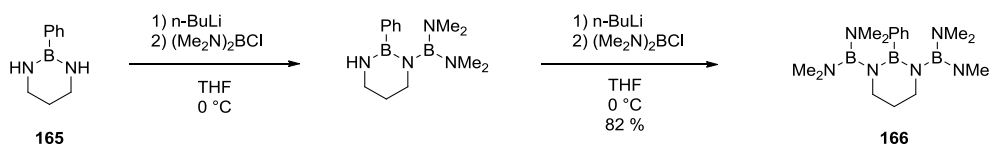
The synthesis illustrated in Scheme 2.16 presents a similar synthetic pathway as the borazine one developed in Scheme 2.4. Mesityl aniline **161** and borane chloride **162** react in refluxing toluene to give intermediate **163**. The steric clash between the mesitylene and the perfluorophenyl group is thought to prevent the formation of the borazole ring, ending up in the formation of borazene **164** after prolonged heating.^[166]

Chapter 2



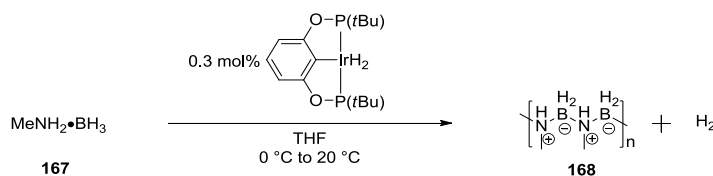
Scheme 2.16 Synthesis of borazene **164** using the synthetic procedure of borazole synthesis.

A distinct synthetic pathway was used for the synthesis of boron-nitrogen chain, avoiding the formation of the thermodynamically stable borazine.^[163,167,168] Starting from cyclic compound **165** (Scheme 2.17), stepwise deprotonation of amine followed by the addition of the electrophilic amino borane, extends the boron-nitrogen backbone to give **166** in good yield (82%).^[167] The crystal structure suggests a steric protection of the boron atoms by the methyl substituents, beside the fact that cyclic borane derivatives are more stable toward hydrolysis.^[168]



Scheme 2.17 Synthesis of borazene **166** starting from cyclic compound **165** and extension of the boron-nitrogen backbone from the amine.

Finally, the synthesis of boron-nitrogen polymers was achieved, by the group of Manners, using iridium catalysis with the aim of producing boron nitride ceramics.^[169–171] Starting from amino-borane Lewis adduct **167** (Scheme 2.18), polymer **168** is synthesized *via* dehydrogenation of **167**, catalyzed by the iridium complex at r.t.^[170] This is in striking contrast with the results reported by the same group with rhodium^[118] catalysis (Scheme 2.3) and iron catalysis from the group of Liu^[121] who reported the synthesis of borazine using the same starting material but a different catalyst. These results highlight the role of the iridium catalyst to avoid borazine or cyclic polymer formation.^[171]



Scheme 2.18 Synthesis of boron-nitrogen polymer **168** through iridium catalyzed dehydrogenation of ammonia borane **167**.

2.2 Synthesis

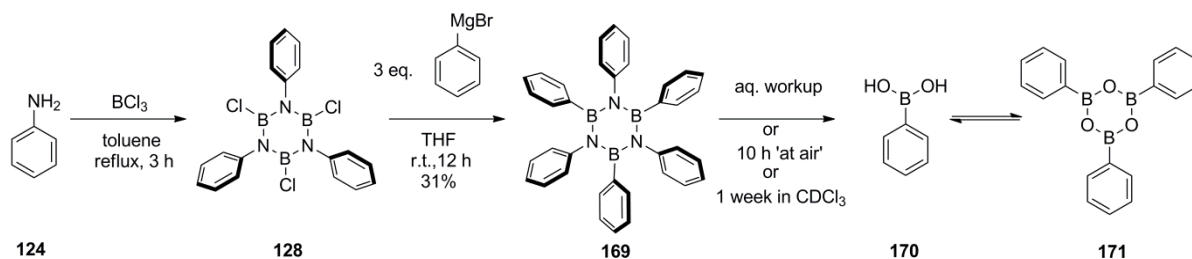
As explained in the introduction, the general aim of this project is to synthesize UV emitters based on hexaarylborazine derivatives. The examples reported in the introduction revealed that hexasubstituted borazine, substituted by anthracenyl units, are emitters around 400 nm. However, reports by Yamagushi and co-workers,^[122] revealed that the fluorescence of these borazine derivatives comes from the anthracenyl group while our goal was to probe and exploit borazine cycle fluorescence deeper in the UV region. Therefore, this project was focused on the synthesis of hexaarylborazine substituted by phenyl or mesityl groups on the boron atoms in order to obtain UV emitters to be incorporated into the luminescent layer of OLED.

The synthetic strategy followed during this work is the one reported in Scheme 2.4. Although the synthetic pathway reported in Scheme 2.5 results in higher yield for the synthesis of hexaarylborazine, it does not offer the needed versatility of the substituents on the nitrogen and boron atoms. The first section (*section 2.2.1*) will concentrate on the synthesis of hexaphenylborazine. The targeted borazine was later changed for sterically hindered borazine (*section 2.2.2*) to afford derivatives stable towards moisture. The steric hindrance was further increased around the boron atom and this leads to the unexpected synthesis of borazene derivatives, exemplified in *section 2.2.3*. Finally *section 2.2.4* will discuss the synthesis of differently substituted borazine.

2.2.1 Synthesis of Hexaphenyl Borazine

Several references in the literature report the synthesis of hexaphenylborazine,^[128,172] nevertheless the stability of this derivative was seldom discussed. The purification procedures vary between different literature references but the uses of aqueous workup or purification on silica gel chromatography were never mentioned. Hence, the synthesis of these derivatives was aimed in exploring their reactivity and moreover their stability. Indeed, for OLED applications compounds stable over a long period of time and ideally stable toward moisture are required in order to allow a preparation of the device under atmospheric conditions, without the need of an inert atmosphere.

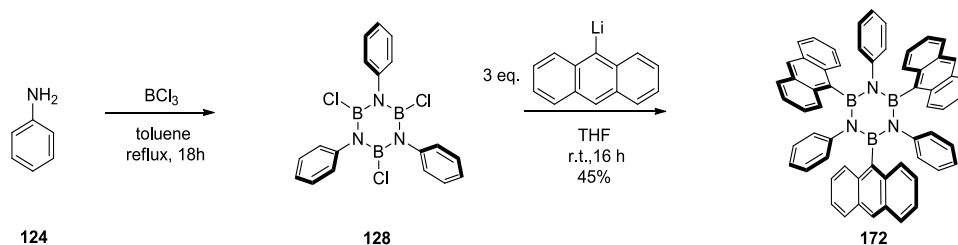
The synthesis of hexaphenylborazine **169** (Scheme 2.19) starts with BCl_3 , which reacts with aniline **124** to form a Lewis adduct. Upon refluxing in toluene, HCl evolves and borazole cycle **128** is formed. The second step involves the nucleophilic substitution on the borazole ring by a Grignard reagent at r.t., which leads to hexasubstituted borazine **169**. Despite the previous reports in the literature,^[172] it was found that hexaphenylborazine **169** is unstable upon exposure to air and therefore difficult to isolate. Compound **169** was also found to be moisture sensitive and degraded into phenylboronic acid **170**, upon aqueous workup or in solution in non anhydrous solvent. The latter boronic acid is in equilibrium with its anhydride form, triphenylboroxine **171**. Therefore, the solid was extracted with anhydrous CH_2Cl_2 using soxhlet extractor. A light brown solid, mixture of hexaphenylborazine and unreacted aniline was recovered. A precipitation in CH_3CN afforded borazine **169** in moderate yield (31%) as a white solid. The average yield could be ascribed to the impurities produced with borazole **128**. Therefore, **128** was recrystallized under inert atmosphere with anhydrous benzene to give pure **128** as a white solid. Borazole **128** is difficult to isolate and to purify owing to the fact that it reacts quickly with moisture, which is in full accordance to what has been reported in the literature.^[123,157,172–174] However, when the purified intermediate was allowed to react with the lithiate species the overall yield did not improve. Therefore it was characterized only by ^{11}B NMR (singlet, δ : 19 ppm) and directly subjected to the second step after three freeze-to-thaw cycles to remove the excess of HCl.



Scheme 2.19 Synthesis of hexaphenylborazine **169** and subsequent degradation into phenylboronic acid **170**, in equilibrium with triphenylboroxine **171**.

2.2.2 Synthesis of Borazines Stable toward Moisture

The lack of stability of the borazine derivatives upon standing at air motivated our research for stable derivatives of borazine for final OLED applications. The degradation of borazines upon addition of H₂O is known to yield the triphenyl boroxine, after nucleophilic addition on the boron atoms.^[154,175] Therefore, a kinetically stable borazine could be expected by blocking the access to the boron atoms. To this end, the steric protection of the boron centers was envisaged by *ortho* substituents on the aryl groups substituting the boron atom. Inspired by the work of Nagasawa,^[154] who described the first example of borazine stable toward hydrolysis (**157**), and by the work of Yamagushi,^[122] who reported the first example of borazine purified on silica gel column chromatography (**130**), the synthesis of borazine **172** was commenced to validate a reproducible synthetic protocol. This synthesis was based on the experimental procedure of the borazine synthesized by the group of Yamagushi which leads to the formation of borazine derivatives stable on silica gel.^[122] Hence, borazole **128** was reacted with the anthracenyl lithiate derivative to give borazine **172**. Product **172** was obtained with moderate yield (45%). Mass spectrometry analysis (Figure 2.5) reveals a peak at $m/z = 837.4$ corresponding to the molecular weight of borazine **172**, the calculated isotopic pattern match the experimental one.



Scheme 2.20 Synthesis of B-trianthracenyl-N-triphenyl borazine **172**.

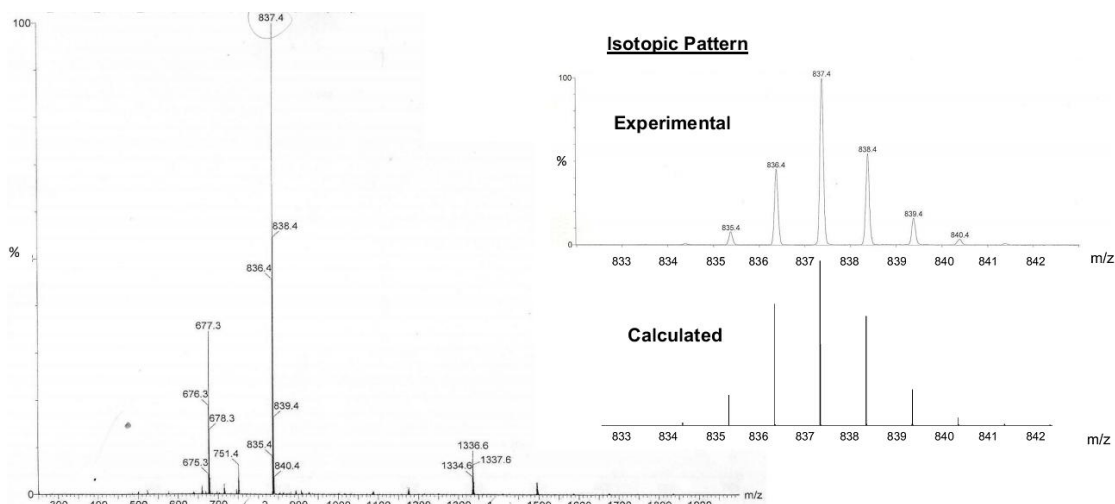
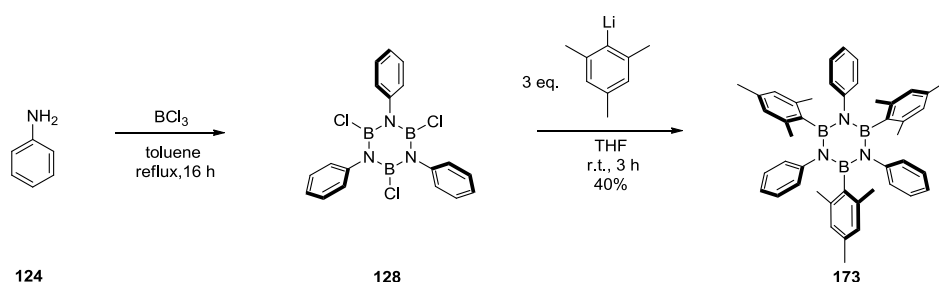


Figure 2.5 Mass spectrum of borazine **172**, corresponding to the molecular formula: C₆₀H₄₂B₃N₃. MALDI, matrix: DCTB.

Chapter 2

Having isolated a stable borazine and confirmed the relation between steric hindrance around the boron atoms and the stability of the derivatives, the anthracenyl substituents were changed for mesityl moieties.

The synthetic route used was identical to the one reported for borazines **169** and **172**, starting with aniline **124**, which was reacted with BCl_3 in refluxing toluene to give borazole **128**. Again, the borazole was not isolated as such due to its sensitivity toward moisture. Hence compound **128** was reacted with MesLi, freshly prepared from the corresponding bromine, to substitute the chlorine atoms on the boron atoms forming desired borazine **173** in average yield (40%). The latter was stable upon aqueous workup and can be purified on silica gel chromatography. The structure was confirmed by ^1H NMR, ^{13}C NMR and ^{11}B NMR, which the last revealed a broad peak at 37 ppm, consistent with a boron substituted by two nitrogen atoms and linked to one carbon atom. IR spectrum revealed a broad band at 1355 cm^{-1} , characteristic of the B-N stretching in the borazine cycle, and high resolution mass spectrometry analysis (Figure 2.6) indicates a peak at $m/z = 663.4138$ whose isotopic pattern corresponds to the one of borazine **173**.



Scheme 2.21 Synthesis of B-trimesityl-N-triphenylborazine **173**, stable toward hydrolysis.

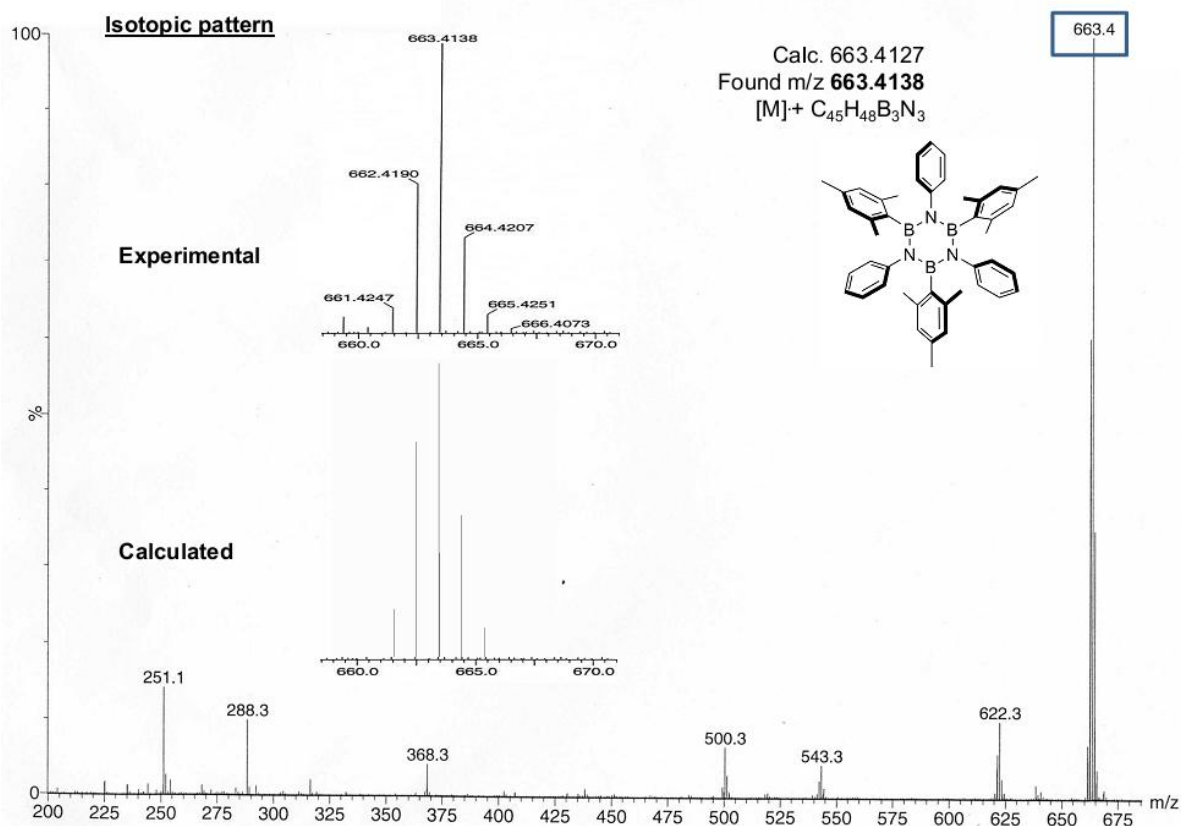


Figure 2.6 Mass spectrum of B-trimesityl-N-triphenylborazine (**173**), corresponding to the molecular formula: $\text{C}_{45}\text{H}_{48}\text{B}_3\text{N}_3$. MALDI HRMS, matrix: DCTB.

Chapter 2

White crystals suitable for X-ray diffraction were obtained by slow evaporation of CH_2Cl_2 , cyclohexane and pentane solutions. They belong to three different space groups, $R\bar{3}2$, $R\bar{3}c$ and $P2_1/n$ respectively. Further details are given in appendix I and in section 2.3.2.

A difference of stability toward moisture between borazine **169** and **173** was therefore noticed experimentally since **169** decomposed upon aqueous workup while **173** did not and was stable on silica gel column chromatography. However, thermogravimetric analysis (TGA) spectra reveal that upon heating under inert atmosphere, borazine **169**, which decomposed at 400 °C, has a better thermal stability than **173**, which decomposed at 360 °C (Figure 2.7). So, under N_2 flow, borazine **169** displays better thermal stability than borazine **173**, even though borazine **169** is less stable upon exposure to air.

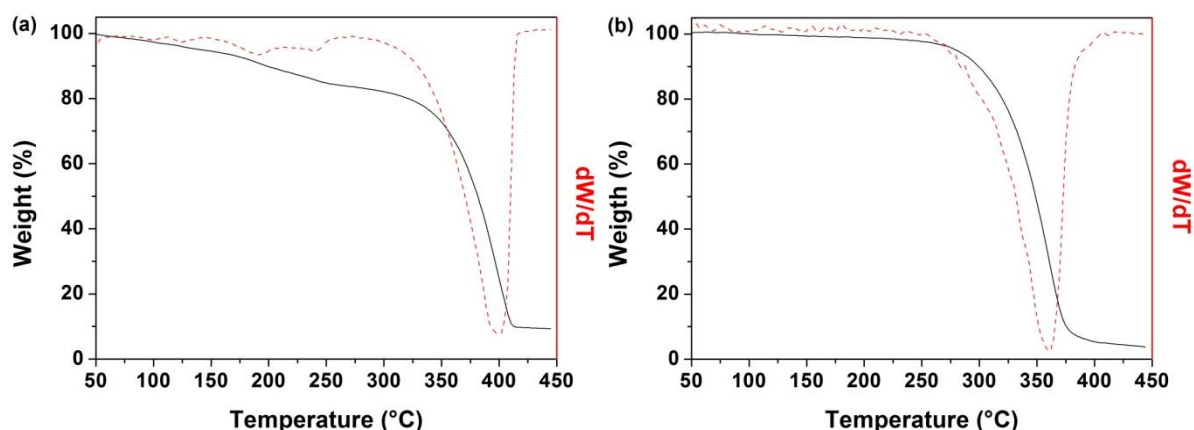
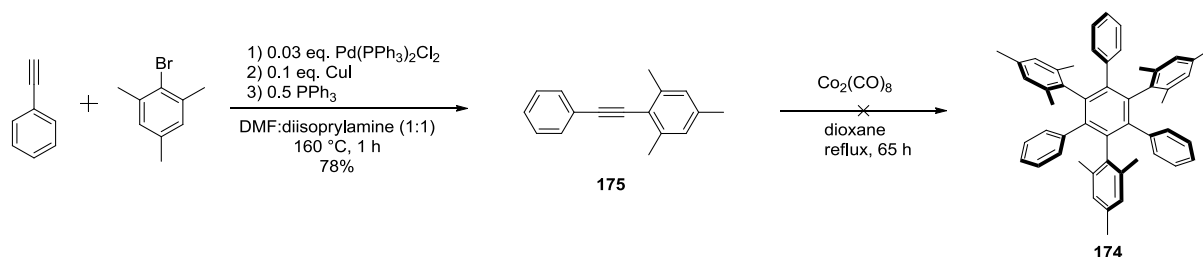


Figure 2.7 TGA, under nitrogen flow, of (a) hexaphenylborazine **169** and (b) B-trimesityl-N-triphenylborazine **173** indicating decomposition at 400 °C and 360 °C respectively.

In order to compare the photophysical properties of borazine **173** to the all carbon analogue, the synthesis of derivative **174** was attempted. The synthesis started with a classical Sonogashira coupling which afforded tolane **175** in good yield (78%) (Scheme 2.22). The next step is the cyclotrimerisation of **175** using cobalt catalyst.^[176] Despite several attempts, including temperature and reaction time modifications, no traces of **174** were observed. Therefore this synthetic strategy was abandoned.



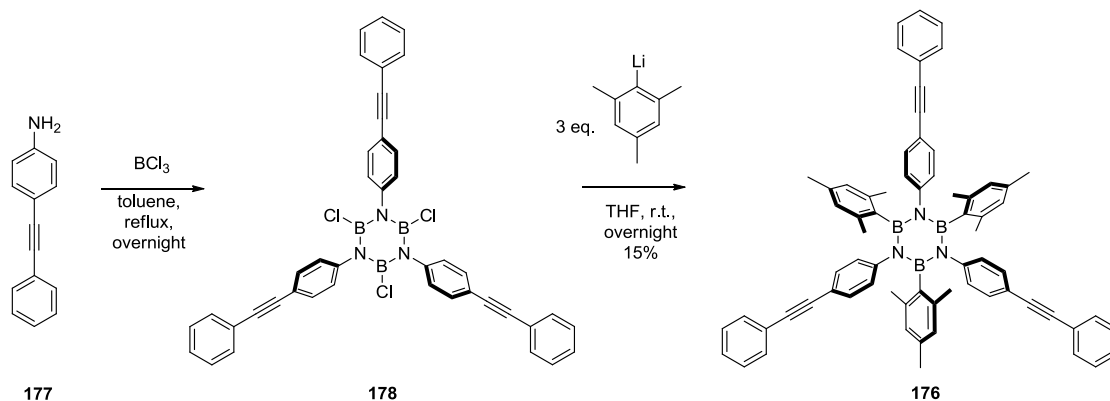
Scheme 2.22 Attempted synthesis of trimesityltriphenylbenzene **174**, analogue of borazine **173**.

So the effect of doping this hexasubstitutedbenzene structure, by inserting a borazine ring, was probed with hexaphenylborazine **169** and the photophysical properties are detailed in section 2.4.1 while the absorption and emission spectra of borazine **173** are detailed in section 2.4.2.

In order to prove the versatility of the synthetic strategy, the synthesis of compound **176** (Scheme 2.23) was envisaged, where the phenyl moiety of the phenylethynyl group could be substituted by electron donor or acceptor groups. Another purpose of this project was the possibility of further functionalization of the triple bond moieties by Diels-Alder reaction, with tetraphenylcyclopentadienone that would have lead to a borazine core decorated by three hexaphenylbenzene substituents. Starting with aniline derivative **177**, which reacts with BCl_3 as described for the borazole **178**. The addition of the borazole solution to the Me_3Li solution afforded borazine **176** in low yield (15%). Analysis by ^1H NMR, ^{13}C NMR, and

Chapter 2

^{11}B NMR confirmed the obtainment of borazine **176**. ^{13}C NMR indicated that hydrogen chloride did not add on the triple bond of the tolane moiety while ^{11}B revealed a broad peak at 37 ppm, consistent with a boron substituted by two nitrogen atoms and linked to one carbon atom. IR spectroscopy revealed the broad B-N stretching characteristic of a borazine ring at 1355 cm^{-1} . Finally, mass spectrometry analysis (Figure 2.8) indicates a mass at $m/z = 963.5086$, corresponding to the molecular weight of borazine **176**. The measured isotopic pattern match the calculated one, the peak at $m/z = 965.5$ corresponds to the mass of the reference used to calibrate the instrument and to one isotope of compound **176**. All these analysis unambiguously confirm the structure. Unfortunately the crystals obtained by slow evaporation in CHCl_3 were too small for X-ray diffraction analysis. The photophysical properties of this derivative were probed and are described in detail in section 2.4.3.



Scheme 2.23 Synthesis of B-trimesityl-N-tri(4-ethynylphenylphenyl) borazine **176**.

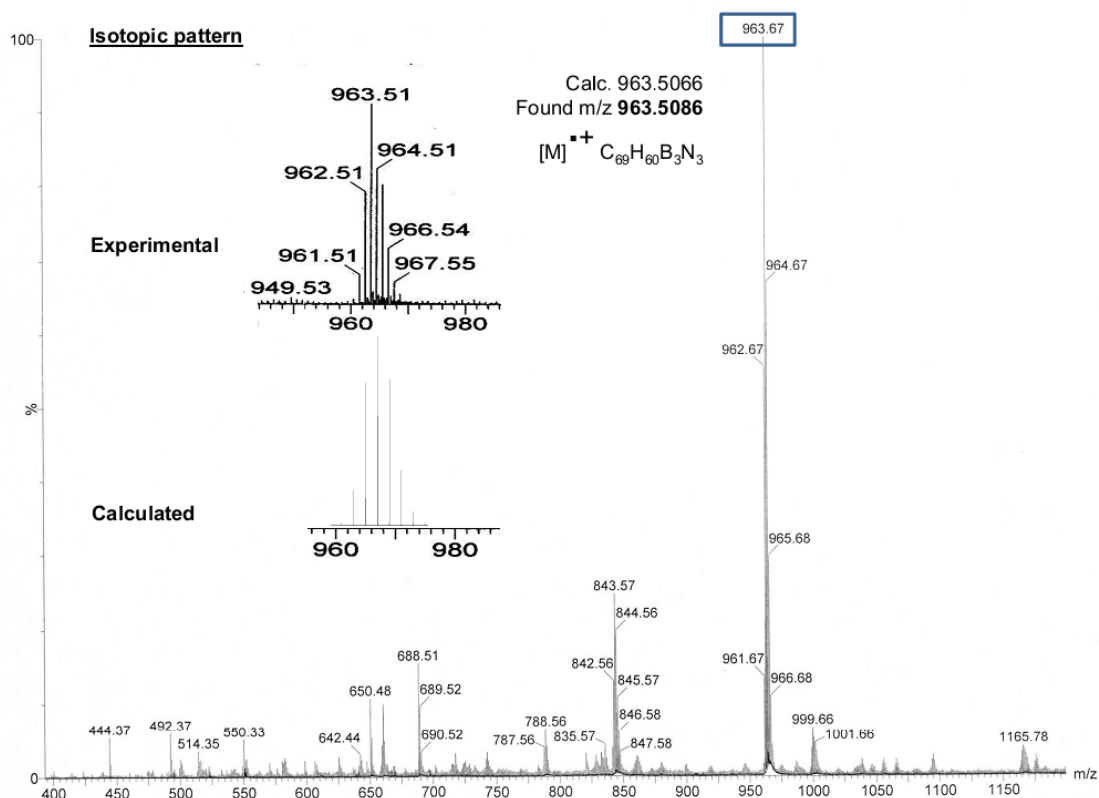
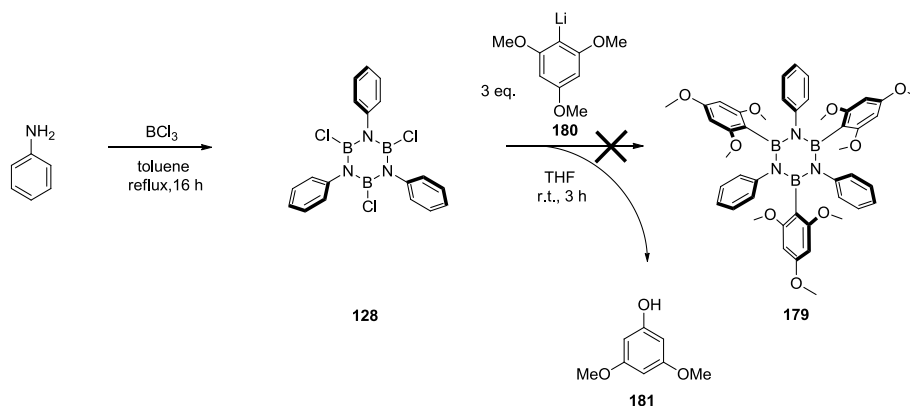


Figure 2.8 Mass spectrum of B-trimesityl-N-tri(4-ethynylphenylphenyl) borazine **176**, corresponding to the molecular formula: $\text{C}_{69}\text{H}_{60}\text{B}_3\text{N}_3$. MALDI-MS, inset: MALDI-HRMS, matrix: DCTB.

In an attempt to change the substituent on the boron atom for electron rich aryl substituents while keeping the steric protection, the synthesis of borazine **179** was envisaged. Using the same strategy as before, a solution of borazole **128** is

Chapter 2

added to a solution of 2,4,6-trimethoxyphenyl lithium **180**. However, borazine **179** could not be observed in the crude but side product **181** was seen by GC-MS. The latter could be due to side reaction of remaining BCl_3 which lead to the deprotection reaction of the methoxy group. An alternative reaction is the deprotection by the borazole ring.

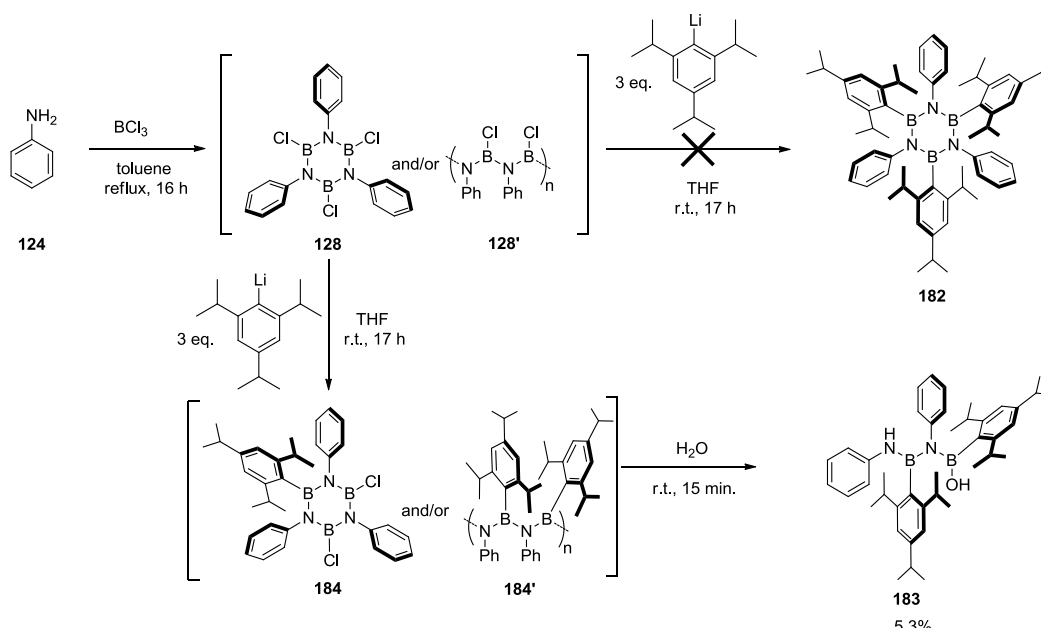


Scheme 2.24 Attempted synthesis of B-tri(1,3,5-trimethoxybenzene)-N-triphenyl borazine **179**.

2.2.3 Synthesis of Sterically Hindered Borazenes

Borazenes are linear modules constituted of boron-nitrogen bonds and are isoelectronic to carbon-carbon double bonds. Their synthesis, as outlined in the introduction, is not well developed and their characterization has been hampered by their instability toward moisture. Herein, in an attempt to increase the steric protection around the borazine cycle, the first borazene stable to hydrolysis and on silica gel column chromatography has been surprisingly obtained rather than the corresponding borazine. In addition of the description of the unexpected products, the stability properties will be discussed.

With the aim of enhancing the steric hindrance on the boron atoms, therefore providing increased stability toward hydrolysis, the synthesis of borazine **182** was attempted, using the same conditions as before. The expected borazine could not be observed in the crude but upon purification by silica gel chromatography unexpected stable borazene **183** was isolated, in very low yield (5.3%), along with the starting materials and traces of unidentified decomposition products.



Scheme 2.25 Synthesis of sterically hindered borazene **183**.

Chapter 2

It was discovered that if the aryl groups attached to the boron atoms bear *ortho* substituents, the too sterically hindered borazine **182** could not be isolated. Instead the decomposition products, after aqueous workup, yield borazene **183** (Scheme 2.25). The proposed reaction pathway suggests that the three boron atoms of borazole ring **128** (Scheme 2.19) cannot be substituted by three aryl groups. Due to the sensitivity towards moisture of intermediate **128**, its exact structure couldn't be determined and the existence of polymeric structure **128'** cannot be ruled out. The next step is the addition of one aryl groups yielding to the differently substituted borazole **184**, the substitution of a chlorine atom by another aryl group is difficult on cyclic intermediate **184** due to the steric hindrance of the isopropyl substituent in *ortho* position. Hence, the intermediate bearing two aryl group on the boron atom would have a steric hindrance between the isopropyl substituent in *ortho* position that could lead to a ring opening. Therefore, an alternative possibility is that borazole ring **184** is not formed but its linear chain equivalent **184'** is rather produced (Scheme 2.25). After aqueous workup, which hydrolyze the asymmetric intermediate **184** or **184'** (Scheme 2.25), a subsequent sequence of ring opening and hydrolysis of the boron-nitrogen bond give access to borazene **183** (Scheme 2.25) with a poor yield (5.3%). The latter compound is stable toward aqueous workup and can be purified by column chromatography. The crystal structure (Figure 2.12) indicates clearly that the boron atoms are sterically hindered by the isopropyl groups, providing a protection against further hydrolysis.

^1H NMR (Figure 2.10) analysis did not allow us to ascribe clearly the structure from the ^1H NMR spectrum. The inset reveals several peaks in the aromatic region corresponding to H_a and H_b resonances (star marked peaks, Figure 2.10) as well as several peaks corresponding to H_c , H_d , H_e and H_f resonances (dot marked peaks, Figure 2.10). The integration of the aromatic signals corresponds to 14 hydrogen atoms (H_a , H_b , and hydrogen atoms of the aniline cycle), while the region between 3.4-2.6 ppm accounts for 6 hydrogen atoms (H_c , H_d , H_e , and H_f), and the region between 1.42-0.80 ppm, attributed to the methyls groups, accounts for a total of 72 hydrogen atoms. Those integration ratios match the hydrogen atoms ratio of borazene **183**. As displayed in the inset of Figure 2.10, several signals corresponding to H_a and H_b resonances overlap, suggesting the existence of rotamers, the possible structures of which are exhibit in Figure 2.10. ^{11}B NMR spectrum indicates a broad signal at 35 ppm, corresponding to a boron atom surrounded by two nitrogen atoms and linked to a carbon atom. Also noticeable, is a shoulder at 25 ppm, indicative of a boron atom bounded to one carbon, one nitrogen and one oxygen atoms. Mass spectrum indicates one major product at $m/z = 628.4735$ whose isotopic pattern corresponds to the one of borazene **183** (Figure 2.10). Moreover, the TLC and HPLC analysis (Figure 2.9) present only one peak using various eluents conditions. Finally, crystals were obtained by slow evaporation in CHCl_3 . After NMR analysis (Figure 2.10 and appendix II), the content of the NMR tube was evaporated and the crystals obtained reveal the presence of only one rotamer. This result suggests the existence of several rotamers in solution but the predominance of one rotamer in solid state. Nevertheless, variable temperature ^1H NMR in benzene- d_6 at 25 °C and 60 °C revealed no change between the spectra, indicating that the rotational barrier between the postulated rotamers is higher than the thermal energy at 60 °C.

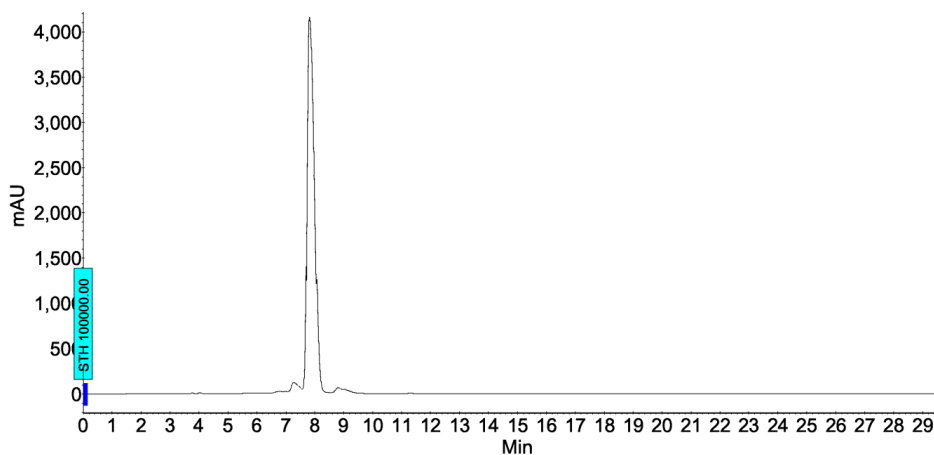


Figure 2.9 HPLC spectrum of borazene **183**. Eluent: CH_3CN , retention time = 7.9 min.

Chapter 2

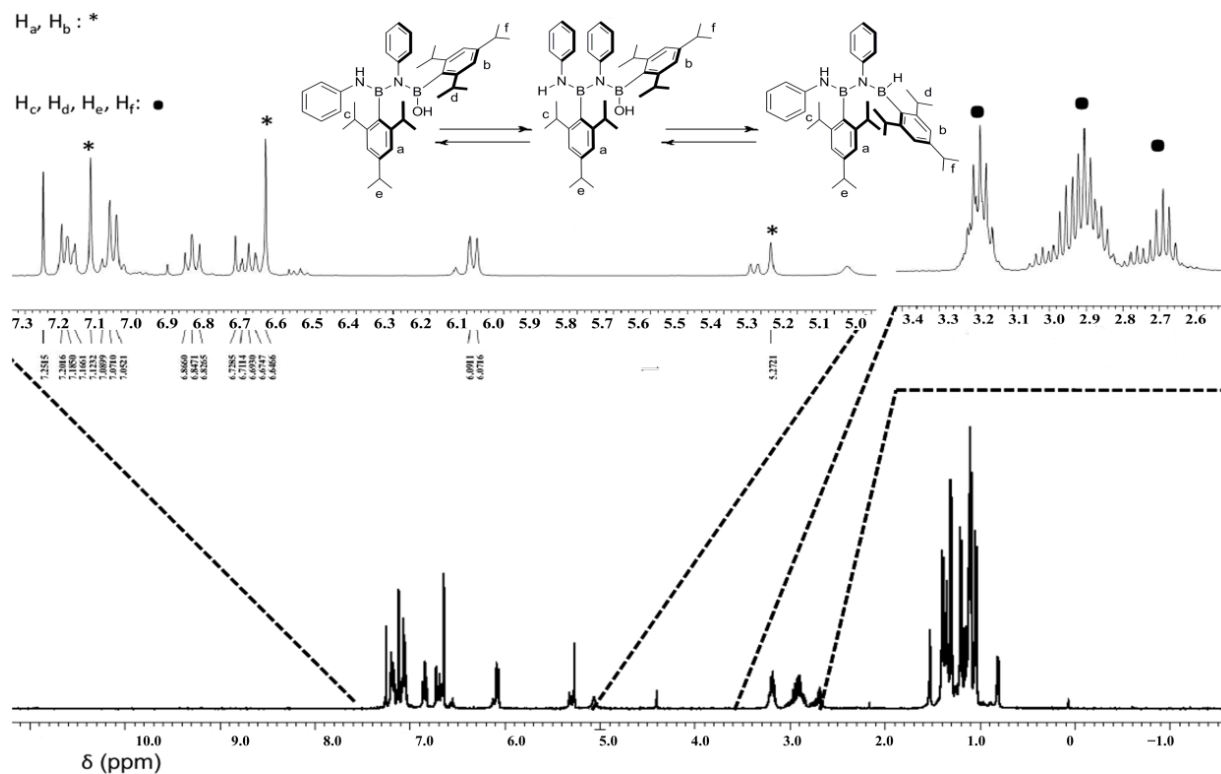


Figure 2.10 ^1H NMR spectrum (400 MHz, CDCl_3) of borazene **183** and its possible rotamers. Inset: zoom of the 7.4-5.0 ppm and 3.4-2.5 ppm areas.

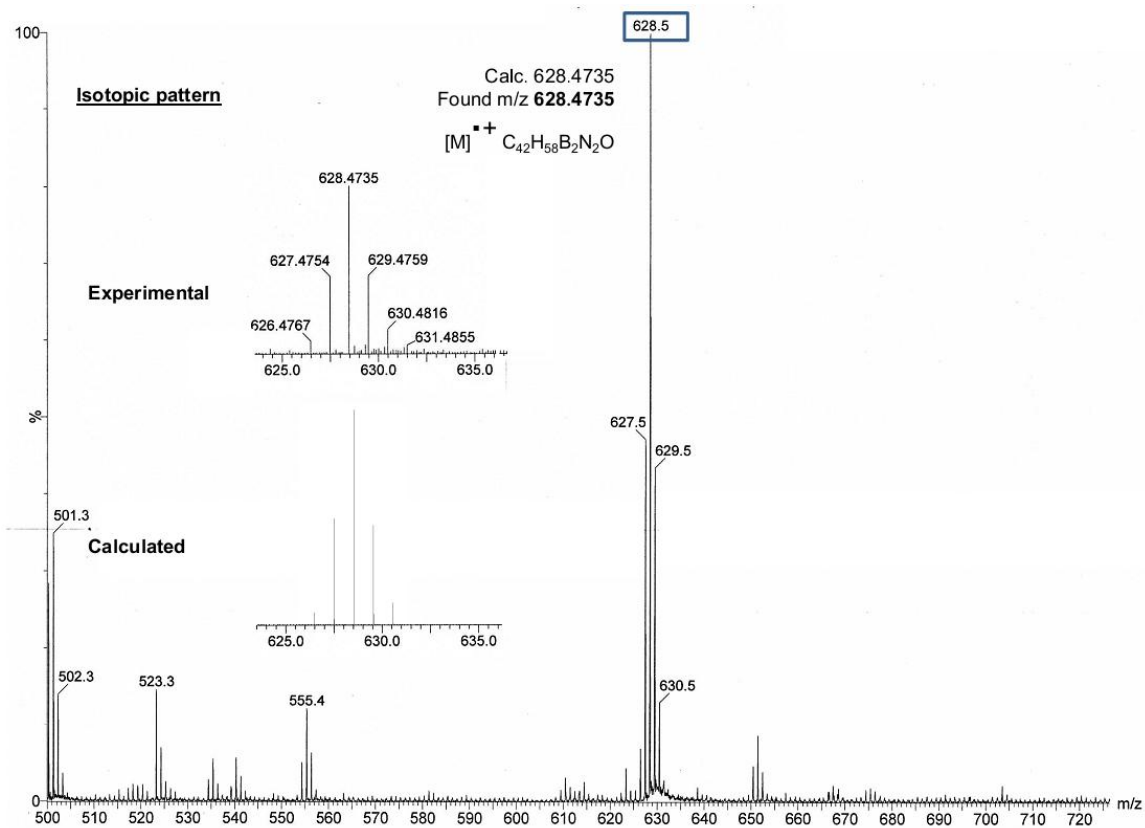


Figure 2.11 Mass spectrum of borazene **183**, corresponding to the molecular formula: $\text{C}_{42}\text{H}_{58}\text{B}_2\text{N}_2\text{O}$. MALDI HRMS, matrix: DCTB.

Crystal structure analysis allowed us to unambiguously assess the structure (Figure 2.12). The boron-nitrogen backbone is nearly planar (B1-N1-B2-O1 torsion angle: $4.4(8)^\circ$), the B1-N1-B2 angle is of 127° and the N2-B1-N1 angle of 117° . All these observations suggest a delocalization of lone pair of electrons of the nitrogen atoms into the empty p orbital of the boron atoms.

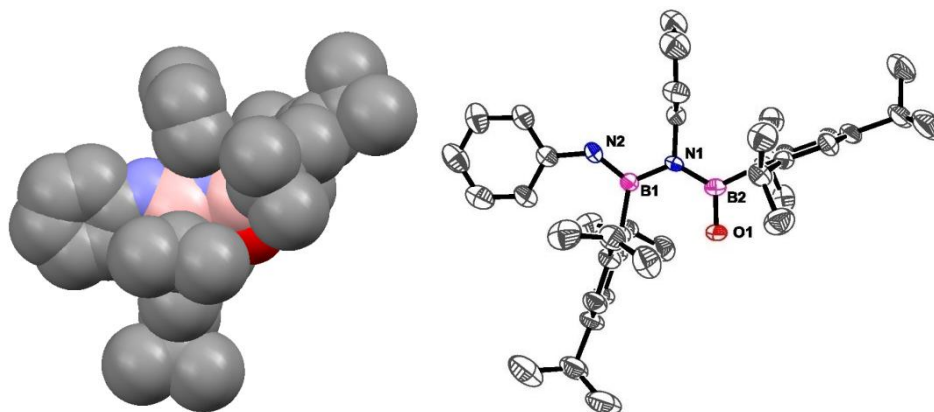
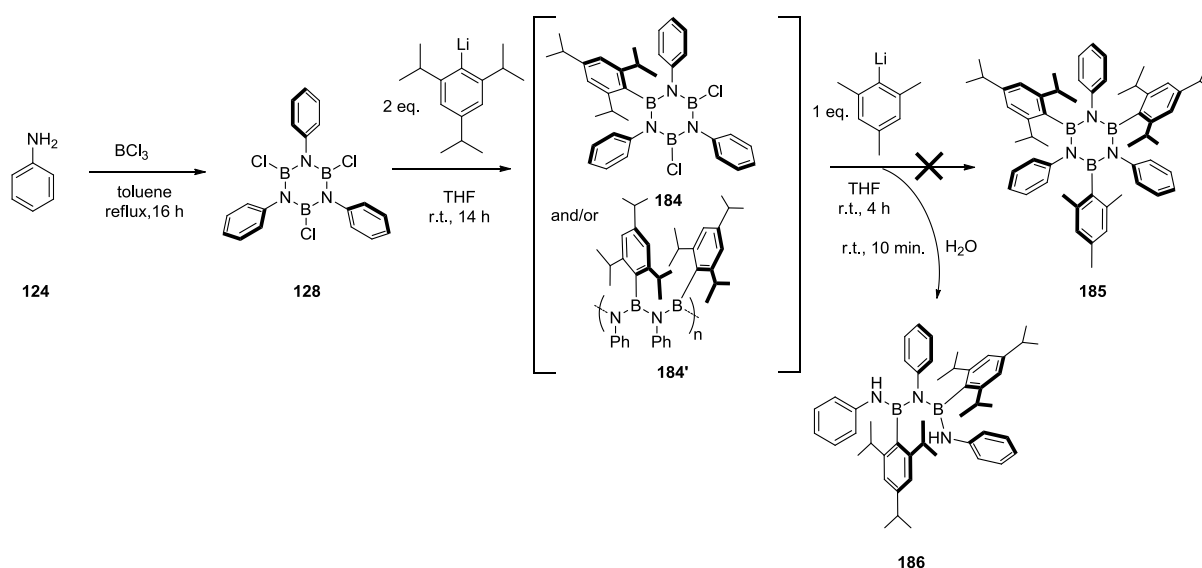


Figure 2.12 Crystal structure of borazene **183**, obtained by slow evaporation in CHCl_3 . Representation: spacefill (left) and ORTEP (right), hydrogen were omitted for the sake of clarity. Color code: grey: C, pink: B, white: H, blue: N, red: O. Space group: P-1.

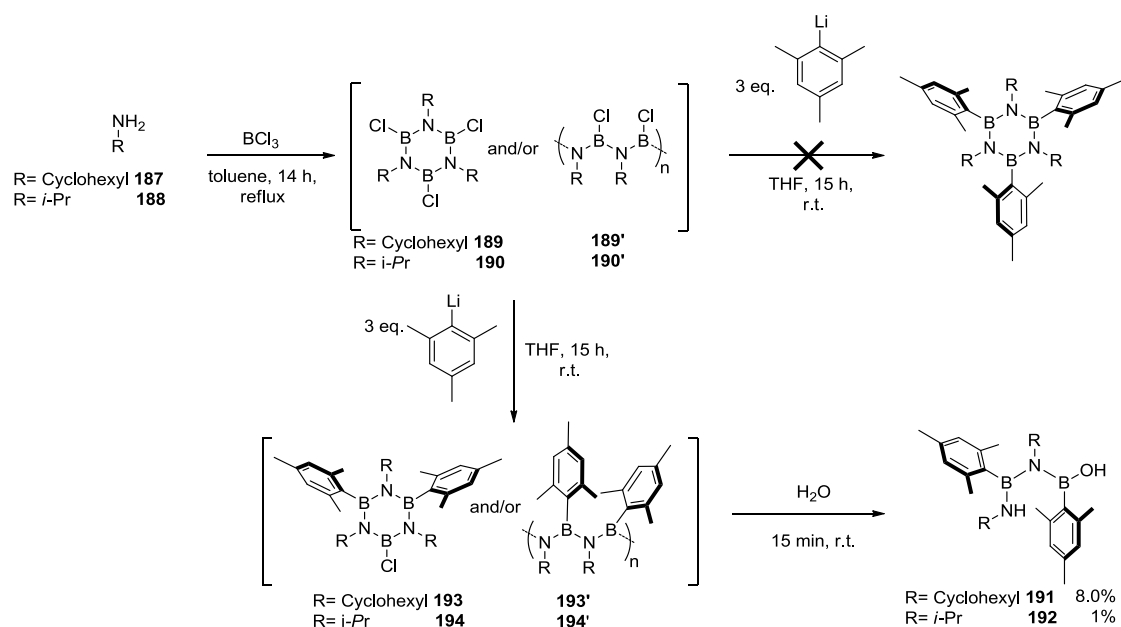
Then we questioned as to what will happen if a sterically hindered substituent is added to the reaction mixture, followed by the addition of MesLi , in order to lead to a differently substituted borazine, on the boron atoms. Hence, the synthesis was commenced using the usual conditions to form the borazole ring, then two equivalents of 2,4,6-triisopropylphenyl lithium were added to form the differently substituted borazole intermediate **184** or its linear chain equivalent **184'**. After 14 h, a second lithiate specie, *i.e.* the MesLi , was added with the aim of forming differently substituted borazine **185** (Scheme 2.26). However, amongst the several products from the crude, borazene **186** was observed with no traces of borazine **185**. This result suggests again that the first two substitution reactions on the borazole ring by lithiate derivative occur rapidly while the steric hindrances due to the isopropyl substituent prevent the substitution by the MesLi . Upon aqueous workup, the unsymmetrical borazole degraded into several unidentified product. The mass spectrum of the crude, before any purification on silica gel chromatography, indicates the presence of the borazene **186** while no traces of borazine **185** has been found.



Scheme 2.26 Synthetic attempt for the synthesis of differently substituted borazine **186**.

Chapter 2

To further explore this peculiar relation between the increase of steric hindrance around boron atoms of the borazine cycle and their synthetic accessibility, the phenyl moieties substituting the nitrogen atoms was changed for bulky alkyl groups. Starting from cyclohexylamine **187** or isopropylamine **188** (Scheme 2.27) and using BCl_3 , borazole rings **189** and **190** were formed under the classical conditions. Another possibility is that borazole rings **189** and **190** are not formed, due to the steric hindrance of the isopropyl and cyclohexyl substituents on the nitrogen atoms, but linear chloro aminoborane **189'** and **190'** would be rather produced. These derivatives are then substituted by MesLi , to provide steric protection without having the problem of the bulky isopropyl groups on the aryls substituting the boron atoms, which cannot yield a borazine, as explained above. Once again, borazine could not be isolated, but instead the decomposition products after aqueous workup yield borazene **191** and **192**. The reaction pathway could be similar to the one already mentioned, passing through the formation of borazole rings **193** and **194**, which are substituted by two mesityl groups. Then the third aryl group cannot add on the last boron atom due to the steric hindrance of the alkyl groups substituting the nitrogen atoms. After aqueous workup, which hydrolyzes the differently substituted cyclic intermediate **193** and **194** or their linear equivalent **193'** and **194'**, the third chlorine atom on the boron atom is substituted for H_2O . This is followed by a sequence of ring opening, or hydrolysis of and/or hydrolysis of the boron-nitrogen bond to give access to the borazene **191** and **192**, in poor yields (8.0% and 1% respectively) along with the starting materials (Scheme 2.27).



Scheme 2.27 Synthesis of sterically hindered borazene **191** and **192**.

These two borazene derivatives are stable upon purification by silica column chromatography and the crystal structure of borazene **192** (Figure 2.16), where the substituents on the nitrogen atoms are isopropyl groups, indicates clearly that the boron atoms are sterically hindered by methyl groups, providing a protection against further hydrolysis. Borazene **191**, where the substituents on the nitrogen atoms are cyclohexyl groups, is a viscous liquid. Once more, ^1H NMR analysis did not allow us to identify clearly the structure for borazene **192** (Figure 2.13). Nevertheless, the integration ratio of the peaks corresponds to the hydrogen atoms ratio of the proposed structure of **192** (see appendix II). The singlets attributed to H_a and H_b account for 4 hydrogen atoms, the peak for H_c for 2 hydrogen atoms and the alkyl region, where the peaks of H_e , H_d , and H_f overlap, for a total of 30 hydrogen atoms. This led us to postulate the existence of one single borazene corresponding to the molecular structure of **192**, in equilibrium between several rotamers resulting in the different ^1H NMR signals observed. Moreover, the ^{11}B NMR spectrum reveals a broad signal at 34 ppm with a shoulder at 26 ppm, corresponding to a boron atom surrounded by two nitrogen atoms and to one boron atom bounded to one carbon, one oxygen and one nitrogen atoms respectively. Mass spectrum (Figure 2.14) reveals a peak at $m/z = 392.3179$, whose isotopic pattern is consistent with the molecular formula:

Chapter 2

$C_{24}H_{38}B_2N_2O$. While IR spectroscopy (Figure 2.15) indicated an oxygen-hydrogen bond stretching characteristic of hydroxyl group (3536 cm^{-1}) and two nitrogen-hydrogen bonds stretching bands (3406 and 3390 cm^{-1}) as well as boron nitrogen stretching (1348 cm^{-1}). Finally single crystal analysis (Figure 2.16) confirmed the structure compound **192**. The NMR spectra presented (Figure 2.13 and appendix II) are the one obtained upon dissolution of the crystals in $CDCl_3$, confirming the existence of one rotamer in solid state but the presence of several in solution.

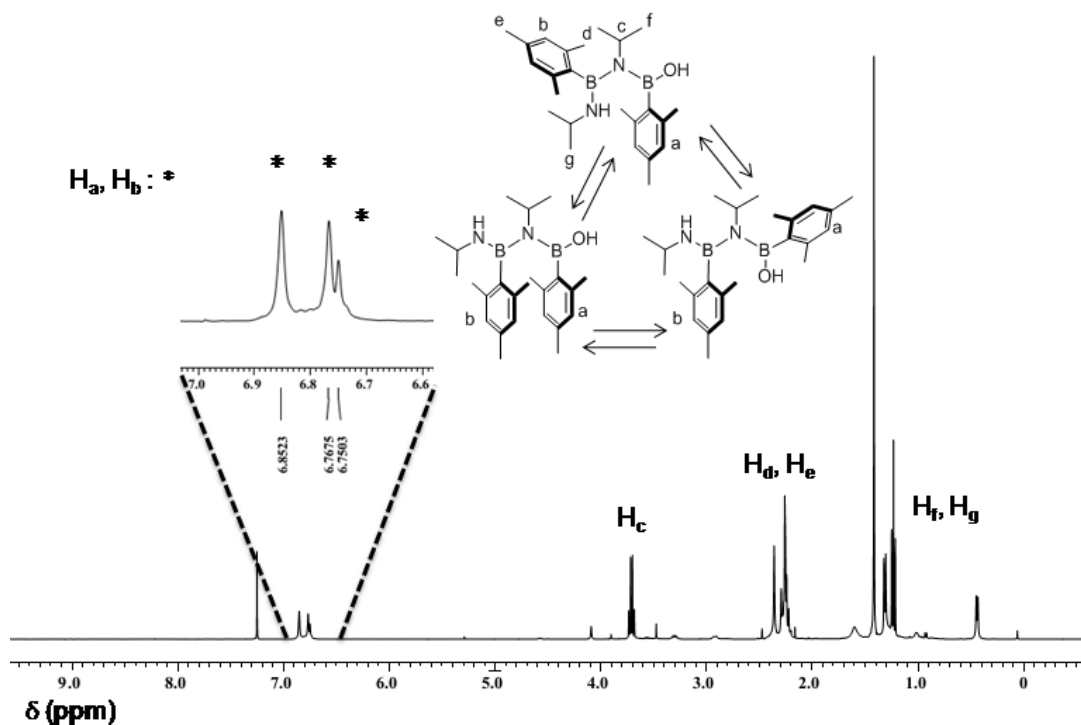


Figure 2.13 1H NMR spectrum (400 MHz, $CDCl_3$) of borazene **192** indicating different signal for proton H_a and H_b and the structure of the possible rotamers. Inset: zoom of the 7.1-6.6 ppm area.

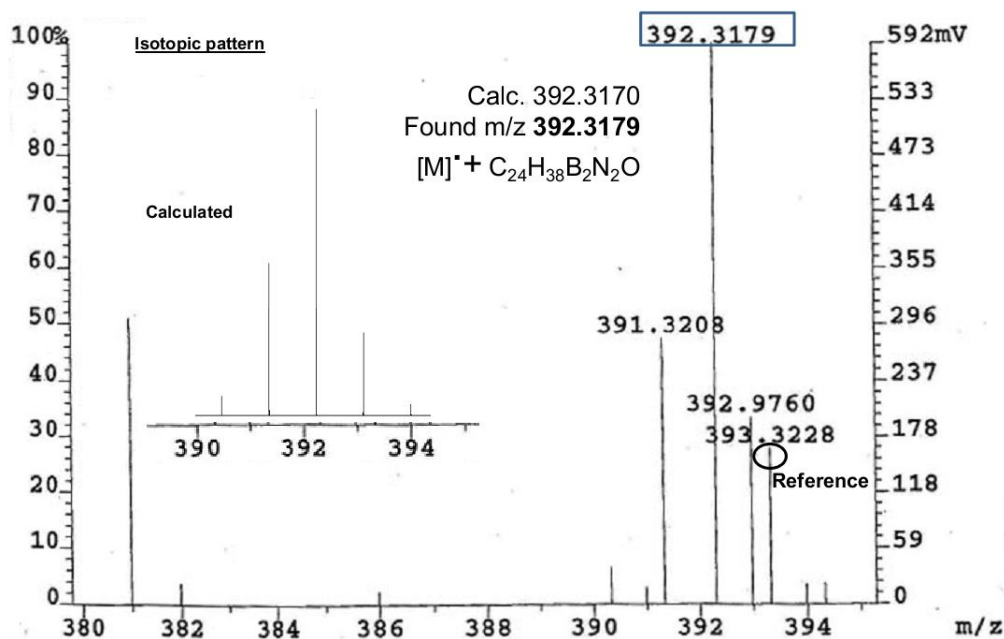


Figure 2.14 Mass spectrum of borazene **192** corresponding to the formula: $C_{24}H_{38}B_2N_2O$. EI-HRMS.

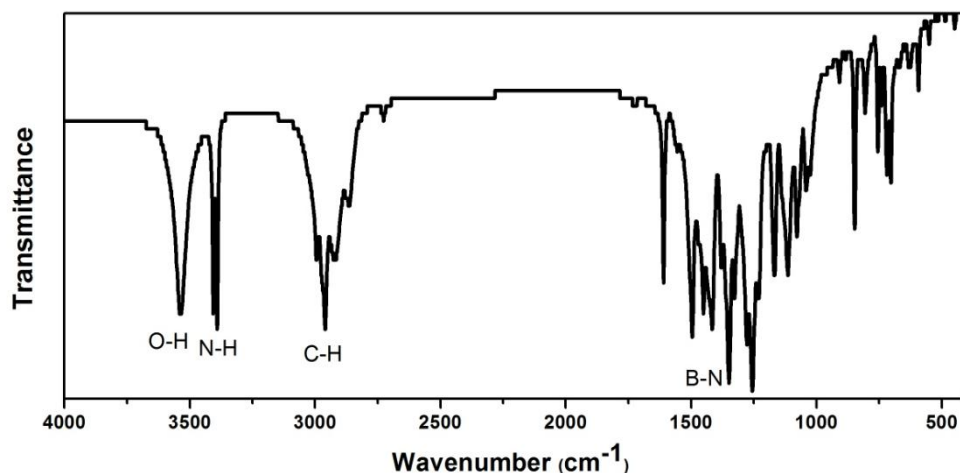


Figure 2.15 IR spectrum of borazene **192** revealing the broad oxygen-hydrogen bond stretching at 3536 cm^{-1} and two nitrogen-hydrogen bonds stretching at 3406 and 3390 cm^{-1} and boron-nitrogen stretching at 1348 cm^{-1} .

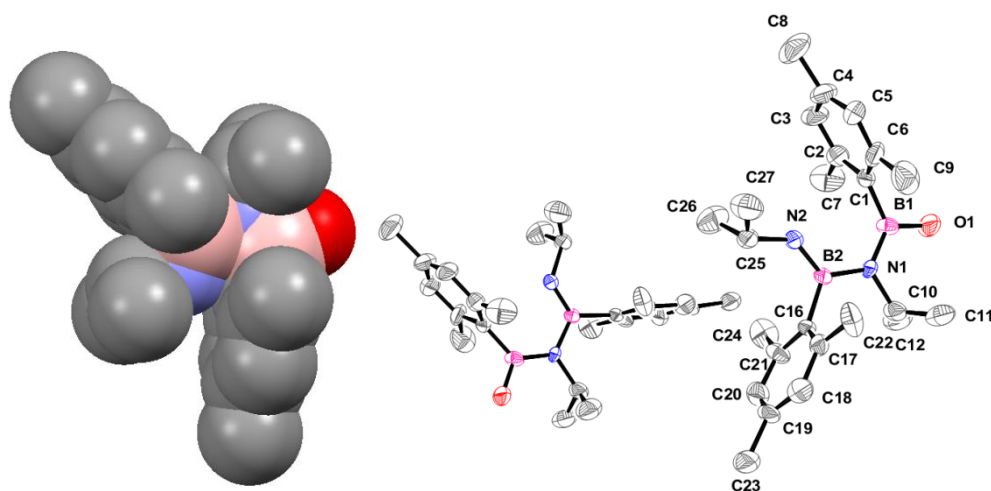


Figure 2.16 Crystal structure of borazene **192**, obtained by slow evaporation in CHCl_3 . Representation: spacefill and ORTEP, hydrogen were omitted for the sake of clarity. Color code: grey: C, pink: B, white: H, blue: N, red: O. Space group: $P2_1/c$.

Since borazene **191** is a liquid and its structure could not be investigated by means of X-ray diffraction, ^1H NMR analysis will be more detailed below. The ^1H NMR spectrum exhibits two regions, the aromatic area, displaying several singlets corresponding to the hydrogen atoms in *meta* position on the mesityl rings, and the alkyl area (Figure 2.17). The integration ratio of the peaks matches the one of the proposed structure. Several singlets (inset in Figure 2.17), attributed to the H_a and H_b account for 4 hydrogens atoms, the hydrogen H_c for 2 and the alkyl region, where the signals of H_e , H_g , and H_f overlap, for a total of 38 hydrogens atoms. Variable temperature ^1H NMR analysis revealed new peaks in the aromatic region (star marked peaks in the inset) at $70\text{ }^\circ\text{C}$, pointing out toward the existence of rotamers (Figure 2.18). The interpretation of the spectra is more complex in the alkyl region, due to the overlap of the signals of the methyl groups and of the cyclohexyl moieties, but again new peaks are present at $70\text{ }^\circ\text{C}$ (dot marked peaks in the inset, Figure 2.18). Nevertheless, few differences between the spectra are noticed and the peaks did not coalesced, which would have indicated the presence of a major rotamer at higher temperature and the presence of several at lower temperature. This suggests that the postulated rotamers should again have a high rotational barrier. After heating, a ^1H NMR spectrum was taken at $25\text{ }^\circ\text{C}$, to verify that no reaction occurred at $70\text{ }^\circ\text{C}$, the spectra at $25\text{ }^\circ\text{C}$ are identical. Moreover, the ^{11}B NMR spectrum indicates a signal at 36 ppm, corresponding to a boron atom surrounded by two nitrogen atoms, and a signal at 30 ppm, consistent with a boron atom substituted by one nitrogen atom, one oxygen atom and linked to a carbon atom. Finally, the mass spectrum reveals several peaks, the first at $m/z = 473.3858$, whose isotopic pattern corresponds to the molecular structure: $\text{C}_{30}\text{H}_{46}\text{B}_2\text{N}_2\text{O}$ and other

Chapter 2

fragmentations at $m/z = 455.3756$, corresponding to the molecular structure: $C_{30}H_{45}B_2N_2$, and $m/z = 353.2930$ (Figure 2.19), corresponding to the molecular structure: $C_{21}H_{35}B_2N_2O$.

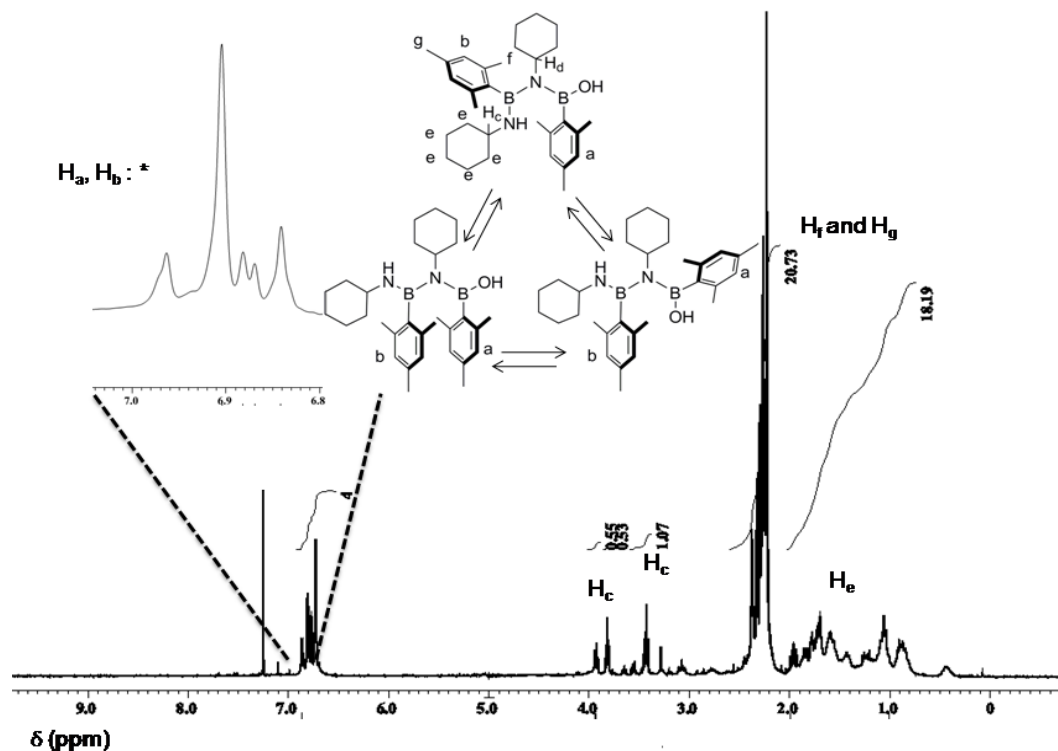


Figure 2.17 ^1H NMR spectrum (400 MHz, CDCl_3) of borazene **191** and the possible rotamers. Inset: zoom of the 7.1-6.8 ppm area.

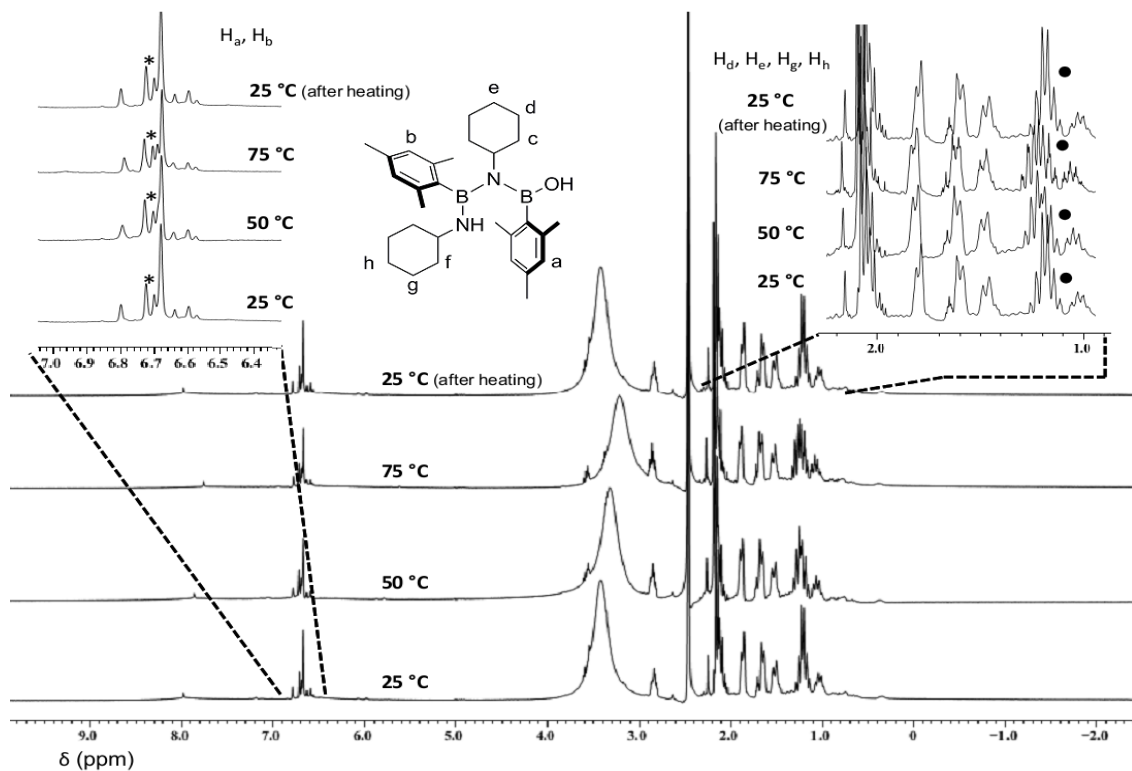


Figure 2.18 Variable temperature ^1H NMR spectra (400 MHz, $\text{DMSO}-d_6$) of borazene **191**, at 25 °C, 50 °C and 70 °C. Inset: zoom of the 7.0-6.4 ppm and 2.2-0.8 ppm areas. Star marked peaks indicate the change in the aromatic region, dot marked peaks in the aliphatic region.

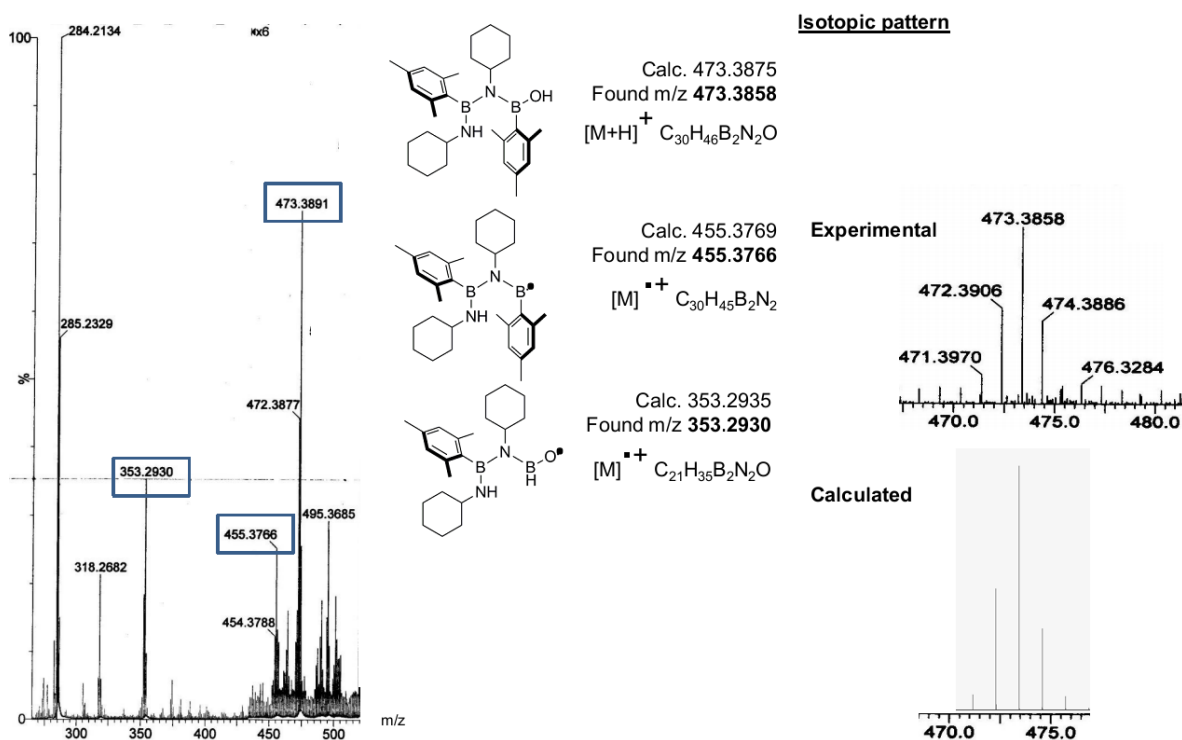
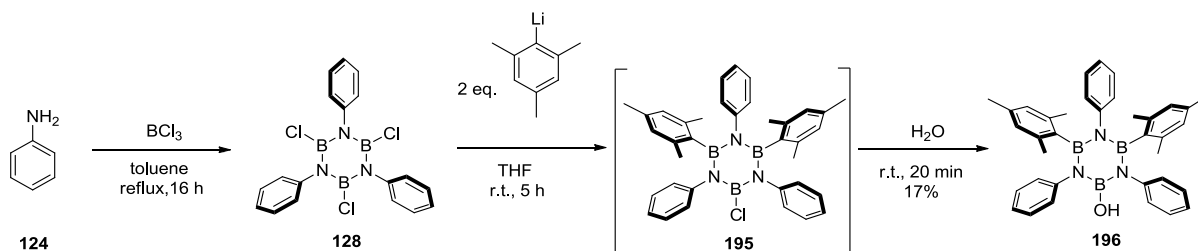


Figure 2.19 Mass spectrum of borazene **191** corresponding to the formula: $C_{30}H_{46}B_2N_2O$ and fragmentation products. MALDI HRMS, matrix: DCTB.

These surprising results of isolation of traces of borazene derivatives after reaction of aniline or amine derivatives with BCl_3 have not been previously reported in the literature. Although, borazene synthesis has been developed, they usually use a different synthetic pathway with a better yield. Inspired by the unexpected results obtained when increasing the steric hindrance around the boron atoms it was decided to further explore the hypothetical mechanistic pathway of the borazene formation. Then, we questioned if it really passed through a borazole ring **128**, which means it could be substituted with only two mesityl groups. The reduced steric hindrance of mesityl groups, as opposed to 2,4,6-isopropylbenzene ring, could avoid the ring opening of the differently substituted intermediate. This intermediate could then be quenched with another nucleophile. This would lead to an unprecedented synthesis of differently substituted borazene and is the subject of the next section.

2.2.4 Differently Substituted Borazine on the Boron Atoms

The synthesis of differently substituted borazine starts as the usual borazine synthesis. Borazole **128** is added dropwise to the solution containing two equivalents of MesLi. It was postulated that the addition of these two equivalents formed intermediate **195**, which, upon aqueous workup, give differently substituted, on the boron atoms, borazine **196**.



Scheme 2.28 Synthesis of differently substituted borazine **196**.

Chapter 2

Surprisingly, borazine **196** is stable on silica gel column chromatography, thanks to the steric hindrance provided by the mesityl groups. Although, one boron atom does not benefit from this steric protection, the mesomeric donor oxygen atom should reduce its electrophilicity, as opposed to borazine **173** in which the boron is substituted by a carbon atom. Interestingly, ^{11}B NMR spectrum indicates two peaks, one at 36 ppm, corresponding to the boron atom substituted by the mesityl and one at 24 ppm, attributed to the boron atom substituted by the hydroxyl group. Mass spectrum indicates a peak at $m/z = 561.3311$ corresponding to the molecular formula: $\text{C}_{36}\text{H}_{38}\text{N}_3\text{B}_3\text{O}$, while IR spectroscopy revealed a peak 3612 cm^{-1} , attributed to the oxygen-hydrogen stretching of a non hydrogen-bonded hydroxyl group, and at 1368 cm^{-1} , the B-N stretching of the borazine ring. Finally, crystal structure (Figure 2.22) confirmed the obtainment of the differently substituted, on the boron atoms, product.

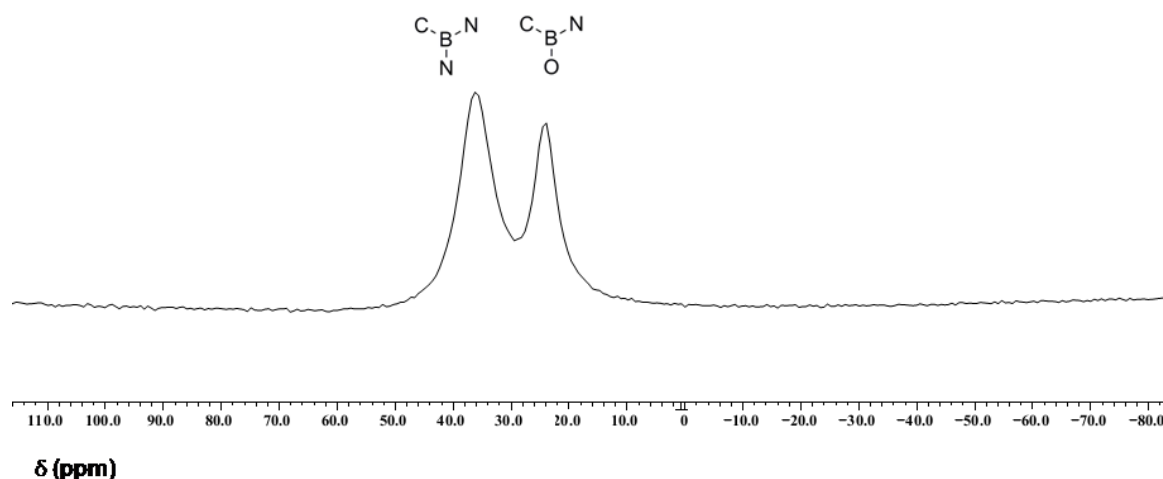
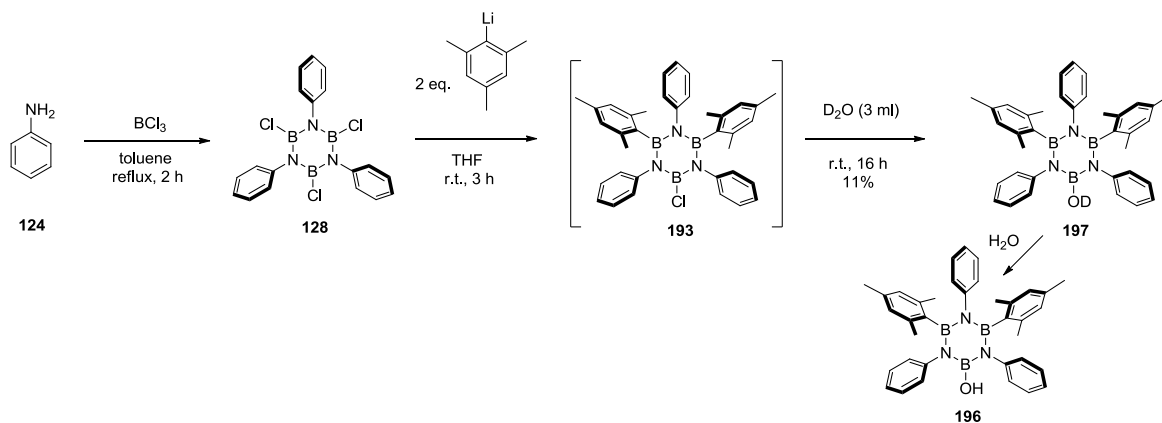


Figure 2.20 ^{11}B NMR spectrum (400 MHz, CDCl_3) of differently substituted borazine **196**.

The borazole derivative was substituted by D_2O , to prove that the hydroxyl group is coming from the aqueous workup, forming borazine **197**. Indeed, BCl_3 is highly reactive towards moisture and it cannot be ruled out that traces of water in toluene could have formed BCl_2OH , which would have reacted with aniline to form an asymmetric borazole, where one boron atom is substituted by one hydroxyl group, instead of symmetric borazole **128**. After performing the reaction in the usual conditions, the non deuterated borazine **196** was obtained in lower yield (11%) (Scheme 2.29). This surprised us but the deuterium of the hydroxyl group is acidic (for comparison, $\text{B}(\text{OH})_3$ have a pK_a of 10) and could have exchange with the proton of H_2O upon aqueous workup. The lower yield can be due to a slight hydrolysis of the borazine cycle during prolonged steering in acidic H_2O ($\text{pH} = 1$).



Scheme 2.29 Synthesis of deuterated differently substituted borazine **197**, which transform into borazine **196** upon aqueous workup.

Chapter 2

Before any surface study, the thermal stability of borazine **196**, bearing a hydroxyl group, was probed and it displays remarkable thermal stability until 286 °C, with a ramp of weight loss until 400 °C (Figure 2.21).

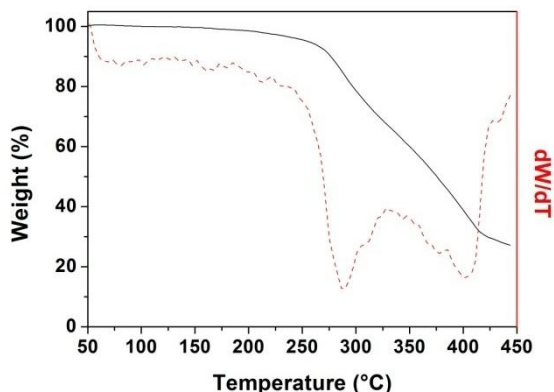


Figure 2.21 TGA, under nitrogen flow, of borazine **196** indicating decomposition at 280 and 400 °C. Solid line: weight, dotted line: dW/dT.

This unexpected synthetic result paved the way for the direct synthesis of differently substituted borazines. A detailed study of the possibility to use various nucleophiles after the addition of two equivalents of MesLi was beyond the scope of this thesis. As a perspective, the use of phenylethynyl lithiate was envisaged. That would allow the conjugation, through the triple bond, between the borazine and the phenyl group. The latter could be substituted by donor or acceptor groups to tune the borazine ring electronic density that would be reflected on UV-Vis absorption and fluorescence spectra. Detailed crystal structure analysis would confirm this influence by measuring the difference in bond lengths, as explain in the next section.

The crystal structure of differently substituted, on the boron atoms, borazine **196** reveals the influence of the hydroxyl group substituting the boron atom. In the crystal structure of B-trimesityl-N-triphenylborazine (**173**, Figure 2.25), there is clear evidence of a delocalization of the lone pair of electrons of the nitrogen atoms into the empty *p* orbital of the boron atoms. What would be then the influence of the hydroxyl group? Boron-oxygen bond distance (1.364(2) Å, similar to the bond length observed for boronic acids derivatives) suggests a delocalization of the lone pair of electrons of the oxygen atom into the empty *p* orbital of the boron atom while the boron-nitrogen bond distances are similar to the symmetrically substituted borazine (Table 2.1).

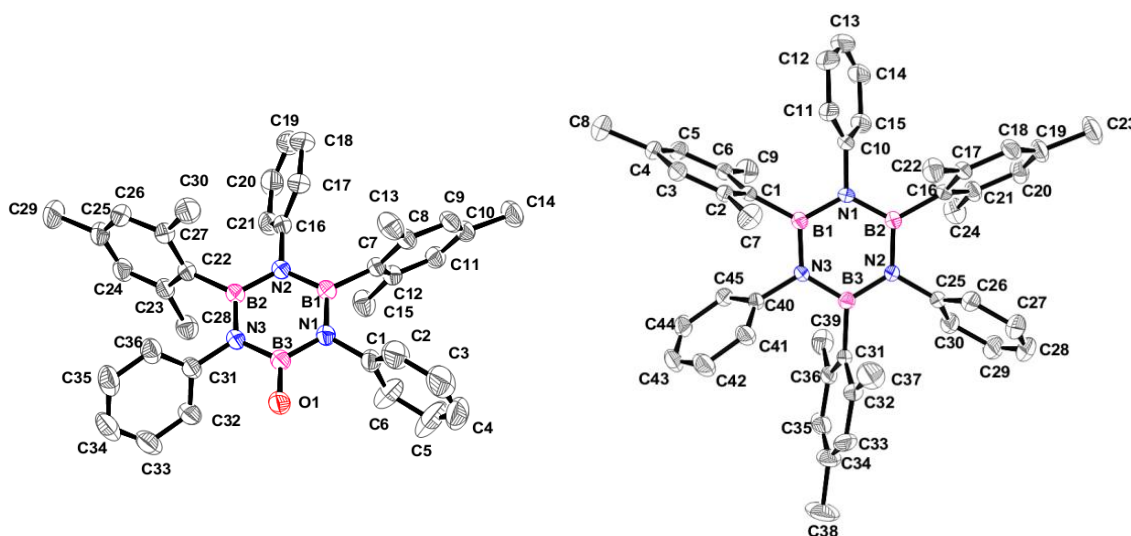


Figure 2.22 ORTEP view of borazine **196** (left), space group $P2_1/c$, and **173** (right), space group $P2_1/n$, hydrogen were omitted for the sake of clarity. Color code: grey: C, pink: B, white: H Blue: N.

Chapter 2

The analysis of bond lengths and angles in the borazine ring revealed little differences between borazine **196** and **173**. Obviously, these results are not statistically relevant, because the comparison is made with only one structure of differently substituted borazine and could be due to packing effects. If the influence of the mesomer donor oxygen is profound there should be an increase of the B3-N3 and B3-N1 distances, while they remain in the average of 1.44 Å. Moreover, the N3-B3-N1 bond angle is slightly higher ($\approx 1^\circ$) than the one observe for borazine **173**, while B2-N3-B3 and B1-N1-B3 angles are slightly lower (less than 1°) than the symmetric borazine **173**.

Borazine 196		Borazine 173 (P2 ₁ /n)	
Bond distance (Å)	Bond angle (°)	Bond distance (Å)	Bond angle (°)
1.431(2) (B1-N1)	117.19(14) (N2-B1-N1)	1.447(3) (B1-N1)	116.43(16) (N1-B2-N3)
1.446(2) (B1-N2)	117.23(14) (N2-B2-N3)	1.438(3) (B1-N3)	116.69(17) (N1-B2-N2)
1.440(2) (B2-N3)	118.55(14) (N3-B3-N1)	1.444(2) (B2-N1)	117.27(18) (N2-B3-N3)
1.450(2) (B2-N2)	122.16(13) (B1-N1-B3)	1.444(3) (B2-N2)	123.13(17) (B1-N1-B2)
1.442(2) (B3-N1)	122.81(13) (B1-N2-B1)	1.435(3) (B3-N2)	122.84(15) (B2-N2-B3)
1.439(2) (B3-N3)	121.69(13) (B2-N3-B3)	1.438(2) (B3-N3)	123.25(16) (B1-N3-B3)
1.364(2) (B3-O3)			

Table 2.1 Selected bond distances and bond angle of borazine **173** and **196**.

2.3 Crystal Structures-Polymorphism

The X-ray diffraction structures have been resolved by *Bernadette Norberg* in the group of *Professor Dr. Johan Wouters*.

The crystal structures of the borazine compounds synthesized were studied to fulfill several objectives. Firstly, this study was performed in order to better understand the steric protection provided by the methyl groups, as observed in solution. These groups sterically hindered the boron atoms due to the fact that the aryl groups are nearly perpendicular to the plane formed by the borazine ring. In addition, this twisted arrangement was further studied on metallic surfaces (*see section 2.5*). The second reason was to study the geometrical parameters, namely the bond lengths, bonds angles and torsion angles of the different structures to compare the hexaaryl borazine to the differently substituted derivative.

2.3.1 Crystal Structure of Hexaphenylborazine 169

After purification with anhydrous solvents, crystals were obtained by slow evaporation of a chloroform solution; which turn brown from white upon standing at air after one night. Crystal structure reveals no steric hindrance around the boron atoms by the hydrogen atoms of the phenyl groups, consistent with our observation of low stability of these derivatives toward moisture (Figure 2.23).

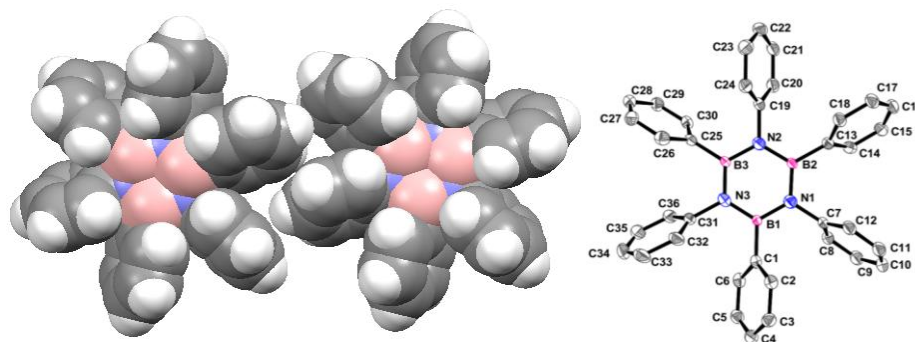


Figure 2.23 Spacefill (left) and ORTEP (right, hydrogen were omitted for the sake of clarity) representation of the crystal structure of hexaphenylborazine **169**. The spacefill representation reveals the two possible turns of **169**, having a propeller shape. Space group Pna2₁. Color code: grey: C, pink: B, white: H Blue: N.

Moreover, the crystal structure indicates equalized boron-nitrogen bond lengths, of 1.439 Å in average, similar to the one reported in the literature.^[100,122] The boron-nitrogen bonds distances of the borazine ring are of: 1.434(4) Å (B1-N1), 1.437(5) Å (B1-N3), 1.443(4) Å (B2-N1), 1.441(4) Å (B2-N2), 1.438(4) Å (B3-N2) and 1.439(5) Å (B3-N3). The angles between the phenyl and the borazine ring are of 73.9(4)°, 64.7(4)° and 67.5(4)° for the phenyls substituting the nitrogen atoms (N1, N2 and N3 respectively) and 62.2(4)°, 60.7(5)° and 65.9(4)° for the phenyls substituting the boron atoms (B1, B2 and B3 respectively). So, the phenyl groups are not perpendicular to the borazine ring, they are all tilted in the same direction, resulting in a propeller shape (Figure 2.23). Interestingly, the two helices of opposite turn are present in the unit cell because the crystal has been grown on achiral substrate. The same observation can be made for B-trimesityl-N-triphenylborazine (**173**) (Figure 2.25), the chirality of this borazine was further studied on metallic surfaces. Other noticeable points are the planarity of the borazine cycle and the close contact distance. The borazine ring deviation of the plane is of 3.2°, close to the range of the standard deviation for aromatic ring. In the crystal packing, one can notice the close contacts, of 2.79 Å between H17 (see ORTEP, Figure 2.23) and a borazine ring. There is also a more distant H- π interaction of 3.17 Å bond between H10 (see ORTEP, Figure 2.23) and a phenyl ring.

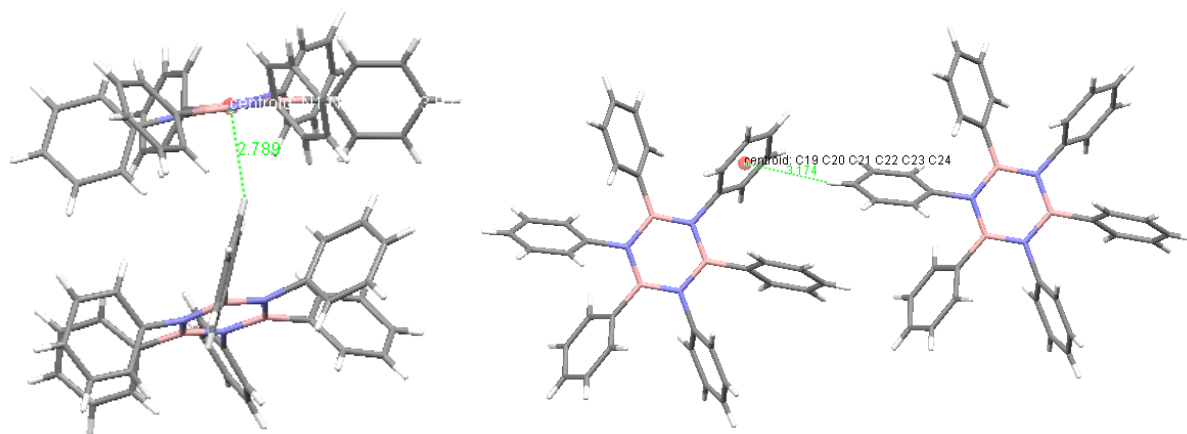


Figure 2.24 Close contacts in hexaphenylborazine **169** structure between H17 and the borazine cycle (left) of 2.79 Å and between H10 and a phenyl ring (right) of 3.17 Å.

2.3.2 Crystal Structures and Polymorph of B-trimesityl-N-triphenylborazine **173**

Similar observations can be made on the crystal structure of B-trimesityl-N-triphenylborazine **173**, which reveals the deviation from orthogonal arrangement of the phenyl rings and the borazine with dihedral angles between 63.14 and 83.68° depending on the polymorph studied. Again the aryl groups are not perpendicular to the borazine ring, they are all tilted in the same direction, resulting in a propeller shape (Figure 2.25b). The boron-nitrogen bonds distances are between 1.40 Å and 1.46 Å, and the internal angles of the borazine cycle are between 114° and 124° as observed in the literature for borazine derivatives.^[100,122] The ring is nearly planar with an average torsion angle of -1.5°. These observations allowed us to confirm the double bond character and the conjugation in the borazine ring, unveiled by both experimental and theoretical experiments.^[99,177–179] The most interesting observation for this structure is the van der Waals radii of the methyl groups (Figure 2.25b), which surround the boron atoms. This is consistent with our observation of the stability of this derivative toward a nucleophilic attack that would yield to the decomposition of the borazine cycle. The C7-B1 and H7a-B1 distances are of 3.0 and 2.4 Å respectively. These distances are comparable to the 2.61 Å between the hydrogen atoms of the anthryl moieties and the boron atoms, reported in the literature (Figure 2.25a).^[122]

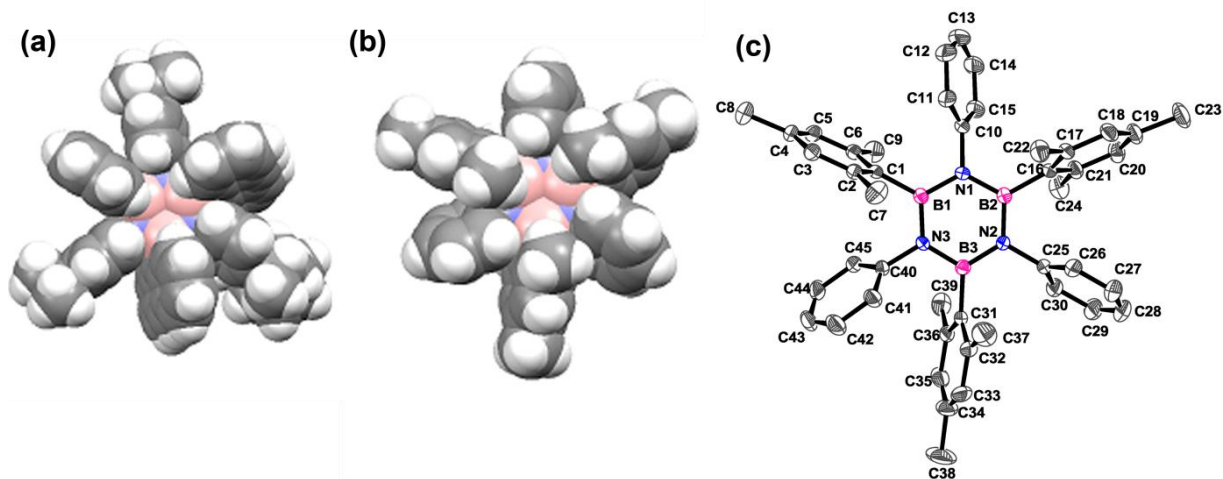


Figure 2.25 Crystal structure of (a) anthracenyl borazine derivative,^[122] (b) borazine **173** indicating the steric hindrance around the boron atoms and (c) ORTEP representation displaying close C7-B1 distance of 3.0 Å, hydrogen were omitted for the sake of clarity. Color code: grey: C, pink: B, white: H, blue: N. Space group: $P2_1/n$.

Colourless crystals were obtained using different solvents for crystallization and in total four polymorphs were obtained. The first three, R32, $R\bar{3}c$ and $P2_1/n$ were obtained using CH_2Cl_2 , cyclohexane and pentane respectively. The differences between the polymorphs can be seen macroscopically (Figure 2.26). Applying a gentle pressure on the first three polymorphs result in them into a new polymorph (powder X), whose 3D crystalline structure could not be determined. Also noticeable, is the conversion of $R\bar{3}c$ polymorph upon redissolution and recrystallisation into the more compact $P2_1/n$ form.

The first two polymorphs, R32 and $R\bar{3}c$, form porous networks and no π - π intermolecular interactions are observed (Figure 2.26 and Figure 2.27), instead short contacts between hydrogen and carbon atoms can be seen in the crystal packing. The dimensions of the voids are best seen by plotting the solvent accessible volume (yellow surfaces in Figure 2.27), which reveals large channels of diameter of 6.0 and 6.8 Å for R32 and $R\bar{3}c$ polymorphs respectively, unlike for the most compact form $P2_1/n$.

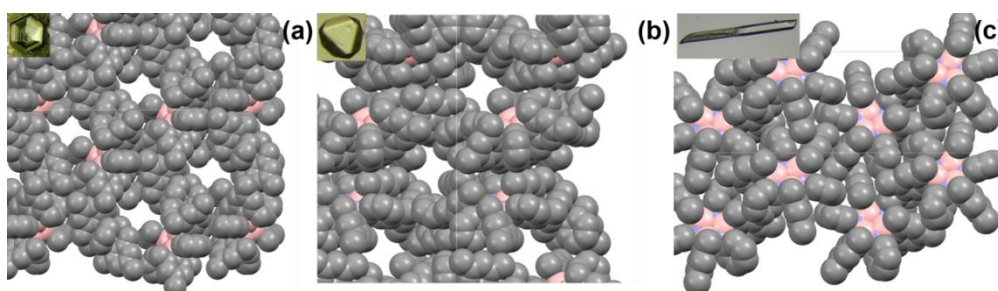


Figure 2.26 Pictures of the crystals and spacefill representation of a) R32, b) $R\bar{3}c$ and c) $P2_1/n$, hydrogen were omitted for the sake of clarity. Color code: grey: C, pink: B, white: H, blue: N.

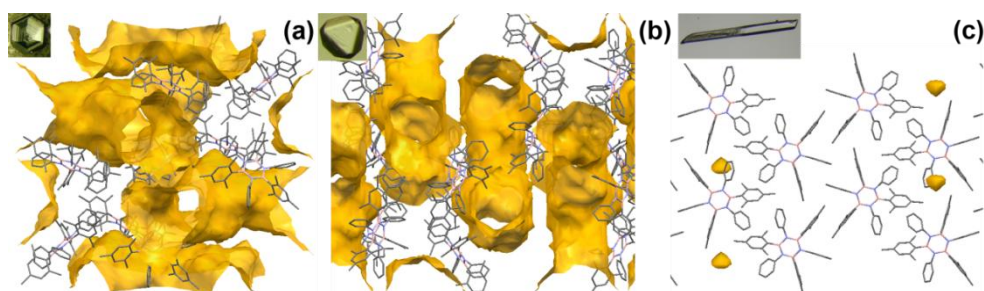


Figure 2.27 Pictures of the crystals and view of the channel of solvent accessible volume (probe radii 1.3 Å) in yellow of the different polymorphs. Space group: a) R32, b) $R\bar{3}c$ and c) $P2_1/n$. Color code: grey: C, pink: B, white: H, blue: N. Hydrogen atoms are omitted for the sake of clarity.

Chapter 2

Simulated powder diffraction patterns agreed with the experimental spectra, which are summarized in Figure 2.28. The polymorphs $R\bar{3}c$, R32 and $P2_1/n$ present peaks around 5° , indicative of a long range order (15 to 17 Å). The R32 and $R\bar{3}c$ have very similar spectra, as verified by the similarity of their 3D structure. Also noticeable, for all polymorphs there is a peak at 8.5° , corresponding to a interplanar distance of 10.3 Å.

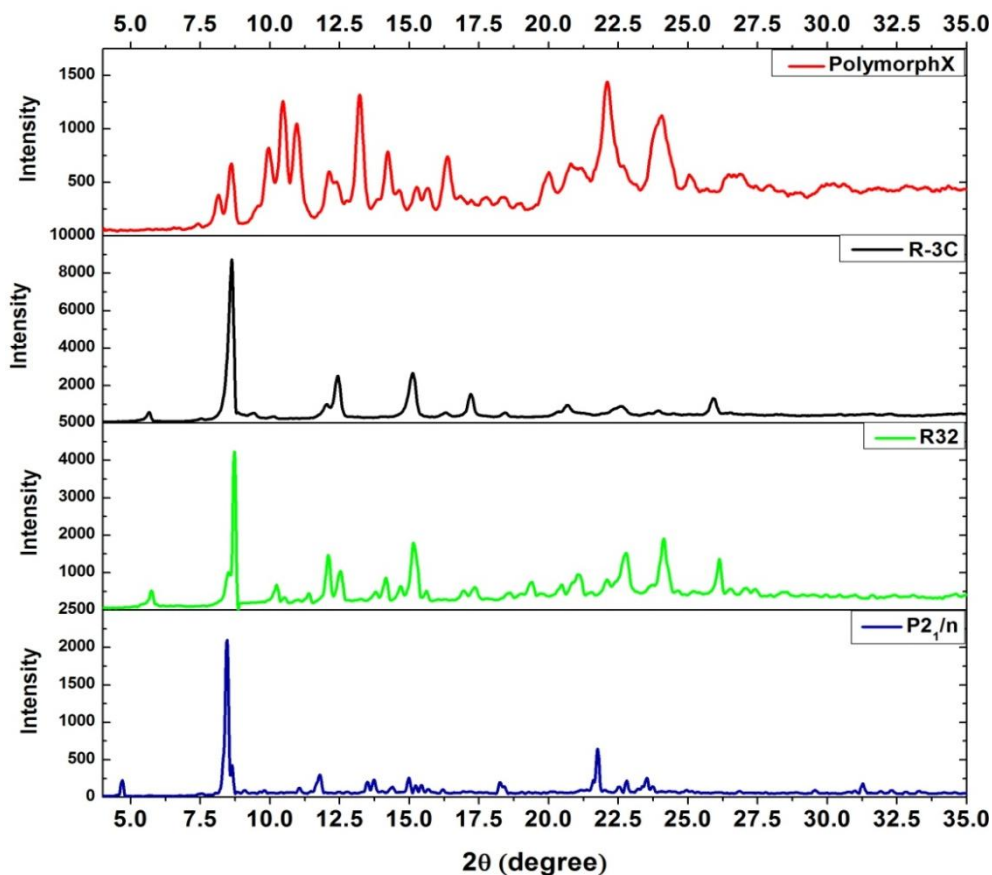


Figure 2.28 Experimental X-ray diffraction pattern of borazine **173** polymorphs, obtained using a copper source ($\lambda = 0.1540$ nm).

The photophysical properties of the different polymorphs were probed and are described in *section 2.4.2.2*.

2.4 UV-Vis Absorption and Fluorescence Properties

The photophysical study was done in collaboration with *Dr. Gianluca Accorsi*, in the group of *Dr. Armaroli*, CNRS, Bologna, Italy.

The photophysical properties of the borazine derivatives were probed in solution and in the solid state. Our aim was to introduce borazine core into π -conjugated structure to see how the doping affect the fluorescence properties. The compounds were analyzed in solution in three different solvents, CH_2Cl_2 , CH_3CN and THF as well as in the solid state prior of the building of OLED.

2.4.1 Analysis of the Doping Effect: HPbenzene vs. HPborazine

The spectra of hexaphenylborazine **169** and of hexaphenylbenzene were compared. The UV-Vis absorption spectra of the two compounds are different. Hexaphenylborazine indicates three bands at 261 nm ($\epsilon = 3850 \text{ mol}^{-1} \text{ cm}^{-1}$ in CH_3CN), 268 nm ($\epsilon = 4100 \text{ mol}^{-1} \text{ cm}^{-1}$ in CH_3CN) and 274 nm ($\epsilon = 3700 \text{ mol}^{-1} \text{ cm}^{-1}$ in CH_3CN) (Figure 2.29) while the UV-Vis absorption spectra of hexaphenylbenzene exhibits a main band at 241 ($\epsilon = 29100 \text{ mol}^{-1} \text{ cm}^{-1}$ in CH_3CN) with a slight shoulder at 269 nm

($\epsilon = 10300 \text{ mol}^{-1} \text{ cm}^{-1}$ in CH_3CN) (Figure 2.29). Borazine **169** reveals to be weakly fluorescent in CH_3CN only while hexaphenylbenzene emits in all three solvents. The lifetimes are very short, less than 2.8 ns for the hexaphenylborazine and less than 0.3 ns for hexaphenylbenzene. The spectra in different solvents do not indicate any evidence for solvatochromism, consistent with a non polarized transition state for both species.

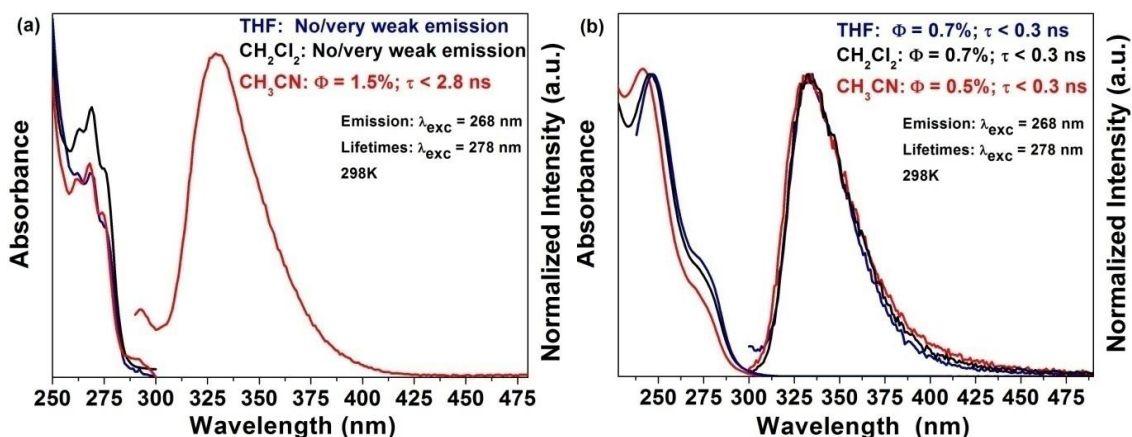


Figure 2.29 UV-Vis and fluorescence profile of (a) hexaphenylborazine **169** and (b) hexaphenylbenzene.

The UV-Vis absorption profiles are different while the emission profiles are very similar (Figure 2.30). Indeed, only a 4 nm ($\Delta E = 0.05 \text{ eV}$) blue shift is observed for the doped analogue of hexaphenylbenzene. However, the quantum yield is improved slightly from 0.5% to 1.5% in CH_3CN . At the contrary, the observation of bathochromic shift and improve quantum yield of fluorescence, upon doping the structure with boron and nitrogen atoms has already been reported in the literature for doped tolane.^[35] As outlined in the introduction, the influence of doping the structure by boron and nitrogen atoms on the fluorescence spectra is complex. However, for the first time the fluorescence spectra of borazine derivative compared to there all carbon analogue have been here reported.

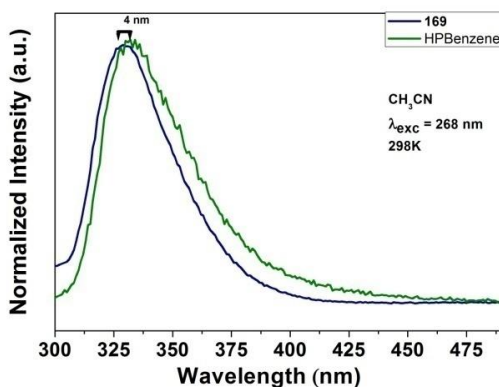


Figure 2.30 Comparison of the fluorescence emission profile of hexaphenylborazine **169** ($\lambda_{\text{em}} = 328 \text{ nm}$) and hexaphenylbenzene ($\lambda_{\text{em}} = 332 \text{ nm}$, $\Delta\lambda = 4 \text{ nm}$, $\Delta E = 0.05 \text{ eV}$).

2.4.2 UV-Vis Absorption and Fluorescence Properties in Solution and in the Solid State of Borazine **173**

2.4.2.1 UV-Vis Absorption and Fluorescence in Solution

The UV-Vis absorption spectrum of B-trimesityl-N-triphenylborazine **173** in CH_3CN reveals three bands at 271 nm ($\epsilon = 2400 \text{ mol}^{-1} \text{ cm}^{-1}$), 265 nm ($\epsilon = 2900 \text{ mol}^{-1} \text{ cm}^{-1}$), 259 nm ($\epsilon = 2600 \text{ mol}^{-1} \text{ cm}^{-1}$) (Figure 2.31a). These bands can be attributed to the vibronic bands of the aromatic ring substituting the borazine (Figure 2.31a inset). The absorption and excitation spectra

Chapter 2

were also recorded in different solvents (CH_2Cl_2 , CH_3CN and THF). No appreciable effect could be detected on the spectral shapes by the solvent polarity (μ = dielectric constant = 1.55, 1.75 and 3.45 for CH_2Cl_2 , THF and CH_3CN , respectively) leading to the lack of charge-transfer processes in solution (Figure 2.31b).

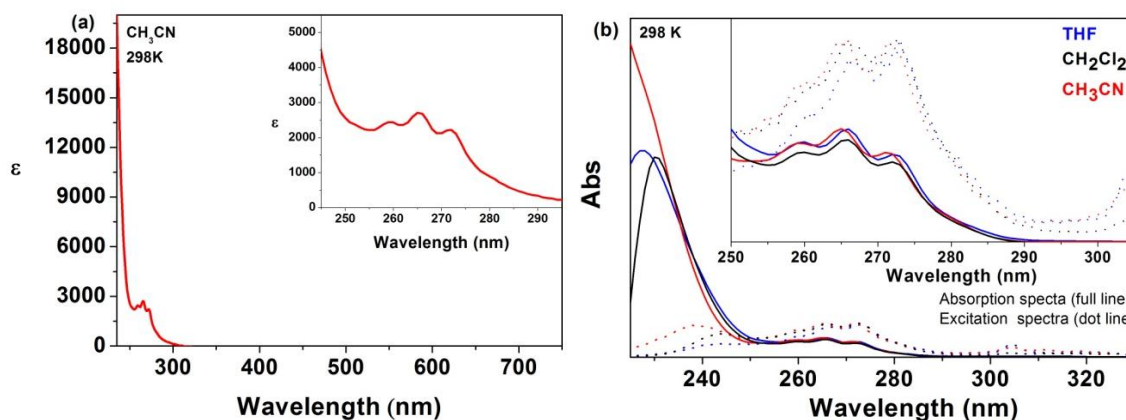


Figure 2.31 (a) UV-Vis absorption spectrum of **173** in CH_3CN . (b) UV-Vis absorption and excitation spectra of **173** in CH_2Cl_2 , CH_3CN and THF displaying the absorption bands between 259 and 271 nm responsible for the fluorescence.

To compare these UV-Vis absorption spectra with the all carbon analogue, the synthesis of compound **174** would have been necessary. However, due to synthetic challenges described in *section 2.2.2*, the synthesis of the carbon analogue could not be achieved (see *section 2.2.2*).

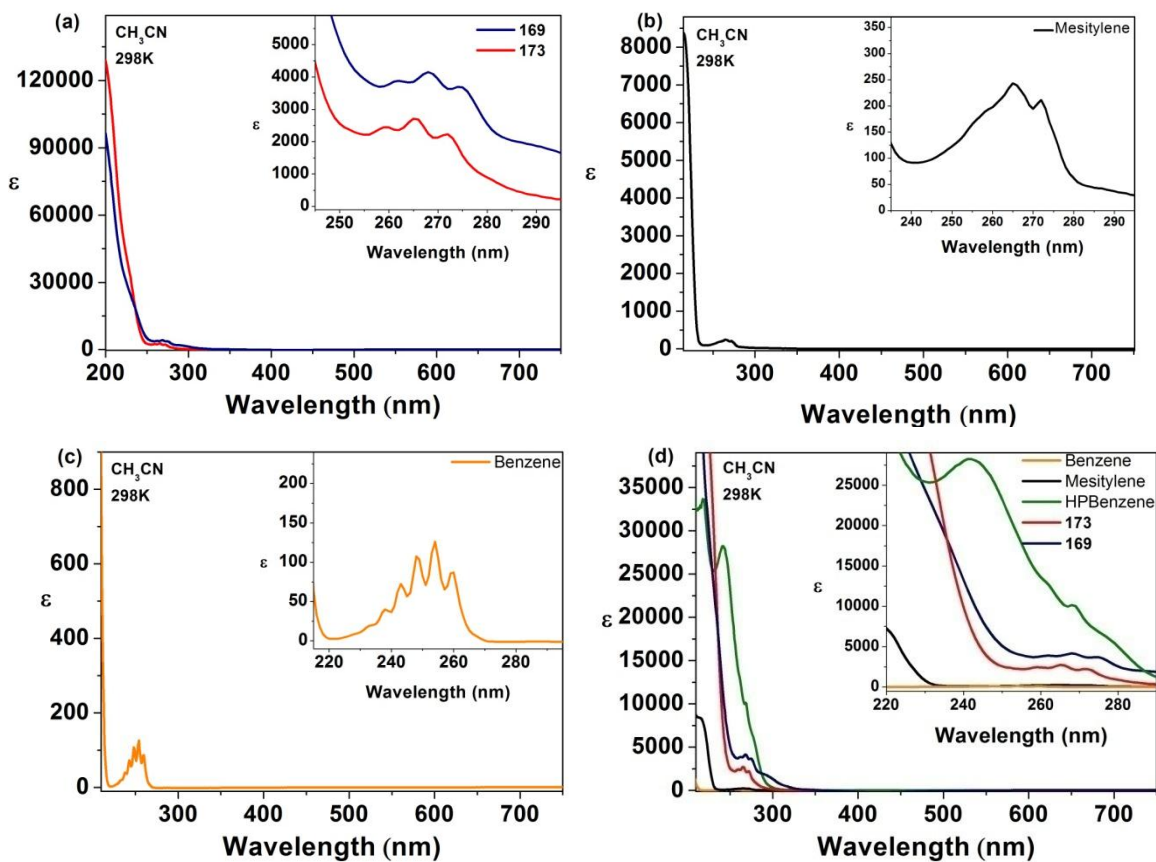


Figure 2.32 UV-Vis absorption spectra of (a) B-trimesityl-N-triphenylborazine (**173**) and hexaphenylborazine (**169**), indicating the slight (3 nm) blue shift and similar molar absorption coefficient. (b) mesitylene. (c) benzene. (d) combined UV-VIS absorption spectra.

Chapter 2

The UV-Vis absorption profile of hexaphenylbenzene can be compared to hexaphenylborazine **169**, in order to measure the shift. The spectra reported in Figure 2.32 exhibit a slight blue shift of 3 nm of B-trimesityl-N-triphenylborazine **173** compared to hexaphenylborazine **169**. To see if the absorption bands are due to the phenyl or mesityl substituents, the UV-Vis spectra of the latter were compared to the corresponding borazine. UV-Vis absorption spectra of mesitylene and benzene present absorption bands at 265 and 250 nm, with a hyperfine vibration shape for the latter. However, combined UV-Vis absorption spectra in Figure 2.32d indicate a higher absorption coefficient for the B-trimesityl-N-triphenyl and hexaphenylborazine, as well as for hexaphenylbenzene, consistent with previous reports of bundle shape chromophores.^[122]

As further evidence, the fluorescence emission was probed in different solvents (Figure 2.33). Moreover, the photoluminescence quantum yields (Φ_{em}) and relative lifetimes (τ) are substantially unchanged ($\Phi_{em} = 7.7\%$, $\tau = 7.1$ ns; $\Phi_{em} = 6.6\%$, $\tau = 7.2$ ns and $\Phi_{em} = 7.2\%$, $\tau = 7.6$ ns in CH_2Cl_2 , THF and CH_3CN respectively) with increasing solvent polarity trend.

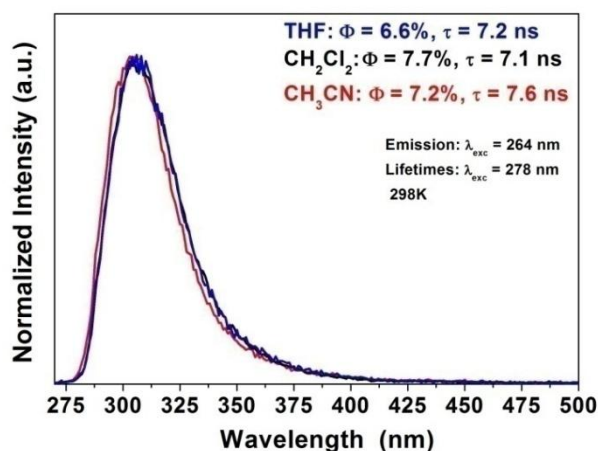
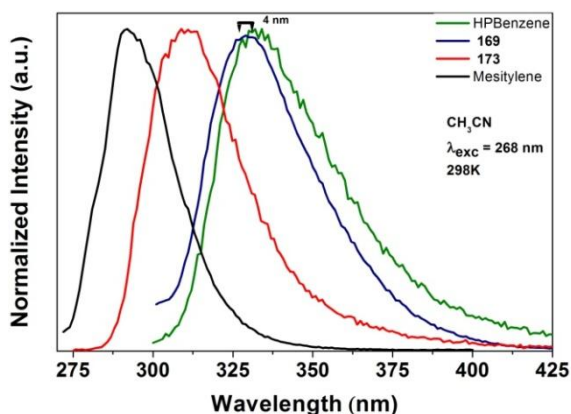


Figure 2.33 Fluorescence of **173** in CH_2Cl_2 , CH_3CN and THF, displaying no solvatochromism, similar quantum yields and lifetimes, consistent with a non polarized transition state ($\lambda_{em} = 310$ nm).

Due to synthetic difficulties, the analogue of this borazine, containing a phenyl group at the center, could not be synthesized (Scheme 2.23). Therefore, the UV-Vis absorption and fluorescence spectra could not be compared. However, B-trimesityl-N-triphenylborazine **173** and hexaphenylborazine **169** UV-Vis absorption spectra are similar (Figure 2.32). While B-trimesityl-N-triphenylborazine fluorescence spectra is blue shifted of 19 nm, being centered at 310 nm, and with an improve fluorescence quantum yield of 7.2%, compare to hexaphenylborazine (1.5%). Mesitylene is also a UV emitter, with a 4.0% fluorescence quantum yield at 292 nm, hypsochromically shifted of 18 nm compare to borazine **173** (Figure 2.34). As outlined earlier, borazine ring influence in hexaphenylborazine is of 4 nm (or 0.05 eV) compare to the carbon analogue.



Compound	Φ (%)	τ (ns)
HPBenzene	0.5	< 0.3
169	1.5	< 2.8
173	7.2	7.6
Mesitylene	4.0	9.7

Figure 2.34 Comparison of the fluorescence in CH_3CN of mesitylene (black), **173** (red), **169** (blue) and hexaphenylbenzene (green).

2.4.2.2 Fluorescence in the Solid State

Solid state fluorescence was probed for the different polymorphs since it is described in the literature that different polymorph can emit at different wavelengths.^[180–184] This has been investigated for applications such as piezochromic sensors^[181] or acids sensors.^[180] Polymorphs R3c and R32 have a very similar, porous structure with no intermolecular interaction between them. Consequently, the fluorescence in the solid state of these polymorphs matches the fluorescence profile in solution, having a peak between 306 and 330 nm (Figure 2.36). While the most compact polymorph, P₂/n and polymorph X, obtained after grinding of R32, have a red-shifted emission of 50 nm, compared to R32. At these wavelengths, this red shift corresponds to an energy of 0.6 eV. Quantum yield emission measurement in the solid state was more difficult, due to technical difficulties. The material of integrating sphere made of PTFE, absorb the UV light below 270 nm, above excitation wavelength. So the integrating sphere used instead is made of BaSO₄. Hence, a quantum yield of 13% at r.t. was measured, while a shoulder band appears between 400 and 500 nm when measuring the fluorescence at 77 K, with the quantum yield improved to 23% (Figure 2.36). The lifetimes are different, depending on the polymorph and are summarized below Figure 2.35.

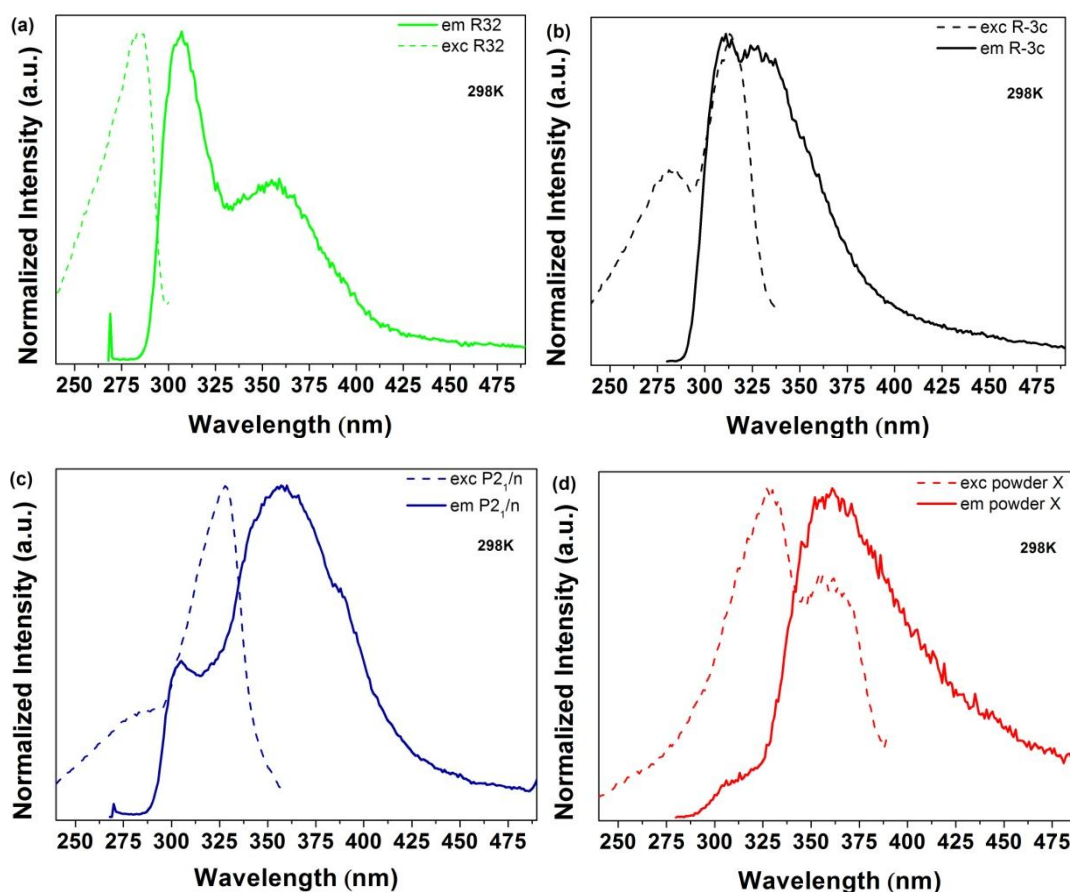


Figure 2.35 Excitation and emission spectra in the solid state of the different polymorph of borazine **173** with the corresponding emission lifetimes. (a) R32, $\lambda_{em} = 307$ nm, $\tau = 11.8$ ns. (b) R3c, $\lambda_{em} = 325$ nm, $\tau = 4.4$ ns. (c) P₂/n $\lambda_{em} = 360$ nm, $\tau = 11.0$ ns. (d) Powder X, $\lambda_{em} = 362$ nm, $\tau_1 = 1.8$ ns (38%), $\tau_2 = 8.3$ ns (62%).

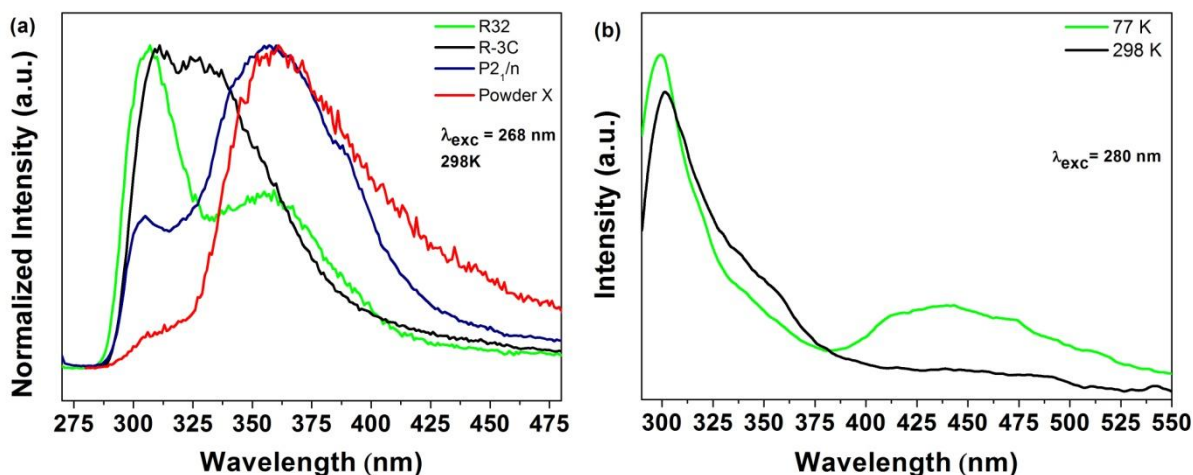


Figure 2.36 (a) Fluorescence profile in the solid state of the different polymorph, indicating the red shifted emission of P2₁/n and powder X. (b) Solid state fluorescence of borazine polymorph R32 at 298 K and 77K, presenting the appearance of a shoulder band between 400 and 500 nm at 77 k.

This solid state fluorescence study was of great importance for the next step, which focuses on OLED devices building (see section 2.6). Indeed, using the same compound, the emission wavelength of the device could be tuned, depending on the solvent used for spin-coating the emissive layer. Before doing any OLED study, the adsorption behavior of borazine **173** on metallic surface (see section 2.5) has to be known in order to be able to choose the best electrode to ensure good electrical conduction in the OLED.

2.4.3 UV-Vis Absorption and Fluorescence Properties in Solution and in the Solid State of Extended Borazine 176

UV-Vis absorption of extended borazine **176** was probed in solution and displays similar characteristic as B-trimesityl-N-triphenylborazine, having a comparatively bathochromic absorption band between 270 and 310 nm (Figure 2.37a). The epsilon values are slightly higher compare to the one of borazine **176**. The band vibronic structure is less defined with two peaks at 288 nm ($\epsilon = 6030 \text{ mol}^{-1} \text{ cm}^{-1}$, in CH_3CN) and at 305 nm ($\epsilon = 5600 \text{ mol}^{-1} \text{ cm}^{-1}$, in CH_3CN). Fluorescence spectra in solution exhibit a very weak emission between 320 and 360 nm with two maximum at 322 and 336 nm. Solid state fluorescence spectrum presents broad bathochromic emission spectrum between 396 and 520 nm (Figure 2.37b). Emissions in solution and in the solid state were too weak to measure the quantum yield.

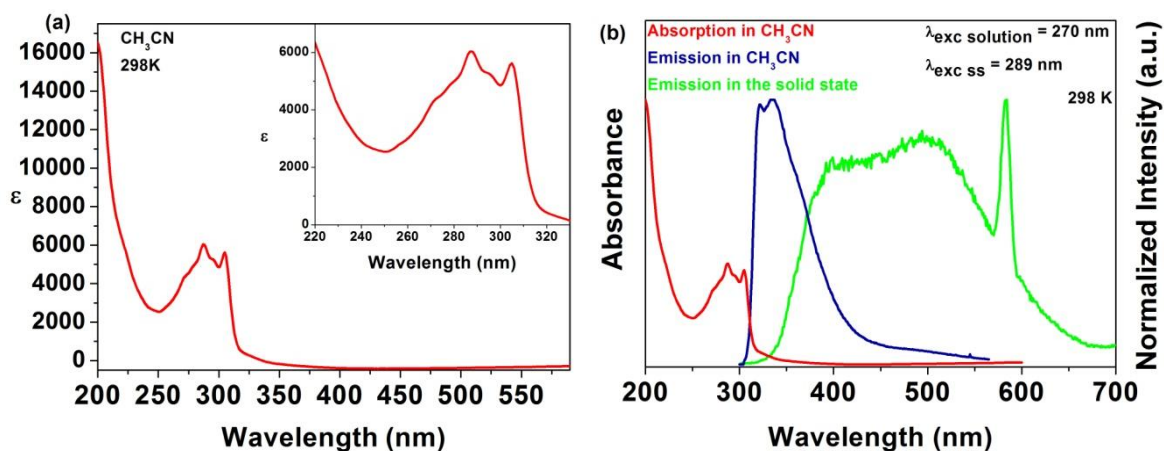


Figure 2.37 (a) UV-Vis absorption spectrum ($\lambda_{abs} = 287$ and 304 nm), (b) fluorescence in solution ($\lambda_{em} = 330$ nm) and in the solid state ($\lambda_{em} = 370$ to 600 nm) of extended borazine **176**.

Lifetimes of the emission in the solid state vary along the emission profile. It is composed of two lifetimes at $\lambda_{em} = 370$ nm ($\tau_1 = 1.5$ ns (37%) and $\tau_2 = 0.4$ ns (63%)) and of two other at $\lambda_{em} = 580$ nm ($\tau_1 = 1.1$ ns (47%) and $\tau_2 = 4.7$ ns (53%)). Crystal structure of the compound could have explained the two lifetimes by two different molecular arrangements in the crystal. However, the small needles obtained by slow evaporation in CH_3CN were not suitable for X-ray diffraction.

2.4.4 UV-Vis Absorption and Fluorescence Properties in Solution and in the Solid State of Differently Substituted Borazine 196

UV-Vis and fluorescence properties of **196** investigation was crucial to determine the influence of the hydroxyl group on the borazine ring. UV-Vis absorption spectra reveals three bands, as observed for borazine **173**, while emission peak at 300 nm, similar to the one of **173** ($\lambda_{max} = 310$ nm). The absorption and emission spectra were measured in different solvents (Figure 2.38) and did not present any solvatochromism. The absorption maxima are at 259, 265 and 271 nm, which are similar to the B-trimesityl-N-triphenylborazine. The fluorescence peak is at 305 nm, the fluorescence quantum yield is of 3.7 to 5.3%, slightly lower than B-trimesityl-N-triphenylborazine **173** (7%) consistent with the loss of one chromophore group, the mesityl, while the lifetimes in different solvents are similar, in the 7 ns range. All these evidence are pointing toward the fact that the emission of these derivatives is due principally to the mesityl rings with a delocalization of the HOMO on the borazine ring. Indeed, the peripheral aryl substituent being conjugated with the borazine ring as evidenced by the LUMO delocalization (Figure 2.51b). Crystal structure did not reveal any intermolecular interactions between the borazine and therefore, the solid state emission matches the emission in solution (Figure 2.38).

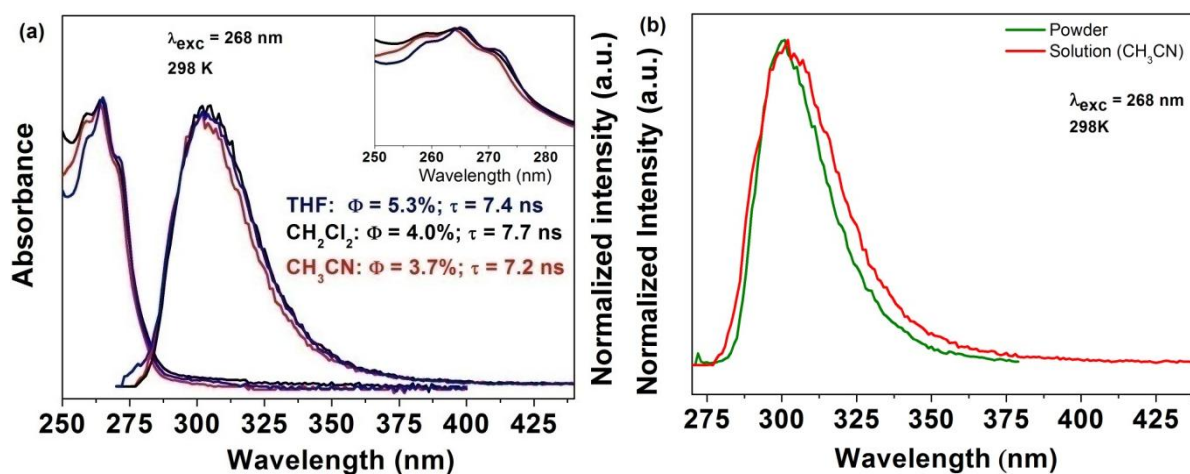


Figure 2.38 (a) UV-Vis absorption spectra and emission of asymmetrically substituted borazine **196** in THF, CH_2Cl_2 and CH_3CN . (b) Fluorescence in solution (red) and in the solid state (green) of differently substituted borazine **196**, displaying similar emission profile ($\lambda_{em} = 300$ nm).

From the photophysical data one can conclude that there is no influence from the hydroxyl group on the UV-Vis absorption and fluorescence spectra of these derivatives. The fluorescence in solution is mainly due to the peripheral aryl substituent, conjugated with the borazine cycle, as evidence from spectra similarity as well as lifetimes values between B-trimesityl-N-triphenylborazine **173** ($\lambda_{em} = 310$ nm, $\Phi = 7.2\%$, $\tau = 7.2$ ns, in CH_3CN) and differently substituted borazine **196** ($\lambda_{em} = 300$ nm, $\Phi = 3.7\%$, $\tau = 7.6$ ns in CH_3CN).

2.5 UHV-STM Characterization of Borazines on Au and Cu Surfaces

Surface analysis, using STM instrument, was achieved by *Dr. Nataliya Kalashnyk* in the group of *Professor Dr. Giovanni Costantini*, University of Warwick, United-Kingdom.

This section describes the adsorption behavior of borazines derivatives on metallic surfaces under UHV conditions, studied by STM and compared to the analogue hexaphenylbenzene. Surfaces like Cu and Au have intermediate interactions strength with aromatic compounds, therefore the 2D molecular assemblies will be governed by the interactions between the aromatic compounds.^[185] So, the first compound adsorbed will influence the disposition and conformation of the following compounds. This allows the creation of homochiral domains on the surface formed by an achiral compound in the gas phase.^[185] The STM study of the borazine derivatives revealed peculiar conformation preferences for **169** and **173** upon adsorption on Cu(111) surfaces. Whereas differently substituted borazine **196** has reacted with the Cu(111) surface to form regular clusters.

2.5.1 UHV-Deposition of Hexaphenylborazine 169

Hexaphenylborazine **169** was deposited on Au(111) by sublimation under ultra high vacuum. The aim was to compare the pattern with the previously reported pattern of hexaphenylbenzene on copper surface.^[186] The deposition of hexaphenylborazine **169** on Au(111) after sublimation at 175 °C exhibits molecular pattern similar to the one described by Gross for hexaphenylbenzene on Cu(111) (Figure 2.39a).^[186] The six lobes of the pattern correspond to the six phenyl groups of the borazine. The molecular 3D model fits in the pattern observed by STM, with two molecules inside the crystal lattice (Figure 2.39c).

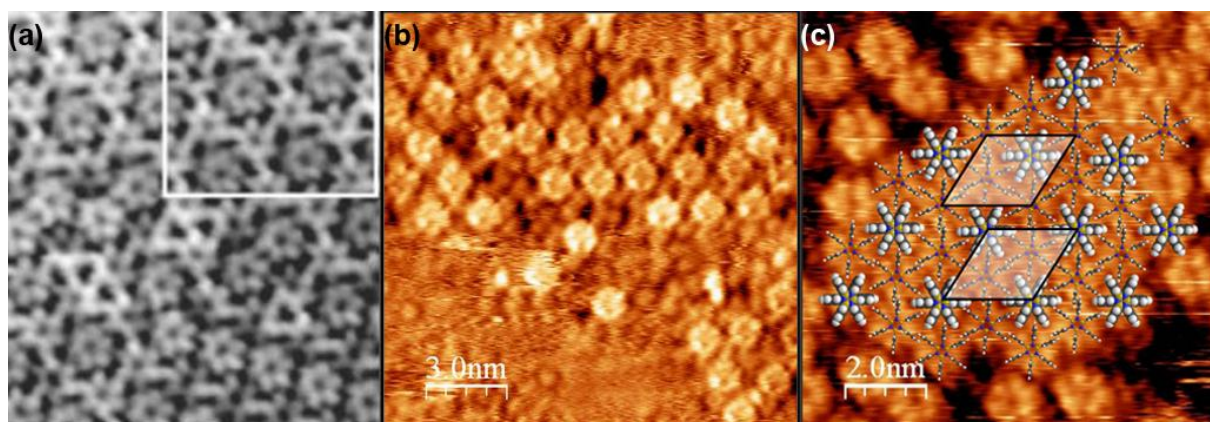


Figure 2.39 (a) Molecular pattern of hexaphenylbenzene on Cu(111). (b) molecular pattern of hexaphenylborazine **169** on Au(111). (c) 3D model of hexaphenylborazine **169** on Au(111) with the unit cell.

Interestingly, the molecular pattern of **169** is different on Cu(111), presenting three fold shape after sublimation at 120 °C. A high resolution STM reveals that the lobes height, corresponding to three phenyl substituents, are different (Figure 2.40b). The steps in height of the phenyl rings on **169** are the proof of the chiral propeller shape of **169**. The borazine derivative now forms a chiral object on the Cu(111) surface, as opposed to the six fold shape on Au(111). Crystal structure of hexaphenylborazine **169** (Figure 2.23) has revealed the propeller shape of **169**, with one clockwise and one anti-clockwise turns while in the cluster studied there is a majority of anticlockwise turn (174) and a minority of clockwise turn (86). Amplification of chirality on an achiral Cu(111) surface has been previously reported for helicene derivatives.^[187] However, in the present case there was no cluster with exclusive clockwise or anti-clockwise chiral molecules (Figure 2.40c).

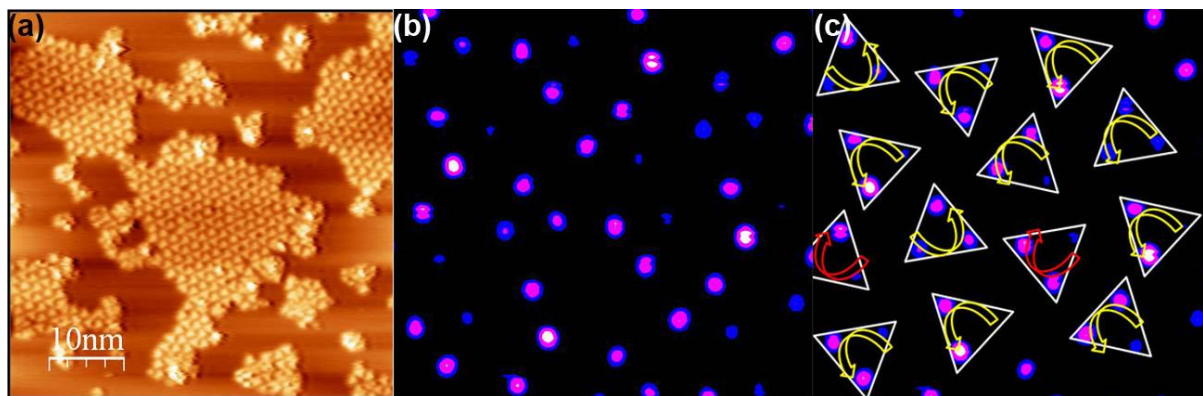


Figure 2.40 STM images of hexaphenylborazine **169** on Cu(111), (a) presenting three fold pattern, (b) different phenyl groups heights, represented by more intense violet color. (c) The disposition can be clockwise or anti-clockwise following the height gradient.

2.5.2 UHV-Deposition of B-trimesityl-N-triphenylborazine **173**

The more stable, toward hydrolysis, B-trimesityl-N-triphenylborazine **173** was studied, to check previously obtained results with hexaphenylborazine **169**, fearing that the latter would have reacted with the metallic surface. Hexaarylbenzene are known to react on Au(111) surfaces to form fused derivatives upon annealing and subsequent cyclodehydrogenation.^[188] A similar reaction could have occurred with hexaphenylborazine **169** to give borazinocoronene. Again, the three fold shape was observed with different heights of the lobes on Cu(111) surface. In this case the lobes can be attributed without ambiguity to the methyl moieties of the mesityl substituents (Figure 2.41d).

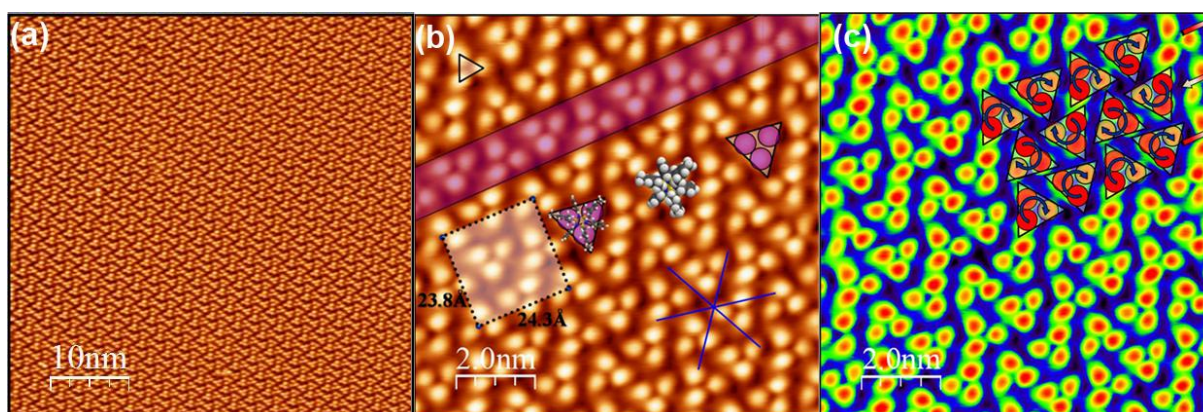


Figure 2.41 STM images of (a) B-trimesityl-N-triphenylborazine **173** on Cu(111) presenting regular high-packing density. (b) zoom in indicating the three lobes corresponding to the mesityl ring on the surface and 3D model of the borazine fitting the measure and the unit cell of Cu(111). (c) Clockwise turns along the different heights of the mesityl substituents.

This study was of importance to observe the adsorption behavior of borazine on metallic surfaces to select the right electrodes for the OLED. Indeed, cathodes are needed for charge injection into organic molecules with a high LUMO level. Amongst them, metallic Au is a promising electrode despite its high work function (5.1 eV).^[189] The adsorption onto the Au surface is crucial to reduce the electron barrier, in order to have an electrical current flow in the OLED.

2.5.3 Surface Study of Differently Substituted Borazine **196**

As observed for the assembly of compound **173** (Figure 2.41), in the modeled hexagonal clusters the aromatic substituents are engaging in non-covalent interactions through perpendicular or offset parallel displacements, with an estimated interaction energy of about 3 kcal mol⁻¹. In principle, once a heptamer is built, it can steadily grow to larger clusters

Chapter 2

upon further accommodation of three molecules. However, this is not the case as only up to 13-mer clusters have been mainly observed suggesting that another interaction, this time repulsive, must be present. With respect to compound **173**, it is possible that the acidic B-OH function of borazine **196** undergoes deprotonation reaction mediated by Cu adatoms, thus leading to negatively-charged molecular species. It is thus conceivable that each hexagonal cluster is composed by a central negatively-charged molecule surrounded by six neutral units through π - π stacking interactions established by the interdigitating phenyl substituents. To support this assumption, a modeled system composed of two hexagonal heptamers on a Cu(111) slab (28.8×28.8 nm) was heated up to 250 K to accelerate the clusters diffusion (for 10 ns). As expected, only the neutral assemblies merged into extended bidimensional architectures, whereas the charged clusters repelled each others.

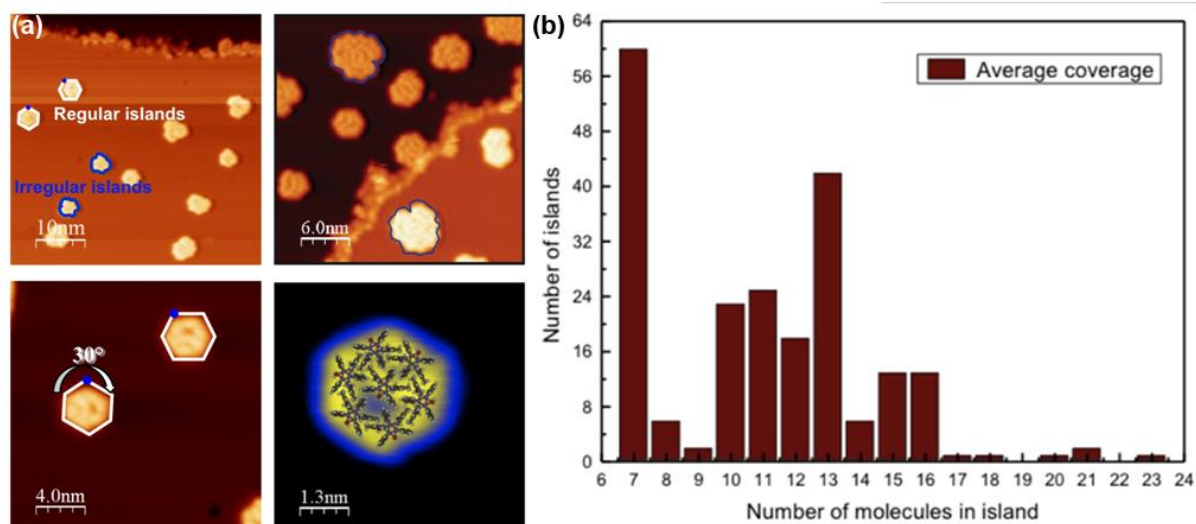


Figure 2.42 (a) STM images of borazine **196** on Cu(111), displaying the regular, hexagonal island constituted of 7 molecules. (b) Distribution of frequency of island vs. the number of molecules constituting them indicates that island constituted of 7, and 13 molecules are most favored.

2.6 OLEDs and LECs, Constructions and Characterizations

OLEDs were built in collaboration with *Dr. Oliver Fenwick* and *Yong Sig Shin*, in the group of *Prof. Dr. Cacialli*, UCLondon, United-Kingdom.

OLEDs are made of several layers, the cathode, the anode, the conductive and the emissive layers (Figure 2.43). The classical anode used in OLED is the Indium-Tin oxide (ITO), due to its good conductivity and appropriate level of energy for positive charge injection. However, as illustrated in Figure 2.43 the absorption profile of ITO will absorb more than half the emission from the borazine down from 350 nm. Therefore sapphire was chosen, which is nearly transparent down to 200 nm. However, the conductivity of sapphire is not optimal and it needs to be improved by depositing a 15 nm layer of silver. This silver layer transmits up to 60% of light between 300 and 350 nm. This layer will be topped by Poly(3,4-ethylenedioxythiophene) (PEDOT), which improves the conductivity and absorbs only 10% of light in this region.

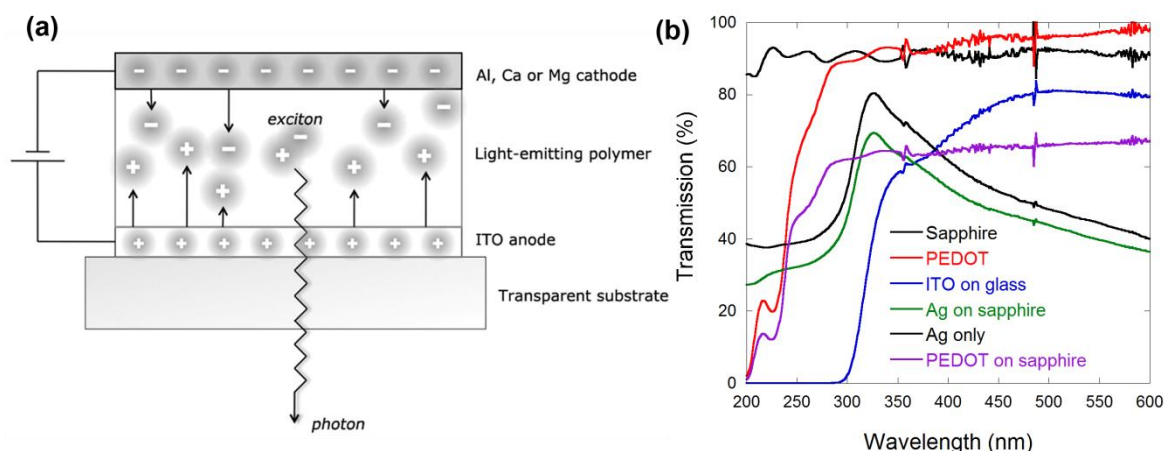


Figure 2.43 (a) Schematic representation of an OLED device. Adapted with permission from the American Chemical Society. Copyright 2009.^[3] (b) absorption spectra of different anode for the OLED.

Therefore, the first prototype devices were built using sapphire as the conductive anode. In order to increase the conductivity of the sapphire, a layer of silver (15 nm) topped by PEDOT (Poly(3,4-ethylenedioxythiophene) (40 nm) was deposited before the borazine layer. The cathode was made of successive layer of LiF (6 nm) followed by a calcium (30 nm) and then an aluminium (150 nm) layer (Figure 2.44a). The first batch of devices reveals that the borazine layer displays good conductivity but no emission of light as probed by the UV-Vis detector.

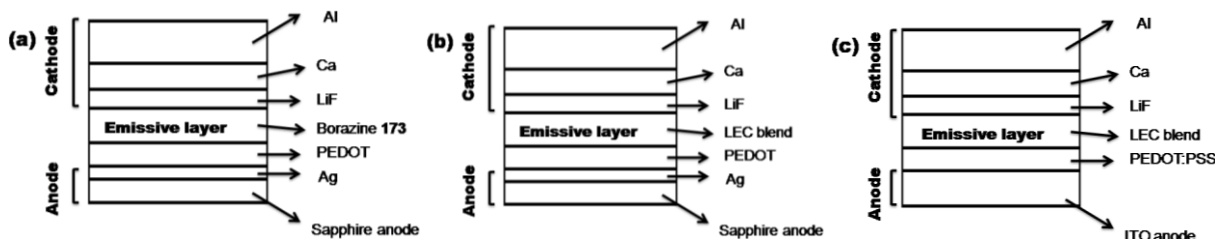


Figure 2.44 Schematic representation of (a) first OLED, (b) second device, an LEC, and (c) second LEC device configurations.

In the second batch of devices, Light Emitting electrochemical Cell (LEC) devices were made in order to increase the conductivity at the interfaces of the different layer.^[189–191] LEC blend replaces the emissive layer while keeping the anode of sapphire and the cathode used for the previous LED. Two competing theories are behind the use of such a blend. The first, is that the ion will separate upon applying the electrical field inside the device, generating a p-n junction which diminishes the barrier potential (Figure 2.45).^[189] The second, is that the potential between the interface is high enough so that an electrochemical reactions can occur, increasing the number of charged species, and diminishing the barrier potential.^[190]

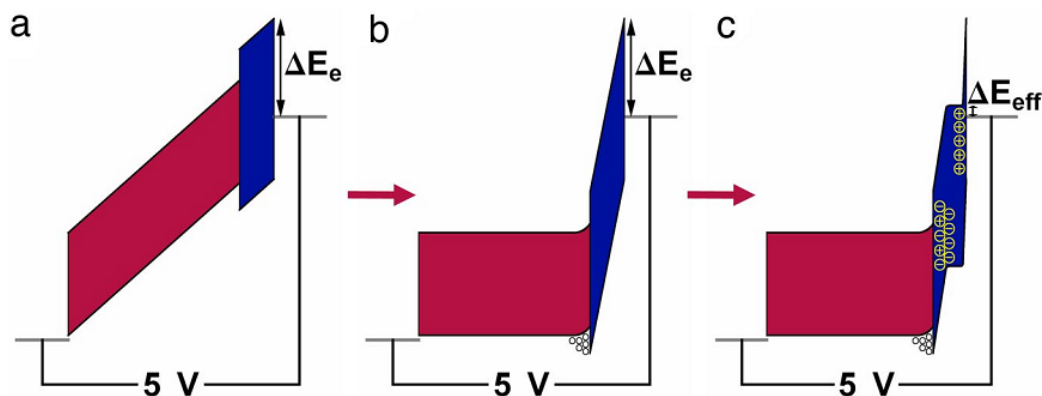


Figure 2.45 Principle of a LEC: (a) the electrical field is evenly distributed across the device, (b) hole accumulate at the interface, screening the electrical field of the other layer, (c) ion redistribute to screen the electrical field, diminishing the injection barrier.^[189] Adapted with permission from the American Chemical Society. Copyright 2008.

Hence, the second batch of devices used identical anode and cathode (Figure 2.44b) but the emissive layer was changed for LEC blend constituted of 25% PEO (2 weight % in chloroform), 25% LiOTf (0.1 weight % in THF) and 50% of B-trimesityl-N-triphenylborazine **173** (2 weight % in toluene) (emissive layer thickness: 80 nm). This turned out to effectively increase the conductivity and present emission of light proportional with the current density (Figure 2.46a). However, the external quantum efficiency is very low ($3 \times 10^{-6}\%$ at 120 mA cm^{-2}) and the electroluminescence spectrum (Figure 2.46b) indicates an emission in the visible.

Finally, using ionic liquid^[192] as the LEC blend and changing the sapphire anode for more conductive ITO (Figure 2.44c), emission of light was achieved. The LEC blend was constituted of 1.5% (w/w) of borazine **173** and TBA-TF (tetrabutyl ammonium nonafluorobutanesulfonate), to wrap our emissive material while maintaining LEC devices advantages, similar electroluminescence spectra were observed (Figure 2.46c), with a slight increase of the external quantum efficiency ($1.3 \times 10^{-5}\%$ at 126 mA cm^{-2}). The cathode layers were kept identical to the previous devices while ITO was used as the conductive anode.

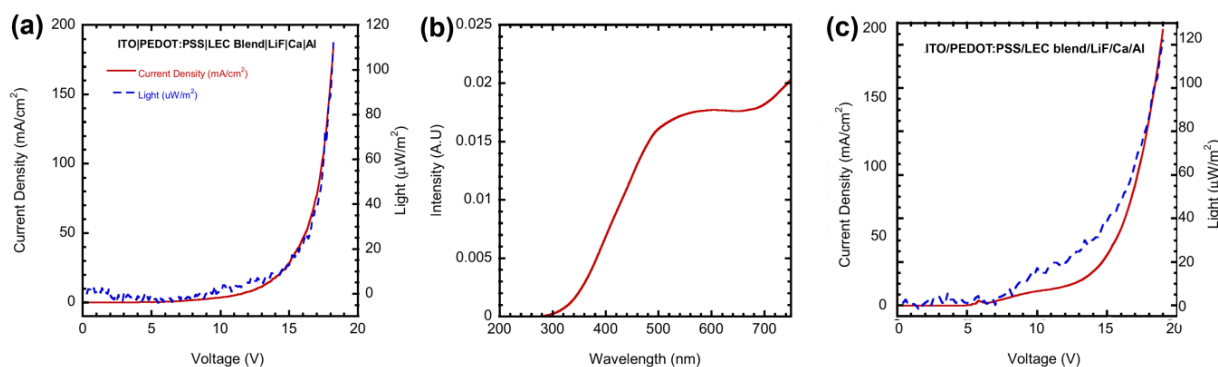


Figure 2.46 a) Current (full line) and radiance Vs. light (dotted line) characteristics of a light-emitting electrochemical cell (LEC) incorporating an active layer of emitter **173**, blended with poly(ethylene oxide) (PEO) as the ion transporter and LiOTf as the salt providing mobile ions. The 3.5 mm^2 device was fabricated with the vertical structure ITO/PEDOT:PSS (80 nm)/active layer/LiF(6 nm)/Ca(30 nm)/Al (150nm), which is indicated schematically as an inset. b) The electroluminescence spectrum obtained at a bias of 17 V of such a device, showing broad emission from the near UV through the visible spectrum. c) Current-voltage-light characteristics of a light-emitting diode (LED) incorporating an active layer of emitter **173**, blended with TBA-TF as the salt providing mobile ions. The 3.5 mm^2 device was fabricated with the vertical structure ITO/PEDOT:PSS (80 nm)/active layer/LiF(6 nm)/Ca(30 nm)/Al(150nm).

2.7 Borazine-Fullerene cocrystal

The properties of **173**·C₆₀ cocrystal were investigated in collaboration with the group of *Dr. Takashi Nakanishi*, National Institute for Material Sciences, Tsukuba, Japan. Theoretical calculations have been performed by *Prof. Dr. Benoît Champagne*, University of Namur.

Being good electron acceptors,^[193–195] [60]fullerene (C₆₀) and its derivatives have revealed fascinating physical properties which display a huge potential for the development of new materials.^[196,197] Amongst others, they have been shown to efficiently trap excited electrons and transfer it to the electrode, thus revealing to be good molecular components for photovoltaic devices.^[198] For organic thin-layer solar cell (OTLSC) applications, classical values for the exciton diffusion length are in the range of 10–20 nm, meaning that the electron donor (D) and the acceptor (A) counterparts should be in a close arrangement. In this respect, bulk heterojunction organic solar cells have allowed an improvement of the OTLSCs's efficiency due to their better charge separation performances.^[199] However, to achieve reproducible and higher efficiencies, the photoactive architecture must possess a precisely controlled molecular organization.^[198] In this respect, the supramolecular route can lead to self-organized materials with an appropriate D-A configuration at controlled distances.^[200] Amongst the different approaches, the cocrystallization of D and A molecular units in bulk heterosystems displaying predictable and tunable distances enabling charge transfer interactions has shown to lead to materials displaying very reproducible physico-chemical properties.^[201,202] B-trimesityl-N-triphenylborazine (**173**, Figure 2.47a) displays high extinction coefficient ($4 \times 10^3 \text{ M}^{-1}\text{cm}^{-1}$ in CH₂Cl₂) in the UV region. As a first demonstration of the use of such hexasubstituted borazines in photoactive materials for photovoltaic applications, herein we report on the study of the supramolecular organization between **173** and C₆₀ in the solid state along with its photophysical measurements.

2.7.1 Structural Studies

B-trimesityl-N-triphenylborazine **173** was solubilized with an equimolar quantity of pristine C₆₀ in *ortho*-dichlorobenzene. The solvent was slowly evaporated at r.t. yielding dark red-purple crystals (Figure 2.47b). Unfortunately, single-crystals X-ray diffraction analysis was unsuccessful to determine the molecular organization in the solid state. In fact, several micrometer-sized bipyramidal crystals revealed to form crystal twinning, as observed by scanning electron microscopy (SEM, JEOL NeoScope JCM-5000) (Figure 2.47b). Therefore, the structure of the nanostructured cocrystals were investigated by means of powder X-ray diffraction (XRD, Rigaku RINT-2200HF Ultima), high-resolution transmission electron microscopy (HR-TEM, JEOL JEM-2100F, 200 kV) and solid-state UV-Vis absorption spectroscopy.

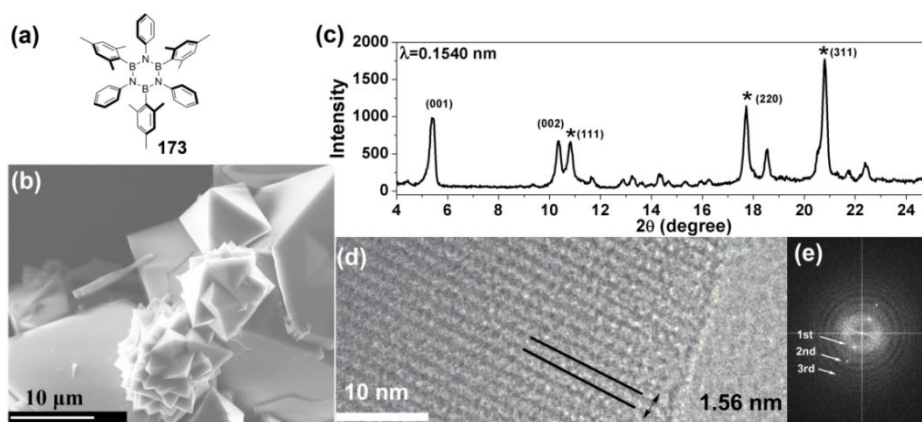


Figure 2.47 a) Chemical structure of B-trimesityl-N-triphenylborazine (**173**). b) SEM image of the cocrystal showing the crystal twinning of bipyramid. c) XRD of the cocrystal, *-marked peaks are the peaks of fcc C₆₀. d) HR-TEM image of the cocrystal indicating the line arrangement of 1.56 nm width. e) The corresponding FFT analysis showing the 1st, 2nd, and 3rd order spots.

Chapter 2

As shown in Figure 2.47c, XRD confirmed the obtention of the cocrystal, the diffraction pattern being different from that of the classical fcc C_{60} crystalline structure^[203] as well as the borazine $R\bar{3}c$ crystal. The cocrystal pattern shows two main peaks at 5.4 and 10.5°, corresponding to d values of 1.60 and 0.84 nm, respectively. These peaks are most likely showing the layer structure as from its (001) and (002) planes. However, small quantities of segregate fcc C_{60} crystal were also observed in the samples (marked * in Figure 2.47c). In addition, HR-TEM analysis of the nanostructures presents a periodic structure of 1.56 nm layer distance (Figure 2.47d). The appearance of third-order spots in the Fast Fourier transform (FFT) analysis indicates a certain degree of periodicity. In particular, the interlayer distance observed in the TEM (1.56 nm) is in good agreement with the plane distance (1.60 nm) observed by XRD (Figure 2.47c). Thermal analysis (TGA and DSC) confirmed the effective cocrystallization of both molecules and the change of their physical properties as a consequence of their interaction. For example, in the DSC profile of the cocrystal (solid line of Figure 2.48a) no endothermic melting point (at 262 °C, dotted curve of Figure 2.48a) has been observed, displaying good homogeneity of the sample and the absence of free borazine in the sample.

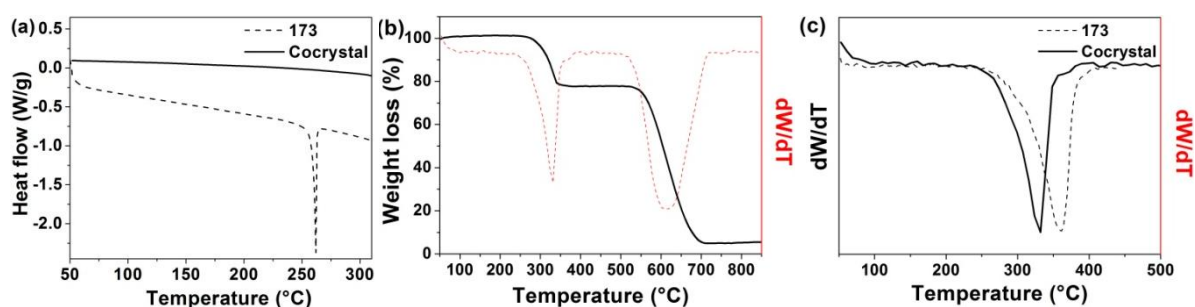


Figure 2.48 (a) DSC profiles for **173**- C_{60} cocrystals (solid) and **173** (dot). The peak at 262 °C corresponds to the melting temperature of **173**. (b) TGA profile of **173**- C_{60} cocrystal showing weight loss corresponding to borazine degradation at 330 °C and sublimation of C_{60} starting at 600 °C. (c) Derivative of the TGA plot showing a degradation of **173**- C_{60} cocrystal at lower temperature than the borazine alone (330 °C Vs. 360 °C).

2.7.2 Photophysical Properties

UV-Vis absorption spectrum of a 1:1 solution of **173** and C_{60} in CH_2Cl_2 (Figure 2.49c) presented no additional features indicating a ground-state charge transfer occurring between the two molecular species. The absorption spectrum of molecule **173** showed three bands at 272, 265 and 257 nm as well as a main peak at 230 nm (Figure 2.49c). The steady-state UV-Vis absorption spectrum of the cocrystal in the solid state (Figure 2.49a) reveals a pronounced tail up to 800 nm, possibly indicating the occurrence of a charge-transfer process between C_{60} and **173**, the latter acting as electron donating specie.^[204] Additionally, a 12-nm blue shift was observed for the fullerene-centered absorption peaks (at 271 and 346 nm), compared to these of crystalline C_{60} . This shift could be attributed to the attenuation of the π - π stacks between neighboring C_{60} molecules in the cocrystal, possibly due to the presence of intercalating borazine molecules.

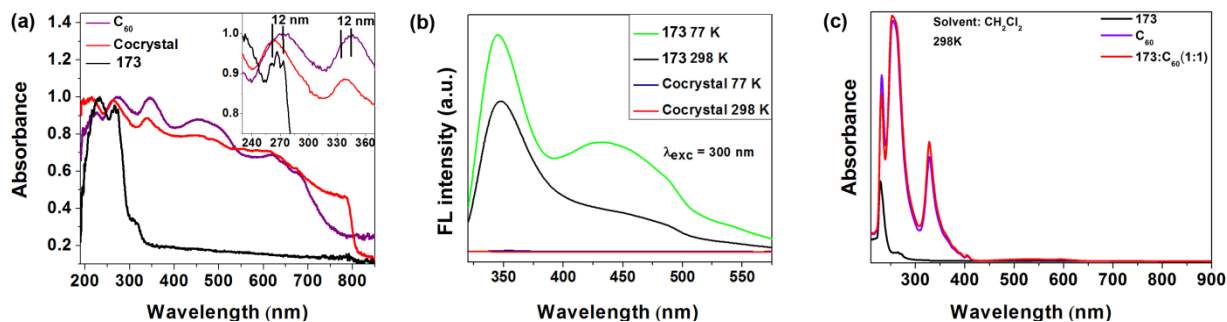


Figure 2.49 (a) Solid-state UV-Vis absorption spectra of **173** (dash), C_{60} (dot) and the cocrystal (solid). (b) Solid-state emission spectra of **173** at 298 K (black), 77 K (green) and of the **173**- C_{60} cocrystal at 298 K (red) and 77 K (blue). (c) UV-Vis absorption spectra of fullerene (purple), borazine (black) and 1:1 equimolar solution of the two (red).

Chapter 2

Borazine derivatives are known to be efficient UV emitters in solution.^[122] Compound **173** revealed to be a good UV emitter also in the solid state, with a fluorescence peak maximum centered at 350 nm (Figure 2.49b). The measured absolute fluorescence quantum yield reveals to be of ca. 13% at r.t., while at 77 K it increases up to 22.9% with the appearance of a broad and novel emission band between 400 and 500 nm. On the contrary, no detectable emissive features have been observed for samples containing the **173**·C₆₀ cocrystals (Figure 2b, red and blue lines). This suggests that a close spatial proximity, allowing strong interchromophoric interactions in the solid state, is adopted. Finally, the charge transporting properties in the solid state of both borazine **173** alone and of that of the **173**·C₆₀ cocrystal were measured by time-resolved microwave conductivity (TRMC)^[205] (Figure 2.50). The measured transient photoconductivity ($\phi\Sigma\mu$ = the product of the quantum efficiency of the charge-carrier generation ϕ and the sum of the nanometer-scale charge-carrier mobility, $\Sigma\mu = \mu_+ + \mu_-$) for the cocrystal ($1.55 \times 10^{-5} \text{ cm}^2 \text{ V}^{-1} \text{ s}^{-1}$) is three time higher than that of compound **173** alone ($0.46 \times 10^{-5} \text{ cm}^2 \text{ V}^{-1} \text{ s}^{-1}$). Such enhanced photoconductivity values can be possibly due to two factors: i) the intrinsic high photoconductivity of C₆₀ and/or ii) the increase of the ϕ value.^[206] A dramatic enhancement of ϕ would most possibly indicate the presence of an additional photoinduced electron transfer processes occurring between compound **173** and C₆₀, which are attenuate in the segregate crystals of the molecular components. Notably, one can observed that the lifetime of the charge-separated species (Figure 2.50) for the cocrystals displays higher values, thus pointing out toward the presence of additional charge-separated states.

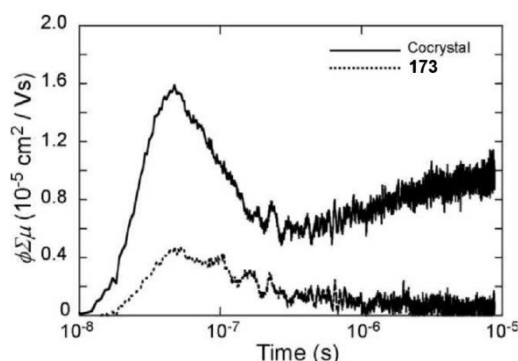


Figure 2.50 TRMC transient decay profiles of the cocrystal (solid) and powder of **173** alone (dot) under excitation at $\lambda_{exc} = 266 \text{ nm}$.

Theoretical investigations (as obtained by DFT level of approximation using M06 exchange-correlation functional and the 6-311G* basis set, Figure 2.51) has shown that borazine **173** has a band gap of 5.8 eV and possess appropriate HOMO and LUMO energy levels to allow photo induced electron transfer from the borazine to C₆₀. In fact, the borazine-centered LUMO is 3.1 eV higher than the LUMO of C₆₀ (Figure 2.51c).

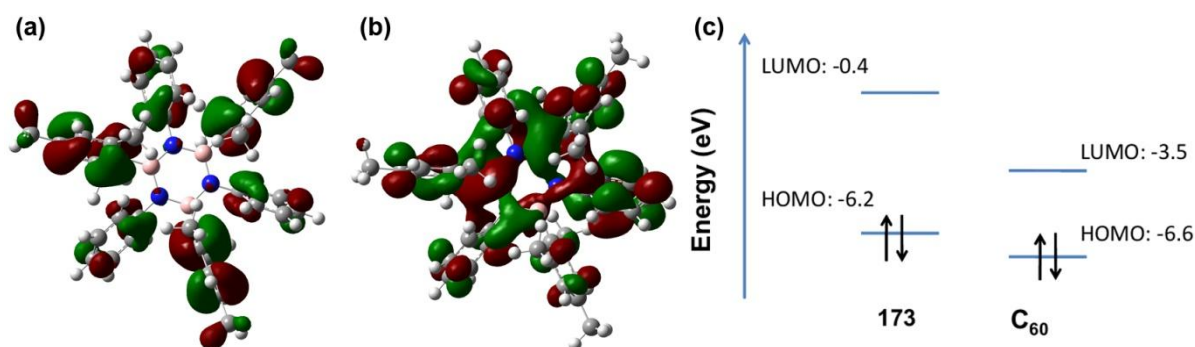


Figure 2.51 (a) HOMO localization. (b) LUMO localization. (c) Energy level of B-trimesityl-N-triphenylborazine **173** and C₆₀.

2.8. Conclusion and Outlooks

With the initial aim of synthesizing stable substituted hexaarylborazine derivatives, the synthesis of hexaphenylborazine **169** was described. Unfortunately, it was demonstrated that hexaphenyl borazine **169** can be degraded quickly, when purified using standard protocols, such as aqueous workup. Hence, the research was focused on the synthesis of sterically hindered derivatives in order to demonstrate the importance of steric hindrance to protect the boron atoms against nucleophilic attack that would lead to borazine cycle degradation. Hence, borazine derivatives **173** and **176** were synthesized and isolated prior to purification by standard silica gel chromatography techniques, proving their stability. Furthermore, crystal structures obtained were investigated and the analysis has clearly pointed out the role of the methyl groups of the mesitylene moieties for steric hindrance around the boron atoms, consistent with the stability toward moisture observed in solution. A detailed crystal structure study has allowed the discovery of several polymorphs whose photophysical properties were studied in detail.

With the aim of increasing the steric protection around the boron atoms, the corresponding borazine could not be obtained but borazene were surprisingly isolated. These observations outline the delicate balance between the steric protection needed and the synthetic accessibility of the borazine. Interestingly, the electronic properties of these boron-nitrogen-doped analogues of butadiene were not deeply studied neither described in the literature. This was out of the range of this thesis but it will be explored in the future. Finally, this discovery and the hypothetical synthetic pathway have turned our focus onto the synthesis of differently substituted borazine **194**. This discovery allows more synthetic versatility for the synthetic pathway previously used for the synthesis of C_3 -symmetry borazine only.

The photophysical study of hexaphenylborazine **169** and its comparison with the one of hexaphenylbenzene has been probed and the measurements revealed that the doping effect is weak, a 4 nm hypsochromic shift. Nevertheless the fluorescence quantum yield improved slightly. The fluorescence of sterically protected borazine was investigated in solution and in the solid state. The fluorescence quantum yield in solution revealed to be improved for B-trimesityl-N-triphenylborazine **173** (7%), compared to hexaphenylborazine **169** (1.5%). Although the quantum yield of fluorescence is modest, the solid state fluorescence study revealed an increase quantum yield of 22%. The different polymorphs of B-trimesityl-N-triphenylborazine display diverse wavelengths of fluorescence due to their different packing arrangement, with a fluorescence emission in the UV ranging from 307 nm to 362 nm.

In order to probe the contact between the metallic electrode of the OLED and the borazine, a STM study of borazine physisorbed on Cu and Au surfaces was performed. Au is a commonly used cathode for organic emitters having a high LUMO position, as for our borazine derivatives. Hexasubstituted borazines, chiral molecules in the solid state as probed by means of X-ray diffraction, forms chiral objects, when adsorbed on chiral surfaces; whereas differently substituted borazine is deprotonated when adsorbed on Cu surfaces and forms regular hexagons. The fundamental part of this work on molecules deposited on surfaces that indicate preferred chiral helices shape could be used in future applications to transfer the chirality in the second dimension, by seeding the surface with one enantiomer^[207] or by preferred orientation of the molecular packing,^[208,209] or into the third dimension,^[210] such as to induce asymmetric growth of crystals.

Having completed the photophysical and surface study of borazine derivatives, the derivative possessing the highest quantum yield in the UV region was selected and inserted into the emissive layer of an OLED. As the fluorescence quantum yield of borazine **173** was low, the OLED devices revealed a good conductivity but a weak emission. However, the emission profile indicated an emission in the visible range. The reasons of the difference between the emission profile at the solid state and the electroluminescence profile remain unclear. As it was observed for the solid state emission, small differences between structural arrangements can lead to an important bathochromic shift of the emission profile (Figure 2.36). Hence it cannot be ruled out that a different arrangement in the OLED could explain this shift. Also, the molecule could have

Chapter 2

degraded into the device. Several technical difficulties have to be overcome for future devices, such as a UV transparent anode and appropriate electron and hole transporting materials matching the borazine HOMO-LUMO levels.

Finally, interactions between borazine **173** and C₆₀ in the crystalline solid state have been studied for the first time. The observed tendency to co-crystallize, together with the decrease in luminescence intensity, provides good evidence for a strong interchromophoric interaction in the solid state between the fullerene and the borazine modules.

3. Boronic Acid Derivatives as new Scaffold for H-Bonded Supramolecular Architectures

This chapter was achieved thanks to a great help from Florence Valtin, Master Student during the last year of my Ph. D. Federica De Leo performed the calculations on boronic acids conformations and complexation enthalpy displayed in Scheme 3.12. Finally, Benoît Georges did the last steps of the synthesis of the diboronic acid derivative exemplified in Scheme 3.21.

The main objective of this chapter is to give a detailed description of the hydrogen bonding properties of boronic acids as a fundamental study, for later use in supramolecular applications. Due to the fact that the definition of the hydrogen bond is subject to debate, the evolution of the successive definitions will be initially reviewed. Furthermore, the characteristics and properties of the hydrogen bond complexes formed and the analytical techniques used to probe them will be described. Boronic acids are able to form hydrogen bonds and can act as DD (Donor-Donor), DA (Donor-Acceptor) or even AA (Acceptor-Acceptor) systems. In the second part of the introduction, the features of boronic acids, their equilibrium with their anhydride and their hydrogen bond properties are exemplified.

Hence, the first objective of this section of the project is to quantify the binding constant and the thermodynamics parameters of complexes formed between boronic acids and hydrogen bond acceptors. To this end, the results and discussion section was divided in four parts. Firstly, the synthesis of boronic acids derivatives, suitable to act as hydrogen bond donors, is described in *section 3.2.1*. In addition, boronic acids are known to be in equilibrium with their anhydrides or boroxine form, which cannot form hydrogen bonds. Boronic acids can be distinguished from their anhydride forms by ^1H NMR spectroscopy. Therefore, this equilibrium and the parameters influencing the latter were studied and are detailed in *section 3.2.2*. In *section 3.2.3*, the geometry, stoichiometry and bond lengths of boroxines, self-interacting boronic acids and in complex with acceptors were studied in the solid state by means of X-ray diffraction. Finally, the binding constant of boronic acids derivatives, in complex with 1,8-naphthyridine, were measured by Isothermal Titration Calorimetry (ITC) and are the subject of the last section.

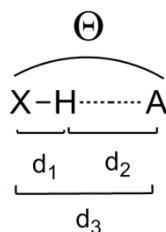
3.1. Introduction

3.1.1. Hydrogen Bonds Features

3.1.1.1. Hydrogen Bond Definition

The discovery of hydrogen bonding cannot be credited to one author. The definition of the hydrogen bond as a directional association between an electronegative atom having a lone pair (the acceptor, A, Scheme 3.1) and a hydrogen linked to a second electronegative atom (the donor, X, Scheme 3.1) was first established in the 1930s by Pauling.^[211] However, the ‘discovery’ of the hydrogen bond interaction can be traced back to 1823, with Faraday studying chlorine hydrate.^[212] The presence of a hydrogen bond can be identified in crystal structures by looking at the distance, between the hydrogen atom and the acceptor (d_2), and at the angle (Θ) formed. However, the experimental values considered for these parameters to determine the hydrogen bond interaction are subject to debate.^[213] In this section, their role will be clarified by considering the successive definitions of the hydrogen bond. Several symbols have been reported in the literature to schematically represent the acceptor and the donor of hydrogen bond. The first literature reports refer to the donor as A (as acid) or X (as an electronegative atom) and the acceptor as B (as a base) or A (as an acceptor). During this thesis, the letter X (representing the hydrogen bond donor) and A (representing the hydrogen bond acceptor) will be used in the general representation of hydrogen bond interaction (Scheme 3.1).

Chapter 3



Scheme 3.1 Representation of a hydrogen bond interaction. X: donor, A: Acceptor. d_1 : donor-hydrogen distance. d_2 : distance of the hydrogen bond interaction from the hydrogen to the acceptor. d_3 : distance of the hydrogen bond from heteroatom to heteroatom. Θ : angle of the hydrogen bond.

The definition of the hydrogen bond changed over time from the first definition from Pauling^[211] in 1931:

‘hydrogen bonds are formed with fluorine supports an ionic structure for HF [and] to some extent by oxygen ((H₂O)_x, ice, etc.) and perhaps also in some cases by nitrogen. The electrostatic structure for the hydrogen bond explains the observation that only these atoms of high electron affinity form such bonds’

This was followed by the definition of Allen^[214] in 1972:

‘Atoms with electronegativity greater than hydrogen have the capability of forming A-H···B hydrogen bonds if B has an unshared pair of electron ...’

Allen’s definition was based on the spectroscopic evidences of hydrogen bond reported in the literature and measured by crystal structures, IR, UV-Vis absorption, and NMR spectroscopy. Hence, it was observed that when a hydrogen bond was present, the crystal structure indicated a d_3 distance shorter than the van der Waals radii. In addition, the IR spectroscopy indicated a X-H stretch lower in frequency in the complex than for the free molecule. This proved the weakening of the X-H bond upon hydrogen bond formation. Moreover, NMR spectroscopy indicated a downfield shift of the X-H proton upon hydrogen bonding. Finally, the UV-Vis absorption spectra of ketone involved in hydrogen bond revealed a blue shift in the $n-\pi^*$ transition, whereas a red shift in the $\pi-\pi^*$ transition of aryl substituting hydrogen bonded groups is observed.

More recently, Desiraju^[215,216] participated to the last hydrogen bond definition elaborated by IUPAC;^[217] the novelty of which is outlined here:

‘The hydrogen bond is an attractive interaction between a hydrogen atom from a molecule or a molecular fragment X–H in which X is more electronegative than H, and an atom or a group of atoms in the same or a different molecule, in which there is evidence of bond formation.’

The differences in the spectroscopic evidence are, for example in crystallography, that the cut-off distance is no longer limited to a distance shorter than the sum of the van der Waal radii. Although, the angle of the hydrogen bond must be close to 180° for short distance hydrogen bond. An additional important criterion is that the Gibbs energy (ΔG) of formation for the hydrogen bond should be greater than the thermal energy of the system for the hydrogen bond to be detected experimentally.’

The features of hydrogen bonds, strengths, geometry and distances are discussed more extensively in the following sections.

3.1.1.2. Hydrogen Bond Strength

The energy of the hydrogen bond interaction is between 0 and 167 kJ mol⁻¹. Hence, hydrogen bonds can be classified depending on their specific energies into strong, normal or weak hydrogen bonds. Firstly, hydrogen bonds can be

Chapter 3

characterized as weak when the energy is below 16 kJ mol^{-1} , such as for a ketone interacting with an aniline derivative, where the donor is slightly more electronegative than the hydrogen atom, and therefore weakly polarized. Secondly, if the interaction is similar in strength to the one between two H_2O molecules, the energy being between 16 and 62 kJ mol^{-1} , they can be described as normal hydrogen bonds, in particular boronic acids or carboxylic acids dimers. Finally, if the energy of the interaction is superior to 62 kJ mol^{-1} , such as for an $\text{N}^+\text{-H}\cdots\text{O-P}$ bond or any complexes where the donor is electron deficient (*e.g.* an ammonium) and the acceptor has excess of an electron (*e.g.* a phosphate), the hydrogen bond is described as strong.^[213,218] The energy of the hydrogen bond interaction is related to several factors. Firstly, the attractive Coulombic interaction between the partial positive charge on the hydrogen atom and the partial negative charge on the acceptor atom is directly dependent of the distance of the hydrogen bond (d_2 , Scheme 3.1). The other parameters are the polarization (E_{pol}), the charge transfer (E_{ct}), the dispersion force (E_{disp}) and the exchange repulsion (E_{er}). The energy of all these parameters varies differently with the distance (r) and the angle of the hydrogen bond. The energy of the interaction decreases rapidly in the following order: Coulomb force decreases as r^{-2} , the polarization term as r^{-4} , and the charge transfer even faster as e^{-r} . The charge transfer consists of the transfer of the lone pair of the donor into the empty σ^* orbital of the X-H bond (Scheme 3.1). The E_{disp} decrease as r^{-6} and the E_{er} increase sharply with reducing distances as r^{-12} , these two latter terms are combined in a ‘van der Waals’ interaction model approximately described by the Lennard-Jones potential.^[213] Depending on the hydrogen bond strength, some parameters dominate in the interaction. The coulombic interaction is the most important parameter in strong hydrogen bonds, while van der Waals interactions are the driving force in weak hydrogen bonds. The varieties of interactions encompassed in the ‘hydrogen bond’ render its definition difficult, as outlined earlier. Nevertheless, Hunter^[219] developed a semiquantitative method to include all these parameters in a single measurable parameter. This can be accomplished by calculating the molecular electrostatic potentials surfaces (MEP), which are plotted on the van der Waals surfaces. Assuming that repulsion, induction and dispersion parameters have negligible effect on the intermolecular interactions, the relationship between the association constant and the dominant electrostatics interactions can be summarized in Equation 3.1.^[220] The association constant can therefore be predicted by calculating the electrostatic charge on the hydrogen bond donor (α parameter) and the one on the acceptor (β parameter).^[219]

$$\log K_a = c_1 \alpha^H \beta^H + c_2$$

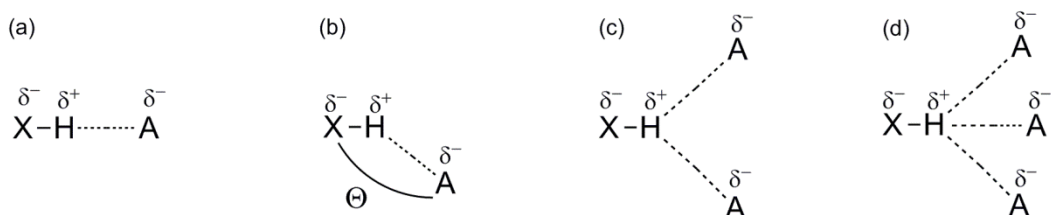
Equation 3.1 Relationship between the association constant (K_a) and the electrostatic charge on the hydrogen bond donor (α), the electrostatic charge on the hydrogen bond acceptors (β), the polarity of the solvent (c_1) and finally the interactions between the two molecules involved in the complexes (c_2).

Solvents also play a role in hydrogen bond strength, as evidenced by the c_1 parameter in Equation 3.1. Polar solvents able to form hydrogen bonds, such as DMSO ($\alpha = 2.5$, sulfoxide group: $\beta = 8.9$), CH_3CN ($\alpha = 1.7$, nitrile group: $\beta = 4.7$), and even CH_2Cl_2 ($\alpha = 1.9$, $\beta = 1.1$) decrease the strength of the interaction by competing with the donor or the acceptor. In contrast, apolar solvents which form weak hydrogen bond complexes, such as benzene ($\alpha = 1.0$, $\beta = 2.2$), favor hydrogen bond assemblies.^[213,219,221]

Finally, the electronegativity of the substituents can also modify the hydrogen bond strength. Electronegative substituents placed on the hydrogen bond donor increase its acidity, *i.e.* the partial charge on the hydrogen atom related to the α parameter. At the contrary, electron donor groups are better placed on the acceptor to enhance its electron density (β parameter). For example, EtOH ($\alpha = 2.7$) is a weaker hydrogen bond donor than perfluoroethanol ($\alpha = 3.7$) in the same manner that perchloroethylacetate ($\beta = 4.5$) is a weaker hydrogen bond acceptor than EtOAc ($\beta = 5.8$).^[222] In conclusion, the energy of the hydrogen bond can be correlated with the pKa value of the donor and the acceptor. The strength of the interaction being increased when the pKa value of the donor and the acceptor are similar, as evidenced by detailed crystallographic and gas-phase bond dissociation enthalpy studies.^[218]

3.1.1.3. Hydrogen Bond Geometry

Hydrogen bonds are a directional interaction. As a result, the angle of the hydrogen bond has a strong influence on the interaction strength (Scheme 3.2). In particular, when the angle is between 90° and 130° the hydrogen bond is usually weak (Scheme 3.2b) while if this angle is closer to 180° , the interaction is strong (Scheme 3.2a). This can be explained by taking into consideration the dipole interactions between the donor and the acceptor. Thus, the repulsion between the two negatively polarized atoms is reduced when the positively charged hydrogen is right between them (Scheme 3.2a).^[213] Exceptions to the preference of linear geometry, exist for hydrogen atoms bonded to two (bifurcated hydrogen bond, Scheme 3.2c) or three acceptors (trifurcated hydrogen bond, Scheme 3.2d).



Scheme 3.2 Representation of different types of hydrogen bonds. (a) Linear hydrogen bond. (b) Bent hydrogen bond. (c) Bifurcated hydrogen bond. (d) Trifurcated hydrogen bond.

Hydroxyl moieties are an important supramolecular synthon for hydrogen bonding, since they can act as hydrogen bond donors or acceptors.^[223] More precisely, hydroxyl moieties bound to a carbon atom, as in alcohol functional moieties, are present in several drugs and carbohydrates. For example, alcohol functional moieties are present in 33 of the top 100 prescribed drugs,^[223] whereas mannose bind through hydrogen bond to C-type lectins, which determine the immune response to pathogens.^[224] More specifically, it is known that alcohol derivatives can form hydrogen bonds with pyridine derivatives, revealing a preference for heterosynthon formation rather than self-interaction with hydroxyl groups.^[223,225] Their ability to act as hydrogen bond donors or acceptors and their hydrogen bond formation with pyridyl derivatives is similar to the features observed for the hydroxyl group of boronic acid derivatives.^[225] Boronic acid possesses two hydroxyl moieties bound to a boron atom. In the aim to observe the differences in angles and bond lengths in hydrogen bonds formed by the hydroxyl moieties of the boronic acids, and self-interacting hydroxyl functional groups, linked to a carbon atom, these data had to be compared. Hence, the data have all been extracted from the Cambridge Structural Database (CSD) with several research filters. Firstly, a search was performed on structures possessing the hydroxyl functional group but by withdrawing the structures containing carboxylic groups. This is due to the fact that the hydrogen bonds formed by carboxylic moieties are not similar to the one of boronic acids, owing to the fact that the carboxylic acid can be easily deprotonated by the hydrogen bond acceptor. Moreover, a second search was performed on the structures collected. This initially involved separating the structures solved by neutron diffraction, to assess precisely the position of the hydrogen atoms (Figure 3.1a and c) and then identical search was performed on structures solved by X-ray diffraction (Figure 3.1b and d). Furthermore, the same search pattern was performed for boronic acid groups. Unfortunately, structures containing boronic acid groups have not yet been solved by neutron diffraction. Therefore, only the structures solved by X-ray diffraction regarding boronic acids were collected in order to be compared with the structures of compounds with hydroxyl moieties solved by the same method. Finally, attempts were made to compare boronic acids to the analogous *gem*-diol. However, due to the reduced number of crystal structures containing *gem*-diol groups, the comparison was abandoned.

The sets of data obtained by neutron and X-ray diffractions revealed identical trend for the angles and distances observed for alcohol moieties implied in hydrogen bonding. Two maxima in the angles distribution, at 110° and 170° are observed while two sets of distances can be distinguished. The first set corresponds to a hydrogen bond distance between 1.6 and 2.2 Å, related to a hydrogen bond angle above 150° . The second set corresponds to a more distant contact, with a bond distance above 2.8 Å and an angle below 130° .

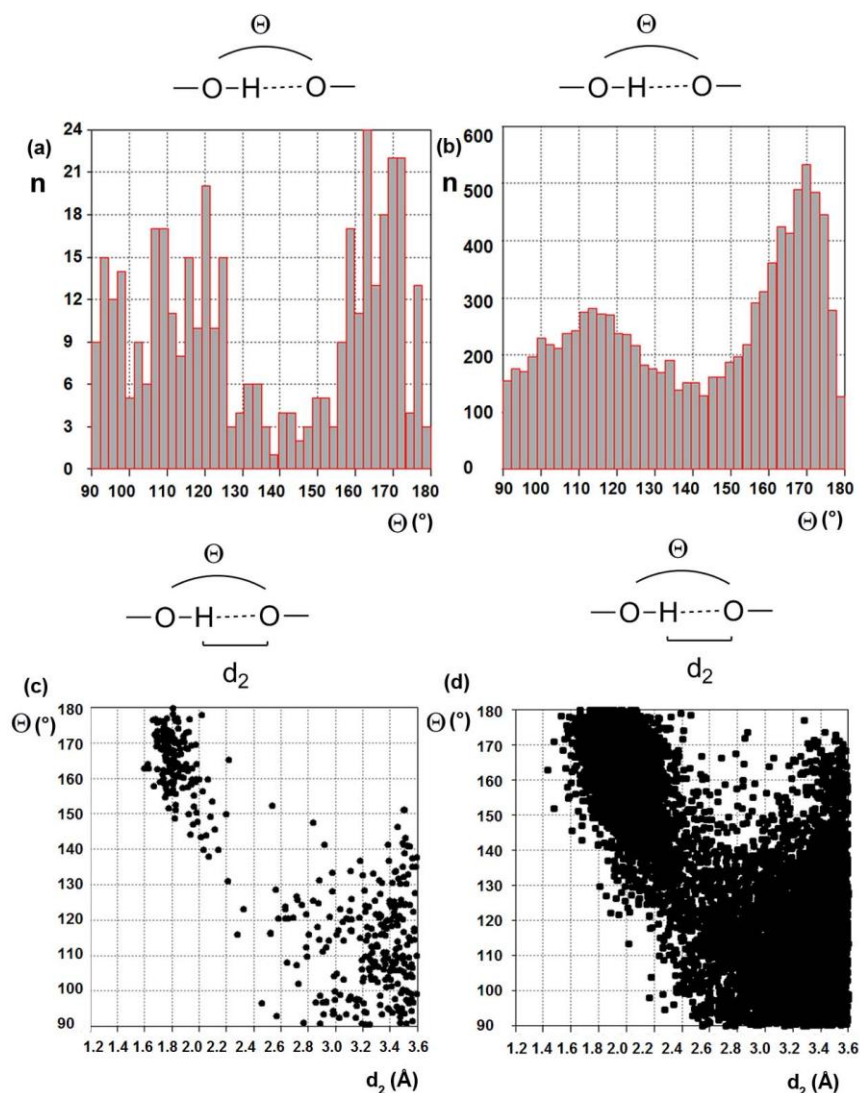


Figure 3.1 Comparison of the data collected by neutron diffraction and X-ray diffraction for hydroxyl group involved in hydrogen bond with another hydroxyl group: bond angles (a) obtained by neutron diffraction; (b) obtained by X-ray diffraction. Maxima are observed at 110° and 170° in both cases. Distribution of the hydrogen angle bond vs. the distance between the donor and the acceptor for hydroxyl group involved in hydrogen bond with another hydroxyl group: (c) obtained by neutron diffraction; (d) obtained by X-ray diffraction.

Furthermore, the data obtained by X-ray diffraction for hydroxyl groups were compared to those measured for boronic acid groups and are presented in Figure 3.2-3.4. The crystalline structures analyzed for boronic acids are related to two types of hydrogen bonds. Firstly, self-interacting boronic acids were studied and secondly the hydrogen bonds formed with nitrogen atoms as acceptors (both this types will be discussed in detail in *section 3.2.3*) were considered. Although, boronic acids are also known to interact with carboxylate moieties (9 examples in the CSD database) phosphate derivatives (2 examples in the CSD database) and other acceptors, the few occurrences did not allow the rational exploitation of the statistics.

Figure 3.2 represents the repartition of number of crystalline structures formed as a function of the angle between donor and acceptor, for (a) hydroxyl groups, (b) self-interacting boronic acids and (c) boronic acids forming hydrogen bonds with nitrogen atoms. In Figure 3.2a, there is a minimum at 140° and two maxima at 110° and 170°, indicating the directionality of the hydrogen bond. A similar trend is presented in Figure 3.2b, where boronic acids form hydrogen bonds with themselves, with a minima at 150° and two maxima at 130° and 175°. Moreover, when the boronic acid is involved in a hydrogen bond

Chapter 3

with a nitrogen atom as acceptor (Figure 3.2c), the small number of structures available in the literature does not allow to draw a definite conclusion, but most of the complexes are forming an angle above 130° .

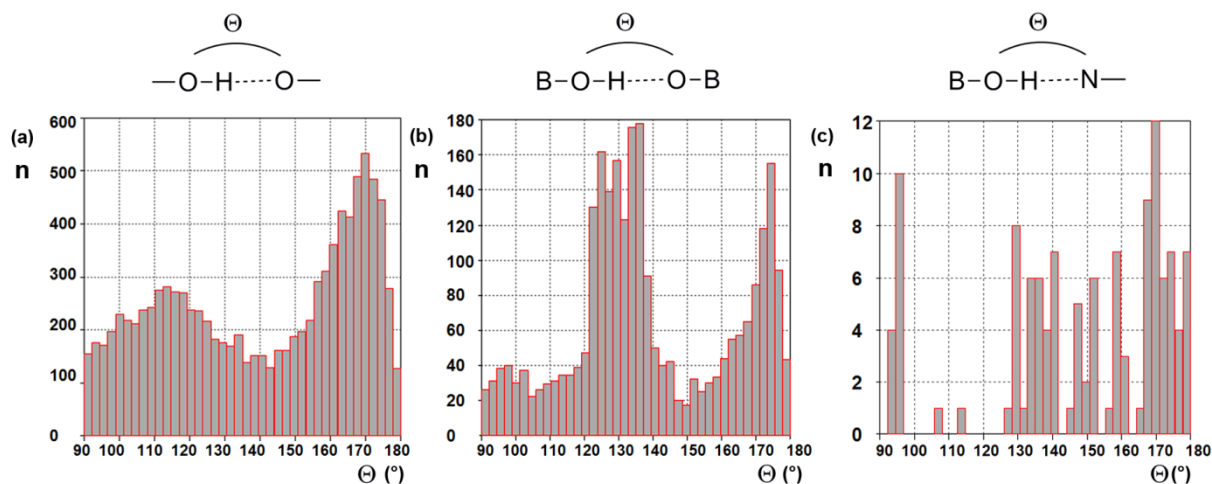


Figure 3.2 Repartition of the number of crystalline structures formed vs. the angle between the donor and the acceptor for (a) hydroxyl group involved in hydrogen bond with another hydroxyl group, maxima are observed at 110° and 170° ; (b) for boronic acid involved in a O-H--O bond, the optimum angles are 130° and 175° ; (c) for boronic acid involved in a O-H--N bond, no optimum angle is observed. Data from CSD.

The angles formed by the hydrogen bonds can also be plotted vs. hydrogen bonds distances (Figure 3.3). The highest number of structures forming hydrogen bond between hydroxyl moieties (Figure 3.3a), having short d_2 distances, is found for an angle above 140° proving the directionality and the preference for the linearity for the hydrogen bond. Finally a second category is found in longer distances (superior to 2.5 \AA) where the angle formed by the hydrogen bond is low (between 90° and 140°). Regarding the boronic acids, two groups can be distinguished whether the boronic acid is involved in a hydrogen bond with an oxygen atom (Figure 3.3b) or a nitrogen atom (Figure 3.3c) as acceptor. The first group is between 1.6 and 2.2 \AA , and corresponds to angles between 140° to 180° . The second group, above 2.7 \AA , corresponds to random contacts without any directionality, as observed with the angles below 140° for hydroxyl moieties. This indicates that the linear hydrogen bonds have the shortest d_2 distances and are the most frequent crystalline arrangements for short hydrogen bond distances.

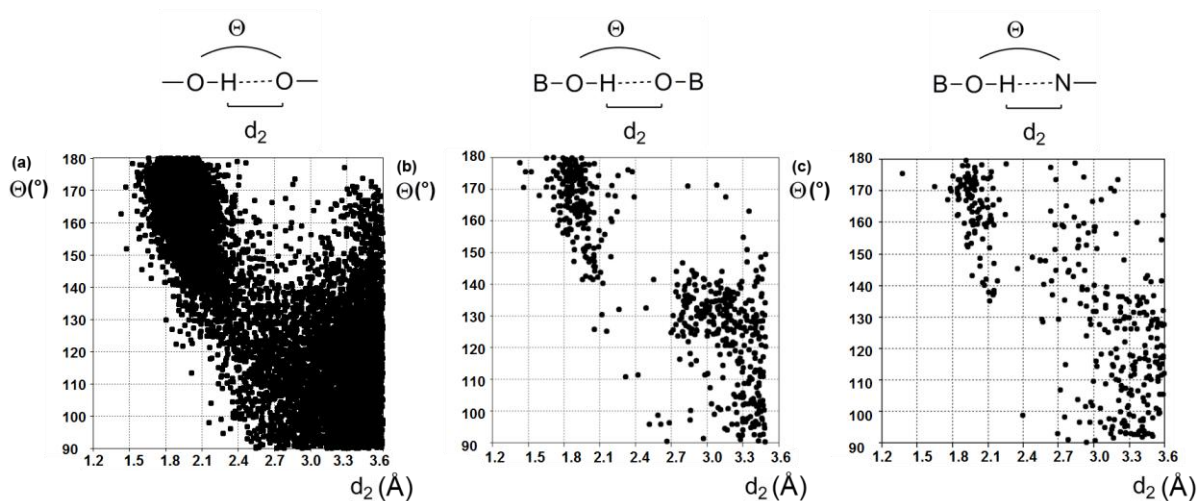


Figure 3.3 (a) Distribution of the hydrogen bond vs. the angle and the distance between the donor and the acceptor for hydroxyl group involved in hydrogen bond with another hydroxyl group; (b) for boronic acid involved in a O-H--O bond; (c) for boronic acid involved in a O-H--N bond. Data from CSD.

3.1.1.4. Hydrogen Bond Distances

Figure 3.4 represents the variation of the distance between the oxygen and the hydrogen atoms of the hydroxyl moieties (d_1) vs. the H-O distance (d_2) of both alcohol moieties implied in hydrogen bonding and in boronic acids. These latter data were taken from the CSD database, from X-ray diffraction analysis, as no neutron diffraction study has been performed to assess the exact d_1 and d_2 distances for boronic acid involved in a hydrogen bond. Two distinct groups can be observed in Figure 3.4a, one from 1.6 to 2.4 Å, corresponding to the group identified in Figure 3.3 for short hydrogen bonds with a high directionality. The other group corresponds to more distant intermolecular interactions, above 2.7 Å (Figure 3.4a). In this two groups, the donor-hydrogen distance varies from 0.6 to 1.2 Å, with an average distance between 0.8 and 1.0 Å. The distribution of the distances is similar for the hydrogen bond implying a nitrogen atom as the acceptor (Figure 3.4b). Similar observation can be made for the hydrogen bond formed by boronic acids interacting with themselves (Figure 3.4c) or with a nitrogen atom (Figure 3.4d). The first group is between 1.6 and 2.2 Å (Figure 3.4c and d) while the second above 2.8 Å which is an interaction without directionality as shown in Figure 3.3. The oxygen-hydrogen distance (d_1) of the hydroxyl group of the boronic acid is always in the same range of 0.7 to 1.0 Å, meaning that the hydrogen involved in the interactions is not delocalized between the donor and the acceptor.

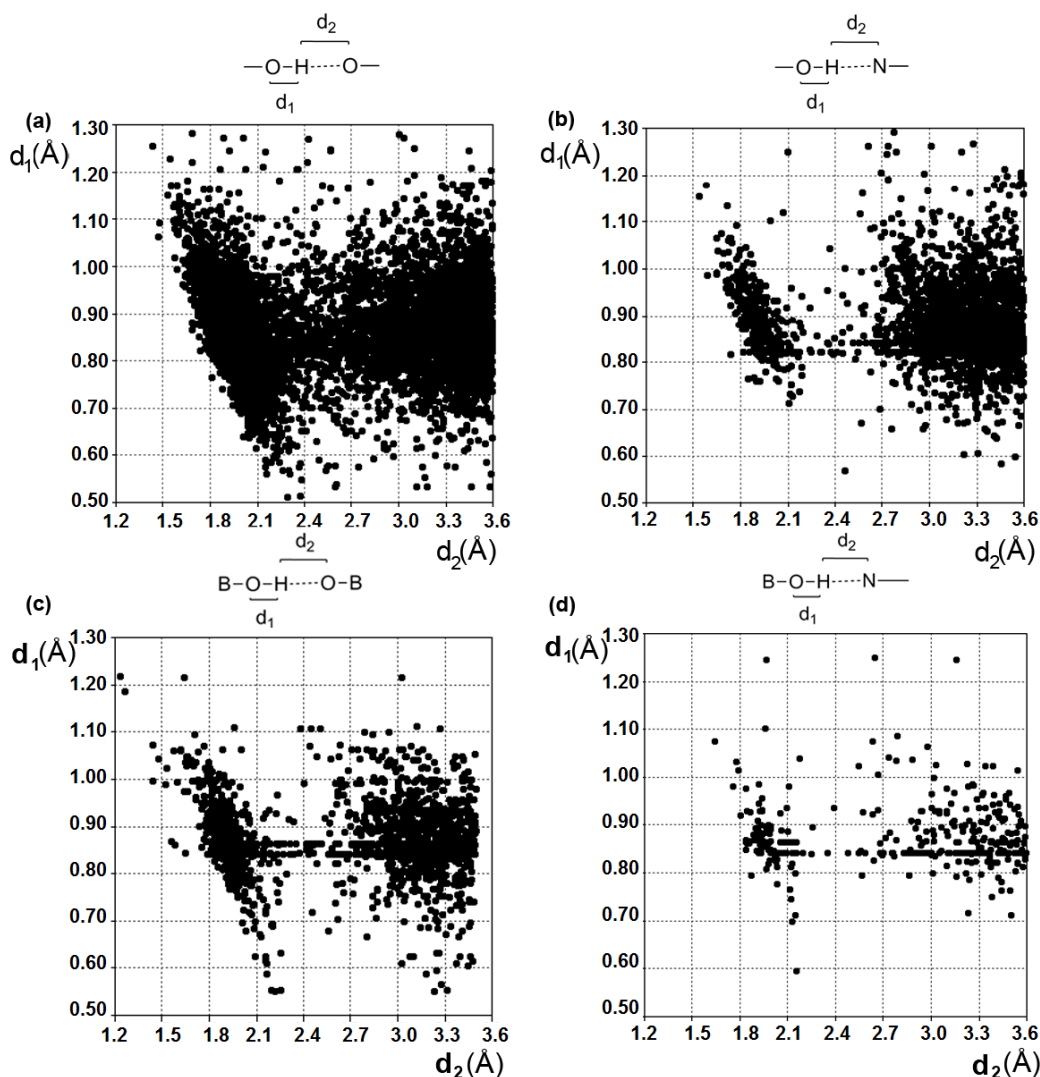


Figure 3.4 a) Variation of the O-H distance vs. the H-O distance in the hydrogen bond of O-H-O for hydroxyl group involved in hydrogen bond with another hydroxyl group.^[213] b) vs. H-N distance in the hydrogen bond formed between an hydroxyl group and a nitrogen atom.^[213] c) vs. the H-O distance in the hydrogen bond formed between boronic acids; d) vs. the H-N distance in the hydrogen bond formed between boronic acids and a nitrogen atom. Data from CSD.

Chapter 3

In conclusion, the boronic acids are able to form highly directional hydrogen bonds as evidenced by angles above 150° for a hydrogen bond distance inferior to 2.4 \AA , for most crystalline structures. Furthermore, the hydrogen atom is tightly linked to the oxygen of the hydroxyl group, as observed for the hydrogen bond formed between hydroxyl groups, linked to a carbon. The only differences of hydrogen bond distance and angles could be explained by the pK_a values of the hydroxyl group, ranging from *para* nitrophenol ($pK_a = 7$) to MeOH ($pK_a = 15$), which means the hydrogen atom is delocalized between the donor and the acceptor moieties, depending on the pK_a of the acceptor. For boronic acid derivatives, the pK_a values are in the same range ($pK_a \approx 8$) with little influence from the substituent (see section 3.1.3).

3.1.1.5 Multiple Hydrogen Bonds

Hydrogen bonds can be classified as single or multiple (Figure 3.5). In the first case a single hydrogen bond occurs when only one hydrogen atom is involved in the hydrogen bond interaction (Figure 3.5a). On the contrary, hydrogen bonds are described as multiple if several hydrogen atoms are organized linearly in a unique recognition moiety (Figure 3.5b and c). The discussion of the current studies will not be extended here on bifurcated and trifurcated hydrogen bonds (Scheme 3.2) since such types of arrangements were not under examination.

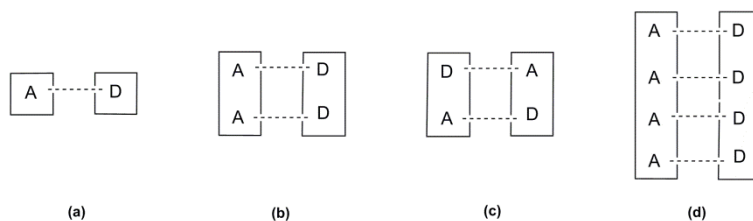
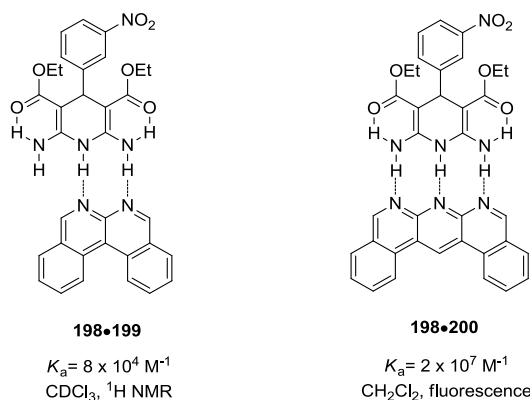


Figure 3.5 Representation of a single (a) and multiple (b, c, and d) hydrogen bonds.

3.1.1.5.1 Effect of the Number of Hydrogen Bonds on the Binding Constant

The first parameter which influences the value of the binding constant is obviously the number of hydrogen bonds formed in the complexes. Complex **198•199** has a binding constant 10^3 times lower than complex **198•200** and this is explained by the formation of an additional hydrogen bond in complex **198•200**. Hence a second parameter which influences the binding constant is the favorable secondary interactions, presented in the next section.



Scheme 3.3 Binding constant for double (**198•199**) and triple (**198•200**) hydrogen bonding.^[226]

3.1.1.5.2. Effect of the Secondary Interactions on the Binding Constant

The stability of complexes formed by multiple hydrogen bonds depends on the spatial arrangement of the donor (D) and acceptor (A) groups. Indeed, secondary interactions (Figure 3.6), and in particular coulombic interactions which are favored between atoms of opposite charge and not favored between atoms of same charge, exist between the heteroatoms involved in the hydrogen bonded contacts. These secondary interactions influence greatly the value of the binding constant. They are

Chapter 3

represented by the Jorgensen model (Figure 3.6),^[227,228] which describes the interactions between the polarized atoms in crossed hydrogen bonds. From this model, the most favorable arrangements can be predicted. As shown in Figure 3.6 these arrangements possess two and four favorable secondary interactions respectively.

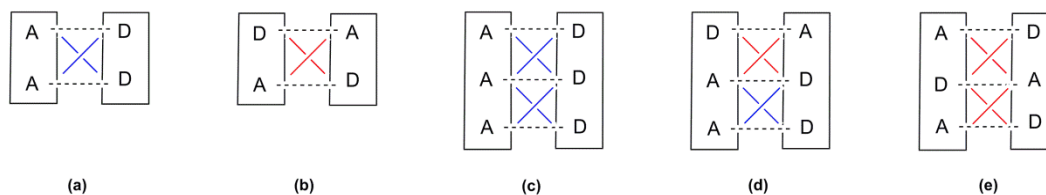
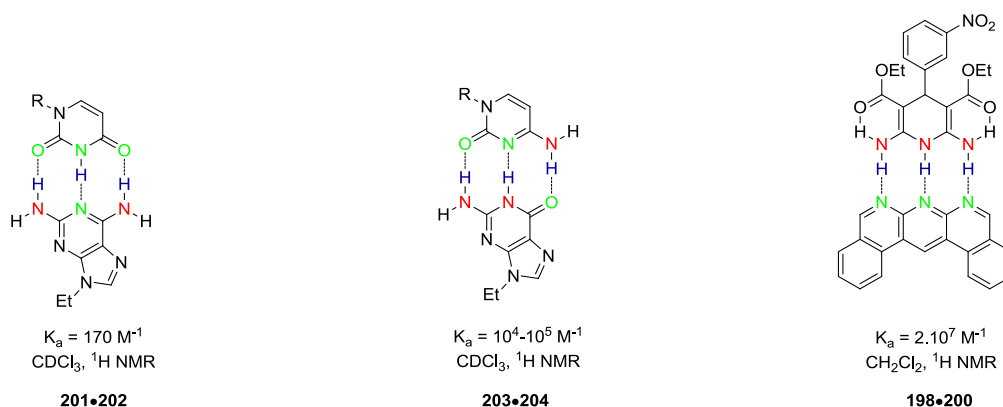


Figure 3.6 Different spatial arrangements possible for double (a, b) and triple (c, d, e) hydrogen bonds. Red: unfavorable secondary interactions, blue: favorable secondary interactions.^[227]

Secondary interactions exert an important influence on the value of the binding constant, as illustrate in Scheme 3.4. The binding constant of a molecule able to form three hydrogen bonds varies from 10^2 to 10^7 M^{-1} depending on the motif of these hydrogen bonds. The lowest value of the constant is observed for complex **201•202** (170 M^{-1} in $CDCl_3$),^[227] having a ADA-DAD arrangement, and an intermediate value is observed for complex **203•204** (10^4 to 10^5 M^{-1} in $CDCl_3$), where the motif is AAD-DDA (Scheme 3.4). The difference of association constant between the two complexes is due to the number and the type of the secondary interactions (Figure 3.6). The first complex has no favorable secondary interactions, and four cross unfavorable secondary interactions, while the second one has two favorable cross secondary interactions and two unfavorable. Moreover, the binding constant is even higher (2×10^7 M^{-1} in CH_2Cl_2) for complex **198•200**, having four favorable cross secondary interactions, as predicted by the Jorgensen model (Figure 3.6c),^[227] consistent with a DDD-AAA arrangement.^[226]



Scheme 3.4 Triple hydrogen bond motif: ADA-DAD (complex **201•202**), AAD-DDA (**203•204**), and AAA-DDD (**198•200**). Color code: red (D) and green (A): negatively polarized atoms; blue: positively polarized atom.^[226-228]

3.1.2. Characterization of the Hydrogen Bond

3.1.2.1. Stoichiometry of the Complexes: Job's plot

The Job's plot is a titration method that allows the determination of the stoichiometry of the complexes formed.^[229] This titration can be performed using different analytical techniques. The possible techniques include UV-Visible, useful for complexes having a change in the absorption spectra upon complexation, and NMR where a change in the chemical shift can be observed. In addition, the stoichiometry can be also determined by ITC, the inflexion point of the curve being where the concentration of the complex is at maxima. The latter technique presents the advantage to allow the measurement of the binding constant (K_a), the enthalpy (ΔH), and the stoichiometry (n) of the complex in one single titration experiment (see section 3.1.2.3., Figure 3.8). The entropy (ΔS) and the ΔG are deduced from the previously determined parameters. An

Chapter 3

overview of the NMR and ITC technique in terms of determining the stoichiometry of the complex will be reported in his section of the introduction. Furthermore, this will be complemented, in the results and discussion part, by experimental results regarding the stoichiometry of boronic acids complexes using the ITC techniques and confirmed by solid state X-ray diffraction analysis in *section 3.4*.

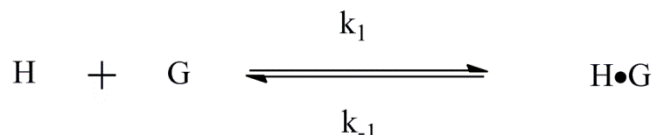
3.1.2.2. Determination of the Thermodynamic Parameters by NMR Spectroscopy

Hydrogen bonds are defined as chemical bonds and can therefore be described by the thermodynamic parameters, ΔG , ΔH , and ΔS , linked by the van't Hoff relation (Equation 3.2). Upon formation of a new hydrogen bond, the ΔH value is augmented, which is reflected by an increase of the K_a , as observed in Scheme 3.3 with 10^3 fold increase of the K_a from complex **198·199** to complex **198·200**.

$$\Delta G^0 = -RT \ln K_a = \Delta H^0 - T\Delta S^0$$

Equation 3.2 van t'Hoff relation between the thermodynamic parameters.

The generation of a complex (H•G) between two species (H and G) is described by the chemical equilibrium reported below (Equation 3.3), where the K_a is proportional to complex concentration and inversely proportional to the concentration of the free species at the equilibrium (Equation 3.4). Some spectroscopic methods, such as UV-Vis and NMR, measure the concentration of the complex and of the free species, permitting therefore the determination of the binding constant (K_a). For slow equilibrium, respective to the NMR timescale, the concentration of the complex and the free species can be measured directly by integration of the signals corresponding to each species and direct comparison to an internal standard. At the contrary, if the equilibrium is rapid, respective to the NMR timescale, and the signals of the guest and the complex are not distinct, the concentration of the complex cannot be measured directly and will be extracted from Equation 3.5 to 3.6.^[230]



Equation 3.3 H: Host, G: Guest, H•G: complex.

$$K_a = \frac{k_1}{k_{-1}} = \frac{[\text{HG}]}{[\text{H}][\text{G}]}$$

Equation 3.4 [H]: concentration of the Host, [G]: concentration of the Guest, [H•G]: concentration of the complex, K_a : binding constant, k: kinetic constant.

If the NMR signals of the host and the guest are not distinct, the concentration of the free species will be measured indirectly. The mass balance relationships are established in Equation 3.5, where the concentration of the free species is equal to the initial concentration minus the concentration of the complex.

$$[\text{H}] = [\text{H}]_0 - [\text{HG}]$$

$$[\text{G}] = [\text{G}]_0 - [\text{HG}]$$

Equation 3.5 [H]: concentration of the Host at the equilibrium, [G]: concentration of the Guest at the equilibrium, [HG]: concentration of the complex, $[\text{H}]_0$: initial concentration of the Host, $[\text{G}]_0$: initial concentration of the Guest.

The titration of the host by the guest is followed by NMR and observed by the change of chemical shift of the host. In a second time, the change of chemical shift ($\Delta\delta$) is plotted vs. the number of equivalent of guest added. The fitting of the curve, using nonlinear least-square method, express by Equation 3.6 allows the evaluation of the unknown association constant (K_a).

$$\Delta\delta = \frac{\Delta\delta_{\text{sat}}}{2[\text{H}]_0} \left\{ \frac{1}{K_a} + [\text{H}]_0 + [\text{G}]_0 - \sqrt{\left(\frac{1}{K_a} + [\text{G}]_0 + [\text{H}]_0 \right)^2 - 4[\text{G}]_0[\text{H}]_0} \right\}$$

Equation 3.6 $\Delta\delta$: difference of chemical shift between the initial signal and the measured signal, $\Delta\delta_{\text{sat}}$: chemical shift observed at saturation, K_a : association constant.

To simplify the resolution of the equation, the titration of the host solution is performed by a guest solution containing the host, so that the host concentration remains constant throughout the titration. The guest concentration inside the NMR tube is therefore defined by Equation 3.7.^[230]

$$[\text{G}] = \frac{V_G \cdot [\text{H}]_0}{V_T}$$

Equation 3.7 V_G : volume of the guest solution, V_T : volume of titrant added.

3.1.2.3. Determination of the Thermodynamic Parameters by ITC

ITC is an analytical method measuring the heat released or absorbed during the formation of a complex and comparing it to a reference cell containing only the same solvent used for the formation of the complex (Figure 3.7).^[231,232] This technique has been used for the determination of binding constant of self-interacting 3,6-diaminopyridazine derivatives,^[233] chloride and bromide anions complexation with cyclohexane 1,3,5-*cis*-trimethanol in water^[234] and DNA base pairs interactions.^[235] The guest is slowly added to the solution containing the host, which lead to the formation of the complex in the cell, releasing or absorbing heat. The outcome of the titration is a curve of the heat release vs. the number of equivalent of guest added (Figure 3.8). The titration allows the direct determination of the ΔH° (heat released at the beginning of the titration), the binding constant (shape of the curve) and the stoichiometry of the complex (inflexion point of the curve) as shown in Figure 3.8. The ΔS and the ΔG are determined from the measured parameters (ΔH° and K_a , Equation 3.2).

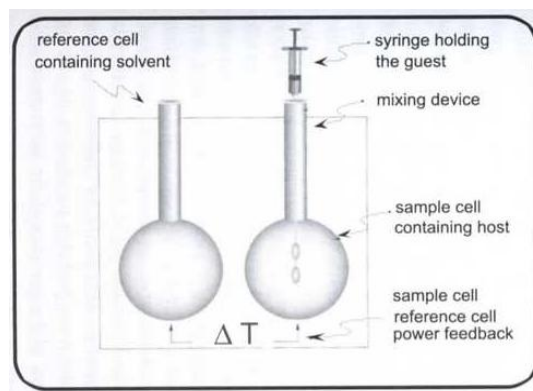


Figure 3.7 Schematic representation of the ITC instrument.^[231] Adapted with permission from the Wiley-VCH Verlag GmbH & Co. KGaA. Copyright 2007.

In Figure 3.8 different exothermic titration curves of ITC are represented. Under ideal conditions a titration should present a sigmoid curve as that depicted in Figure 3.8, curve (b). This allows a precise determination of the ΔH , stoichiometry, and the binding constant. The ΔH is directly measured from the peak height at the beginning of the titration. The stoichiometry is determined by the inflexion point of the curve and the association constant is evaluated by the shape of the curve. Titration of a system having a low binding constant gives a curve similar to (a), where the estimation of the ΔH will be obtained with a low precision. Also, the fitting of the curve will not give a precise estimation of the binding constant and the inflexion point of the curve will not be estimated with enhanced precision. At the contrary, titration of high binding

constant system will give a curve similar to (c), where the ΔH can be measured directly with a high precision and the inflexion point is clearly marked, so as the stoichiometry. However, the binding constant cannot be estimated precisely in this case as the change of slope of the curve at the equivalence is so abrupt that it cannot be fitted with the wished precision.^[236]

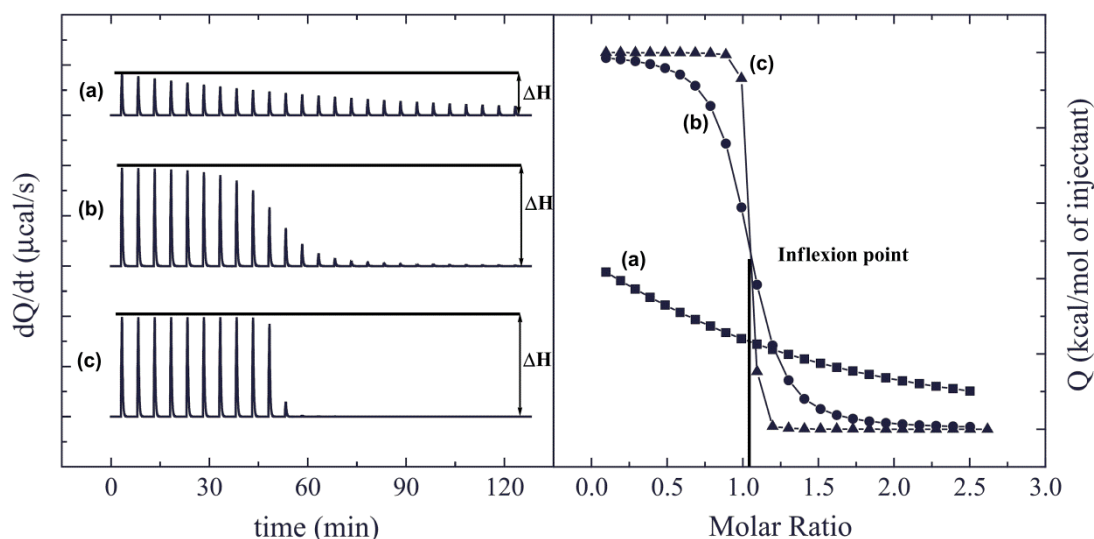


Figure 3.8 Titration curve obtained by ITC, for complexes having (a) a low ($K_a = 10^4 \text{ M}^{-1}$), (b) moderate ($K_a = 10^6 \text{ M}^{-1}$), and (c) high ($K_a = 10^8 \text{ M}^{-1}$) binding constant.^[236] Adapted with permission from the Elsevier. Copyright 2005.

As explained above, the analysis by ITC has to be performed in a certain range of binding constant. It was observed experimentally that dilution of the system can provide the desired sigmoid shape. In fact the concentration, stoichiometry and the binding constant are related by Equation 3.8. The ‘c’ value is an experimental constant that has to be between 5 and 500 (Equation 3.8). If the value of the constant ‘c’ is below 5, the characteristic sigmoid curve is not observed and is similar to the one observed in Figure 3.8a. The same problem is posed for a value of ‘c’ higher than 500, where the change at the equivalence is so abrupt that the slope of the curve cannot be plotted (Figure 3.8c). The concentration of the host and the guest in the cell (M_{tot}) can be changed to move the complex’s titration in the experimental windows of the ITC. Nevertheless, a higher M_{tot} will be reflected by a greater value of the heat released, which can be out of the detector range.

$$c = K_a \times M_{\text{Tot}} \times n$$

Equation 3.8 Calculation of the ‘c’ value for ITC. K_a : binding constant, M_{tot} : total concentration of the host and the guest in the cell, n: stoichiometry.

If the ‘c’ value is below 5, the data known by alternative spectroscopic methods, can be implemented into the program to have a better precision on the other parameters.^[237,238] For example, the stoichiometry can be known by crystallographic analysis, assuming that the complexes formed in the solid state will be the same in solution, or by doing a Job’s plot using ^1H NMR. The ΔH of complexation can also be determined by ^1H NMR and these two parameters can be implemented into the program fitting the curve to reduce the number of unknown parameters to one: the association constant. Furthermore, a system with a low association constant means that not all the guests are complexed at the equivalence. So, the titration should be performed until a large excess of guest is injected to drive the equilibrium toward the complexation of the entirety of the host.^[238] These approaches were used during this studies which will be discussed in detail in sections 3.4 and 3.5.

3.1.3. Boronic Acids Features

Since their first synthesis from $\text{B}(\text{OH})_3$ by Frankland in 1860,^[239] boronic acids, a moiety composed of a boron atom linked to a carbon atom and two hydroxyl groups, have been an important functional group for several research fields.^{[11,240-}

Chapter 3

^{243]} The large array of application of boronic acids is bound to the particular topology of this functional group. The boron atom has an empty *p* orbital perpendicular to the plane formed by the other substituents, making it a Lewis acid. This Lewis acidity is exploited in several applications. Firstly, in organometallic chemistry where the Lewis acidity of the boron atom and the capacity to form tetragonal complexes are exploited in the Suzuki-Miyaura coupling, in favor toward the transmetalation reaction step.^[11] Secondly, in biology, boronic acid are used to form stable tetragonal complexes with a free alcohol moiety present in the active site of the enzyme, able to act as antifungal agents^[240] or suicide protease inhibitors.^[241,242] An additional application of boronic acids is as Lewis acids in supramolecular chemistry,^[243] forming reversible tetragonal complexes with pyridine when the hydroxyl group are protected as to form a boronic ester^[244] or with protected phosphine^[245] and unprotected boronic acid.^[245] Another utilization in supramolecular chemistry has been reported by the group of Reetz,^[246] which has proved that the two hydroxyl groups can act as hydrogen bond donors (Figure 3.9).

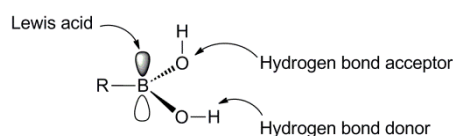
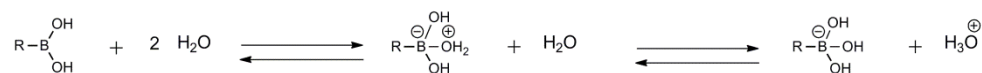


Figure 3.9 Configuration of the boronic acid (R = alkyl or aryl group).

The aim of the present study is the use of boronic acid as hydrogen bond donor and acceptor, ability which is related, as mentioned earlier, to the pKa of the donor and the acceptor.^[218] The pKa value of the hydroxyl group has been measured, by potentiometric titration, and is of 8.8 for phenylboronic acid and of 7.1 for 4-nitrophenylboronic acid, slightly lower than B(OH)₃ (pKa = 9).^[247] The pKa value measured is the one of deprotonation of the tetragonal complex in Scheme 3.5. This explains the weak difference in pKa between boronic acids substituted by phenyl or substituted by 4-nitrophenyl groups. Since the intermediate is tetragonal, no mesomeric effects influence the value of the pKa, which is dependent on inductive effects only.

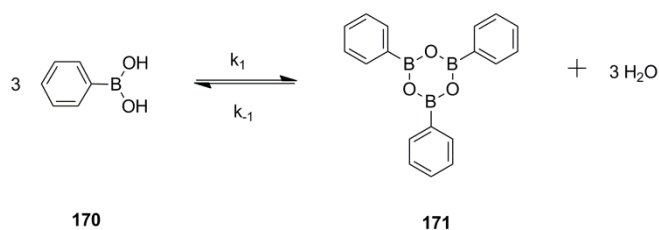


Scheme 3.5 Ionization equilibrium of boronic acid in aqueous solutions as Lewis and Brønsted acid.

3.1.3.1. Boronic Acids-Boroxines

3.1.3.1.1. Equilibrium between Boronic Acid and Boroxine Forms

Boronic acids are in equilibrium with their anhydrides, called boroxines (Scheme 3.6). These six-membered rings, composed of alternating boron and oxygen atoms, are planar and show equalization of the boron-oxygen bond distances. The lone pair of electrons of the oxygen atoms are delocalized in the empty *p* orbital of the boron atoms, which is surrounded by two oxygen atoms, as in the boronic acid form. Nevertheless, there is one mesomeric donor oxygen atom for one boron atom in the anhydride form instead of two in the acid form, increasing the electron affinity of the electrophilic boron atom. Therefore, the presence of an electron donating group on the aromatic ring will favor the formation of boroxine by reducing the Lewis acidity of the boron atom.



Scheme 3.6 Equilibrium between the acid (**170**) and the anhydride (**171**) of phenylboronic acid.^[248]

Chapter 3

Boroxines are used as flame retardant for polystyrene,^[249] since their incorporation results in better heat stability of the polymer, for the formation of COF^[250] (Covalent Organic Framework, as explained in Scheme 3.9), and for charge transporting polymer for lithium battery.^[251] In the latter application, the addition of substituted boroxine enhances the conductivity of electrolyte, by complexation of the anion in solution, therefore reducing the association of ion pair and increasing the number of free charges.^[251]

3.1.3.1.2. Distinction between Boronic acid and Boroxine Forms by Spectroscopic Methods

One possible method for observing the difference of the boron-oxygen bonds between the boronic acid and the boroxine is IR spectroscopy. In the case of the anhydride, the bond has more of a double bond character. For example the stretching frequency of phenylboronic acid is at 1350 cm⁻¹ while the one of the boroxine form is at 1370 cm⁻¹. Moreover, the hydrogen-oxygen bond vibration of the acid is observed at 3280 cm⁻¹, but this frequency overlaps with the one of the oxygen-hydrogen stretching of H₂O and can be misleading if water is present or if the boroxine is highly hygroscopic.^[252] Unfortunately, only a single publication has been reported by Shurvell and co-workers examining precisely the difference in boron-oxygen stretching frequency between the acid and the anhydride.^[252]

Alternatively, the difference of chemical environment between the boroxines and the boronic acids can be probed by the difference of chemical shifts in ¹H NMR spectra of aryl boronic acids, since the equilibrium is slow respective to the NMR time scale.^[253] For instance, the peaks of 4-toluyboronic acid ($\delta_{acid} = 7.23$ ppm and 7.63 ppm, in CDCl₃)^[253] are at lower field if compare to those of the corresponding boroxine ($\delta_{boroxine} = 8.12$ ppm and 7.31 ppm, in CDCl₃)^[253] and this trend is also observed for 3,4,5-trifluorophenylboronic acid ($\delta_{acid} = 7.35$ ppm, in CDCl₃) and its corresponding boroxine ($\delta_{boroxine} = 7.77$ ppm, in CDCl₃)^[254] but the opposite tendency appears for 2,3,5,6-tetrafluorophenylboronic acid ($\delta_{acid} = 7.11$ ppm, $\delta_{boroxine} = 6.74$ ppm, in ether).^[254] Once again, the lack of data reported in the literature does not allow to draw conclusions on the trend of the chemical shifts observed between boronic acids and boroxines.

3.1.3.1.3. Parameters Favoring the Formation of Boroxine

The formation of boroxine is favored from both an enthalpic and an entropic point of view.^[248,255-257] From an enthalpic point of view, three molecules of boronic acid posses six boron-oxygen bonds and six oxygen-hydrogen bonds while the equivalent boroxine posses six boron-oxygen bonds and the three H₂O molecules formed have six oxygen-hydrogen bonds. Therefore, the difference in energy is in the slight change of energy of these bonds. From an entropic point of view, the liberation of three molecules of H₂O in the solvent is highly favored, although the formation of the rigid boroxine cycle reduces the ΔS of the system. One factor can therefore influence the boronic acid/boroxine ratio: the temperature (Equation 3.9). Low temperature, increase the ΔG for the boroxine formation, which in turn favors the acid form, as determined by the group of Tokunaga for heteroboroxine.^[255]

$$\Delta G = \Delta H - T\Delta S$$

Equation 3.9 *G*: Gibbs free energy, *H*: enthalpy, *S*: entropy.

As outlined earlier, boronic acids and boroxines have different chemical shifts in the ¹H NMR, hence the thermodynamic parameters of the equilibrium can be determined by integrating the signals of the ¹H NMR spectra (Equation 3.10).

$$K = \frac{[\text{boroxine}][\text{H}_2\text{O}]^3}{[\text{boronic acid}]^3}$$

Equation 3.10 *K*: constant of the reaction.

Tokunaga and co-workers determined the thermodynamic parameters, by ¹H NMR in CDCl₃, of the boronic acid-boroxine equilibrium for boronic acids substituted by electron donating and withdrawing groups (Table 3.1). From these data,

Chapter 3

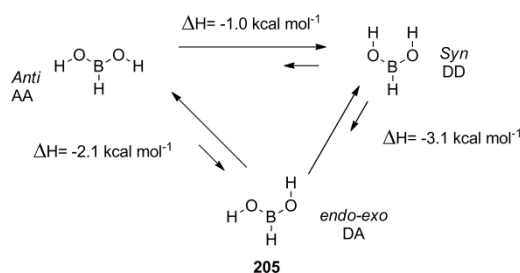
the influence of the substituent is clearly demonstrated. The ΔG values, demonstrates that electrons donating groups, such as methoxy ($\Delta G = -0.83 \text{ kJ mol}^{-1}$) group favors the formation of the boroxine. At the contrary of electron withdrawing groups, such as bromine ($\Delta G = 2.46 \text{ kJ mol}^{-1}$) or ketone ($\Delta G = 5.47 \text{ kJ mol}^{-1}$), which favor the acid form. The enthalpies of formation are always negative and greatly vary depending on the substituents while the ΔS is nearly constant (between 0.08 and $0.16 \text{ J K}^{-1} \text{ mol}^{-1}$). This can be explained by the fact that the major contribution comes from the liberation of three molecules of H_2O and the formation of a planar, rigid, cycle, independent of the substituent properties. The Hammett parameter (σ) was determined and is of course negative for boronic acids substituted by electron withdrawing groups, such as methyl ($\sigma = -0.17$) and methoxy ($\sigma = -0.27$) groups. It is worth noting that the reaction constant has been measured for the formation of a boroxine having a methyl substituent in *ortho* and revealed a K value of 0.28 M^{-1} . This value is lower than the one observed for the derivative bearing a methyl group in *para* position and closer to the one observed for electron withdrawing bromine substituent. This striking difference between the *para* and *ortho* substituted boronic acids was attributed to stereoelectronic effect, due to the fact that the aryl ring is no anymore in the plane of boroxine ring and therefore the conjugation is essentially reduced.^[257]

<i>para</i> substituents	$K (\text{M}^{-1})$	$\Delta G (\text{kJ mol}^{-1})$	$\Delta H (\text{kJ mol}^{-1})$	$\Delta S (\text{J K}^{-1} \text{mol}^{-1})$	σ
H	0.32	2.82	-14.3	0.158	0
Me	0.45	1.98	-15.2	0.175	-0.17
OMe	1.40	-0.83	-8.3	0.127	-0.27
Cl	0.45	1.98	-7.7	0.0782	0.23
Br	0.37	2.46	-10.8	0.116	0.23
COMe	0.11	5.47	-16.4	0.149	0.5

Table 3.1 Selected thermodynamic parameter for the formation of the boroxine cycle.^[257]

3.1.3.2. Conformations of the Boronic Acids

Hydrogen bonds are directional interactions that drive the predictable self-assembly and spatial organization of molecular donors and acceptors, allowing the creation of supramolecular structures. The advantages of hydrogen bonded networks over covalent frameworks are their versatility in strength, tuned by the solvent, the charge, the substituent anchored on the functional moiety, the number of hydrogen bonds involved and finally their motif, as depicted by the Jorgensen model (see Figure 3.6, b and c, DA, DD systems). The hydrogen bond motif is of extreme importance; examples showing dramatic strength changes depending on the hydrogen bond motif abound in the literature (see Scheme 3.4, ADA-DAD, DAD-ADA, AAA-DDD systems). Interestingly, boronic acids demonstrate this versatility by presenting three different conformations, *endo-exo* (DA), *syn* (DD) and *anti* (AA) depending on the involved partner (Figure 3.10, Figure 3.11, Figure 3.12). In the literature, the energies of the three conformations has been calculated for boronic acid **205**, substituted by a hydrogen atom, and reveal the slight difference in energy between the conformations.^[256] The *endo-exo* conformation is the most favorable from an energetic point of view for boronic acid **205**, the repulsion between the two positively charged hydrogen atoms are minimized, as presented in Scheme 3.7. Therefore, this is the conformation adopted in crystal structures of self-interacting boronic acids (Figure 3.10). The *syn* conformation is the most disfavored due to the repulsive interactions between the two positively polarized hydrogen atoms (Figure 3.11). The last conformation (*anti*), is disfavored by the repulsion between the substituent on the boron atom, in this case an hydrogen atom, and the hydroxyl groups. This is the most rare conformation and only three examples, in the solid state, appear in the CSD.^[258-260] In addition this conformation is found when the boronic acid is interacting with a DD hydrogen bond system (Figure 3.12).^[260]



Scheme 3.7 The three different conformations of boronic acid **205** and their respective differences in energy. Calculated by MP2/aug-cc-pVTZ computational level.^[256]

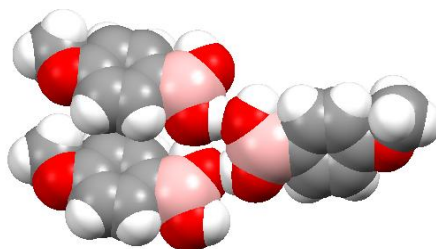


Figure 3.10 Crystalline structure of the complex formed between paramethoxyphenylboronic acids. DA or *endo-exo* conformation of boronic acid interacting, through hydrogen bond interactions with themselves, revealing a 'tapes' arrangement. Color code: red: oxygen, gray: carbon, white, hydrogen, pink: boron. Space group $P2_1/n$.^[261]

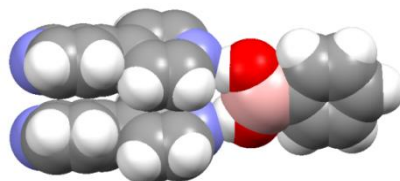


Figure 3.11 Crystalline structure of the complex formed between phenylboronic acid and 4,4'-dipyridyl. DD or *syn* conformation of the boronic acid, interacting with a AA. Color code: red: oxygen, gray: carbon, white, hydrogen, pink: boron, blue: nitrogen. Space group $Fdd2$.^[261]

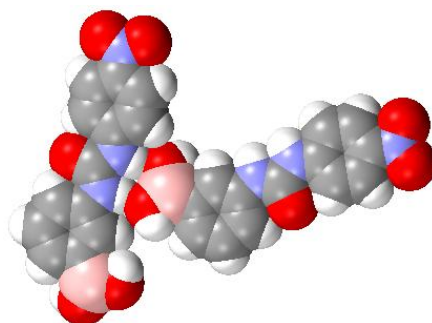
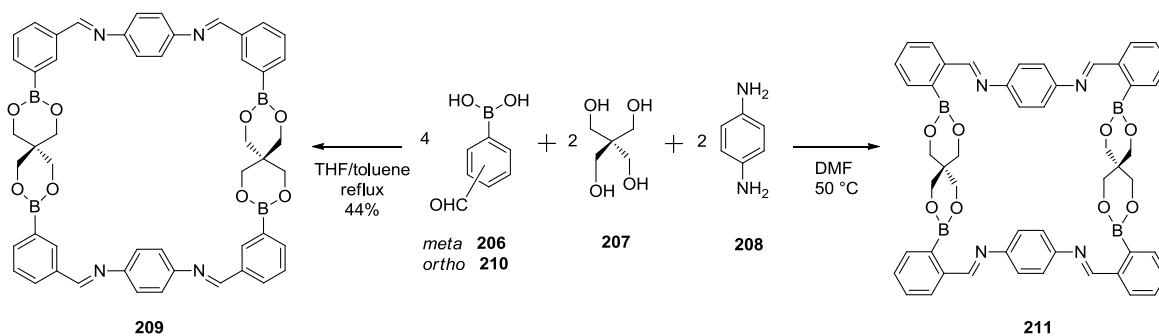


Figure 3.12 Crystalline structure of the complex formed between boronic acid and an urea group. AA or *anti* conformation of the boronic acid, interacting with a DD-type urea moiety. Color code: red: oxygen, gray: carbon, white, hydrogen, pink: boron, blue: nitrogen. Space group $P2_1/c$.^[260]

3.1.3.3. Boronic acids in Supramolecular Chemistry

3.1.3.3.1. Boronic Esters

As outlined in the introduction, boronic acids can form ester bonds with diols and can therefore be used as sugar sensors (compound **12**, Figure 1.5). Exploiting this reactivity, the formation of macrocycles by condensation of boronic acid with an alcohol moiety has been demonstrated. In particular, **206** reacts with pentaerythritol **207** while the aniline moiety of 1,4-diaminobenzene **208** will react with the aldehyde moiety in THF/toluene to form macrocycle **209** (Scheme 3.8).^[262] On the other hand, starting from *ortho* substituted boronic acid **210**, the reaction in DMF leads to macrocycle **211** (Scheme 3.8).^[263]



Scheme 3.8 Synthesis of macrocycle **209** and **211** from boronic acids **206** and **210** respectively.

The advantage of the use of boronic acids is the reversibility of the boronic ester formation allowing the so-called ‘self-healing’ process. This process occurs when reagents are mixed and heated over an extensive period, to give the time to a series of esterification followed by hydrolysis reactions until the desired product is formed. This is of fundamental importance to obtain a majority of macrocycles over polymeric products. These macrocycles form highly porous network which can be of great potential for future sensors or adsorbent applications. The advantage of COF formed of boronic esters over those constituted of boroxines, is the resistance toward hydrolysis, paving the way for their applications in ambient conditions.^[264,265]

3.1.3.3.2. Spiroborates

Spiroborates are tetravalent complexes of boronic esters, where the boron bridges the two rings, forming a tetragonal center analogous to the *spiro* carbon derivatives. Their ease of synthesis from B(OH)_3 and phenol derivatives along with their special geometrical shape make them attractive candidates for utilization in supramolecular chemistry. Starting from chiral (-)-1,1'-bi-2-naphthol **212**, spiroborate **213** is obtained in good yield (Figure 3.13).^[266] The latter, owing to its double bowl shape, forms supramolecular assemblies, with iridium complex **214** which has a ball shape, that result in a temperature-responsive gel (Figure 3.13). The gel formation occurs when heated above 80 °C in HMPA and reverts to solution state rapidly upon cooling.^[266]

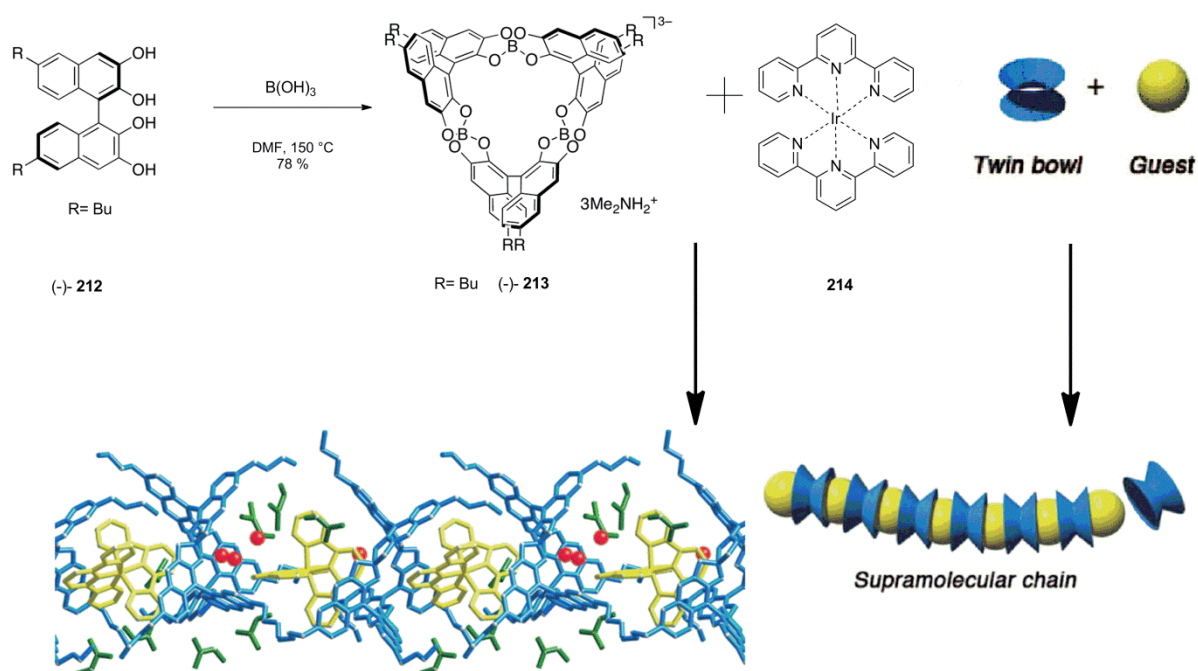


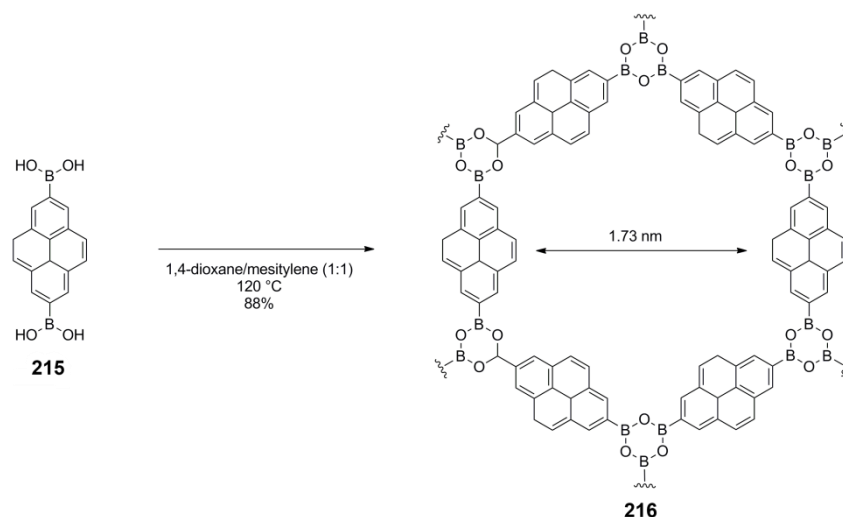
Figure 3.13 Synthesis of spiroborate **213** which forms supramolecular gel with complex **214** upon heating.^[266]

Chapter 3

The supramolecular gel illustrated in Figure 3.13 is one of several applications^[266,267] of spiroborates and pave the way for its use in supramolecular chemistry.

3.1.3.3. Boroxines

As outlined in *section 3.1.3.1*, the formation of boroxine ring is reversible and they are in equilibrium with their corresponding boronic acid. This reactivity has been exploited to build SCOFs (Self-assembled Covalent Organic Frameworks), porous 2D and 3D crystalline materials, whose structure depends on the geometrical properties of the organic angular unit.^[265] In order to have a regular network, the condensation reaction was carried out under reversible conditions (at 120 °C as suspension in apolar solvent) to allow a self-healing process, and thus condensation of compound **215** into the regular porous network **216** (Scheme 3.9). The crystalline structure of **216** has high pore volume ($0.7907 \text{ cm}^3 \text{ g}^{-1}$), thus usable as gas storages or hosts for luminescent molecules.^[268] In particular, hexameric units pile through π - π stacking interactions (intersheets distance: 3.4 \AA) to give an anisotropic, conductive, and fluorescent ($\lambda_{em} = 484 \text{ nm}$, $\lambda_{ex} = 414 \text{ nm}$, solid state) porous material.^[268-270] Notably, when the crystalline structure is excited by polarized light, the emitted light is depolarized due to the exciton migration within the lifetime of the molecular excited state.^[269] An identical synthetic strategy was also used to build fluorescent self-assembling polymers.^[271]



Scheme 3.9 Formation of a pyrenyl COF material **216**.

In another example, SCOFs formed under Ultra-high vacuum (UHV) conditions on Ag(111) surfaces were reported by the group of Zwaneveld, exploiting condensation reactions between boronic acid derivatives.^[250] Condensation reactions involving 1,4-benzenediboronic acid (**217**) led to boroxine ring (Figure 3.14) arranged into ordered porous hexagonal arrays with cavity diameters of $15 \pm 1 \text{ \AA}$ (sublimation of benzenediboronic acid at 300-500 K, surface coverage ranging from <1% to near-complete monolayer). The stability of the assembly was tested by thermal annealing at 750 K. No degradation was observed after 5 min, however, following prolonged period (12 h) significant degradation occurred and only small islands of the intact assembly were observed. Hexagonal networks with larger pore sizes (29 \AA) were also obtained upon co-deposition of 1,4-benzenediboronic acid **217** and 2,3,6,7,10,11-hexahydroxytriphenylene **218**, and once again, annealing at 750 K did not degrade the network, thus confirming the covalent nature of the assembly (Figure 3.14).

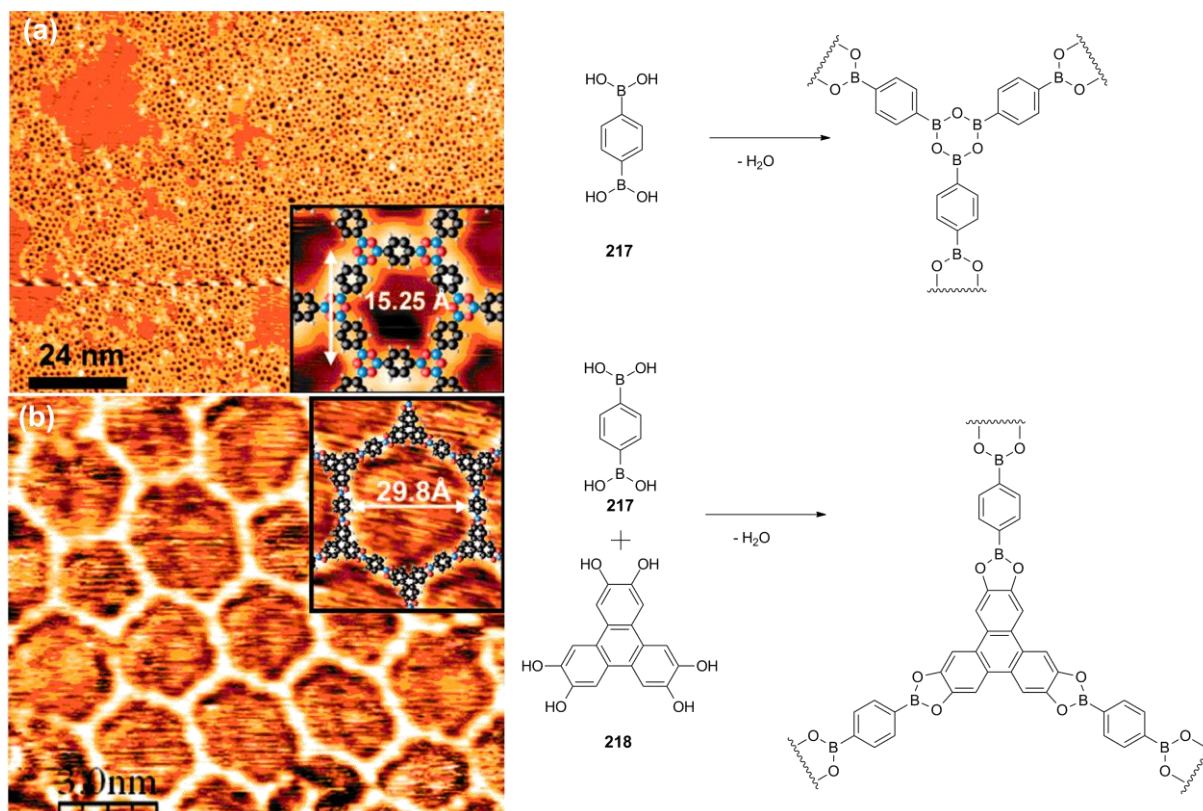


Figure 3.14 a) STM images of a covalent network formed upon deposition of 1,4-benzenediboronic acid on Ag(111) at near-complete monolayer coverage; b) STM image of the SCOF formed upon co-deposition of 1,4-benzenediboronic acid **217** and 2,3,6,7,10,11-hexahydroxy triphenylene **218** on Ag(111). The insets in both images show the theoretical pore diameter obtained by DFT calculations.

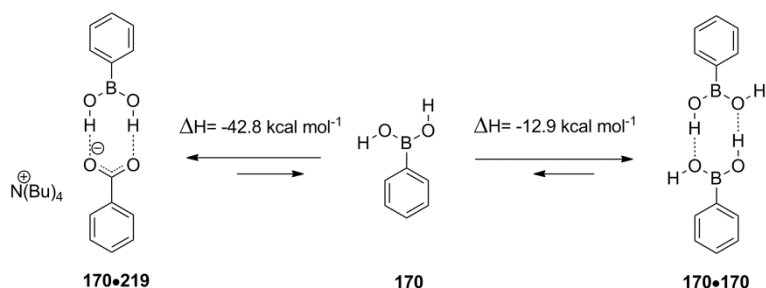
A detailed discussion of the COF formation by boroxines formation is beyond the scope of this thesis and the interested reader is addressed to the specialized literature.^[265,271–273]

3.1.3.3.4. Hydrogen Bonded Complexes

A search in the CSD reveals 174 crystalline structures having a boronic acid functional group. However, most of the literature references of crystal structures involving boronic acids have overlooked the possibility of exploiting this moiety for hydrogen bond self-assembly.^[260] Moreover, only few research groups have investigated their potentiality by studying their crystal structures arrangements.^[225,261,274] Notable examples have described DA-AD assemblies of self-interacting boronic acids (Figure 3.10),^[261] DD conformation when forming complexes with pyridyl^[261] (Figure 3.11) or pyridazine derivatives^[275] (Figure 3.16) and finally few examples revealed a AA arrangement^[258–260] (Figure 3.12). So, the solid state studies have revealed the three possible conformations of the hydroxyl groups (DA, DD or AA), which depending on the acceptor molecules, can lead, in principle, to different recognition motifs (DA \cdots AD, DD \cdots AA and AA \cdots DD). The energy difference between the different conformations being low, typically inferior to 2.8 kcal mol⁻¹ (Scheme 3.7), the boronic acids can dynamically adapt to different acceptors systems. As the total energy of the self-assembly is ranking from 15 to 37 kcal mol⁻¹, and is therefore by far superior to the difference in energy between the different conformations, boronic acids have this advantage of being flexible systems able to adapt to the counterpart involved in the hydrogen bonds. Therefore, several functional groups are found in the CSD database to form complexes with boronic acids, such as pyridyls, carboxylates, sulfates, amides and halogens.^[276] Amongst them, pyridyl and carboxylate derivatives are interesting because they are DD systems, able to form stable complexes. Inspired by the work of Pedireddi^[261] (Figure 3.11), a search in the crystal database revealed additional examples of boric or boronic acids binding with pyridyl derivatives,^[277–279] often with no description of the hydrogen bond, the latter being overlooked^[275] (Figure 3.16). An extensive search revealed that B(OH)₃ was also

Chapter 3

described to bind with amino acid.^[280] This has been the inspiration for an impressive work by the group of Reetz,^[246] who designed a boronic acid able to enhance the transfer of amino acids through biomembranes (Figure 3.17). Finally, these synthetic efforts and solid state studies have been complemented by computing the energy of the self-interaction of boronic acids or when in complex with phenyl carboxylate.^[281,282] The energetic values are reported in Scheme 3.10. They revealed that the strong complexation of phenylboronic acid **170** should be obtained with carboxylate derivatives ($\Delta H = -42.8$ kcal mol⁻¹). Whereas the energy of the interaction of boronic acid with itself ($\Delta H = -12.9$ kcal mol⁻¹) is not negligible and has to be overcome to observe the formation of complexes with phenylcarboxylate **219**.^[281]



Scheme 3.10 Energies of the different conformations of boronic acid and the complexation enthalpies with boronic acid **170**, and phenylcarboxylate **219**. Computed by MP2/6-31G(d,p) level of theory by the GAUSSIAN 98 program.^[281]

The group of Wuest explored the use of boronic acid as ‘tecton’ (the equivalent of a synthon group, for supramolecular chemistry) to direct supramolecular structures.^[274] Using boronic acid derivative **220** (Figure 3.15), they obtained crystals with large pore volume, of diameter of up to 9.0 Å, able to adsorb ethylacetate and exchange it for diethylmalonate upon standing in THF/hexane (1:9). The boronic acid in this study acts as a donor-acceptor with itself, in an *endo-exo* conformation.

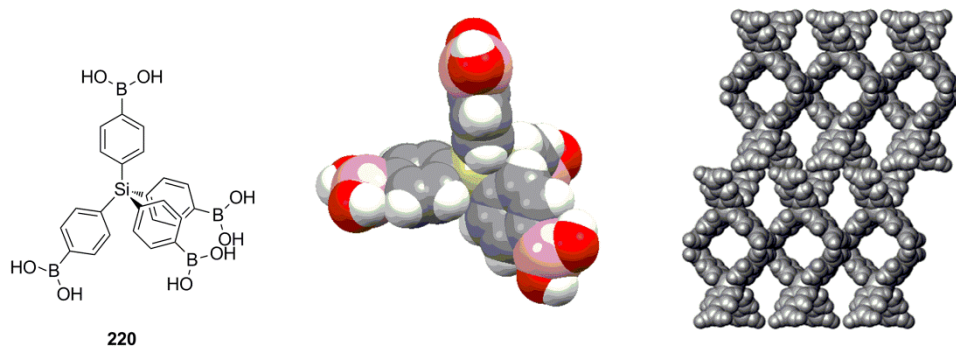


Figure 3.15 Tetraboronic acid derivative **220** forming highly porous crystalline network. Color code: red: oxygen, gray: carbon, white, hydrogen, pink: boron. Space group I4₁/a.^[283]

The *syn* conformation of boronic acid derivatives has been mainly explored with acceptors possessing a nitrogen atom. To this regard, several complexes are known with pyridyl derivatives^[225,261,279,284] but only one with pyridazyl derivative and the formation of the complex at the solid state was not discussed.^[275] The advantage of the pyridazyl derivative over the pyridyl is the smaller ΔS upon complex formation. Indeed, the electrostatic repulsion between the two acceptors atoms, which disfavored the formation of complexes with pyridyl derivatives, does not influence the formation of complexes with pyridazyl derivatives, the two nitrogen atoms being covalently linked. Nevertheless, the drawback of this functional group is that the angle formed, between the nitrogen atoms and the oxygen atoms, is not optimal. Indeed, the two nitrogen atoms are separated by a 1.376(2) Å distance while the two oxygen atoms of the boronic acid group are distant of 2.403(2) Å. This distance difference forces the two, positively polarized, hydrogen atoms closer (Figure 3.16).

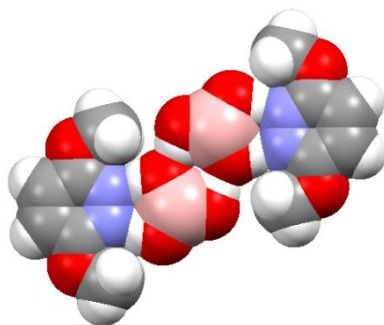


Figure 3.16 Crystalline structure of the complex formed between $B(OH)_3$ and a pyridazyl derivative. Conformation *syn* of the boronic acid, interacting with an AA. Color code: red: oxygen, gray: carbon, white, hydrogen, pink: boron, blue: nitrogen. Space group $P2_1/c$.^[275]

In the literature, few occurrences of crystal structures of boronic acids complexed with carboxylates have been reported.^[281,285] The most accomplished work has been done by the group of Reetz, on the use of boronic acids to complex the carboxylate of phenylalanine (Figure 3.17). The boronic acid can be judiciously placed close to the crown ether, mimic of a membrane transporter in cell membrane, to enhance the speed of transfer of amino acids through hydrophobic membranes.^[246] The hydrogen bond of the boronic acid interacting with carboxylate moiety has a better geometry than in the previous DD example (Figure 3.16), with the oxygen-oxygen atoms of the carboxylate being separated by 2.221(3) Å while the oxygen-oxygen atoms of the boronic acid are separated by 2.41(3) Å.

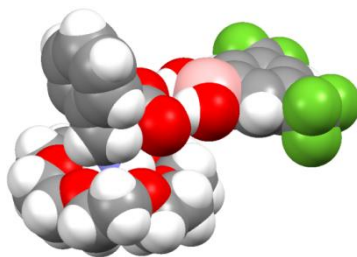
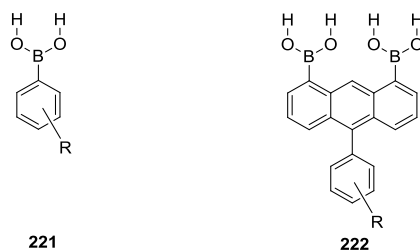


Figure 3.17 Crystalline structure of the complex formed between 3,5-trifluorophenylboronic acid and L-phenylalanine. Conformation *syn* of the boronic acid, interacting with an AA. Representation: spacefill. Color code: red: oxygen, gray: carbon, white, hydrogen, pink: boron, green-yellow: fluorine. Space group $P1$.^[246]

3.2. Synthesis

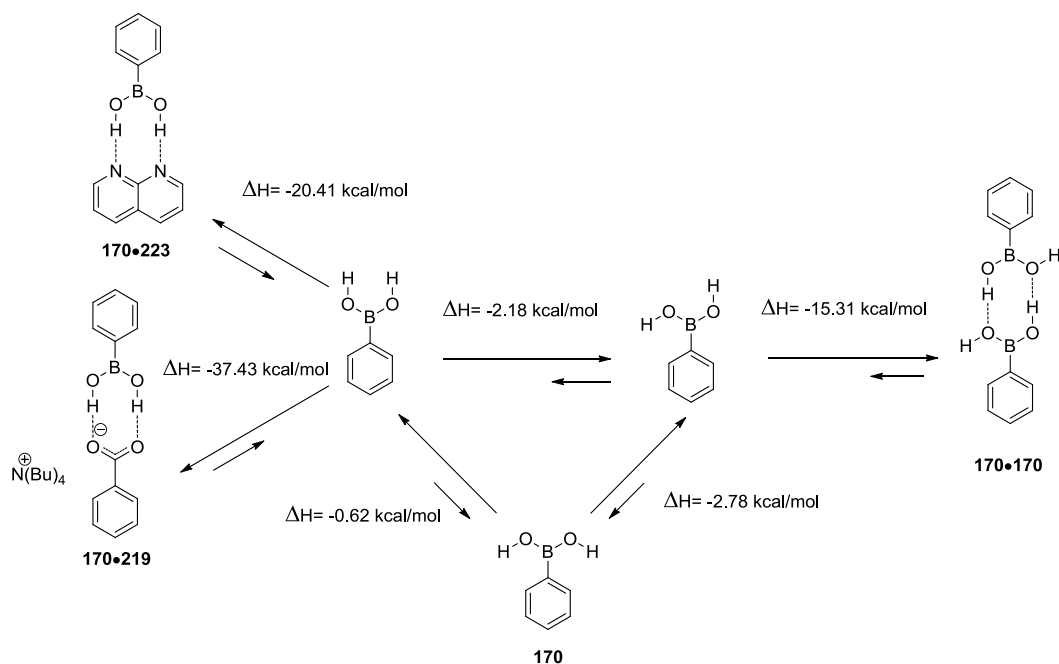
The aim of this work is therefore to explore the potential of boronic acids as hydrogen bonding moieties for material organization. In particular, the first system to be studied will be a DD system (**221**), bearing one boronic acid functional group, however, subsequently, the work will be further developed with the synthesis of a DDDD system (**222**), having two boronic acid groups (Scheme 3.11). The latter systems should display a higher binding constant between the donor and acceptor due to the favorable secondary interactions. Moreover, in order to tune the binding constant, and hence the strength of the hydrogen bonds, the 'R' group would be changed from an electron withdrawing to an electron donating group.



Scheme 3.11 DD system (compound **221**) and DDDD (compound **222**). R: solubilizing group, electron donating or withdrawing group in *ortho*, *meta* or *para* position.

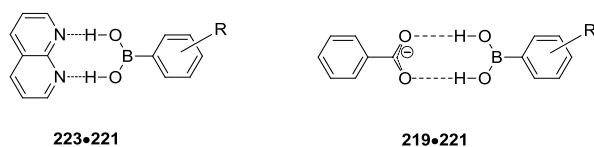
In section 3.1.3.3.4. the reader has been introduced to the acceptor molecules previously reported in the literature, for hydrogen bonding with boronic acids. Few literature reports computed the energy of the different conformations^[256] (see section 3.1.3.2.) as well as the binding interactions with the acceptor.^[281,282] Nevertheless, the work reported did not take into account the energy of the possible conformations neither the energy of self-interacting boronic acids. In addition, the calculations did not include acceptors bearing nitrogen atoms. Pyridyl^[225,261,279,284] and pyridazyl^[275] derivatives have been reported to bind with boronic acids. The latter compound has the advantage to be a DD system, which forms stronger hydrogen bonded complex, due to favorable secondary interactions. Inspired by the work with pyridazyl derivatives, this work envisaged the possibility to use 1,8-naphthyridine **223** as an acceptor. Indeed, the acceptor molecule used in this work possesses two covalently linked nitrogen atoms separated by 2.300(2) Å (Figure 3.17), a value closer to the oxygen-oxygen distance found in boronic acids. This should reduce the repulsion between the two positively polarized hydrogen atoms, as opposed to pyridazyl derivatives where the nitrogen atoms are separated by 2.403(2) Å (Figure 3.16). In addition, inspired by the work of Höpfl,^[281] who described the hydrogen bonding between boronic acid and benzoates derivatives, an alternative DD acceptor was envisaged. Theoretical calculations previously reported predicted a binding energy of -42.8 kcal mol⁻¹ between benzoate and phenylboronic acid. Several benzoates derivatives were synthesized and are described in section 3.2.3.. In order to gain more information into these systems, computational predictions, involving the preferred conformation of phenylboronic acid and the complexation enthalpies in the presence of 1,8-naphthyridine **223** and tetrabutylammonium benzoate **219**, were performed during this work and are summarized in Scheme 3.12.

Regarding the relative energy of the conformations, an opposite tendency, to the one reported in Scheme 3.7, is observed for the least favored conformations. Indeed, it was found that when the boronic acid is substituted by a phenyl, as opposed to a hydrogen atom, the *anti* conformation ($\Delta H = -2.78$ kcal mol⁻¹) is the least favored, followed by the *syn* conformation ($\Delta H = -2.18$ kcal mol⁻¹), respective to the *endo-exo* conformation. This is consistent with the increase in steric hindrance due to the phenyl ring that disfavors the *anti* conformation. In addition, the calculations regarding the hydrogen bonding energy revealed that the strongest complexation of phenylboronic acid **170** should be obtained with carboxylate derivatives. Even more, the energy of the interaction of boronic acid with itself is not negligible and has to be overcome in order to observe the formation of complexes with 1,8-naphthyridine **223** or phenylcarboxylate **219**.



Scheme 3.12 Energies of the different conformations of boronic acid and the complexation enthalpies with boronic acid **170**, 1,8-naphthyridine **223** and phenylcarboxylate **219**. Computed by B3LYP/6-311G** level of theory by the GAUSSIAN 09 program.^[286]

The computational predictions reported in Scheme 3.12 revealed that 1,8-naphthyridine **223** and phenylcarboxylate **219** are suitable acceptors for self-assembly with boronic acid derivatives. Therefore, the acceptors chosen to be studied were 1,8-naphthyridine and carboxylate moieties (Scheme 3.13), and the complexes forms are presented in detail in *sections 3.4.3* and *3.5* (**223•221** and **219•221**).



Scheme 3.13 Hydrogen bonding interactions between boronic acid derivative **221** and 1,8-naphthyridine **223** or benzoate derivative **219**. R: electron donating or withdrawing groups in *ortho*, *meta* or *para* positions.

3.2.1. Synthesis of Boronic Acids (DD Systems)

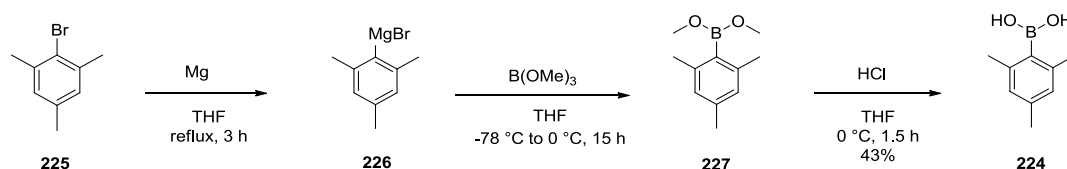
Several methods are described in the literature for the synthesis of boronic acids involving the formation of C_{sp^2} -B bonds.^[287] A first methodology takes advantage of the nucleophilic substitution on $B(OMe)_3$ by a Grignard^[288] or an organo lithiate^[289] derivative, generated from the corresponding bromide or iodide. This leads to the formation of a boronic ester which can be subsequently hydrolyzed in the aqueous workup to afford the boronic acid. A second method takes advantage of the electrophilic aromatic substitution of an aryl by BCl_3 , catalyzed by Lewis acids such as $AlCl_3$, to furnish the corresponding boronic acid after hydrolysis of the halogenoborane formed.^[290] Finally, boronic acids can also be obtained by Pd-catalyzed coupling of halogeno aryls and diboron reagents, the Miyaura borylation reaction, and again subsequent hydrolysis of the ester.^[291] Finally, additional metal catalyzed methods reported in the literature, include the C-H activation through iridium catalysis.^[292,293]

As already mentioned, one of the aims of this project is to measure the binding constant of DD systems, constituted by boronic acids, with various acceptors. Hence, in the following section a detailed discussion of the synthetic pathway leading to the formation of mesitylboronic acid, tri-*i*-propyl boronic acid, and durene-1,4-diboronic acid will be reported. As outlined

Chapter 3

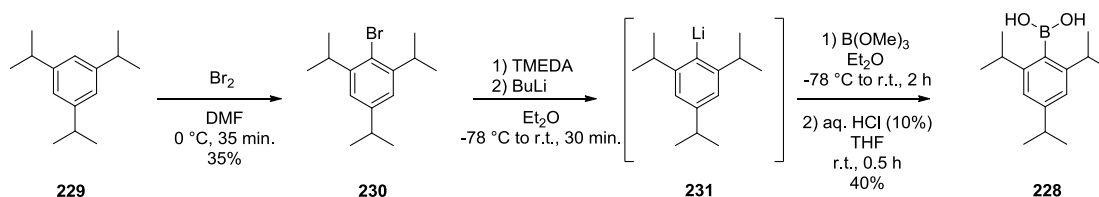
in section 3.1.3.1, this sterically encumbered group will disfavor the formation of the corresponding boroxine. The absence of boroxine form will be of fundamental importance for the ITC measurement of the binding constant. Moreover, the presence of the alkyl substituents will improve the solubility of the compounds in the solvents used for ITC measurement.

Firstly, 1-mesityl boronic acid (compound **224**, Scheme 3.14) was synthesized from 1-bromomesitylene **225**, which was reacted with magnesium to give the corresponding Grignard intermediate **226**. Grignard derivative **226** produced, through a nucleophilic substitution with $B(OMe)_3$, boronic ester **227**. The latter was hydrolyzed during an acidic aqueous work-up to give boronic acid **224** in 43% yield from **225** (Scheme 3.14).



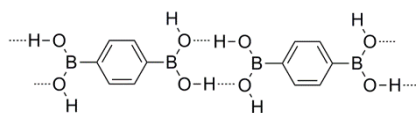
Scheme 3.14 Synthesis of 1-mesityl boronic acid **224**.

The second arylboronic acid, aimed to be synthesized was **228**. This boronic acid possesses isopropyl substituents in *ortho* and *para* positions, respective to the boronic acid moiety. As a result, arylboronic acid **228** has been synthesized according to the strategy disclosed in Scheme 3.15. Starting from 1,3,5-triisopropylbenzene **229**, reacting it with Br_2 in the absence of light gave brominated derivative **230** in a 35% yield. The latter, through a metal-halogen exchange using *n*-BuLi in the presence of TMEDA, furnished lithiated intermediate **231**. This intermediate produced, which was immediately reacted through a nucleophilic substitution with $B(OMe)_3$. Finally, hydrolysis of the ester during the aqueous work-up, allowed the isolation of desired boronic acid **228** in average yield (40%) from **230**.^[289]



Scheme 3.15 Synthesis of 2,4,6-triisopropylphenylboronic acid **228**.

The focus of this study was then concentrated on the synthesis of a third compound, having two boronic acid moieties in *para* position, both sterically hindered by methyl groups, derivative **232**. This compound would allow the formation of linear networks of hydrogen-bonded complexes. For example, complexation of 1,4-phenylenediboronic acid (Scheme 3.16, compound **217**) has been described in the literature.^[279] However, its exploitation has been hampered by its low solubility, since it is soluble only in hot H_2O or EtOH.^[276,279,294] As a result, the introduction of methyl groups in the *ortho* position would not only improve the solubility but would also prevent the boroxine formation and result in the formation of linear networks by forming hydrogen-bonded complexes.



217•217

Scheme 3.16 Linear DA hydrogen bonded network formed by 1,4-phenylenediboronic acid **217**.

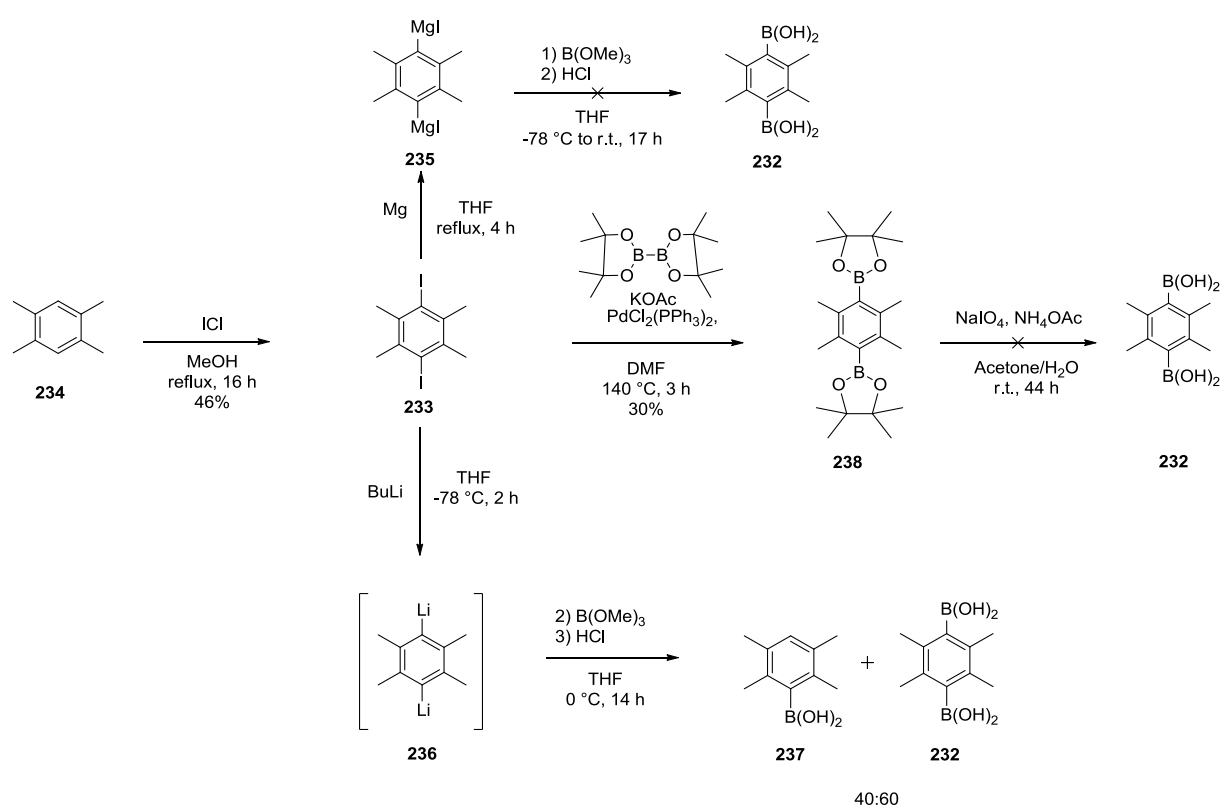
The synthesis of durene-1,4-diboronic acid (Scheme 3.17, compound **232**) was attempted using several methods. Firstly, diiododurene **233** was obtained in moderate yield (46%) from the reaction of durene **234** with ICl in MeOH.^[295] Intermediate **233** was initially treated with magnesium to give Grignard derivative **235**, which precipitated in solution and did not react

Chapter 3

with $\text{B}(\text{OMe})_3$ in order to afford boronic acid **232**.^[288] Aqueous workup, after protonation of Grignard **235**, resulted in the isolation of durene **234**.

In a second attempt to form desired boronic acid **232**, compound **233** was reacted with *n*-BuLi to give intermediate **236** that, after the addition of $\text{B}(\text{OMe})_3$ and subsequent hydrolysis of the ester, gave the diboronic acid **232** and the monoboronic acid **237** derivatives in a 40:60 ratio as determined by GC-MS.^[289] Nevertheless, due to the fact that these two compounds were difficult to separate on silica gel column chromatography, an alternative synthetic pathway was attempted.

The last attempt involved using the classical Miyaura reaction conditions. Hence, diiododurene **232** was reacted with a Pd complex in the presence of B_2pin_2 and heated up by MW irradiation, to give boronic ester **238** in a 30% yield.^[296] Unfortunately, the ester could not be hydrolyzed in the presence of NaIO_4 and NH_4OAc and the starting material was recovered.^[297]



Scheme 3.17 Attempted synthesis of durene-1,4-diboronic acid **231**.

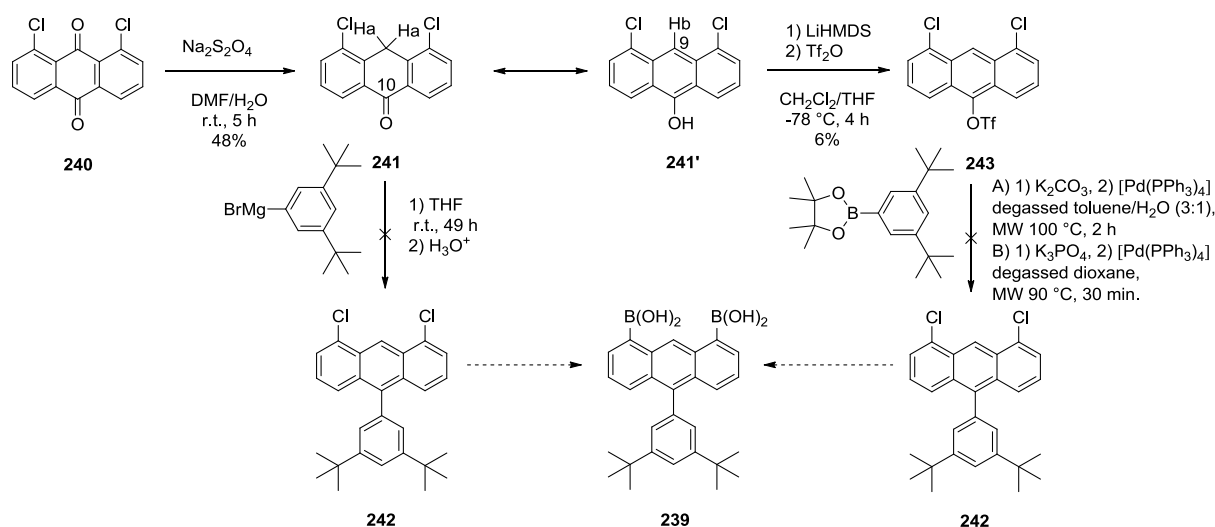
3.2.2. Synthesis of Multiple Boronic Acids (DDDD Systems)

With the aim of increasing the binding constant of boronic acid derivatives with acceptor derivatives the synthesis of a DDDD boronic acid system of hydrogen bonds was envisaged. This compound, able to form DDDD motif, would be useful for applications, such as the formation of robust auto organized networks able to resist ambient humidity and polar solvents.^[272] The compound envisaged is based on an anthracene core bearing two boronic acid groups, in 1 and 8 positions, hence the four hydroxyl moieties of the boronic acids functional groups will be aligned (compounds **239**, Scheme 3.18) The synthesis of these anthracenyl derivatives revealed to be a challenge from the synthetic point of view and will be discussed extensively in this section.

The first compound attempted was anthracene-based diboronic acid **239**. Apart from introducing two boronic acid moieties in order to accomplish a DDDD system and additional aromatic ring bearing two *t*-butyl moieties will be introduced

Chapter 3

in order to improve the solubility of desired product **239**. The first synthetic pathway envisaged for the synthesis of derivative **239** was commenced with the reduction of 1,8-dichloroanthraquinone **240** with $\text{Na}_2\text{S}_2\text{O}_4$ yielding 1,8-dichloroanthracen-9-one **241** in moderate yield (48%). This ketone was then subjected to the next step, by mixing with the Grignard reagent in THF. However, the addition of the Grignard on the ketone led to a complex mixture of products, as already described in the literature.^[298,299] A potential pitfall for this reaction is that ketone **241** could be in equilibrium with its enol form (**241'**), therefore preventing the addition reaction of the Grignard reagent to occur. The ^1H NMR spectrum of **241** in CDCl_3 reveals a peak at 3.15 ppm corresponding to the hydrogen atom of the enol function, while the integration of the peak for the hydrogen atom in position 9 corresponded to one proton but appeared at 6.40 ppm. This chemical shift corresponded to an average between the hydrogen atom in benzylic position (H_a , expected chemical shift: 5 ppm) and the enol form (H_b , expected chemical shift: 9 ppm). Moreover, the ^{13}C NMR spectrum revealed a peak at 182.6 ppm, attributed to the carbon of the ketone form, while the IR spectra indicated a carbonyl stretching band (1660 cm^{-1}). Hence, all these analysis proved that product **241** is in equilibrium with its enol form **241'**. Therefore, a possible alternative synthetic pathway would allow a Suzuki coupling that will anchor the solubilizing *t*-butyl group yielding **242**, a precursor of boronic acid **239**, from triflate **243** after activation of the enol (Scheme 3.18). As a result, the alcohol functional group of **241'** was transformed to triflate **243**, using TF_2O , with an extremely low yield of 6%.^[300] The Suzuki coupling to yield to derivative **242** was attempted using $\text{Pd}(\text{PPh}_3)_4$ in the presence of K_2CO_3 (conditions A, Scheme 3.18) or K_3PO_4 (conditions B, Scheme 3.18) as a base, without any success, recovering starting material **242**.^[301,302] In the literature, it is reported that the coupling reaction is extremely sensitive toward oxygen on this particular substrate and oxygen scavengers are required to improve the yield for this product.^[301] Therefore, judging by the poor yield obtained for the triflate derivative and also the difficult coupling reaction, this synthetic strategy was abandoned.

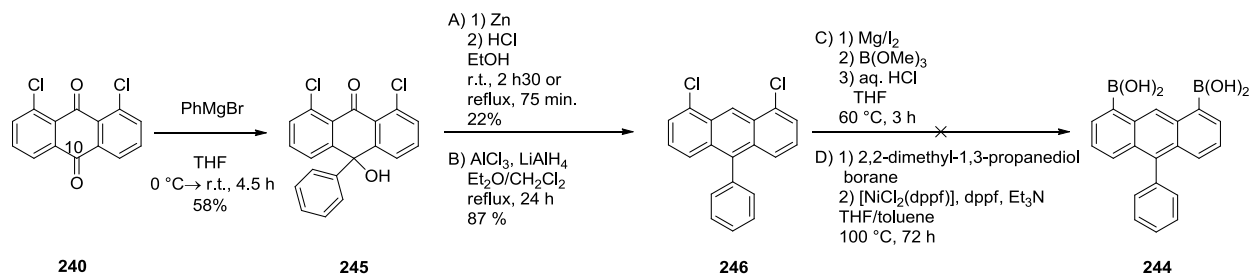


Scheme 3.18 First synthetic pathway to yield to bisboronic acid **239**, a DDDD system.

In a second synthetic pathway, the synthesis of compound **244**, an analogue of our target compound **239**, bearing a simple phenyl group in position 10 was attempted. The key step of this strategy is the selective addition of a Grignard species on the ketone in *meta* position respective to the chlorine. Hammett σ values for the hydrolysis of benzoate substituted in *para* or *meta* by chlorine atoms are of 0.227 and of 0.373 respectively.^[303] Fortunately, the reaction of diketone with the relevant Grignard reagent afforded selectively mono addition compound **245** in 58% yield (Scheme 3.19), along with starting material with no traces of double addition product.^[299] The interpretation of the ^1H NMR spectrum indicated a mono reduction of the ketone (Figure 3.18), as evidenced by the hydrogen atom peak of the alcohol moiety at 2.88 ppm. Furthermore, the ^{13}C NMR spectrum indicated that only one ketone was reduced (one peak at 183.2 ppm) but the attribution to which of the ketone

Chapter 3

wasn't possible. Therefore, crystals were grown and the X-ray diffraction allowed us to unambiguously establish the regioselectivity of the addition reaction (compound **245**, Scheme 3.19, Figure 3.19), which proceeded in position 10.



Scheme 3.19 Second synthetic pathway, trial on a model compounds **244**.

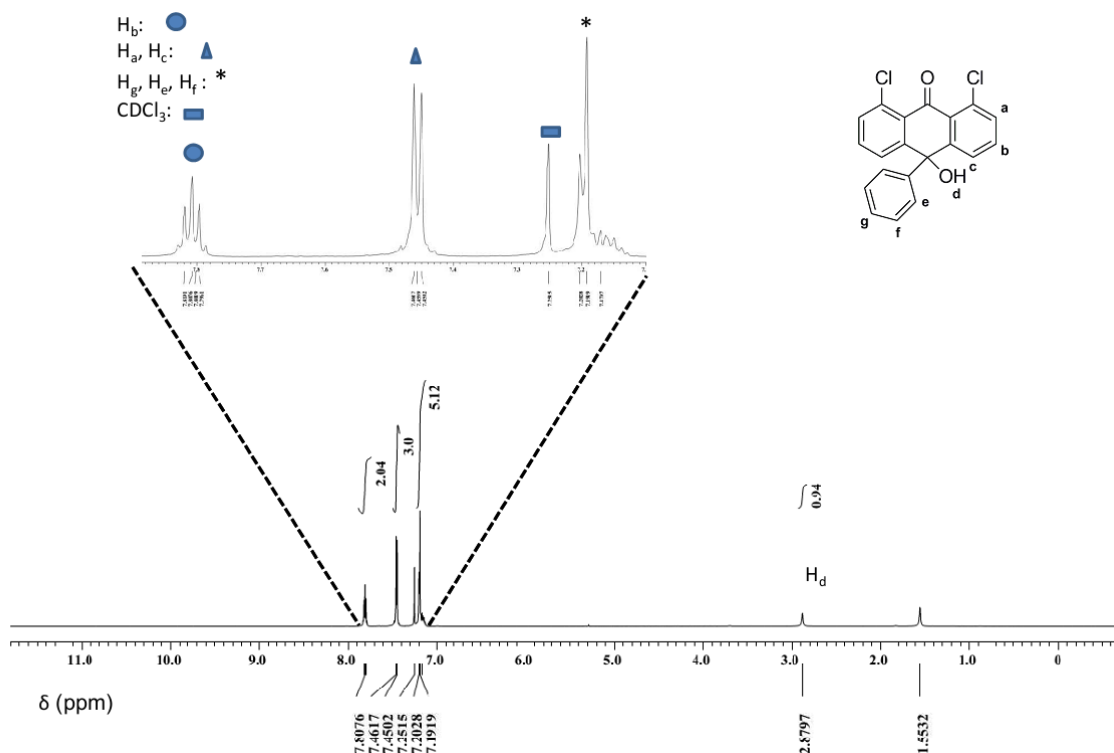


Figure 3.18 ¹H NMR spectrum (400 MHz, CDCl₃) of compound **244**. Inset: zoom of the 7.9-7.0 ppm area.

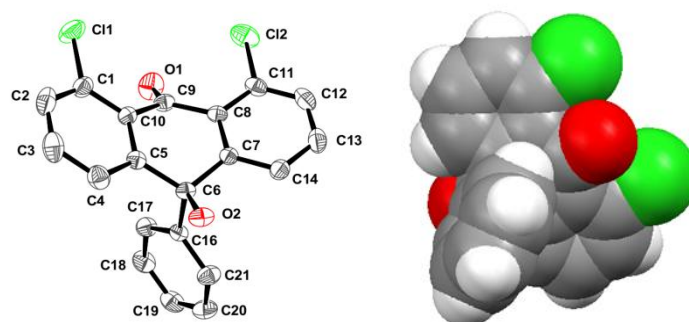


Figure 3.19 Crystal structure of **245**, obtained by slow evaporation in CH₂Cl₂. Representation: left: ORTEP (drawn at the 30% probability level), right: spacefill. Color code: red: oxygen, grey: carbon, white: hydrogen, green: chlorine. Space group P2₁/c.

Then, derivative **246** was obtained by a tandem Clemmensen reduction of the ketone, using zinc, followed by the elimination of the hydroxyl group of **245** by the addition of concentrated HCl to produce **246** in low yield (22%) (conditions

Chapter 3

A, Scheme 3.19).^[304] Therefore, alternative reaction conditions were tried which could afford the desired product in a one step reaction. Reduction of the ketone with LiAlH_4 in the presence of AlCl_3 , gave expected product **246** after a tandem reduction/elimination reaction in 87% yield (conditions B, Scheme 3.19). The HMQC NMR spectrum of the product revealed the apparition of one peak at 9.39 ppm, linked to an aromatic carbon atom (121.1 ppm), corresponding to the hydrogen atom in position 9, in pseudo-*para* of the phenyl group (Figure 3.20). The structure was also confirmed by X-ray diffraction (Figure 3.21).

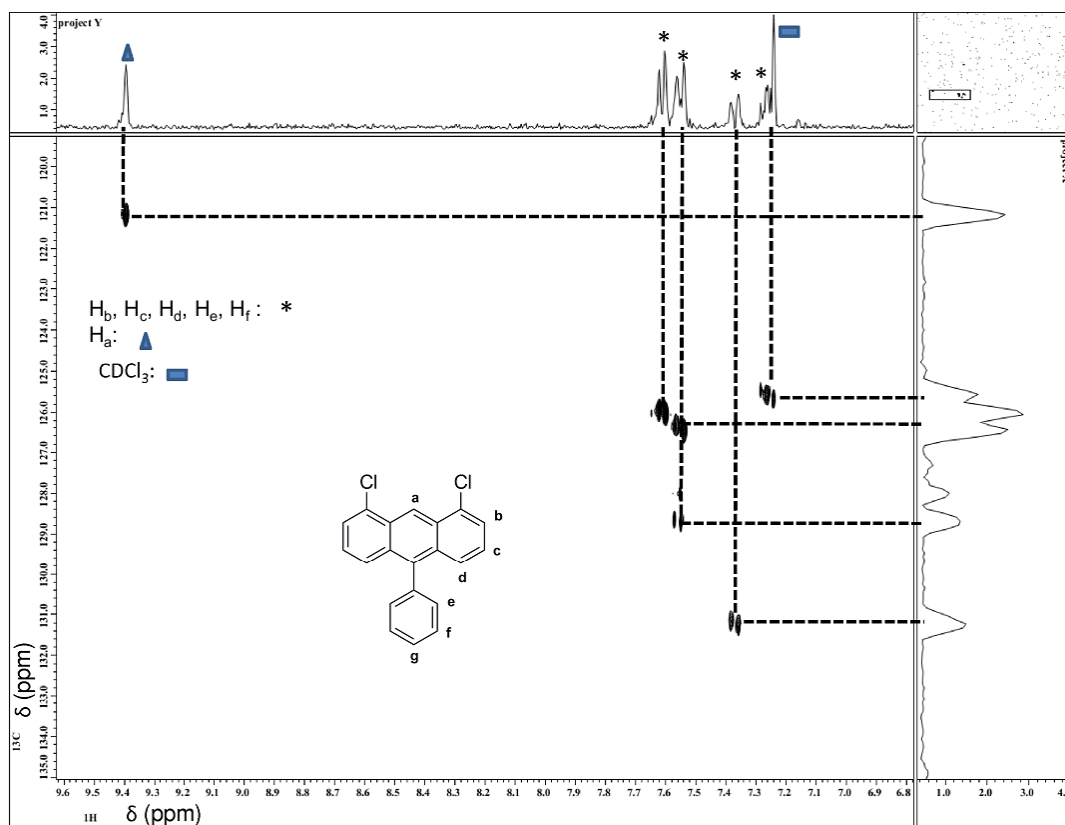


Figure 3.20 HMQC NMR spectrum (400 MHz, CDCl_3) of derivative **246**.

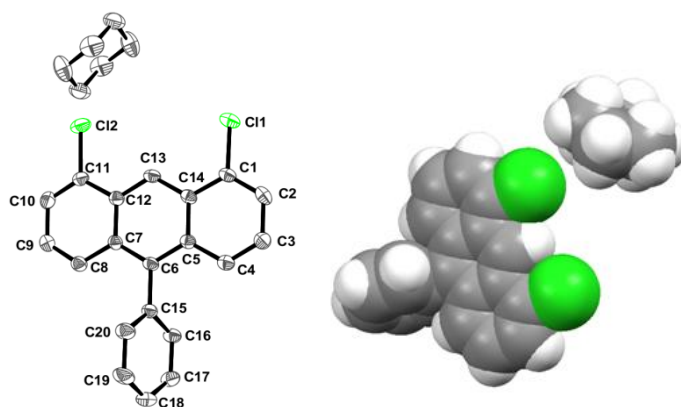


Figure 3.21 Structure of compound **246** with one molecule of cyclohexane. Crystals obtained by slow evaporation in cyclohexane Representation: left: ORTEP (drawn at the 30% probability level), right: spacefill. Color code: red: oxygen, grey: carbon, white, hydrogen, green: chlorine. Space group $P2_1/n$.

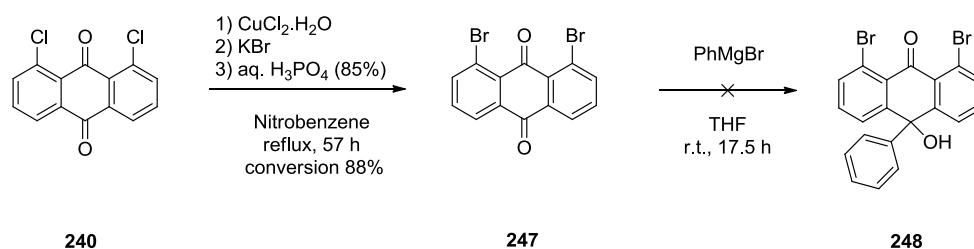
Unfortunately, the last step to substitute the chlorine atoms of **246** by boronic acids, leading to **244**, revealed to be unsuccessful. The first attempt to transform chlorinated derivative **246** to a Grignard species followed by a nucleophilic substitution on $\text{B}(\text{OMe})_3$, a reaction analogous to the synthesis of derivative **224** (Scheme 3.14), did not furnish the desired

Chapter 3

product (Scheme 3.19, conditions C).^[305] An alternative reaction condition attempted was the nickel catalyzed reaction with $[\text{NiCl}_2(\text{dppf})]$ ^[306] (Scheme 3.19, conditions D) but once again, only the starting material was recovered. A possible pitfall for this reaction is the sensitivity of the nickel catalyst to traces of oxygen that oxidized readily the phosphine ligand.^[306]

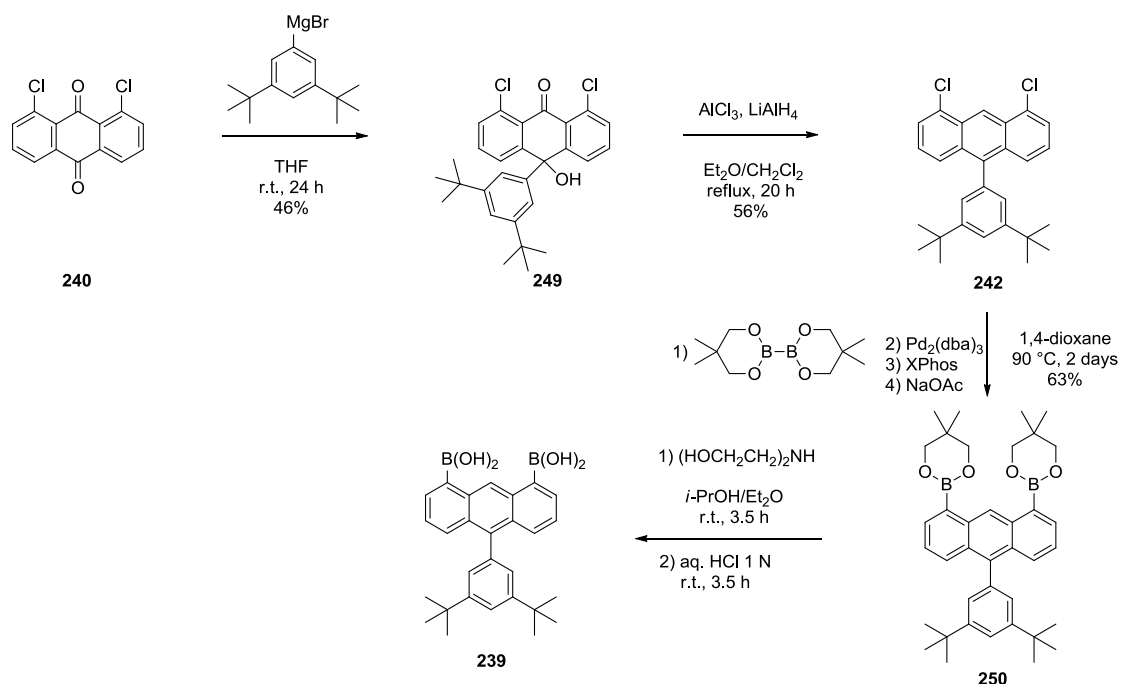
At this point, since the method allowing the transformation of chlorine atoms to boronic acids have been unsuccessful, other synthetic options were explored, such as the possibility to restart the synthesis of boronic acid **244** from bromine derivative **247**. This would allow us the examination of a variety of borylation conditions for the last step; amongst them a Grignard formation,^[288] lithiate exchange followed by nucleophilic addition on $\text{B}(\text{OMe})_3$,^[289] and a Miyaura coupling,^[296] using palladium catalysis (see Scheme 3.17, compound **224**).

Hence, the synthesis was commenced with the transformation of 1,8-dichloroanthraquinone **240** into 1,8-dibromoanthraquinone **247** by nucleophilic substitution in *beta* of the ketone by bromide, catalyzed by Cu (II) in presence of H_3PO_4 . This reaction gave 1,8-dibromoanthraquinone **247** in low yield (12%) under harsh reaction conditions (57 h at reflux in nitrobenzene).^[307] The compound was purified by sublimation, being almost insoluble. The next step involves the reaction of dibromocompound **247** with the relevant Grignard reagent. Unfortunately, this resulted in a complex mixture of products for the addition reaction and compound **248** was not isolated, even though the σ values for the hydrolysis of benzoate substituted in *para* or *meta* by bromine atoms are of 0.232 and of 0.391 and therefore the addition reaction should have been selective. As a result, this strategy for the synthesis of diboronic acid **244** was not further investigated.



Scheme 3.20 Attempted synthesis of bromine derivative **248**.

Taking into consideration the synthetic attempts for diboronic acid **244** (Scheme 3.19), the synthesis of diboronic acid **238**, bearing solubilizing *t*-butyl groups, was reexamined. Hence, the key step of this synthetic pathway is again, the selective addition on the ketone in position 10 of a Grignard intermediate bearing solubilizing *tert*-butyl groups in *meta*. Compound **249** was synthesized, *via* the addition of the Grignard derivative, obtained from 1-bromo-3,5-di-*tert*-butylbenzene on compound **240**, with 46% yield, (Figure 3.19) in similar reaction conditions as developed for the model compound (Scheme 3.19). Once again, the X-ray analysis allowed us an unambiguous determination of product **249** (Figure 3.22). Following the same synthetic procedure outlined in Scheme 3.19, compound **249** was subjected to a tandem reduction/elimination that produced **242** in good yield (56%). Finally, previously attempted conditions for the borylation steps on model compound **246** (Scheme 3.19) having been unsuccessful, other reactions conditions were tried. Hence, the key borylation step was achieved by using palladium catalysis in presence of the diboryl reagent and NaOAc .^[308] Starting from **242**, boronic ester **250** was obtained in good yield (63%). After purification on silica gel chromatography, the ester was hydrolyzed in presence of diethanolamine and by a subsequent suspension in aqueous HCl to give desired boronic acid **239**.^[308]



Scheme 3.21 Second synthetic pathway for the synthesis of compound **239**.

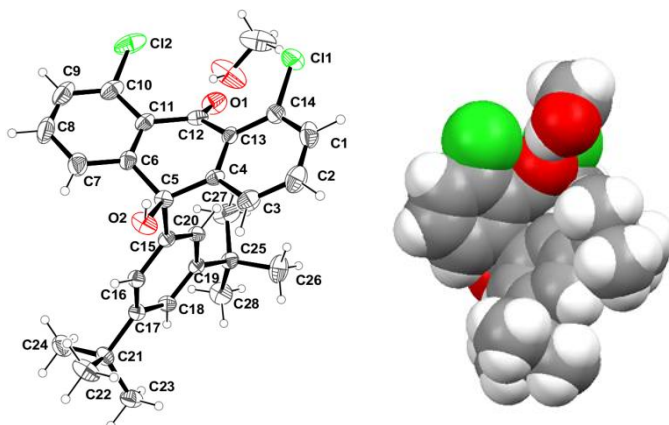


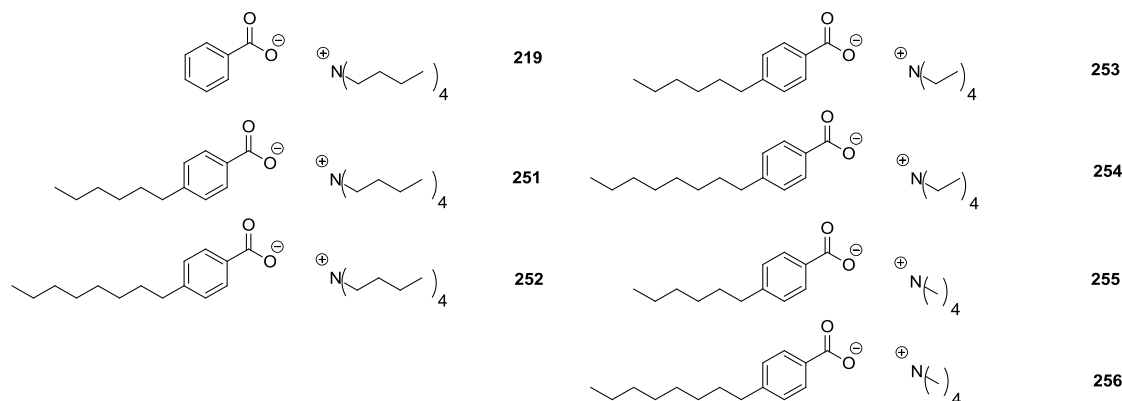
Figure 3.22 Structure of compound **249** with one molecule of MeOH. Crystals obtained by slow evaporation in MeOH. Representation: left: ORTEP (drawn at the 30% probability level), right: spacefill. Color code: red: oxygen, grey: carbon, white, hydrogen, green: chlorine. Space group P-1.

3.2.3. Synthesis of Hydrogen Bond Acceptors

As previously mentioned in the introduction of *section 3.2.*, boronic acids are known to bind with carboxylates, as demonstrated by theoretical computation^[281,282] and crystal structures studies.^[281] The computational study performed during this work further confirmed the high energy ($-37.43 \text{ kcal mol}^{-1}$) of the hydrogen bond interactions between phenylboronic acid and phenyl carboxylate. With the aim of studying the binding constant of boronic acid with other hydrogen bond acceptors, such as alkylammonium benzoates (Scheme 3.22, and Scheme 3.23, compound **219** to **256**), the latter were synthesized. They were obtained by acid-base reactions from the corresponding acids reacting with tetraalkylammonium hydroxide. Due to the fact that the solubility plays a great role in ITC measurement, the solubility of the salts was tuned by varying the lengths of the alkyl chains. Indeed, a first trial performed with benzoate **219** reveal that its solubility does not exceed 70 mM in toluene at r.t., while ITC measurement needs a very high concentration of the titrant (200 mM) in order to stay in the experimental window of the instrument. Moreover, the determination of the thermodynamic parameter and the

Chapter 3

stoichiometry is more accurate with a higher concentration of titrant. To this end, derivatives **251** and **252**, bearing solubilizing alkyl chains, were synthesized. However, they turned out to be viscous hygroscopic liquids. Consequently, in order to facilitate their manipulation, the alkyl chain length on the ammonium moiety and hence compounds **253**, **254**, **255** and **256** were isolated as solids, keeping the alkyl chain on the benzoate identical.



Scheme 3.22 Hydrogen bond acceptors: benzoate of tetraalkylammonium, bearing alkyl chains of various lengths to enhance their solubility in toluene.

With the aim of forming linear arrangement of AA and DD hydrogen bond acceptors systems,^[281] using **257** and diboronic acid **217**, the dicarboxylate derivative having two carboxylate groups in *para* position was obtained. In the same vein, compound **258** was obtained to form bidimensionnal networks by complexation with diboronic acid **218**.^[281]



Scheme 3.23 Hydrogen bond acceptors substituted by several carboxylate moieties, tetrabutylammonium 1,4-dicarboxybenzoate (compound **257**) and tetrabutylammonium trimesic benzoate (compound **257**).

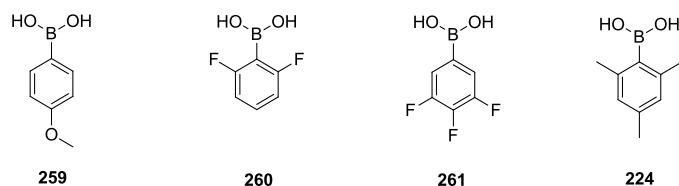
3.3. Equilibrium between Boronic Acids and Boroxines

Boronic acid derivatives are known to be in equilibrium between their acid and their anhydride form. During the ITC analysis, measuring the association constant of the acid form with AA acceptors, it is crucial that the derivatives is on its acid form. As developed in *section 3.1.3.1.* of the introduction, several parameters influence the equilibrium such as the temperature and the substituents on the aryl group. The influence of the substituent on the acid/boroxine ratio was studied in the aim to confirm that the derivative studied by ITC were in their acid form at the beginning of the titration. As outlined in the introduction, the boronic acids and the corresponding boroxines can be differentiated by ^1H NMR^[253] and IR^[252] spectroscopy. The two forms exist in equilibrium in solution but this equilibrium can also be shifted to the preferred form. For example, the boronic acid can be converted into the anhydride by reaction with thionyl chloride in toluene or by heating them in a drying pistol.^[254]

3.3.1. Analysis of Boroxines by ^1H NMR Spectroscopy

Taking all these into consideration, commercially available boronic acids **259**, **260** and **261** and boronic acid **224**, which has been synthesized for the purpose of this study and described in *section 3.2.1.*, (Scheme 3.24) were converted, by heating them in a drying pistol in presence of P_2O_5 , into their boroxine form and later analyzed by ^1H NMR spectroscopy. The ratio between the acid and the anhydride was determined by integrating the aromatic ^1H signals of the acid or the boroxine, and the results are summarized in Table 3.2.

Chapter 3



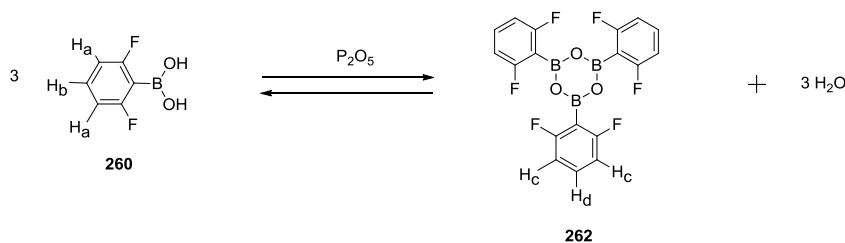
Scheme 3.24 Boronic acids studied in their anhydride form. 4-methoxyphenylboronic acid (compound **259**), 2,6-difluorophenylboronic acid (compound **260**), 3,4,5-trifluorophenylboronic acid (compound **261**), mesitylboronic acid (compound **224**).

Boronic acid derivative	Reaction time (h)	Ratio of acid/boroxine before reaction	Ratio of acid/boroxine after reaction	δ (ppm) of the acid (solvent)	δ (ppm) of the boroxine (solvent)
259	2h	0/100	0/100	6.93, 7.68, 3.84 (CDCl ₃) ¹ 7.63, 6.75, 3.19 (C ₆ D ₆) ¹	8.16, 7.01, 3.89 (CDCl ₃) 8.29, 6.98, 3.29 (C ₆ D ₆)
260	5h	100/0	15.3/84.7	6.62, 6.33 (toluene- <i>d</i> ₈)	6.78, 6.50 (toluene- <i>d</i> ₈)
261	5h	64.7/35.3	18.0/82.0	6.88 (benzene- <i>d</i> ₆)	7.31 (benzene- <i>d</i> ₆)
224	5h	100/0	5.7/94.3	6.83, 2.35, 2.27 (CDCl ₃)	6.85, 2.45, 2.28 (CDCl ₃)

Table 3.2 Ratio of boronic acid/boroxine determined by ¹H NMR after treatment of the acid in a drying pistol with P₂O₅, 150 mbar, 150 °C. ¹spectral data obtained after solubilizing the boroxine into a THF/H₂O solution and subsequent analysis of the powder obtained by NMR.

The analysis of the results reveals that the equilibrium can be shifted toward the boroxine form upon treatment with P₂O₅ (Table 3.2). Moreover, the kinetic of the equilibrium between the acid and the boroxine form is slow respective to the ¹H NMR time scale, as evidenced by the two sets of chemical shifts corresponding respectively to the boroxine and the boronic acid. Also, it appears from the results outlined in Table 3.2 that boronic acid **259**, which is substituted by a methoxy group in *para* is completely in the anhydride form before treatment. Indeed, electron donating substituents favor the boroxine form, as already outlined in section 3.1.3.1.^[255]

In addition, the ¹H NMR spectra of 2,6-difluorophenylboronic acid **260** (Figure 3.23) before and after treatment with P₂O₅ reveals two peaks, one corresponding to the free acid form at 6.62 ppm (H_a) and one at 6.33 ppm (H_b). However, after drying, two additional peaks are present at 6.78 ppm (H_d) and 6.50 ppm (H_c), corresponding to the boroxine form **262**.



Scheme 3.25 Equilibrium between 2,6-difluorophenylboronic acid **260** and its anhydride form **262**.

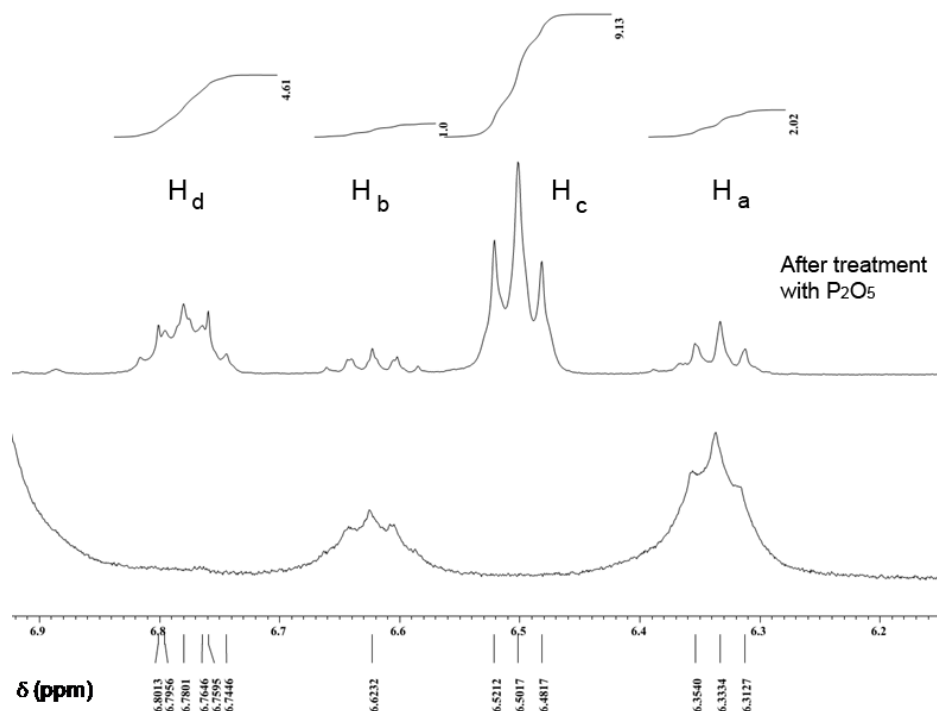
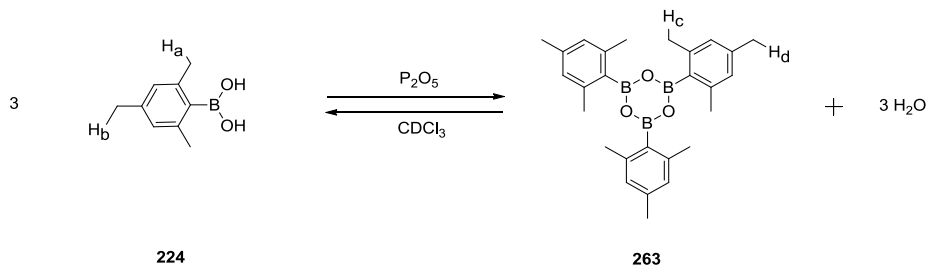


Figure 3.23 ^1H NMR spectra of 2,6-difluorophenylboronic acid (**260**) before (below) and after (above) treatment on P_2O_5 . Solvent: toluene- d_8 .

Moreover, a closer examination of mesitylboroxine **263** revealed that it could also be slowly hydrolyzed in CDCl_3 to yield again the corresponding acid **224**. ^1H NMR analysis of mesitylboroxine **263** in CDCl_3 revealed slow hydrolysis after several hours as summarized in Table 3.3. The ratio of the two species was determined by integration of the hydrogen atoms of the methyl group peaks, corresponding to the two species (Scheme 3.26, Table 3.3).



Scheme 3.26 Equilibrium between the acid (compound **224**) and the boroxine (compound **263**) forms of mesitylboronic acid.

The data summarized in Table 3.3 lead to the conclusion that boroxine **263** could be transformed into the acid form **224** in CDCl_3 without the addition of H_2O , base or acid. After 14 h30, the ratio is nearly 1:1 and the evolution is toward the predominant acid form. Indeed, the presence of the two *ortho* substituents on the aromatic ring disfavored the boroxine form. This is of fundamental importance for the ITC study, necessary to determine the binding constant of the boronic acid with 1,8-naphthyridine. In the present case, the presence of boroxine in the solid state will not be a problem, since it will transform into the acid upon dissolution in solvent.

Time (min.)	acid/boroxine ratio	¹ H NMR Spectra
0	5.7/94.3	
3	6.0/94.0	
9	6.3/93.7	
18	6.5/93.5	
34	7.4/92.6	
69	7.4/92.6	
355	18.0/82.0	
869	52.0/48.0	

Table 3.3 Evolution of the acid/boroxine ratio with time for mesityl boronic acid, determined by ¹H NMR in CDCl₃.

3.3.2. Analysis of Boroxines by IR Spectroscopy

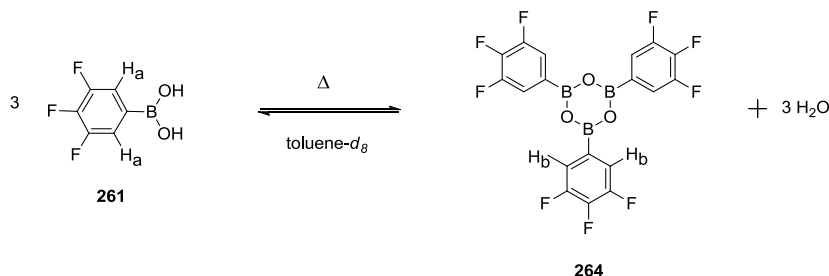
The second analysis technique used to distinguish between the acid and the boroxine is IR spectroscopy.^[252] The literature data revealed that phenylboronic acid gives an absorption band at 1350 cm⁻¹,^[252] while phenylboroxine has an absorption band at higher energy, at 1370 cm⁻¹.^[252] Unfortunately, this is the only example reported in the literature. Therefore, in this thesis reports the first account on the IR stretching frequencies comparison between differently substituted boronic acid and boroxine derivatives. The results summarized in Table 3.2 have underlined that the 4-methoxyphenylboronic acid **259** is completely in the anhydride form without subjecting it to drying treatment, while 2,6-difluorophenylboronic acid **260** is totally in the acid form. IR spectroscopy analysis of these molecules has allowed us to determine the exact position of the B-O stretching band for the compound **259** and **260**. Firstly, 2,6-difluorophenylboronic acid **260** (Scheme 3.25) reveal an absorption band at 1346 cm⁻¹, this value is lower than the one for the reference compound, phenylboronic acid, with a $\Delta\nu = 4$ cm⁻¹. Secondly, the boroxine form of 4-methoxyphenylboroxine **259** (Scheme 3.28) present a B-O stretching absorption band even lower in energy, at 1338 cm⁻¹. This value is lower than the one reported in the literature for phenylboroxine, with a $\Delta\nu = 32$ cm⁻¹. This difference could come from the influence of the mesomeric donor substituent in *para* position, which weakens the B-O bond, reducing its double bond character, therefore shifting the B-O stretching to lower wavenumber, *i.e.* lower energy. Hence the attribution of the stretching frequency of the B-O bond to the anhydride or the acid has to take into account the substituent on the phenyl ring.

3.3.3. Influence of the Temperature on the Equilibrium

As outlined in the introduction, the equilibrium between acid and boroxine forms is affected by the temperature. At lower temperature, the ΔG of the formation of boroxine increases (Scheme 3.6, equation 4, section 3.1.2.2),^[255] therefore shifting the equilibrium toward the acid form. Taking this into consideration, the ¹H NMR analysis of 3,4,5-trifluorophenylboronic

Chapter 3

acid **261** was carried out at different temperatures. As evidenced by the ^1H NMR spectra of boronic acid **261** at r.t. and 90 °C, at higher temperature the boroxine form is favored. The peak corresponding to the acid form **261** is observed at 6.90 ppm (H_a) whereas the one corresponding to the boroxine **264** is present at 7.42 ppm (H_b). Hence, upon heating, the hydrogen atoms peak corresponding to the boroxine increases while the one corresponding to the acid diminishes.



Scheme 3.27 Equilibrium between 3,4,5-trifluorophenylboronic acid **261** and its boroxine form **264**.

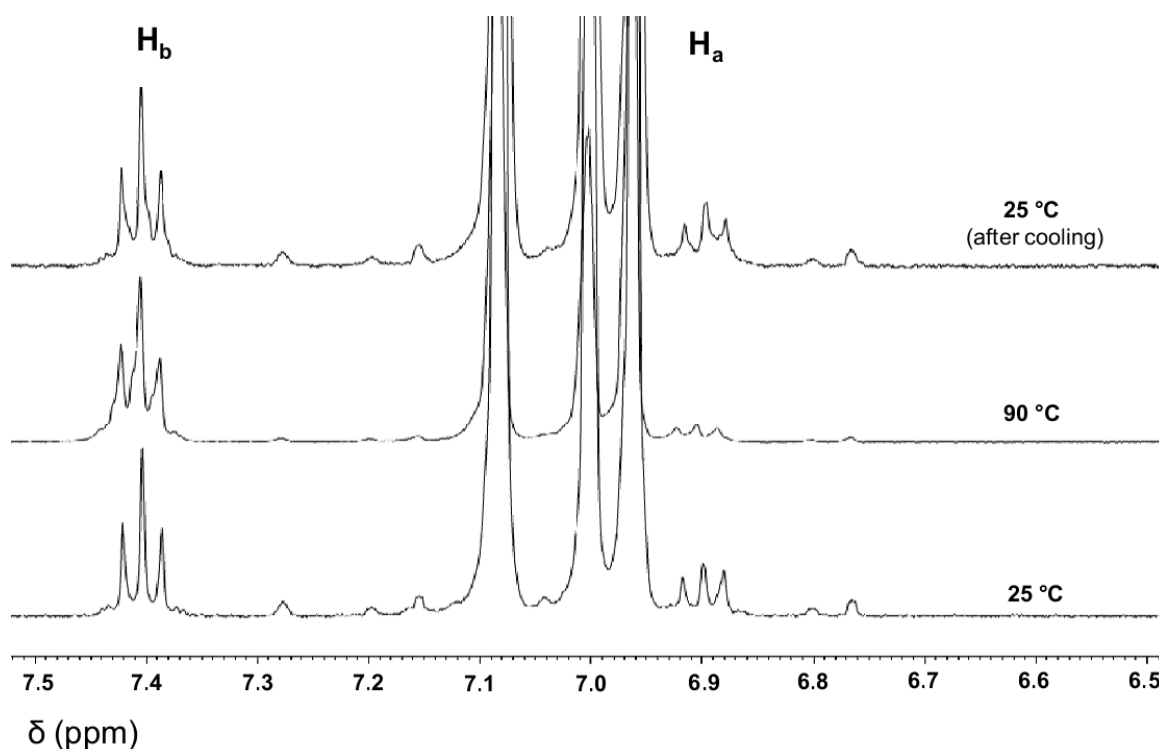


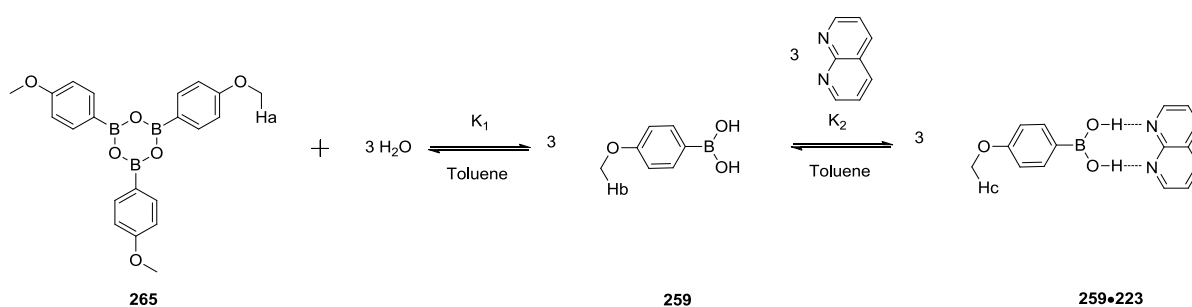
Figure 3.24 ^1H NMR spectra of 3,4,5-trifluorophenylboronic acid **261** at 25 °C (below), 90 °C (middle), and at 25 °C after cooling. The spectra display the transformation of the acid (H_a) into boroxine form (H_b) with a higher temperature. Solvent: $\text{toluene-}d_8$.

Whereas lower temperatures favor the acid form, as evidenced by the analysis of the acid/boroxine ratio. For instance, 4-methoxyphenylboronic acid **259** (Scheme 3.28) is completely in its anhydride form at r.t.. However, upon cooling at -30 °C, two peaks were observed in deuterated toluene, the new peak at higher field was attributed to the acid form. Hence, upon addition of 0.08 eq. of 1,8-naphthyridine **223** at -30 °C, the peak attributed to the acid form and the complex form is observed (Figure 3.25). Two peaks can be noticed and are attributed to the hydrogen atoms of the methoxy group, corresponding to the anhydride **265** ($\text{H}_a = 3.54$ ppm, Figure 3.25) or the acid **259** and complex **259**·**223** species (H_b and $\text{H}_c = 3.48$ ppm). Moreover, upon further addition of 1,8-naphthyridine **223**, a shift of the peak toward lower field is noticed, typical of a formation of a hydrogen bonded complex. Finally, the addition of 0.50 eq. is sufficient to observed a single peak, corresponding to the average between the chemical shift of the free acid and the complexed species. The addition of a double

Chapter 3

acceptor of hydrogen bond displaced the acid-anhydride equilibrium toward the acid form, as proven by the diminution of the peak intensity, corresponding to the anhydride (H_a , Figure 3.25, Scheme 3.28).

The presence of one peak for the free acid and the complexed species indicates that the equilibrium is rapid respective to ^1H NMR time scale (Figure 3.25). In contrast, the equilibrium between the acid and the boroxine form is slow and two peaks can be observed (Scheme 3.28, compound **265** and **259**). Unfortunately, the difference in chemical shift measured (0.05 ppm) was too low to allow a precise determination of the binding constant.



Scheme 3.28 Equilibriums present in solution, between boroxine **265**, acid **259** forms, and the complex **259•223**, during the titration of 4-methoxyphenylboronic acid **259** by 1,8-naphthyridine **223**.

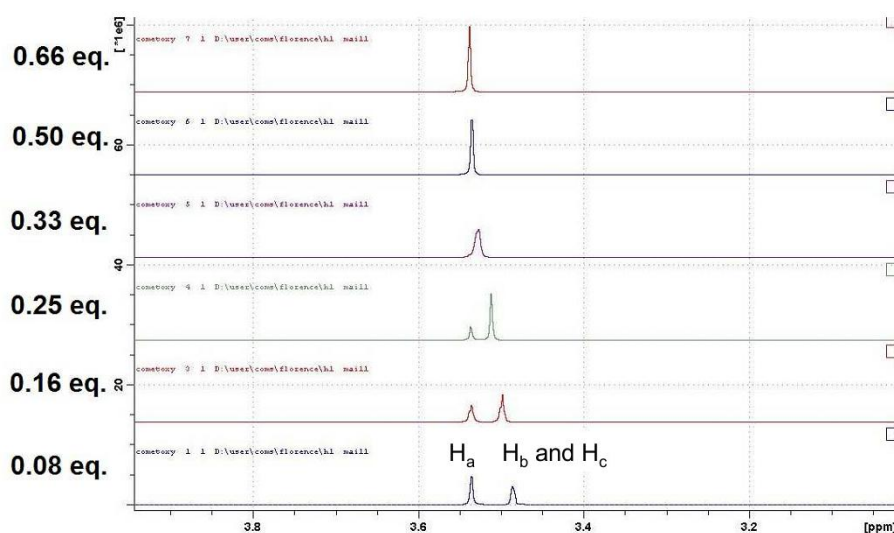


Figure 3.25 Overlay of ^1H NMR spectra taken during the titration experiment of 4-methoxyphenylboronic acid **259** by 1,8-naphthyridine **223** at -30°C in $\text{toluene-}d_8$. a: boroxine form, b: free acid form, c: complex.

3.4. Crystal Structures Study

The group of Professor Dr. Johan Wouters has resolved all X-ray diffraction structures. More particularly, the crystal structures have been solved by Bernadette Norberg.

With the aim of studying hydrogen bonds geometry and lengths of self-interacting boronic acid as DA system, a systematic study has been carried out for both commercially available and synthesized boronic acids, in the solid state by means of X-ray diffraction. As outlined earlier, boronic acids which do not possess *ortho* substituents on the aryl moieties have their equilibrium shifted toward the boroxine forms in solution, as probed by ^1H NMR spectroscopy. Thus the crystal structures of these boronic acids were not obtained in the solid state and their hydrogen bonding interactions were not studied. However, the crystal structures of their boroxine forms were studied instead.

3.4.1. Crystal Structure of Boroxines

Crystal structures of boroxines obtained from the corresponding boronic acids such as 4-methoxyphenylboronic acid (Figure 3.26), 4-dimethylaminophenylboronic acid (Figure 3.27), 3,4,5-trifluorophenylboronic acid (Figure 3.29), 4-fluorophenylboronic acid (Figure 3.28) were studied by means of X-ray diffraction. This study was performed with the aim of confirming that the products were the boroxines in the solid state and not the acids, allowing us to correctly attribute the IR stretching frequencies. Moreover, the dissolution of the compounds in solutions and their analysis by ^1H NMR spectroscopy allowed us to confirm the chemical shifts attributed to the boroxine form.

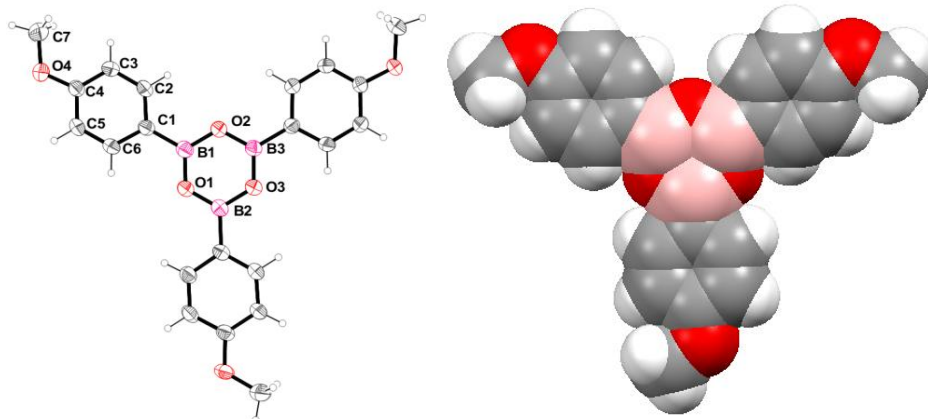


Figure 3.26 Crystal structure of 4-methoxyphenylboronic acid in its anhydride form **265**. Obtained by slow evaporation in CHCl_3 . Representation: left: ORTEP (drawn at the 30% probability level), right: spacefill. Color code: red: O, grey: C, pink: B, white: H. Space group: $P2_1/C$.

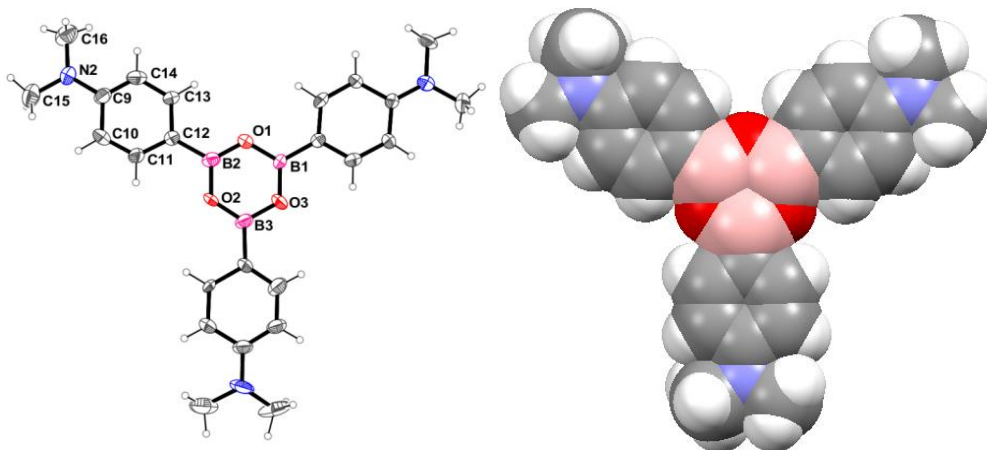


Figure 3.27 Crystal structure of 4-dimethylaminophenylboronic acid in its anhydride form. Obtained by slow evaporation in toluene. Representation: left: ORTEP (drawn at the 30% probability level), right: spacefill. Color code: red: O, grey: C, pink: B, white: H, blue: N. Space group: $P2_1$.

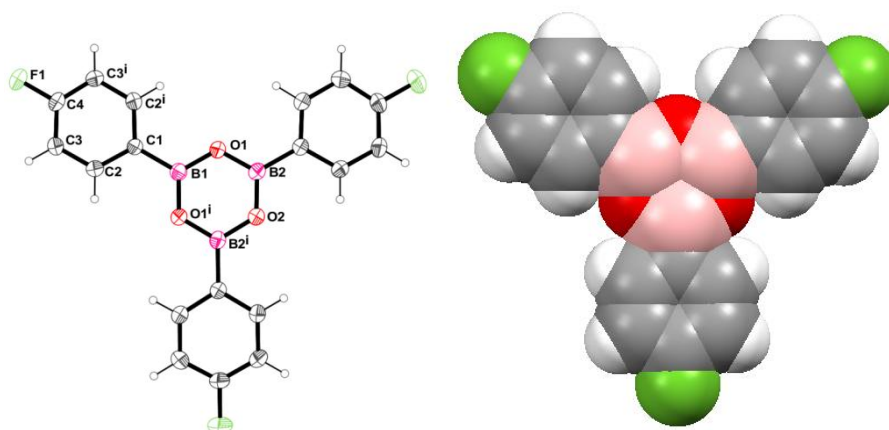


Figure 3.28 Crystal structure of 4-fluorophenylboronic acid in its anhydride form. Obtained by slow evaporation in toluene. Representation: left: ORTEP (drawn at the 30% probability level), right: spacefill. Color code: red: O, grey: C, pink: B, white: H green-yellow: F. Space group: $P2_1/m$.

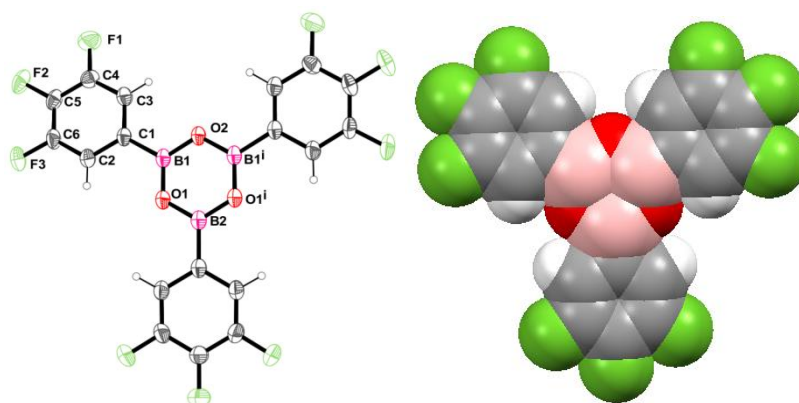


Figure 3.29 Crystal structure of 3,4,5-trifluorophenylboronic acid in its anhydride form **264**. Obtained by slow evaporation in CH_2Cl_2 . Representation: left: ORTEP (drawn at the 30% probability level), right: spacefill. Color code: red: O, grey: C, pink: B, white: H green-yellow: F. Space group: $C2/c$.

The crystals were obtained by slow evaporation of a solution containing the products. The first two crystal structures of the anhydrides of 4-methoxyphenylboronic acid (Figure 3.26) and 4-dimethylaminophenylboronic acid (Figure 3.27) were obtained from a solution containing both the anhydride in equilibrium with its acid form. Unfortunately, all other crystallization conditions tested, by varying the solvents used, could not afford crystal structures of the corresponding boronic acids. Surprisingly, the boroxine form of derivatives bearing electron withdrawing groups were also obtained for 4-fluorophenylboronic acid (Figure 3.28) and 3,4,5-trifluorophenylboronic acid (Figure 3.29). Indeed, these compounds are in equilibrium between the acid and the boroxine form in solution, as revealed during our study using ^1H NMR spectroscopy. In conclusion, it was observed that boroxine rings are planar, and the aryl groups are in the same plane, indicating a possible conjugation between the boroxine and the aromatic ring.

3.4.2. Crystal Structures of Self-Interacting Boronic Acids

In the literature, crystal structures of boronic acids have been systematically studied as DA systems of hydrogen bonds in order to measure the hydrogen bond lengths and observe the conformations adopted by the hydroxyl groups. The computational prediction discussed in the introduction of *section 3.2*. revealed that boronic acids interact preferably in a DA fashion. Moreover, the study of the boronic acid-boroxine equilibrium described in *section 3.3.*, outlined the importance of

the *ortho* substituents to favor the acid form. Hence, this section will focus on boronic acids which can act as DA systems substituted in *ortho* positions.

The crystal structures of mesitylboronic acid **224** (Figure 3.30), 2,6-dichlorophenylboronic acid (Figure 3.31), 2,6-difluorophenylboronic acid (Figure 3.32), pentafluorophenylboronic acid (Figure 3.33) and 2-fluoropyridine-3-boronic acid (Figure 3.35) all possessing substituents in *ortho* positions display DA arrangements. Due to the presence of the sterically hindered *ortho* substituents, no π - π stacking interactions were observed between the aryl groups. An additional effect of the presence of these *ortho* substituents is that the boronic acid group is not in the same plane as the aryl group. A direct consequence of this is that the conjugation between the π orbitals of the aryl moiety and the empty *p* orbital of the boronic acid group is reduced. Therefore, the effects of mesomeric donor or acceptor substituents of the aryl rings, on hydrogen bonds strengths, will be reduced. This is due to the break of the π -conjugation between the π orbitals of the aryl and the empty *p* orbital of the boron atom. Consequently, the study was focused on arylboronic acids bearing inductive donor, *e.g.* methyl or isopropyl, or attractor, *e.g.* fluorine or chlorine atoms, substituents in *ortho* positions.

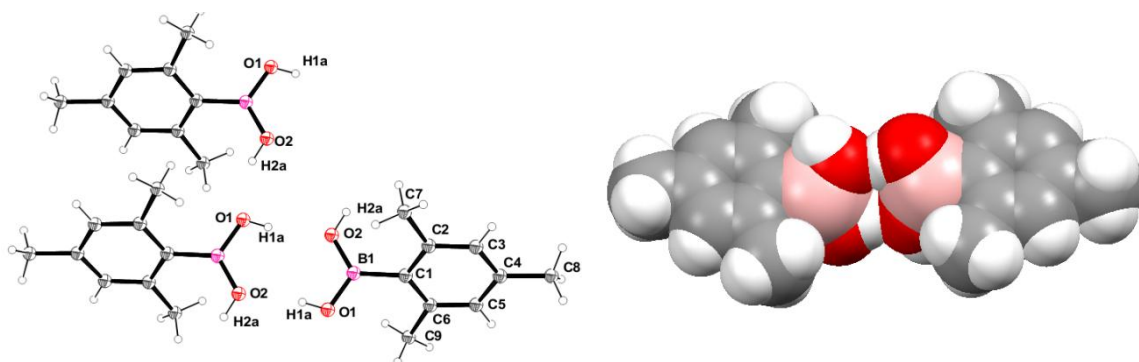


Figure 3.30 Crystal structure of mesitylboronic acid **224** obtained from slow evaporation in CHCl_3 . The dihedral angle formed by the aryl ring and the boronic acid moiety is: 51.55° . Distances of the hydrogen bonds (angle of the interactions): O1-H1-O2: $2.770(2) \text{ \AA}$ (169°), O2-H2-O1: $2.6868(18) \text{ \AA}$ (156°). Hydrogen bond system: DA-AD. Representation: left: ORTEP (drawn at the 30% probability level), right: spacefill. Color code: red: O, grey: C, pink: B, white: H. Space group: P-1.

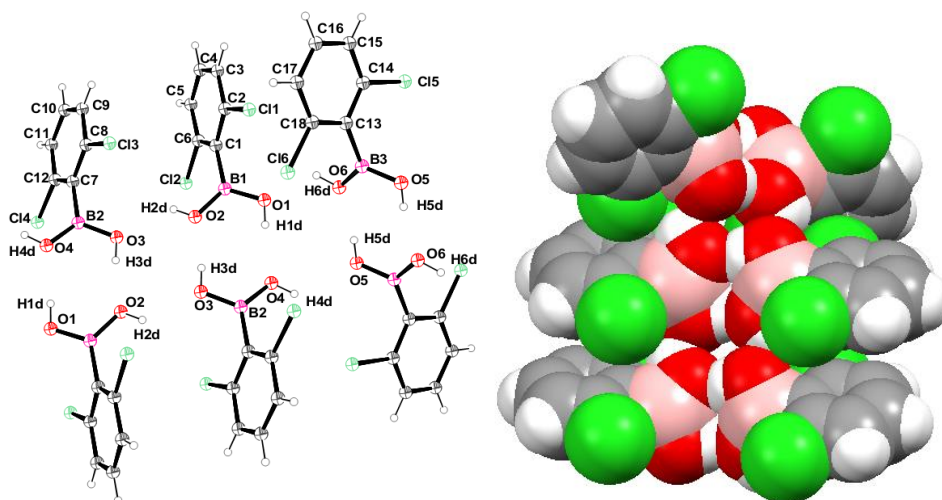


Figure 3.31 Crystal structure of 2,6-dichlorophenylboronic acid obtained from slow evaporation in toluene. The dihedral angle formed by the aryl ring and the boronic acid moiety is: 74.26° . Distances of the hydrogen bonds (angle of the interactions): O1-H1-O4: $2.797(3) \text{ \AA}$ (173°), O2-H2-O3: $2.754(3) \text{ \AA}$ (135°), O3-H3-O2: $2.726(3) \text{ \AA}$ (170°), O4-H4-O5: $2.873(3) \text{ \AA}$ (123°), O5-H5-O6: $2.772(3) \text{ \AA}$ (172°), O6-H6-O1: $2.830(3) \text{ \AA}$ (125°). Hydrogen bond system: DA-AD. Representation: left: ORTEP (drawn at the 30% probability level), right: spacefill. Color code: red: O, grey: C, pink: B, white: H, green: Cl. Space group: $P2_1/C$.

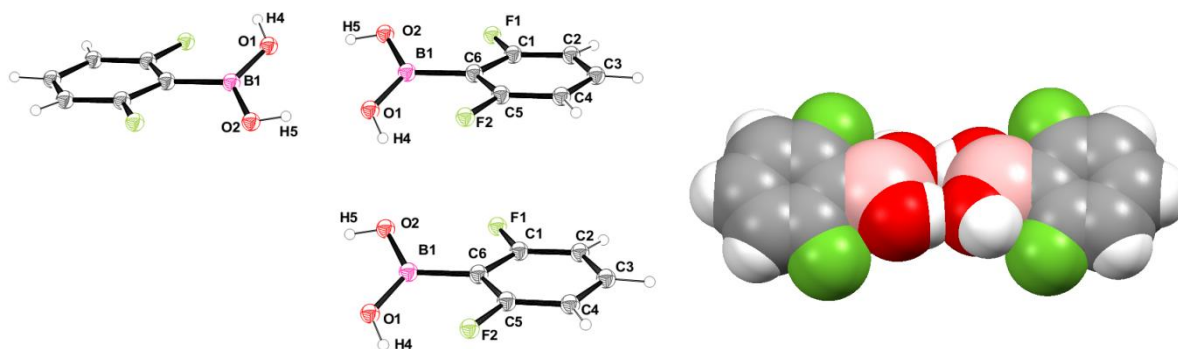


Figure 3.32 Crystal structure of 2,6-fluorophenylboronic acid **260**. The dihedral angle formed by the aryl ring and the boronic acid moiety is: 26.59° . Distances of the hydrogen bonds (angle of the interactions): O1-H4-O2: $2.849(6)$ Å (152°), O2-H5-O1: $2.798(6)$ Å (174°). Hydrogen bond system: DA-AD. Representation: left: ORTEP (drawn at the 30% probability level), right: spacefill. Color code: red: O, grey: C, pink: B, white: H, green-yellow: F. Space group: $P2_1/n$.^[245]

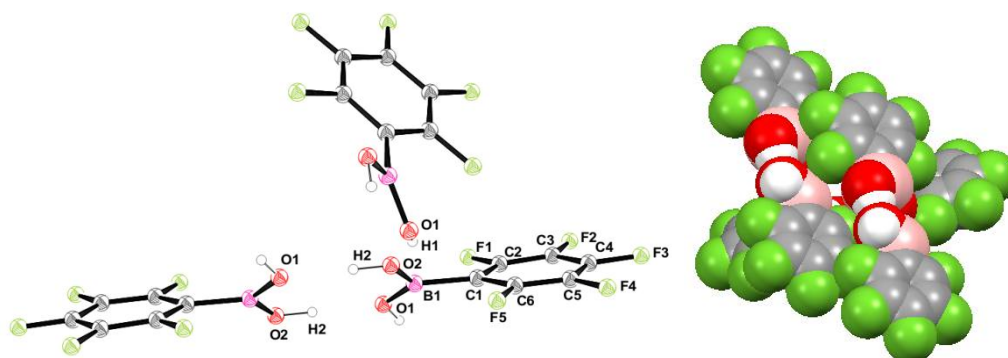


Figure 3.33 Crystal structure of pentafluorophenylboronic acid. The dihedral angle formed by the aryl ring and the boronic acid moiety is: 37.55° . Distances of the hydrogen bonds and close contacts (angle of the interactions): O1-H1-O2: $2.7651(19)$ Å (159°), O1-H2-O2: $2.7328(19)$ Å (177°). Hydrogen bond system: DA-AD. Representation: left: ORTEP (drawn at the 30% probability level), right: spacefill. Color code: red: O, grey: C, pink: B, white: H, green-yellow: F. Space group: $P2_1/n$.

Finally, in an attempt to observe the π - π stacking between the electron deficient ring of pentafluorophenylboronic acid and the electron rich ring of phenylboronic acid, the two components were mixed. However, they organized through hydrogen bonds in two separate networks and no π - π stacking interactions are observed (Figure 3.34). The arrangement is peculiar for phenylboronic acid, the ‘tape’ motif is not formed, as observed in the crystal structure of phenylboronic acid alone.^[309] Moreover, the boronic acid group is not in the same plane as the phenyl group, having a torsion angle between the hydroxyl group and the aryl moiety of 32.1° . Regarding pentafluorophenylboronic acid, the torsion angle (36.4°) is similar to the one observed in the crystal structure of pentafluorophenylboronic acid alone (37.5°) (Figure 3.33). Even more noticeable is the hydrogen bond distances, the one formed by self-interacting phenylboronic acid (O4-H4-O3: $2.867(1)$ Å and O3-H3-O4: $2.817(1)$ Å) are slightly shorter compared to these formed between pentafluorophenylboronic acid (H1-O2: $2.914(1)$ Å and O2-H2-O1: $2.804(1)$ Å). The contrary was expected based on the idea that five electron withdrawing substituents would increase the partial charge on the hydrogen atoms, resulting in a stronger hydrogen bond. This surprising observation can be explained by the presence of the fluorine atoms in *ortho* positions, which have close contacts with the hydroxyl groups (O1-H1-F5: $2.9038(6)$ Å, O2-H2-F1: $2.817(2)$ Å, O1-H1-F1: $2.915(1)$ Å), in the case of pentafluorophenylboronic acid. Also, this could be due to packing effects since the hydrogen bond distances are slightly longer than the one measured on the crystal structure of pentafluorophenylboronic acid alone.

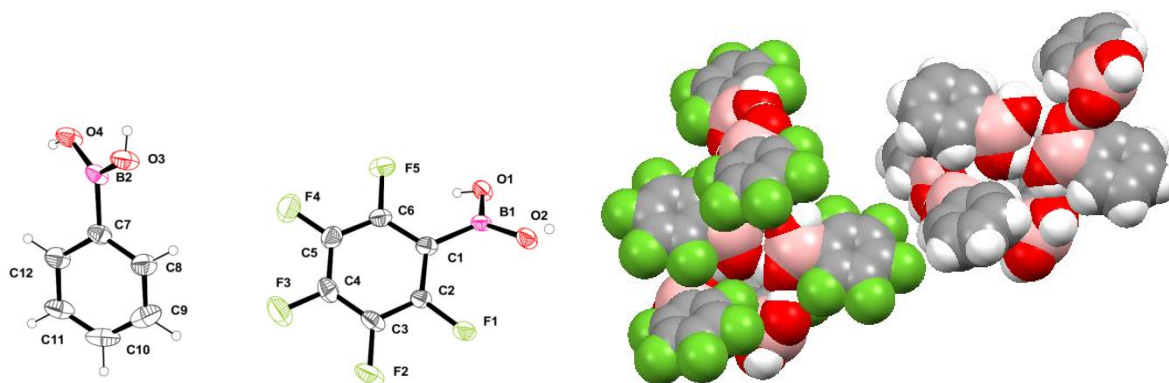


Figure 3.34 Crystal structure of 2,3,4,5,6-pentafluorophenylboronic acid and phenylboronic acid. The dihedral angle formed by the aryl ring and the boronic acid moiety is: 36.4° and 32.1° for pentafluorophenylboronic acid and phenylboronic acid respectively. Distances of the hydrogen bonds and close contacts (angle of the interactions): O1-H1-O2: $2.914(1) \text{ \AA}$ (151°), O2-H2-O1: $2.804(1) \text{ \AA}$ (171°), O1-H1-F5: $2.9038(6) \text{ \AA}$ (107°), O2-F5: $2.817(2) \text{ \AA}$, O1-H1-F1: $2.915(1) \text{ \AA}$ (111°) for pentafluorophenylboronic acid and O4-H4-O3: $2.867(1) \text{ \AA}$ (176°), O3-H3-O4: $2.817(1) \text{ \AA}$ (166°) for phenylboronic acid. Hydrogen bond system: DA-AD. Representation: left: ORTEP (drawn at the 30% probability level), right: spacefill. Color code: red: O, grey: C, pink: B, white: H, green-yellow: fluorine. Space group: $P2_1/c$.

Some conclusions can be drawn from the first five structures regarding the effect of the inductive attractor substituents on the oxygen-oxygen distances between the hydroxyl groups involved in hydrogen bonding. The hydrogen bond distances vary but no correlations can be found with the presence of inductive attractor groups on the aryl moieties (Table 3.4). The shorter hydrogen bond distances can be explained by the differences in the angles formed by the oxygen-hydrogen-oxygen involved in the hydrogen bond. Indeed, when the angle is below 180° , for bent hydrogen bond, the distance between the two heteroatoms is reduced (see bent hydrogen bonds in Scheme 3.2). The other reason is the type of crystal packing, as observed for Figure 3.31 and Figure 3.33, where the ‘tape’ arrangement is twisted to the contrary of linear tape arrangement observed in Figure 3.30 and Figure 3.32. In the first case, 2,6-dichlorophenylboronic acid is not in the plane of the other aryl groups (Figure 3.31). In the second case, one pentafluorophenylboronic acid is perpendicular to its neighbor in the tape formation (Figure 3.33).

Boronic acid derivative	Shortest O-O distance (\AA)	Longest O-O distance (\AA)
mesitylboronic acid 224	2.6868(18)	2.770(2)
2,6-dichlorophenylboronic acid	2.726(3)	2.830(3)
2,6-difluorophenylboronic acid 260	2.798(6)	2.849(6)
pentafluorophenylboronic acid	2.7328(19) (Figure 3.33)/ 2.804(1) (Figure 3.34)	2.7651(19) (Figure 3.33)/ 2.914(1) (Figure 3.34)

Table 3.4 Hydrogen bond distances of self-interacting boronic acids.

3.4.3. Crystal structure of Complexes

The aim of this extensive crystal structure study was to gain access to the stoichiometry, geometry and bond distances of the complexes formed between the boronic acids and the hydrogen bond acceptors in the solid state. Even though, the stoichiometry of the complex can be determined by ITC titration, when the binding constants of the complexes are low, resulting in a small ‘c’ value (Equation 3.8, page 71), the measurement cannot be obtained with precision, as outlined in the introduction (section 3.1.2.3.). Therefore, parameters, such as the stoichiometry, need to be obtained from through an alternative analysis. Consequently, a systematic study of the stoichiometry, the bond distances and the geometry of the complex was undertaken by X-ray diffraction analysis, assuming that the stoichiometry of the complex will be identical in solution. Even more interestingly, the geometry of the complexes in the solid state can indicate the dihedral angle formed between the boronic acid moiety and the phenyl group. This could inform on the effective conjugation between mesomeric

donor groups substituting the phenyl and the boronic acid moiety, influencing the energy of the hydrogen bond interaction. Finally, a detailed measure of the hydrogen bond distances in the solid state could be correlated to the energy of the hydrogen bond, as measured by ITC.

3.4.3.1. Complexes with Pyridyl or Naphthyridine as Acceptors (1:1 stoichiometry)

The complexes formed between boronic acids and pyridyl or 1,8-naphthyridine derivatives were studied in the solid state, in order to gain access to the stoichiometry and geometry of the complexes. Initially, the single hydrogen bond, formed when boronic acid moieties interact with pyridyl acceptors, was studied for 2-fluoropyridine-3-boronic acid (Figure 3.35) and 2-fluoropyridine-5-boronic acid (Figure 3.36). Furthermore, the study was focused on the double hydrogen bonds formed between boronic acid derivatives and 1,8-naphthyridine. In addition, boronic acids substituted in *ortho* positions were investigated, followed by the one substituted in *meta* or *para* positions.

Firstly, in order to study the effect of only one substituent in *ortho* position on the torsion angle between the aryl group and the boronic acid moiety, the crystal structure of 2-fluoropyridine-3-boronic acid (Figure 3.35) was studied. The second purpose of this study was to measure the hydrogen bond distances between the hydroxyl group and the pyridyl moieties, in order to compare the latter with the value obtained when boronic acids form a double hydrogen bond with 1,8-naphthyridine (see Table 3.6). Hence, it was observed that the acid moiety is in the same plane as the pyridyl ring, with no influence from the fluorine atom in *ortho* position. In addition, the first hydroxyl group is involved in a hydrogen bond with the nitrogen atom of the pyridyl group of another boronic acid molecule while the second hydroxyl group is not involved in a hydrogen bond with another hydroxyl group but has a close contact with the fluorine atom in *ortho* position within the same molecule (O2-F1: 2.816(8) Å). The system formed is a D-A system of hydrogen bond.

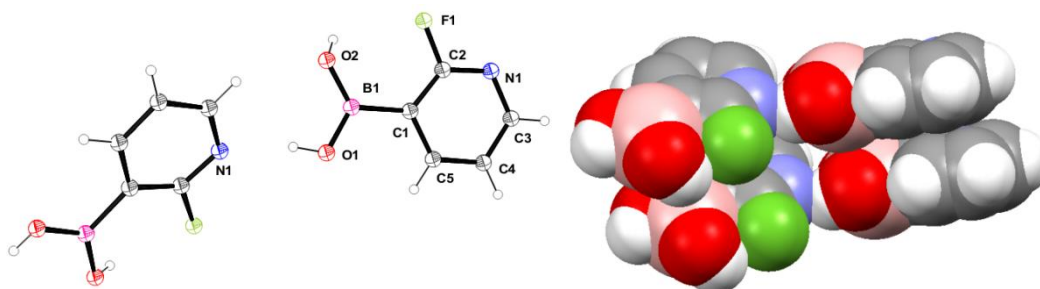


Figure 3.35 Crystal structure of 2-fluoropyridine-3-boronic acid. The dihedral angle formed by the aryl ring and the boronic acid moiety is: 0°. Distances of the hydrogen bonds and close contacts (angle of the interactions): O1-N1: 2.829(8) Å (155°), O2-F1: 2.816(8) Å (111°). Hydrogen bond system: D-A. Distance between the aryl groups centroid involved in π - π stacking: 3.76 Å. Representation: left: ORTEP (drawn at the 30% probability level), right: spacefill. Color code: red: O, grey: C, pink: B, white: H, blue: N, green-yellow: F. Space group: P2₁/c.

Secondly, 2-fluoropyridine-5-boronic acid (Figure 3.36) was crystallized, with the aim of comparing the hydrogen bond distances between the heteroatoms with a derivative having no substituent in *ortho* but in *para* position. The crystal structure reveals the presence of hydrogen bonds between the hydroxyl groups of boronic acid, in a DA-AD fashion together with a hydroxyl-pyridyl hydrogen bond. The distance of the hydrogen bond between the oxygen and the nitrogen atoms is shorter (from 2.829(8) Å to 2.7167(13) Å) when there is no fluorine atom in *ortho* to distort the hydroxyl group.

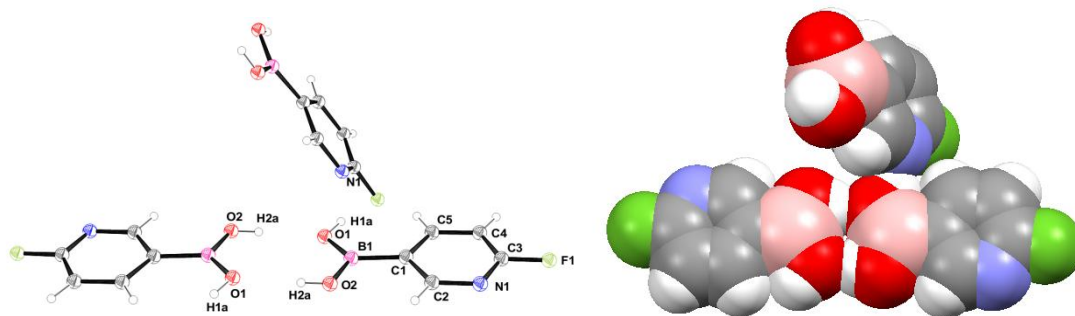


Figure 3.36 Crystal structure of 2-fluoropyridine-5-boronic acid. The dihedral angle formed by the aryl ring and the boronic acid moiety is: 0° . Distances of the hydrogen bonds (angle of the interactions): O1-N1: 2.7167(13) Å (144°), O1-O2: 2.7630(15) Å (175°). Hydrogen bond system: DA-AD. Representation: left: ORTEP (drawn at the 30% probability level), right: spacefill. Color code: red: O, grey: C, pink: B, white: H, blue: N, green-yellow: F. Space group: $P2_1/c$.

Furthermore, the second aim of this studies involved boronic acids forming double hydrogen bonds with 1,8-naphthyridine in an attempt to act as AA-DD systems. Firstly, boronic acids bearing *ortho* substituents (mesitylboronic acid **224**, 2,6-dichlorophenylboronic acid, and 2,6-difluorophenylboronic acid) were studied, in the solid state, while in complexes with 1,8-naphthyridine. In theory, the presence of substituents in *ortho* position on aryl boronic acids will force the boronic acid moiety to have a torsion angle with the aryl group. As a result, the angles observed are higher, when boronic acids form a complex with 1,8-naphthyridine, than compared to the angle measured in crystal structure of boronic acid alone (Table 3.5). The torsion angles measured are high enough to reduce the conjugation between mesomeric acceptors groups, on the aryl, and the boronic acid moiety. Therefore, only boronic acids bearing inductive donor groups, such as methyl (Figure 3.37) or isopropyl, and attractor groups, such as chlorine atoms (Figure 3.38) or fluorine atoms (Figure 3.39), were studied. Another interesting observation is the influence of the *ortho* groups on the hydrogen bond distances between the donor and the acceptor. The expected trend, without taking into account packing effect or influence of the steric hindrance from the groups in *ortho* position, is a reduced distance with the increase of electronegativity of the substituents. This is the trend observed, as outlined in Table 3.6, with the shortest hydrogen bonds distances for the 2,6-difluorophenylboronic acid (Figure 3.39).

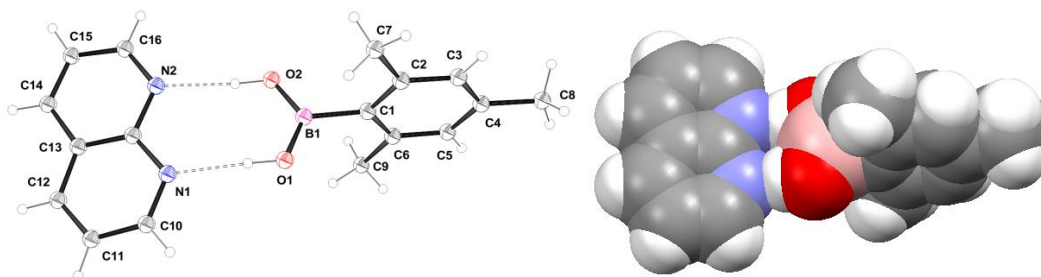


Figure 3.37 Crystal structure of the complex formed between mesitylboronic acid **224** and 1,8-naphthyridine **223**. Crystals were obtained by slow evaporation in toluene. Distances of the hydrogen bonds: N1-O1: 2.839(3) Å, N2-O2: 2.878(2) Å. Dihedral angle formed between the aryl group and the boronic acid group: 88.94° . Hydrogen bond system: DD-AA. Representation: left: ORTEP (drawn at the 30% probability level), right: spacefill. Color code: red: O, grey: C, pink: B, white: H, blue: N. Space group: $P2_1/C$.

The presence of methyl groups, in the case of mesitylboronic acid, prevents the π - π stacking interactions with other aryl groups, while the π - π stacking is observed in the crystal packing of 2,6-dichlorophenylboronic acid and 2,6-difluorophenylboronic acid, when forming complex with 1,8-naphthyridine. In this case, the π - π stacking interactions are observed between the rings of aryl boronic acids and the centroid to centroid distances are of 3.63 Å and 3.86 Å when substituted with chlorine and fluorine atoms respectively.

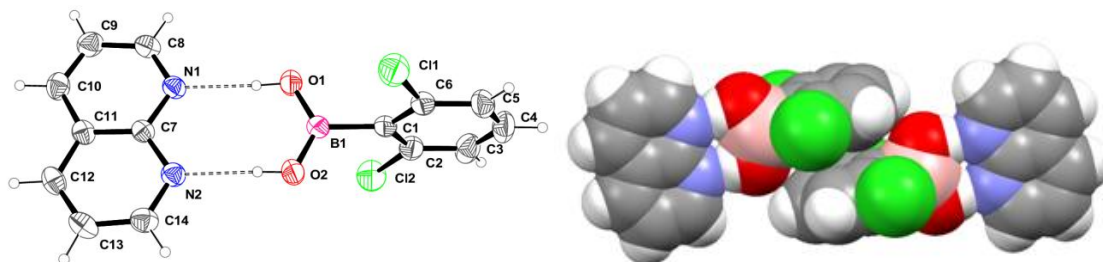


Figure 3.38 Crystal structure of the complex formed between 2,6-dichlorophenylboronic acid and 1,8-naphthyridine **223**. Crystals were obtained by slow evaporation in toluene. Distances of the hydrogen bonds: N1-O1: 2.812(2) Å, N1-O1: 2.802(2) Å. Distance between the aryl groups centroid involved in π - π stacking interactions: 3.63 Å. Dihedral angle formed between the aryl group and the boronic acid group: 88.77°. Hydrogen bond system: DD-AA. Representation: left: ORTEP (drawn at the 30% probability level), right: spacefill. Color code: red: O, grey: C, pink: B, white: H, blue: N, green: Cl. Space group: $P2_1/C$.

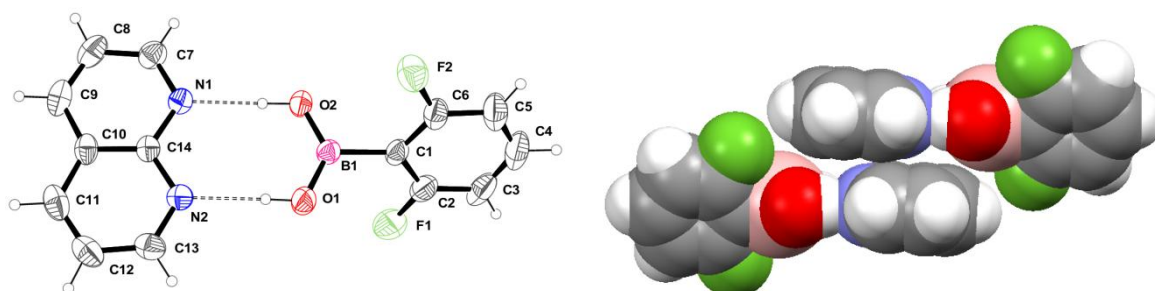


Figure 3.39 Crystal structure of the complex formed between 2,6-difluorophenylboronic acid **260** and 1,8-naphthyridine **223**. Crystals were obtained by slow evaporation in toluene. Distances of the hydrogen bonds: N1-O2: 2.7862(19) Å, N2-O1: 2.798(2) Å. Distance between the aryl groups centroid involved in π - π stacking interactions: 3.86 Å. Dihedral angle formed between the aryl group and the boronic acid group: 62.46°. Hydrogen bond system: DD-AA. Representation: left: ORTEP (drawn at the 30% probability level), right: spacefill. Color code: red: O, grey: C, pink: B, white: H, blue: N, yellow: F. Space group: $P2_1/c$.

Finally, pentafluorophenylboronic acid was dissolved in toluene with 1,8-naphthyridine. However, the derivative decomposed into $B(OH)_3$, due to a hydrolysis of the carbon-boron bond, catalyzed in presence of a base.^[310] The hydrogen bond distances (between 2.771(2) Å and 2.865(2) Å, Figure 3.40) are comparable to the one observed with arylboronic acid in complex with 1,8-naphthyridine. Also noticeable is the DA system of hydrogen bond between the $B(OH)_3$, with similar hydrogen bonds distances to the one measured between self-interacting boronic acids (Table 3.4). The stoichiometry is 1:1 in the complex implying two molecules of $B(OH)_3$ and two molecules of 1,8-naphthyridine.

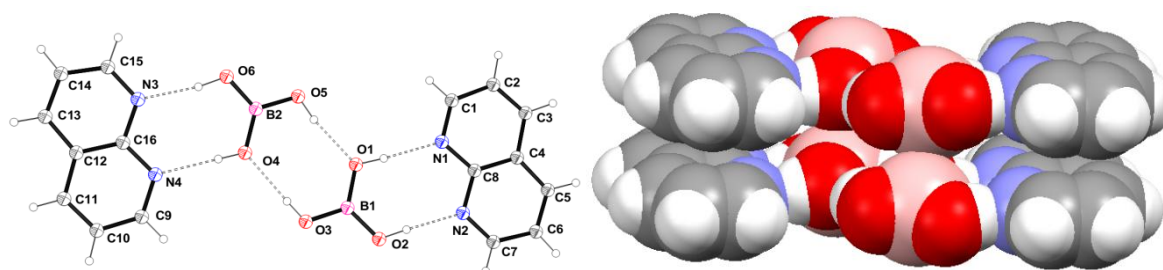


Figure 3.40 Crystal structure of the complex formed between $B(OH)_3$ and 1,8-naphthyridine **223**. Crystals were obtained by slow evaporation in toluene. Distances of the hydrogen bonds: N1-O1: 2.790(2) Å, N2-O2: 2.823(2) Å, N3-O6: 2.771(2) Å, N4-O4: 2.865(2) Å, O5-O1: 2.755(2) Å, O4-O3: 2.797(2) Å. Distance between the aryl groups centroid involved in π - π stacking interactions: 3.80 Å. Hydrogen bond system: DD-AA. Representation: left: ORTEP (drawn at the 30% probability level), right: spacefill. Color code: red: O, grey: C, pink: B, white: H, blue: N. Space group: $P-1$.

The torsion angles between the boronic acid groups and the aryl groups follow the trend outlined in Table 3.5. The highest angle is observed for 2,6-dichlorophenylboronic acid (74.26°), while the lower angle is measured in the crystal structure of 2,6-difluorophenylboronic acid (26.59°). The low angle value obtained with the latter compound let us hoped that

Chapter 3

we could design a boronic acids substituted in *ortho* position by substituent that disfavored the formation of boroxines, and in *para* position by mesomeric donor and acceptor groups. The mesomeric donor and acceptors would be used to tune the strength of the hydrogen bonds. However, the values of the torsion angles obtained when boronic acids are complexed by 1,8-naphthyridine are higher than the one observed for self-interacting boronic acids. These high torsion angles would result in a breaking of conjugation between the mesomeric groups and the boronic acid moieties, assuming that the geometry of the complexes in solution will be similar to the one observed in the solid state.

Boronic acid derivative	Torsion angles of self-interacting boronic acid	Torsion angles of boronic acid in complex with 1,8-naphthyridine
2,6-difluorophenylboronic acid 260	26.59°	62.46°
pentafluorophenylboronic acid	37.55° (Figure 3.33)/ 36.4° (Figure 3.34)	Not obtained.
mesitylboronic acid 224	51.55°	88.94°
2,6-dichlorophenylboronic acid	74.26°	88.77°

Table 3.5 Torsion angles between the boronic acid groups and the aryl moieties, for boronic acids substituted in *ortho* positions.

Moreover, crystal structures of complex formed between aryl boronic acids, substituted in *meta* or *para* positions, and 1,8-naphthyridine were investigated. Again, these complexes have a 1:1 stoichiometry and interact in a DD-AA fashion. In these cases, the aryl group of the boronic acid and 1,8-naphthyridine are on the same plane due to the absence of *ortho* substituent, that provokes a distortion between the aryl groups and the boronic acid moieties. The distances are summarized in Table 3.7 and no clear trend can be drawn from these data and a statistically more significant study is needed, on a larger sample.

Also noticeable, in the following complex, is the presence of π - π stacking interactions between the phenyl group substituted by the boronic acid and 1,8-naphthyridine. For example, when in complex with phenylboronic acid, 4-fluorophenylboronic acid, and 4-methoxyphenylboronic acid, the distances are of 3.62 Å, 3.76 Å and 3.94 Å respectively (Figure 3.41, Figure 3.42 and Figure 3.44). In the complex formed between 3,4,5-trifluorophenylboronic acid or 4-thiomethylphenylboronic acid and 1,8-naphthyridine, the centroid-centroid distances between naphthyridine-naphthyridine rings and phenyl-phenyl rings are of 3.87 Å and 3.87 Å, (Figure 3.43) of 3.83 Å and 3.89 Å (Figure 3.45), respectively.

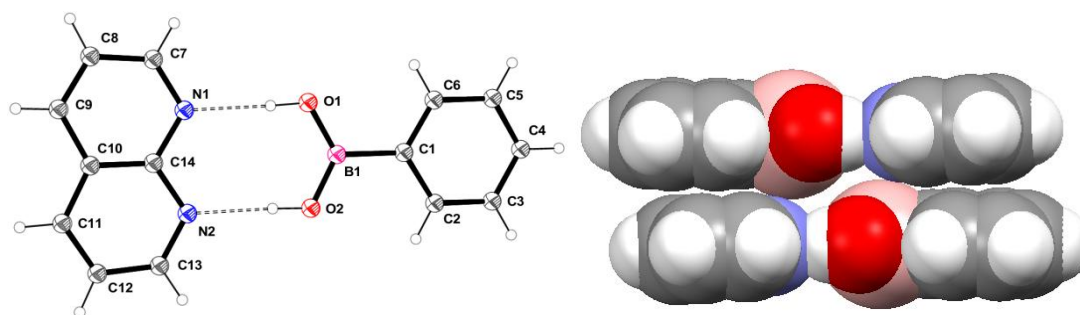


Figure 3.41 Crystal structure of the complex formed between phenylboronic acid **170** and 1,8-naphthyridine **223**. Obtained by slow evaporation in CDCl_3 . Distances of the hydrogen bonds: N1-O1: 2.8219(14) Å, N2-O2: 2.8270(14) Å. Distance between aryl group centroid involved in π - π stacking: 3.62 Å. Hydrogen bond system: DD-AA. Representation: left: ORTEP (drawn at the 30% probability level), right: spacefill. Color code: red, O, grey, C, pink, B, white, H. Space group: $P2_1/C$.

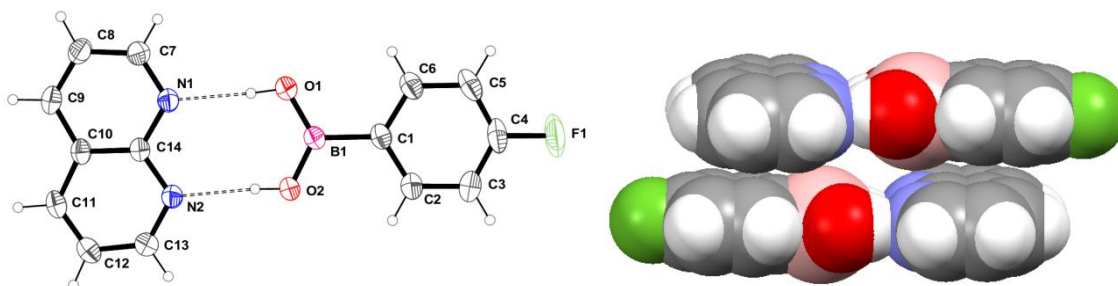


Figure 3.42 Crystal structure of the complex formed between 4-fluorophenylboronic acid and 1,8-naphthyridine **223**. Crystals were obtained by slow evaporation in toluene. Distance N1-O1: 2.8273(18) Å, N2-O2: 2.8250(19) Å. Distance between the aryl groups centroid involved in π - π stacking interactions: 3.76 Å. Hydrogen bond system: DD-AA. Representation: left: ORTEP (drawn at the 30% probability level), right: spacefill. Color code: red: O, grey: C, pink: B, white: H, blue: N, green-yellow: F. Space group: $P2_1/C$.

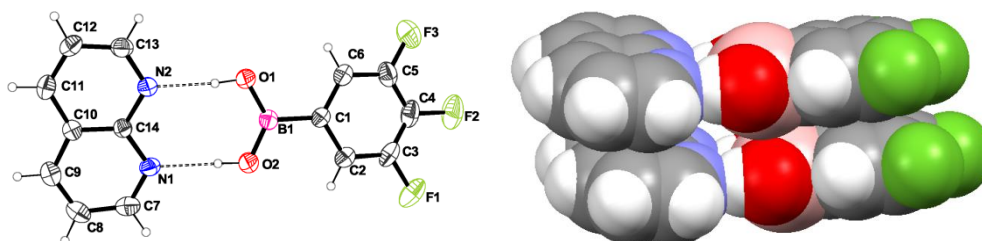


Figure 3.43 Crystal structure of the complex formed between 3,4,5-trifluorophenylboronic acid and 1,8-naphthyridine **223**. Crystals were obtained by slow evaporation in toluene. Distance N1-O2: 2.820(3) Å, N2-O1: 2.829(3) Å. Distances between the aryl groups centroid involved in π - π stacking interactions between the naphthyridine rings: 3.87 Å, between the phenyl rings: 3.87 Å. Hydrogen bond system: DD-AA. Representation: left: ORTEP (drawn at the 30% probability level), right: spacefill. Color code: red: O, grey: C, pink: B, white: H, blue: N, yellow: F. Space group: $P2_1/C$.

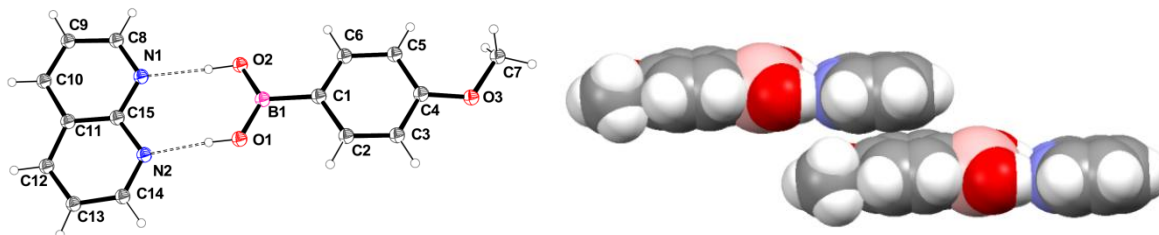


Figure 3.44 Crystal structure of the complex formed between 4-methoxyphenylboronic acid and 1,8-naphthyridine **223**. Crystals were obtained by slow evaporation in toluene. Distance N1-O2: 2.8445(19) Å, N2-O1: 2.819(2) Å. Distance between the aryl groups centroid involved in π - π stacking interactions: 3.94 Å. Hydrogen bond system: DD-AA. Representation: left: ORTEP (drawn at the 30% probability level), right: spacefill. Color code: red: O, grey: C, pink: B, white: H, blue: N. Space group: $P2_1/C$.

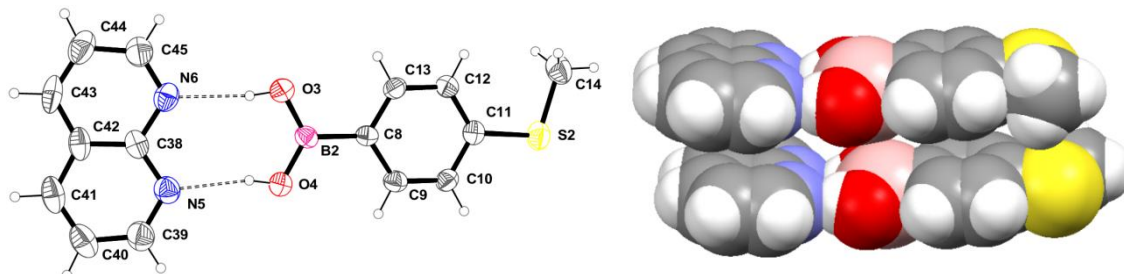


Figure 3.45 Crystal structure of the complex formed between 4-thiomethylphenylboronic acid and 1,8-naphthyridine **223**. Crystals were obtained by slow evaporation in MeOH. Distance N6-O3: 2.869(5) Å, N5-O4: 2.879(5) Å. Distances between the aryl groups centroid involved in π - π stacking interactions between the naphthyridine rings: 3.83 Å, between the phenyl rings: 3.89 Å. Hydrogen bond system: DD-AA. Representation: left: ORTEP (drawn at the 30% probability level), right: spacefill. Color code: red: O, grey: C, pink: B, white: H, blue: N, yellow: S. Space group: $Pbcn$.

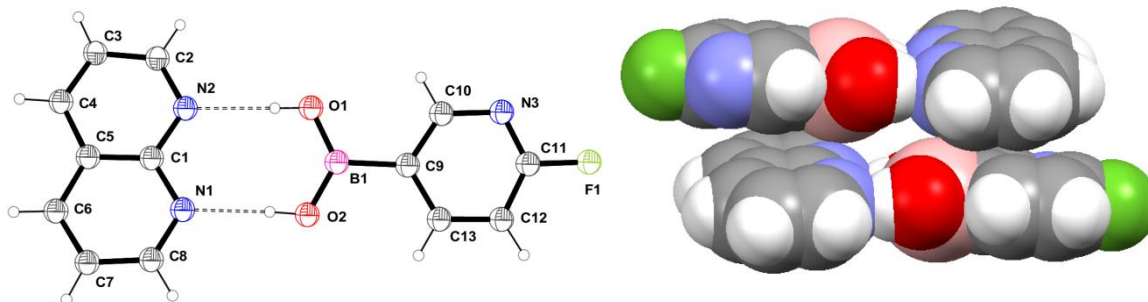


Figure 3.46 Crystal structure of the complex formed between 2-fluoropyridyl-4-boronic acid and 1,8-naphthyridine **223**. The dihedral angle formed by the aryl ring and the boronic acid moiety is: 0° . Distance N1-O2: 2.7831(14) Å, N2-O1: 2.8288(14) Å. Hydrogen bond system: DD-AA. Distance between the aryl groups centroid involved in π - π stacking: 3.792 Å. Representation: left: ORTEP (drawn at the 30% probability level), right: spacefill. Color code: red: O, grey: C, pink: B, white: H, green-yellow: fluorine. Space group: $P2_1/c$.

As a summary, hydrogen bond distances vary slightly within the series of boronic acids. For boronic acids possessing *ortho* substituents, the variation follows the trend outlined in Table 3.6. The increase of the electronegativity of the substituent enhances the hydrogen atoms polarization, reducing the hydrogen bond distances.

Boronic acid derivative	First O-N distance (Å)	Second O-N distance (Å)
mesitylboronic acid 224	2.839(3)	2.878(2)
2,6-dichlorophenylboronic acid	2.802(2)	2.812(2)
2,6-difluorophenylboronic acid 260	2.798(6)	2.849(6)
2-fluoropyridine-3-boronic acid	2.829(8)	/
2-fluoropyridine-5-boronic acid	2.7167(13)	/

Table 3.6 Hydrogen bond distances of *ortho* substituted aryl boronic acids complexed by 1,8-naphthyridine.

The same trend is not observed for *meta* or *para* substituted phenylboronic acids, the variation of distances are more likely due to packing effects (Table 3.7). However, one can notice that the hydrogen bond distances in the complex form by 3,4,5-trifluorophenylboronic acid and 1,8-naphthyridine of 2.830(2) Å and 2.829(3) Å (Figure 3.43) are relatively shorter than the one in the complex with 4-thiomethylphenylboronic acid, with distances of 2.869(5) Å and 2.879(5) Å respectively (Figure 3.45). These shorter distances can be attributed to the presence of three electron withdrawing atoms that increase the positive charge on the hydrogen atoms as opposed to an electron donating group, such as the thiomethyl group.

Boronic acid derivative	First O-N distance (Å)	Second O-N distance (Å)
phenylboronic acid 170	2.8219(14)	2.8270(14)
4-fluorophenylboronic acid	2.8250(19)	2.8273(18)
3,4,5-trifluorophenylboronic acid 261	2.820(3)	2.829(3)
4-methoxyphenylboronic acid 259	2.819(2)	2.8445(19)
4-thiomethylphenylboronic acid	2.869(5)	2.879(5)

Table 3.7 Distances of the hydrogen bonds of *meta* or *para* substituted aryl boronic acids complexed by 1,8-naphthyridine.

3.4.3.2. Bidentate Hydrogen Bond Motifs

With the aim of studying infinite linear arrangement of boronic acids with their acceptor counterparts, several complexes having two hydrogen bond donor groups or two hydrogen bond acceptors groups were studied. For example, the first complex represents the binding of 1,4-phenylenediboronic acid with 1,8-naphthyridine in a AA-DD arrangement (Figure 3.47). The complex formed is planar, letting us hope that a planar, infinite structure can be obtained. One can observe π - π

stacking interactions, between the aryls bearing the boronic acid and between 1,8-naphthyridine rings with a distance of 3.92 Å and 3.75 Å respectively. Another interesting feature of this complex is the presence of a parallel network of boronic acid, involved in hydrogen bonding interactions with the oxygen atoms of an additional boronic acid molecule, acting as an acceptor.

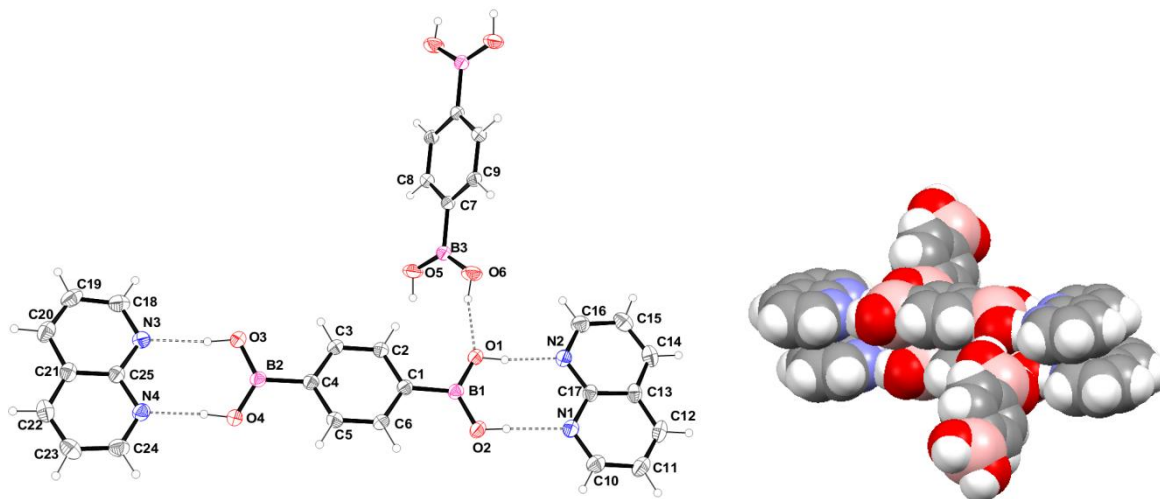


Figure 3.47 Crystal structure of the complex formed between 1,4-phenylenediboric acid **257** and 1,8-naphthyridine. Crystals were obtained by slow evaporation in hot H₂O. Distance N1-O2: 2.8736(16) Å, N2-O1: 2.7420(16) Å, N3-O3: 2.8766(16) Å, N4-O4: 2.7527(16) Å, O5-O4: 2.7776(17) Å, O6-O1: 2.7326(18) Å. Distance between the aryl groups involved in π - π stacking interactions: 3.92 Å. Hydrogen bond system: DD-AA. Representation: left: ORTEP (drawn at the 30% probability level), right: spacefill. Color code: red: O, grey: C, pink: B, white: H, blue: N. Space group: P-1.

At the contrary, the complex formed between 2,5-thiophenediboric acid and 1,8-naphthyridine is not planar and the dihedral angle observed between the plane of the boronic acid group and the plane of the thiophene ring is of 11.56°. Even more, no π - π stacking interactions neither side hydrogen bonding interactions are observed.

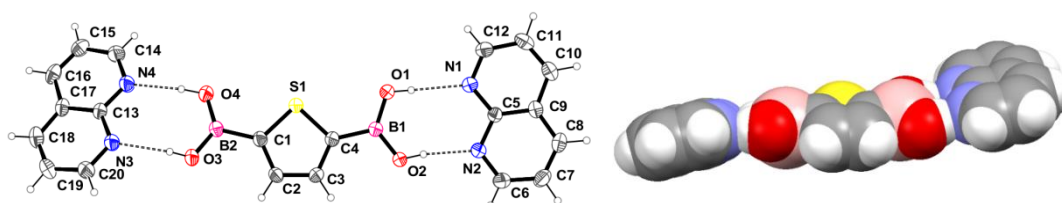


Figure 3.48 Crystal structure of the complex formed between 2,5-thiophenediboric acid and 1,8-naphthyridine. Crystals were obtained by slow evaporation in MeOH. Distance N1-O1: 2.889(2) Å, N2-O2: 2.759(2) Å, N3-O3: 2.825(2) Å, N4-O4: 2.832(2) Å. Hydrogen bond system: DD-AA. Representation: left: ORTEP (drawn at the 30% probability level), right: spacefill. Color code: red: O, grey: C, pink: B, white: H, blue: N, yellow: S. Space group: P2₁/C.

In order to extend our study of complex of boronic acids with other acceptors, the crystal structures of boronic acids in complex with benzoate derivatives were investigated. The latter can behave as AA systems and these are soluble in organic solvents when a suitable counter ion is chosen. For example, the complex formed between mesitylboronic acid **224** and tetrabutylammonium 1,4-dicarboxybenzoate **257** (Figure 3.49), previously synthesized (see *section 3.2.3.*), was obtained by slow evaporation in toluene. The aryl groups are not in the same plane due to the presence of methyl groups in *ortho* of the boronic acid group. More particularly, the torsion angle is of 66.94°, smaller than the angle observed when in complex with 1,8-naphthyridine (Figure 3.37). The oxygen-oxygen distances are of 2.578(4) Å to 2.691(4) Å, shorter than the one observed in the complex formed with 1,8-naphthyridine (Figure 3.37) which had nitrogen-oxygen distances of 2.839(3) Å to 2.878(2) Å. Interestingly, side hydrogen bonding interactions are also involved in these complex involving another molecule of

mesitylboronic acid. The expected stoichiometry, 1:2, is not observed but the exact stoichiometry is 1:3 (1,4-dicarboxybenzoate **257**: mesitylboronic acid **224**).

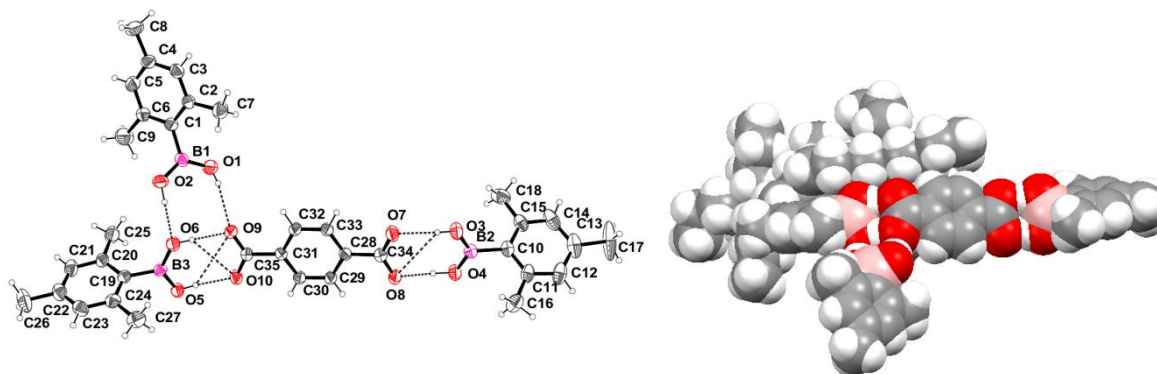


Figure 3.49 Crystal structure of the complex formed between mesitylboronic acid **224** and tetrabutylammonium 1,4-dicarboxybenzoate (omitted for sake of clarity). Crystals were obtained by slow evaporation in toluene. Distances of the hydrogen bonds: O1-O9: 2.915(4) Å, O2-O6: 2.727(4) Å, O3-O7: 2.691(4) Å, O4-O8: 2.617(4) Å, O5-O10: 2.628(4) Å, O6-O9: 2.578(4) Å. Dihedral angle formed between the aryl group and the boronic acid group: 66.94°. Hydrogen bond system: DD-AA. Representation: left: ORTEP (drawn at the 30% probability level), right: spacefill. Color code: red: O, grey: C, pink: B, white: H, blue: N. Space group: $P2_1/c$.

In order to form an infinite, mono dimensional, network connected through hydrogen bonds, tetrabutylammonium 1,4-dicarboxybenzoate and 1,4-phenylenediboronic acid were mixed in MeOH. However, the components combined in two separate networks connected through hydrogen bonds between the boronic acid and the carboxylate. The two networks, made of boronic acid and carboxylate, form linear and planar arrangement.

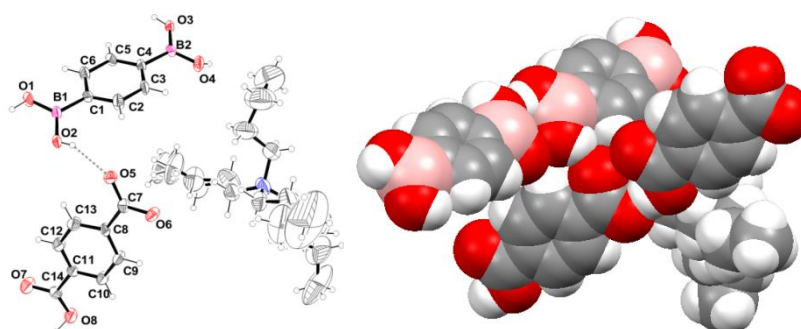


Figure 3.50 Crystal structure of the complex formed between 1,4-phenylenediboronic acid **217** and tetrabutylammonium 1,4-monocarboxybenzoate **257**. Crystals were obtained by slow evaporation in MeOH. Distances O1-O3: 2.787(10) Å, O2-O4: 2.801(10) Å, O6-O8: 2.644(6) Å, O2-O5: 2.728(8) Å, O5-O7: 2.6502(1) Å. Hydrogen bond system: DA-AD. Representation: left: ORTEP (drawn at the 30% probability level), right: spacefill. Color code: red: O, grey: C, pink: B, white: H, blue: N. Space group: Cc.

Finally, starting with a diboronic acid, 2,5-thiophenediboronic acid, and tetrabutylammonium benzoate (Scheme 3.22, molecule **219**), an unexpected cocrystals was observed. The expected stoichiometry was 2:1 but again, side hydrogen bonding interactions are present in the complex so that the exact stoichiometry is 1:2 were two 2,5-thiophenediboronic acid molecules form hydrogen bonds with each other and the carboxylate group. The distances between the two heteroatoms involved in the hydrogen bond are of 2.651(5) Å and 2.551(5) Å, again shorter than when 2,5-thiophenediboronic acid form a complex with 1,8-naphthyridine (of 2.759(2) Å and 2.889(2) Å), represented in Figure 3.48.

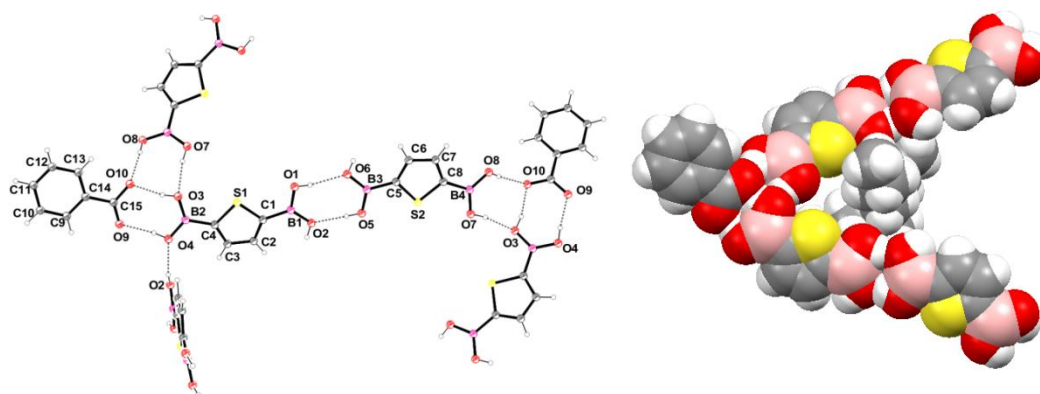


Figure 3.51 Crystal structure of the complex formed between 2,5-dithiopheneboronic acid and tetrabutylammonium benzoate **219**. Crystals were obtained by slow evaporation in toluene. Distance O1-O6: 2.820(4) Å, O2-O4: 2.709(5) Å, O3-O10: 2.551(5) Å, O4-O9: 2.651(5) Å, O1-O6: 2.820(4) Å, O5-O2: 2.734(5) Å, O6-O8: 2.765(4) Å, O7-O3: 2.769(6) Å, O8-O10: 2.751(5) Å. Hydrogen bond systems: DD-AA, with the carboxylate, DA-AD, between boronic acids. Representation: left: ORTEP (drawn at the 30% probability level, ammonium not represented for sake of clarity), right: spacefill. Color code: red: O, grey: C, pink: B, white: H, blue: N, yellow: S. Space group: P2₁2₁2₁.

The present study regarding crystal structures has allowed us to collect data on the geometry of the complex, their stoichiometry, some of which were unexpected, and the hydrogen bond distances. The analysis of the hydrogen bond distances reveals two sets of distances. The first set corresponds to the hydrogen bonding of boronic acid derivatives with a neutral acceptor, that is with themselves or with 1,8-naphthyridine. The second set corresponds to boronic acids hydrogen bonded with a charged carboxylate moiety. The first group as an average hydrogen bond distance of 2.8 Å from heteroatom to heteroatom and the second group as a shorter distance of 2.6 Å. Within the groups, the distances could not be correlated to the electron withdrawing or donating capacity of the substituents to the exception for ortho substituted boronic acid in complexes with 1,8-naphthyridine (Table 3.6).

All these data were necessary to measure the stoichiometry and to confirm and compare the trend observed with the data obtained by ITC, on the energy values of the hydrogen bonds, presented in the *section 3.5*.

3.5. Binding constant measurement by ITC

ITC titrations were performed in the group of *Professor Dr. Bartik*, with *Dr. Gilles Bruylants*, in ULB, Belgium.

The binding constant (K_a), the stoichiometry (n) and thermodynamic parameters (ΔG^0 , ΔH^0 and ΔS^0) of the complex can be obtained by ^1H NMR or by ITC. However, in our case the chemical shifts observed during the titration of phenylboronic acid and 4-methoxyphenylboronic acid by 1,8-naphthyridine, using ^1H NMR spectroscopy (Figure 3.25) were too small to determine precisely the value of the binding constant. The observed variation of chemical shift from the beginning to the end of the titration was less than 0.05 ppm. Therefore, ITC was chosen as an alternative methodology to give access to the K_a , n , and ΔH^0 of the interaction in one single titration experiment. The strength of the association varies with the solvent, particularly with polar, protic, solvents that can form hydrogen bonds and will compete with the complex, as explained in *section 3.1.1.2*. This will result in a diminution of the association constant. Furthermore, non-volatile solvents are needed for ITC titration to avoid evaporation which would change the concentration values, during the lengthy titration (over 5 h). Hence, all titrations analysis were performed in toluene, an apolar ($\epsilon = 2.38$), high boiling point solvent, which is a weak hydrogen bond donor (as a comparison, benzene as a $\alpha = 1.0$) and acceptor (as a comparison, benzene as a $\beta = 2.2$). The toluene solutions were non-anhydrous since the titration could not be performed under anhydrous conditions. The titrant solutions were prepared at different concentrations (letter code in Table 3.8 and Table 3.9) from non-anhydrous toluene from different bottles. Similar results were obtained.

At first, this study was aimed at measuring the binding constant of boronic acid derivatives, as DD and even DDDD systems of hydrogen bonds. Unfortunately, derivative **239** revealed to be insoluble in toluene and only slightly soluble in THF, therefore it could not be used for ITC measurements. Therefore, all the systems studied were of DD hydrogen bond type, titrated by AA acceptors (1,8-naphthyridine **223** and tetrabutylammonium of phenylcarboxylate **219**). 1,8-naphthyridine **223** (Scheme 3.13) was envisaged as a suitable hydrogen bond acceptor, owing to its ability to form double hydrogen bonds, compared to the simple pyridine, previously used in other studies as excellent hydrogen bond acceptor ($\beta = 7.0$).^[219]

A systematic study was undertaken with boronic acid derivatives that are in their acid form in toluene and not in the boroxine form (Table 3.2). The choice of boronic acids was limited since only derivatives substituted by *ortho* groups (*e.g.* compounds **224**, **228**, **260**, and **266**) or substituted by several electron withdrawing groups (*e.g.* compound **261**) were in their acid form. ^1H NMR spectra were taken before the titration to evaluate the stability of the derivative upon addition of 1,8-naphthyridine. The first trial with pentafluorophenylboronic acid, dissolved in deuterated chloroform and titrated with 1,8-naphthyridine, revealed that it quickly decomposes upon addition of 1,8-naphthyridine. The latter acts as a base and catalyzes, in the presence of traces of H_2O , the degradation into $\text{B}(\text{OH})_3$. $\text{B}(\text{OH})_3$ forms a hydrogen bonded complex with 1,8-naphthyridine (Figure 3.40).^[310] All the other boronic acids studied were stable under the titration conditions.

Figure 3.52 indicates a typical thermogram of the titration of 2,6-dichlorophenylboronic acid derivative with 1,8-naphthyridine using ITC. Initially, it was observed that the binding constant was low and the heat released by the addition of the guest diminishes continuously, meaning that the guest was not fully complexed by the host, even for the first injections where the host excess in the cell is large. Another effect of this uncompleted complexation is that there was free guest after the equivalence point, this is observable by the heat of dilution that was still released after this point. Therefore, in order to have precise measurement of the thermodynamic parameters, three modifications were applied to the titration protocol. First, the guest was added in large excess beyond the equivalence point, reaching 3 equivalents, so that the equilibrium will be driven toward the formation of the complex. Secondly, the stoichiometry will be determined by crystallography, in the solid state assuming that the complex formed will be identical in solution. This will allow the fixation of the equivalence point on the curve, enhancing the precision of the measured binding constant (shape of the curve). Thirdly, due to the fact that the measured heat exchange was extremely large due to the high concentrations, the volume of injection was reduced (from a

Chapter 3

typical injection of 10 μl to injections of 3 μl) to obtain more points on the binding curve and heat exchanges in the desired range.

After the application of the optimum ITC conditions, the titration of 2,6-dichlorophenylboronic acid with 1,8-naphthyridine indicates a sharper titration curve (Figure 3.53), which is reflected in the highest binding constant value (Table 3.8) for the formation of this complex. The binding constant is calculated by plotting the heat released per injection and fitting the curve (Figure 3.54). The ΔH° is measured on the plateau determined for the first point of the curve and the inflexion point of the curve gives the stoichiometry (see section 3.1.2.3).

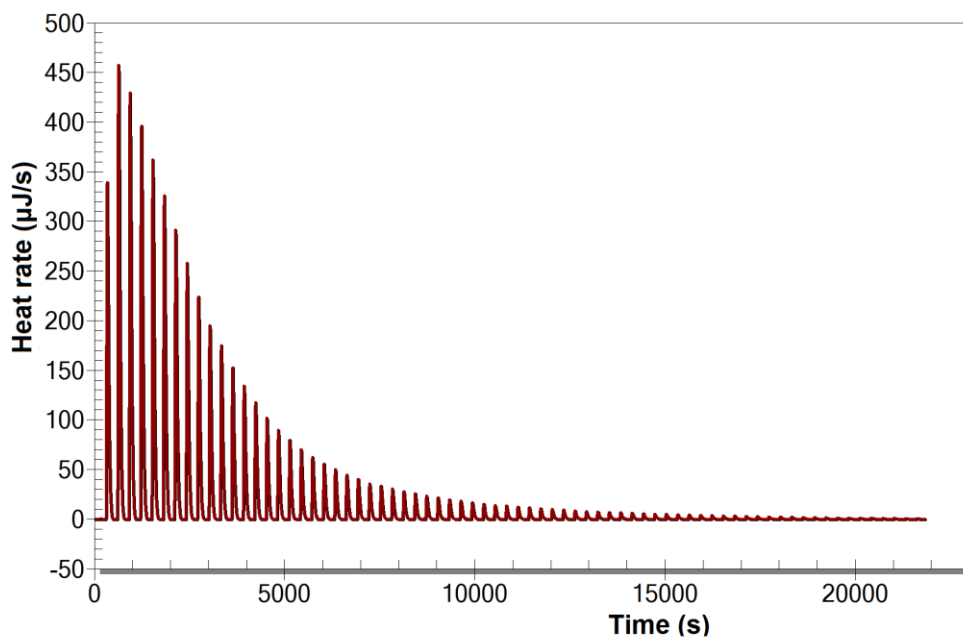


Figure 3.52 ITC titration: 25 injections of 10 μl of a 200 mM solution 1,8-naphthyridine **223** into 1300 μl of a 3.8 mM solution of 2,6-difluoroboronic acid **260**.

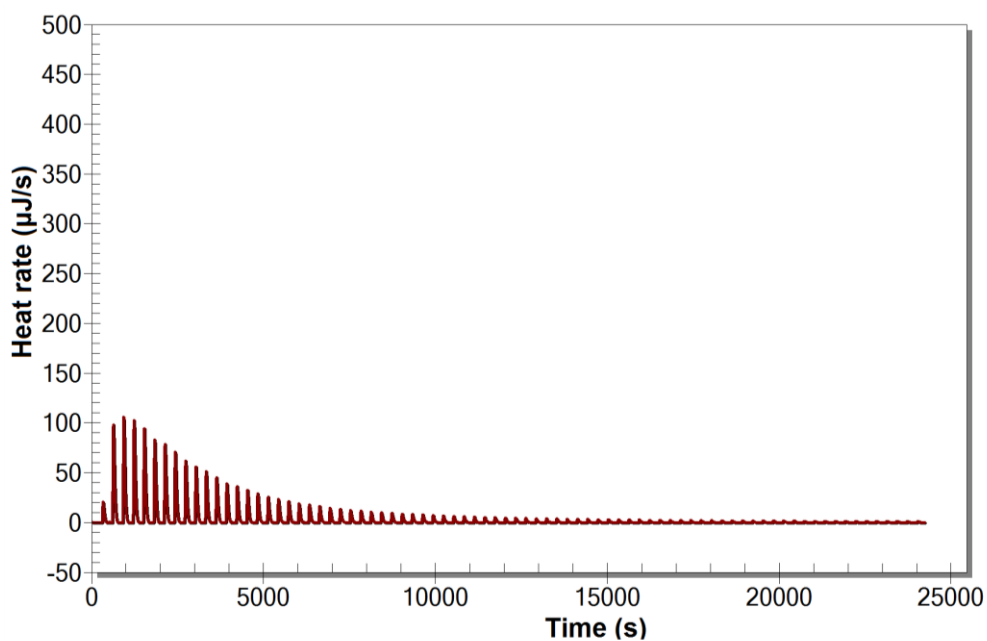


Figure 3.53 ITC titration: 50 injections of 3 μl of a 78 mM solution 1,8-naphthyridine **223** into 1300 μl of a 1.5 mM solution of 2,6-dichlorophenylboronic acid **266**.

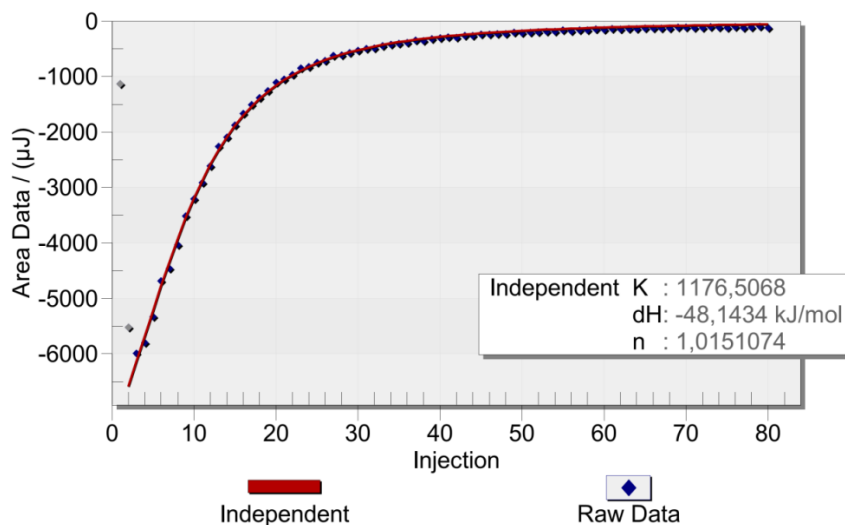


Figure 3.54 ITC plot of the heat released per injection for the titration of a 1.5 mM solution of 2,6-dichlorophenylboronic acid by a 78 mM solution of 1,8-naphthyridine **223**.

For the first injection of the titration, 1,8-naphthyridine is in a 1:6 ratio respective to the boronic acid, and therefore totally complexed by the boronic acid. So the heat released during the first injections corresponds to the ΔH° of formation of the complex multiplied by the amount of complex formed and is seen as a plateau in the system having an important binding constant. On the other end, at the end of the analysis, the heat released corresponds to the heat of dilution of the guest into the solution of the host. By consequence, the heat of dilution of the guest into toluene as well as the heat of dilution of host by injection of toluene should be measured and subtracted to the titration curve. The dilution curve of 1,8-naphthyridine is presented in Figure 3.55 and is endothermic but the value is negligible compare to the heat released during the titration. The solution of aryl boronic acid in the cell was also diluted by injection of toluene from the syringe and again the heat released revealed to be negligible.

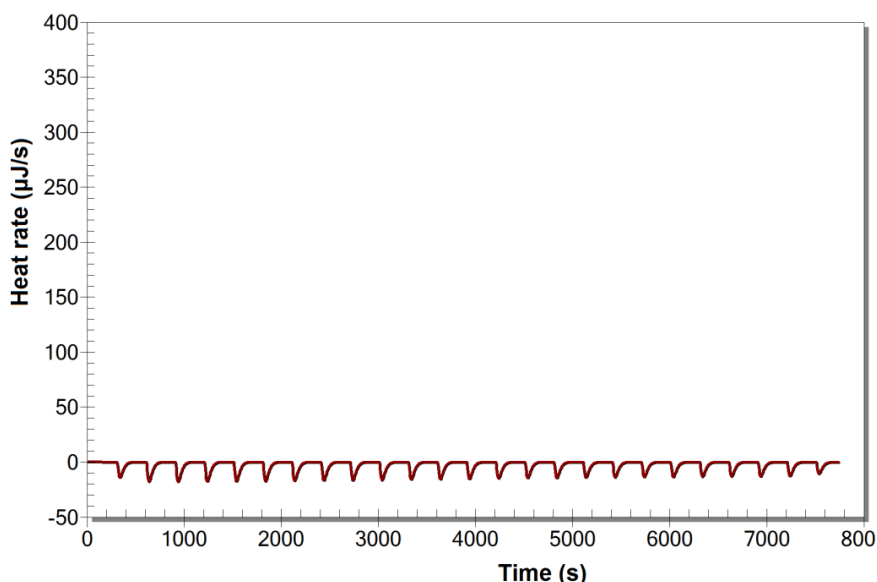


Figure 3.55 Dilution of the 200 mM solution of 1,8-naphthyridine **223**, in the cell containing 1300 μL of toluene, by 80 injections of 10 μL .

Since the binding constant of the aryl boronic acid measured is low, and therefore no plateau allowing the precise determination of the ΔH° is observed, it is only possible to obtain the ΔH° of interaction with a poor precision. Another way

Chapter 3

to have a plateau and therefore determine precisely the ΔH^0 is to reverse the titration. By injecting small quantities of mesitylboronic acid (guest – 10 μl of a 200 mM solution) in a large excess of 1,8-naphthyridine (host – 1300 μl of a 5 mM solution), the heat decay should come after several peaks. The titration was reproducible with a low but constant heat released (Figure 3.56). However, performing the blank experiment, by dilution of the 5 mM solution of mesitylboronic acid into the cell containing toluene, irreproducible results were obtained (Figure 3.57), possibly due to various amount of H_2O in the toluene solutions, which can form hydrogen bond with boronic acids. It should be stressed that the value of the heat released by the dilution of mesitylboronic acid into the cell is quasi equivalent to the heat released when the same mesityl boronic acid is injected in the cell containing the 200 mM solution of 1,8-naphthyridine (Figure 3.56). It is worth to point out that in these conditions the mesitylboronic acid is diluted in a large volume of solvent and that any traces of impurities, and in particular H_2O , will interact with a non negligible fraction of the host molecule.

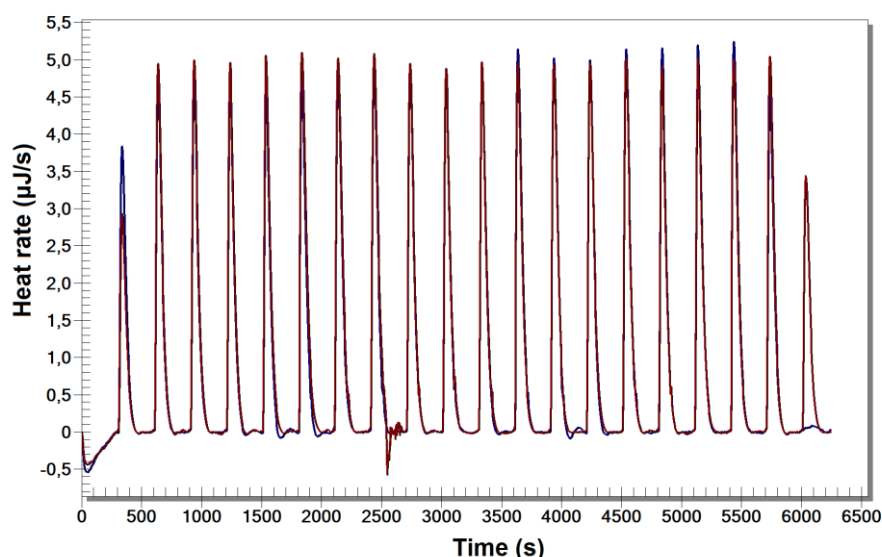


Figure 3.56 Injections of 5 μl of a 5 mM solution of mesitylboronic acid **224** in the 1300 μl cell containing a 200 mM solution of 1,8-naphthyridine **223**. Blue: first titration, red: second titration.

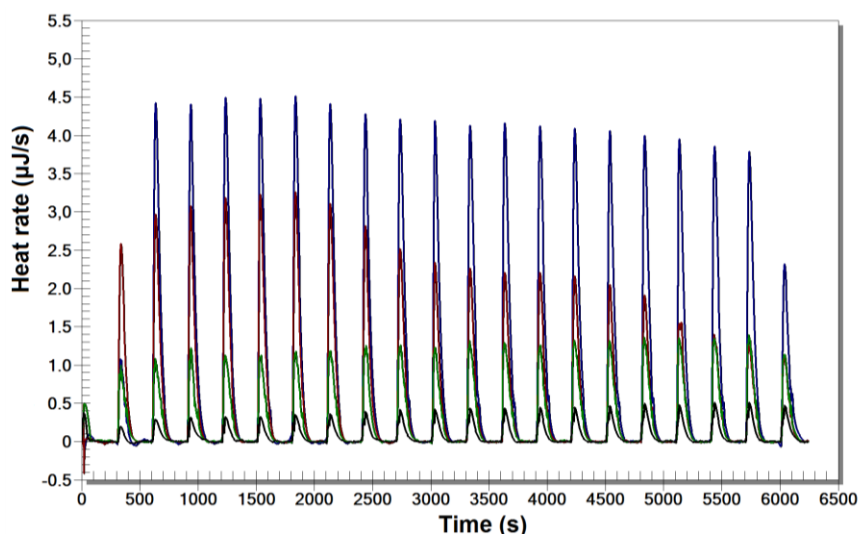
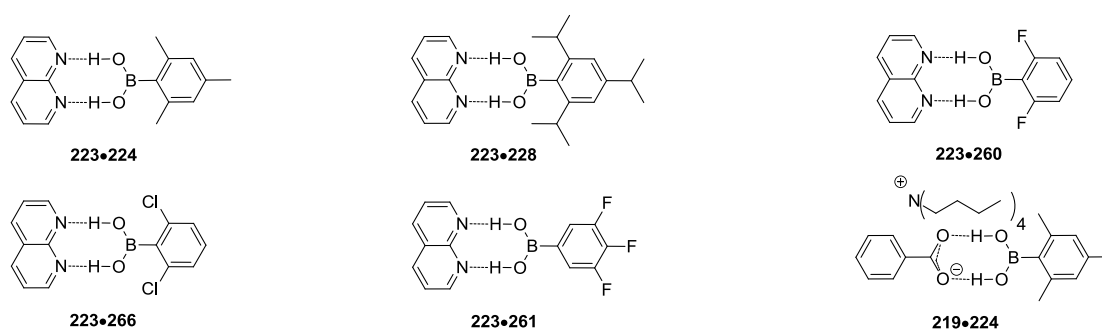


Figure 3.57 Injections of 5 μl of a 5 mM solution of mesitylboronic acid **224** in the 1300 μl cell containing toluene. Blue: first titration, black: second titration, red: third titration, green: fourth titration.

Therefore, the ΔH^0 of the formation of the complex could not be measured precisely and can only be estimated on the basis of the full titrations with a large excess of the guest molecules, *i.e.* 1,8-naphthyridine **223**. The systems measured are

Chapter 3

summarized in Scheme 3.29 and the mean results, obtained over three titrations, gathered in Table 3.8 and Table 3.9. Titration of mesitylboronic acid with tetrabutylammonium of benzoate revealed a stoichiometry 1:2 while a 1:1 was expected base on the computational predictions described in Scheme 3.12 and on the previously reported crystal structure of phenylboronic acid in complex with tetrabutylammonium benzoate.^[281] The problem of accuracy could come from various water content in the toluene solution. Indeed, benzoate **219** can form hydrogen bond with water. Hence, a new complex stoichiometry, comprising a molecule of water and one of boronic acid, could be formed with carboxylate. This could be verified in future experiment by quantifying the quantity of water by NMR before the ITC titration experiment. Nevertheless, the K_a value obtained for mesityl boronic acid ($2100 \pm 110 \text{ M}^{-1}$) is higher than the one measured for the titration with 1,8-naphthyridine ($300 \pm 60 \text{ M}^{-1}$), as expected by the theoretical predictions.



Scheme 3.29 Boronic acid derivatives complexes with 1,8-naphthyridine **223** or phenyl carboxylate **219**, whose K_a were measured by ITC.

Complex	Concentration of aryl boronic acid	Concentration of acceptor (solution code)	K_a (M^{-1})	ΔH^0 (kJ mol^{-1})	n	ΔG^0 (kJ mol^{-1})	$-T\Delta S^0$ (kJ mol^{-1})
223•224	8.80	53.5 (A)	250	-37.4	1.0	-13.7	23.7
	4.92	200 (B)	290	-38.3	1.0	-14.0	24.3
	4.90	200 (B)	350	-35.8	0.9	-14.5	21.4
Mean value and confidence interval (95%)			300±60	-37.2±1.4	0.95	-14.1±0.5	23.1±1.8
223•228	4.25	200 (B)	550	-35.6	1.0	-15.6	20.6
	4.25	200 (C)	380	-40.4	1.0	-14.7	25.5
	1.95	78 (D)	430	-33.7	1.0	-15.0	18.7
Mean value and confidence interval (95%)			450±100	-37±4	1	-15.1±0.5	23±4
223•260	4.94	200 (B)	780	-44.6	1.1	-16.5	28.1
	3.81	200 (B)	800	-42.6	1.0	-16.6	26.0
	3.81	200 (C)	630	-45.6	1.0	-16.0	29.7
Mean value and confidence interval (95%)			740±100	-44.3±1.7	1.0	-16.4±0.4	28±2.1
223•266	1.50	78.0 (D)	1200	-48.1	1.0	-17.5	30.6
	1.68	78.0 (D)	1030	-48.9	0.9	-17.2	31.7
Mean value and confidence interval (95%)			1100±170	-48.5±0.8	1.0	-17.4±0.3	31±1.1
223•261	4.65	200 (B)	5400	-54.3	1.0	-21.3	33.0
	4.96	200 (C)	19000	-49.8	1.0	-24.5	25.4
	4.96	200 (E)	13000	-48.9	1.0	-23.5	25.4
Mean value and confidence interval (95%)			12400±7700	-52±3.2	1.0	-23.4±1.8	29±5.0

Table 3.8 Thermodynamic parameters measured by ITC at 25 °C, under atmospheric pressure using 1,8-naphthyridine as acceptor.

Chapter 3

Complex	Concentration of aryl boronic acid	Concentration of acceptor (solution code)	K_a (M^{-1})	ΔH^0 ($kJ\ mol^{-1}$)	n	ΔG^0 ($kJ\ mol^{-1}$)	$-T\Delta S^0$ ($kJ\ mol^{-1}$)
219•224	1.10	40.1 (F)	1600	-13	2.1	-18.3	-5.3
	1.10	40.1 (G)	4000	-10	1.8	-20.5	-10.5
	1.10	47.9 (I)	1850	-20	2.1	-18.6	1.4
	1.10	38.5 (J)	800	-29	2.1	-16.6	12.4
Mean value and confidence interval (95%)			2100±1100	-18±8.3	2.0	-18.5±1.6	-0.5±9.7

Table 3.9 Thermodynamic parameters measured by ITC at 25 °C, under atmospheric pressure using **219** as acceptor.

The ITC data revealed the following trends:

- 1) Boronic acid derivatives bearing electron withdrawing groups have a higher ΔH^0 of formation of the complex.
- 2) When the crystal structure revealed a planar complex (*e. g.* **223•261**) the complex ΔH^0 of formation increases and the binding constant value soars. Unfortunately, these boronic acid derivatives tend to be on the boroxine form, as outlined earlier, although the presence of three electron withdrawing groups on this boronic acid favored the formation of the acid. As a consequence, the K measured is the equilibrium constant of the two equilibrium.

3.6. Conclusions and Outlooks

The synthesis of ortho-substituted boronic acids **224** and **228** were performed with the aim to study their complexation constant with 1,8-naphthyridine and carboxylate derivatives. The synthesis of the anthracene-based boronic acid DDDD system, compound **239** and **244**, revealed to be a challenge and the synthesis of others derivatives, bearing more solubilizing groups, such as longer alkyl chains, has yet to be performed in order to measure its K_a with AAAA acceptors.

Crystal structure analysis of self-interacting boronic acids and complexes formed between boronic acid derivatives and 1,8-naphthyridine gave access to the complex geometry and distances. The torsion angles, measured between the boronic acid moieties and the aryls rings, indicate that the conjugation between the orbitals of the respective groups could be blocked. This led us to investigate, during our ITC studies, boronic acid derivatives bearing only inductive attractor groups.

ITC analysis afforded the first measure of association constant of supramolecular complex using boronic acid moieties. The association constants measured are middling for a double hydrogen bond donor. Nevertheless, a slight increase of the K_a was noticed when methyl substituents were changed for electron withdrawing chlorine or fluorine atoms. Finally, boronic acids bearing hydrogen atoms in *ortho* positions, form planar complexes in the solid state and a tenfold increase of the association constant is noticed by ITC titration, principally due to an augmentation of the ΔH^θ . Moreover, the titration of mesitylboronic acid **224** by benzoate **219** revealed an even higher binding constant, as predicted by theoretical calculations. However, the stoichiometry obtained by ITC is not supported by these calculations neither by crystal structures studies at the solid state. The complexation of boronic acid derivatives by benzoates moieties will be further studied in the future.

As a perspective, this work will be continued by measuring K_a of DDDD system of hydrogen bond and by measuring the K_a with other DD systems (*e. g.* carboxylate). Obviously, binding constant measurements serve only the development of supramolecular application to organize materials at the nano level, preliminary studies of formation of complex on surfaces have to be developed in the future.

4. Experimental part

4.1. Instrumentation

Thin layer chromatography (TLC) was conducted on pre-coated aluminum sheets with 0.20 mm *Machevery-Nagel* Alugram SIL G/UV254 with fluorescent indicator UV254. Column chromatography was carried out using Merck Gerduran silica gel 60 (particle size 40-63 μm). **Microwave reactions** were performed on a *Biotage AB Initiator microwave instrument* producing controlled irradiation at 2.450 GHz. **Melting points (M.p.)** were measured on a *Büchi Melting Point B-545* in open capillary tubes and have not been corrected. **Nuclear magnetic resonance (NMR)** ^1H , ^{13}C , ^{11}B spectra were obtained on a 400 MHz NMR (*Jeol JNM EX-400*) or 270 MHz (*Jeol JNM EX-270*). Chemical shifts were reported in ppm according to tetramethylsilane using the solvent residual signal as an internal reference (CDCl_3 : $\delta_{\text{H}} = 7.26$ ppm, $\delta_{\text{C}} = 77.16$ ppm, $\text{DMSO}-d_6$: $\delta_{\text{H}} = 2.50$ ppm, $\delta_{\text{C}} = 39.52$ ppm, CD_2Cl_2 : $\delta_{\text{H}} = 5.32$ ppm, $\delta_{\text{C}} = 53.80$ ppm, $\text{THF}-d_8$: $\delta_{\text{H}} = 3.58$ ppm, $\delta_{\text{C}} = 67.57$ ppm). Coupling constants (J) were given in Hz (J_1 : ortho, J_2 : meta, J_3 : para). Resonance multiplicity was described as s (singlet), d (doublet), t (triplet), dd (doublet of doublets), dt (doublet of triplets), q (quartet), m (multiplet) and br (broad signal). Carbon spectra were acquired with a complete decoupling for the proton. **Infrared spectra (IR)** in KBr were recorded on a *Perkin-Elmer spectrum RX I FT-IR System*. **UV-Vis spectra** were recorded in quartz cuvettes using a *Cary-Varian 5000*. **Liquid chromatography mass spectrometry (LC-MS)** measurements were conducted on an *Agilent 6200 series TOF mass spectrometer* equipped with ESI and APCI ionization sources and a Time Of Flight (TOF) detector, operating in positive mode. The analyte solutions were delivered to the ESI or APCI source by an Agilent 1200 series LC system at a flow rate of 0.25 mL/min. Typical elution gradient start from H_2O (90%) to CH_3CN (100%) for 20 min. ESI mode: Typical ESI conditions were capillary voltage 2.0 kV, cone voltage 65 V, source temperature 150 °C, desolvation temperature 250 °C, drying gas 5 L/min, nebulizer 60 psig. APCI: Typical APCI conditions were, capillary voltage 2.0 kV, cone voltage 65 V, source temperature 250 °C, desolvation temperature 350°C, drying gas 5L/min, nebuliser 60 psig. Dry nitrogen was used as the ESI and APCI gas. **Mass spectrometry** was generally performed by the *Centre de spectrométrie de masse at the Université de Mons in Belgium* where they performed EI-MS and MALDI-MS, using the following instrumentation. EI-MS measurements were performed on a *Waters AutoSpec 6 F mass spectrometer* operating in positive mode. Typical source conditions are 70 eV, 200 μA trap current and 8 kV accelerating voltage. The source temperature is 200°C. The liquid samples are injected *via* a heated (160 °C) septum inlet and the solid samples are introduced directly in the ion source *via* a direct insertion probe (DIP). The mass spectrometer presents an original EBEEBE configuration with E and B being respectively electrostatic and magnetic sectors. The mass measurements are performed by scanning the field of the first magnetic sector. MALDI-MS were recorded using a *Waters QToF Premier mass spectrometer* equipped with a nitrogen laser, operating at 337 nm with a maximum output of 500 mW delivered to the sample in 4 ns pulses at 20 Hz repeating rate. Time-of-flight analyses were performed in the reflectron mode at a resolution of about 10,000. The matrix solution (1 μl) was applied to a stainless steel target and air dried. Analyte samples were dissolved in a suitable solvent to obtain 1 mg/mL solutions. 1 μl aliquots of these solutions were applied onto the target area already bearing the matrix crystals, and air dried. For the recording of the single-stage MS spectra, the quadrupole (rf-only mode) was set to pass ions from 100 to 1000 THz and all ions were transmitted into the pusher region of the time-of-flight analyzer where they were analyzed with 1 s integration time. **HPLC** analyses were performed to check the purity of the compounds investigated in this thesis and were carried out on a *Varian 940-LC liquid chromatography system*. The column used was a *Varian Pursuit C18*, 5 μm , 4.6 \times 250 mm column. CH_3CN was used as eluent.

4.2. Materials and General Methods

Chemicals were purchased from Sigma Aldrich, Acros Organics, Fluorochem and ABCR and were used as received. Solvents were purchased from Sigma Aldrich, while deuterated solvents from Eurisotop. Anhydrous solvents as Et_2O , THF

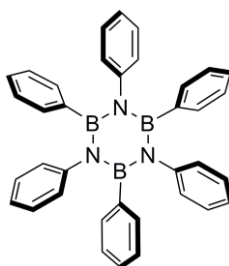
Chapter 4

and toluene were distilled from Na/benzophenone, CH_2Cl_2 , CHCl_3 and CH_3CN from CaH_2 . Anhydrous DMF was purchased from Acros Organics. Hydrogen peroxide (H_2O_2 , 15%) was obtained from Riedel-de Haën, whereas sulfuric acid (H_2SO_4 , 95%) nitric acid (HNO_3 , 62%) and hydrochloric acid (HCl , 32%) were purchased from Fischer Scientific. Pyridine was purchased from Acros Organics. MeOH, CHCl_3 , acetone were purchased as reagent-grade and used without further purification. Low temperature baths were prepared using different solvent mixtures depending on the desired temperature: -78°C with acetone/liquid N_2 or acetone/dry ice, -40°C with CH_3CN /liquid N_2 , -10°C with ice- H_2O / NaCl , and 0°C with ice- H_2O . Anhydrous conditions were achieved by drying Schlenk flask or 2-neck flasks by flaming with a heat gun under vacuum and then purging with Argon. The inert atmosphere was maintained using Argon-filled balloons equipped with a syringe and needle that was used to penetrate the silicon stoppers used to close the flasks' necks. Additions of liquid reagents were performed using dried plastic or glass syringes.

4.3. Experimental Procedure

4.3.1. Borazine and Borazene Derivatives

Hexaphenylborazine 169



In a flame-dried 50 mL Schlenk flask, anhydrous aniline (1.862 g, 20 mmol) was diluted with 2 mL of anhydrous toluene and cooled to -5°C (ice-salt bath). Then BCl_3 (24 mL, 24 mmol, 1 M solution in toluene) was added dropwise which yield to a white precipitate. The septum was changed for a flame-dried condenser topped by a CaCl_2 tube. The reaction mixture was heated up to reflux for 3 h. After this period the reaction mixture was cooled down to 0°C , the condenser was changed for a septum, and the flask subjected to three freeze-to-thaw cycle to remove the remaining HCl . The borazole was cannulated dropwise to the schlenk containing a solution of PhMgBr (22 mL, 22 mmol, 1 M in THF) at 0°C and allowed to react at r.t.. After 12 h the solution was transparent with a grey precipitate. Solvents were removed under reduce pressure. The solid was then extracted with 100 mL anhydrous CH_2Cl_2 using a soxhlet apparatus during 5 h. Then the solvents were distilled off to give a light brown solid. This solid was triturated with 25 mL of CH_3CN , and the solid was filtered to afford a white solid. The supernate solution was distilled off and a second trituration allowed the recovery of extra white solid (1.120 g, 31% yield). M.p.: $>300^\circ\text{C}$. ^1H NMR (400 MHz, CDCl_3 , 25°C) δ (ppm) 6.85-6.73 (m, 30H). ^{13}C NMR (100 MHz, CDCl_3 , 25°C) δ (ppm) 146.7, 132.5, 129.6 (overlap of two signals), 127.4, 126.3, 124.0 (the ^{13}C resonance corresponding to the carbon atom bonded to the boron atom is not observed due to the quadrupolar relaxation). ^{11}B NMR (128 MHz, CDCl_3 , 25°C) δ (ppm) 34.4 (br) Solid IR. KBr. ν (cm^{-1}) 3026 (C-H aromatic), 1599, 1492, 1452, 1432, 1368 (B-N), 1310, 756. UV-Vis (CH_3CN , 25°C) λ_{max} (ϵ , $\text{mol}^{-1}\text{cm}^{-1}$) 275 (3680), 268 (4150), 262 (3880) nm. HRMS (MALDI, matrix: DCTB, m/z): $[\text{M}+\text{Na}^+]$ calc. for $\text{C}_{36}\text{H}_{30}\text{N}_3\text{B}_3\text{Na}$, 560.2617; found, 560.2638. Crystals suitable for X-ray diffraction were obtained by slow evaporation in CHCl_3 , space group: $\text{Pna}2_1$.

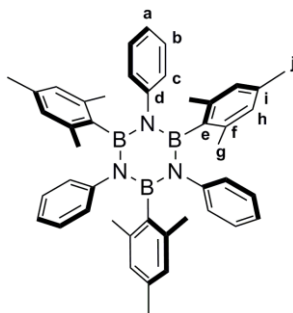
Chapter 4

N-triphenyl-B-trianthryl borazine 172



In a flame-dried 25 mL Schlenk flask, anhydrous aniline (932 mg, 10 mmol) was diluted with 3 mL of anhydrous toluene and cooled to $-5\text{ }^{\circ}\text{C}$ (ice-salt bath). Then BCl_3 (1 M solution in toluene, 13 mL, 13 mmol) was added dropwise which yield to a white precipitate. The septum was changed for a flame-dried condenser topped by a CaCl_2 tube. The reaction mixture was heated up to reflux for 18 h. After this period the reaction mixture was cooled down to $0\text{ }^{\circ}\text{C}$, the condenser was changed for a septum, and the flask subjected to three freeze-to-thaw cycle to remove the remaining HCl. In parallel, to a flame-dried 50 mL Schlenk flask, 9-bromoanthracene (2.571 g, 10 mmol) was dissolved in 10 mL of anhydrous THF and freshly-titrated *t*-BuLi (13 mL, 22 mmol, 1.7 M in hexanes) added dropwise at $-78\text{ }^{\circ}\text{C}$. The flask was allowed to warm up at $0\text{ }^{\circ}\text{C}$ and stirred for 1 h (the color changed from transparent to pale yellow). The borazole was then cannulated dropwise to the lithiate solution at $0\text{ }^{\circ}\text{C}$ and allowed to react at r.t. for 16 h. The reaction mixture was diluted with 40 mL of H_2O , extracted with EtOAc ($3 \times 15\text{ mL}$) and the combined organic phases dried over MgSO_4 and the solvents removed under reduced pressure. The yellow solid (1.250 g, 45% yield) obtained was washed with EtOAc and CH_2Cl_2 and is insoluble in all solvents. M.p. $> 300\text{ }^{\circ}\text{C}$. Solid-state IR (KBr) ν (cm^{-1}) 3045 (C-H aromatic), 1596, 1492, 1416, 1379, 1338 (B-N), 731. MS (MALDI, matrix: DCTB, m/z) = 837.4 [M^+].

B-trimesityl-N-triphenylborazine 173

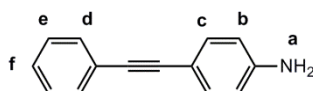


In a flame-dried 25-mL Schlenk flask, aniline (370 mg, 4 mmol) was diluted with 8 mL of anhydrous toluene and cooled to $-5\text{ }^{\circ}\text{C}$ (ice-salt bath). A solution of BCl_3 (5.2 mL, 5.2 mmol, 1M solution in toluene) was added dropwise. The septum was changed for a flame-dried condenser topped by a CaCl_2 tube and the resulting mixture refluxed for 16 h. The reaction solution was cooled down to $0\text{ }^{\circ}\text{C}$, the condenser was changed for a septum, and the flask subjected to three freeze-to-thaw cycle to remove the remaining HCl. In parallel, to a flame-dried 50 mL Schlenk flask, MesBr (876 mg, 4.4 mmol) was dissolved in 10 mL of anhydrous THF and freshly-titrated *n*-BuLi (3.8 mL, 5.2 mmol, 1.36 M in hexanes) added dropwise at $-78\text{ }^{\circ}\text{C}$. The flask was allowed to warm up at $0\text{ }^{\circ}\text{C}$ and stirred for 1 h (the color changed from transparent to pale yellow). The borazole was then cannulated dropwise to the lithiate solution at $0\text{ }^{\circ}\text{C}$ and allowed to react at r.t. for 24 h. The reaction mixture was diluted with 20 mL of H_2O , extracted with EtOAc ($3 \times 20\text{ mL}$) and the combined organic phases dried over MgSO_4 and the solvents removed under reduced pressure. The crude solid was purified by silica gel chromatography (EtOAc/CHX, 1:5; $R_f = 0.5$, retention time (HPLC): 8.7 min with CH_3CN at a flow rate of 20 mL min^{-1}) yielding **1** as a white solid (352 mg, 40% yield). M.p.: $262\text{ }^{\circ}\text{C}$ (powder X). Suitable crystals (M.p.: $295\text{ }^{\circ}\text{C}$) for X-ray diffraction were obtained by

Chapter 4

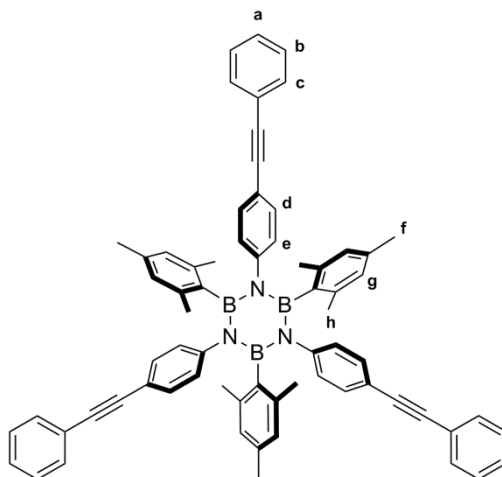
slow evaporation at r.t. from: a) CH_2Cl_2 at r.t. (needles or hexagons, space group: $R\bar{3}2$), b) CHX (hexagonal parallelepiped, space group: $R\bar{3}c$) and c) pentane, hexane or EtOAc (parallelograms, space group: $P2_1/n$). ^1H NMR (400 MHz, CDCl_3 , 25 °C) δ (ppm) 6.82-6.80 (m, 6H, H_c), 6.77-6.71 (m, 9H, H_b and H_d), 6.32 (s, 6H, H_h), 2.22 (s, 18H, H_g), 1.96 (s, 9H, H_j). ^1H NMR (400 MHz, C_6D_6 , 25 °C) δ (ppm) 7.16 (d, $J = 7.1$ Hz, 6H, H_c), 6.78 (t, $J = 7.6$ Hz, 6H, H_b), 6.58 (t, $J = 7.3$ Hz, 3H, H_d), 6.47 (s, 6H, H_h), 2.51 (s, 18H, H_g), 1.86 (s, 9H, H_j). ^{13}C NMR (100MHz, CDCl_3 , 25 °C) δ (ppm) 146.4 (C_d), 137.3, 136.1, 127.1, 126.8, 126.2, 124.2, 23.1 (C_g), 21.1 (C_j) (the ^{13}C resonance corresponding to the carbon atom bonded to the boron atom is not observed due to the quadrupolar relaxation). ^{11}B NMR (128 MHz, CDCl_3 , 25 °C) δ (ppm) 36.8 (br). Solid-state IR (KBr) ν (cm^{-1}) (C-H aromatic), 2915, 2856 (C-H alkyl), 1597, 1491, 1356 (B-N), 1308. UV-Vis (CH_3CN , 25 °C) λ_{max} (ϵ , $\text{mol}^{-1} \text{cm}^{-1}$) 271 (2400), 265 (2900), 259 (2600) nm. Quantum yield: 0.7 ($\lambda_{\text{exc}} = 300\text{nm}$). HRMS (MALDI, matrix: DCTB, m/z): $[\text{M}^+]$ calc. for $\text{C}_{45}\text{H}_{48}\text{N}_3\text{B}_3$, 663.4127; found, 663.4138.

4-ethynylphenyl aniline



In a 250 mL two necked flask, 4-ethynylphenylnitrobenzene (8.5 mg, 0.038 mmol) was suspended in concentrated HCl (50 mL). The mixture was heated up to 60 °C under stirring to get homogenous suspension. Then, tin powder (5 g, 42 mmol) was added slowly and the mixture was stirred at 60 °C for 6 h. After this period, a TLC shows complete conversion of the starting material and the solution was poured into 250 mL of ice (H_2O) and stirred to get a yellow suspension. Aqueous solution of NaOH (10%) was added to basify the suspension to pH 14. The crude was extracted with EtOAc (3×100 mL), the combined organic layers were dried over MgSO_4 , filtered and the solvents removed under reduced pressure. M.p.: 126-128°C. Yield: 99%. ^1H NMR (400 MHz, C_6D_6 , 25 °C) δ (ppm) 7.50-7.48 (m, 2H, H_d), 7.34-7.32 (m, 5H, H_c , H_e , H_f), 6.63 (d, $J = 8$ Hz, 2H, H_b), 3.83 (br, 2H, H_a); ^{13}C NMR (100 MHz, CDCl_3 , 25 °C) δ (ppm) 146.6, 133.0, 131.4, 128.3, 127.7, 124.0, 114.8, 112.7, 90.2 (overlap of two signals). All other spectroscopic and analytical properties were identical to those reported in the literature.^[311]

B-trimesityl-N-tri(4-ethynylphenylphenyl)borazine 176

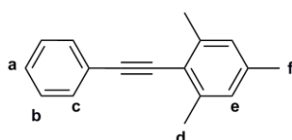


In a flame-dried 25 mL Schlenk flask, anhydrous 4-ethynylphenyl aniline (773 mg, 4 mmol) was diluted with 4 mL of anhydrous toluene and cooled to -5 °C (ice-salt bath). Then BCl_3 (4.8 mL, 4.8 mmol, 1M solution in toluene) was added dropwise yielding to a white precipitate. The septum was changed for a dry condenser topped by a CaCl_2 tube. The reaction mixture was heated up to reflux overnight. After this period the flask was cooled down and subject to three freeze-to-thaw cycle to remove the HCl. In parallel, in a flame-dried 50mL Schlenk flask, MesBr (877 mg, 4.4 mmol) was diluted with 15

Chapter 4

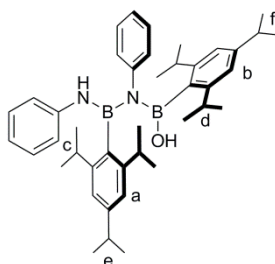
mL of anhydrous THF. The solution was cooled down to $-78\text{ }^{\circ}\text{C}$ and freshly titrated *n*-BuLi (3.4 mL, 4.8 mmol) was added dropwise. The flask was allowed to warm up to $0\text{ }^{\circ}\text{C}$ for 1 h. The color changed from transparent to light yellow. The borazole was cannulated dropwise to the lithiate at $0\text{ }^{\circ}\text{C}$ and allowed to react at r.t.. After 17 h the reaction was quenched by H_2O . The aqueous layer was extracted with EtOAc ($3 \times 20\text{ mL}$). The combined organic layers were dried over MgSO_4 , filtered and the solvents removed under reduced pressure. The crude was purified by silica gel chromatography, $\text{CHX}:\text{CH}_2\text{Cl}_2$ (1:1) Rf: 0.5, to afford a white solid (195 mg, 15% yield). M.p.: $>300\text{ }^{\circ}\text{C}$. ^1H NMR (400 MHz, C_6D_6 , $25\text{ }^{\circ}\text{C}$) δ (ppm) 7.24-7.22 (m, 6H, H_d), 6.99 (d, $J = 8\text{ Hz}$, 6H, H_c), 6.95 (d, $J = 8\text{ Hz}$, 6H, H_b), 6.87-6.85 (m, 9H, H_a , H_e), 6.42 (s, 6H, H_g), 2.31 (s, 18H, H_h), 1.80 (s, 9H, H_j); ^{13}C NMR (100 MHz, C_6D_6 , $25\text{ }^{\circ}\text{C}$) δ (ppm) 146.5, 137.2, 137.1, 131.4, 130.6, 128.1, 127.8, 127.4, 127.0, 123.7, 119.9, 89.7, 89.6, 23.0, 20.9 (the ^{13}C resonance corresponding to the carbon atom bonded to the boron atom is not observed due to the quadrupolar relaxation). ^{11}B NMR (128 MHz, CDCl_3 , $25\text{ }^{\circ}\text{C}$) δ (ppm) 37.4 (br). Solid-state IR (KBr) ν (cm^{-1}) 2916 (C-H aromatic), 1510, 1356 (B-N) 1301, 836, 754. HRMS (MALDI, m/z): $[\text{M}^+]$ calc. for $\text{C}_{69}\text{H}_{60}\text{N}_3\text{B}_3$, 963.5066; found, 963.5086.

Mesitylethynylbenzene 175



In a 20 mL microwave sealable flask, $\text{Pd}(\text{PPh}_3)\text{Cl}_2$ (195 mg, 0.3 mmol), CuI (180 mg, 1 mmol) and PPh_3 (1.300 g, 5 mmol) were added and the flask was purge with three vacuum-argon cycles. Then, phenylacetylene (1.040 g, 10 mmol) and MesBr (2.380 g, 12 mmol), diluted in 20 mL of degassed $\text{DMF}:\text{diisopropylamine}$ (1:1) were added. The reaction was then allowed to proceed at $160\text{ }^{\circ}\text{C}$ for 30 min. After this period, conversion was not complete and it further reacts for 30 min. After 1 h the reaction was quenched by 20 mL of H_2O . The aqueous layer was extracted with pentane ($3 \times 20\text{ mL}$). The combined organic layers were dried over MgSO_4 , filtered and the solvents removed under reduced pressure. The crude was purified on silica gel column chromatography (eluent: pentane), affording a white solid (1.718 g, 78% yield). ^1H NMR (400 MHz, CDCl_3 , $25\text{ }^{\circ}\text{C}$) δ (ppm) 7.54-7.53 (m, 2H, H_b), 7.36-7.34 (m, 3H, H_c , H_a), 6.91 (s, 2H, H_e), 2.48 (s, 6H, H_d), 2.31 (s, 3H, H_j). All other spectroscopic and analytical properties were identical to those reported in the literature.^[312]

B-hydroxy-B-(2,4,6-triisopropyl-benzene)- B'-(2,4,6-triisopropyl-benzene)- N-phenyl-N'-phenyl borazene 183

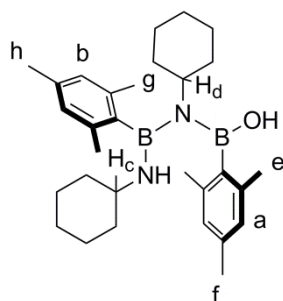


In a flame-dried 25 mL Schlenk flask, anhydrous aniline (335.26 mg, 3.6 mmol) was diluted with 4 mL of anhydrous toluene and cooled to $-5\text{ }^{\circ}\text{C}$ (ice-salt bath). Then BCl_3 (4.7 mL, 4.7 mmol, 1 M solution in toluene) was added dropwise. The septum was changed for a dry condenser topped by a CaCl_2 tube. The reaction mixture was heated up for 17 h. After this period the flask was cooled down and subject to three freeze-to-thaw cycle to remove the HCl . In parallel, in a flame-dried 50 mL Schlenk flask, 1-bromo-2,4,6-triisopropylbenzene (1,230 mg, 4 mmol) was diluted with 20 mL of anhydrous THF. The solution was cooled down to $-78\text{ }^{\circ}\text{C}$ and freshly titrated *n*-BuLi (3.5 mL, 4.3 mmol, 1.2 M) was added dropwise. The flask was allowed to warm up to $0\text{ }^{\circ}\text{C}$ for 1 h. The color changes from transparent to light yellow. The borazole was cannulated dropwise to the lithiate at $0\text{ }^{\circ}\text{C}$ and allowed to react at r.t.. After 20 h the reaction was quenched by 20 mL of H_2O . The

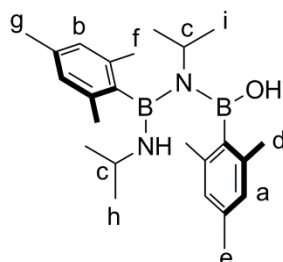
Chapter 4

aqueous layer was extracted with EtOAc (3 × 40 mL). The organic layer was dried over MgSO₄, filtered and the solvents removed under reduced pressure. The crude was purified by silica gel chromatography to obtain a white solid (60 mg, 5.3% yield). Eluent: CHX:CH₂Cl₂ (1:1). M.p.: 40 °C, decomposition at 122 °C. ¹H NMR (400 MHz, CDCl₃, 25 °C) δ (ppm) (rotamer) 7.20-7.17 (m), 7.12 (s), 7.09-7.03 (m), 6.90 (s), 6.84 (t, 8.0 Hz), 6.72-6.65 (m), 6.64 (s), 6.08 (d, 7.8 Hz), 5.32 (d, 8.0 Hz), 5.27 (s) (total aromatic: 36H, *H_a*, *H_b*, *H_{aromatic}*), 5.06 (s, 1H, PhNH), 3.21-2.65 (m, 6H, *H_c*, *H_d*, *H_e*, *H_f*), 1.45-0.80(m, 42H, CHCH₃). ¹³C NMR (400 MHz, CDCl₃, 25 °C) δ (ppm) (rotamers) 151.1, 148.8, 148.0, 145.3, 143.4, 129.3, 129.1, 128.8, 128.5, 128.0, 125.7, 122.0, 121.6, 121.6, 119.4, 119.1, 118.8, 35.6, 35.3, 35.2, 35.0, 34.5, 34.1, 26.8, 25.3, 25.2, 24.7, 24.25, 24.2, 24.0, 23.8, 22.7 (the ¹³C resonance corresponding to the carbon atom bonded to the boron atom is not observed due to the quadrupolar relaxation). ¹¹B NMR (400 MHz, CDCl₃, 25 °C) δ (ppm) 33.77. Solid-state IR (KBr) ν (cm⁻¹) 3373 (O-H) 2959 (C-H aromatic), 2869 (C-H alkyl), 1517, 1462, 1361 (B-N), 1312, 1196. HRMS (MALDI, *m/z*): [M⁺] calc. for C₄₂H₅₈N₂O_B₂, 628.4735; found, 628.4735. Crystal suitable for X-ray diffraction was obtained by slow evaporation in CHCl₃. Space group P-1.

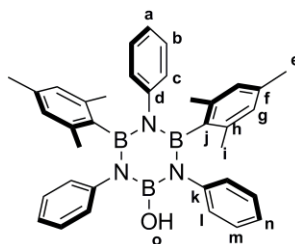
B-hydroxy-B-mesityl- B'-mesityl- N-cyclohexyl-N'- cyclohexylborazene 191



In a flame-dried 25 mL Schlenk flask, anhydrous cyclohexylamine (992 mg, 10 mmol) was diluted with 2 mL of anhydrous toluene and cooled to -5 °C (ice-salt bath). Then BCl₃ (12 mL, 512 mmol, 1 M solution in toluene) was added dropwise which yield to a white precipitate. The septum was changed for a dry condenser topped by a CaCl₂ tube. The reaction mixture was heated up for 16 h. After this period the flask was cooled down and subject to three freeze-to-thaw cycle to remove the HCl. In parallel, in a flame-dried 50 mL Schlenk flask, MesBr (2,189 mg, 11 mmol) was added dropwise to a suspension of magnesium turning in anhydrous THF (30 mL). Magnesium turning was previously activated by washing with HCl followed by a drying at 120 °C. The borazole was cannulated dropwise to the Grignard at 0 °C and allowed to react at r.t.. After 16 h the reaction was quenched by 20 mL of H₂O. The aqueous layer was extracted with EtOAc (3 × 20 mL). The combined organic layers were dried over MgSO₄, filtered and the solvents removed under reduced pressure. The crude was purified by silica gel chromatography, CH₂Cl₂/CHX (1:1) (R_f = 0.5) to afford a transparent oil (200 mg, 8% yield). ¹H NMR (400 MHz, CDCl₃, 25 °C) δ (ppm) 6.86 (s), 6.81 (s), 6.77 (s), 6.73 (s) (total: 4H, *H_a*, *H_b*), 3.93 (t, 6.2 Hz), 3.81 (t, 6.2 Hz), 3.45-3.41 (m) (total: 2H, *H_c*, *H_d*), 2.38-2.21 (m, 18H, *H_e*, *H_e*, *H_f*, *H_h*), 2.00-0.78 (m, 20H, CH₂). ¹H NMR (400 MHz, DMSO-*d*₆, 25 °C) δ (ppm) 6.78 (s), 6.72 (s), 6.70 (s), 6.68 (s), 6.67 (s), 6.63 (s), 6.60 (s) (aromatic signal), 2.18-1.19 (m, alkyl). ¹³C NMR (100 MHz, CDCl₃, 25 °C) δ (ppm) 138.4, 136.9, 127.2, 127.0, 126.9, 126.7, 116.5, 56.7, 35.9, 34.6, 33.7, 27.2, 26.6, 25.9, 25.8, 22.4, 22.2, 22.1, 21.6, 21.3 (the ¹³C resonance corresponding to the carbon atom bonded to the boron atom is not observed due to the quadrupolar relaxation). ¹¹B NMR (128 MHz, CDCl₃, 25 °C) δ (ppm) 34.4 and 30.1 (br). Solid-state IR (KBr) ν (cm⁻¹) 3393 (N-H) 2928 (C-H aromatic), 2854 (C-H alkyl), 1610, 1486, 1450, 1356 (B-N) 1283, 1239, 848. HRMS (MALDI, *m/z*): [M⁺] calc. for C₃₀H₄₇N₂O_B₂, 473.3875; found, 473.3858.

B-hydroxy-B-mesityl- B'-mesityl- N-isopropyl-N'- isopropylborazene 192

In a flame-dried 25 mL Schlenk flask, anhydrous isopropylamine (298 mg, 5 mmol) was diluted with 2 mL of anhydrous toluene and cooled to $-5\text{ }^{\circ}\text{C}$ (ice-salt bath). Then BCl_3 (6 mL, 6 mmol, 1 M solution in toluene) was added dropwise. The septum was changed for a dry condenser topped by a CaCl_2 tube. The reaction mixture was heated up for 16 h. After this period the flask was cooled down and subject to three freeze-to-thaw cycle to remove the HCl. In parallel, the in a flame-dried 50 mL Schlenk flask, MesBr (1,094 mg, 5.5 mmol) was diluted with 20 mL of anhydrous THF. The solution was cooled down to $-78\text{ }^{\circ}\text{C}$ and freshly titrated *n*-BuLi (3 mL, 6 mmol) was added dropwise. The flask was allowed to warm up to $0\text{ }^{\circ}\text{C}$ for 1 h. The colour changes from transparent to light yellow. The borazole was cannulated dropwise to the lithiate at $0\text{ }^{\circ}\text{C}$ and allowed to react at r.t.. After 15 h the reaction was quenched by 10 mL of H_2O . The aqueous layer was extracted with EtOAc (3×20 mL). The organic layer was dried over MgSO_4 , filtered and the solvents removed under reduced pressure. The crude was purified by chromatography column so as to obtain a white solid (10 mg, 1% yield). Eluent: $\text{CH}_2\text{Cl}_2/\text{CHX}$ (1:1). Crystal obtained by slow evaporation in pentane. Space group: $\text{P2}_1/\text{n}$. ^1H NMR (400 MHz, CDCl_3 , $25\text{ }^{\circ}\text{C}$) δ (ppm) (rotamers) 6.85 (s), 6.77 (s), 6.75 (s) (total: 4H, H_a, H_b), 3.71 (sex, 6.9 Hz, 2H, H_c), 2.36-2.21 (m, 18H, H_d, H_e, H_f, H_g), 1.31 (d, 6.9 Hz, 3H), 1.23, (dd, 6.9 Hz, 6H) 0.44 (d, 6.9 Hz, 3H) (total: 12H, H_h, H_i). ^{13}C NMR (400 MHz, CDCl_3 , $25\text{ }^{\circ}\text{C}$) δ (ppm) (rotamers) 138.8, 138.6, 138.0, 127.5, 126.9, 50.1, 43.7, 25.9, 23.9, 21.6, 21.2 (the ^{13}C resonance corresponding to the carbon atom bonded to the boron atom is not observed due to the quadrupolar relaxation). ^{11}B NMR (400 MHz, CDCl_3 , $25\text{ }^{\circ}\text{C}$) δ (ppm) 34.4 (br). Solid-state IR (KBr) ν (cm^{-1}) 3536 (O-H), 3390 (N-H) 2993 (CH aromatic), 2863 (CH alkyl), 1609, 1450, 1348 (B-N), 1327, 1277. HRMS (EI, m/z): $[\text{M}^+]$ calc. for $\text{C}_{24}\text{H}_{38}\text{N}_2\text{OB}_2$, 392.3170; found, 392.3179. Crystal suitable for X-ray diffraction was obtained by slow evaporation in CHCl_3 . Space group $\text{P2}_1/\text{c}$.

B-hydroxy-B'-mesityl-B''-mesityl-N-phenyl-N'-phenyl-N''-phenylborazine 196

Procedure a) In a flame-dried 100 mL Schlenk flask, anhydrous aniline (3.730 g, 40 mmol) was diluted with 25 mL of anhydrous toluene and cooled to $-5\text{ }^{\circ}\text{C}$ (ice-salt bath). Then BCl_3 (48 mL, 48 mmol, 1M solution in toluene) was added dropwise which yield to a white precipitate. The septum was changed for a flame-dried condenser topped by a CaCl_2 tube and the resulting mixture refluxed for 15 h. The reaction solution was cooled down to $0\text{ }^{\circ}\text{C}$ and subjected to three freeze-to-thaw cycles to remove the excess of HCl. In parallel, in a flame-dried 100 mL Schlenk flask, MesBr (8.760 g, 44 mmol) was diluted with 20 mL of anhydrous THF. The solution was cooled down to $-78\text{ }^{\circ}\text{C}$ and freshly titrated *n*-BuLi (24 mL, 48 mmol) was added dropwise. The flask was allowed to warm up to $0\text{ }^{\circ}\text{C}$ for 1 h. The color changes from transparent to light yellow. The borazole was then cannulated dropwise to the organometallic-containing solution at $0\text{ }^{\circ}\text{C}$ and allowed to react at

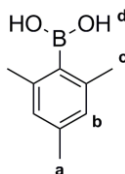
Chapter 4

r.t.. Aliquots were taken to follow the reaction, after 17 h the reaction was quenched by 20 mL of H₂O. The aqueous layer was extracted with of EtOAc (3 × 50 mL). The combined organic layers were dried over MgSO₄, filtered and the solvents removed under reduced pressure. The crude was purified by precipitation in MeOH and affords a white powder (1.238 g, 17% yield). TLC: CH₂Cl₂/CHX (1:1) (R_f = 0.5). M.p.: 240 °C. ¹H NMR (400 MHz, CDCl₃, 25 °C) δ (ppm) 7.13-7.02 (m, 10H, *H_{l-n}*), 6.79-6.70 (m, 5H, *H_{a-c}*), 6.33 (s, 4H, *H_g*), 2.21 (s, 12H, *H_i*) 1.97 (s, 6H, *H_e*) ¹³C NMR (100 MHz, CDCl₃, 25 °C) δ (ppm) 146.4, 144.0, 137.4, 136.2, 128.4, 127.5, 127.0, 126.8, 126.3, 125.3, 124.2, 23.0, 21.1 (the ¹³C resonance corresponding to the carbon atom bonded to the boron atom is not observed due to the quadrupolar relaxation). ¹¹B NMR (128 MHz, CDCl₃, 25 °C) δ (ppm) 36.2 (br), 23.9 (br). Solid-state IR (KBr) ν (cm⁻¹) = 3612 (O-H) 2915 (C-H aromatic), 1611, 1597, 1490, 1453, 1429, 1368 (B-N) 1325, 907, 729. HRMS (MALDI, *m/z*): [*M*⁺] calc. for C₃₆H₃₈N₃B₃O, 561.3294; found, 561.3311. Crystal suitable for X-ray diffraction was obtained by slow evaporation in CHCl₃. Space group P2₁/c.

Procedure b) In a flame-dried 50 mL Schlenk flask, anhydrous aniline (940 mg, 10 mmol) was diluted with 25 mL of anhydrous toluene. The solution was cooled to -5 °C (ice-salt bath). Then BCl₃ (12 mL, 12 mmol, 1 M solution in toluene) was added dropwise which yield to a white precipitate. The septum was changed for a flame-dried condenser topped by a CaCl₂ tube and the resulting mixture refluxed for 2 h. After this period, solution was cooled down to 0 °C, the condenser was changed for a septum, and the flask subjected to three freeze-to-thaw cycle to remove the remaining HCl. In parallel, in a flame-dried 100 mL Schlenk flask, MesBr (1310 mg, 6.5 mmol) was diluted with 15 mL of anhydrous THF. The solution was cooled down to -78 °C and freshly titrated *n*-BuLi (4.0 mL, 7.2 mmol, 1.8 M) was added dropwise. The flask was allowed to warm up to 0 °C for 1h. The color changes from transparent to light yellow. The borazole was then cannulated dropwise to the organometallic-containing solution at 0 °C and allowed to react at r.t. for 3 h. After this period, deuterated H₂O (180 μL, 10 mmol) was added dropwise and the reaction was allowed to proceed for 16 h at r.t., after which it was quenched by 20 mL of H₂O. The aqueous layer was extracted with CH₂Cl₂ (3 × 20 mL). The combined organic layers were dried over MgSO₄, filtered and the solvents removed under reduced pressure. The crude was purified by precipitation in MeOH and affords a white powder (210 mg, 11% yield). The characterizations correspond to the non-deuterated borazine **194**.

4.3.2. Boronic Acids and Carboxylates Derivatives

Mesityleneboronic acid **224**

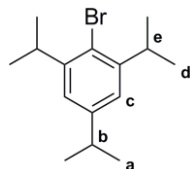


In a 100 mL flame-dried schlenk flask, MesBr (5 g, 25.1 mmol) was added dropwise to a suspension of metallic Mg (0.80 g, 33.1 mmol) with a iodine crystal in 50 mL of anhydrous THF at 0 °C under argon atmosphere. The reaction was then heated up to reflux for 3 h and then cool down to -78 °C. Then, boron B(OMe)₃ (4.87 g, 46.8 mmol) was added dropwise to the cooled solution. The reaction was then stirred for 3 h at r.t. and then quenched by the addition of a solution of hydrochloric acid (80 mL, 1 M) at 0 °C. The reaction was stirred for 2 h after which the aqueous phase was extracted with Et₂O (3 × 50 mL). The organic phases are combined, washed with brine (40 mL), dried over MgSO₄, filtered and the solvents are removed under reduced pressure. The crude obtained (2.38 g) was purified by recrystallization in hot cyclohexane. A white solid was collected by filtration and after rinsing with cold pentane (1.77 g, 44%). M.p.: 144-146 °C, after continuous heating, second melting point at 192-195 °C.^[313] ¹H NMR (400 MHz, CDCl₃, 25 °C) δ (ppm) 6.82 (s, 2H, *H_b*), 4.51 (br, 2H, *H_d*), 2.34 (s, 6H, *H_c*), 2.27 (s, 3H, *H_a*). ¹³C NMR (100 MHz, CDCl₃, 25 °C) δ (ppm), 139.8, 138.8, 127.4, 22.2, 21.2 (the ¹³C resonance corresponding to the carbon atom bonded to the boron atom is not observed due to the quadrupolar relaxation). ¹¹B

Chapter 4

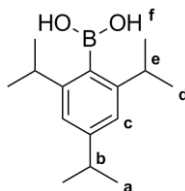
NMR (128 MHz, CDCl₃, 25 °C) δ (ppm) 30.7 (s). Solid-state IR (KBr) ν (cm⁻¹) 3315 (BO-H), 2918 (C-H), 1344 (B-O). HRMS (EI, m/z): [M⁺] calc. for C₉H₁₃O₂B, 163.1045; found, 163.1046.

Bromo-2,4,6-triisopropylbenzene 230



To a light-protected solution of bromine (6.39 g, 40 mmol) in DMF (6 mL) at 0 °C, a solution of triisopropylbenzene (2.04 g, 10 mmol) in DMF (2 mL) was added dropwise. After 45 min of stirring, the reaction mixture was added to a 20 mL saturated solution of Na₂SO₃ at 0 °C. The aqueous layer was extracted with pentane (3 x 10 mL). The organic phases were combined, dried over MgSO₄, filtered and the solvents were removed under reduced pressure. The crude (2.74 g) was purified by distillation (180 °C, 13 mbar) to afford a transparent liquid (0.99 g, 35%). ¹H NMR (400 MHz, CDCl₃, 25 °C) δ (ppm) 7.03 (s, 2H, H_c), 3.50 (septuplet, J = 6.6 Hz, 2H, H_e), 2.90 (septuplet, J = 6.9 Hz, 1H, H_b), 1.27 (d, 6.9 Hz, 18H, H_a, H_d). ¹³C NMR (100 MHz, CDCl₃, 25 °C) δ (ppm), 147.9, 147.5, 123.8, 122.4, 34.2, 33.7, 24.2, 23.3. Mass (GC-MS) calc. for C₁₅H₂₃Br, 282.09; found, 281.94 (R.T.: 12.58 min, starting temperature: 60 °C, ramp: 10 °C/min.). All other spectroscopic and analytical properties were identical to those reported in the literature.^[289]

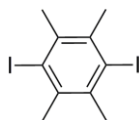
2,4,6-triisopropylphenylboronic acid 228



To a solution of 1-bromo-2,4,6-triisopropylbenzene (10.60 g, 10.6 mmol) in anhydrous THF under argon atmosphere, TMEDA was added (2.5 mL) at -5 °C. Then, the solution was cooled down to -78 °C and *n*-BuLi (9 mL, 1.43 M, 12.8 mmol) was added dropwise. After 1 h of stirring at r.t., the solution was cooled down again to -78 °C and B(OMe)₃ (2.20 g, 21.2 mmol) was added dropwise and the solution turns brown upon addition. The reaction was thawed to r.t. after 30 min. of stirring at -78 °C and followed by GC-MS. There was a 40% conversion after 20 h. The solution was then heated up to reflux for 4 h and then quenched by H₂O. The aqueous layer was extracted with Et₂O (3x15 mL). The organic phases are combined, dried over MgSO₄, filtered and the solvents are removed under reduced pressure. The crude dimethyl boronic ester (1.385 g) was hydrolyzed by the addition an aqueous solution of HCl (6 mL, 10%). After 1 h, the aqueous layer was extracted with CH₂Cl₂ (3 x 15 mL). The organic phases are combined, dried over MgSO₄, filtered and the solvents are removed under reduced pressure. The white solid was purified by sublimation (85 °C, 0.1 mbar) to afford a pure white solid (1.05 g, 40%). M.p.: 159-161 °C. ¹H NMR (400 MHz, CDCl₃, 25 °C) δ (ppm) 6.99 (s, 2H, H_c), 4.48 (br, 2H, H_f) 2.88 (septuplet, 6.7 Hz, 3H, H_b, H_e), 1.25 (m, 18H, H_d et H_a). ¹³C NMR (100 MHz, CDCl₃, 25 °C) δ (ppm) 150.7, 150.0, 120.4, 35.1, 34.5, 24.8, 24.1 (the ¹³C resonance corresponding to the carbon atom bonded to the boron atom is not observed due to the quadrupolar relaxation). ¹¹B NMR (128 MHz, CDCl₃, 25 °C) δ (ppm) 30.7. Solid-state IR (KBr) ν (cm⁻¹) 3580, 3354 (BO-H), 2959, 2870 (C-H), 1362, 1327 (B-O), 1297. HRMS (EI, m/z): [M⁺] calc. for C₁₅H₂₅O₂B, 247.1984; found, 247.1983. All other spectroscopic and analytical properties were identical to those reported in the literature.^[289]

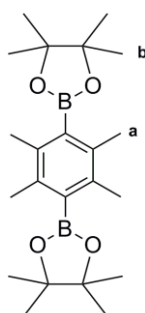
Chapter 4

1,4-diiodo-2,3,5,6-tetramethylbenzene 233



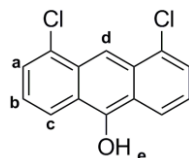
In a 250 mL flask equipped with a condenser, durene (6.71 g, 50 mmol) was added at 0 °C to a solution of ICl (35.06 g, 216 mmol) in MeOH (100 mL). The reaction mixture was then heated up to reflux for 16 h. The precipitate obtained (12.93 g) was filtered and washed with MeOH. The crude was purified by two recrystallizations in hot EtOAc. After filtration, the desired product was obtained as a white solid (8.83 g, 46%). M.p.: 137 °C. ¹H NMR (400 MHz, CDCl₃, 25 °C) δ (ppm) 2.62 (s, 12H, CH₃). ¹³C NMR (100 MHz, CDCl₃, 25 °C) δ (ppm) 138.0, 112.3, 29.9 (CH₃). Solid-state IR (KBr) ν (cm⁻¹) 2916 (C-H), 1398, 1379, 1162, 974. Mass (GC-MS) calc. for C₁₀H₁₂I₂, 385.90; found, 385.9 (R.T.: 13.32 min, starting temperature: 100 °C, ramp: 10 °C/min.).

2,3,5,6-tetramethyl-1,4-phenylenediboronic acid 238



In a 10 mL microwave flask, PdCl₂(PPh₃)₂ (0.098 g, 0.14 mmol), KOAc (0.59 g, 6 mmol), diiododurene (0.39 g, 1 mmol) and bis(pinacol)diboron (0.56 g, 2.2 mmol) are dissolved in DMF. The reaction proceeds under microwave irradiation, 3 h at 140 °C. The solution was filtered on celite, organic phase was washed with 10 mL of brine, the aqueous layer extracted with CH₂Cl₂ (3 × 10 mL). The organic phases are combined, washed with brine, dried over MgSO₄, filtered and the solvents are removed under reduced pressure. The crude solid obtained (0.16 g) was purified by recrystallization in hot EtOH. To afford a white solid (0.12 g, 30%). M.p.: degradation at 300 °C. TLC Rf: 0.47 et 0.58 (eluents: cyclohexane/ CH₂Cl₂ 1:1). ¹H NMR (400 MHz, CDCl₃, 25 °C) δ (ppm) 2.20 (s, 12H, H_a), 1.38 (s, 24H, H_b). ¹³C NMR (100 MHz, CDCl₃, 25 °C) δ (ppm), 135.9, 83.7, 25.2, 19.5 (one peak for the carbon atoms bonding to the boron atoms was not observed due to quadrupolar relaxation). ¹¹B NMR (128 MHz, CDCl₃, 25 °C) δ (ppm) 31.3. Solid-state IR (KBr) ν (cm⁻¹) 2977 (C-H), 1372, 1325 (B-O), 1309, 1141, 858. HRMS (EI, *m/z*): [M⁺] calc. for C₂₂H₃₆O₄B₂ 384.2872; found 384.2868.

4,5-dichloro-9-anthracenone 241

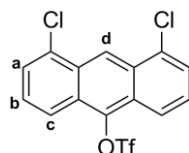


In a 250 mL flask, Na₂S₂O₄ (15.91 g, 89.7 mmol) was added to a suspension of de 1,8-dichloroanthraquinone (2.77 g, 10 mmol) in a 1:1 mixture of DMF and H₂O under argon atmosphere. After 5 h at r.t., the solution was poured into 200 mL of H₂O and the aqueous layer was extracted with CH₂Cl₂ (3 × 200 mL). The organic phases are combined, washed with brine, dried over MgSO₄, filtered and the solvents were removed under reduced pressure. The orange solid obtained was purified by recrystallization in refluxing CCl₄. After filtration, an orange solid was obtained (1.28 g, 48%). M.p. 220 °C. TLC Rf: 0.34

Chapter 4

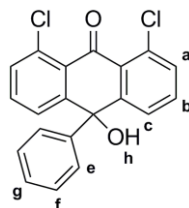
(eluent: CH₂Cl₂/cyclohexane 1:1). ¹H NMR (400 MHz, CDCl₃, 25 °C) δ (ppm) 8.19 (d, *J* = 7.8 Hz, 2H, *H_d*), 7.73 (d, *J* = 8.0 Hz, 2H, *H_c*), 7.51 (t, *J* = 7.8 Hz and 8.0 Hz, 2H, *H_b*), 6.40 (s, 1H, *H_d*), 3.15 (br, 1H, *H_e*). ¹³C NMR (100 MHz, CDCl₃, 25 °C) δ (ppm), 182.6, 138.4, 135.0, 134.9, 132.8, 130.1, 126.6, 61.7. Solid-state IR (KBr) ν (cm⁻¹) 3517 (O-H), 3100 (C-H), 1660 (C=O), 1311, 1135. HRMS (EI, *m/z*): [*M*⁺] Calc. for C₁₄H₈OCl₂, 260.9874; found, 260.9881.

4,5-dichloroanthracen-9-yl trifluoromethanesulfonate 243



In a 5 mL flame-dried schlenk flask, a solution of LiHMDS (3 mL, 3 mmol, 1 M) in anhydrous THF was added to a solution of 4,5-dichloro-9-anthracenone (132 mg, 0.5 mmol) in anhydrous dichloromethane (2 mL) under argon atmosphere at -78 °C. After 2 h of stirring at -78 °C, triflic anhydride was added (1 mL, 1 mmol, 1 M in CH₂Cl₂) dropwise. After 2 h of stirring the reaction was quenched with H₂O (5 mL). The aqueous layer was extracted with CH₂Cl₂ (3 × 5 mL). The organic phases were combined, dried over MgSO₄, filtered and the solvents were removed under reduced pressure. The crude (219 mg) was purified on silica gel column chromatography (eluent: cyclohexane/CH₂Cl₂ 1:1) to give the desired product in 6% yield (11.4 mg). ¹H NMR (400 MHz, CDCl₃, 25 °C) δ (ppm) 9.31 (s, 1H, *H_d*), 8.46 (d, *J* = 8.9 Hz, 2H, *H_d*), 7.69 (d, *J* = 7.1 Hz, 2H, *H_c*), 7.54 (t, *J* = 8.9 Hz, 2H, *H_b*).

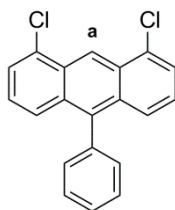
1,8-dichloro-10-hydroxy-10-phenyl-10,10a-dihydroanthracen-9-one 245



In a 250 mL flame-dried flask, PhMgBr (23.6 mL, 23.6 mmol, 1 M in THF) was added to a solution of 1,8-dichloroanthraquinone (6 g, 21.6 mmol) in anhydrous THF, under argon atmosphere at 0 °C. After 4 h 30 of stirring, the color of the solution changes from yellow to red and was quenched with H₂O (30 mL). The aqueous layer was extracted with CH₂Cl₂ (3 × 40 mL). The organic phases are combined, dried over MgSO₄, filtered and the solvents are removed under reduced pressure. The crude was purified by recrystallization in hot CH₂Cl₂ and a white solid was filtered, washed with cold pentane to give a pure white solid (4.48 g, 58.3%). M.p.: 204 °C. TLC Rf: 0.10 (eluent: CH₂Cl₂/cyclohexane 1:1). ¹H NMR (400 MHz, CDCl₃, 25 °C) δ (ppm) 7.81 (t, *J* = 4.6 Hz, 2H, *H_b*), 7.45 (d, *J* = 4.6 Hz, 4H, *H_a*, *H_c*), 7.19-7.16 (m, 5H, *H_e*, *H_f*, *H_g*), 2.88 (s, 1H, *H_d*). ¹³C NMR (100 MHz, CDCl₃, 25 °C) δ (ppm) 183.2, 170.9, 148.2, 145.0, 133.0, 131.3, 130.4, 128.8, 127.9, 125.5, 124.5, 74.2. Solid-state IR (KBr) ν (cm⁻¹) 3460 (O-H), 1668 (C=O), 1584, 1447, 1252. HRMS (EI, *m/z*): [*M*⁺] calc. for C₂₀H₁₂O₂Cl₂ 354.0214; found, 354.0227. Crystals suitable for X-ray diffraction were obtained by slow evaporation in CH₂Cl₂, space group: P2₁/c.

Chapter 4

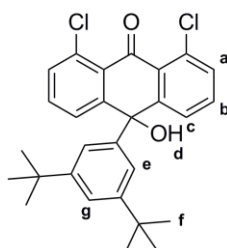
1,8-dichloro-10-phenylanthracene 246



Procedure A) To a suspension of zinc dust (4.03 g, 61.9 mmol) in EtOH (190 mL), 1,8-dichloro-10-hydroxy-10-phenyl-10,10a-dihydroanthracen-9-one was added (2 g, 5.6 mmol) and the reaction mixture was heated up to reflux for 45 min. After this period, 10% aq. HCl (150 mL) was added to the hot solution. The reaction was monitored by TLC and shows no more evolution after 2 h of stirring. The aqueous layer was extracted with Et₂O (3 x 100 mL). The organic phases are combined, dried over MgSO₄, filtered and the solvents are removed under reduced pressure. The crude (1.88 g) was directly subjected to another reduction. The crude was mixed with a suspension of zinc (3.81 g, 58.3 mmol) in EtOH (190 mL) and heated up to reflux for 45 min. After this period, 10% aq. HCl (125 mL) was added to the hot solution. The reaction was monitored by TLC and shows no more evolution after 2h of stirring. The aqueous layer was extracted with CH₂Cl₂ (3 x 100 mL). The organic phases are combined, dried over MgSO₄, filtered and the solvents are removed under reduced pressure. The crude (2.29 g) was purified by a first precipitation in MeOH and a white solid was recovered (322 mg). A second precipitation MeOH after evaporation of the crystallization liquor affords the product in total yield of 22% (371 mg). M.p.: 121 °C. TLC Rf: 0.89 (eluent: CH₂Cl₂/cyclohexane 1:1). ¹H NMR (400 MHz, CDCl₃, 25 °C) δ (ppm) 9.40 (s, 1H, H_a), 7.63-7.53 (m, 7H, H_{arom}), 7.39-7.34 (m, 2H, H_{arom}) 7.29-7.23 (m, 2H (overlap with solvent signal), H_{arom}). ¹³C NMR (100 MHz, CDCl₃, 25 °C) δ (ppm) 132.7, 131.5, 131.1, 129.2, 128.8, 128.6, 128.3, 128.0, 126.3, 125.9, 125.5, 121.1. Solid-state IR (KBr) ν (cm⁻¹) 3052, 1660, 1591, 1391, 1311, 1136, 743. HRMS (EI, m/z): [M⁺] calc. for C₂₀H₁₂Cl₂, 322.0316; found, 322.0312. Crystal suitable for X-ray diffraction was obtained by slow evaporation in cyclohexane, space group: P2₁/C. Experimental data agree with previously reported data.^[314]

Procedure B): In a flame-dried 5 mL schlenk flask, LiAlH₄ (18.7 mg, 0.49 mmol) was suspended in anhydrous Et₂O (3 mL), under argon atmosphere, and the reaction mixture was cooled down to 0 °C. To this mixture, a solution of **245** (50 mg, 0.141 mmol) in anhydrous CH₂Cl₂ (1 mL) and a solution of AlCl₃ (150.4 mg, 1.13 mmol) in anhydrous Et₂O (4 mL) are added. Then, the reaction was heated up to reflux for 24 h and quenched by the addition of 20 mL of MeOH at 0 °C, then by 10 mL of H₂O. The aqueous layer was extracted with CH₂Cl₂ (3 x 20 mL). The organic phases are combined, dried over MgSO₄, filtered and the solvents are removed under reduced pressure. A pure product was obtained in 87% yield (40 mg) whose spectral data match the one of the product obtained by Clemmensen reduction. Experimental data agree with previously reported data.^[314]

1,8-dichloro-10-(3,5-di-tert-butylphenyl)-10-hydroxy-10,10a-dihydroanthracen-9-one 249



In a 25 mL flame-dried schlenk flask, a solution of 1-bromo-3,5-di-tert-butylbenzene (1.065 g, 3.96 mmol) in anhydrous THF, was added dropwise to a suspension of metallic Mg (105 mg, 4.32 mmol) with a iodine crystal in 6 mL of anhydrous THF under argon atmosphere. The reaction mixture was then heated up to 60 °C for 3 h. Then the Grignard solution is added

Chapter 4

dropwise to a suspension of 1,8-dichloroanthraquinone in 3 mL of anhydrous THF. The color of the solution changes from yellow to green. After 24 h of stirring at r.t., the reaction was quenched by the addition of 2 mL of H₂O. The aqueous layer was extracted with CH₂Cl₂ (3 × 15 mL). The organic phases are combined, dried over MgSO₄, filtered and the solvents are removed under reduced pressure. The crude (1.993 g) was purified by three recrystallisation in hot Et₂O to give a white solid (0.588 g) in 49% yield. M.p.: 195 °C. TLC Rf: 0.26 (eluents: CH₂Cl₂/cyclohexane 1:1). ¹H NMR (400 MHz, CDCl₃, 25 °C) δ (ppm) 7.84-7.82 (m, 2H, H_b), 7.45-7.44 (m, 4H, H_a, H_c), 7.21 (s, 1H, H_g), 6.98 (s, 2H, H_e), 3.46 (s, 1H, H_d) 1.16 (s, 18H, H_f). ¹³C NMR (100 MHz, CDCl₃, 25 °C) δ (ppm) 183.2, 151.2, 148.4, 144.3, 132.7, 132.6, 131.1, 130.9, 124.1, 122.0, 119.9, 75.0, 35.0, 31.4. Solid-state IR (KBr) ν (cm⁻¹) 3465 (O-H), 2962 (C-H), 1674 (C=O), 1587, 1249. HRMS (EI, *m/z*): [M⁺] calc. for C₂₈H₂₈O₂Cl₂₂, 466.1466; found, 466.1462. Crystal suitable for X-ray diffraction was obtained by slow evaporation in CH₂Cl₂, space group: P-1.

The synthesis of anthracene diboronic acid **238**, starting from **249**, as outlined in Scheme 3.21 has been carried out by Mr. Benoît Georges and will be reported in a future publication.

General procedure for the formation of alkyammonium benzoate

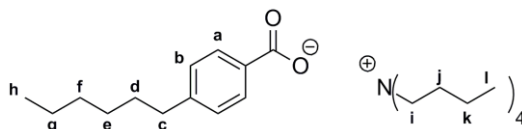
Benzoic acid derivatives (1 equivalent) were mixed with a tetralkylammonium hydroxide derivative (1 equivalent) in H₂O and the solutions were stirred for 15 min. After this period, the H₂O was removed by azeotropic distillation with EtOH, repeated three times.

Tetrabutylammonium benzoate **219**



¹H NMR (400 MHz, CDCl₃, 25 °C) δ (ppm) 7.84-7.81 (m, 2H, H_a), 7.04-7.02 (m, 3H, H_c, H_b), 2.91-2.87 (m, 8H, H_d), 1.29-1.21 (m, 8H, H_e), 1.09 (q, *J* = 7.4 Hz, 8H, H_f), 0.68 (t, *J* = 7.4 Hz, 12H, H_g). M.p.: 64-67 °C. ¹³C NMR (100 MHz, CDCl₃, 25 °C) δ (ppm) 170.4, 131.6, 129.9, 128.0, 58.8, 24.1, 19.8, 13.7. Solid-state IR (KBr) ν (cm⁻¹) 2958, 2874 (C-H), 1698, 1599, 1575, 1450, 1312, 718.

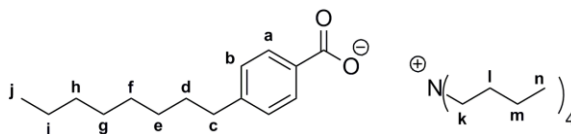
Tetrabutylammonium 4-hexylbenzoate **251**



¹H NMR (400 MHz, CDCl₃, 25 °C) δ (ppm) 7.92 (d, *J* = 8.0 Hz, 2H, H_a), 7.04 (d, *J* = 8.0 Hz, 2H, H_b), 3.19-3.15 (m, 8H, H_i), 2.53 (t, 8.0 Hz, 2H, H_c), 1.53-1.45 (m, 10H, H_d, H_j), 1.33-1.22 (m, 14H, H_e, H_f, H_g et H_k), 0.88 (t, *J* = 7.3 Hz, 12H, H_l), 0.82 (t, *J* = 6.6 Hz, 3H, H_h). ¹³C NMR (100 MHz, CDCl₃, 25 °C) δ (ppm) 171.3, 143.9, 137.2, 129.6, 127.3, 58.6, 35.9, 31.8, 31.5, 29.1, 24.0, 22.7, 19.7, 14.2, 13.7. Solid-state IR (KBr) ν (cm⁻¹) 2960, 2874 (C-H), 1596, 1553, 1461, 1371, 1104.

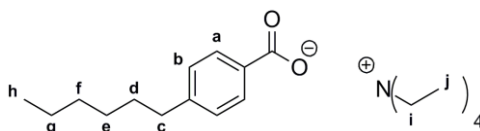
Chapter 4

Tetrabutylammonium 4-octylbenzoate 252



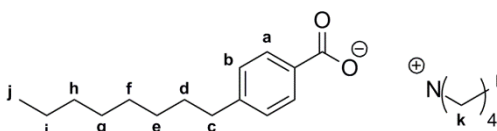
^1H NMR (400 MHz, CDCl_3 , 25 °C) δ (ppm) 7.97 (d, $J = 8.0$ Hz, 2H, H_a), 7.08 (d, $J = 8.0$ Hz, 2H, H_b), 3.27-3.32 (m, 2H, H_k), 2.55 (t, $J = 7.8$ Hz, 8H, H_c), 1.64-1.57 (m, 12H, H_d , H_e , H_f , H_g , H_h , H_i), 1.35-1.41 (m, 8H, H_m), 1.28-1.24 (m, 8H, H_l), 0.93 (t, $J = 7.3$ Hz, 12H, H_n), 0.87 (t, $J = 6.9$ Hz, 3H, H_j). ^{13}C NMR (100 MHz, CDCl_3 , 25 °C) δ (ppm) 166.9, 148.5, 129.7, 128.6, 128.5, 64.7, 36.1, 31.9, 31.3, 30.9, 29.5, 29.3, 24.3, 22.7, 19.4, 14.2, 13.9. Solid-state IR (KBr) ν (cm^{-1}) 2958, 2926, 2855 (C-H), 1718, 1273, 1106.

Tetraethylammonium 4-hexylbenzoate 253



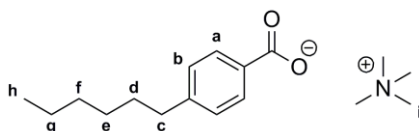
^1H NMR (400 MHz, CDCl_3 , 25 °C) δ (ppm) 7.98 (d, $J = 8.0$ Hz, 2H, H_a), 7.10 (d, $J = 8.0$ Hz, 2H, H_b), 3.39 (q, $J = 7.33$ Hz, 8H, H_i), 2.60-2.56 (m, 2H, H_c), 1.60-1.57 (m, 2H, H_d), 1.31-1.28 (m, 18H, H_j , H_e , H_f et H_g), 0.86 (t, $J = 6.9$ Hz, 3H, H_h). ^{13}C NMR (100 MHz, CDCl_3 , 25 °C) δ (ppm) 171.1, 144.5, 136.2, 129.6, 127.6, 52.7, 35.9, 31.8, 31.5, 29.1, 22.7, 14.2, 7.8. Solid-state IR (KBr) ν (cm^{-1}) 2924, 2853 (C-H), 1595, 1552, 1357.

Tetraethylammonium 4-octylbenzoate 254



^1H NMR (400 MHz, CDCl_3 , 25 °C) δ (ppm) 7.97 (d, $J = 8.0$ Hz, 2H, H_a), 7.09 (d, $J = 8.0$ Hz, 2H, H_b), 3.36 (q, $J = 7.3$ Hz, 8H, H_c), 2.56 (t, $J = 7.8$ Hz, 2H, H_k), 1.59-1.55 (m, 2H, H_d), 1.30-1.24 (m, 22H, H_e , H_f , H_g , H_h , H_i , H_l), 0.85 (t, $J = 6.9$ Hz, 3H, H_j). ^{13}C NMR (100 MHz, CDCl_3 , 25 °C) δ (ppm) 170.8, 144.2, 136.8, 129.5, 127.5, 52.6, 35.9, 32.0, 31.5, 29.6, 29.5, 29.4, 22.8, 14.2, 7.7. Solid-state IR (KBr) ν (cm^{-1}) 2922, 2851 (C-H), 1593, 1551, 1365, 1174, 776.

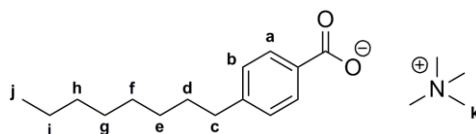
Tetramethylammonium 4-hexylbenzoate 255



^1H NMR (400 MHz, CDCl_3 , 25 °C) δ (ppm) 7.84 (d, $J = 8.0$ Hz, 2H, H_a), 7.02 (d, $J = 8.0$ Hz, 2H, H_b), 3.19-3.15 (s, 12H, H_i), 2.50 (t, 7.6 Hz Hz, 2H, H_c), 1.55-1.48 (m, 2H, H_d), 1.30-1.24 (m, 6H, H_e , H_f , H_g), 0.86 (m, 3H, H_h). ^{13}C NMR (100 MHz, CDCl_3 , 25 °C) δ (ppm) 171.6, 145.4, 135.9, 129.5, 127.9, 55.8, 36.0, 31.8, 31.4, 29.1, 22.7, 14.2. Solid-state IR (KBr) ν (cm^{-1}) 2929 (C-H), 1680, 1379, 1128, 1083, 949, 843.

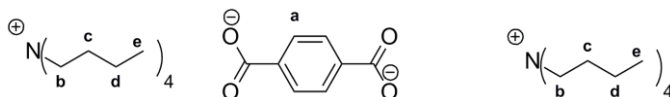
Chapter 4

Tetramethylammonium 4-octylbenzoate 256



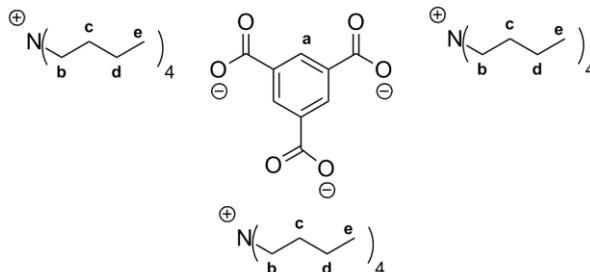
^1H NMR (400 MHz, CDCl_3 , 25 °C) δ (ppm) 7.96 (d, $J = 8.0$ Hz, 2H, H_a), 7.14 (d, $J = 8.0$ Hz, 2H, H_b), 3.46 (s, 12H, H_k), 2.58 (t, 8.0 Hz, 2H, H_c), 1.62-1.57 (m, 2H, H_d), 1.28-1.24 (m, 10H, H_e , H_f , H_g , H_h , H_i), 0.86 (t, 7.1 Hz, 3H, H_j). ^{13}C NMR (100 MHz, CDCl_3 , 25 °C) δ (ppm) 171.7, 145.2, 135.3, 129.5, 127.8, 56.0, 36.0, 32.0, 31.5, 29.6, 29.5, 29.4, 22.8, 14.2. Solid-state IR (KBr) ν (cm^{-1}) 2924, 2853 (C-H), 1594, 1552, 1367.

Tetrabutylammonium terephthalate 257



^1H NMR (400 MHz, CDCl_3 , 25 °C) δ (ppm) 7.97 (s, 4H, H_a), 3.14-3.06 (m, 16H, H_b), 1.49-1.42 (m, 16H, H_c), 1.36-1.29 (m, 16H, H_d), 0.93-0.88 (m, 24H, H_e). M.p.: 108-110 °C. ^{13}C NMR (100 MHz, CDCl_3 , 25 °C) δ (ppm) 170.8, 140.4, 127.9, 57.9, 23.2, 19.0, 13.0. Solid-state IR (KBr) ν (cm^{-1}) 2960, 2873 (C-H), 1576, 1484, 1351, 749.

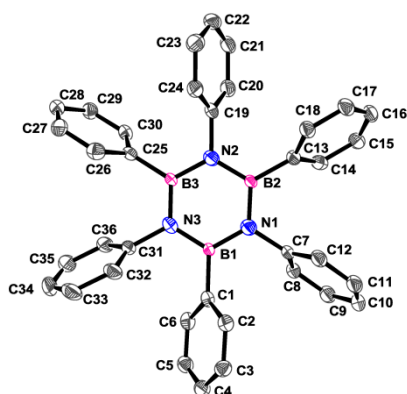
Tetrabutylammonium benzene-1,3,5-tricarboxylate 258



^1H NMR (400 MHz, CDCl_3 , 25 °C) δ (ppm) 8.59 (s, 3H, H_a), 3.37-3.32 (m, 24H, H_b), 1.65-1.59 (m, 24H, H_c), 1.36-1.32 (m, 24H, H_d), 0.89-0.86 (m, 36H, H_e). ^{13}C NMR (100 MHz, CDCl_3 , 25 °C) δ (ppm) 171.9, 138.1, 131.8, 58.9, 24.1, 19.7, 13.8. Solid-state IR (KBr) ν (cm^{-1}) 2971 (C-H), 1721, 1378, 1125, 1047.

Appendix I-Crystal Structures

X-Ray Analysis of 169



Crystal Data

Identification code: **169**
 Empirical formula: $C_{36}H_{30}B_3N_3$
 Formula weight: 537.09
 Temperature (°K): 150
 Crystal system, space group: Orthorhombic, Pna21
 Unit cell dimension a, b, c (Å):
 10.9138(2), 21.8912(5), 12.4977(4)
 Angle α , β , γ (°):
 90, 90, 90
 Volume (Å³): 2985.90(13)
 Z, calculated density (g cm⁻³): 4, 1.195
 F(000): 1128
 Crystal size (mm): 0.07 x 0.07 x 0.20

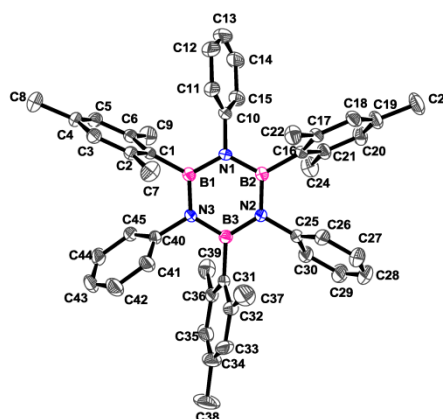
Data Collection

Radiation: 1.54184 Å
 Θ range for data collection (°): 4.0, 62.1
 Total, Unique data, R(int): 5931, 3670, 0.033
 Observed data: 3041

Refinement

SHELXS-86 program
 Refinement method: F^2 using SHELXS-97 program
 Nref, Npar: 3670, 379
 R, wR2, S: 0.0467, 0.1229, 1.00
 $w = 1/[\sigma^2(F_o^2) + (0.0769P)^2]$ where
 $P = (F_o^2 + 2F_c^2)/3$
 Min. and Max. Resd. Dens. (electron Å⁻³): -0.24, 0.16

X-Ray Analysis of 173



Crystal Data

Identification code: **173**
 Empirical formula: $C_{45}H_{48}B_3N_3$
 Formula weight: 663.29
 Temperature (°K): 293
 Crystal system, space group: Monoclinic, P2₁/c
 Unit cell dimension a, b, c (Å):
 8.256(1), 38.855(4), 14.1685(18)
 Angle α , β , γ (°):
 90, 119.191(7), 90
 Volume (Å³): 3967.8(9)
 Z, calculated density (g cm⁻³): 4, 1.110
 F(000): 1416
 Crystal size (mm): 0.12 x 0.14 x 0.37

Data Collection

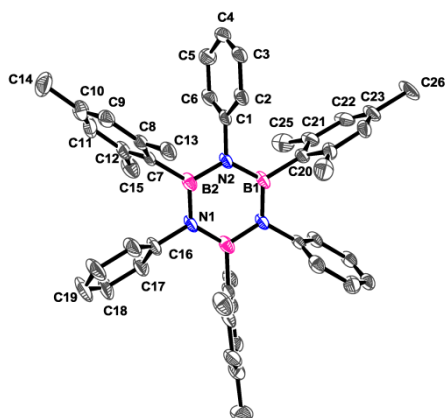
Radiation: 0.71073 Å
 Θ range for data collection (°): 3.2, 33.0
 Total, Unique data, R(int): 32464, 13517, 0.066
 Observed data: 3962

Refinement

SHELXS-86 program
 Refinement method: F^2 using SHELXS-97 program
 Nref, Npar: 13517, 469
 R, wR2, S: 0.0582, 0.1505, 0.76
 $w = 1/[\sigma^2(F_o^2) + (0.0631P)^2]$ where
 $P = (F_o^2 + 2F_c^2)/3$
 Min. and Max. Resd. Dens. (electron Å⁻³): -0.17, 0.18

Appendix I-Crystal Structures

X-Ray Analysis of 173



Crystal Data

Identification code: **173**
 Empirical formula: $C_{45}H_{48}B_3N_3$
 Formula weight: 663.29
 Temperature (°K): 293
 Crystal system, space group: Trigonal, $R\bar{3}c$
 Unit cell dimension a, b, c (Å):
 20.9058(6) 20.9058(6) 60.951(3)
 Angle α, β, γ (°):
 90 90 120
 Volume (Å³): 23069.9(15)
 Z, calculated density (g cm⁻³): 18, 0.859
 F(000): 6372
 Crystal size (mm): 0.02 x 0.13 x 0.20

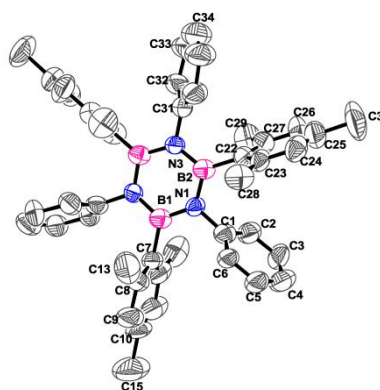
Data Collection

Radiation: 0.71073 Å
 Θ range for data collection (°): 3.4, 28.1
 Total, Unique data, R(int): 55976, 5994, 0.090
 Observed data: 2708

Refinement

SHELXS-86 program
 Refinement method: F^2 using SHELXS-97 program
 Nref, Npar: 5994, 241
 R, wR2, S: 0.0582, 0.1505, 0.76
 $w = 1/[\sigma^2(F_o^2) + (0.0631P)^2]$ where
 $P = (F_o^2 + 2F_c^2)/3$
 Min. and Max. Resd. Dens. (electron Å⁻³): -0.22, 0.31

X-Ray Analysis of 173



Crystal Data

Identification code: **173**
 Empirical formula: $C_{45}H_{48}B_3N_3$
 Formula weight: 663.29
 Temperature (°K): 293
 Crystal system, space group: Trigonal, R32
 Unit cell dimension a, b, c (Å):
 21.2055(12) 21.2055(12) 31.176(4)
 Angle α, β, γ (°):
 90 90 120
 Volume (Å³): 12140.8(18)
 Z, calculated density (g cm⁻³): 9, 0.813
 F(000): 3159
 Crystal size (mm): 0.14 x 0.15 x 0.20

Data Collection

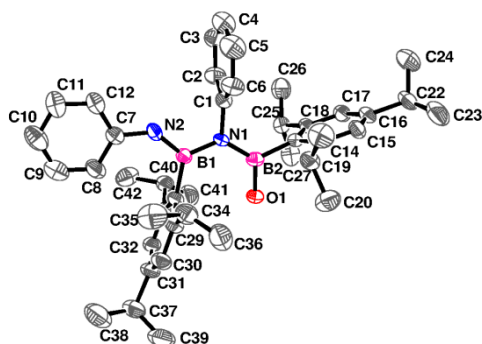
Radiation: 1.54184 Å
 Θ range for data collection (°): 2.8, 61.8
 Total, Unique data, R(int): 7608, 3996, 0.030
 Observed data: 1360

Refinement

SHELXS-86 program
 Refinement method: F^2 using SHELXS-97 program
 Nref, Npar: 3996, 199
 R, wR2, S: 0.0514, 0.1456, 0.68
 $w = 1/[\sigma^2(F_o^2) + (0.0631P)^2]$ where
 $P = (F_o^2 + 2F_c^2)/3$
 Min. and Max. Resd. Dens. (electron Å⁻³): -0.08, 0.10

Appendix I-Crystal Structures

X-Ray Analysis of 183



Crystal Data

Identification code: **183**
 Empirical formula: $C_{42}H_{58}B_2N_2O_2$
 Formula weight: 628.52
 Temperature (°K): 293
 Crystal system, space group: Triclinic, $\bar{P}1$
 Unit cell dimension a, b, c (Å):
 10.2850(4) 19.5420(8) 23.4478(10)
 Angle α , β , γ (°):
 105.064(4) 96.730(3) 98.352(3)
 Volume (Å³): 4442.9(3)
 Z, calculated density (g cm⁻³): 4, 0.940
 F(000): 1368
 Crystal size (mm): 0.07 x 0.25 x 0.30

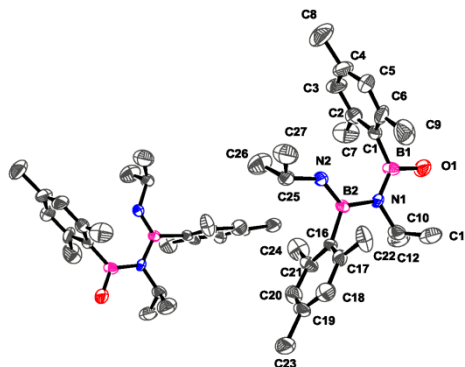
Data Collection

Radiation: 0.71073 Å
 Θ range for data collection (°): 3.3, 25.0
 Total, Unique data, R(int): 41530, 15675, 0.054
 Observed data: 5432

Refinement

SHELXS-86 program
 Refinement method: F^2 using SHELXS-97 program
 Nref, Npar: 15675, 483
 R, wR2, S: 0.1186, 0.3808, 1.00
 $w = 1/[\sigma^2(F_o^2) + (0.0631P)^2]$ where
 $P = (F_o^2 + 2F_c^2)/3$
 Min. and Max. Resd. Dens. (electron Å⁻³): -0.39, 0.54

X-Ray Analysis of 192



Crystal Data

Identification code: **192**
 Empirical formula: $C_{24}H_{38}B_2N_2O_2$
 Formula weight: 392.18
 Temperature (°K): 293
 Crystal system, space group: Monoclinic, $P2_1/c$
 Unit cell dimension a, b, c (Å):
 17.6292(18) 12.3662(12) 27.781(3)
 Angle α , β , γ (°):
 90 119.964(7) 90
 Volume (Å³): 5246.9(10)
 Z, calculated density (g cm⁻³): 8, 0.993
 F(000): 1712
 Crystal size (mm): 0.08 x 0.09 x 0.10

Data Collection

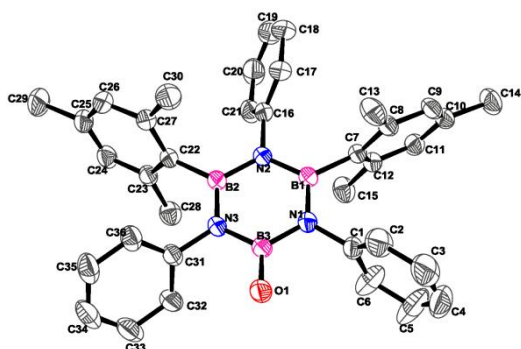
Radiation: 0.71073 Å
 Θ range for data collection (°): 3.1, 25.0
 Total, Unique data, R(int): 26083, 9023, 0.121
 Observed data: 1488

Refinement

SHELXS-86 program
 Refinement method: F^2 using SHELXS-97 program
 Nref, Npar: 9023, 369
 R, wR2, S: 0.1562, 0.4681, 0.84
 $w = 1/[\sigma^2(F_o^2) + (0.0631P)^2]$ where
 $P = (F_o^2 + 2F_c^2)/3$
 Min. and Max. Resd. Dens. (electron Å⁻³): -0.43, 0.40

Appendix I-Crystal Structures

X-Ray Analysis of 194



Crystal Data

Identification code: **194**
 Empirical formula: $C_{36}H_{38}B_3N_3O$
 Formula weight: 561.12
 Temperature (°K): 293
 Crystal system, space group: Monoclinic, $P2_1/c$
 Unit cell dimension a, b, c (Å):
 8.7087(1) 21.9290(4) 16.9669(3)
 Angle α, β, γ (°):
 90 94.153(2) 90
 Volume (Å³): 3231.71(9)
 Z, calculated density (g cm⁻³): 4, 1.153
 F(000): 1192
 Crystal size (mm): 0.15 x 0.15 x 0.20

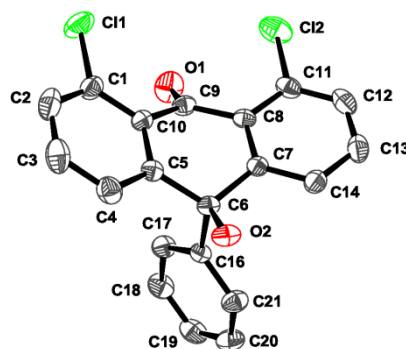
Data Collection

Radiation: 1.54184 Å
 Θ range for data collection (°): 3.3, 66.6
 Total, Unique data, R(int): 17425, 5695, 0.020
 Observed data: 4625

Refinement

SHELXS-86 program
 Refinement method: F^2 using SHELXS-97 program
 Nref, Npar: 5695, 394
 R, wR2, S: 0.0477, 0.1561, 1.04
 $w = 1/[\sigma^2(F_o^2) + (0.0631P)^2]$ where
 $P = (F_o^2 + 2F_c^2)/3$
 Min. and Max. Resd. Dens. (electron Å⁻³): -0.21, 0.20

X-Ray Analysis of 244



Crystal Data

Identification code: **244**
 Empirical formula: $C_{20}H_{12}Cl_2O_2$
 Formula weight: 355.20
 Temperature (°K): 293
 Crystal system, space group: Monoclinic, $P2_1/c$
 Unit cell dimension a, b, c (Å):
 13.4573(4) 15.2847(4) 16.0328(5)
 Angle α, β, γ (°):
 90 93.333(3) 90
 Volume (Å³): 3292.22(17)
 Z, calculated density (g cm⁻³): 8, 1.433
 F(000): 1456
 Crystal size (mm): 0.08 x 0.10 x 0.30

Data Collection

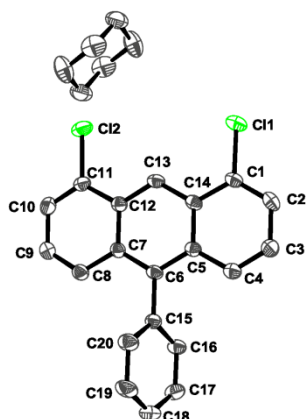
Radiation: 0.71073 Å
 Θ range for data collection (°): 3.3, 29.4
 Total, Unique data, R(int): 36679, 7989, 0.045
 Observed data: 5252

Refinement

SHELXS-86 program
 Refinement method: F^2 using SHELXS-97 program
 Nref, Npar: 7989, 441
 R, wR2, S: 0.0527, 0.1218, 1.02
 $w = 1/[\sigma^2(F_o^2) + (0.0431P)^2 + 1.1974P]$ where
 $P = (F_o^2 + 2F_c^2)/3$
 Min. and Max. Resd. Dens. (electron Å⁻³): -0.34, 0.24

Appendix I-Crystal Structures

X-Ray Analysis of 245



Crystal Data

Identification code: **245**
 Empirical formula: $C_{20}H_{12}Cl_2 \cdot C_6H_{12}$
 Formula weight: 365.30
 Temperature (°K): 293
 Crystal system, space group: Monoclinic, $P2_1/c$
 Unit cell dimension a, b, c (Å):
 13.4573(4) 15.2847(4) 16.0328(5)
 Angle α , β , γ (°):
 90 93.333(3) 90
 Volume (Å³): 3292.22(17)
 Z, calculated density (g cm⁻³): 8, 1.433
 F(000): 1456
 Crystal size (mm): 0.08 x 0.10 x 0.30

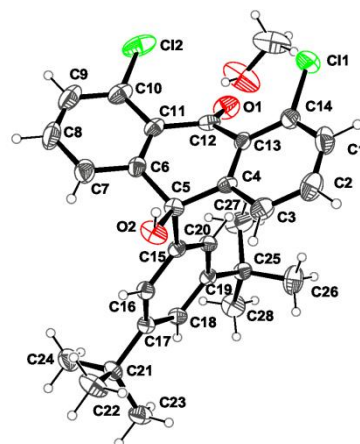
Data Collection

Radiation: 0.71073 Å
 Θ range for data collection (°): 3.3, 29.4
 Total, Unique data, R(int): 36679, 7989, 0.045
 Observed data: 5252

Refinement

SHELXS-86 program
 Refinement method: F^2 using SHELXS-97 program
 Nref, Npar: 7989, 441
 R, wR2, S: 0.0527, 0.1218, 1.02
 $w = 1/[\sigma^2(F_o^2) + (0.0431P)^2 + 1.1974P]$ where
 $P = (F_o^2 + 2F_c^2)/3$
 Min. and Max. Resd. Dens. (electron Å⁻³): -0.34, 0.24

X-Ray Analysis of 248



Crystal Data

Identification code: **248**
 Empirical formula: $C_{20}H_{12}Cl_2 \cdot C_6H_{12}$
 Formula weight: 365.30
 Temperature (°K): 293
 Crystal system, space group: Triclinic, $\bar{P}1$
 Unit cell dimension a, b, c (Å):
 9.2626(19) 11.044(3) 13.955(3)
 Angle α , β , γ (°):
 103.65(2) 104.360(19) 91.748(18)
 Volume (Å³): 1337.9(6)
 Z, calculated density (g cm⁻³): 2, 1.240
 F(000): 528
 Crystal size (mm): 0.09 x 0.09 x 0.30

Data Collection

Radiation: 0.71073 Å
 Θ range for data collection (°): 3.1, 25.0
 Total, Unique data, R(int): 10028, 4710, 0.085
 Observed data: 2409

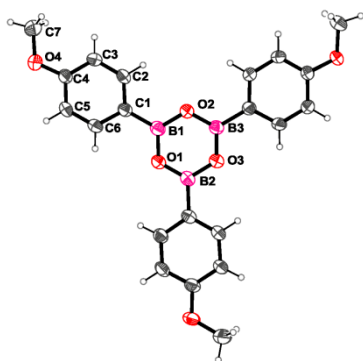
Refinement

SHELXS-86 program
 Refinement method: F^2 using SHELXS-97 program
 Nref, Npar: 4710, 309
 R, wR2, S: 0.0640, 0.1423, 0.98
 $w = 1/[\sigma^2(F_o^2) + (0.0358P)^2]$ where
 $P = (F_o^2 + 2F_c^2)/3$
 Min. and Max. Resd. Dens. (electron Å⁻³): -0.21, 0.19

Appendix I-Crystal Structures

Crystal structures of boroxines

X-Ray Analysis of 4-methoxyphenylboroxine



Crystal Data

Identification code: **264**
Empirical formula: $C_{21}H_{21}B_3O_6$
Formula weight: 401.81
Temperature (°K): 293
Crystal system, space group: Monoclinic, $P2_1/c$
Unit cell dimension a, b, c (Å):
9.0803(4) 14.0659(5) 17.1586(11)
Angle α , β , γ (°):
90 106.676(5) 90
Volume (Å³): 2099.37(19)
Z, calculated density (g cm⁻³): 4, 1.271
F(000): 840
Crystal size (mm): 0.02 x 0.20 x 0.36

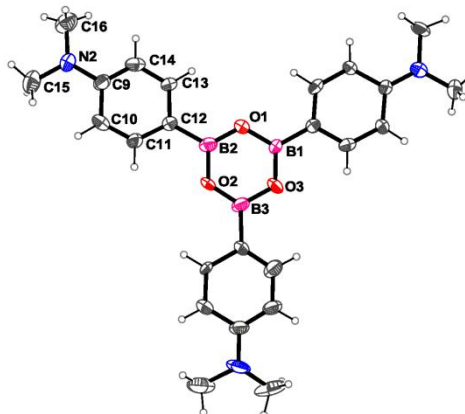
Data Collection

Radiation: 0.71073 Å
 Θ range for data collection (°): 3.2, 25.0
Total, Unique data, R(int): 9743, 3703, 0.034
Observed data: 2352

Refinement

SHELXS-86 program
Refinement method: F^2 using SHELXS-97 program
Nref, Npar: 3703, 274
R, wR2, S: 0.0747, 0.2246, 1.07
 $w = 1/[\sigma^2(F_o^2) + (0.1083P)^2 + 0.5303P]$ where
 $P = (F_o^2 + 2F_c^2)/3$
Min. and Max. Resd. Dens. (electron Å⁻³): -0.16, 0.44

X-Ray Analysis of 4-dimethylaminophenylboroxine



Crystal Data

Empirical formula: $C_{24}H_{30}B_3N_3O_3$
Formula weight: 440.94
Temperature (°K): 293
Crystal system, space group: Monoclinic, $P2_1/m$
Unit cell dimension a, b, c (Å):
6.5459(9) 24.599(3) 7.6627(14)
Angle α , β , γ (°):
90 97.335(15) 90
Volume (Å³): 1223.8(3)
Z, calculated density (g cm⁻³): 2, 1.197
F(000): 468
Crystal size (mm): 0.11 x 0.02 x 0.02

Data Collection

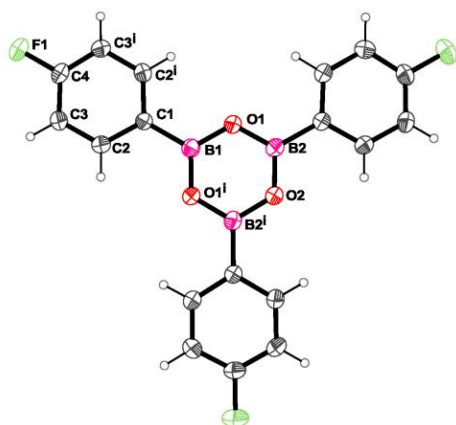
Radiation: 1.54184 Å
 Θ range for data collection (°): 3.6, 67.8
Total, Unique data, R(int): 5115, 2206, 0.162
Observed data: 1121

Refinement

SHELXS-86 program
Refinement method: F^2 using SHELXS-97 program
Nref, Npar: 2206, 158
R, wR2, S: 0.1561, 0.5172, 1.61
 $w = 1/[\sigma^2(F_o^2) + (0.2000P)^2]$ where
 $P = (F_o^2 + 2F_c^2)/3$
Min. and Max. Resd. Dens. (electron Å⁻³): -0.58, 0.34

Appendix I-Crystal Structures

X-Ray Analysis of 4-fluorophenylboroxine



Crystal Data

Empirical formula: $C_{18}H_{12}B_3F_3O_3$
 Formula weight: 365.71
 Temperature (°K): 293
 Crystal system, space group: Monoclinic, $P2_1/m$
 Unit cell dimension a, b, c (Å):
 3.9151(5) 20.916(4) 10.4868(15)
 Angle α , β , γ (°):
 90 97.858(12) 90
 Volume (Å³): 850.7(2)
 Z, calculated density (g cm⁻³): 2, 1.428
 F(000): 372
 Crystal size (mm): 0.06 x 0.06 x 0.36

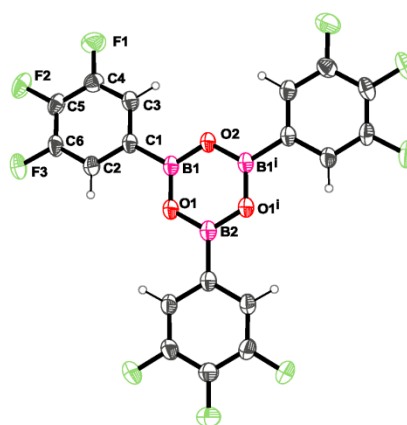
Data Collection

Radiation: 0.71073 Å
 Θ range for data collection (°): 3.5, 25.0
 Total, Unique data, R(int): 3645, 1550, 0.023
 Observed data: 1060

Refinement

SHELXS-86 program
 Refinement method: F^2 using SHELXS-97 program
 Nref, Npar: 1550, 130
 R, wR2, S: 0.0462, 0.1037, 1.05
 $w = 1/[\sigma^2(F_o^2) + (0.0409P)^2]$ where
 $P = (F_o^2 + 2F_c^2)/3$
 Min. and Max. Resd. Dens. (electron Å⁻³): -0.17, 0.11

X-Ray Analysis of 3,4,5-fluorophenylboroxine



Crystal Data

Empirical formula: $C_{18}H_6B_3F_9O_3$
 Formula weight: 473.66
 Temperature (°K): 293
 Crystal system, space group: Monoclinic, $C2/c$
 Unit cell dimension a, b, c (Å):
 12.852(1) 12.673(1) 12.921(1)
 Angle α , β , γ (°):
 90 119.025(10) 90
 Volume (Å³): 1840.2(3)
 Z, calculated density (g cm⁻³): 4, 1.710
 F(000): 936
 Crystal size (mm): 0.15 x 0.28 x 0.35

Data Collection

Radiation: 0.71073 Å
 Θ range for data collection (°): 3.2, 32.5
 Total, Unique data, R(int): 6202, 3046, 0.015
 Observed data: 1888

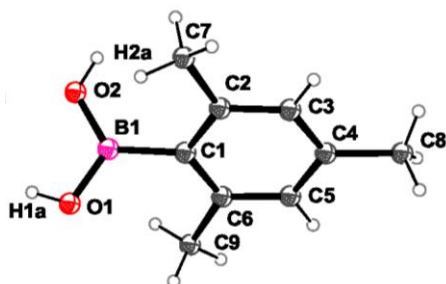
Refinement

SHELXS-86 program
 Refinement method: F^2 using SHELXS-97 program
 Nref, Npar: 3046, 152
 R, wR2, S: 0.0518, 0.1470, 1.06
 $w = 1/[\sigma^2(F_o^2) + (0.0562P)^2 + 0.3773P]$ where
 $P = (F_o^2 + 2F_c^2)/3$
 Min. and Max. Resd. Dens. (electron Å⁻³): -0.19, 0.26

Appendix I-Crystal Structures

Crystal structures of boronic acids

X-Ray Analysis of 224 (mesitylboronic acid)



Crystal Data

Identification code: **224**
Empirical formula: $C_9H_{13}BO_2$
Formula weight: 164.00
Temperature ($^{\circ}K$): 293
Crystal system, space group: Triclinic, $\bar{P}1$
Unit cell dimension a, b, c (\AA):
4.9491(4) 6.5516(4) 15.2409(12)
Angle α , β , γ ($^{\circ}$):
85.128(6) 82.152(6) 89.729(5)
Volume (\AA^3): 487.77(6)
Z, calculated density (g cm^{-3}): 2, 1.117
F(000): 176
Crystal size (mm): 0.06 x 0.20 x 0.40

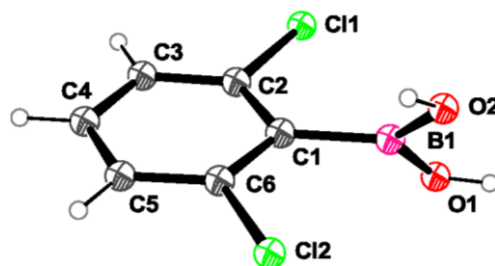
Data Collection

Radiation: 0.71073 \AA
 Θ range for data collection ($^{\circ}$): 3.1, 29.3
Total, Unique data, R(int): 4084, 2262, 0.030
Observed data: 1366

Refinement

SHELXS-86 program
Refinement method: F^2 using SHELXS-97 program
Nref, Npar: 2262, 112
R, wR2, S: 0.0658, 0.1872, 1.06
 $w = 1/[\sigma^2(F_o^2) + (0.0771P)^2 + 0.0410P]$ where
 $P = (F_o^2 + 2F_c^2)/3$
Min. and Max. Resd. Dens. (electron \AA^{-3}): -0.15, 0.19

X-Ray Analysis of 2,6-dichlorophenylboronic acid



Crystal Data

Empirical formula: $C_6H_5BCl_2O_2$
Formula weight: 190.81
Temperature ($^{\circ}K$): 293
Crystal system, space group: Monoclinic, $P2_1/c$
Unit cell dimension a, b, c (\AA):
14.4847(5) 12.6336(4) 13.9157(5)
Angle α , β , γ ($^{\circ}$):
90 90.889(3) 90
Volume (\AA^3): 2546.18(15)
Z, calculated density (g cm^{-3}): 12, 1.493
F(000): 1152
Crystal size (mm): 0.16 x 0.20 x 0.30

Data Collection

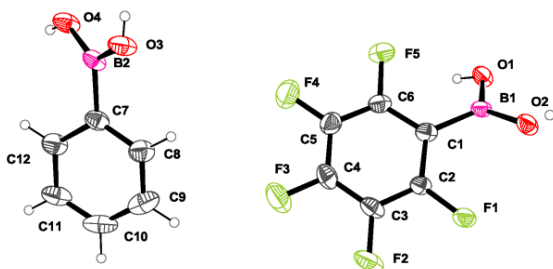
Radiation: 0.71073 \AA
 Θ range for data collection ($^{\circ}$): 3.2, 25.0
Total, Unique data, R(int): 12449, 4484, 0.026
Observed data: 3729

Refinement

SHELXS-86 program
Refinement method: F^2 using SHELXS-97 program
Nref, Npar: 4484, 298
R, wR2, S: 0.0562, 0.1567, 1.02
 $w = 1/[\sigma^2(F_o^2) + (0.0721P)^2 + 2.3137P]$ where
 $P = (F_o^2 + 2F_c^2)/3$
Min. and Max. Resd. Dens. (electron \AA^{-3}): -0.51, 0.56

Appendix I-Crystal Structures

X-Ray Analysis of pentafluorophenylboronic acid·phenylboronic acid cocrystal



Crystal Data

Empirical formula: $C_6H_2BF_5O_2 \cdot C_6H_7BO_2$
 Formula weight: 333.81
 Temperature (°K): 293
 Crystal system, space group: Monoclinic, $P2_1/c$
 Unit cell dimension a, b, c (Å):
 20.004(5) 7.352(5) 9.566(5)
 Angle α , β , γ (°):
 90 94.721(5) 90
 Volume (Å³): 1402.1(13)
 Z, calculated density (g cm⁻³): 4, 1.581
 F(000): 672
 Crystal size (mm): 0.03 x 0.33 x 0.37

Data Collection

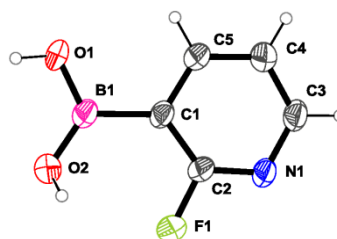
Radiation: 0.71073 Å
 Θ range for data collection (°): 3.4, 25.0
 Total, Unique data, R(int): 4084, 2262, 0.030
 Observed data: 1366

Refinement

SHELXS-86 program
 Refinement method: F^2 using SHELXS-97 program
 Nref, Npar: 2262, 112
 R, wR2, S: 0.0658, 0.1872, 1.06
 $w = 1/[\sigma^2(F_o^2) + (0.0771P)^2 + 0.0410P]$ where
 $P = (F_o^2 + 2F_c^2)/3$
 Min. and Max. Resd. Dens. (electron Å⁻³): -0.15, 0.19

Crystal structures of boronic acids in complexes

X-Ray Analysis of 2-fluoropyridine-3-boronic acid



Crystal Data

Empirical formula: $C_5H_5BFNO_2$
 Formula weight: 140.91
 Temperature (°K): 293
 Crystal system, space group: Monoclinic, $P2_1/c$
 Unit cell dimension a, b, c (Å):
 3.7591(14) 11.554(4) 14.469(4)
 Angle α , β , γ (°):
 90 101.47(3) 90
 Volume (Å³): 615.9(4)
 Z, calculated density (g cm⁻³): 4, 1.520
 F(000): 288
 Crystal size (mm): 0.4 x 0.04 x 0.04

Data Collection

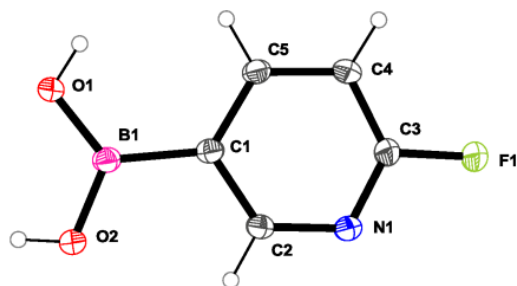
Radiation: 1.54184 Å
 Θ range for data collection (°): 4.9, 66.6
 Total, Unique data, R(int): 2028, 1085, 0.043
 Observed data: 676

Refinement

SHELXS-86 program
 Refinement method: F^2 using SHELXS-97 program
 Nref, Npar: 1085, 92
 R, wR2, S: 0.1510, 0.4759, 1.67
 $w = 1/[\sigma^2(F_o^2) + (0.2000P)^2]$ where
 $P = (F_o^2 + 2F_c^2)/3$
 Min. and Max. Resd. Dens. (electron Å⁻³): -0.34, 0.86

Appendix I-Crystal Structures

X-Ray Analysis of 4-fluoropyridine-3-boronic acid



Crystal Data

Empirical formula: $C_5H_5BFNO_2$
 Formula weight: 140.91
 Temperature (°K): 293
 Crystal system, space group: Monoclinic, $P2_1/c$
 Unit cell dimension a, b, c (Å):
 7.4576(2) 7.7607(2) 12.4337(3)
 Angle α , β , γ (°):
 90 119.790(2) 90
 Volume (Å³): 624.52(3)
 Z, calculated density (g cm⁻³): 4, 1.499
 F(000): 288
 Crystal size (mm): 0.08 x 0.08 x 0.22

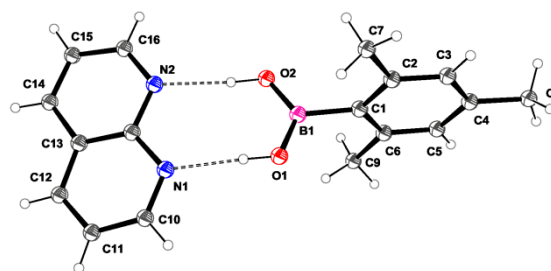
Data Collection

Radiation: 1.54184 Å
 Θ range for data collection (°): 6.8, 67.5
 Total, Unique data, R(int): 2312, 1108, 0.016
 Observed data: 1040

Refinement

SHELXS-86 program
 Refinement method: F^2 using SHELXS-97 program
 Nref, Npar: 1108, 91
 R, wR2, S: 0.0319, 0.0986, 1.13
 $w = 1/[\sigma^2(F_o^2) + (0.0555P)^2 + 0.1145P]$ where
 $P = (F_o^2 + 2F_c^2)/3$
 Min. and Max. Resd. Dens. (electron Å⁻³): -0.22, 0.26

X-Ray Analysis of Mesitylboronic acid 224 in complex with 1,8-naphthyridine



Crystal Data

Identification code: **223•224**
 Empirical formula: $C_9H_{13}BO_2 \cdot C_8H_6N_2$
 Formula weight: 294.15
 Temperature (°K): 293
 Crystal system, space group: Monoclinic, $P2_1/c$
 Unit cell dimension a, b, c (Å):
 7.6712(4) 19.9377(13) 10.8372(6)
 Angle α , β , γ (°):
 90 99.292(5) 90
 Volume (Å³): 1635.76(17)
 Z, calculated density (g cm⁻³): 4, 1.194
 F(000): 624
 Crystal size (mm): 0.07 x 0.10 x 0.20

Data Collection

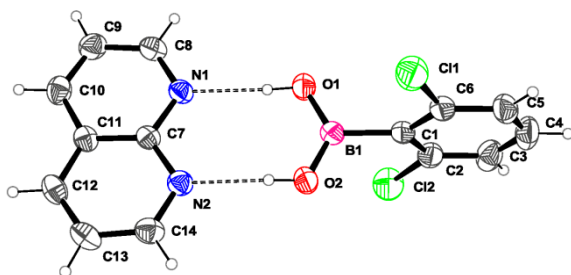
Radiation: 0.71073 Å
 Θ range for data collection (°): 3.4, 25.0
 Total, Unique data, R(int): 5806, 2861, 0.026
 Observed data: 1853

Refinement

SHELXS-86 program
 Refinement method: F^2 using SHELXS-97 program
 Nref, Npar: 2861, 210
 R, wR2, S: 0.0522, 0.1243, 1.04
 $w = 1/[\sigma^2(F_o^2) + (0.0452P)^2 + 0.1807P]$ where
 $P = (F_o^2 + 2F_c^2)/3$
 Min. and Max. Resd. Dens. (electron Å⁻³): -0.11, 0.13

Appendix I-Crystal Structures

X-Ray Analysis of 2,6-dichlorophenylboronic acid in complex with 1,8-naphthyridine



Crystal Data

Empirical formula: $C_6H_5BCl_2O_2 \cdot C_8H_6N_2$
 Formula weight: 320.96
 Temperature (°K): 293
 Crystal system, space group: Monoclinic, $P2_1/c$
 Unit cell dimension a, b, c (Å):
 13.0892(6) 13.9674(4) 8.3002(4)
 Angle α , β , γ (°):
 90 96.400(4) 90
 Volume (Å³): 1508.00(11)
 Z, calculated density (g cm⁻³): 4, 1.414
 F(000): 656
 Crystal size (mm): 0.07 x 0.28 x 0.33

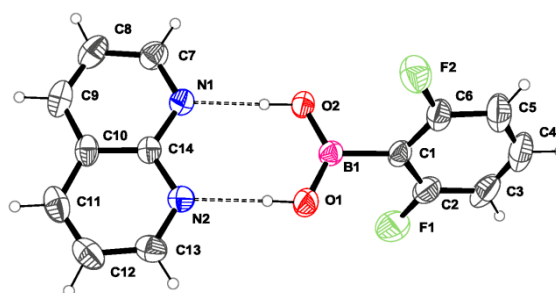
Data Collection

Radiation: 0.71073 Å
 Θ range for data collection (°): 3.3, 25.0
 Total, Unique data, R(int): 6937, 2659, 0.016
 Observed data: 2251

Refinement

SHELXS-86 program
 Refinement method: F^2 using SHELXS-97 program
 Nref, Npar: 2659, 198
 R, wR2, S: 0.0387, 0.0978, 1.04
 $w = 1/[\sigma^2(F_o^2) + (0.0383P)^2 + 0.4668P]$ where
 $P = (F_o^2 + 2F_c^2)/3$
 Min. and Max. Resd. Dens. (electron Å⁻³): -0.36, 0.25

X-Ray Analysis of 2,6-difluorophenylboronic acid in complex with 1,8-naphthyridine



Crystal Data

Identification code: **223-259**
 Empirical formula: $C_6H_5BF_2O_2 \cdot C_8H_6N_2$
 Formula weight: 288.06
 Temperature (°K): 293
 Crystal system, space group: Monoclinic, $P2_1/c$
 Unit cell dimension a, b, c (Å):
 6.7753(3) 24.5789(11) 9.4800(6)
 Angle α , β , γ (°):
 90 117.015(4) 90
 Volume (Å³): 1406.44(14)
 Z, calculated density (g cm⁻³): 4, 1.360
 F(000): 592
 Crystal size (mm): 0.08 x 0.20 x 0.20

Data Collection

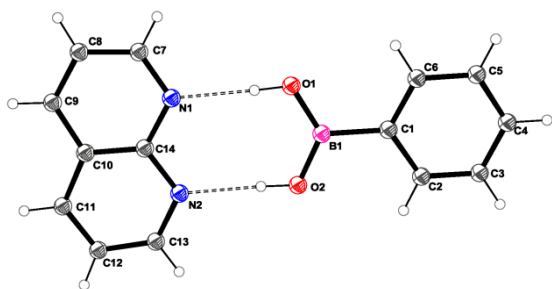
Radiation: 0.71073 Å
 Θ range for data collection (°): 3.3, 25.0
 Total, Unique data, R(int): 7142, 2482, 0.021
 Observed data: 1835

Refinement

SHELXS-86 program
 Refinement method: F^2 using SHELXS-97 program
 Nref, Npar: 2482, 198
 R, wR2, S: 0.0455, 0.1221, 1.05
 $w = 1/[\sigma^2(F_o^2) + (0.0558P)^2 + 0.1438P]$ where
 $P = (F_o^2 + 2F_c^2)/3$
 Min. and Max. Resd. Dens. (electron Å⁻³): -0.20, 0.10

Appendix I-Crystal Structures

X-Ray Analysis of phenylboronic acid in complex with 1,8-naphthyridine



Crystal Data

Empirical formula: $C_6H_7BO_2 \cdot C_8H_6N_2$
 Formula weight: 252.08
 Temperature ($^{\circ}K$): 293
 Crystal system, space group: Monoclinic, $P2_1/c$
 Unit cell dimension a, b, c (\AA):
 10.8694(3) 8.7104(2) 14.4710(3)
 Angle α , β , γ ($^{\circ}$):
 90 103.501(2) 90
 Volume (\AA^3): 1332.21(6)
 Z, calculated density (g cm^{-3}): 4, 1.257
 F(000): 528
 Crystal size (mm): 0.12 x 0.14 x 0.28

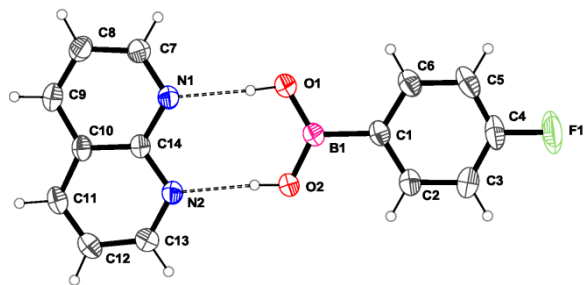
Data Collection

Radiation: 1.54184 \AA
 Θ range for data collection ($^{\circ}$): 6.0, 67.6
 Total, Unique data, R(int): 6704, 2399, 0.017
 Observed data: 2133

Refinement

SHELXS-86 program
 Refinement method: F^2 using SHELXS-97 program
 Nref, Npar: 2399, 181
 R, wR2, S: 0.0379, 0.1181, 1.04
 $w = 1/[\sigma^2(F_o^2) + (0.0673P)^2 + 0.0811P]$ where
 $P = (F_o^2 + 2F_c^2)/3$
 Min. and Max. Resd. Dens. (electron \AA^{-3}): -0.13, 0.12

X-Ray Analysis of 4-fluorophenylboronic acid in complex with 1,8-naphthyridine



Crystal Data

Empirical formula: $C_6H_6BFO_2 \cdot C_8H_6N_2$
 Formula weight: 270.07
 Temperature ($^{\circ}K$): 293
 Crystal system, space group: Monoclinic, $P2_1/c$
 Unit cell dimension a, b, c (\AA):
 12.354(2) 8.628(1) 14.2421(19)
 Angle α , β , γ ($^{\circ}$):
 90 116.121(10) 90
 Volume (\AA^3): 1363.0(3)
 Z, calculated density (g cm^{-3}): 4, 1.316
 F(000): 560
 Crystal size (mm): 0.13 x 0.17 x 0.40

Data Collection

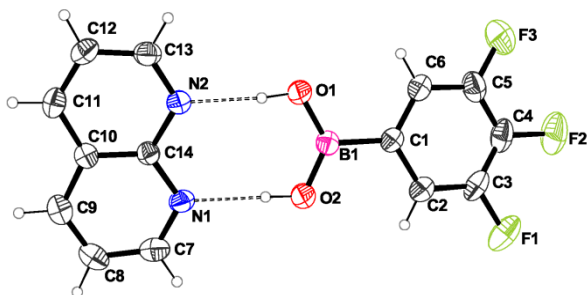
Radiation: 0.71073 \AA
 Θ range for data collection ($^{\circ}$): 3.7, 25.0
 Total, Unique data, R(int): 6777, 2404, 0.017
 Observed data: 1993

Refinement

SHELXS-86 program
 Refinement method: F^2 using SHELXS-97 program
 Nref, Npar: 2399, 181
 R, wR2, S: 0.0396, 0.1053, 1.04
 $w = 1/[\sigma^2(F_o^2) + (0.0483P)^2 + 0.1809P]$ where
 $P = (F_o^2 + 2F_c^2)/3$
 Min. and Max. Resd. Dens. (electron \AA^{-3}): -0.17, 0.10

Appendix I-Crystal Structures

X-Ray Analysis of 3,4,5-trifluorophenylboronic acid in complex with 1,8-naphthyridine



Crystal Data

Identification code: **223·260**
 Empirical formula: $C_6H_4BF_3O_2 \cdot C_8H_6N_2$
 Formula weight: 306.05
 Temperature (°K): 293
 Crystal system, space group: Monoclinic, $P2_1/c$
 Unit cell dimension a, b, c (Å):
 3.8701(4) 12.5606(14) 28.597(2)
 Angle α , β , γ (°):
 90 93.811(9) 90
 Volume (Å³): 1387.1(2)
 Z, calculated density (g cm⁻³): 4, 1.465
 F(000): 624
 Crystal size (mm): 0.05 x 0.06 x 0.40

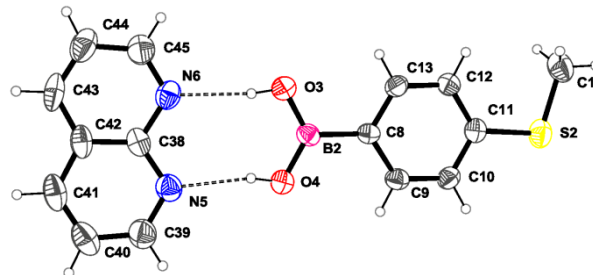
Data Collection

Radiation: 0.71073 Å
 Total, Unique data, R(int): 5650, 2623, 0.015
 Observed data: 2081

Refinement

SHELXS-86 program
 Refinement method: F^2 using SHELXS-97 program
 Nref, Npar: 2623, 199
 R, wR2, S: 0.0408, 0.1061, 1.01
 $w = 1/[\sigma^2(F_o^2) + (0.0478P)^2 + 0.1667P]$ where
 $P = (F_o^2 + 2F_c^2)/3$
 Max. and Av. Shift/Error: 0.00, 0.00
 Min. and Max. Resd. Dens. (electron Å⁻³): -0.14, 0.11

X-Ray Analysis of 4-thiomethylphenylboronic acid in complex with 1,8-naphthyridine



Crystal Data

Empirical formula: $C_7H_9BO_2S \cdot C_8H_6N_2$
 Formula weight: 298.16
 Temperature (°K): 293
 Crystal system, space group: Orthorhombic, Pbcn
 Unit cell dimension a, b, c (Å):
 24.7752(15) 13.4269(8) 27.4783(14)
 Angle α , β , γ (°):
 90 90 90
 Volume (Å³): 9140.8(9)
 Z, calculated density (g cm⁻³): 24, 1.300
 F(000): 3744
 Crystal size (mm): 0.04 x 0.20 x 0.42

Data Collection

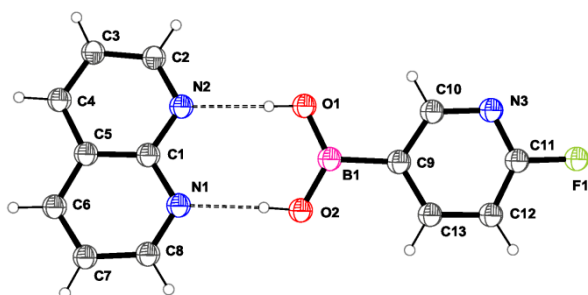
Radiation: 0.71073 Å
 Θ range for data collection (°): 3.2, 25.0
 Dataset: -27: 29 ; -15: 15 ; -29: 32
 Total, Unique data, R(int): 29942, 8051, 0.069
 Observed data: 4102

Refinement

SHELXS-86 program
 Refinement method: F^2 using SHELXS-97 program
 Nref, Npar: 8051, 568
 R, wR2, S: 0.0848, 0.1913, 1.04
 $w = 1/[\sigma^2(F_o^2) + (0.0505P)^2 + 4.7241P]$ where
 $P = (F_o^2 + 2F_c^2)/3$
 Min. and Max. Resd. Dens. (electron Å⁻³): -0.22, 0.39

Appendix I-Crystal Structures

X-Ray Analysis of 2-fluoropyridyl-4-boronic acid in complex with 1,8-naphthyridine



Crystal Data

Empirical formula: $C_5H_5BFNO_2 \cdot C_8H_6N_2$

Formula weight: 271.06

Temperature (°K): 293

Crystal system, space group: Monoclinic, $P2_1/n$

Unit cell dimension a, b, c (Å):

8.874(1) 12.358(2) 12.186(2)

Angle α , β , γ (°):

90 104.83(2) 90

Volume (Å³): 1291.9(4)

Z, calculated density (g cm⁻³): 4, 1.394

F(000): 560

Crystal size (mm): 0.15 x 0.20 x 0.25

Data Collection

Radiation: 1.54184 Å

Θ range for data collection (°): 5.2, 67.5

Total, Unique data, R(int): 5704, 2310, 0.016

Observed data: 2203

Refinement

SHELXS-86 program

Refinement method: F^2 using SHELXS-97 program

Nref, Npar: 2310, 190

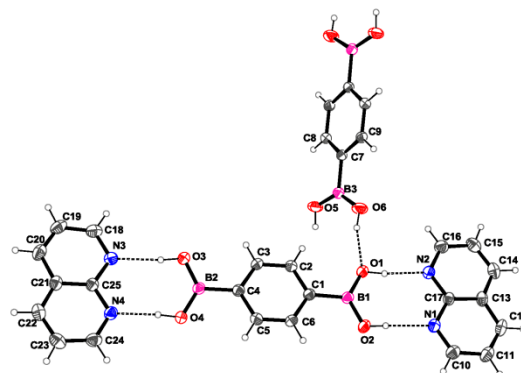
R, wR2, S: 0.0354, 0.1054, 1.03

$w = 1/[\sigma^2(F_o^2) + (0.0645P)^2 + 0.1176P]$ where

$P = (F_o^2 + 2F_c^2)/3$

Min. and Max. Resd. Dens. (electron Å⁻³): -0.13, 0.17

X-Ray Analysis of 1,4-phenylenediboronic acid in complex with 1,8-naphthyridine



Crystal Data

Identification code: **223-217**

Empirical formula: $3(C_6H_8B_2O_4) \cdot 4(C_8H_6N_2)$

Formula weight: 1017.82

Temperature (°K): 293

Crystal system, space group: Triclinic, $\bar{P}1$

Unit cell dimension a, b, c (Å):

10.1517(6) 11.1294(8) 11.3910(7)

Angle α , β , γ (°):

80.742(6) 86.043(5) 80.122(6)

Volume (Å³): 1250.25(14)

Z, calculated density (g cm⁻³): 1, 1.352

F(000): 530

Crystal size (mm): 0.05 x 0.10 x 0.40

Data Collection

Radiation: 0.71073 Å

Θ range for data collection (°): 3.3, 25.0

Total, Unique data, R(int): 10041, 4414, 0.021

Observed data: 23450

Refinement

SHELXS-86 program

Refinement method: F^2 using SHELXS-97 program

Nref, Npar: 4414, 375

R, wR2, S: 0.0418, 0.1184, 0.96

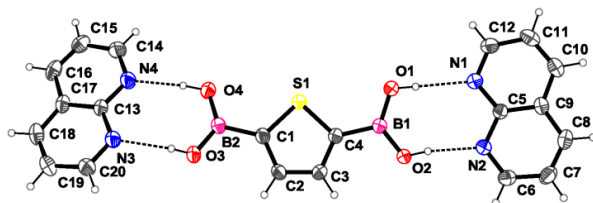
$w = 1/[\sigma^2(F_o^2) + (0.0699P)^2 + 0.0643P]$ where

$P = (F_o^2 + 2F_c^2)/3$

Min. and Max. Resd. Dens. (electron Å⁻³): -0.21, 0.16

Appendix I-Crystal Structures

X-Ray Analysis of 2,5-thiophenediboronic acid in complex with 1,8-naphthyridine



Crystal Data

Empirical formula: $C_4H_6B_2O_4S \cdot 2(C_8H_6N_2)$
 Formula weight: 432.06
 Temperature (°K): 293
 Crystal system, space group: Monoclinic, $P2_1/c$
 Unit cell dimension a, b, c (Å):
 14.9982(6) 10.8389(3) 13.0251(5)
 Angle α, β, γ (°):
 90 93.653(3) 90
 Volume (Å³): 2113.11(13)
 Z, calculated density (g cm⁻³): 4, 1.358
 F(000): 896
 Crystal size (mm): 0.09 x 0.10 x 0.21

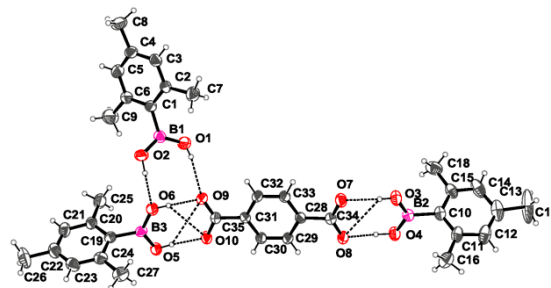
Data Collection

Radiation: 0.71073 Å
 Θ range for data collection (°): 3.3, 25.0
 Total, Unique data, R(int): 11224, 3721, 0.032
 Observed data: 2970

Refinement

SHELXS-86 program
 Refinement method: F^2 using SHELXS-97 program
 Nref, Npar: 3721, 296
 R, wR2, S: 0.0429, 0.1100, 1.06
 $w = 1/[\sigma^2(F_o^2) + (0.0503P)^2 + 0.2005P]$ where
 $P = (F_o^2 + 2F_c^2)/3$
 Min. and Max. Resd. Dens. (electron Å⁻³): -0.15, 0.19

X-Ray Analysis of mesitylboronic acid 224 in complex with tetrabutylammonium 1,4-dicarboxylate



Crystal Data

Identification code: **257-224**
 Empirical formula: $2(C_{16}H_{36}N) \cdot 3(C_9H_{13}BO_2) \cdot C_8H_4O_4$
 Formula weight: 1139.02
 Temperature (°K): 293
 Crystal system, space group: Monoclinic, $P2_1/c$
 Unit cell dimension a, b, c (Å):
 22.2500(7) 18.7204(5) 17.2638(4)
 Angle α, β, γ (°):
 90 100.782(3) 90
 Volume (Å³): 7063.9(3)
 Z, calculated density (g cm⁻³): 4, 1.071
 F(000): 2496
 Crystal size (mm): 0.10 x 0.20 x 0.25

Data Collection

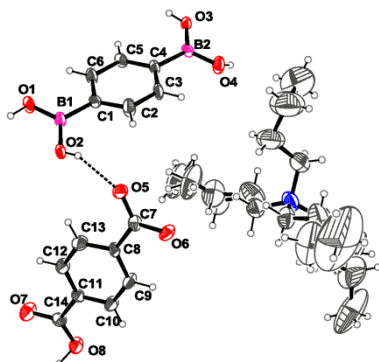
Radiation: 0.71073 Å
 Θ range for data collection (°): 3.3, 25.0
 Total, Unique data, R(int): 45159, 12474, 0.054
 Observed data: 7201

Refinement

SHELXS-86 program
 Refinement method: F^2 using SHELXS-97 program
 Nref, Npar: 12474, 780
 R, wR2, S: 0.1034, 0.2773, 1.06
 $w = 1/[\sigma^2(F_o^2) + (0.1047P)^2 + 5.8904P]$ where
 $P = (F_o^2 + 2F_c^2)/3$
 Min. and Max. Resd. Dens. (electron Å⁻³): -0.96, 0.83

Appendix I-Crystal Structures

X-Ray Analysis of 1,4-phenylenediboronic acid in complex with tetrabutylammonium 4-carboxybenzoate



Crystal Data

Empirical formula: $C_{16}H_{36}N \cdot 3(C_6H_8B_2O_4) \cdot C_8H_5O_4$

Formula weight: 572.31

Temperature (°K): 293

Crystal system, space group: Monoclinic, Cc

Unit cell dimension a, b, c (Å):

17.7745(11) 9.7874(4) 21.0288(13)

Angle α , β , γ (°):

90 113.726(7) 90

Volume (Å³): 3349.1(4)

Z, calculated density (g cm⁻³): 4, 1.135

F(000): 1236

Crystal size (mm): 0.03 x 0.20 x 0.32

Data Collection

Radiation: 0.71073 Å

Θ range for data collection (°): 3.5, 25.0

Total, Unique data, R(int): 6939, 4430, 0.034

Observed data: 3308

Refinement

SHELXS-86 program

Refinement method: F^2 using SHELXS-97 program

Nref, Npar: 4430, 384

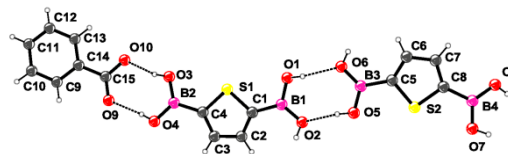
R, wR2, S: 0.0726, 0.2139, 1.07

$w = 1/[\sigma^2(F_o^2) + (0.1242P)^2 + 0.8831P]$ where

$P = (F_o^2 + 2F_c^2)/3$

Min. and Max. Resd. Dens. (electron Å⁻³): -0.25, 0.31

X-Ray Analysis of 2,5-thiophenediboronic acid in complex with tetrabutylammonium benzoate



Crystal Data

Empirical formula: $C_{16}H_{36}N \cdot 2(C_4H_6B_2O_4S) \cdot C_7H_5O_2$

Formula weight: 707.10

Temperature (°K): 293

Crystal system, space group: Orthorhombic, P2₁2₁2₁

Unit cell dimension a, b, c (Å):

10.4582(4) 18.1866(7) 20.9983(8)

Angle α , β , γ (°):

90 90 90

Volume (Å³): 3993.9(3)

Z, calculated density (g cm⁻³): 4, 1.176

F(000): 1512

Crystal size (mm): 0.03 x 0.20 x 0.25

Data Collection

Radiation: 0.71073 Å

Θ range for data collection (°): 3.5, 25.0

Total, Unique data, R(int): 14329, 6535, 0.053

Observed data: 4428

Refinement

SHELXS-86 program

Refinement method: F^2 using SHELXS-97 program

Nref, Npar: 6535, 434

R, wR2, S: 0.0757, 0.1817, 1.03

$w = 1/[\sigma^2(F_o^2) + (0.0781P)^2 + 1.6466P]$ where

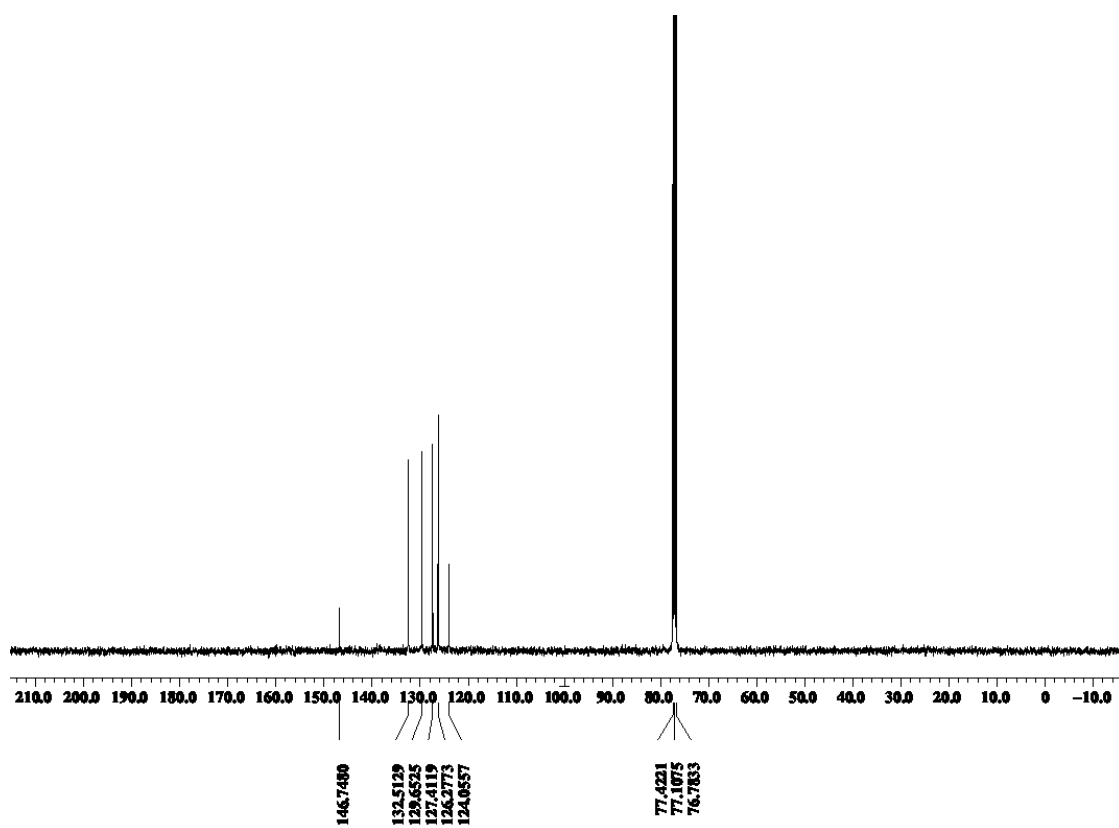
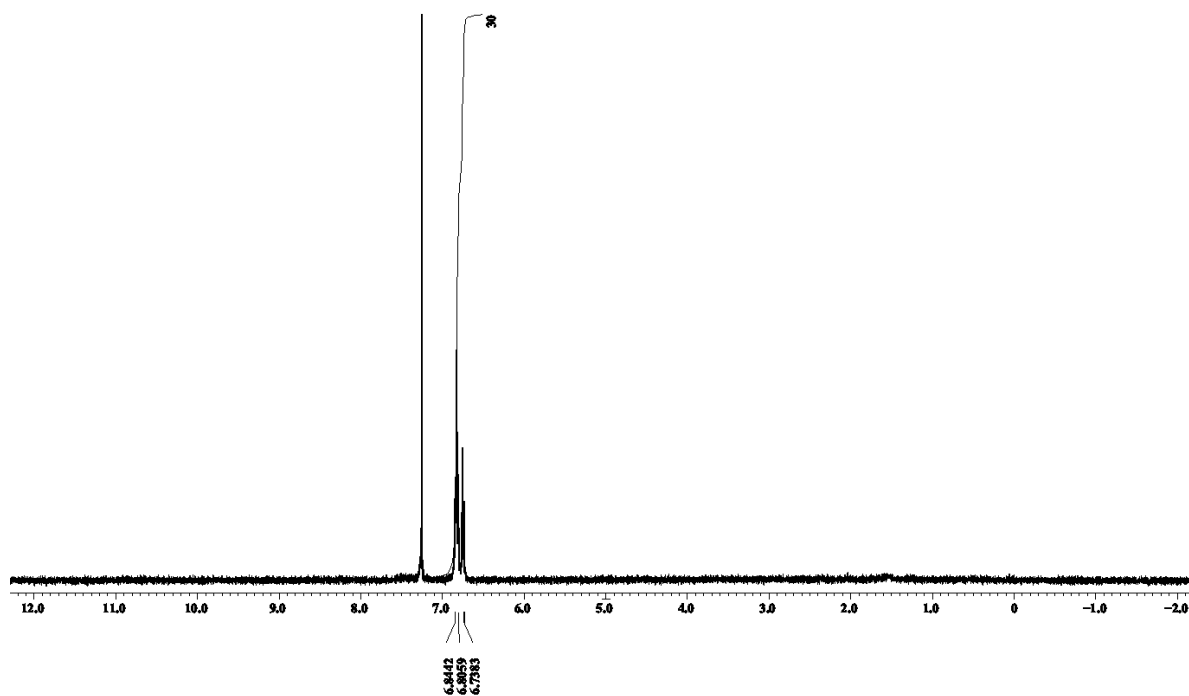
$P = (F_o^2 + 2F_c^2)/3$

Min. and Max. Resd. Dens. (electron Å⁻³): -0.23, 0.43

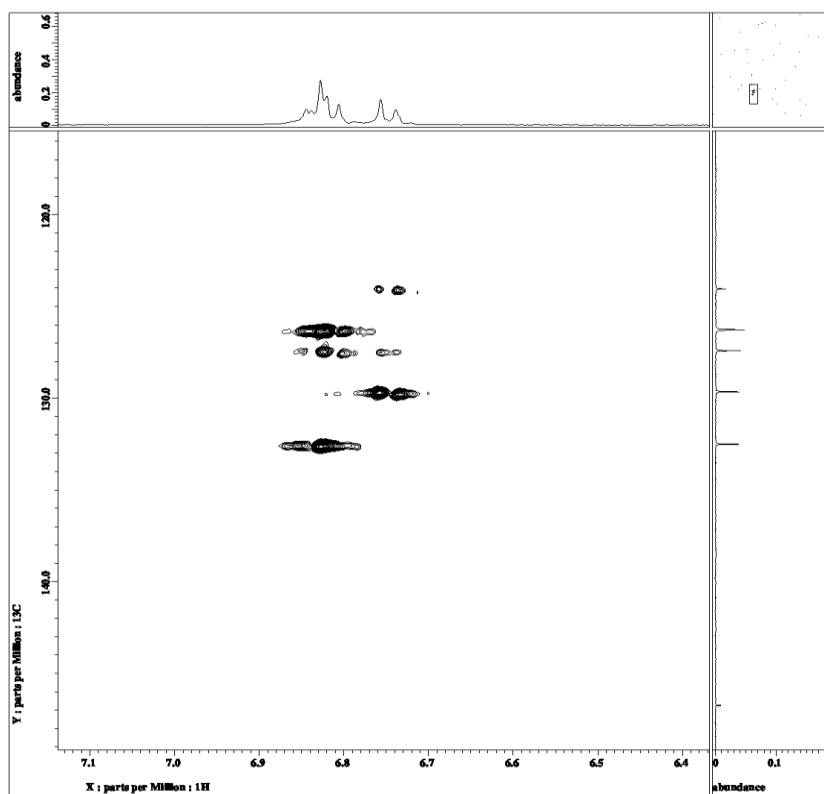
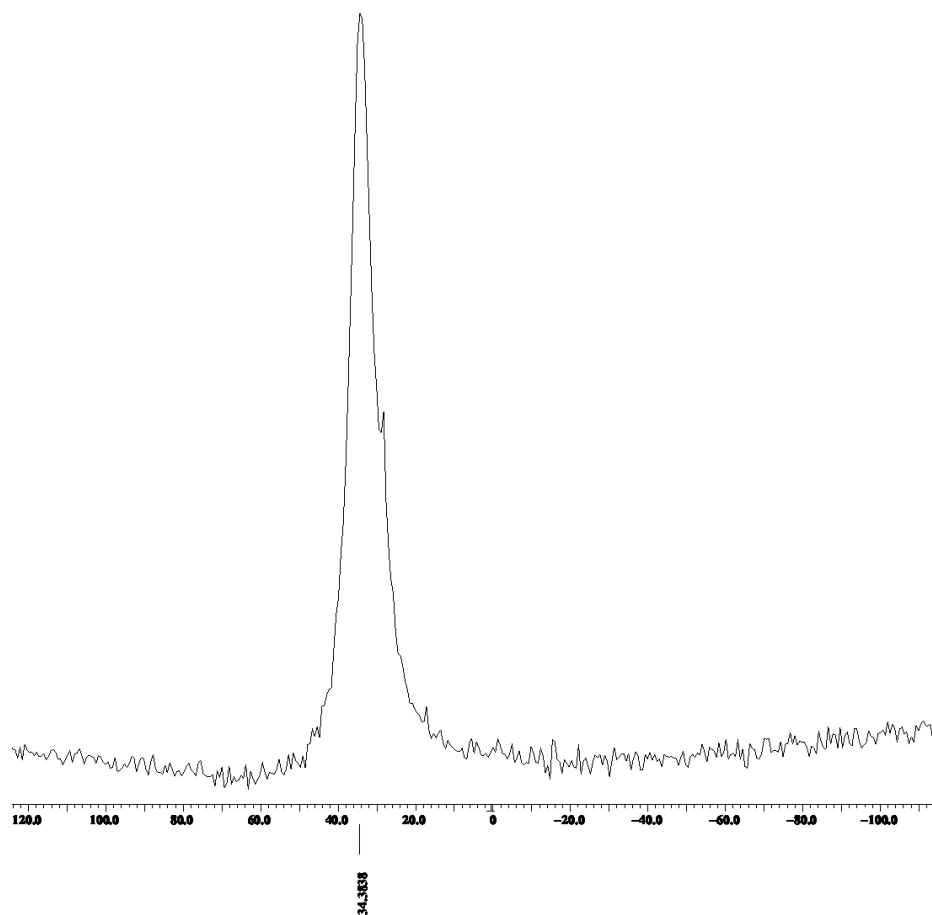
Appendix II-NMR Spectra

1. Borazine and borazene derivatives

Compound **169**: ^1H NMR, ^{13}C NMR, ^{11}B NMR and HMQC NMR in CDCl_3

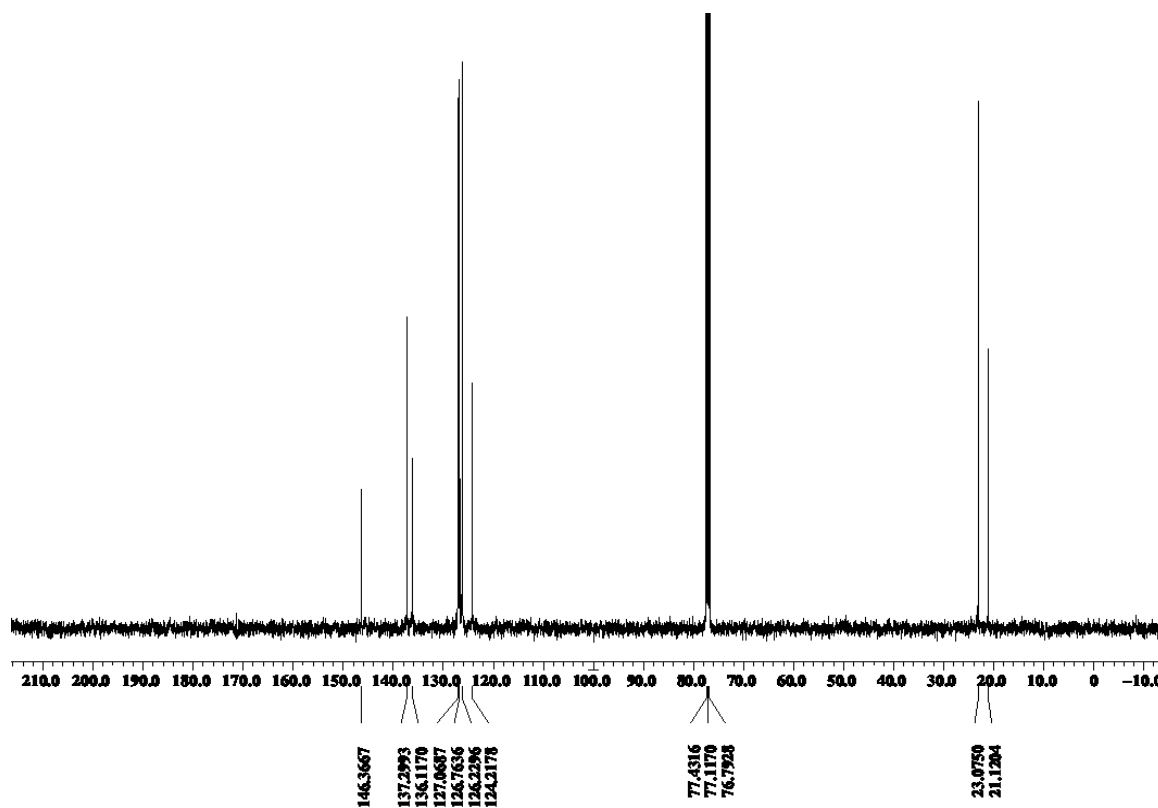
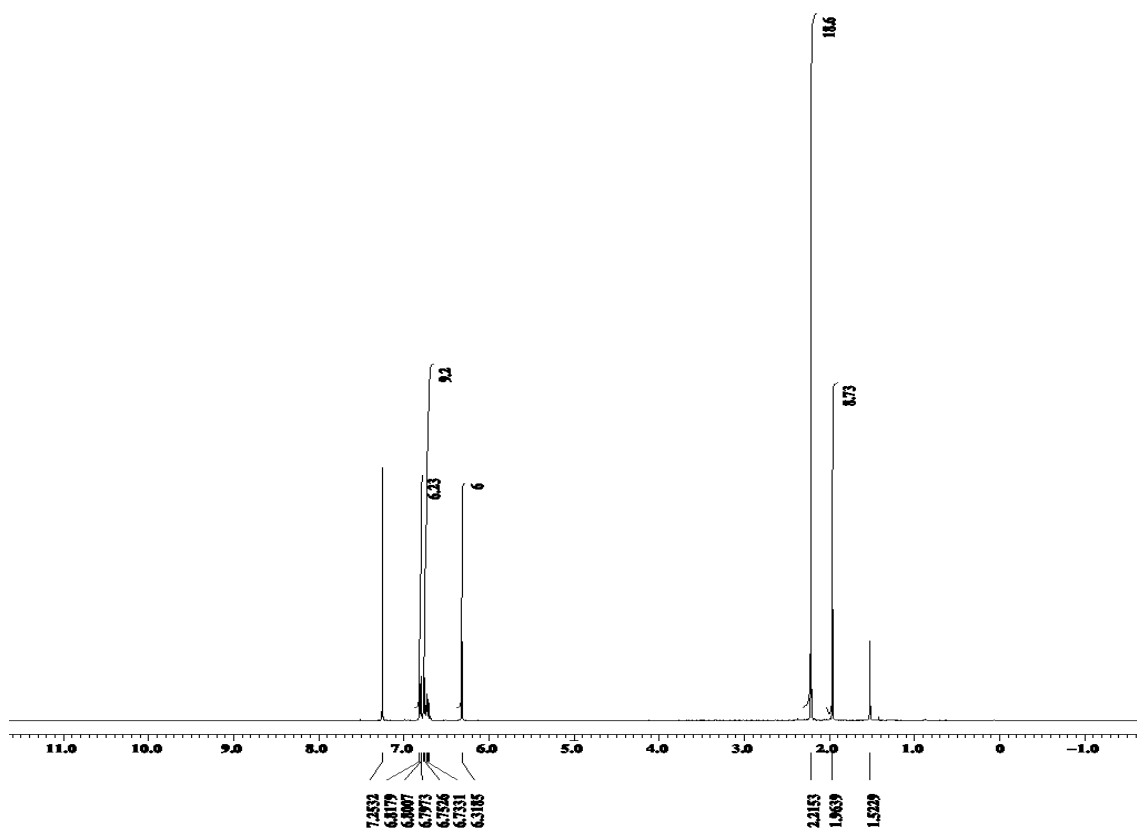


Appendix II-NMR Spectra

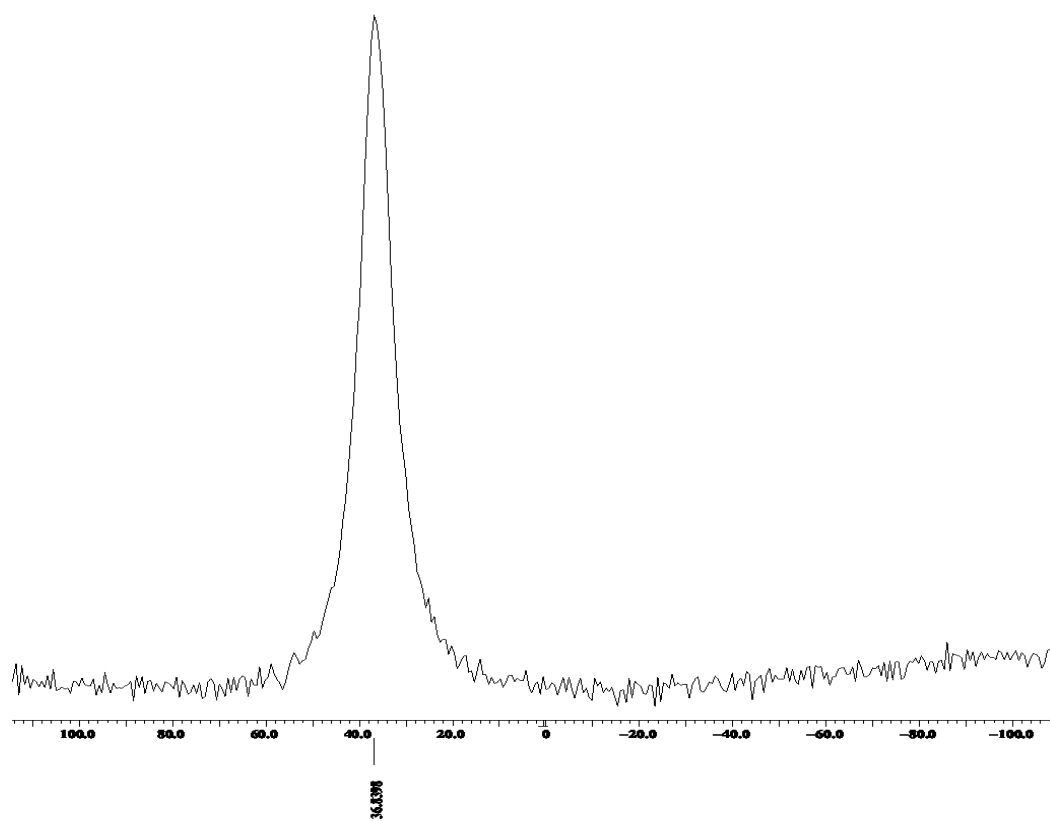


Appendix II-NMR Spectra

Compound 173: ^1H NMR, ^{13}C NMR, and ^{11}B NMR in CDCl_3

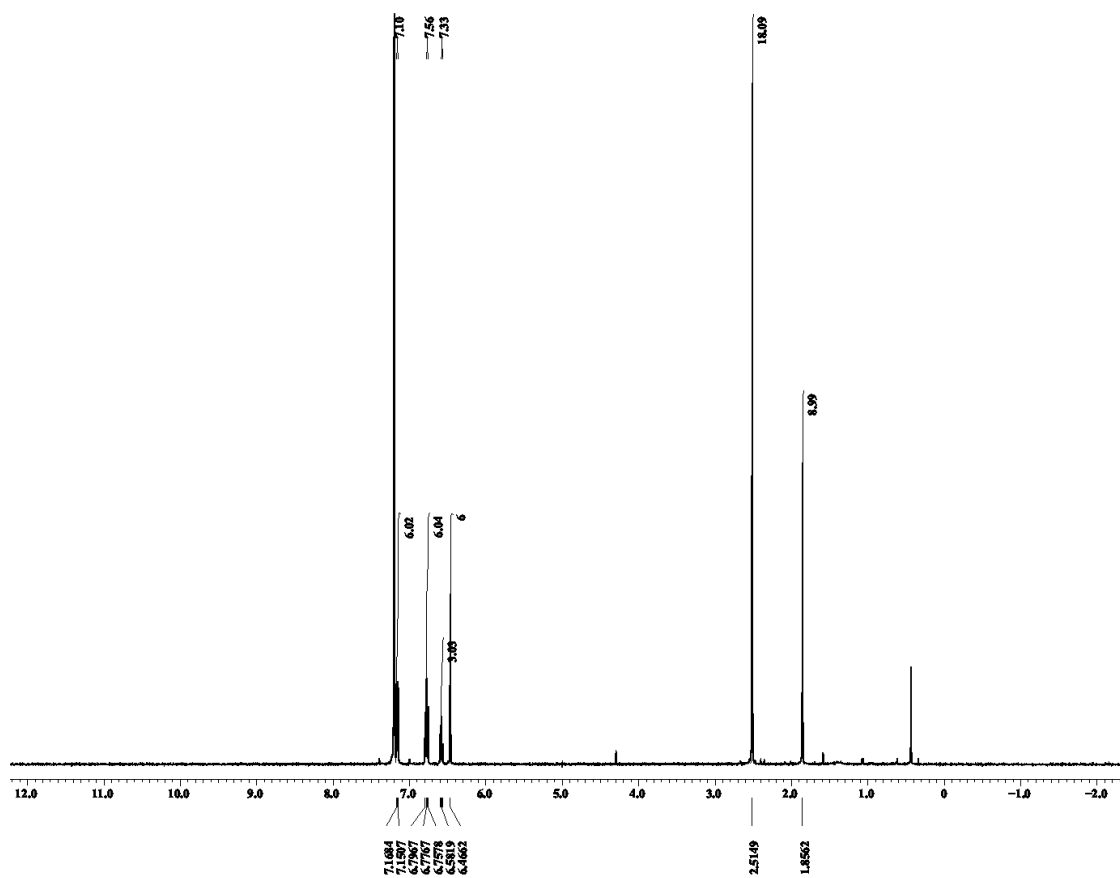


Appendix II-NMR Spectra



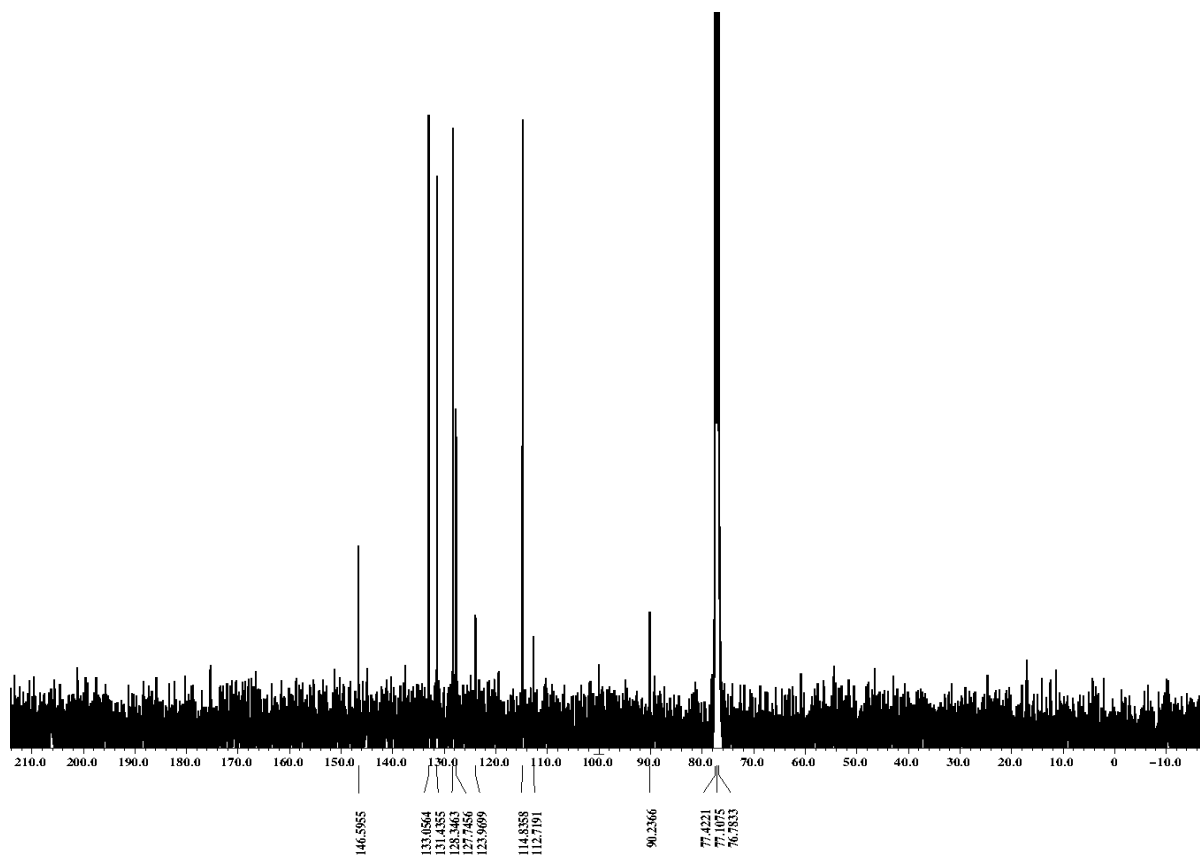
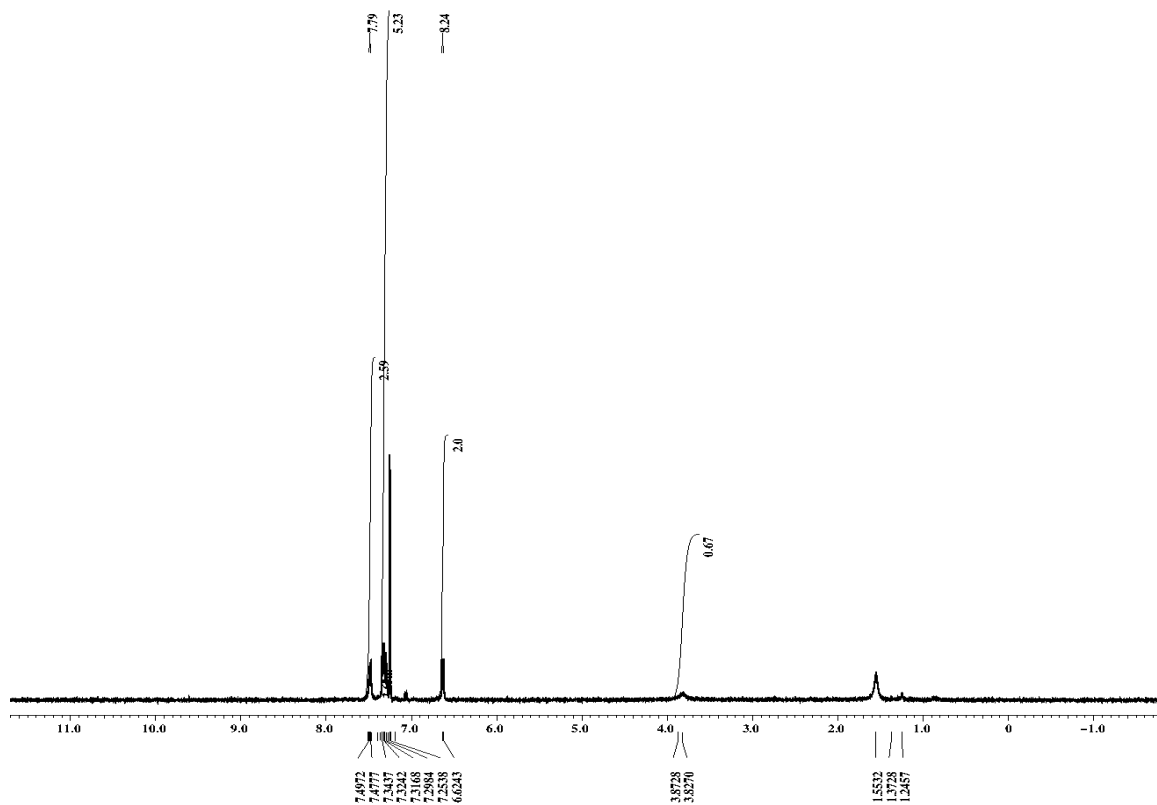
Appendix II-NMR Spectra

Compound **173**: ^1H NMR, ^{13}C NMR, and ^{11}B NMR in C_6D_6



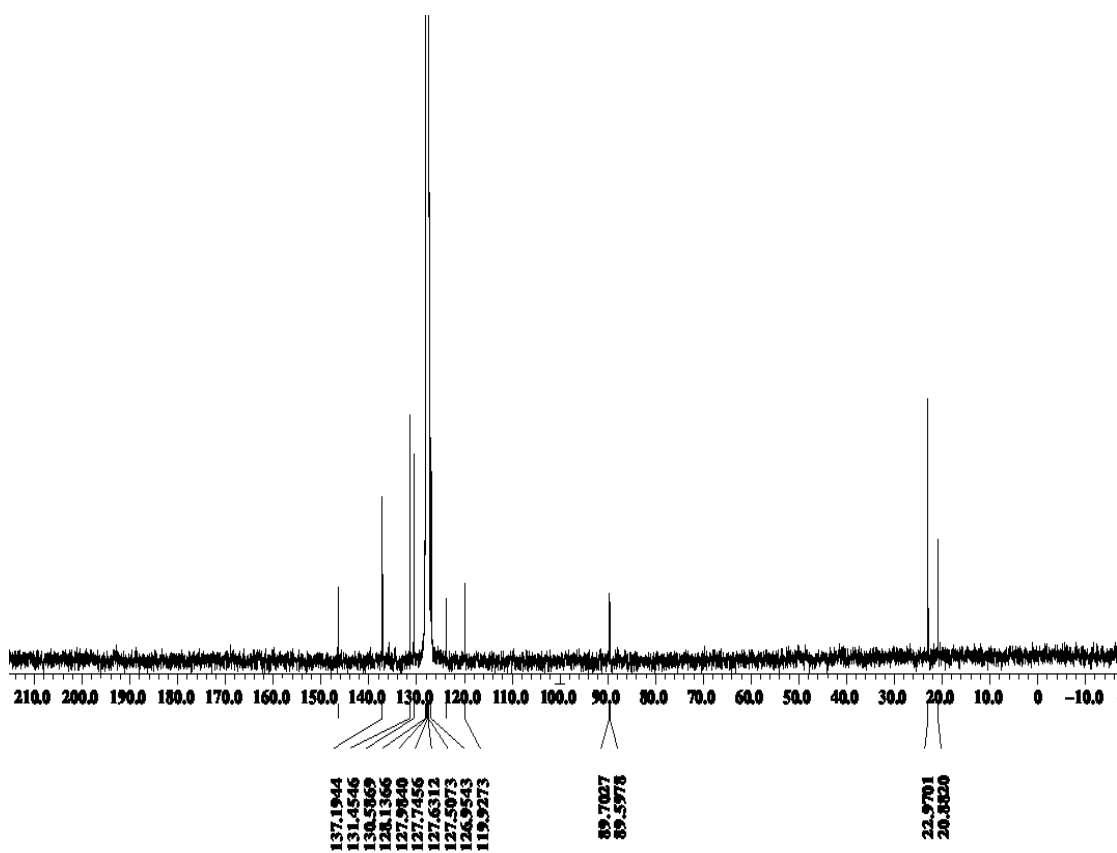
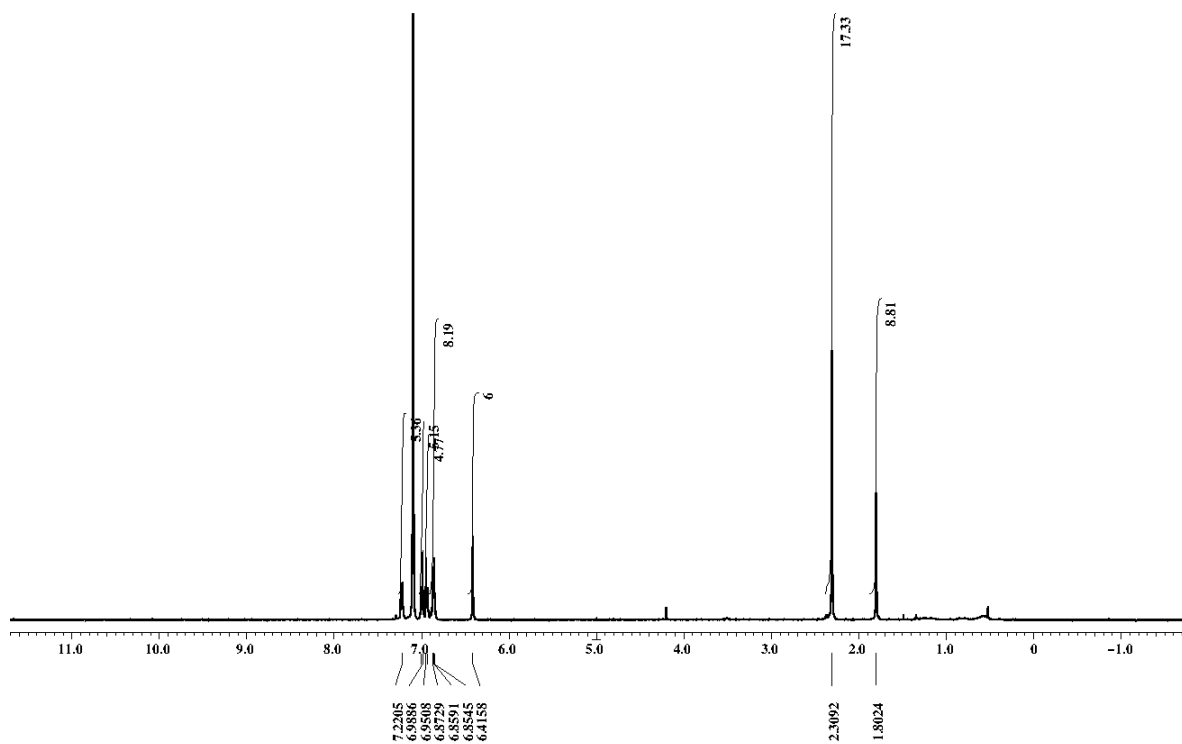
Appendix II-NMR Spectra

Compound 177: 4-ethynylaniline ^1H NMR and ^{13}C NMR, in CDCl_3

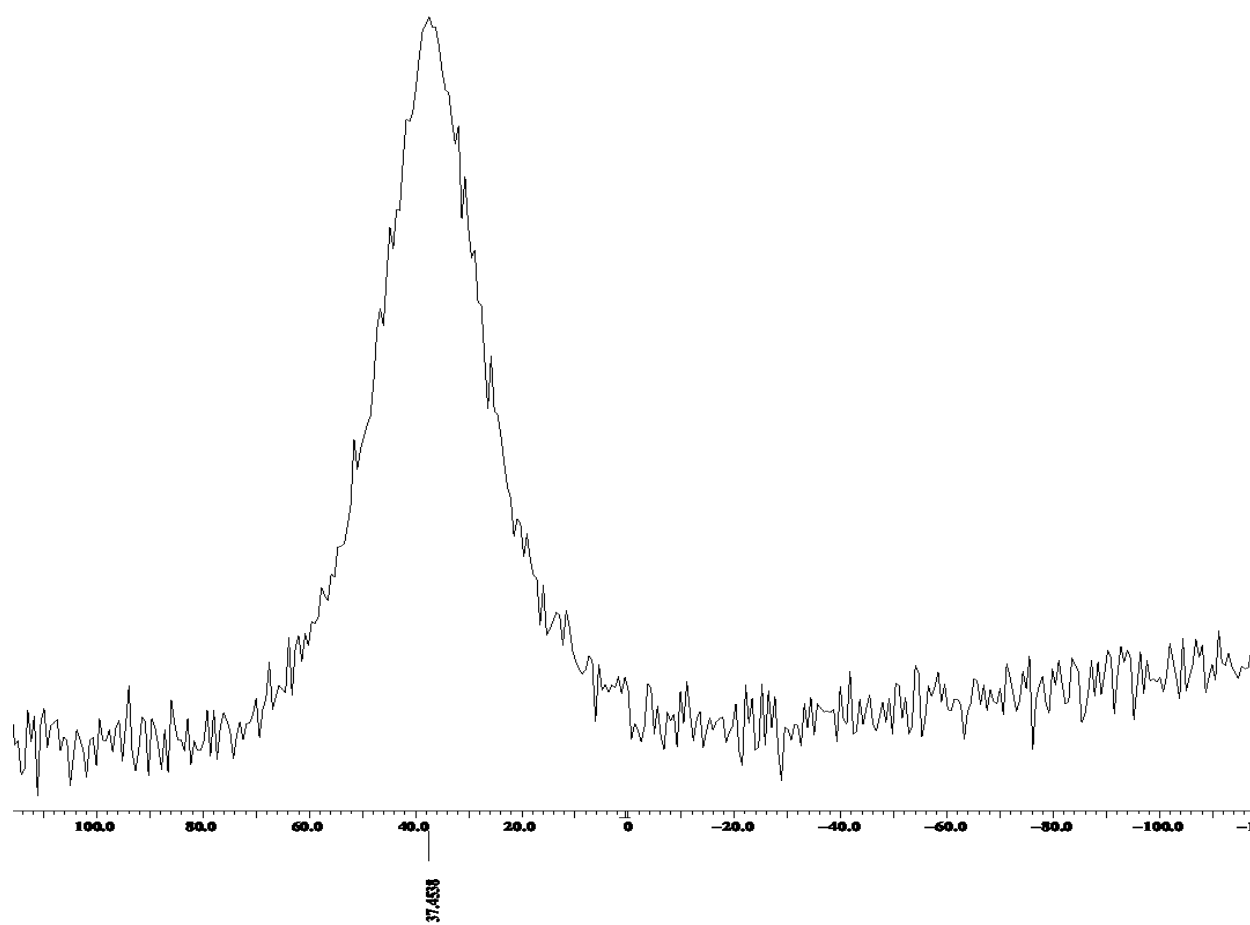


Appendix II-NMR Spectra

Compound **176**: ^1H NMR, ^{13}C NMR, and ^{11}B NMR in C_6D_6

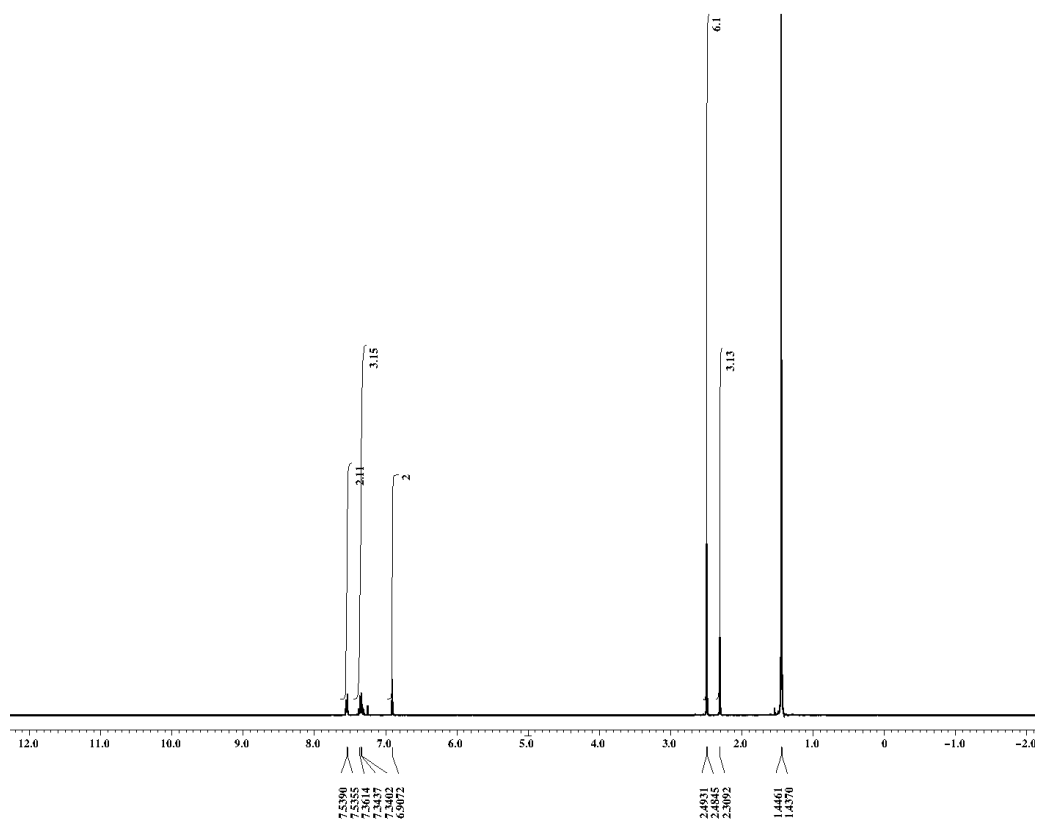


Appendix II-NMR Spectra



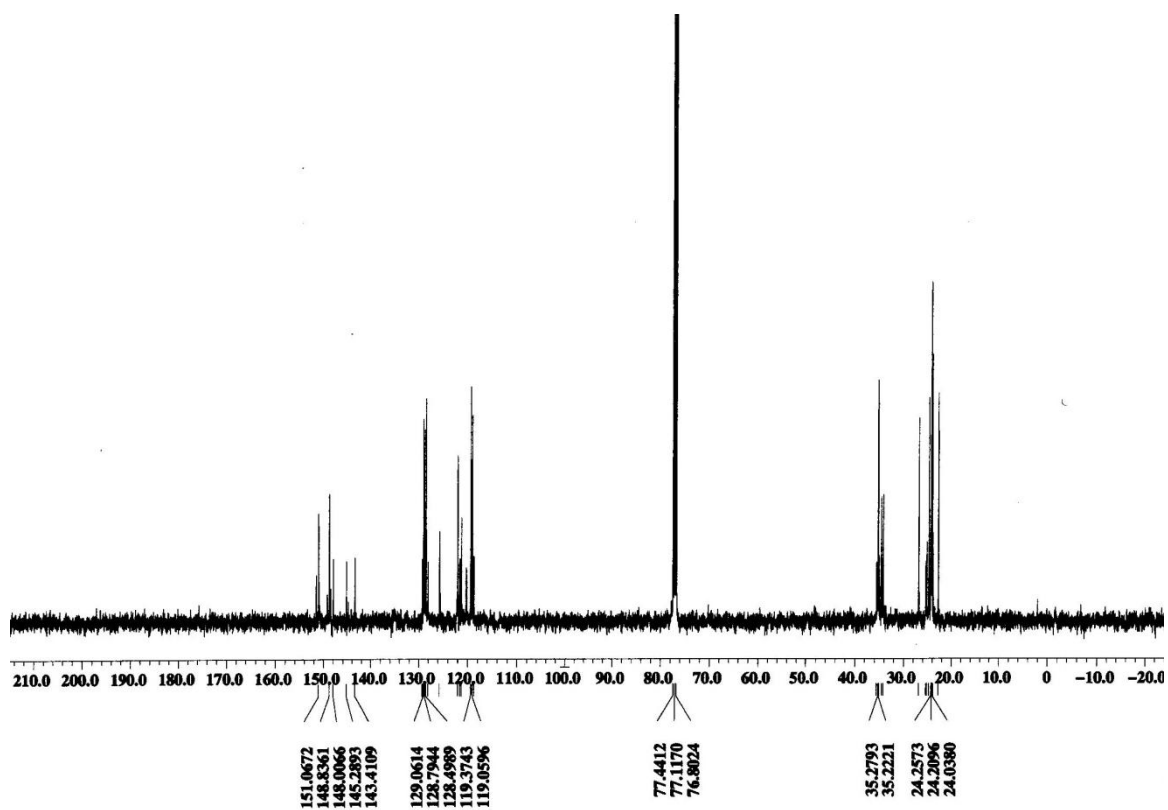
Appendix II-NMR Spectra

Compound **175**: ^1H NMR in CDCl_3

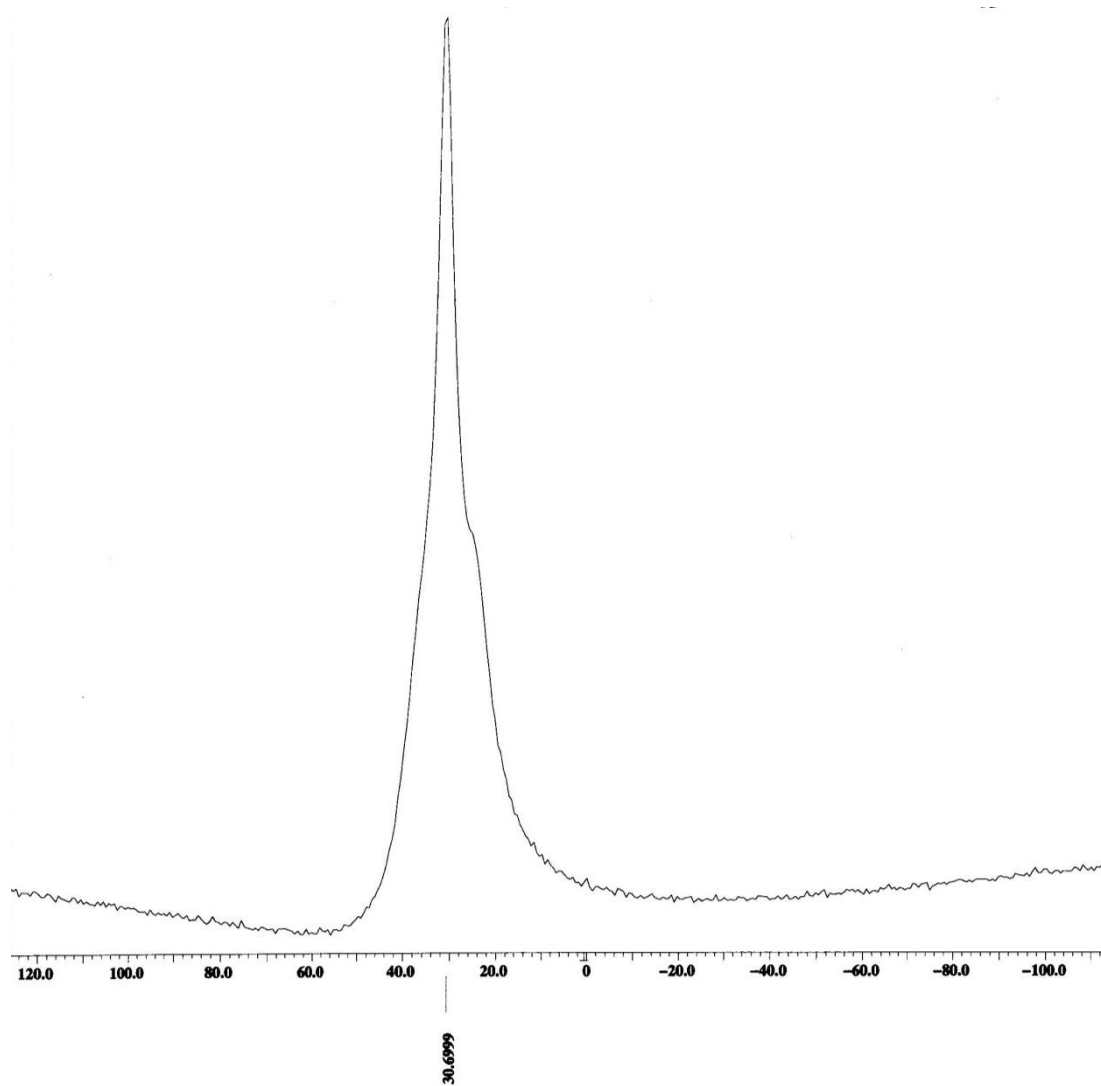


Appendix II-NMR Spectra

Compound **183**: ^1H NMR, ^{13}C NMR, and ^{11}B NMR in CDCl_3

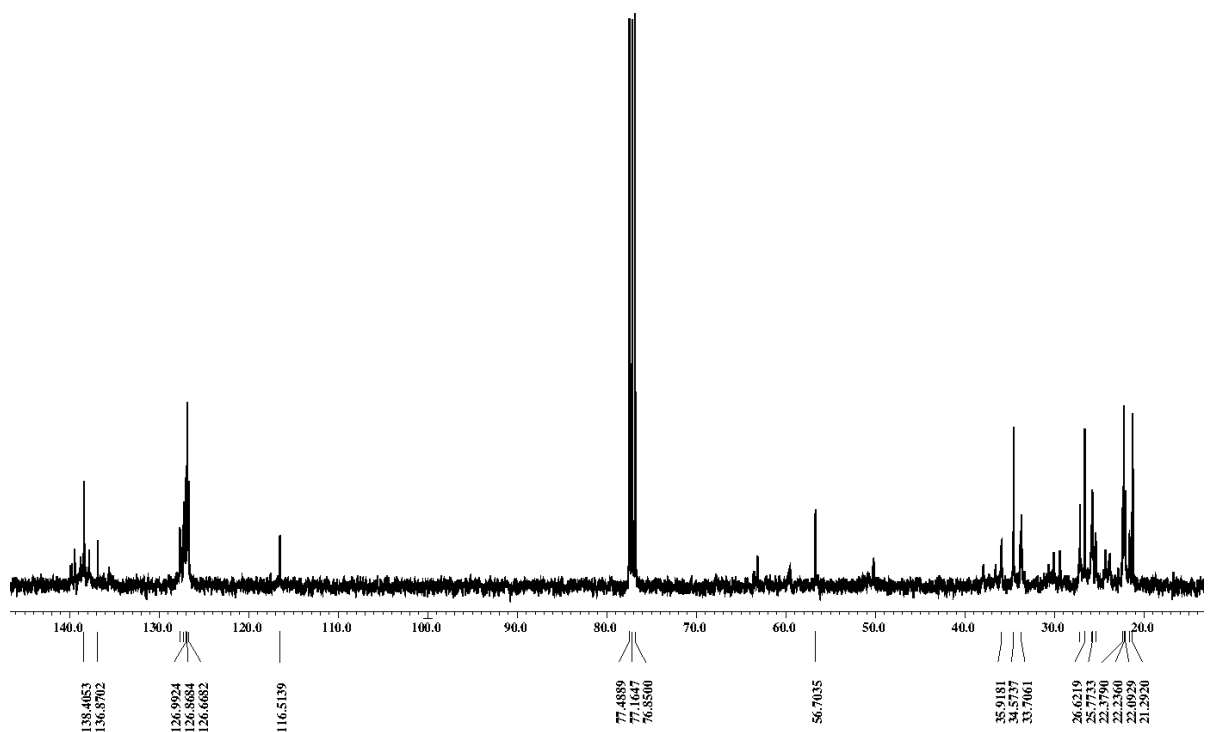
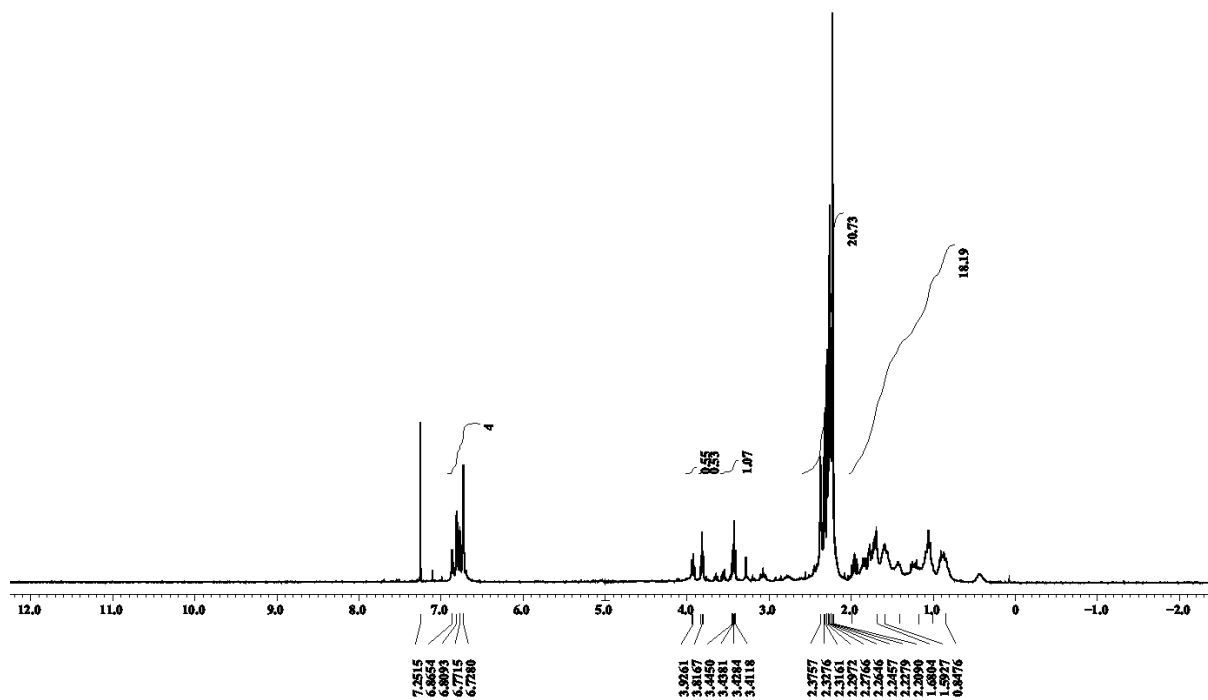


Appendix II-NMR Spectra

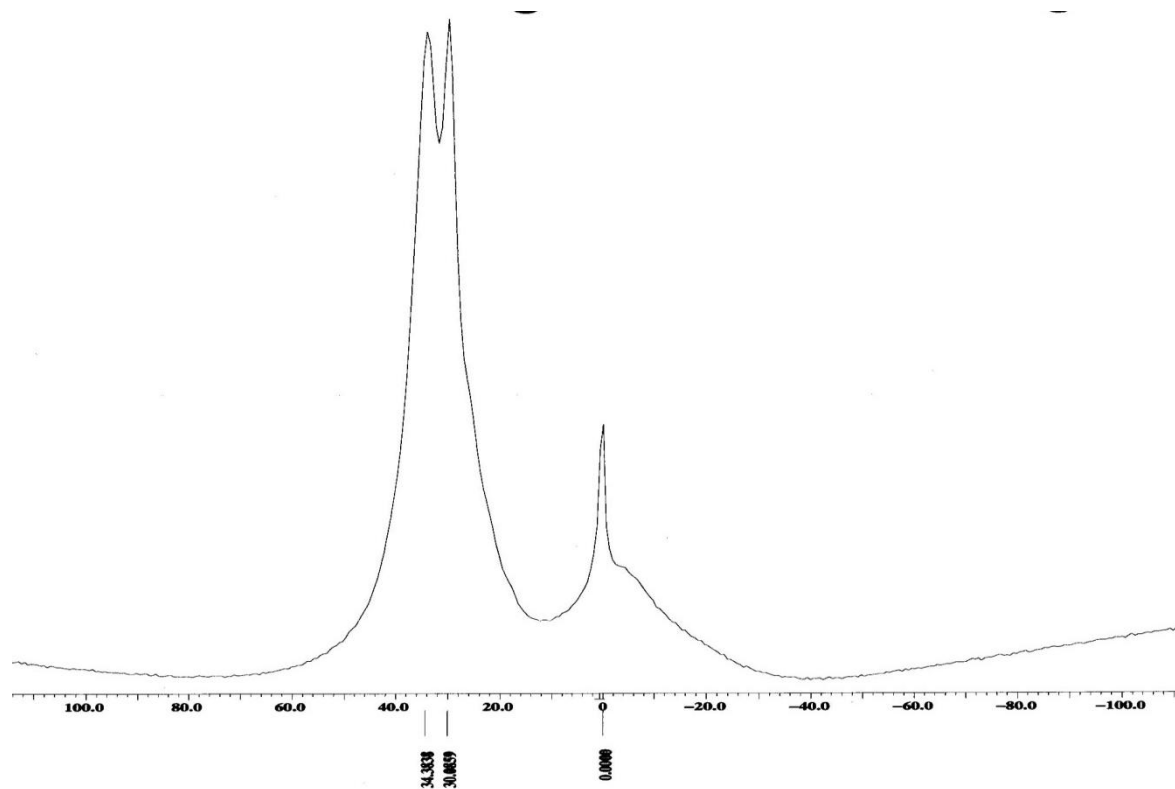


Appendix II-NMR Spectra

Compound **191**: ^1H NMR, ^{13}C NMR, and ^{11}B NMR in CDCl_3

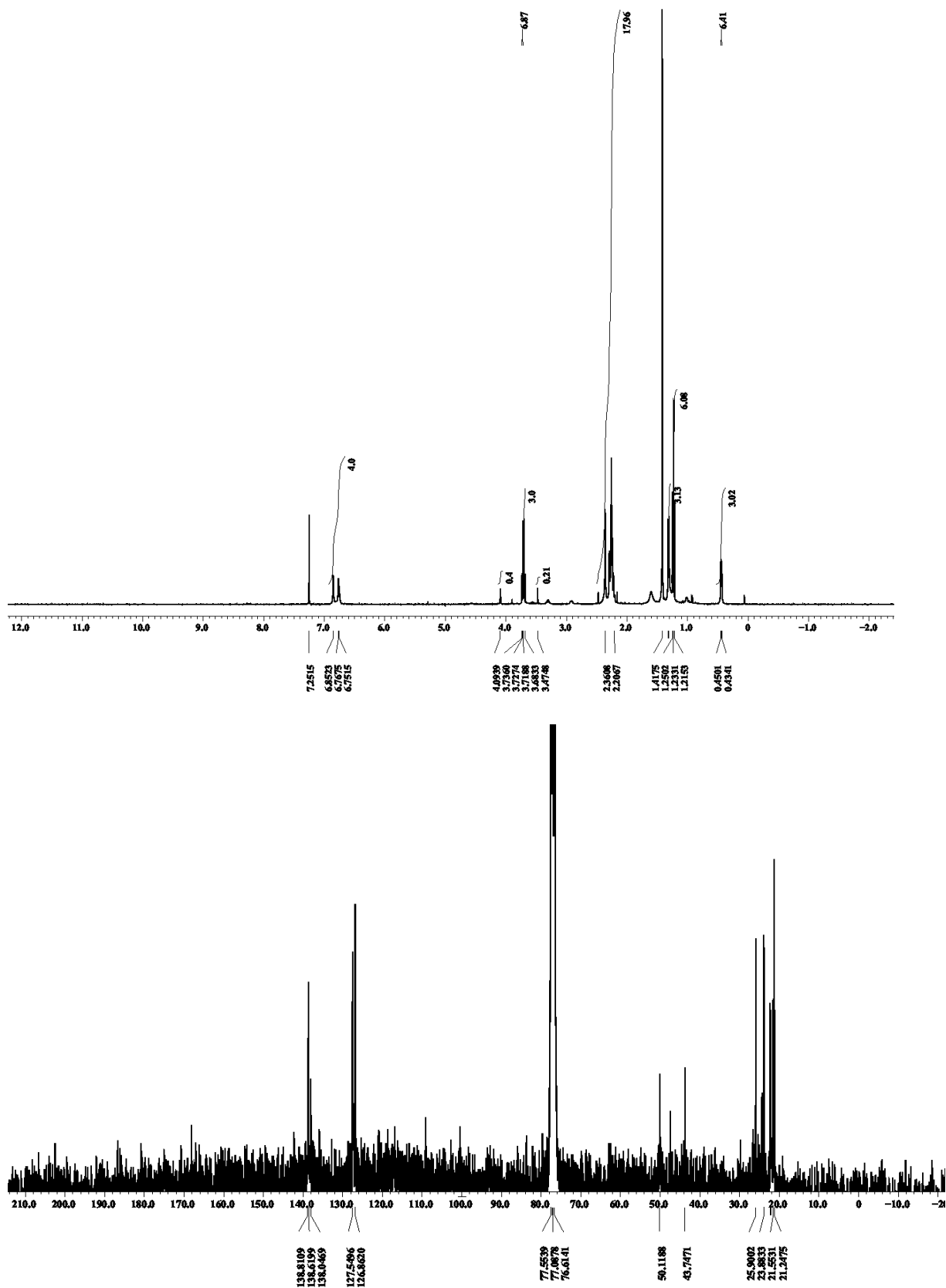


Appendix II-NMR Spectra

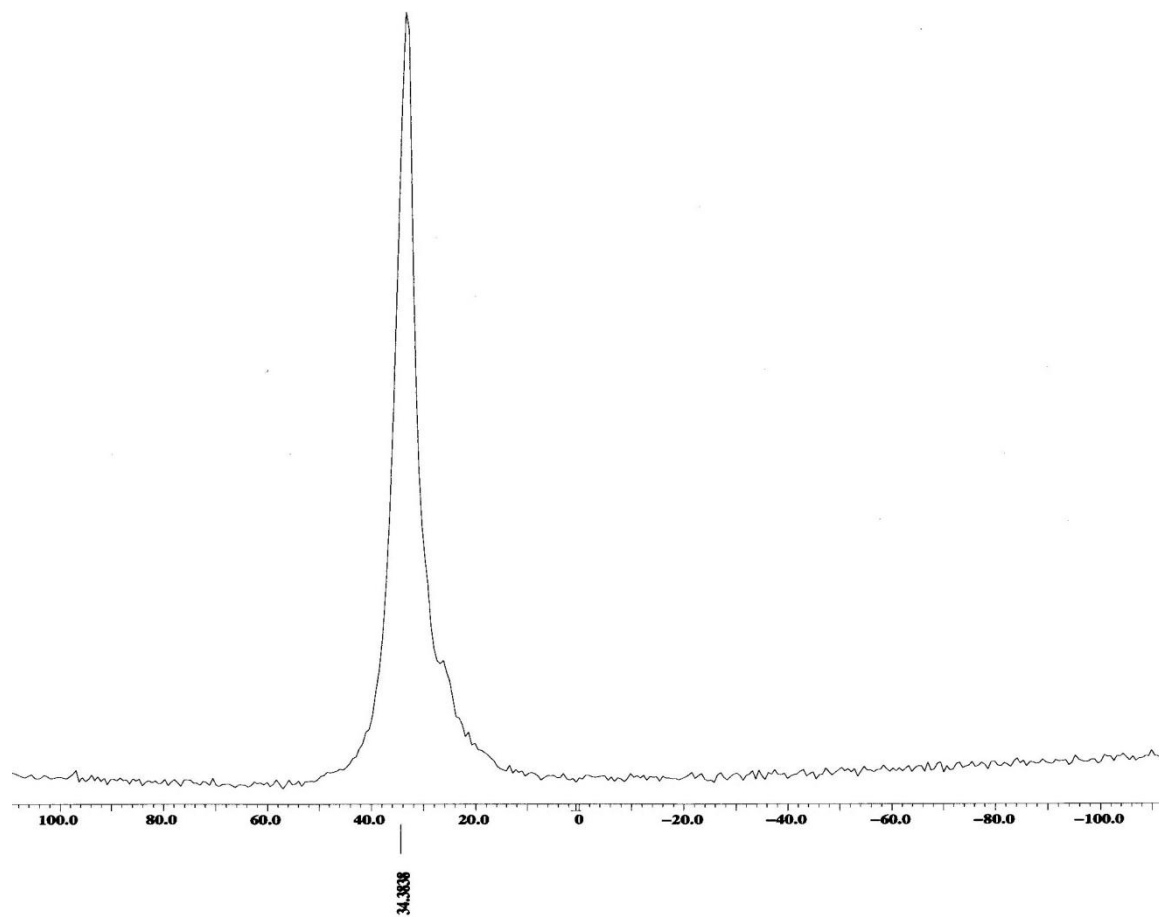


Appendix II-NMR Spectra

Compound **192**: ^1H NMR, ^{13}C NMR, and ^{11}B NMR in CDCl_3

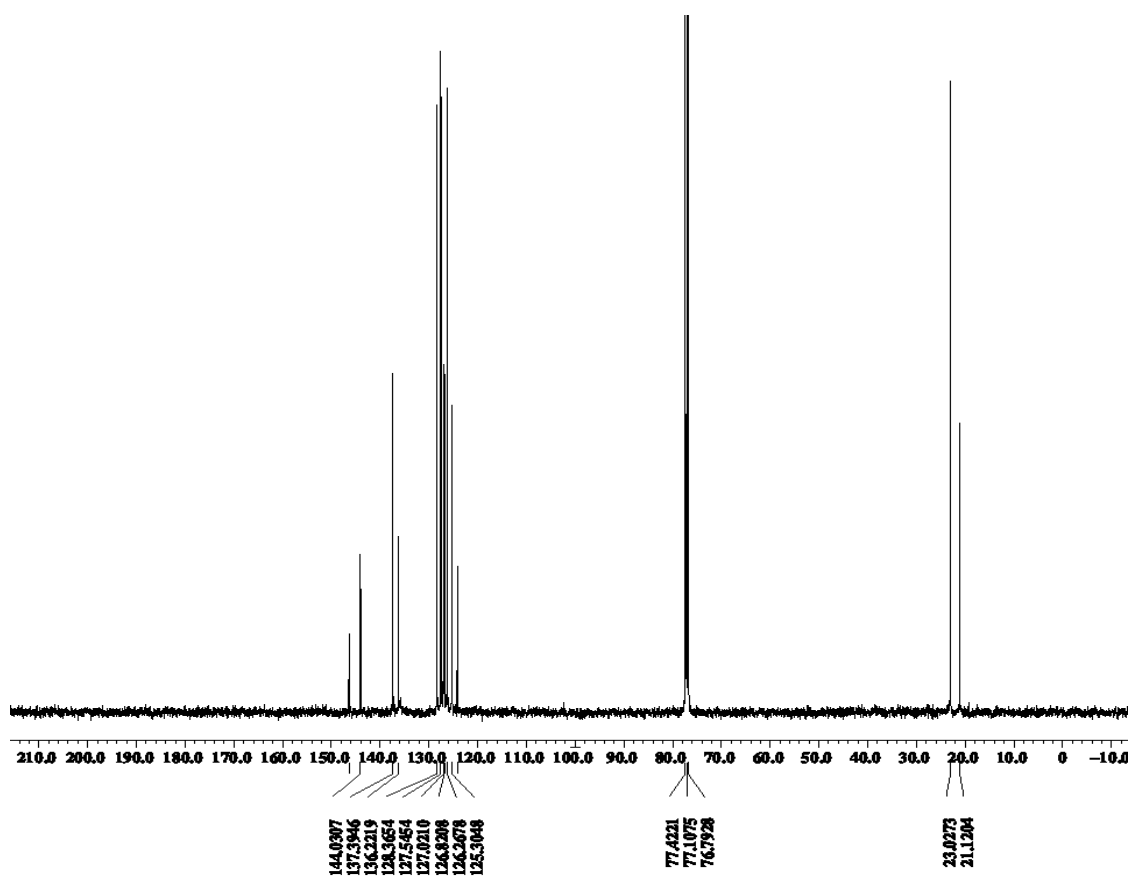
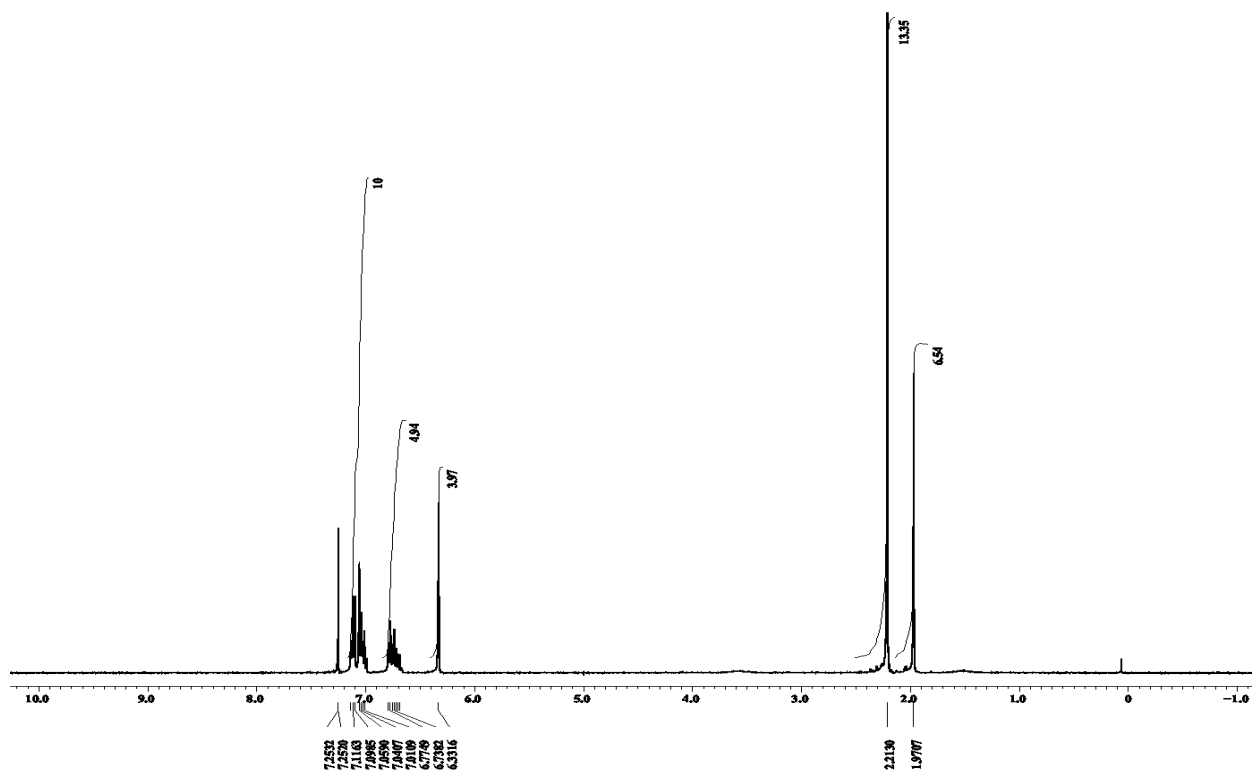


Appendix II-NMR Spectra

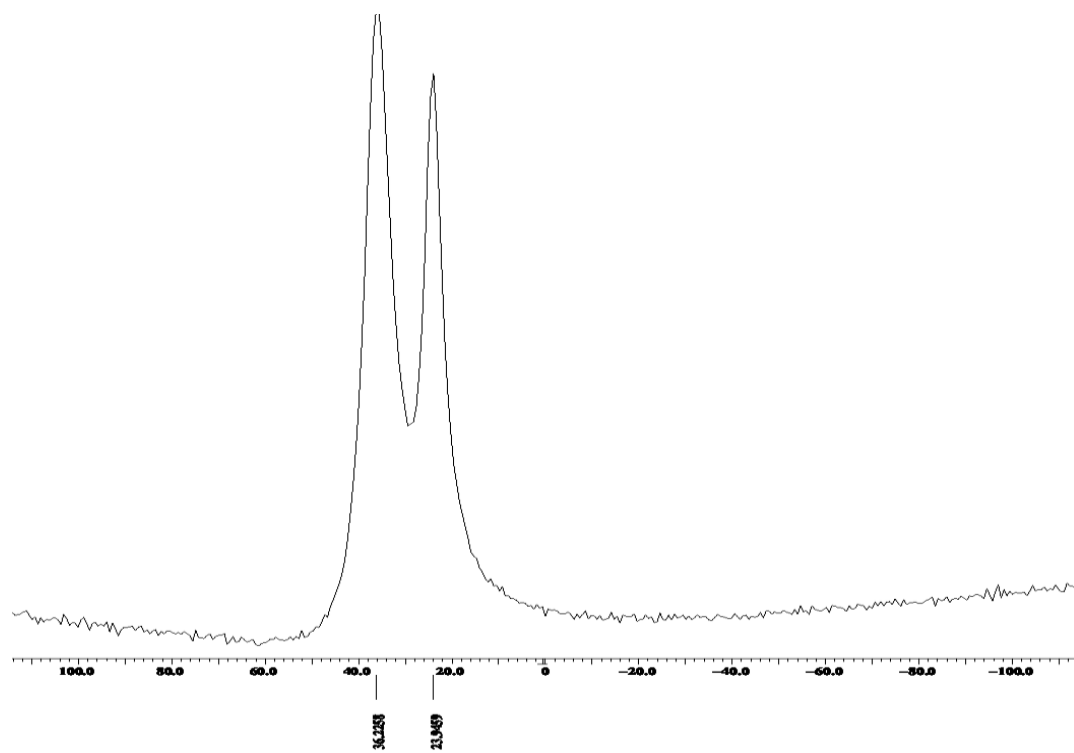


Appendix II-NMR Spectra

Compound **194**: ^1H NMR, ^{13}C NMR, and ^{11}B NMR in CDCl_3



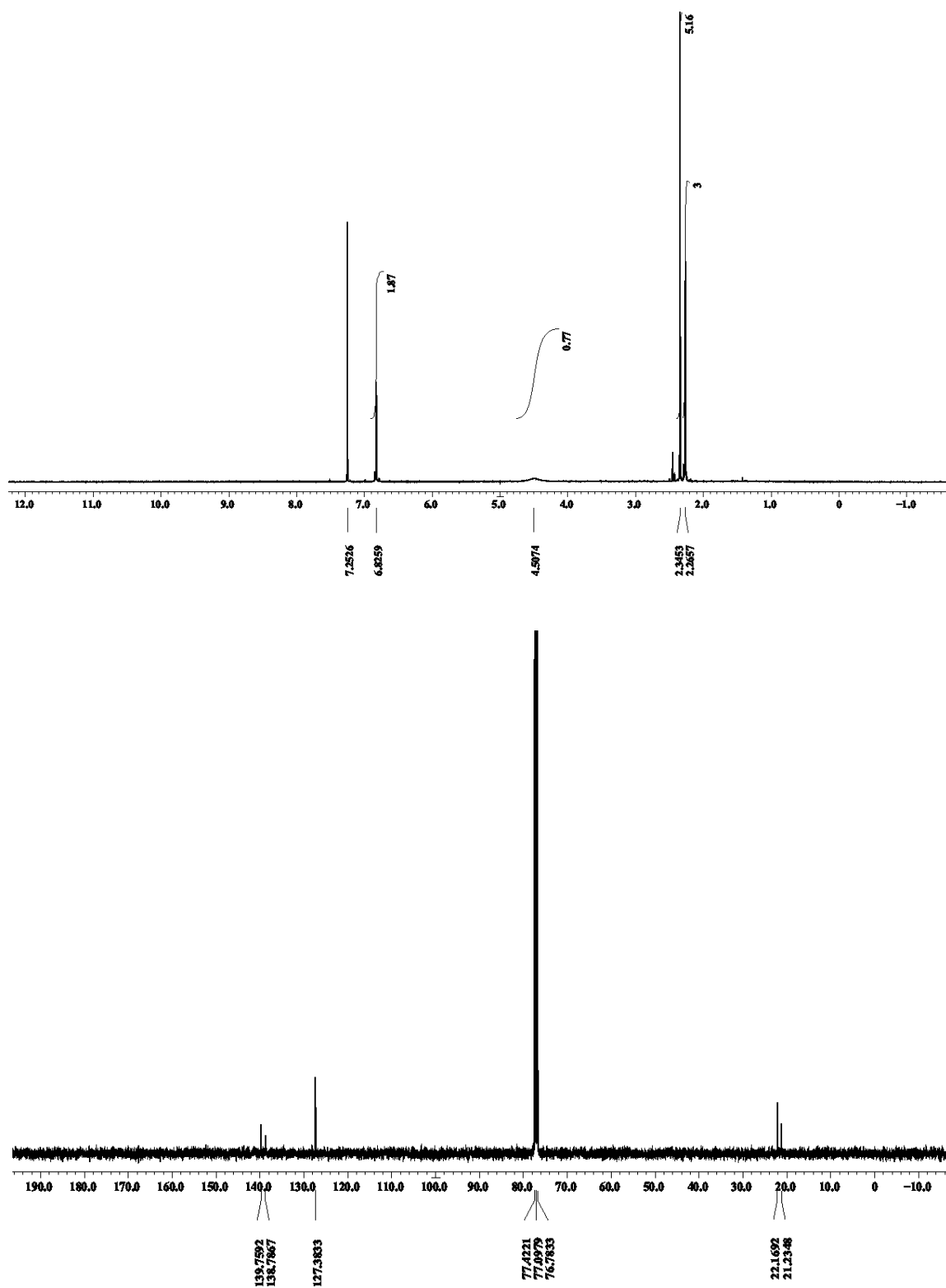
Appendix II-NMR Spectra



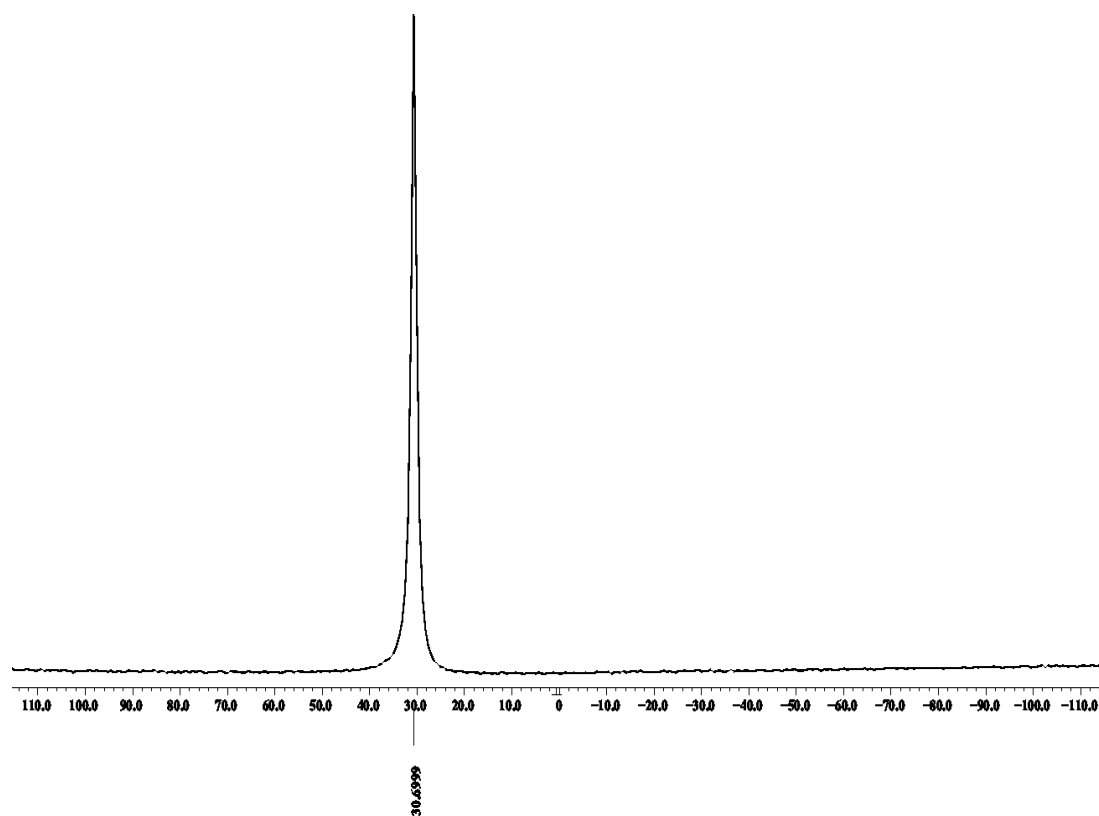
Appendix II-NMR Spectra

2. Boronic Acids and Carboxylates Derivatives

Compound 224: ^1H NMR, ^{13}C NMR, ^{11}B NMR and HMQC NMR in CDCl_3

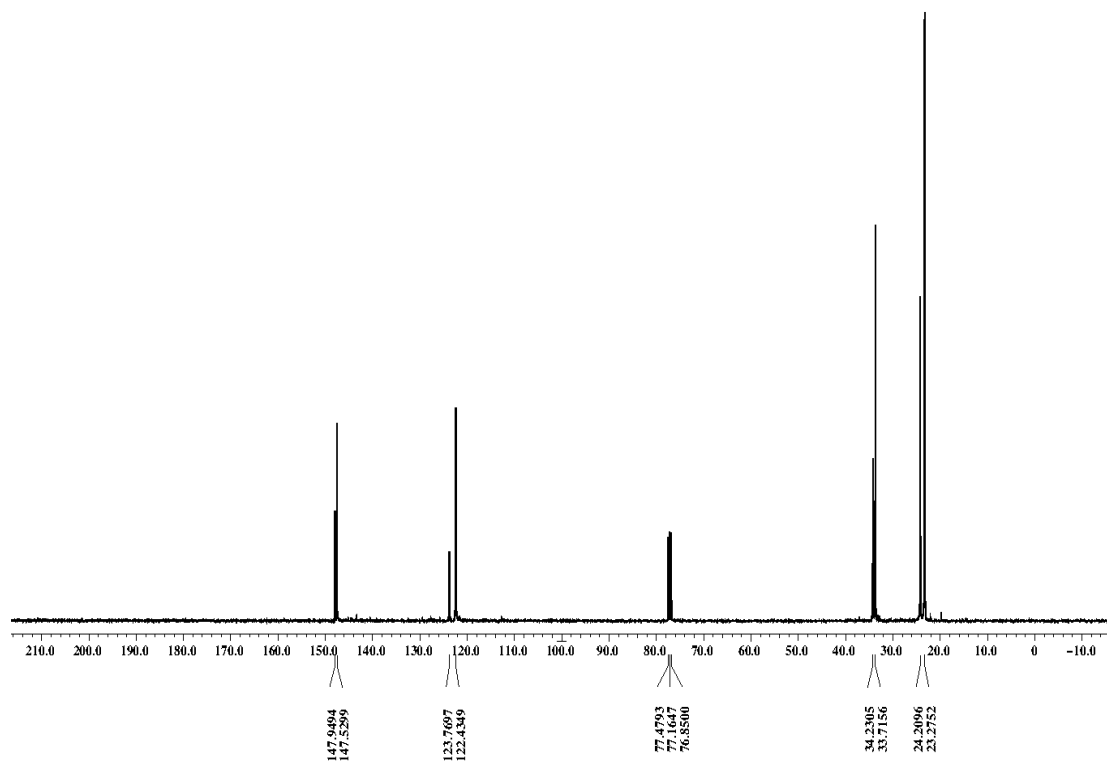
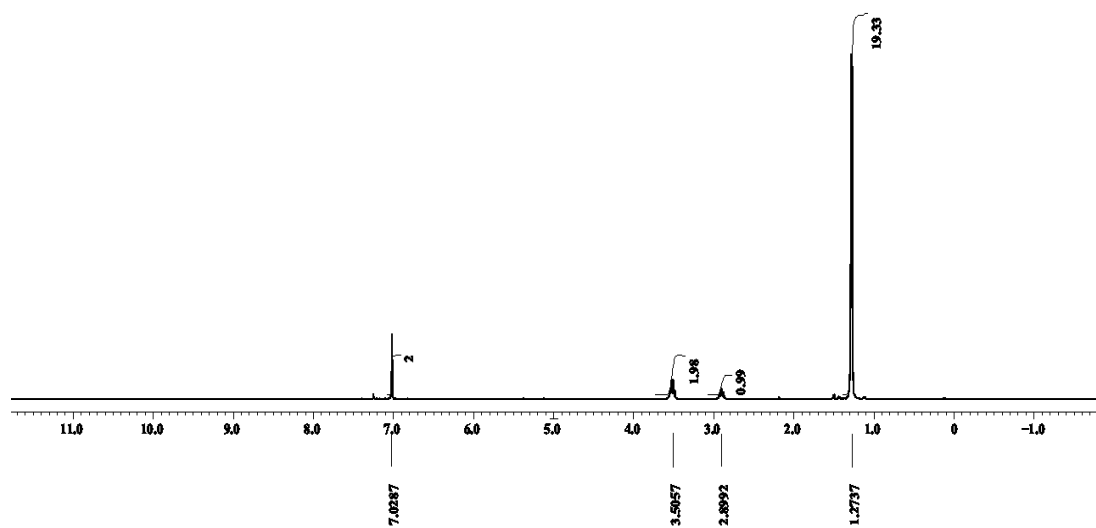


Appendix II-NMR Spectra



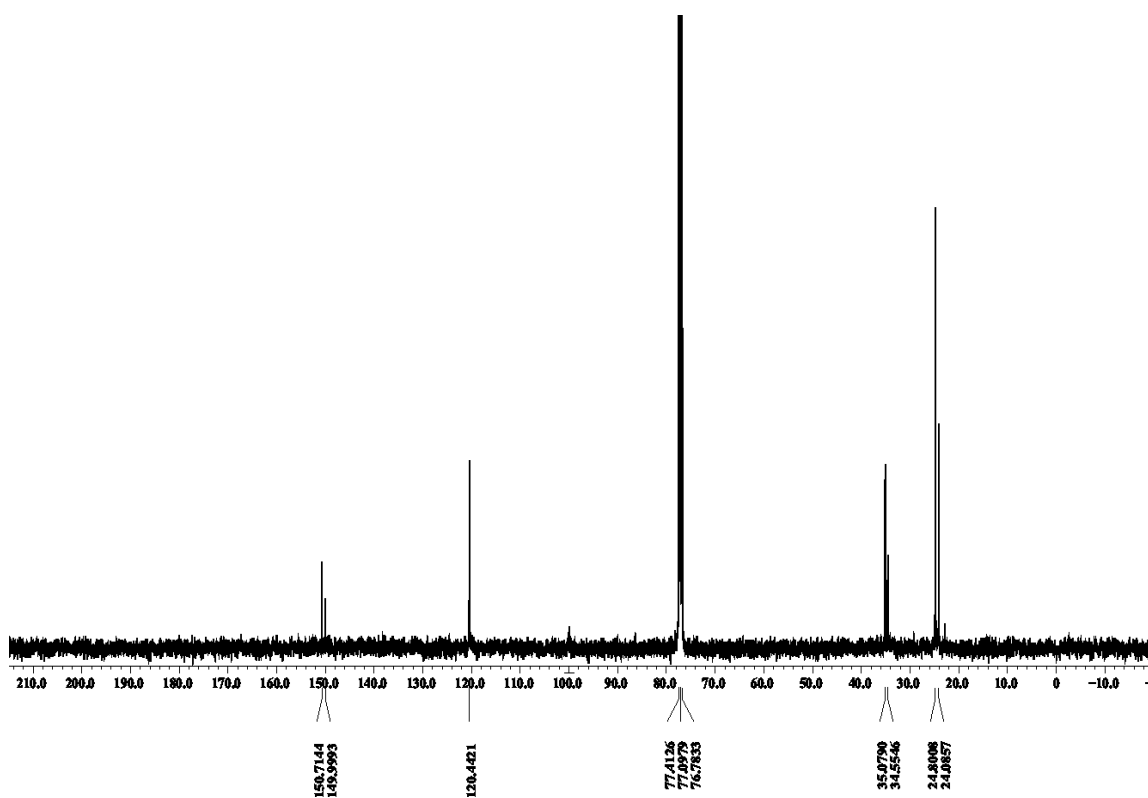
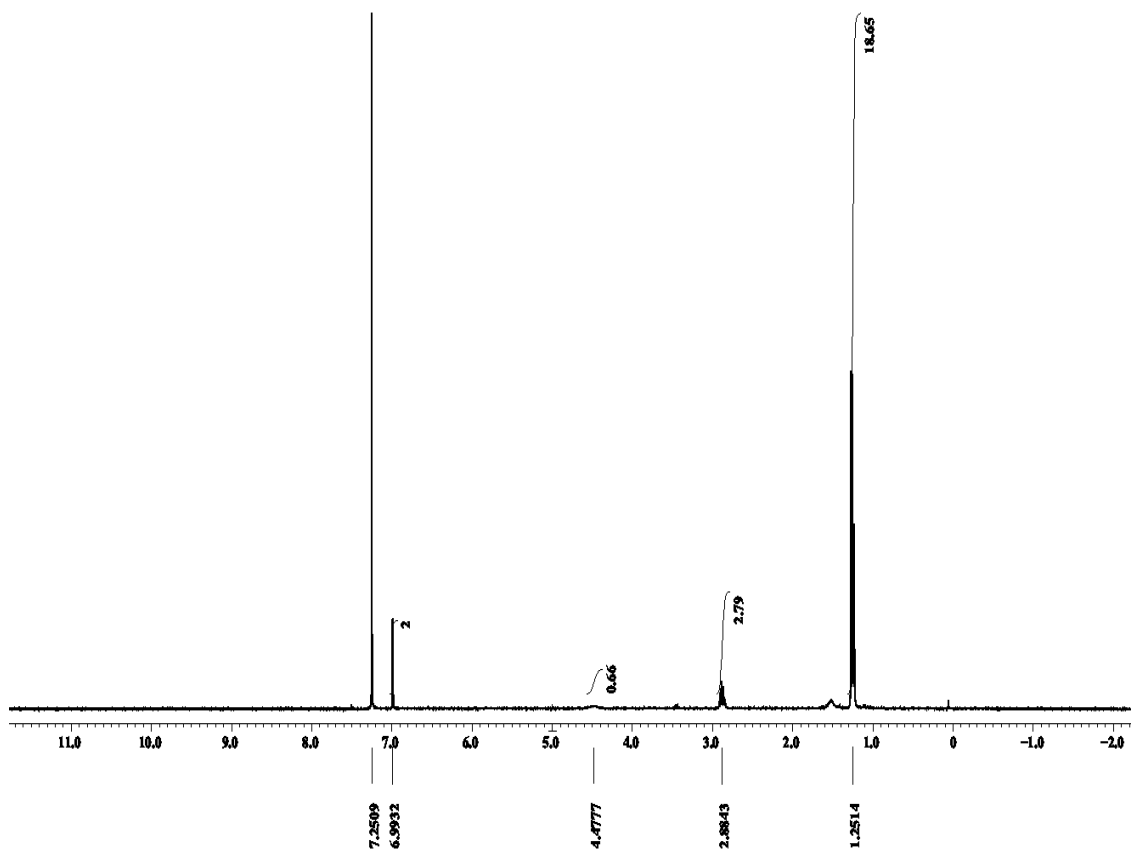
Appendix II-NMR Spectra

Compound 229: ^1H NMR, ^{13}C NMR, ^{11}B NMR and HMQC NMR in CDCl_3

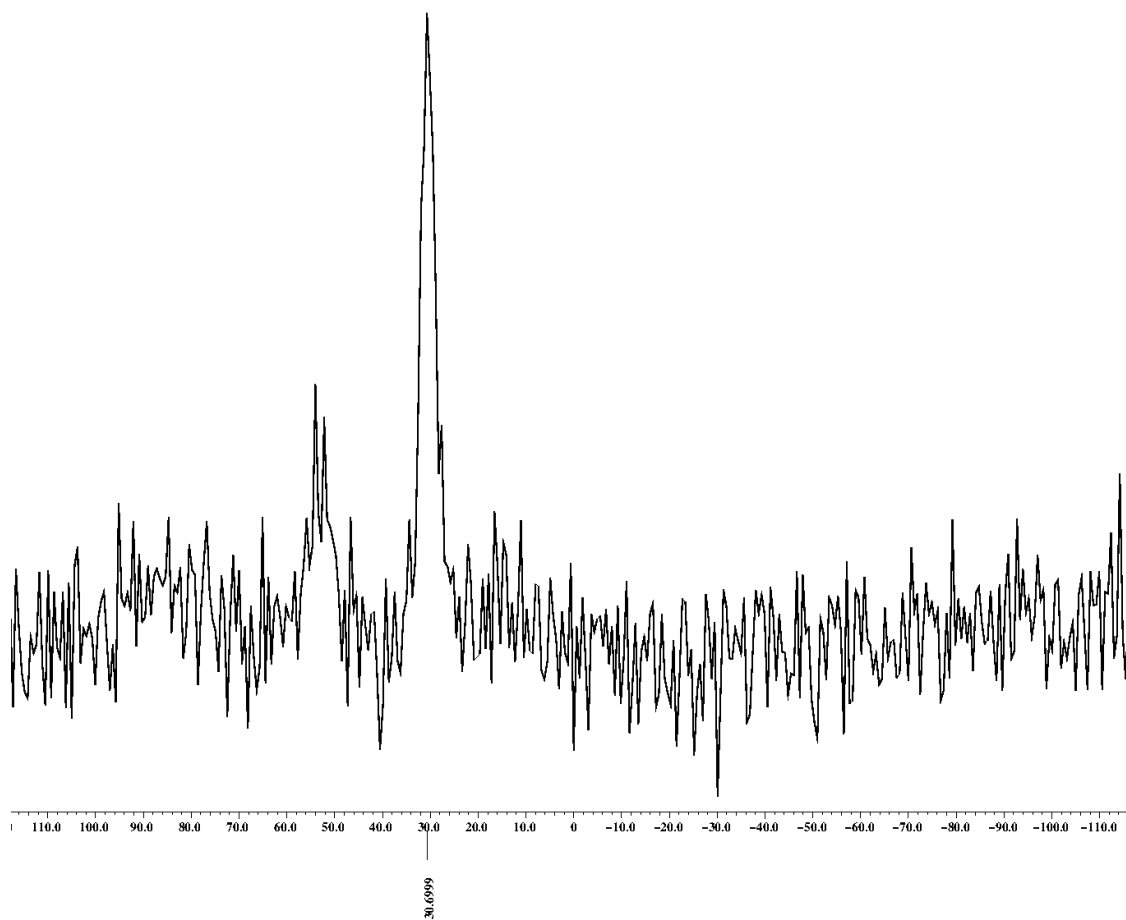


Appendix II-NMR Spectra

Compound 228: ^1H NMR, ^{13}C NMR, ^{11}B NMR and HMQC NMR in CDCl_3

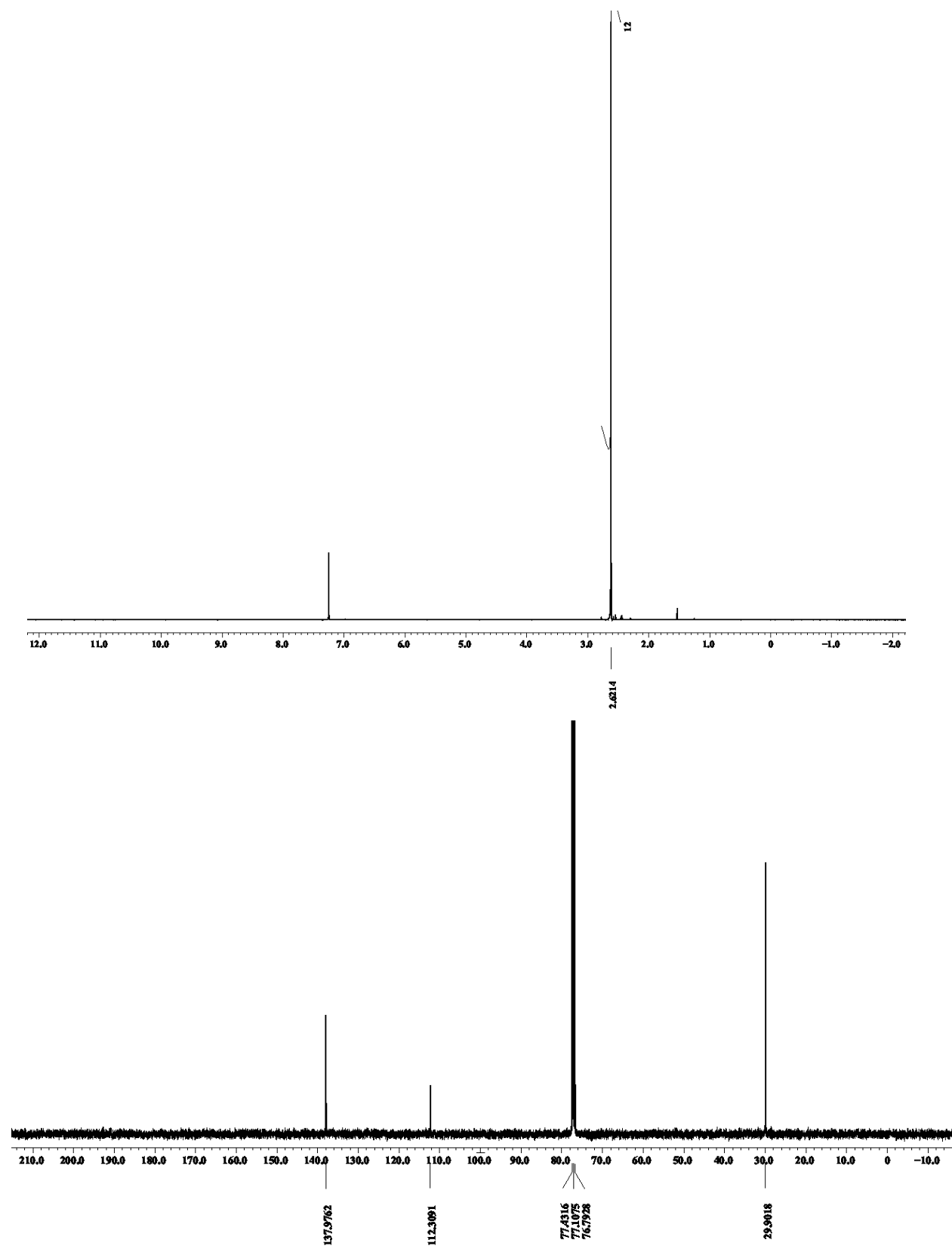


Appendix II-NMR Spectra



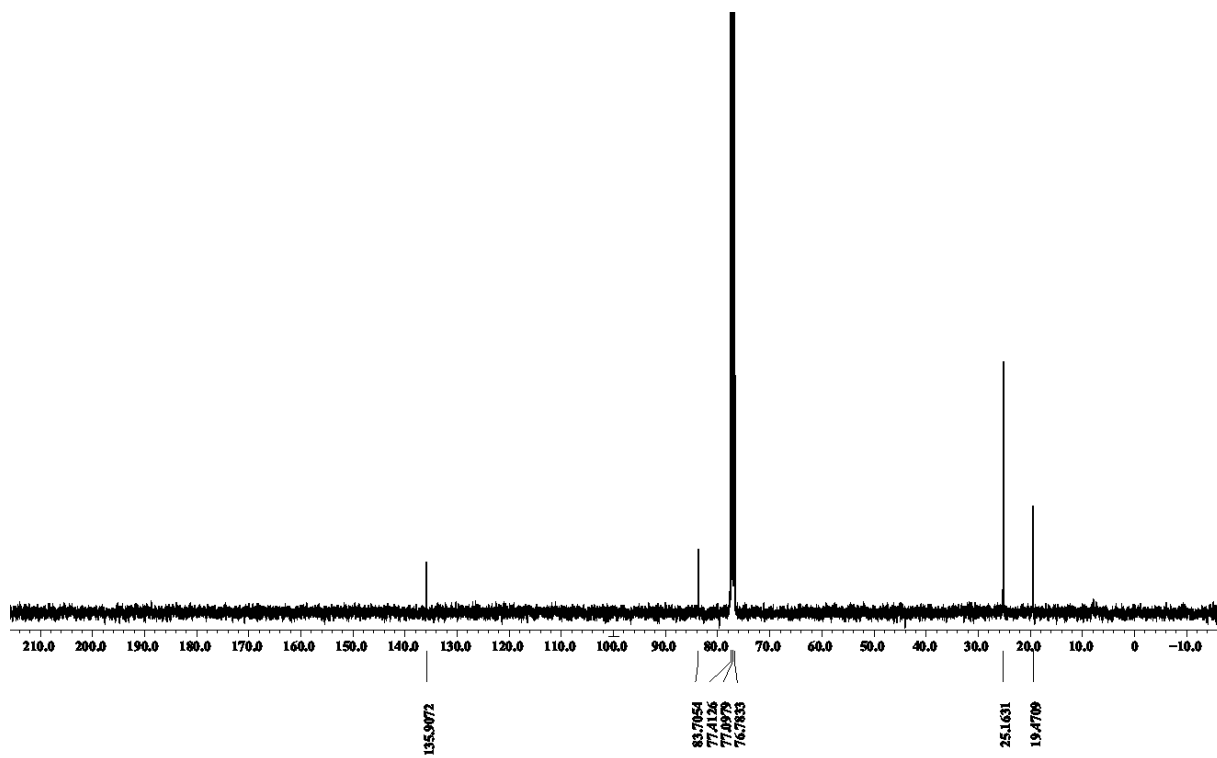
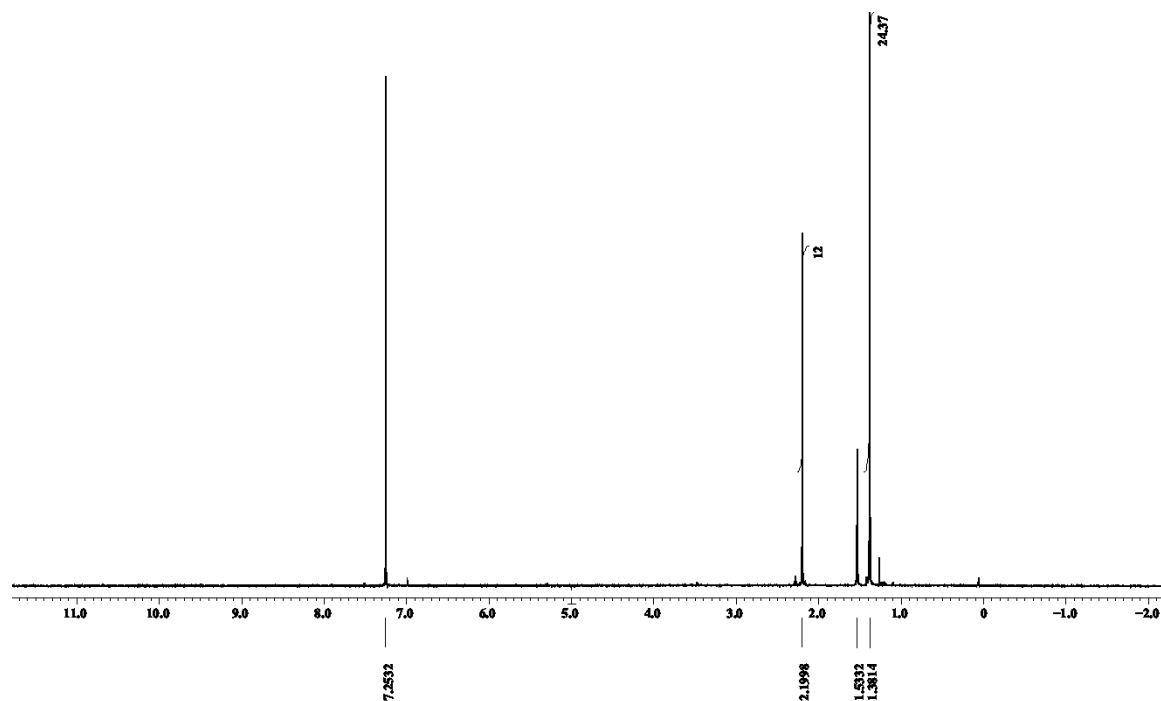
Appendix II-NMR Spectra

Compound 232: ^1H NMR and ^{13}C NMR in CDCl_3

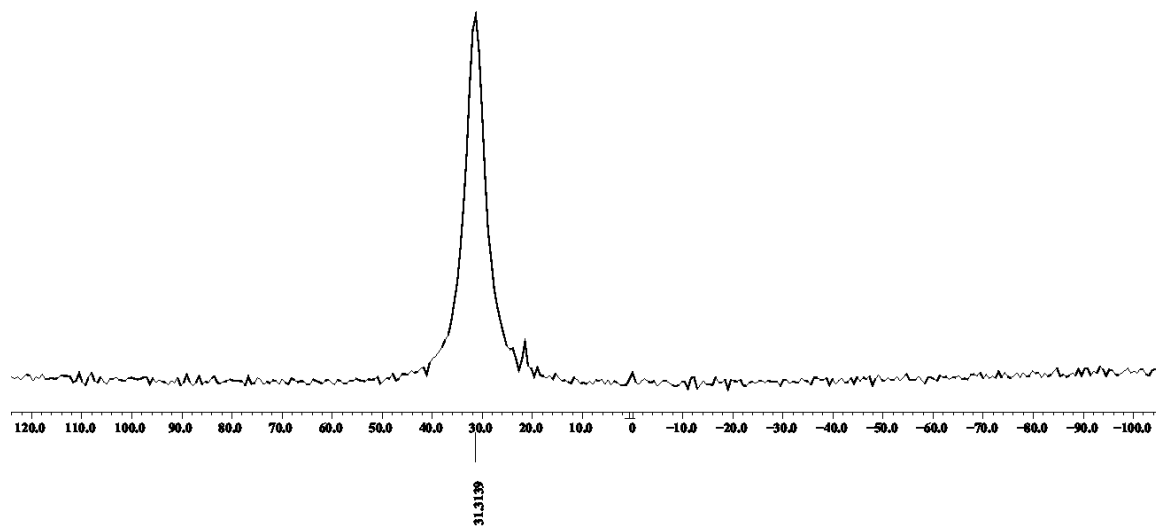


Appendix II-NMR Spectra

Compound 238: ^1H NMR, ^{13}C NMR, and ^{11}B NMR in CDCl_3

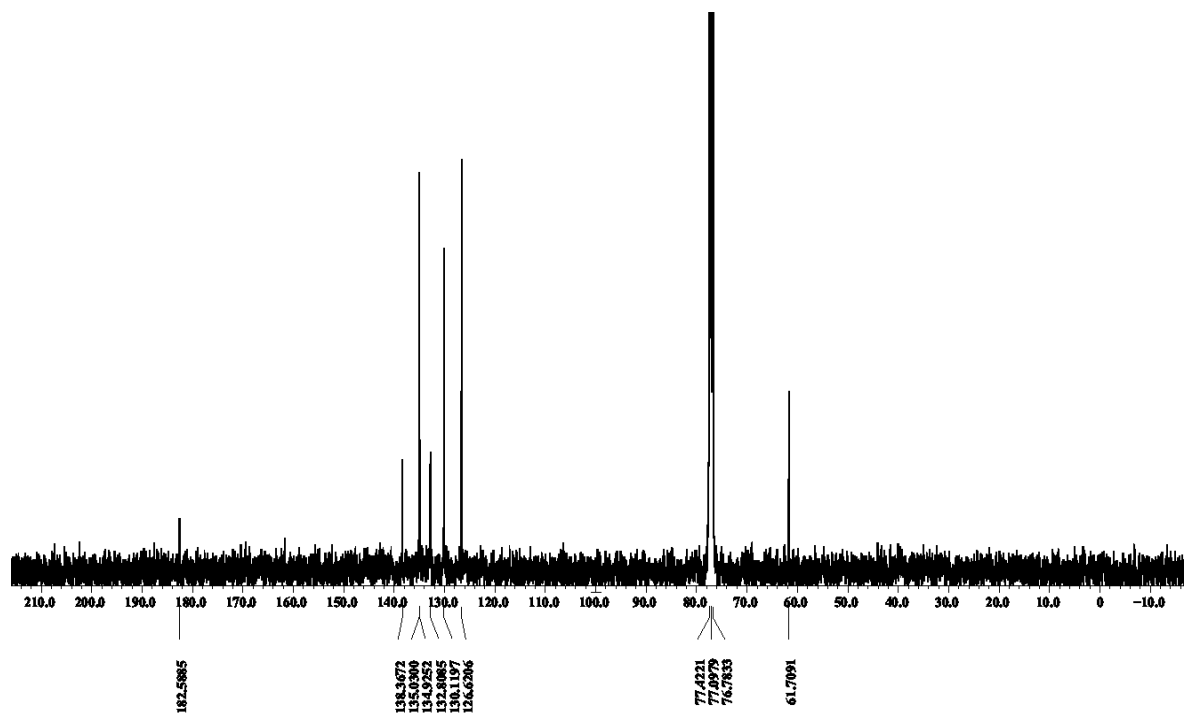
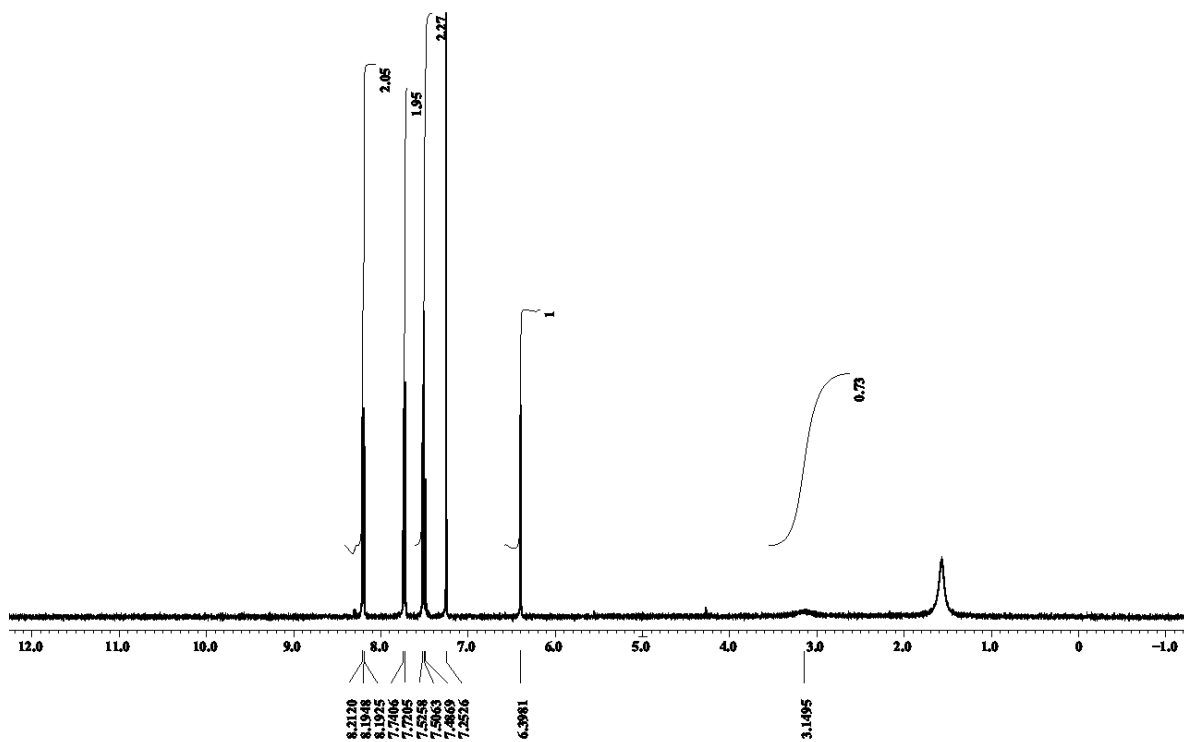


Appendix II-NMR Spectra



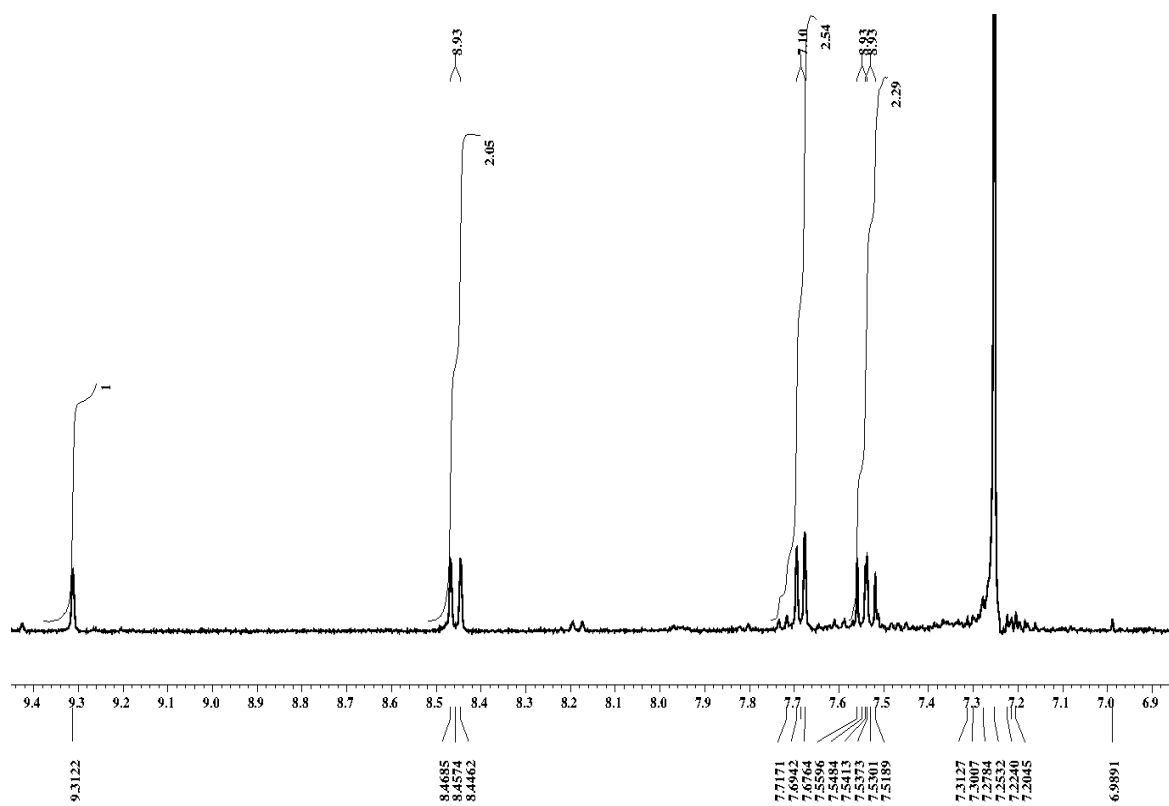
Appendix II-NMR Spectra

Compound 241: ^1H NMR and ^{13}C NMR in CDCl_3



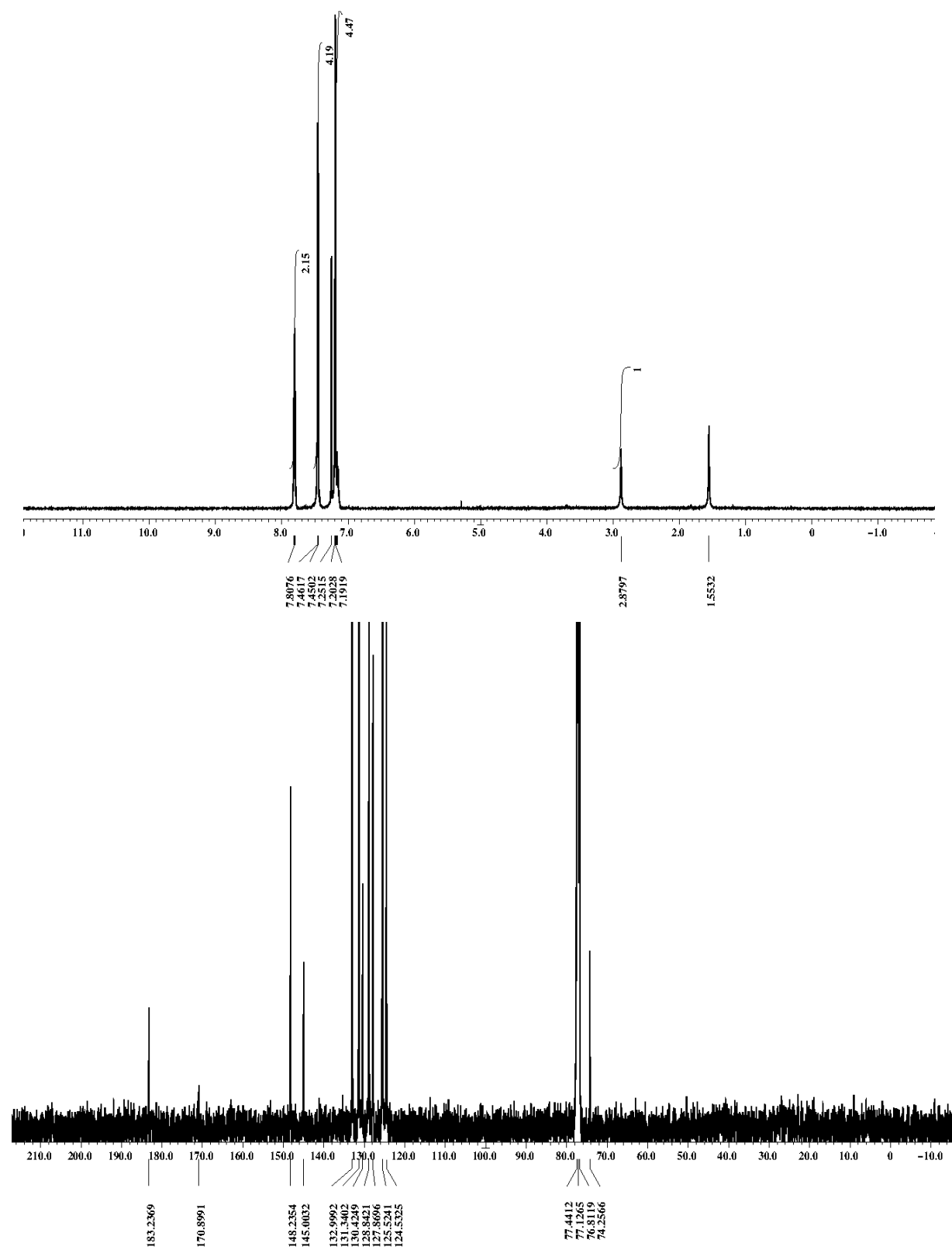
Appendix II-NMR Spectra

Compound 243: ^1H NMR in CDCl_3



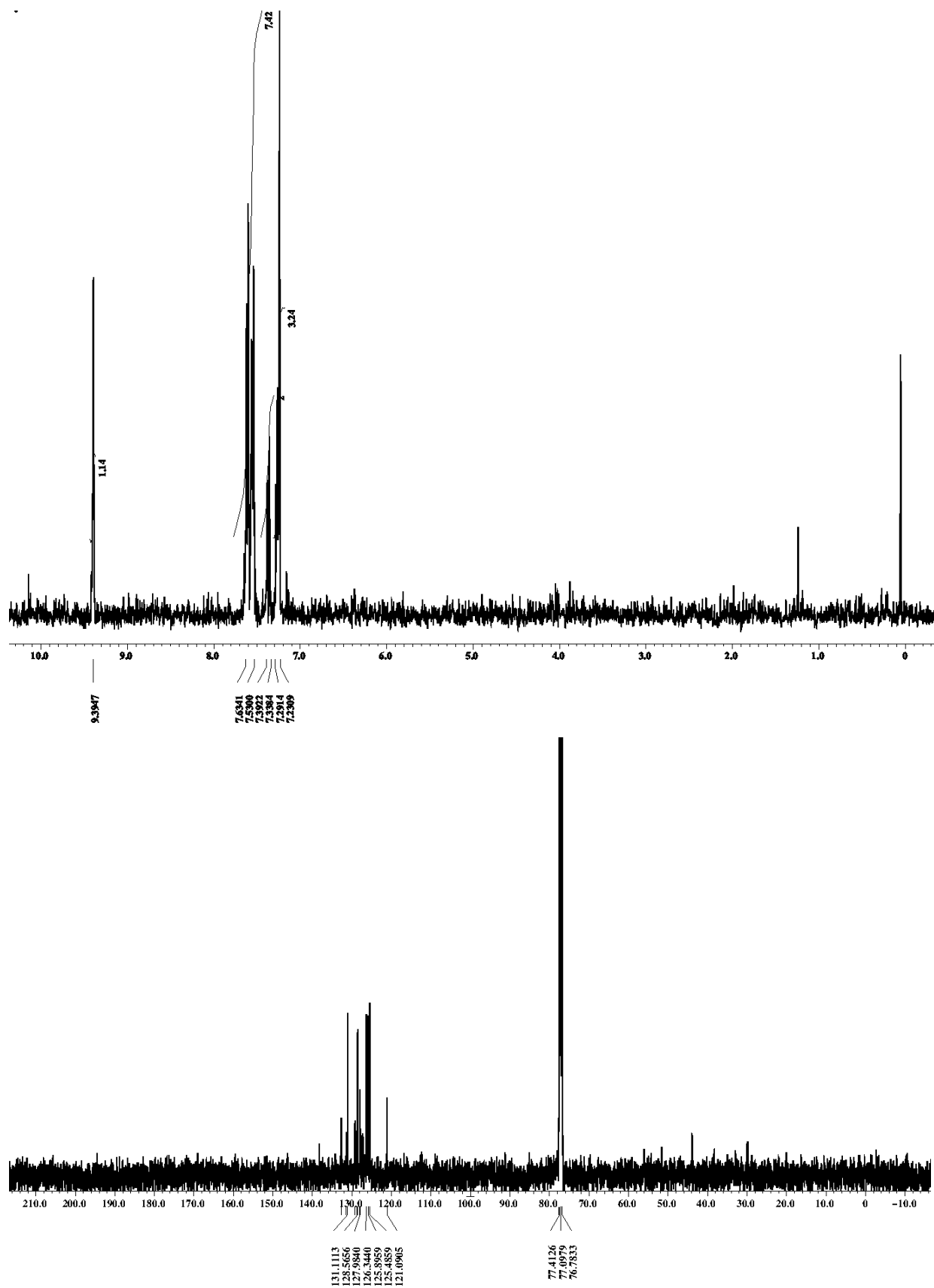
Appendix II-NMR Spectra

Compound **245**: ^1H NMR and ^{13}C NMR in CDCl_3



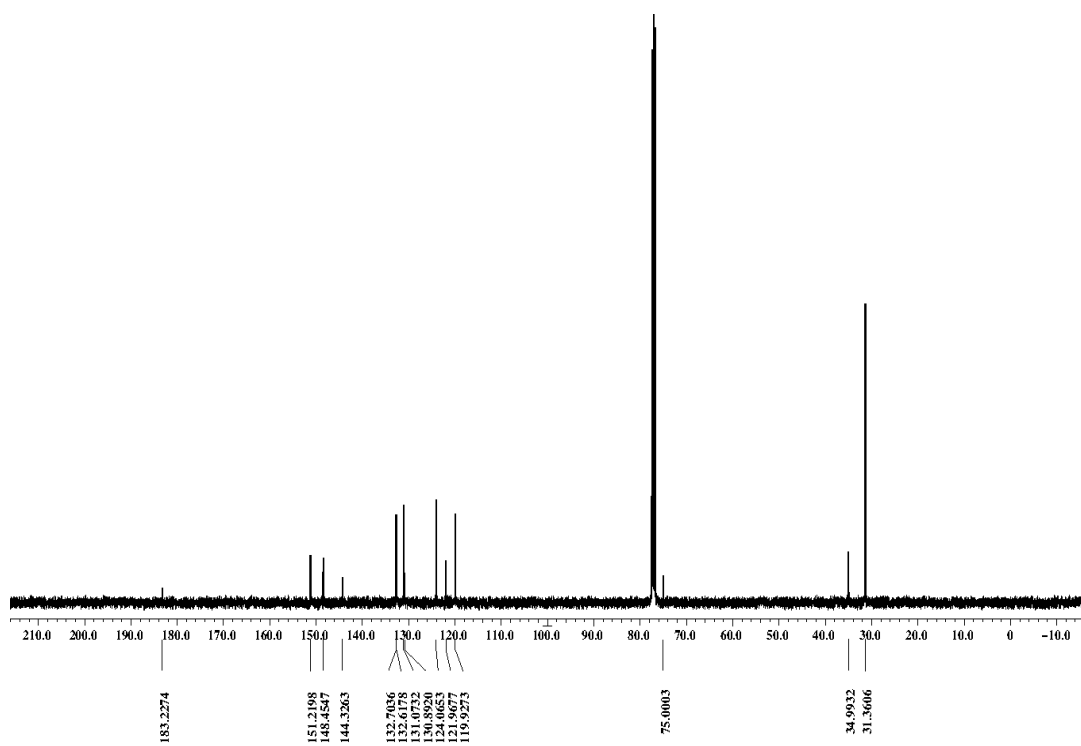
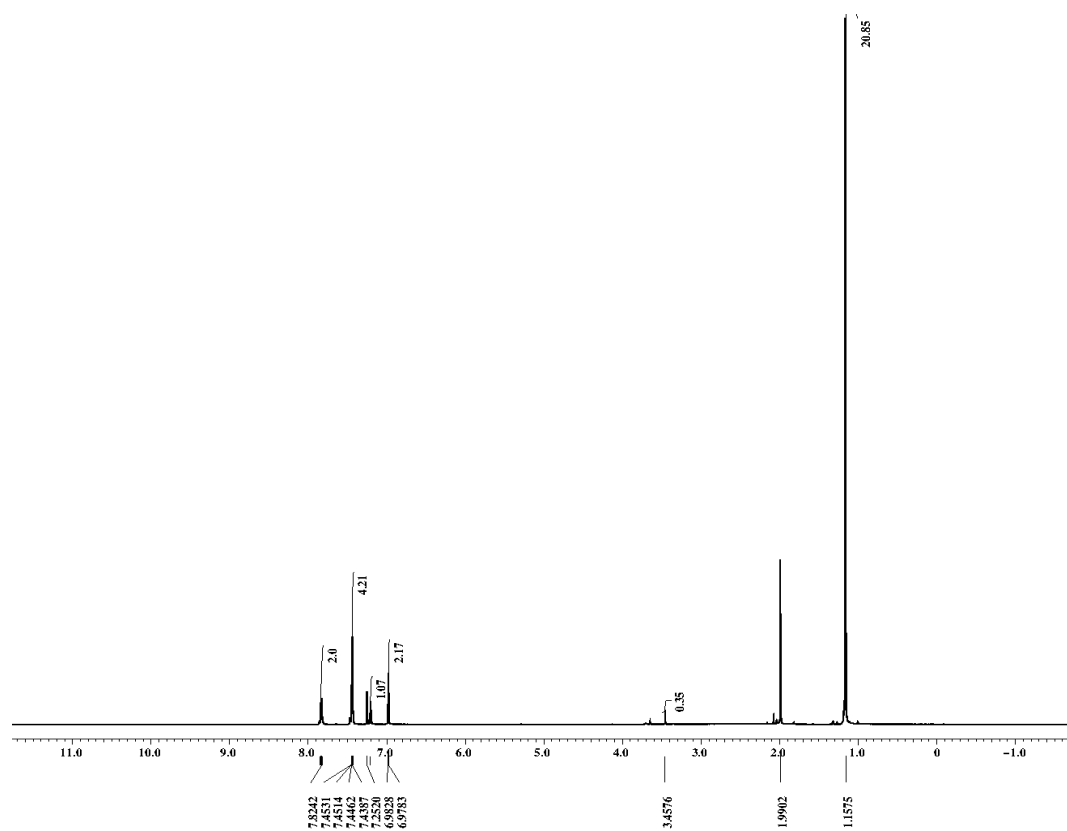
Appendix II-NMR Spectra

Compound 246: ^1H NMR and ^{13}C NMR in CDCl_3



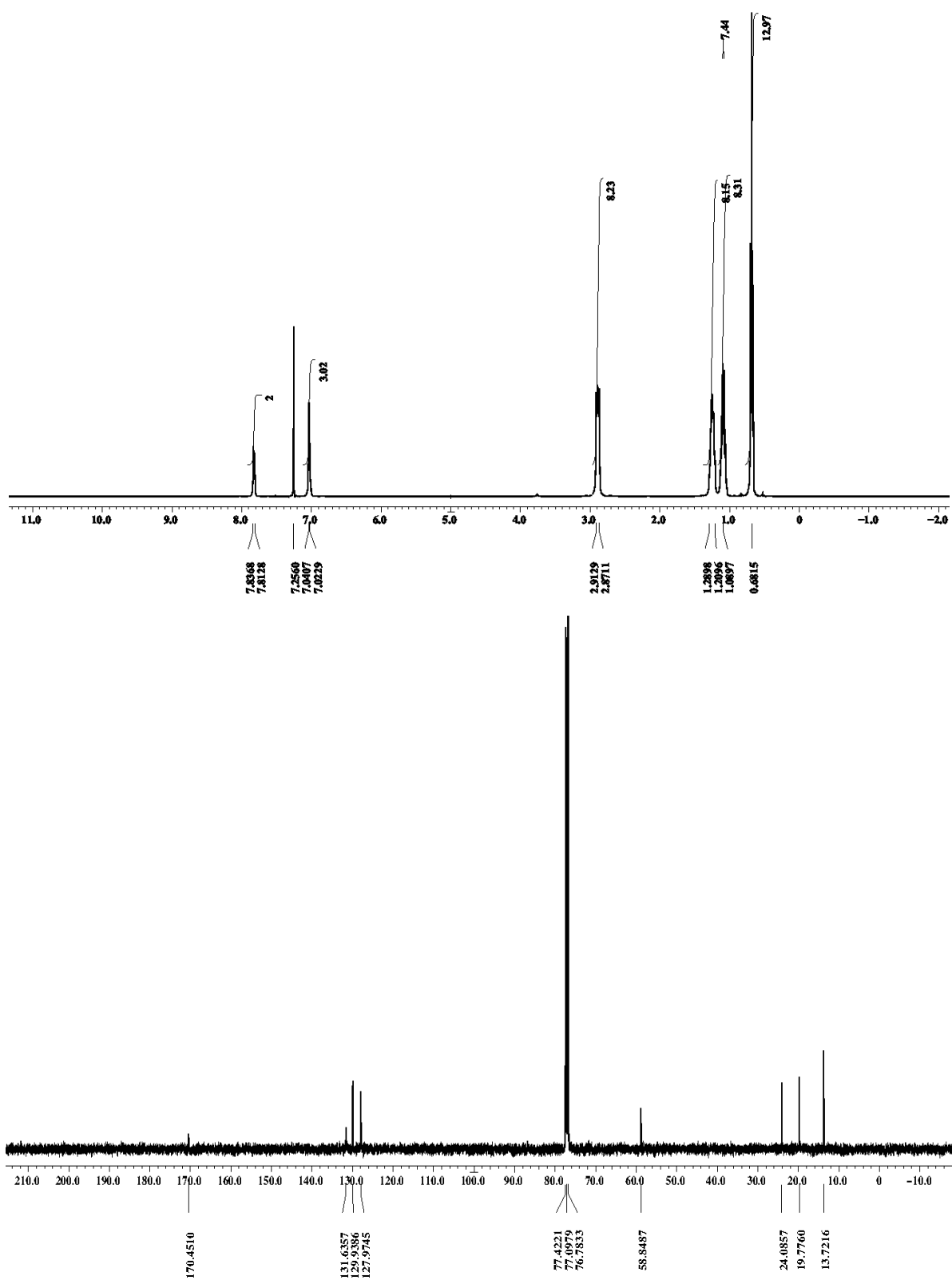
Appendix II-NMR Spectra

Compound 249: ^1H NMR and ^{13}C NMR in CDCl_3



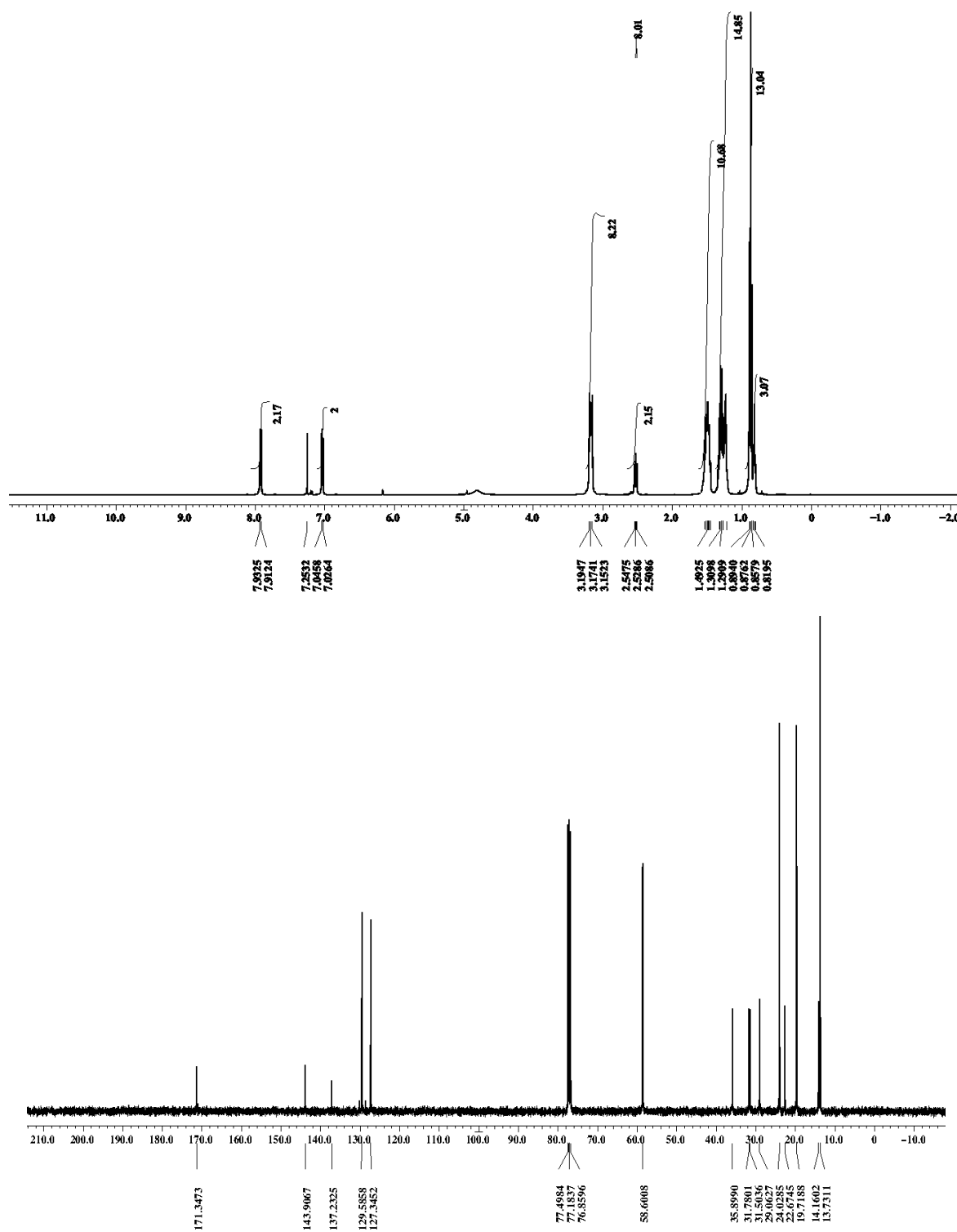
Appendix II-NMR Spectra

Compound 219: ^1H NMR and ^{13}C NMR in CDCl_3



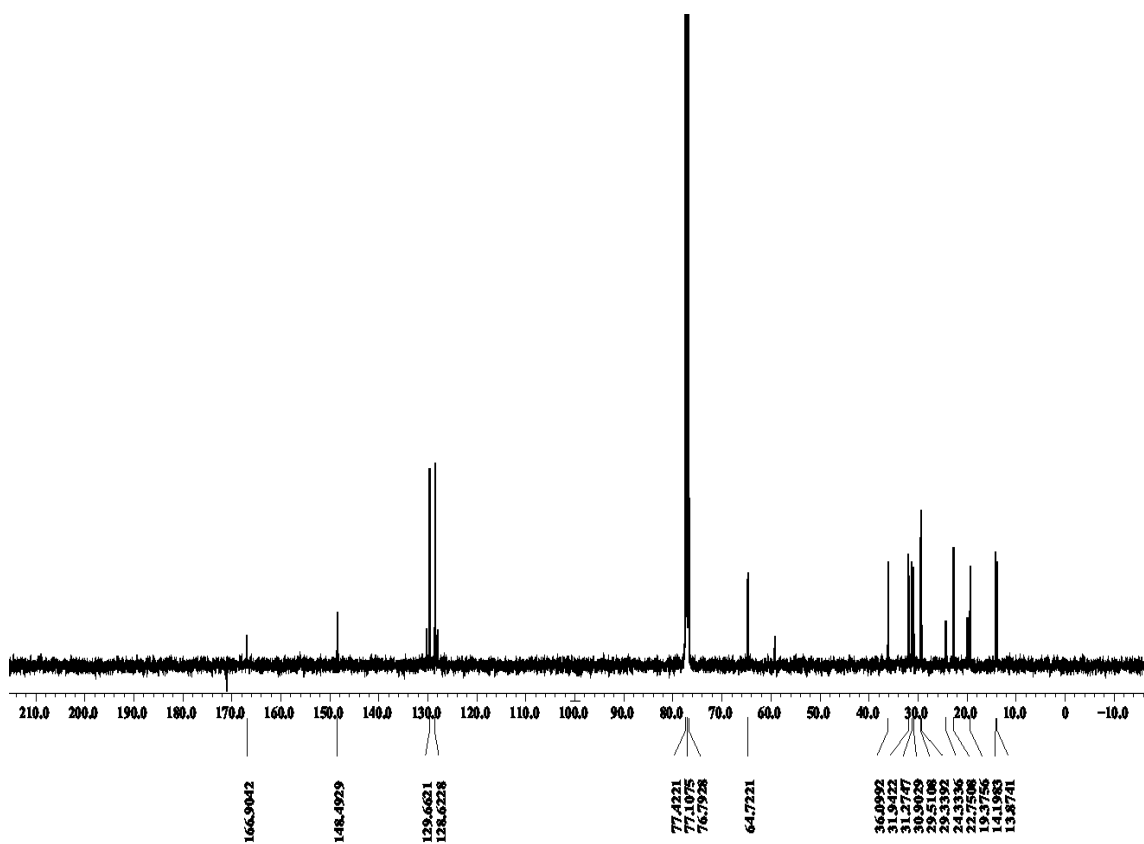
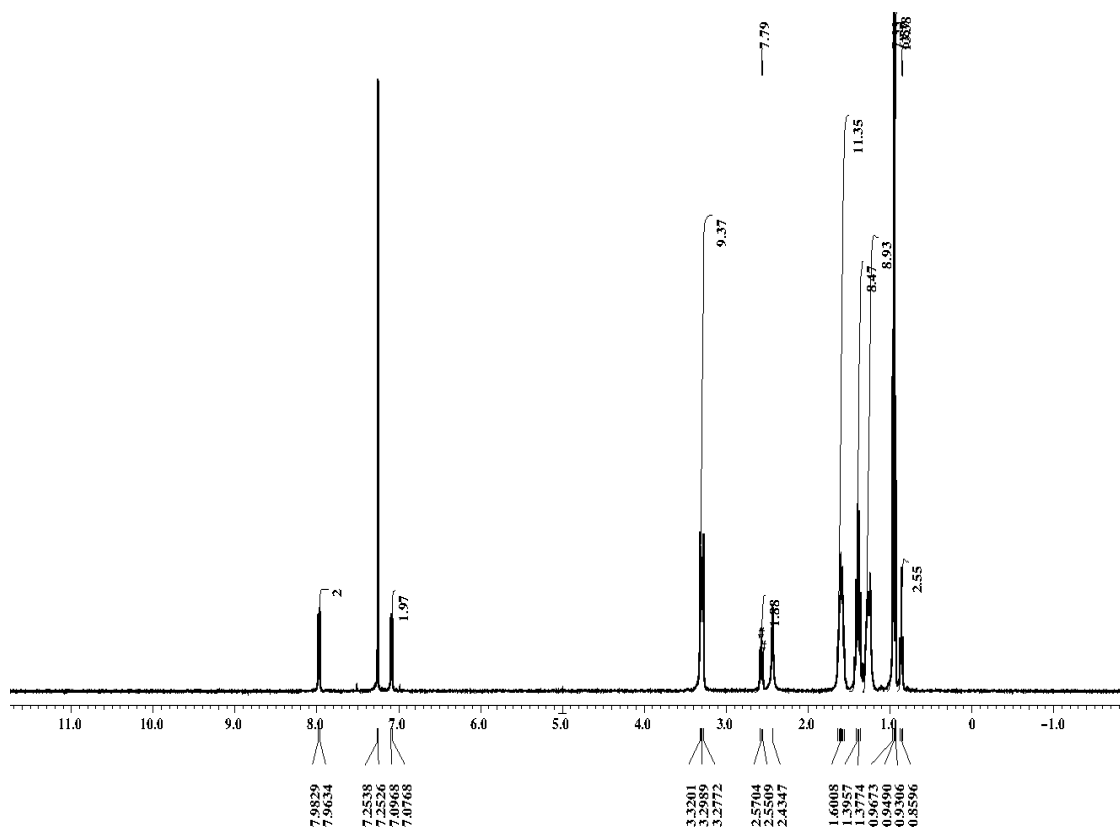
Appendix II-NMR Spectra

Compound 251: ^1H NMR and ^{13}C NMR in CDCl_3



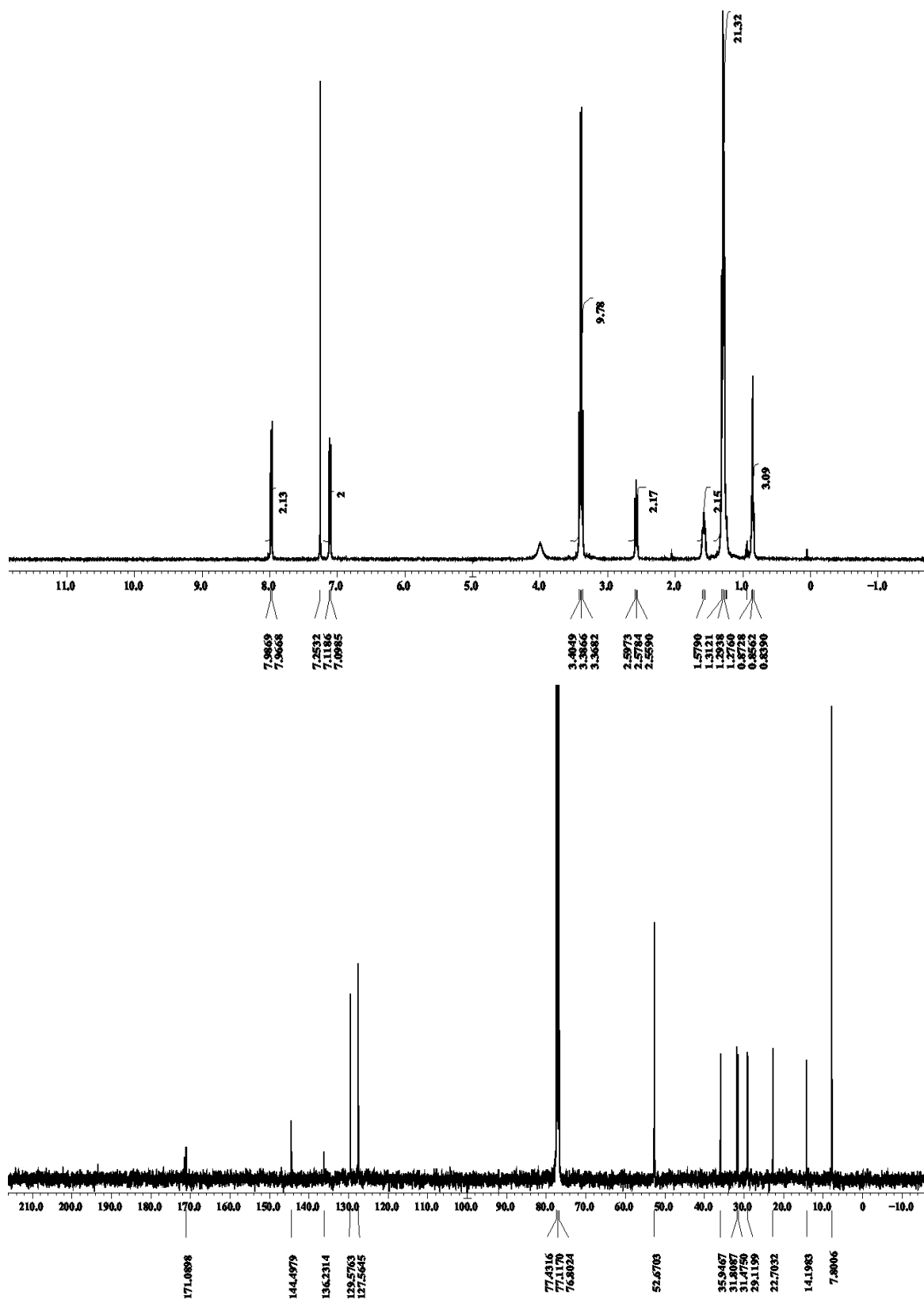
Appendix II-NMR Spectra

Compound 252: ^1H NMR and ^{13}C NMR in CDCl_3



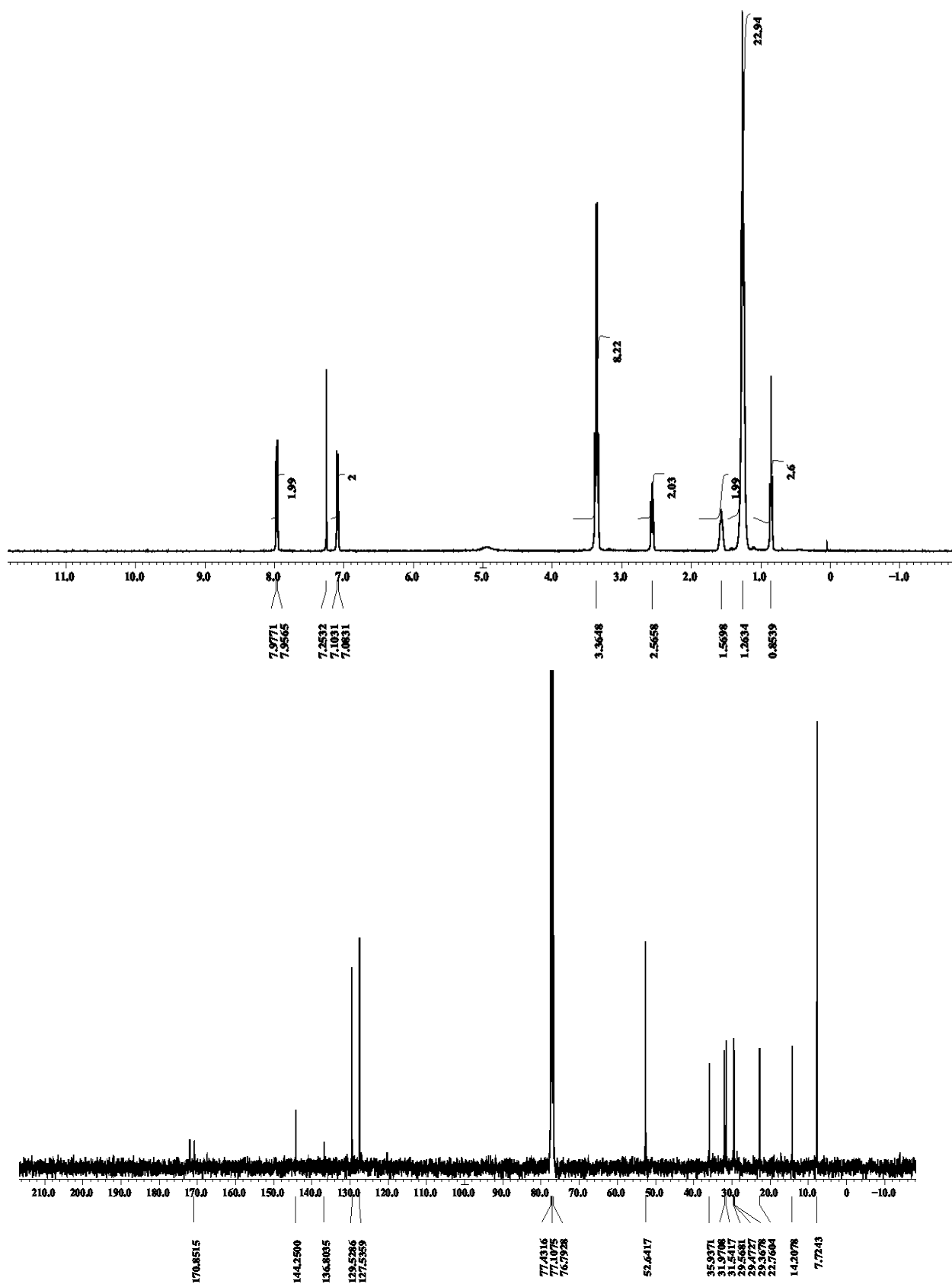
Appendix II-NMR Spectra

Compound 253: ^1H NMR and ^{13}C NMR in CDCl_3



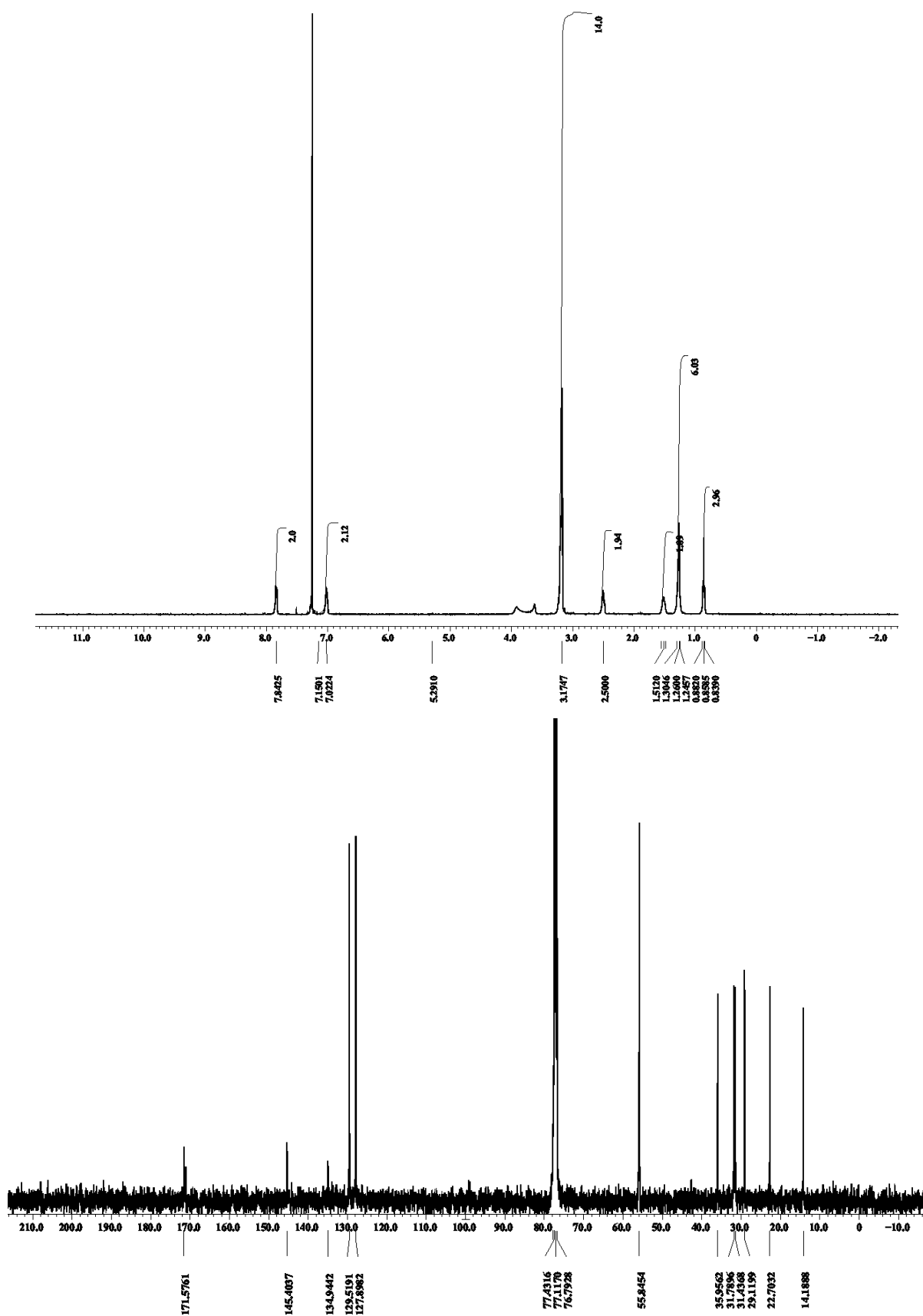
Appendix II-NMR Spectra

Compound 254: ^1H NMR and ^{13}C NMR in CDCl_3



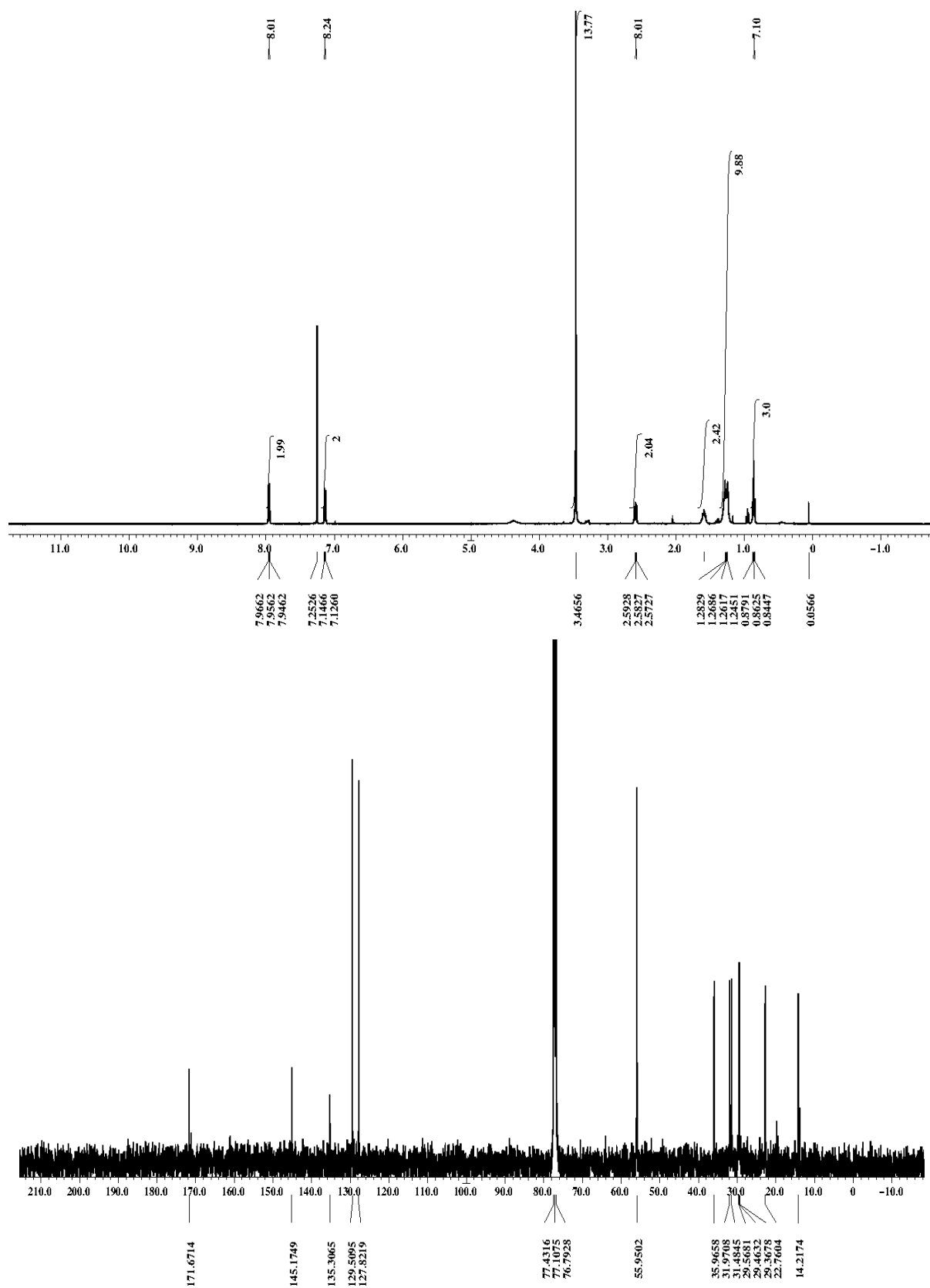
Appendix II-NMR Spectra

Compound 255: ^1H NMR and ^{13}C NMR in CDCl_3



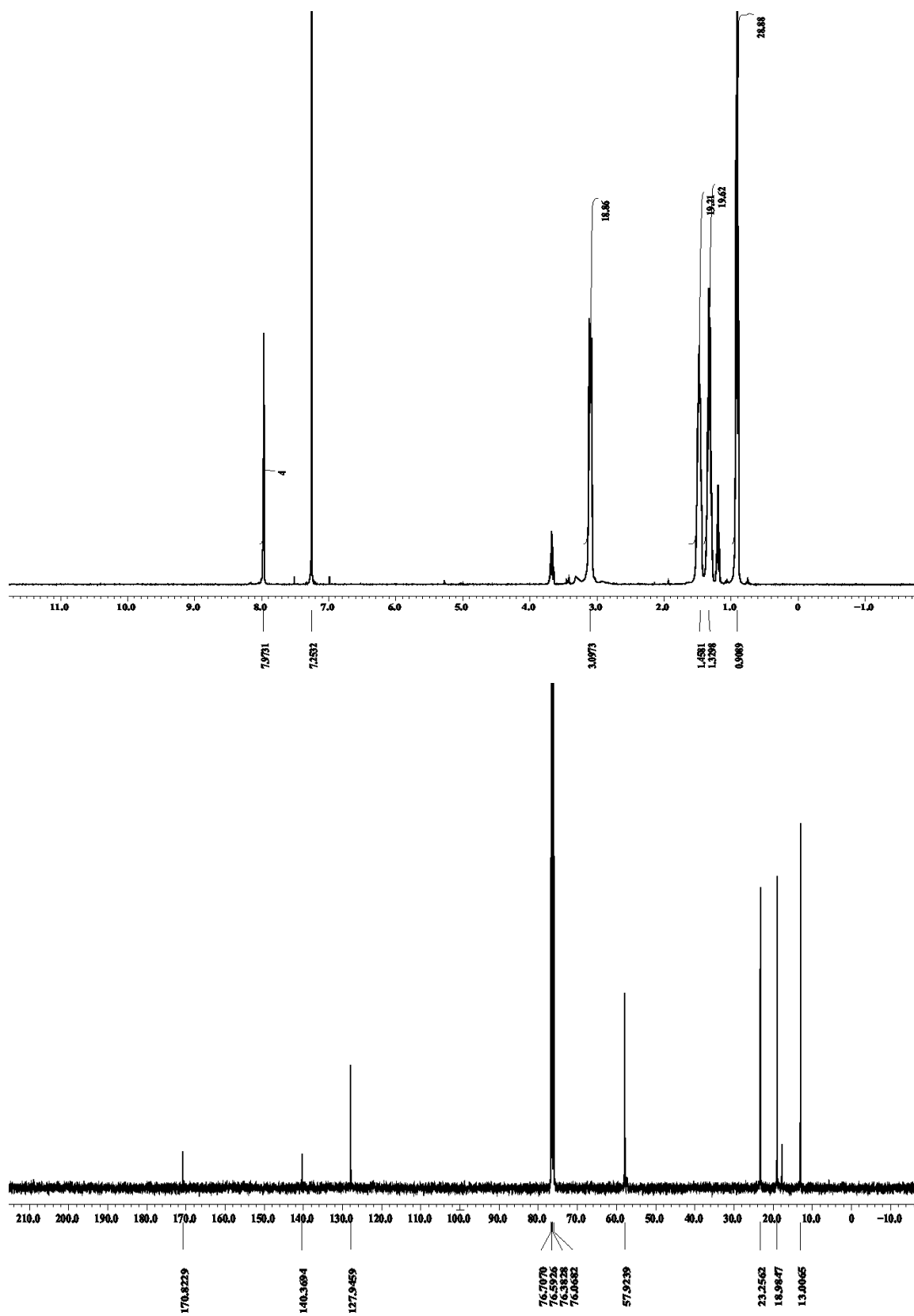
Appendix II-NMR Spectra

Compound 256: ^1H NMR and ^{13}C NMR in CDCl_3



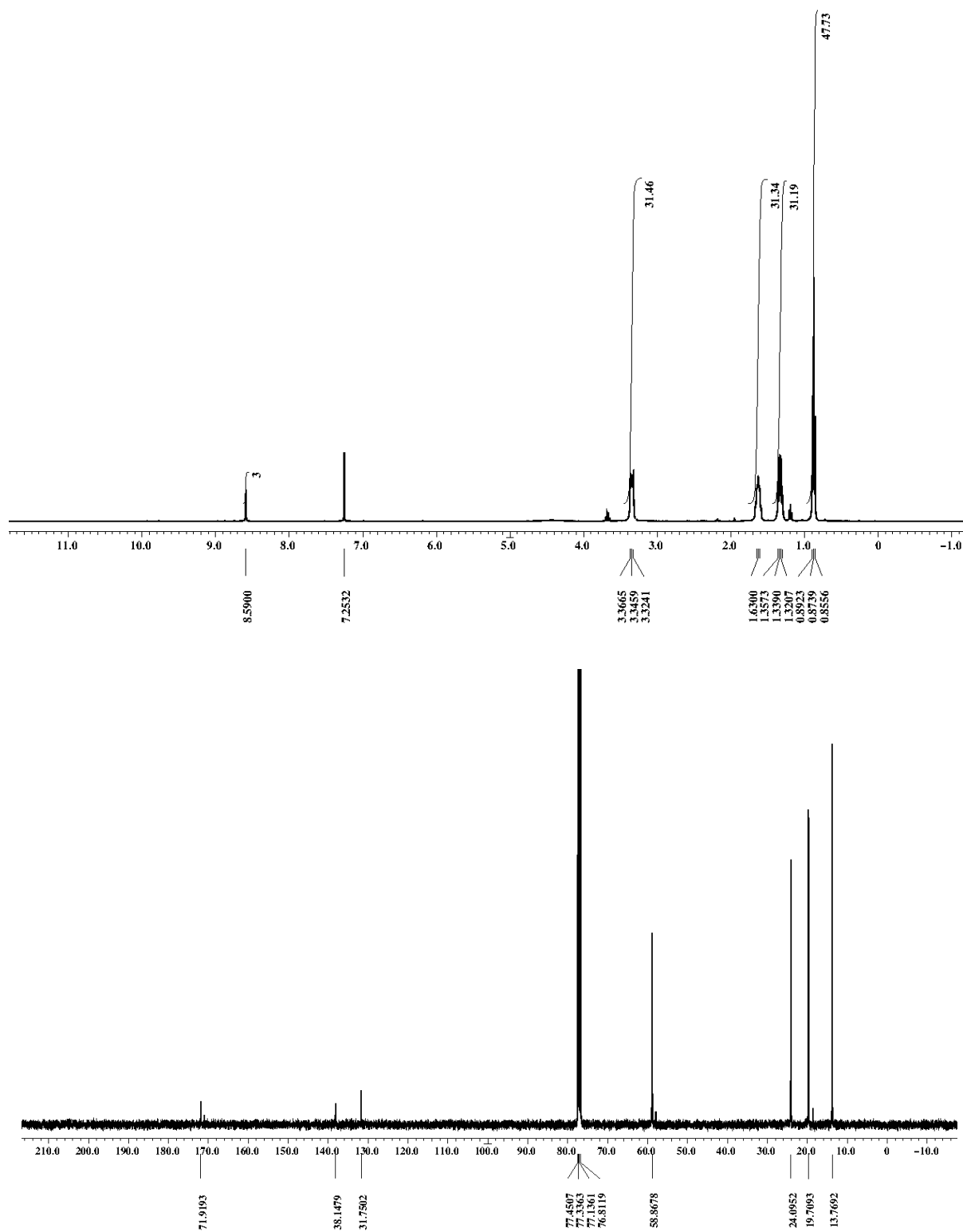
Appendix II-NMR Spectra

Compound 257: ^1H NMR and ^{13}C NMR in CDCl_3



Appendix II-NMR Spectra

Compound **258**: ^1H NMR and ^{13}C NMR in CDCl_3



Bibliography

- [1] V. Coropceanu, J. Vornil, D. A. da Silva Filho, Y. Olivier, R. Silbey, J.-L. Brédas, *Chem. Rev.* **2007**, *107*, 926–952. 'Charge Transport in Organic Semiconductors'.
- [2] S. R. Marder, *J. Mater. Chem.* **2009**, *19*, 7392–7393. 'Themed Issue: Nonlinear Optics. The Evolving Field of Nonlinear Optics—a Personal Perspective'.
- [3] A. C. Grimsdale, K. Leok Chan, R. E. Martin, P. G. Jokisz, A. B. Holmes, *Chem. Rev.* **2009**, *109*, 897–1091. 'Synthesis of Light-Emitting Conjugated Polymers for Applications in Electroluminescent Devices'.
- [4] M. B. Nielsen, F. Diederich, *Chem. Rev.* **2005**, *105*, 1837–1867. 'Conjugated Oligoenynes Based on the Diethynylethene Unit'.
- [5] Y. Huang, L. Huo, S. Zhang, X. Guo, C. C. Han, Y. Li, J. Hou, *Chem. Commun.* **2011**, *47*, 8904–8906. 'Sulfonyl: A New Application of Electron-withdrawing Substituent in Highly Efficient Photovoltaic Polymer'.
- [6] C. A. Cutler, A. K. Burrell, D. L. Officer, C. O. Too, G. G. Wallace, *Synth. Met.* **2002**, *128*, 35–42. 'Effect of Electron Withdrawing or Donating Substituents on the Photovoltaic Performance of Polythiophenes'.
- [7] Y. Liang, D. Feng, Y. Wu, S. Tsai, G. Li, C. Ray, L. Yu, *J. Am. Chem. Soc.* **2009**, *131*, 7792–7799. 'Highly Efficient Solar Cell Polymers Developed via Fine-Tuning of Structural and Electronic Properties'.
- [8] G. Daoust, M. Leclerc, *Macromolecules* **1991**, *24*, 455–459. 'Structure-Property Relationships in Alkoxy-Substituted Polythiophenes'.
- [9] W. Jiang, H. Qian, Y. Li, Z. Wang, *J. Org. Chem.* **2008**, *73*, 7369–7372. 'Heteroatom-Annulated Perylenes: Practical Synthesis, Photophysical Properties, and Solid-State Packing Arrangement'.
- [10] R. N. Grimes, *Chem. Rev.* **1992**, *92*, 251–268. 'Boron-Carbon Ring Ligands in Organometallic Synthesis'.
- [11] N. Miyaura, A. Suzuki, *Chem. Rev.* **1995**, *95*, 2457–2483. 'Palladium-Catalyzed Cross-Coupling Reactions of Organoboron Compounds'.
- [12] W. Kaim, N. S. Hosmane, *J. Chem. Sci.* **2010**, *122*, 7–18. 'Multidimensional Potential of Boron-containing Molecules in Functional Materials'.
- [13] F. Issa, M. Kassiou, L. M. Rendina, *Chem. Rev.* **2011**, *111*, 5701–5722. 'Boron in Drug Discovery: Carboranes as Unique Pharmacophores in Biologically Active Compounds'.
- [14] E. D. Jemmis, E. G. Jayasree, *Acc. Chem. Res.* **2003**, *36*, 816–824. 'Analogies Between Boron and Carbon'.
- [15] S. Kervyn, C. Aurisicchio, D. Bonifazi 'Synthesis and Design of π -Conjugated Organic Architectures Doped with Heteroatoms'. In 'Functional Supramolecular Architectures: for Organic Electronics and Nanotechnology'.; Samorì, P.; Cacialli, F., Eds.; Wiley, 2010; pp. 233–277.
- [16] T. W. Hudnall, C.-W. Chiu, F. P. Gabbai, *Acc. Chem. Res.* **2009**, *42*, 388–397. 'Fluoride Ion Recognition by Chelating and Cationic Boranes'.
- [17] Z. M. Hudson, S. Wang, *Acc. Chem. Res.* **2009**, *42*, 1584–1596. 'Impact of Donor-Acceptor Geometry and Metal Chelation on Photophysical Properties and Applications of Triarylboranes'.
- [18] M. F. Hawthorne, A. Maderna, *Chem. Rev.* **1999**, *99*, 3421–3434. 'Applications of Radiolabeled Boron Clusters to the Diagnosis and Treatment of Cancer'.
- [19] S. Wang, *Coord. Chem. Rev.* **2001**, *215*, 79–98. 'Luminescence and Electroluminescence of Al(III), B(III), Be(II) and Zn(II) Complexes with Nitrogen Donors'.

Bibliography

- [20] C. D. Entwistle, T. B. Marder, *Chem. Mater.* **2004**, *16*, 4574–4585. 'Applications of Three-Coordinate Organoboron Compounds and Polymers in Optoelectronics'.
- [21] S. Yamaguchi, S. Akiyama, K. Tamao, *J. Am. Chem. Soc.* **2001**, *123*, 11372–11375. 'Colorimetric Fluoride Ion Sensing by Boron-containing π -Electron Systems'.
- [22] C. Branger, M. Lequan, R. M. Lequan, M. Barzoukas, A. Fortb, *J. Mater. Chem.* **1996**, *6*, 555–558. 'Boron Derivatives Containing a Bithiophene Bridge as new Materials for Non-linear Optics'.
- [23] M. Lequan, R. M. Lequan, K. C. Ching, M. Barzoukas, A. Fort, H. Lahoucine, G. Bravic, D. Chasseau, J. Gaultier, *J. Mater. Chem.* **1992**, *2*, 719–725. 'Crystal Structures and Non-linear Optical Properties of Borane Derivatives'.
- [24] L. Yang, S. Jiang, Y. Zhao, L. Zhu, S. Chen, X. Wang, Q. Wu, J. Ma, Y. Ma, Z. Hu, *Angew. Chem. Int. Ed.* **2011**, *50*, 7132–7135. 'Boron-doped Carbon Nanotubes as Metal-free Electrocatalysts for the Oxygen Reduction Reaction'.
- [25] A. J. Ashe, E. Meyers, P. Shu, T. Von Lehmann, J. Bastide, *J. Am. Chem. Soc.* **1975**, *97*, 6865–6866. 'Bis(1-substituted-borabenzene)iron Complexes'.
- [26] A. J. Ashe, X. Fang, J. W. Kampf, *Organomet. Chem.* **1999**, *18*, 466–473. 'Synthesis and Properties of 1-Substituted 1-Boratanaphthalenes'.
- [27] C. Fan, W. E. Piers, M. Parvez, *Angew. Chem. Int. Ed.* **2009**, *48*, 2955–2958. 'Perfluoropentaphenylborole'.
- [28] J. J. Eisch, J. E. Galles, B. Shafih, A. L. Rheingoldt, *Organomet.* **1990**, *9*, 2342–2349. 'Thermal Generation and Transformation of the Borepin Ring'.
- [29] B. Y. Lee, S. Wang, M. Putzer, G. P. Bartholomew, X. Bu, G. C. Bazan, *J. Am. Chem. Soc.* **2000**, *122*, 3969–3970. 'Borastilbene : Synthesis , Structural Characterization , and Photophysics'.
- [30] T. K. Wood, W. E. Piers, B. A. Keay, M. Parvez, *Angew. Chem. Int. Ed.* **2009**, *48*, 4009–4012. '9-Boraanthracene Derivatives Stabilized by N-heterocyclic Carbenes'.
- [31] A. Lorbach, M. Bolte, H. Li, H.-W. Lerner, M. C. Holthausen, F. Jäkle, M. Wagner, *Angew. Chem. Int. Ed.* **2009**, *48*, 4584–4588. '9,10-Dihydro-9,10-diboraanthracene: Supramolecular Structure and use as a Building Block for Luminescent Conjugated Polymers'.
- [32] L. Ci, L. Song, C. Jin, D. Jariwala, D. Wu, Y. Li, A. Srivastava, Z. F. Wang, K. Storr, L. Balicas, F. Liu, P. M. Ajayan, *Nat. Mater.* **2010**, *9*, 430–435. 'Atomic Layers of Hybridized Boron Nitride and Graphene Domains'.
- [33] S. Wang, E. Iyyamperumal, A. Roy, Y. Xue, D. Yu, L. Dai, *Angew. Chem. Int. Ed.* **2011**, *50*, 11756–11760. 'Vertically Aligned BCN Nanotubes as Efficient Metal-Free Electrocatalysts for the Oxygen Reduction Reaction: A Synergetic Effect by Co-Doping with Boron and Nitrogen'.
- [34] M. J. D. Bosdet, C. A. Jaska, W. E. Piers, T. S. Sorensen, M. Parvez, *Org. Lett.* **2007**, *9*, 1395–1398. 'Blue Fluorescent 4a-Aza-4b-boraphenanthrenes'.
- [35] A. J. V. Marwitz, A. N. Lamm, L. N. Zakharov, M. Vasiliu, D. A. Dixon, S.-Y. Liu, *Chem. Sci.* **2012**, *3*, 825–829. 'BN-substituted Diphenylacetylene: a Basic Model for Conjugated π -systems Containing the BN Bond Pair'.
- [36] M. Côté, P. D. Haynes, C. Molteni, *J. Phys.: Condens. Matter* **2002**, *14*, 9997–10009. 'Material Design from First Principles : the Case of Boron Nitride Polymers'.
- [37] M. Goursaud, P. De Bernardin, A. Dalla Cort, K. Bartik, G. Bruylants, *Eur. J. Org. Chem.* **2012**, *2012*, 3570–3574. 'Monitoring Fluoride Binding in DMSO: Why is a Singular Binding Behavior Observed?'.
- [38] X. Y. Liu, D. R. Bai, S. Wang, *Angew. Chem. Int. Ed.* **2006**, *45*, 5475–5478. 'Charge-Transfer Emission in Nonplanar Three- Coordinate Organoboron Compounds for Fluorescent Sensing of Fluoride'.

Bibliography

- [39] W. L. Jia, X. D. Feng, D. R. Bai, Z. H. Lu, S. Wang, G. Vamvounis, *Chem. Mater.* **2005**, *17*, 164–170. 'Mes2B (p-4,4'-biphenyl-NPh(1-naphthyl)): A Multifunctional Molecule for Electroluminescent Devices'.
- [40] D. R. Bai, X. Y. Liu, S. Wang, *Chem. Eur. J.* **2007**, *13*, 5713–5723. 'Charge-Transfer Emission Involving Three-Coordinate Organoboron: V-Shape versus U-Shape and Impact of the Spacer on Dual Emission and Fluorescent Sensing'.
- [41] A. Pron, G. Zhou, H. Norouzi-arasi, M. Baumgarten, K. Müllen, *Org. Lett.* **2009**, *11*, 3550–3553. 'Controlling the Charge Transfer in π -Conjugated Systems'.
- [42] R. Stahl, C. Lambert, C. Kaiser, R. Wortmann, R. Jakober, *Chem. Eur. J.* **2006**, *12*, 2358–2370. 'Electrochemistry and Photophysics of Donor-Substituted Triarylboranes: Symmetry Breaking in Ground and Excited State'.
- [43] G. Zhou, M. Baumgarten, K. Müllen, *J. Am. Chem. Soc.* **2008**, *130*, 12477–12484. 'Mesitylboron-Substituted Ladder-Type Pentaphenylenes: Charge-Transfer, Electronic Communication, and Sensing Properties'.
- [44] S. Yamaguchi, S. Akiyama, K. Tamao, *J. Am. Chem. Soc.* **2000**, *122*, 6335–6336. 'Tri-9-anthrylborane and Its Derivatives: New Boron-Containing π -Electron Systems with Divergently Extended π -Conjugation through Boron'.
- [45] Y. Kim, H. Zhao, F. P. Gabbaï, *Angew. Chem. Int. Ed.* **2009**, *48*, 4957–4960. 'Sulfonium Boranes for the Selective Capture of Cyanide Ions in Water'.
- [46] T. W. Hudnall, P. Gabbaï, *J. Am. Chem. Soc.* **2007**, *129*, 11978–11986. 'Ammonium Boranes for the Selective Complexation of Cyanide or Fluoride Ions in Water'.
- [47] S. M. Levonis, M. J. Kiefel, T. A. Houston, *Chem. Commun.* **2009**, 2278–2280. 'Boronolectin with Divergent Fluorescent Response Specific for Free Sialic Acid'.
- [48] H. Li, F. Jäkle, *Angew. Chem. Int. Ed.* **2009**, *48*, 2313–2316. 'Universal Scaffold for Fluorescent Conjugated Organoborane Polymers'.
- [49] M. Elbing, G. C. Bazan, *Angew. Chem. Int. Ed.* **2008**, *47*, 834–838. 'A New Design Strategy for Organic Optoelectronic Materials by Lateral Boryl Substitution'.
- [50] D. Reitzenstein, C. Lambert, *Macromolecules* **2009**, *42*, 773–782. 'Localized versus Backbone Fluorescence in N-p-(Diarylboryl)phenyl-Substituted 2,7- and 3,6-Linked Polycarbazoles'.
- [51] A. Sundararaman, M. Victor, R. Varughese, F. Jäkle, *J. Am. Chem. Soc.* **2005**, *127*, 13748–13749. 'A Family of Main-Chain Polymeric Lewis Acids: Synthesis and Fluorescent Sensing Properties of Boron-Modified Polythiophenes'.
- [52] T. Renk, W. Ruf, W. Siebert, W. Rulf, *J. Organomet. Chem.* **1976**, *120*, 1–25. 'Metallocenylborane III. Darstellung und eigenschaften von ferrocenyl- und cymantrenylboranen'.
- [53] J. B. Heilmann, M. Scheibitz, Y. Qin, A. Sundararaman, F. Jäkle, T. Kretz, M. Bolte, H. Lerner, M. C. Holthausen, M. Wagner, *Angew. Chem. Int. Ed.* **2006**, *45*, 920–925. 'A Synthetic Route to Borylene-Bridged Poly(ferrocenylene)s'.
- [54] M. Scheibitz, J. W. Bats, M. Bolte, H. Lerner, M. Wagner, *Organomet.* **2004**, *23*, 940–942. 'Ferrocenylborane-Amine and Monomeric Diferrocenylborane: Novel Organometallic Hydroborating Reagents'.
- [55] C. Bresner, S. Aldridge, I. A. Fallis, C. Jones, L.-L. Ooi, *Angew. Chem. Int. Ed.* **2005**, *44*, 3606–3609. 'Selective Electrochemical Detection of Hydrogen Fluoride by Amphiphilic Ferrocene Derivatives'.
- [56] G. Marr, R. E. Moore, B. W. Rockett, *J. Chem. Soc. C* **1968**, 24–27. 'Unsymmetrically Disubstituted Ferrocenes. Part IV. The Synthesis and Reactivity of 2-(NN-Dimethylaminomethyl)ferroceneboronic acid'.
- [57] J. Chen, J. W. Kampf, A. J. Ashe, *Organomet.* **2008**, *27*, 3639–3641. 'Syntheses and Structures of 6, 13-Dihydro-6,13-diborapentacenes: π -Stacking in Heterocyclic Analogues of Pentacene'.

Bibliography

- [58] A. J. Ashe, P. Shu, *J. Am. Chem. Soc.* **1971**, *93*, 1804–1805. '*1-Phenylborabenzene Anion*'.
- [59] G. C. Bazan, G. Rodriguez, A. J. Ashe, S. Al-Ahmad, C. Müller, *J. Am. Chem. Soc.* **1996**, *118*, 2291–2292. '*Aminoboratabenzene Derivatives of Zirconium : A New Class of Olefin Polymerization Catalysts*'.
- [60] X. Zheng, B. Wang, G. E. Herberich, *Organomet.* **2002**, *21*, 1949–1954. '*Borabenzene Adducts of Ylidic Lewis Bases. Syntheses and Structures of 3,5-Me₂C₅H₃BCH₂PPh₃, 3,5-Me₂C₅H₃BCH(SiMe₃)PPh₃, and C₅H₅BN(Ph)PPh₃*'.
- [61] J. Tweddell, D. A. Hoic, G. C. Fu, *J. Org. Chem.* **1997**, *62*, 8286–8287. '*First Synthesis and Structural Characterization of an Enantiomerically Pure Planar-Chiral Lewis Acid Complex*'.
- [62] B. Y. Lee, G. C. Bazan, *J. Organomet. Chem.* **2002**, *642*, 275–279. '*Zirconocene Compounds Derived from Boratastilbene, 4-Boratastyrylstilbene, and 1,4-bis(boratastyryl)benzene and their Reactivities to the Ethylene Polymerization*'.
- [63] B. Y. Lee, G. C. Bazan, *J. Am. Chem. Soc.* **2000**, *122*, 8577–8578. '*1,4-Bis(boratastyryl)benzene : Synthesis, Structural Characterization, and Photophysics*'.
- [64] G. E. Herberich, E. Cura, J. Ni, *Inorg. Chem. Commun.* **1999**, *2*, 503–506. '*A New Synthetic Route to 2-Boratanaphthalenes*'.
- [65] A. J. Ashe, W. Klein, R. Rousseau, *Organomet.* **1993**, *12*, 3225–3231. '*Borepin Aromaticity*'.
- [66] A. Caruso, J. D. Tovar, *J. Org. Chem.* **2011**, *76*, 2227–2239. '*Functionalized Dibenzoborepins as Components of Small Molecule and Polymeric π -Conjugated Electronic Materials*'.
- [67] A. Caruso, J. D. Tovar, *Org. Lett.* **2011**, *13*, 3106–3109. '*Conjugated "B-entacenes": Polycyclic Aromatics Containing Two Borepin Rings*'.
- [68] J. Eisch, John, J. E. Galle, *J. Am. Chem. Soc.* **1975**, *97*, 4436–4437. '*The Synthesis of Heptaphenylborepin via the Thermal Rearrangement of Heptaphenyl-7-borabicyclo[2.2.1]heptadiene*'.
- [69] H. Braunschweig, I. Fernandez, G. Frenking, T. Kupfer, *Angew. Chem. Int. Ed.* **2008**, *47*, 1951–1954. '*Structural Evidence for Antiaromaticity in Free Boroles*'.
- [70] C. So, D. Watanabe, A. Wakamiya, S. Yamaguchi, *Organomet.* **2008**, *27*, 3496–3501. '*Synthesis and Structural Characterization of Pentaarylboroles and Their Dianions*'.
- [71] J. Wu, M. Baumgarten, M. G. Debije, J. M. Warman, K. Müllen, *Angew. Chem. Int. Ed.* **2004**, *43*, 5331–5335. '*Arylamine-substituted hexa-peri-hexabenzocoronenes: facile synthesis and their potential applications as "coaxial" hole-transport materials*'.
- [72] M. J. D. Bosdet, W. E. Piers, T. S. Sorensen, M. Parvez, *Angew. Chem. Int. Ed.* **2007**, *46*, 4940–4943. '*10a-Aza-10b-borapyrenes: Heterocyclic Analogues of Pyrene with Internalized BN Moieties*'.
- [73] A. J. V Marwitz, M. H. Matus, L. N. Zakharov, D. A. Dixon, S.-Y. Liu, *Angew. Chem. Int. Ed.* **2009**, *48*, 973–937. '*A Hybrid Organic/Inorganic Benzene*'.
- [74] C. A. Jaska, W. E. Piers, R. McDonald, M. Parvez, *J. Org. Chem.* **2007**, *72*, 5234–5243. '*Synthesis, Characterization, and Fluorescence Behavior of Twisted and Planar B₂N₂-Quaterphenyl Analogues*'.
- [75] C. A. Jaska, D. J. H. Emslie, M. J. D. Bosdet, W. E. Piers, T. S. Sorensen, M. Parvez, *J. Am. Chem. Soc.* **2006**, *128*, 10885–10896. '*Triphenylene Analogues with B₂N₂C₂ Cores: Synthesis, Structure, Redox Behavior, and Photophysical Properties*'.
- [76] J. Pan, J. W. Kampf, A. J. Ashe, *Organomet.* **2006**, *25*, 197–202. '*Switchable Haptotropic Migrations of Tricarbonylchromium Complexes of 1,2-Dihydro-2-phenyl-1,2-azaborine*'.

Bibliography

- [77] J. Pan, J. W. Kampf, A. J. Ashe, *Org. Lett.* **2007**, *9*, 679–681. 'Electrophilic Aromatic Substitution Reactions of 1,2-Dihydro-1,2-azaborines.'
- [78] X. Fang, H. Yang, J. W. Kampf, M. M. Banaszak Holl, A. J. Ashe, *Organomet.* **2006**, *25*, 513–518. 'Syntheses of Ring-Fused B–N Heteroaromatic Compounds'.
- [79] M. J. S. Dewar, V. P. Kubba, R. Pettit, *J. Chem. Soc.* **1958**, 3073–3076. 'New Heteroaromatic Compounds. Part I. 9-Aza-10-boraphenanthrene'.
- [80] R. Carion, V. Liégeois, B. Champagne, D. Bonifazi, S. Pelloni, P. Lazzeretti, *J. Phys. Chem. Lett.* **2010**, *1*, 1563–1568. 'On the Aromatic Character of 1,2-Dihydro-1,2-azaborine According to Magnetic Criteria'.
- [81] M. Kranz, T. Clark, *J. Org. Chem.* **1992**, *57*, 5492–5500. 'Azaborines: An ab Initio Study'.
- [82] A. J. Ashe, T. R. Diephouse, M. Y. El-sheikh, *J. Am. Chem. Soc.* **1982**, *88*, 5693–5699. 'Stabilization of Stibabenzene and Bismabenzene by 4-Alkyl Substituents'.
- [83] J. Chen, Z. Bajko, J. W. Kampf, A. J. Ashe, *Organomet.* **2007**, *26*, 1563–1564. '1,2-Dihydro-1,2-oxaborin: A Boron-Oxygen Heterocycle Isoelectronic with Benzene'.
- [84] A. J. Ashe III, *Organomet.* **2009**, *28*, 4236–4248. 'Aromatic Borataheterocycles : Surrogates for Cyclopentadienyl in Transition-Metal Complexes'.
- [85] S. Xu, L. N. Zakharov, S.-Y. Liu, *J. Am. Chem. Soc.* **2011**, *133*, 20152–20155. 'A 1,3-dihydro-1,3-azaborine debuts.'
- [86] M. Kranz, F. Hampel, T. Clark, *J. Chem. Soc., Chem. Commun.* **1992**, 1247–1248. 'N-Methyl-B-mesityldibenzo-1,4-azaborine: the First Experimental Structure of a 1,4-Azaborinine Derivative'.
- [87] H. Braunschweig, A. Damme, J. O. C. Jimenez-Halla, B. Pfaffinger, K. Radacki, J. Wolf, *Angew. Chem. Int. Ed.* **2012**, *51*, 10034–10037. 'Metal-Mediated Synthesis of 1,4-Di-tert-butyl-1,4-azaborine'.
- [88] L. J. Liu, A. J. V Marwitz, B. W. Matthews, S. Y. Liu, *Angew. Chem. Int. Ed.* **2009**, *48*, 6817–6819. 'Boron Mimetics: 1,2-Dihydro-1,2-azaborines Bind inside a Nonpolar Cavity of T4 Lysozyme'.
- [89] P. G. Campbell, E. R. Abbey, D. Neiner, D. J. Grant, D. A. Dixon, S.-Y. Liu, *J. Am. Chem. Soc.* **2010**, *132*, 18048–18050. 'Resonance Stabilization Energy of 1,2-Azaborines: A Quantitative Experimental Study by Reaction Calorimetry'.
- [90] P. G. Campbell, L. N. Zakharov, D. J. Grant, D. A. Dixon, S.-Y. Liu, *J. Am. Chem. Soc.* **2010**, *132*, 3289–3291. 'Hydrogen Storage by Boron-Nitrogen Heterocycles: A Simple Route for Spent Fuel Regeneration'.
- [91] E. R. Abbey, L. N. Zakharov, S.-Y. Y. Liu, *J. Am. Chem. Soc.* **2008**, *130*, 7250–7252. 'Crystal Clear Structural Evidence for Electron Delocalization in 1,2-Dihydro-1,2-azaborines'.
- [92] A. N. Lamm, E. B. Garner, D. A. Dixon, S.-Y. Liu, *Angew. Chem. Int. Ed.* **2011**, *50*, 8157–8160. 'Nucleophilic Aromatic Substitution Reactions of 1,2-Dihydro-1,2-Azaborine'.
- [93] A. J. V Marwitz, E. R. Abbey, J. T. Jenkins, L. N. Zakharov, *Org. Lett.* **2007**, *9*, 4905–4908. 'Diversity through Isosterism : The Case of Boron-Substituted'.
- [94] K. M. Waggoner, P. P. Power, *J. Am. Chem. Soc.* **1991**, *113*, 3385–3393. 'Reactions of Trimethylaluminum or Trimethylgallium with Bulky Primary Amines: Structural Characterization of the Thermolysis Products'.
- [95] A. B. Burg, P. J. Slota, *J. Am. Chem. Soc.* **1960**, *82*, 2148–2151. 'Chemistry of the C₄H₈P Ring: the Aminophosphine (CH₃)₂NPC₄H₈, the Cyclophosphine C₄H₈PH and the Tetracyclic Trimer (C₄H₈PBH₂)₃'.

Bibliography

- [96] R. A. Bartlett, H. V. R. Dias, X. Feng, P. P. Power, *J. Am. Chem. Soc.* **1989**, *111*, 1306–1311. 'Synthesis and Spectroscopic and X-ray Structural Characterization of Compounds Involving Boron-Phosphorus Multiple Bonds: Lithium Salts of Boryl Phosphides and Their Precursors'.
- [97] H. V. R. Dias, P. P. Power, *J. Am. Chem. Soc.* **1989**, *111*, 144–148. 'Boron-Phosphorus Analogues of Benzene and Cyclobutadiene. Synthesis and Characterization of the Boraphosphabenzenes (RBPR)₃ (R = Mes, Ph; R' = Ph, Mes, C₆H₁₁, t-Bu) and the diphosphadiboretane (ThexylBPMes)₂'.
- [98] A. Stock, E. Pohland, *Ber. Dtsch. Chem. Ges.* **1926**, *59B*, 2215–2223. 'Borwasserstoffe, IX.: B₃N₃H₆'.
- [99] A. Y. Timoshkin, G. Frenking, *Inorg. Chem.* **2003**, *42*, 60–69. '"True" Inorganic Heterocycles: Structures and Stability of Group 13-15 Analogues of Benzene and their Dimers'.
- [100] R. Boese, A. H. Maulitz, P. Stellberg, *Chem. Ber.* **1994**, *127*, 1887–1889. 'Solid-State Borazine: Does it Deserve to be Entitled "Inorganic Benzene"?'.
- [101] E. D. Jemmis, B. Kiran, *Inorg. Chem.* **1998**, *37*, 2110–2116. 'Aromaticity in X₃Y₃H₆ (X = B, Al, Ga; Y = N, P, As), X(3)Z(3)H(3) (Z = O, S, Se), and Phosphazenes. Theoretical Study of the Structures, Energetics, and Magnetic Properties'.
- [102] J. P. Doering, A. Gedanken, A. P. Hitchcock, P. Fischer, J. Moore, J. K. Olthoff, J. Tossel, K. Raghavachari, M. B. Robin, *J. Am. Chem. Soc.* **1986**, *108*, 3602–3608. 'Electronic Excitation and π -Electron Interaction in Borazine'.
- [103] J. A. Tossell, J. H. Moore, K. McMillan, C. K. Subramaniam, M. A. Coplan, *J. Am. Chem. Soc.* **1992**, *114*, 1114–1115. 'The Electron Momentum Density in the Highest Energy Occupied Molecular-Orbital of Borazine, B₃n₃h₆ - Evidence for Localization'.
- [104] T. B. Jones, J. P. Maier, O. Marthaler, *Inorg. Chem.* **1979**, *18*, 2140–2142. 'Emission Spectrum of Tri-B-fluoroborazine Radical Cation in the Gas Phase: a₂A₂" \rightarrow X₂E" Band System'.
- [105] V. V. Pokropivny, V. L. Bekenev, *Semiconductors* **2006**, *40*, 636–641. 'Electronic Properties and Bulk Moduli of New Boron Nitride Polymorphs, i.e., Hyperdiamond B₁₂N₁₂ and Simple Cubic B₂₄N₂₄, B₁₂N₁₂ Fulborenites'.
- [106] B. Toury, C. Duriez, D. Cornu, P. Miele, C. Vincent, M. Vaultier, B. Bonnetot, *J. Solid State Chem.* **2000**, *154*, 137–140. 'Influence of Molecular Precursor Structure on the Crystallinity of Boron Nitride'.
- [107] E. Framery, M. Vaultier, *Heteroat. Chem.* **2000**, *11*, 218–225. 'Efficient Synthesis and NMR Data of N- or B-Substituted Borazines'.
- [108] D. Cornu, P. Miele, B. Toury, B. Bonnetot, H. Mongeot, J. Bouix, *J. Mater. Chem.* **1999**, *9*, 2605–2610. 'Boron Nitride Matrices and Coatings from Boryl Borazine Molecular Precursors'.
- [109] C. Zhi, Y. Bando, T. Terao, C. Tang, H. Kuwahara, D. Golberg, *Adv. Funct. Mater.* **2009**, *19*, 1857–1862. 'Towards Thermoconductive, Electrically Insulating Polymeric Composites with Boron Nitride Nanotubes as Fillers'.
- [110] O. R. Lourie, C. R. Jones, B. M. Bartlett, P. C. Gibbons, R. S. Ruoff, W. E. Buhro, *Chem. Mater.* **2000**, *12*, 1808–1810. 'CVD Growth of Boron Nitride Nanotubes'.
- [111] B. Zhong, X. Huang, G. Wen, L. Xia, H. Yu, H. Bai, *J. Phys. Chem. C* **2010**, *114*, 21165–21172. 'Preparation and Ultraviolet-Visible Luminescence Property of Novel BN Whiskers with a Cap-Stacked Structure'.
- [112] K. Watanabe, T. Taniguchi, H. Kanda, *Nat. Mater.* **2004**, *3*, 404–409. 'Direct-Bandgap Properties and Evidence for Ultraviolet Lasing of Hexagonal Boron Nitride Single Crystal'.
- [113] K. Watanabe, T. Taniguchi, T. Niiyama, K. Miya, M. Taniguchi, *Nat. Photonics* **2009**, *3*, 591–594. 'Far-Ultraviolet Plane-Emission Handheld Device Based on Hexagonal Boron Nitride'.
- [114] A. Khan, K. Balakrishnan, T. Katona, *Nat. Photonics* **2008**, *2*, 77–84. 'Ultraviolet Light-Emitting Diodes Based on Group Three Nitrides'.

Bibliography

- [115] C. E. Nebel, *Nat. Photonics* **2009**, 3, 564–566. 'Light Sources: Tackling the Deep Ultraviolet'.
- [116] A. Stock, E. Wiberg, H. Martini, *Ber. Dtsch. Chem. Ges.* **1930**, 63B, 2927–2936. 'Borwasserstoffe, XIV.: Zur Kenntnis des B₄H₁₀'.
- [117] J. Kroner, D. Proch, W. Fuss, H. Bock, *Tetrahedron* **1972**, 28, 1585–1600. 'Ionisierungs und Anregungsenergien Methyl und Fluor-Substituierter Borazine'.
- [118] C. A. Jaska, K. Temple, A. J. Lough, I. Manners, *J. Am. Chem. Soc.* **2003**, 125, 9424–9434. 'Transition Metal-Catalyzed Formation of Boron-Nitrogen Bonds: Catalytic Dehydrocoupling of Amine-Borane Adducts to Form Aminoboranes and Borazines'.
- [119] T. E. Reich, K. T. Jackson, S. Li, P. Jena, H. M. El-Kaderi, *J. Mater. Chem.* **2011**, 21, 10629–10632. 'Synthesis and Characterization of Highly Porous Borazine-Linked Polymers and their Performance in Hydrogen Storage Application'.
- [120] K. T. Jackson, M. G. Rabbani, T. E. Reich, H. M. El-Kaderi, *Polym. Chem.* **2011**, 2, 2775–2777. 'Synthesis of Highly Porous Borazine-Linked Polymers and their Application to H₂, CO₂, and CH₄ Storage'.
- [121] W. Luo, P. G. Campbell, L. N. Zakharov, S.-Y. Liu, *J. Am. Chem. Soc.* **2011**, 133, 19326–1939. 'A Single-Component Liquid-Phase Hydrogen Storage Material'.
- [122] A. Wakamiya, T. Ide, S. Yamaguchi, *J. Am. Chem. Soc.* **2005**, 127, 14859–14866. 'Toward π -Conjugated Molecule Bundles: Synthesis of a Series of B,B',B"-Trianthryl-N,N',N"-triarylborazines and the Bundle Effects on their Properties'.
- [123] C. A. Brown, A. W. Laubengayer, *J. Am. Chem. Soc.* **1955**, 77, 3699–3700. 'B-Trichloroborazole'.
- [124] H. Watanabe, T. Totani, T. Yoshizaki, *Inorg. Chem.* **1965**, 4, 657–660. 'Preparation and Conformation of B-Triethynylborazine Derivatives'.
- [125] F. Cheng, B. Toury, S. J. Archibald, J. S. Bradley, *J. Organomet. Chem.* **2002**, 657, 71–74. 'Synthesis and structure of 2,4,6-tris[tris(dimethylamino)silylamino] borazine'.
- [126] E. A. Rojo, G. J. Videla, M. A. Molinari, O. A. Lires, L. H. Casas, *Int. J. Appl. Radiat. Isot.* **1964**, 15, 611–616. 'Borazarenes and Borazole. Fluorescence spectrometry and Quantum Efficiencies in Relation to Slow Neutron Counting'.
- [127] M. A. Molinari, A. E. Rojo, G. J. Videla, *IEEE Trans. Nucl. Sci.* **1967**, 14, 393–401. 'Borazine and Borazarene Derivatives as Scintillators'.
- [128] I. H. T. Sham, C. C. Kwok, C. M. Che, N. Y. Zhu, *Chem. Commun.* **2005**, 3547–3549. 'Borazine Materials for Organic Optoelectronic Applications'.
- [129] P. Paetzold, R. Truppat, *Chem. Ber.* **1983**, 116, 1531–1539. 'Borimide beim thermischen Zerfall der Diarylazidoborane'.
- [130] W. Fraenk, T. M. Klapötke, B. Krumm, H. Nöth, M. Suter, M. Warchhold, *J. Chem. Soc., Dalton Trans.* **2000**, 4635–4638. 'Oligomeric Pentafluorophenylboron Azides'.
- [131] H. J. Emeléus, K. Wade, *J. Chem. Soc.* **1960**, 2614–2617. 'Reaction of Diborane with Volatile Cyanides'.
- [132] A. Meller, G. Beer, *Monatsh. Chem.* **1973**, 104, 1055–1063. 'Die Reaktion von Diboran mit 2-aminobenzonitril und 2-amino-1-cyclopenten-1-carbonsäurenitril'.
- [133] C. F. Lane, *Chem. Rev.* **1976**, 76, 773–799. 'Reduction of Organic Compounds with Diborane'.
- [134] K. M. Davies, M. J. S. Dewar, P. Rona, *J. Am. Chem. Soc.* **1967**, 89, 6294–6297. 'New Heteroaromatic Compounds XXVI. Synthesis of Borazarenes'.

Bibliography

- [135] R. J. Brotherton, H. Steinberg, *J. Org. Chem.* **1961**, 26, 4632–4634. 'Direct Preparation of Some Cyclic Boron-Nitrogen Compounds from Alkoxyborane'.
- [136] K. Pilgram, F. Korte, F. Kortb, *Tetrahedron* **1963**, 19, 137–141. 'Über Die Umsetzung von triarylphosphiten, triarylphosphoniten und triarylboraten mit aromatischen diaminen'.
- [137] R. H. Cragg, A. F. Weston, *J. Chem. Soc., Dalton Trans.* **1975**, 1761–1764. 'Organoboron Compounds. Part X. Polycyclic Borazines'.
- [138] R. H. Cragg, A. F. Weston, *J. Chem. Soc., Chem. Commun.* **1972**, 79–80. 'Thioboranes: Their Use in the Synthesis of Borazines'.
- [139] R. H. Cragg, A. F. Weston, *J. Chem. Soc., Dalton Trans.* **1975**, 93–95. 'Organoboron Compounds. Part IX. Synthesis and Properties of Some 2-Phenyl-1,3,2-oxazaborolans'.
- [140] T. Chivers, C. Fedorchuk, M. Parvez, *Acta Crystallogr. C* **2005**, 61, o47–o49. 'An Asymmetrically Substituted Borazine'.
- [141] Y. Lei, Y. Wang, Y. Song, C. Deng, *Ceram. Int.* **2011**, 37, 3005–3009. 'Novel Processable Precursor for BN by the Polymer-Derived Ceramics Route'.
- [142] Y. Ye, U. Graupner, R. Krüger, *Chem. Vapor Depos.* **2011**, 17, 221–227. 'Hexagonal Boron Nitride from a Borazine Precursor for Coating of SiBNC Fibers using a Continuous Atmospheric Pressure CVD Process'.
- [143] Y. Lei, Y. Wang, Y. Song, C. Deng, H. Wang, *Ceram. Int.* **2011**, 37, 1795–1800. 'Nearly Stoichiometric BN Fiber by Curing and Thermolysis of a Novel Poly[(alkylamino)borazine]'.
- [144] S. Frueh, R. Kellett, C. Mallery, T. Molter, W. S. Willis, C. King'ondou, S. L. Suib, *Inorg. Chem.* **2011**, 50, 783–792. 'Pyrolytic Decomposition of Ammonia Borane to Boron Nitride'.
- [145] D. L. Coursen, J. L. Hoard, *J. Am. Chem. Soc.* **1951**, 74, 1742–1750. 'The Structure of B-Trichloroborazole'.
- [146] K. Lonsdale, *Nature* **1959**, 184, 1060–1060. 'Intermolecular Distances and Diamagnetic Anisotropy in Crystals as Measures of the Polarity of Benzene and Borazole Substituents'.
- [147] A. W. Laubengayer, O. T. Beachley, R. F. Porter, *Inorg. Chem.* **1965**, 4, 578–582. 'The Reactions of Borazanaphthalene and Borazine with Anhydrous Hydrogen Bromide and Hydrogen Chloride'.
- [148] B. Chiavarino, M. E. Crestoni, S. Fornarini, *J. Am. Chem. Soc.* **1999**, 121, 2619–2620. 'Electrophilic Substitution of Gaseous Borazine'.
- [149] B. Chiavarino, M. E. Crestoni, A. Di Marzio, S. Fornarini, M. Rosi, *J. Am. Chem. Soc.* **1999**, 121, 11204–11210. 'Gas-phase Ion Chemistry of Borazine, an Inorganic Analogue of Benzene'.
- [150] R. I. Wagner, J. L. Bradford, I. Ross, *Inorg. Chem.* **1962**, 1, 93–97. 'Preparation of Some Unsymmetrically Substituted Borazines'.
- [151] H. Nöth, A. Troll, *Eur. J. Org. Chem.* **2005**, 2005, 3524–3535. 'The N-lithiation of 2,4,6-triphenylborazine'.
- [152] H. Nöth, B. Gemünd, R. T. Paine, *Eur. J. Inorg. Chem.* **2007**, 2007, 4282–4297. 'N-(2,4,6-Trimethylborazinyl)-Substituted Phosphanes, Arsanes, and Stibanes'.
- [153] P. J. Fazen, L. G. Sneddon, *Organomet.* **1994**, 13, 2867–2877. 'Transition Metal-Promoted Reactions of Boron Hydrides. 14. A New Synthetic Route to B-Substituted Mono-, Di-, and B-Alkylpolyborazylenes via Rhodium-Catalyzed Borazine/Olefin Hydroboration Reactions'.
- [154] K. Nagasawa, *Inorg. Chem.* **1966**, 5, 442–445. 'Borazines Stable to Hydrolysis'.

Bibliography

- [155] J. H. Smalley, F. Stafiej, *J. Am. Chem. Soc.* **1955**, *77*, 582–586. 'Organoboron Compounds. II. The B-Alkylation of N-Trisubstituted Borazole'.
- [156] H. C. Kelly, F. R. Marchelli, M. B. Giusto, *Inorg. Chem.* **1964**, *3*, 431–437. 'The Kinetics and Mechanism of Solvolysis of Amineboranes'.
- [157] R. G. Jones, C. R. Kinney, *J. Am. Chem. Soc.* **1939**, *61*, 1378–1381. 'Organoboron-Nitrogen Compounds. I. The Reaction of Boron Chloride with Aniline'.
- [158] H. Werner, R. Prinz, E. Deckelmann, *Chem. Ber.* **1969**, *102*, 95–103. 'Synthese und Eigenschaften von Hexaalkylborazolchromtricarbylen'.
- [159] H. Gottfried, K. Bernhard, *Angew. Chem. Int. Ed.* **1971**, *10*, 512–513. 'Crystal and Molecular Structure of Tricarbonyl(hexaethylborazine)chromium(0)'.
- [160] L. Li, A. Decken, B. G. Sayer, M. J. McGlinchey, P. Bregaint, J. Y. Thepot, L. Toupet, J. R. Hamon, C. Lapinte, *Organomet.* **1994**, *13*, 682–689. 'Multiple Fluxional Processes in Chiral (Pentaphenylcyclopentadienyl)iron Complexes: X-ray Crystal Structure of (C5Ph5)Fe(CO)(PMe3)(HC:O) and the Barriers to Aryl, Phosphine, and Tripodal Rotation in (C5Ph5)Fe(CO)(PMe2Ph)C(O)Er'.
- [161] N. L. Armanasco, M. V. Baker, M. R. North, B. W. Skelton, A. H. White, *J. Chem. Soc., Dalton Trans.* **1997**, 1363–1368. 'Chromium(0) Tricarbonyl Complexes of 1,3,5-Triazacyclohexanes'.
- [162] H. Koide, M. Uemura, *Tet. Lett.* **1999**, *40*, 3443–3446. 'Axially Chiral Benzamides: Diastereoselective Nucleophilic Additions to Planar Chiral (N, N-diethyl-2-acyl-6-methylbenzamide)chromium Complexes'.
- [163] P. Schreyer, P. Paetzold, R. Boeseb, *Chem. Ber.* **1988**, *121*, 195–205. 'Reaktionen der Cyclobutadien-homologen Diazadiboretidine'.
- [164] J. Münster, P. Paetzold, E. Schröder, H. Schwan, T. von Bennigsen-Mackiewicz, *Z. Anorg. Allg. Chem.* **2004**, *630*, 2641–2651. 'Cyclic Iminoboranes: Analogues of Cycloalkynes'.
- [165] G. R. Whittell, I. Manners, *Angew. Chem. Int. Ed.* **2011**, *50*, 10288–10289. 'Advances with Ammonia-Borane: Improved Recycling and Use as a Precursor to Atomically Thin BN Films'.
- [166] J. G. Morse, W. K. Glanville, *Inorg. Chem.* **1984**, *23*, 11–13. 'Dehydrohalogenation of Adducts of Dichloro(pentafluorophenyl)borane with Mesidine and p-Asidine: A Reinvestigation'.
- [167] S. Y. Shaw, R. H. Neilson, *Inorg. Chem.* **1994**, *33*, 3239–3245. 'Skeletally Stabilized Diborylamines: N-Boryl and N-Silyl Derivatives of the 1,3,2-Diazaboracyclohexane Ring System'.
- [168] Y. S. Shaw, D. A. Dubois, W. H. Watson, R. H. Neilson, *Inorg. Chem.* **1988**, *27*, 974–976. 'Boron-Nitrogen Polymer Precursors. Synthesis, Structure and Stereochemistry of N-Boryl Derivatives of the 1,3,2-Diazaboracyclohexane Ring System'.
- [169] J. R. Vance, A. P. M. Robertson, K. Lee, I. Manners, *Chem. Eur. J.* **2011**, *17*, 4099–4103. 'Photoactivated, Iron-Catalyzed Dehydrocoupling of Amine-Borane Adducts: Formation of Boron-Nitrogen Oligomers and Polymers'.
- [170] A. Staubitz, A. Presa Soto, I. Manners, *Angew. Chem. Int. Ed.* **2008**, *47*, 6212–6215. 'Iridium-Catalyzed Dehydrocoupling of Primary Amine-Borane Adducts: A Route to High Molecular Weight Polyaminoboranes, Boron-Nitrogen Analogues of Polyolefins'.
- [171] V. Pons, R. T. Baker, *Angew. Chem. Int. Ed.* **2008**, *47*, 9600–9602. 'Soluble Boron-Nitrogen High Polymers from Metal-Complex-Catalyzed Amine Borane Dehydrogenation'.
- [172] S. J. Groszos, S. F. Stafiej, *J. Am. Chem. Soc.* **1958**, *80*, 1357–1360. 'Organoboron Compounds. I. A New Synthesis of B-Trialkyl and Triaryl-N-triphenylborazoles'.
- [173] C. R. Kinney, M. J. Kolbezen, *J. Am. Chem. Soc.* **1942**, *64*, 1584–1585. 'Organoboron-Nitrogen Compounds. II. The Reaction of Boron Chloride with p-Toluidine'.

Bibliography

- [174] K. Niedenzu, J. W. Dawson, *J. Am. Chem. Soc.* **1959**, *81*, 5553–5555. 'Boron-Nitrogen Compounds. II.1,2 Aminoboranes, Part 1: The Preparation of Organic Substituted Aminoboranes through a Grignard Reaction'.
- [175] R. G. Jones, C. R. Kinney, *J. Am. Chem. Soc.* **1939**, *61*, 1378–1381. 'Organoboron-Nitrogen Compounds. I. The Reaction of Boron Chloride with Aniline'.
- [176] K. P. C. Vollhardt, *Acc. Chem. Res.* **1977**, *10*, 1–8. 'Transition-Metal-Catalyzed Acetylene Cyclizations in Organic Synthesis'.
- [177] P. V Schleyer, H. J. Jiao, N. Hommes, V. G. Malkin, O. L. Malkina, *J. Am. Chem. Soc.* **1997**, *119*, 12669–12670. 'An Evaluation of the Aromaticity of Inorganic Rings: Refined Evidence from Magnetic Properties'.
- [178] J. J. Engelberts, R. W. A. Havenith, J. H. van Lenthe, L. W. Jenneskens, P. W. Fowler, *Inorg. Chem.* **2005**, *44*, 5266–5272. 'The Electronic Structure of Inorganic Benzenes: Valence Bond and Ring-Current Descriptions'.
- [179] W. R. Nutt, M. L. McKeen, *Inorg. Chem.* **2007**, *46*, 7633–7645. 'Theoretical Study of Reaction Pathways to Borazine'.
- [180] M. Ghedini, M. La Deda, I. Aiello, A. Grisolia, *Inorg. Chim. Acta* **2004**, *357*, 33–40. 'Fine-Tuning the Luminescent Properties of Metal-Chelating 8-Hydroxyquinolines Through Amido Substituents in 5-Position'.
- [181] Y. Sagara, T. Mutai, I. Yoshikawa, K. Araki, *J. Am. Chem. Soc.* **2007**, *129*, 1520–1521. 'Material Design for Piezochromic Luminescence: Hydrogen-Bond-Directed Assemblies of a Pyrene Derivative'.
- [182] Y. Dong, J. W. Y. Lam, A. Qin, Z. Li, J. Sun, H. H.-Y. Sung, I. D. Williams, B. Z. Tang, *Chem. Commun.* **2007**, 40–42. 'Switching the Light Emission of (4-Biphenyl)phenyldibenzofulvene by Morphological Modulation: Crystallization-Induced Emission Enhancement'.
- [183] Z. Fei, N. Kocher, C. J. Mohrschladt, H. Ihmels, D. Stalke, *Angew. Chem. Int. Ed.* **2003**, *42*, 783–787. 'Single Crystals of the Disubstituted Anthracene 9,10-(Ph₂P=S)2C₁₄H₈ Selectively and Reversibly Detect Toluene by Solid-State Fluorescence Emission'.
- [184] Y. Mizobe, H. Ito, I. Hisaki, M. Miyata, Y. Hasegawa, N. Tohnai, *Chem. Commun.* **2006**, 2126–2128. 'A Novel Strategy for Fluorescence Enhancement in the Solid-State: Affording Rigidity to Fluorophores Packing'.
- [185] T. G. Gopakumar, F. Matino, B. Schwager, A. Bannwarth, F. Tuczek, J. Kröger, R. Berndt, *J. Phys. Chem. C* **2010**, *114*, 18247–18251. 'Coverage Driven Formation of Homochiral Domains of an Achiral Molecule on Au (111)'.
- [186] L. Gross, F. Moresco, P. Ruffieux, A. Gourdon, C. Joachim, K.-H. Rieder, *Phys. Rev. B* **2005**, *71*, 165428–165435. 'Tailoring Molecular Self-Organization by Chemical Synthesis: Hexaphenylbenzene, Hexa-peri-hexabenzocoronene, and Derivatives on Cu (111)'.
- [187] R. Fasel, M. Parschau, K.-H. Ernst, *Nature* **2006**, *439*, 449–452. 'Amplification of Chirality in Two-Dimensional Enantiomorphous Lattices'.
- [188] J. Cai, P. Ruffieux, R. Jaafar, M. Bieri, T. Braun, S. Blankenburg, M. Muoth, A. P. Seitsonen, M. Saleh, X. Feng, K. Müllen, R. Fasel, K. Mu, *Nature* **2010**, *466*, 470–473. 'Atomically Precise Bottom-Up Fabrication of Graphene Nanoribbons'.
- [189] C. V Hoven, R. Yang, A. Garcia, V. Crockett, A. J. Heeger, G. C. Bazan, T.-Q. Nguyen, *Proc. Natl. Acad. Sci. U.S.A.* **2008**, *105*, 12730–12735. 'Electron Injection into Organic Semiconductor Devices from High Work Function Cathodes'.
- [190] Q. Pei, G. Yu, C. Zhang, Y. Yang, A. J. Heeger, *Science* **1995**, *269*, 1086–1088. 'Polymer Light-Emitting Electrochemical Cells'.
- [191] P. Matyba, K. Maturova, M. Kemerink, N. D. Robinson, L. Edman, *Nat. Mater.* **2009**, *8*, 672–676. 'The Dynamic Organic p-n Junction'.

Bibliography

- [192] J.-H. Shin, S. Xiao, A. Fransson, L. Edman, *Appl. Phys. Lett.* **2005**, *87*, 43503–43506. 'Polymer Light-Emitting Electrochemical Cells: Frozen-Junction Operation of an "Ionic Liquid" Device'.
- [193] D. Bonifazi, A. Kiebele, M. Stöhr, F. Cheng, T. Jung, F. Diederich, H. Spillmann, *Adv. Funct. Mater.* **2007**, *17*, 1051–1062. 'Supramolecular Nanostructuring of Silver Surfaces via Self-Assembly of [60]Fullerene and Porphyrin Modules'.
- [194] X. Quigshan, E. Perez-Cordero, L. Echegoyen, *J. Am. Chem. Soc.* **1992**, *114*, 3978–3980. 'Electrochemical detection of C₆₀ 6- and C₇₀ 7-: Enhanced Stability of Fullerides in Solution'.
- [195] T. Nakanishi, H. Ohwaki, H. Tanaka, H. Murakami, T. Sagara, N. Nakashima, *J. Phys. Chem. B* **2004**, *108*, 7754–7762. 'Electrochemical and Chemical Reduction of Fullerenes C₆₀ and C₇₀ Embedded in Cast Films of Artificial Lipids in Aqueous Media'.
- [196] A. Montellano López, A. Mateo-Alonso, M. Prato, *J. Mater. Chem.* **2011**, *21*, 1305–1321. 'Materials Chemistry of Fullerene C₆₀ Derivatives'.
- [197] D. M. Guldi, B. M. Illescas, C. M. Atienza, M. Wielopolski, N. Martín, *Chem. Soc. Rev.* **2009**, *38*, 1587–1597. 'Fullerene for Organic Electronics'.
- [198] T. M. Clarke, J. R. Durrant, *Chem. Rev.* **2010**, *110*, 6736–6767. 'Charge Photogeneration in Organic Solar Cells'.
- [199] P. W. M. Blom, V. D. Mihailetschi, L. J. A. Koster, D. E. Markov, *Adv. Mater.* **2007**, *19*, 1551–1566. 'Device Physics of Polymer: Fullerene Bulk Heterojunction Solar Cells'.
- [200] L. Schmidt-Mende, A. Fechtenkötter, K. Müllen, E. Moons, R. H. Friend, J. D. MacKenzie, *Science* **2001**, *293*, 1119–1122. 'Self-Organized Discotic Liquid Crystals for High-Efficiency Organic Photovoltaics'.
- [201] Y. Shibano, H. Imahori, C. Adachi, *J. Phys. Chem. C* **2009**, *113*, 15454–15466. 'Organic Thin-Film Solar Cells Using Electron-Donating Perylene Tetracarboxylic Acid Derivatives'.
- [202] T. Wakahara, P. D'Angelo, K. Miyazawa, Y. Nemoto, O. Ito, N. Tanigaki, D. D. C. Bradley, T. D. Anthopoulos, *J. Am. Chem. Soc.* **2012**, *134*, 7204–7206. 'Fullerene/Cobalt Porphyrin Hybrid Nanosheets with Ambipolar Charge Transporting Characteristics'.
- [203] X. Zhang, M. Takeuchi, *Angew. Chem. Int. Ed.* **2009**, *48*, 9646–9651. 'Controlled Fabrication of Fullerene C₆₀ into Microspheres of Nanoplates through Porphyrin-Polymer-Assisted Self-Assembly'.
- [204] T. Wakahara, M. Sathish, K. Miyazawa, C. Hu, Y. Tateyama, Y. Nemoto, T. Sasaki, O. Ito, *J. Am. Chem. Soc.* **2009**, *131*, 9940–9944. 'Preparation and Optical Properties of Fullerene/Ferrocene Hybrid Hexagonal Nanosheets and Large-Scale Production of Fullerene Hexagonal nanosheets'.
- [205] A. Saeki, S. Seki, T. Takenobu, Y. Iwasa, S. Tagawa, *Adv. Mater.* **2008**, *20*, 920–923. 'Mobility and Dynamics of Charge Carriers in Rubrene Single Crystals Studied by Flash-Photolysis Microwave Conductivity and Optical Spectroscopy'.
- [206] X. Zhang, T. Nakanishi, T. Ogawa, A. Saeki, S. Seki, Y. Shen, Y. Yamauchi, M. Takeuchi, *Chem. Commun.* **2010**, *46*, 8752–8755. 'Flowerlike Supramolecular Architectures Assembled from C₆₀ Equipped with a Pyridine Substituent'.
- [207] F. Masini, N. Kalashnyk, M. M. Knudsen, J. R. Cramer, E. Laegsgaard, F. Besenbacher, K. V. Gothelf, T. R. Linderoth, *J. Am. Chem. Soc.* **2011**, *133*, 13910–13913. 'Chiral Induction by Seeding Surface Assemblies of Chiral Switches'.
- [208] E. V. Iski, H. L. Tierney, A. D. Jewell, E. C. H. Sykes, *Chem. Eur. J.* **2011**, *17*, 7205–7212. 'Spontaneous Transmission of Chirality through Multiple Length Scales'.
- [209] M. Parschau, R. Fasel, K.-H. Ernst, *Cryst. Growth Des.* **2008**, *8*, 1890–1896. 'Coverage and Enantiomeric Excess Dependent Enantioselectivity on Two-Dimensional Molecular Crystals'.

Bibliography

- [210] G. Contini, S. Turchini, S. Sanna, D. Catone, J. Fujii, I. Vobornik, T. Prosperi, N. Zema, *Physical Review B* **2012**, *86*, 1–6. 'Transfer of Chirality from Adsorbed Chiral Molecules to the Substrate Highlighted by Circular Dichroism in Angle-Resolved Valence Photoelectron Spectroscopy'.
- [211] L. Pauling, *J. Am. Chem. Soc.* **1931**, *455*, 1367–1400. 'The Nature of the Chemical Bond. Application of Results Obtained from the Quantum Mechanics and from a Theory of Paramagnetic Susceptibility to the Structure of Molecules'.
- [212] M. Faraday, *J. Svi. Liter. Arts* **1823**, 71–90. 'On the Hydrate of Chlorine'.
- [213] T. Steiner, *Angew. Chem. Int. Ed.* **2002**, *41*, 48–76. 'The Hydrogen Bond in the Solid State'.
- [214] P. A. Kollman, L. C. Allen, *Chem. Rev.* **1972**, *72*, 283–303. 'The Theory of the Hydrogen Bond'.
- [215] G. R. Desiraju, *Angew. Chem. Int. Ed.* **2011**, *50*, 52–59. 'A Bond by Any Other Name'.
- [216] G. R. Desiraju, *Cryst. Growth Des.* **2011**, *11*, 896–898. 'Reflections on the Hydrogen Bond in Crystal Engineering'.
- [217] E. Arunan, G. R. Desiraju, R. A. Klein, J. Sadlej, S. Scheiner, I. Alkorta, D. C. Clary, R. H. Crabtree, J. J. Dannenberg, P. Hobza, H. G. Kjaergaard, A. C. Legon, B. Mennucci, D. J. Nesbitt, *Pure Appl. Chem.* **2011**, *83*, 1637–1641. 'Defining the Hydrogen Bond'.
- [218] P. Gilli, L. Pretto, V. Bertolasi, G. Gilli, *Acc. Chem. Res.* **2009**, *42*, 33–44. 'Predicting Hydrogen-Bond Strengths from Acid-Base Molecular Properties. The pK Slide Rule: Toward the Solution of a Long-Lasting Problem'.
- [219] C. A. Hunter, *Angew. Chem. Int. Ed.* **2004**, *43*, 5310–5324. 'Quantifying Intermolecular Interactions: Guidelines for the Molecular Recognition Toolbox'.
- [220] M. H. Abraham, J. A. Platts, *J. Org. Chem.* **2001**, *66*, 3484–3491. 'Hydrogen Bond Structural Group Constants'.
- [221] R. Cabot, C. A. Hunter, *Org. Biomol. Chem.* **2010**, *8*, 1943–1950. 'A Thermodynamic Study of Selective Solvation in Solvent Mixtures'.
- [222] J. Marco, J. M. Orza, R. Notario, J.-L. M. Abboud, *J. Am. Chem. Soc.* **1994**, *116*, 8841–8842. 'Hydrogen Bonding of Neutral Species in the Gas Phase: The Missing Link'.
- [223] T. R. Shattock, K. K. Arora, P. Vishweshwar, M. J. Zaworotko, *Cryst. Growth Des.* **2008**, *8*, 4533–4545. 'Hierarchy of Supramolecular Synthons: Persistent Carboxylic Acid...Pyridine Hydrogen Bonds in Cocrystals That also Contain a Hydroxyl Moiety'.
- [224] K. Drickamer, *Nature* **1992**, *360*, 183–186. 'Engineering Galactose-Binding Activity into a C-type Mannose-Binding Protein'.
- [225] M. Talwelkar, V. R. Pedireddi, *Tetrahedron Lett.* **2010**, *51*, 6901–6905. '-B(OH)₂ Versus -OH in Supramolecular Synthesis: Molecular Complexes of 4-Hydroxyphenylboronic Acid with Aza-Donor Compounds'.
- [226] S. Djurdjevic, D. A. Leigh, H. McNab, S. Parsons, G. Teobaldi, F. Zerbetto, *J. Am. Chem. Soc.* **2007**, *129*, 476–477. 'Extremely Strong and Readily Accessible AAA–DDD Triple Hydrogen Bond Complexes'.
- [227] W. L. Jorgensen, J. Pranata, *J. Am. Chem. Soc.* **1990**, *112*, 2008–2010. 'Importance of Secondary Interactions in Triply Hydrogen Bonded Complexes: Guanine-Cytosine vs Uracil-2,6-Diaminopyridine'.
- [228] S. Kawahara, T. Uchamaru, *J. Comput. Chem. Jpn.* **2004**, *3*, 41–48. 'Secondary Interaction Contribution in Hydrogen-Bonded Complex: Theoretical Model Study in Hydrogen Fluoride Trimer'.
- [229] E. J. Olson, P. Bühlmann, *J. Org. Chem.* **2011**, *76*, 8406–8412. 'Getting More out of a Job Plot: Determination of Reactant to Product Stoichiometry in Cases of Displacement Reactions and n:n Complex Formation'.

Bibliography

- [230] A. P. Bisson, C. A. Hunter, J. C. Morales, K. Young, *Chem. a Eur. J.* **1998**, *4*, 845–851. 'Cooperative Interactions in a Ternary Mixture'.
- [231] F. P. Schmitchen 'Analytical Methods in Supramolecular Chemistry'. In 'Analytical methods in Supramolecular Chemistry'.; Schalley, C. A., Ed.; 2007; pp. 55–78.
- [232] A. Ababou, J. E. Ladbury, *J. Mol. Recognit.* **2006**, *19*, 79–89. 'Survey of the year 2004: literature on applications of isothermal titration calorimetry'.
- [233] H. Gong, M. J. Krische, *J. Am. Chem. Soc.* **2005**, *127*, 1719–1725. 'Duplex molecular strands based on the 3,6-diaminopyridazine hydrogen bonding motif: amplifying small-molecule self-assembly preferences through preorganization and iterative arrangement of binding residues'.
- [234] S. G. Tajc, B. L. Miller, *J. Am. Chem. Soc.* **2006**, *128*, 2532–2533. 'A Designed Receptor for pH-Switchable Ion Binding in Water'.
- [235] O. Khakshoor, S. E. Wheeler, K. N. Houk, E. T. Kool, *J. Am. Chem. Soc.* **2012**, *134*, 3154–3163. 'Measurement and Theory of Hydrogen Bonding Contribution to Isosteric DNA Base Pairs'.
- [236] A. Velázquez Campoy, E. Freire, *Biophys. Chem.* **2005**, *115*, 115–124. 'ITC in the Post-Genomic Era...? Priceless'.
- [237] W. B. Turnbull, A. H. Daranas, *J. Am. Chem. Soc.* **2003**, *125*, 14859–14866. 'On the Value of c: Can Low Affinity Systems be Studied by Isothermal Titration Calorimetry?'.
- [238] J. Tellinghuisen, *J. Phys. Chem. B* **2007**, *111*, 11531–11537. 'Optimizing Experimental Parameters in Isothermal Titration Calorimetry: Variable Volume Procedures'.
- [239] E. Frankland, B. F. Duppa, *Liebigs Ann. Chem.* **1860**, *115*, 319–322. 'Borathyl'.
- [240] Q. Tan, A. M. Ogawa, R. E. Painter, Y.-W. Park, K. Young, F. P. DiNinno, *Bioorg. Med. Chem. Lett.* **2010**, *20*, 2622–2624. '4,7-Dichloro Benzothien-2-yl sulfonylaminomethyl Boronic Acid: First Boronic Acid-Derived Beta-Lactamase Inhibitor with Class A, C, and D Activity'.
- [241] R. Smoum, A. Rubinstein, V. M. Dembitsky, M. Srebnik, *Chem. Rev.* **2012**, *112*, 4156–4220. 'Boron Containing Compounds as Protease Inhibitors'.
- [242] W. Yang, X. Gao, B. Wang, *Med. Res. Rev.* **2003**, *23*, 346–368. 'Boronic Acid Compounds as Potential Pharmaceutical Agents'.
- [243] M. Sánchez, T. S. Keizer, S. Parkin, H. Höpfl, D. A. Atwood, *J. Organomet. Chem.* **2002**, *654*, 36–43. 'Salen-Supported Dinuclear and Trinuclear Boron Compounds'.
- [244] R. Nishiyabu, Y. Kubo, T. D. James, J. S. Fossey, *Chem. Commun.* **2011**, 1124–1150. 'Boronic Acid Building Blocks: Tools for self Assembly'.
- [245] D. C. Bradley, I. S. Harding, A. D. Keefe, M. Motevalli, D. H. Zheng, *J. Chem. Soc., Dalton Trans.* **1996**, 3931–3936. 'Reversible Adduct Formation Between Phosphines and Triarylboron Compounds'.
- [246] M. T. Reetz, J. Huff, J. Rudolph, K. Tollner, A. Deege, R. Goddard, *J. Am. Chem. Soc.* **1994**, *116*, 11588–11589. 'Highly Efficient Transport of Amino Acids through Liquid Membranes'.
- [247] L. Yabroff, G. E. K. Branch, H. J. Almquist, *J. Am. Chem. Soc.* **1933**, *55*, 2935–2941. 'The Interaction of the Boron Sextet with Adjacent Groups'.
- [248] Y. Tokunaga, H. Ueno, Y. Shimomura, *Heterocycles* **2007**, *74*, 219–223. 'Formation of Hetero-Boroxines: Dynamic Combinatorial Libraries Generated Through Trimerization of Pairs of Arylboronic Acids'.
- [249] P. Armitage, J. R. Ebdon, B. J. Hunt, M. S. Jones, F. G. Thorpe, *Polym. Degrad. Stab.* **1996**, *54*, 387–393. 'Chemical Modification of Polymers to Improve Flame Retardance-I. The influence of Boron-Containing Groups'.

Bibliography

- [250] N. A. A. Zwaneveld, R. Pawlak, M. Abel, D. Catalin, D. Gignes, D. Bertin, L. Porte, *J. Am. Chem. Soc.* **2008**, *130*, 6678–6679. 'Organized Formation of 2D Extended Covalent Organic Frameworks at Surfaces'.
- [251] M. Forsyth, J. Sun, F. Zhou, D. R. Macfarlane, *Electrochim. Acta* **2003**, *48*, 2129–2136. 'Enhancement of Ion Dissociation in Polyelectrolyte Gels'.
- [252] J. A. Faniran, H. F. Shurvell, *Can. J. Chem.* **1968**, *46*, 2089–2095. 'Infrared Spectra of Phenylboronic Acid (Normal and Deuterated) and Diphenyl Phenylboronate'.
- [253] T. M. B. Islam, K. Yoshino, H. Nomura, T. Mizuno, A. Sasane, *Anal. Sci.* **2002**, *18*, 363–366. '¹H and ¹¹B NMR Study of p-Toluene Boronic Acid and Anhydride'.
- [254] H. Frohn, N. Y. Adonin, V. V. Bardin, V. F. Starichenko, *Z. Anorg. Allg. Chem.* **2002**, *628*, 2827–2833. 'Polyfluorinated Aryl (Dihydroxy)boranes'.
- [255] Y. Tokunaga, T. Ito, H. Sugawara, R. Nakata, *Tetrahedron Lett.* **2008**, *49*, 3449–3452. 'Dynamic Covalent Chemistry of a Boronylammonium Ion and a Crown Ether: Formation of a C₃-Symmetric [4]Rotaxane'.
- [256] J. D. Larkin, K. L. Bhat, G. D. Markham, B. R. Brooks, H. F. Schaefer, C. W. Bock, *J. Phys. Chem. A* **2006**, *110*, 10633–10642. 'Structure of the Boronic Acid Dimer and the Relative Stabilities of its Conformers'.
- [257] Y. Tokunaga, H. Ueno, Y. Shimomura, T. Seo, *Heterocycles* **2002**, *57*, 787–790. 'Formation of Boroxine: Its Stability and Thermodynamic Parameters in Solution'.
- [258] M. Regueiro-Figueroa, K. Djanashvili, D. Esteban-Gómez, A. de Blas, C. Platas-Iglesias, T. Rodríguez-Blas, *Eur. J. Org. Chem.* **2010**, *2010*, 3237–3248. 'Towards Selective Recognition of Sialic Acid Through Simultaneous Binding to Its cis-Diol and Carboxylate Functions'.
- [259] K. B. Anderson, R. A. Franich, H. W. Kroese, R. Meder, *Polyhedron* **1995**, *14*, 1149–1153. 'The Structure of Biguanide Complexes of boron'.
- [260] J. Y. Yang, J. Bachmann, D. G. Nocera, *J. Org. Chem.* **2006**, *71*, 8706–8714. 'Hangman Salen Platforms Containing two Xanthene Scaffolds'.
- [261] V. R. R. Pedireddi, N. Seethalekshmi, *Tetrahedron Lett.* **2004**, *45*, 1903–1906. 'Boronic Acids in the Design and Synthesis of Supramolecular Assemblies'.
- [262] N. Christinat, R. Scopelliti, K. Severin, *Angew. Chem. Int. Ed.* **2008**, *47*, 1848–1852. 'Multicomponent Assembly of Boronic Acid Based Macrocycles and Cages'.
- [263] M. Hutin, G. Bernardinelli, J. R. Nitschke, *Chem. Eur. J.* **2008**, *14*, 4585–4593. 'An Iminoboronate Construction Set for Subcomponent Self-Assembly'.
- [264] M. Dogru, A. Sonnauer, A. Gavryushin, P. Knochel, T. Bein, *Chem. Commun.* **2011**, 1707–1709. 'A Covalent Organic Framework with 4 nm Open Pores'.
- [265] H. M. El-Kaderi, J. R. Hunt, J. L. Mendoza-Cortés, A. P. Côté, R. E. Taylor, M. O'Keeffe, O. M. Yaghi, *Science* **2007**, *316*, 268–272. 'Designed Synthesis of 3D Covalent Organic Frameworks'.
- [266] H. Danjo, K. Hirata, S. Yoshigai, I. Azumaya, K. Yamaguchi, *J. Am. Chem. Soc.* **2009**, *131*, 1638–1639. 'Back to Back Twin Bowls of D₃-Symmetric Tris(spiroborate)s for Supramolecular Chain Structures'.
- [267] E. Voisin, T. Maris, J. D. Wuest, *Cryst. Growth Des.* **2008**, *8*, 308–318. 'Crystal Structures of Spiroborates Derived from 2,2'-Dihydroxybiphenyl'.
- [268] M. Mastalerz, *Angew. Chem. Int. Ed.* **2008**, *47*, 445–447. 'The Next Generation of Shape-Persistent Zeolite Analogues: Covalent Organic Frameworks'.

Bibliography

- [269] S. Wan, J. Guo, J. Kim, H. Ihee, D. Jiang, *Angew. Chem. Int. Ed.* **2009**, *48*, 5439–5442. 'Photoconductive Structures A Photoconductive Covalent Organic Framework: Self-Condensed Arene Cubes Composed of Eclipsed 2D Polypyrene Sheets for Photocurrent Generation'.
- [270] S. Wan, J. Guo, J. Kim, H. Ihee, D. Jiang, *Angew. Chem. Int. Ed.* **2008**, *47*, 8826–8830. 'A Belt-Shaped, Blue Luminescent, and Semiconducting Covalent Organic Framework'.
- [271] W. Niu, M. D. Smith, J. J. Lavigne, *J. Am. Chem. Soc.* **2006**, *128*, 16466–16467. 'Self-Assembling Poly(dioxaborole)s as Blue-Emissive Materials'.
- [272] J. W. Colson, A. R. Woll, A. Mukherjee, M. P. Levendorf, E. L. Spitler, V. B. Shields, M. G. Spencer, J. Park, W. R. Dichtel, *Science* **2011**, *332*, 228–231. 'Oriented 2D Covalent Organic Framework Thin Films on Single-Layer Graphene'.
- [273] F. J. Uribe-Romo, J. R. Hunt, H. Furukawa, C. Klöck, M. O'Keeffe, O. M. Yaghi, *J. Am. Chem. Soc.* **2009**, *131*, 4570–4571. 'A Crystalline Imine-Linked 3-D Porous Covalent Organic Framework'.
- [274] K. E. Maly, N. Malek, J.-H. Fournier, P. Rodríguez-Cuamatzi, T. Maris, J. D. Wuest, *Pure Appl. Chem.* **2006**, *78*, 1305–1321. 'Engineering Crystals Built from Molecules Containing Boron'.
- [275] K. M. Clapham, A. S. Batsanov, R. D. R. Greenwood, M. R. Bryce, E. Amy, B. Tarbit, S. Page, A. E. Smith, *J. Org. Chem.* **2008**, *3*, 2176–2181. 'Derivatives via Palladium-Catalyzed Cross-Coupling Methodology'.
- [276] J. J. Campos-Gaxiola, A. Vega-Paz, P. Román-Bravo, H. Höpfl, M. Sánchez-Vázquez, *Cryst. Growth Des.* **2010**, *10*, 3182–3190. 'Pyridineboronic Acids as Useful Building Blocks in Combination with Perchloroplatinate(II) and -(IV) Salts: 1D, 2D, and 3D Hydrogen-Bonded Networks Containing X-H...Cl 2 Pt - (X = C, N +), B(OH) 2 ...Cl 2 Pt -, and B(OH) 2 ... (HO)2B Synthons'.
- [277] P. Rodríguez-Cuamatzi, R. Luna-García, A. Torres-huerta, M. I. Bernal-Uruchurtu, V. Barba, H. Höpfl, *Cryst. Growth Des.* **2009**, *9*, 1575–1583. 'On the Organizing Role of Water Molecules in the Assembly of Hydrogen-Bonded Architectures Containing Cyclophane-Type Motifs'.
- [278] K. M. Clapham, A. E. Smith, A. S. Batsanov, L. McIntyre, A. Pountney, M. R. Bryce, B. Tarbit, *Eur. J. Org. Chem.* **2007**, *2007*, 5712–5716. 'New Pyrimidylboronic Acids and Functionalized Heteroarylpyrimidines by Suzuki Cross-Coupling Reactions'.
- [279] A. Vega, M. Zarate, H. Tlahuext, H. Höpfl, *Acta Crystallogr. C* **2010**, *66*, o219–o221. 'Benzene-1,4-diboronic acid-4,4'-bipyridine-water (1/2/2)'.
- [280] E. Zobetz, A. Preisinger, *Monatsh. Chem.* **1989**, *298*, 291–298. 'Kristallstruktur und Phasenumwandlung von Betain-Borat, (CH₃)₃NCH₂COO•B(OH)₃'.
- [281] P. Rodríguez-Cuamatzi, O. I. Arillo-Flores, M. I. Bernal-Uruchurtu, H. Höpfl, *Cryst. Growth Des.* **2005**, *5*, 167–175. 'Theoretical and Experimental Evaluation of Homo- and Heterodimeric Hydrogen-Bonded Motifs Containing Boronic Acids, Carboxylic Acids, and Carboxylate Anions: Application for the Generation of Highly Stable Hydrogen-Bonded Supramolecular Systems'.
- [282] M. K. Cyranski, A. Jezierska, P. Klimentowska, J. J. Panek, A. Sporzynski, M. K. Cyrański, A. Sporzynski, *J. Phys. Org. Chem.* **2008**, *21*, 472–482. 'Impact of Intermolecular Hydrogen Bond on Structural Properties of Phenylboronic acid: Quantum Chemical and X-Ray Study'.
- [283] J.-H. H. Fournier, T. Maris, J. D. Wuest, W. Z. Guo, E. Galoppini, *J. Am. Chem. Soc.* **2003**, *125*, 1002–1006. 'Molecular tectonics. Use of the Hydrogen Bonding of Boronic Acids to Direct Supramolecular Construction'.
- [284] M. Abe, M. Tanaka, K. Umakoshi, Y. Sasaki, *Inorg. Chem.* **1999**, *38*, 4146–4148. 'Enhanced Kinetic Lability of Ru(III) Centers in Oxo-Centered Mixed-Metal Ru₂M Trinuclear Complexes (M = Zn and Mg)'.
- [285] P. Rogowska, M. K. Cyrański, A. Sporzynski, A. Ciesielski, *Tetrahedron Lett.* **2006**, *47*, 1389–1393. 'Evidence for Strong Heterodimeric Interactions of Phenylboronic Acids with Amino Acids'.

Bibliography

- [286] 2009. M. J. Frisch, G. W. Trucks, H. B. Schlegel, G. E. Scuseria, M. A. Robb, J. R. Cheeseman, G. Scalmani, V. Barone, B. Mennucci, G. A. Petersson, H. Nakatsuji, M. Caricato, X. Li, H. P. Hratchian, A. F. Izmaylov, J. Bloino, G. Zheng, J. L. Sonnenberg, M. Had.
- [287] G. Hall, *Denisboronic Acids*; Hall, D. G., Ed.; Wiley VCH, 2005; p. 545.
- [288] P. Wipf, J. K. Jung, *J. Org. Chem.* **2000**, *65*, 6319–6337. 'Formal Total Synthesis of (+)-Diepoxin σ '.
- [289] H. Chaumeil, S. Signorella, C. Le Drian, *Tetrahedron* **2000**, *56*, 9655–9662. 'Suzuki Cross-Coupling Reaction of Sterically Hindered Aryl Boronates with 3-Iodo-4-methoxybenzoic Acid Methyl Ester'.
- [290] E. L. Muetterties, *J. Am. Chem. Soc.* **1960**, *82*, 4163–4166. 'Synthesis of Organoboranes'.
- [291] A. R. Miller, D. Y. Curtin, *J. Am. Chem. Soc.* **1976**, *98*, 1860–1865. 'Locked aryl rotation in cis-diarylacenaphthenes, torsionally rigid analogues of cis-1,2-diarylcyclopentanes'.
- [292] T. Teraoka, S. Hiroto, H. Shinokubo, *Organic Letters* **2011**, *13*, 2532–2535. 'Iridium-Catalyzed Direct Tetraborylation of Perylene Bisimides'.
- [293] T. M. Boller, J. M. Murphy, M. Hapke, T. Ishiyama, N. Miyaura, J. F. Hartwig, *J. Am. Chem. Soc.* **2005**, *127*, 14263–14278. 'Mechanism of the Mild Functionalization of Arenes by Diboron Reagents Catalyzed by Iridium Complexes. Intermediacy and Chemistry of Bipyridine-Ligated Iridium Trisboryl Complexes'.
- [294] P. Rodríguez-Cuamatzi, G. Vargas-Díaz, T. Maris, J. D. Wuest, H. Höpfl, *Acta crystallogr. E* **2004**, *60*, o1316–o1318. '1,4-Phenylenediboronic Acid'.
- [295] K. Wariishi, S. Morishima, Y. Inagaki, *Org. Process Res. Dev.* **2003**, *7*, 98–100. 'A Facile Synthesis of 1,4-Dialkoxy-2,5-diiodobenzenes: Reaction of Dialkoxybenzenes with Iodine Monochloride in Alcoholic Solvents'.
- [296] A. M. Elder, D. H. Rich, *Org. Lett.* **1999**, *1*, 1443–1446. 'Two Syntheses of the 16- and 17-Membered DEF Ring Systems of Chloropeptin and Complestatin'.
- [297] T. Itoh, K. Hirai, H. Tomioka, *J. Am. Chem. Soc.* **2004**, *2*, 1130–1140. 'Preparation of Oligodiazo Compounds by Using the Suzuki Coupling Reaction and Characterization of Their Photoproducts'.
- [298] H. O. House, J. A. Hrabie, D. VanDerveer, *J. Org. Chem.* **1986**, *51*, 921–929. 'Unsymmetrically Substituted 1,8-Diarylanthracene'.
- [299] S. Toyota, H. Miyahara, M. Goichi, S. Yamasaki, T. Iwanaga, *Bull. Chem. Soc. Jpn.* **2009**, *82*, 931–945. 'Chemistry of Anthracene-Acetylene Oligomers. XIII. Synthesis, Structures, and Spectroscopic Properties of All Possible 1,8-Anthrylene Cyclic Tetramers With Acetylene and Diacetylene Linkers'.
- [300] N. K. S. Davis, A. L. Thompson, H. L. Anderson, *Org. Lett.* **2010**, *12*, 2124–2127. 'Bis-Anthracene Fused Porphyrins: Synthesis, Crystal Structure, and Near-IR Absorption'.
- [301] C. Coudret, V. Mazenc, *Tetrahedron Lett.* **1997**, *38*, 5293–5296. 'Heteroarylation of Anthraquinone-Triflate by Suzuki Cross-Coupling'.
- [302] D. S. Zinad, M. Hussain, O. A. Akrawi, A. Villinger, P. Langer, *Tetrahedron Lett.* **2011**, *52*, 3451–3454. 'Site-Selective Suzuki–Miyaura Reactions of the Bis(triflate) of 1,3-Dihydroxythioxanthone'.
- [303] C. G. Swain, E. C. Lupton, *J. Am. Chem. Soc.* **1968**, *90*, 4328–4337. 'Field and Resonance Components of Substituent Effects'.
- [304] I. A. Pearl, *J. Org. Chem.* **1957**, *22*, 1229–1232. 'Reactions of Vanillin and Its Derived Compounds. XXVII. Synthesis in the Syringyl Series'.
- [305] C. P. Butts, E. Filali, G. C. Lloyd-Jones, P.-O. Norrby, D. A. Sale, Y. Schramm, *J. Am. Chem. Soc.* **2009**, *131*, 9945–9957. 'Structure-Based Rationale for Selectivity in the Asymmetric Allylic Alkylation of Cycloalkenyl Esters'.

Bibliography

- Employing the Trost "Standard Ligand" (TSL): Isolation, Analysis and Alkylation of the Monomeric form of the Cationic η^3 -Cyclohexenyl Complex [(η^3 -c-C₆H₉)⁺].*
- [306] C. Moldoveanu, D. A. Wilson, C. J. Wilson, P. Corcoran, B. M. Rosen, V. Percec, *Org. Lett.* **2009**, *11*, 4974–4977. 'Neopentylglycolborylation of Aryl Chlorides Catalyzed by the Mixed Ligand System NiCl₂ (dppp)/dppf'.
- [307] W. Nakanishi, S. Hayashi, N. Itoh, *J. Org. Chem.* **2004**, *69*, 1676–1684. 'Extended Hypervalent 5c-6e Interactions: Linear Alignment of Five C-Se---O---Se-C Atoms in Anthraquinone and 9-Methoxyanthracene Bearing Arylselanyl Groups at the 1,8-Positions'.
- [308] T. Wada, *Dalton Trans.* **2011**, *40*, 2225–2233. 'Substituents Dependent Capability of Bis(ruthenium-dioxolene-terpyridine) Complexes Toward Water Oxidation'.
- [309] J. Rettig, J. Trotter, *Can. J. Chem.* **1977**, *55*, 3071–3074. 'Crystal and Molecular structure of Phenylboronic Acid, C₆H₅B(OH)₂'.
- [310] H. Frohn, N. Y. Adonin, V. V. Bardin, V. F. Starichenko, *Z. Anorg. Allg. Chem.* **2002**, *628*, 2834–2838. 'Base-catalysed Hydrodeboration of Polyfluorophenyl(dihydroxy)boranes'.
- [311] G. Adjabeng, T. Brenstrum, C. S. Frampton, A. J. Robertson, J. Hillhouse, J. McNulty, A. Capretta, *J. Org. Chem.* **2004**, *69*, 5082–5086. 'Palladium Complexes of 1,3,5,7-Tetramethyl-2,4,8-trioxa-6-phenyl-6-phosphaadamantane: Synthesis, Crystal Structure and Use in the Suzuki and Sonogashira Reactions and the α -Arylation of Ketones'.
- [312] J. Moon, M. Jang, S. Lee, *J. Org. Chem.* **2009**, *74*, 1403–1406. 'Palladium-Catalyzed Decarboxylative Coupling of Alkynyl Carboxylic Acids and Aryl Halides'.
- [313] M. F. Hawthorne, *J. Org. Chem.* **1958**, *23*, 1579–1580. 'Preparation and Reactions of Mesitylene-boronic Acid'.
- [314] J. Chmiel, I. Heesemann, A. Mix, B. Neumann, H.-G. Stammler, N. W. Mitzel, *Eur. J. Org. Chem.* **2010**, *2010*, 3897–3907. 'The Effect of Bulky Substituents on the Formation of Symmetrically Trisubstituted Triptycenes'.

SIMON KERVYN DE MEERENDRE

Address: Rue du Paradis, 20, 5030 Gembloux, Belgium.

+32 472701089 (private)

E-mail: simonkervyn@hotmail.com

Date of birth: 06.07.1984

Nationality: French and Belgian

EDUCATION

- Oct07-Oct12** **PhD in Organic Chemistry – University of Namur, Chemistry Department**
Specializing in Organic Supramolecular Chemistry under the supervision of Prof. Davide Bonifazi.
- Sep05-Jul07** **Master in Chemistry – University of Namur, Chemistry Department**
Specialized in organic chemistry. Dissertation title: “Transformation of Carboxylic Esters into Acids using Microreactors”. Succeeded with ‘Grande Distinction’. (Belgian equivalent of ‘Magna cum laude’).
- Sept03-Jun05** **Bachelor in Chemistry – University of Namur, Chemistry Department.**
Succeeded with ‘Grande Distinction’ (Belgian equivalent of ‘Magna cum laude’).

EXPERIENCES

- Jan12-Mar12** **Invited researcher – NIMS Tsukuba (Japan)**
Research activity in the laboratory of Dr. Takashi Nakanishi, characterizations of cocrystal at the solid state (TEM, fluorescence, solid state conductivity, DSC).
- Feb11-Dec11** **Supervision of Master student – FUNDP.**
Guide and teach a master student (Florence Valtin) in supramolecular organic chemistry.
- Sep10** **Visiting researcher – ISOF-CNR Bologna (Italy)**
Research activity in the laboratory of Dr. Nicola Armaroli, working with solid state fluorimeter under the supervision of Dr. Gianluca Accorsi.
- Nov09** **Visiting researcher – UCL London (UK)**
Research activity in the laboratory of Prof. Franco Cacialli, working on the construction of OLED under the supervision of Dr. Olly Fenwick.
- Oct07-Oct12** **Research activity in the Supramolecular Organic Chemistry Laboratory (COMS) of Prof. Davide Bonifazi, University of Namur (Belgium), Chemistry Department – PhD in Chemistry.**
- Feb07-Jun07** **Research activity in the Organic Chemistry Laboratory of Prof. Thomas Wirth – University of Cardiff, Cardiff School of Chemistry**
Completion of master-thesis research activity.

- Sept06-Jan07** **Research activity in the Organic Chemistry Laboratory of Prof. Alain Krief – University of Namur, Chemistry Department**
Completion of master-thesis research activity.
- Sept05-Jun05** **Student representative – University of Namur Chemistry Department.**
- Summer 2002** **Work in a Start-Up producing heat exchanger.**
- 2000-03** **Student representative – High School ‘Institut Saint Albert’, Jodoigne, Belgium.**

RESEARCH PROJECTS

- Jan12-Mar12** **Research activity NIMS – “Cocrystal of fullerene and borazines and liquid crystals”.**
- Oct11-Dec11** **Research activity FUNDP – “New H-bonding units for supramolecular materials”.**
- Oct07-Sep11** **Research activity FRIA-FNRS – “Synthesis of Extended π -conjugated Organic Multiads Using Hexasubstituted Borazine Cores”.**
- Sept06-Jul07** **Research activity-Master Thesis – “Transformation of Carboxylic Esters into Acids using Microreactors”.**

AWARDS AND FELLOWSHIP

- 2012-2013** **BAEF ‘honorary fellowship’**
- Jan12-Mar12** **NIMS internship award, Tsukuba Japan.**
- Oct11-Dec11** **FUNDP-fellowship.**
- Oct09-Sep011** **Fonds pour la Recherche dans l’Industrie et l’Agriculture (F.R.I.A.)**
Two years fellowship for Ph.D. student. First candidate selected by the Jury.
- Oct07-Oct09** **Fonds pour la Recherche dans l’Industrie et l’Agriculture (F.R.I.A.)**
Two years fellowship for Ph.D. student.

ADDITIONAL SKILLS

Languages: French (native), English (fluent), Dutch (basic).

Technical Skills: Scientific and technical responsible of GC and LC-MS, mass spectrometry responsible.

Techniques: IR, (solution and solid state), NMR, UV (solution and solid state), fluorimeter (Solution and solid state), GC-MS, LC-MS.

Computing: Operating systems (Windows 95/98/00/NT/XP/Vista); Applications (Microsoft Office 2007, Origin, ChemOffice, Mercury, CSD database, Espacenet)

PUBLICATIONS

S. Kervyn, T. Nakanishi, J. Aimi, A. Saeki, S. Seki, B. Champagne, D. Bonifazi, *Chem. Lett.*, **2012, *41*, 1210-1212. ‘Nanostructured Cocrystal of a Borazine with [60]Fullerene’.**

PATENTS

S. Kervyn, D. Bonifazi, ‘Borazine’, PCT/EP2012/054670 filed in March 2011.

S. Kervyn, D Bonifazi, ‘Borazene oligomers’, PCT/EP2012/054689 filed in March 2012.

SUBMITTED:

S. Kervyn, O. Fenwick, F. Di Stasio, Y.S. Shin, J. Wouters, G. Accorsi, S. Osella, D. Beljonne, F. Cacialli and D. Bonifazi. 'Polymorphism, fluorescence and optoelectronic properties of a borazine derivative'.

IN PREPARATION:

S. Kervyn, N. Kalashnyk, M. Riello, J. Wouters, A. De Vita, G. Costantini and D. Bonifazi, 'Magic self-assembly of borazines on metal surfaces'.

S. Kervyn, F. Valtin, I. Georgiou, F. de Leo, G. Bruylants, K. Bartik, J. Wouters, D. Bonifazi, 'Boronic acids scaffoldings for complementary AA-DD H-bonding arrays'.

BOOK

S. Kervyn, C. Aurisicchio, D. Bonifazi 'Synthesis and design of π -conjugated architectures doped with heteroatoms', in F. Cacialli and P. Samori 'Functional Supramolecular Architecture for Organic Electronics and nanotechnology' Wiley – WCH, 2010.

ORAL COMMUNICATIONS

S. Kervyn (2011) ' π -conjugated organic UV emitters doped with Boron and Nitrogen', in proceeding of the 15th Sigma-Aldrich Organic Synthesis Meeting, Spa, Belgium, 1st-2nd of December.

S. Kervyn (2011) 'BN doped π -conjugated organic emitters' in proceedings of the 14th ISNA, Eugene, USA, 24nd-30rd of July.

S. Kervyn (2010) 'Properties of Borazine derivatives' in proceedings of the FNRS contact group in supramolecular chemistry, ULB, Brussels, 13th of September.

S. Kervyn (2010) 'Borazines Derivatives as New UV Emitters' in proceedings of the workshop on Organic Emitters, CNR Bologna, Italy, 19th of May.

REFEREES

Prof. Davide Bonifazi (Ph.D. Supervisor) – Dept. de Chimie, Facultés Universitaires Notre-Dame de la Paix (F.U.N.D.P), Rue de Bruxelles 61, Namur, Belgium, Tel: +32 81725452, Fax: +32 81725433, Email : davide.bonifazi@fundp.ac.be

Prof. Thomas Wirth (Master thesis Supervisor) – Cardiff school of chemistry, Cardiff University, Main Building, Park Place, Cardiff CF10 3AT, United Kingdom, Tel./Fax: +44 292087 6968, Email: wirth@cf.ac.uk

Prof. Alain Krief (Master thesis Supervisor) - Dept. de Chimie, Facultés Universitaires Notre-Dame de la Paix (F.U.N.D.P), Rue de Bruxelles 61, Namur, Belgium, Tel: +32 81724539, Fax: +32 81724536, Email : alain.krief@fundp.ac.be